U.PORTO

FACULDADE DE CIÊNCIAS
UNIVERSIDADE DO PORTO

Combining Earth Observation and predictive modelling for multi-scale and multi-level biodiversity assessment and monitoring

João Francisco Fernandes Gonçalves

Tese de Doutoramento apresentada à
Faculdade de Ciências da Universidade do Porto

Departamento de Biologia

2017

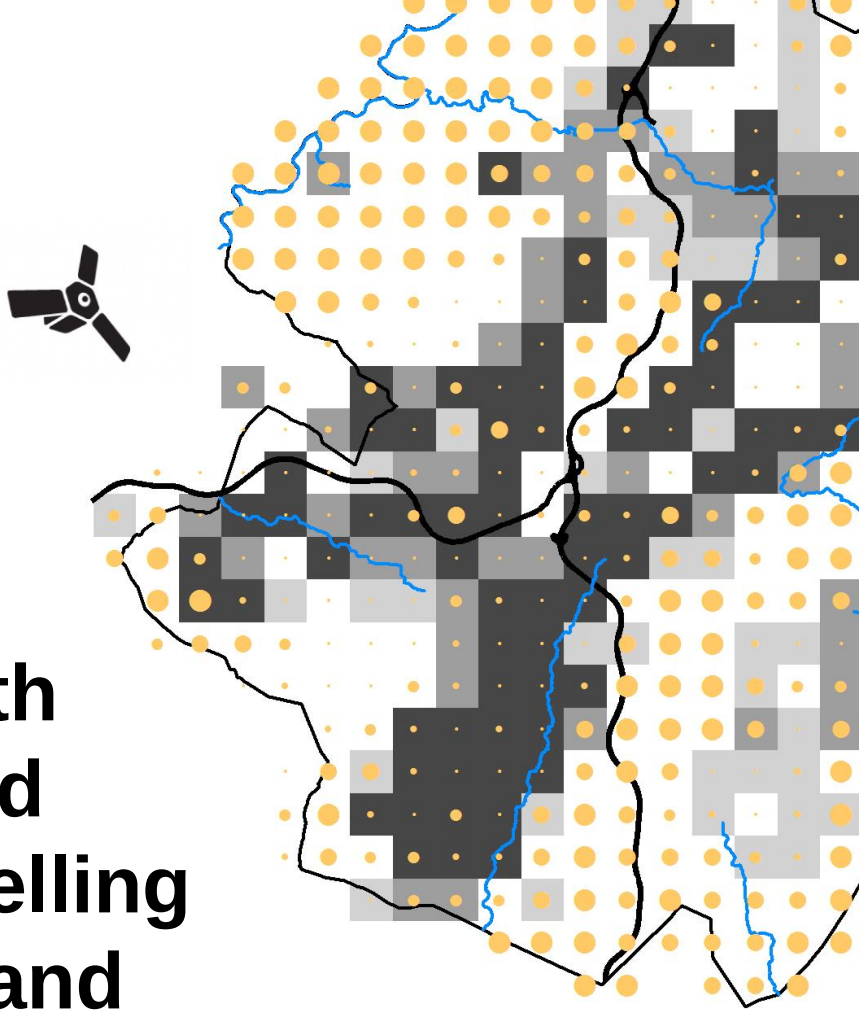

Combining Earth Observation and predictive modelling for multi-scale and multi-level biodiversity assessment and monitoring

João Francisco Fernandes Gonçalves
Plano Doutoral em Biodiversidade, Genética e Evolução
Departamento de Biologia
Faculdade de Ciências da Universidade do Porto
2017

Orientador
João P. Honrado, Professor Auxiliar e Investigador, Faculdade de Ciências
Universidade do Porto

Coorientador
Caspar A. Mücher, Dr. Ir., Wageningen Environmental Research (Alterra)
Wageningen University and Research

Nota Prévia

Na elaboração desta tese, e nos termos do número 2 do Artigo 4º do Regulamento Geral dos Terceiros Ciclos de Estudos Universidade do Porto e do Artigo 31º do Decreto-Lei 74/2006, de 24 de março, com a nova redação introduzida pelo Decreto-Lei 230/2009, de 14 de setembro, foi efetuado o aproveitamento total de um conjunto coerente de trabalhos de investigação já publicados, submetidos ou em fase final de preparação para publicação em revistas internacionais indexadas e com arbitragem científica, os quais integram alguns dos capítulos da presente tese. Tendo em conta que os referidos trabalhos foram realizados com a colaboração de outros autores, o candidato esclarece que, em todos eles, participou ativamente na sua conceção, na obtenção de dados e/ ou no seu processamento e análise, na discussão e interpretação dos resultados obtidos bem como na elaboração e redação dos artigos científicos aqui apresentados.

A Faculdade de Ciências da Universidade do Porto foi a instituição de origem do candidato, tendo o trabalho sido realizado sob a supervisão do orientador Prof. João Pradinho Honrado (CIBIO/InBIO – Faculdade de Ciências da Universidade do Porto), do coorientador Casper A. Mücher (Alterra – Wageningen University and Research, Holanda) e da coorientadora Isabel Pôças (LEAF/ISA – Universidade de Lisboa e CICGE – Faculdade de Ciências da Universidade do Porto). Os trabalhos foram realizados nas instalações do CIBIO/InBIO e noutras associadas aos investigadores que colaboraram no âmbito desta tese.

A elaboração desta tese de Doutoramento foi apoiada pela Fundação para a Ciência e a Tecnologia (FCT) através da bolsa de doutoramento nr.: SFRH/BD/90112/2012 do Fundo Social Europeu (FSE) e POPH-QREN (2007-2013).

Summary (EN)

Earth Observation (EO) technologies are a powerful tool to monitor biodiversity status and change, with a vast collection of available platforms with different spatial, spectral and temporal resolutions. This variety of EO data sources is opening a wide range of opportunities for biodiversity research and for developing multi-level (from genes to landscapes), multi-scalar (from local to regional) and multi-faceted (from structure, composition up to function) monitoring systems, supported by the integration of EO data and robust modelling frameworks. Based on a comprehensive framework including those multiple biodiversity dimensions, this thesis research plan aimed to contribute to fundamental and applied research around the analysis, assessment and monitoring of biodiversity patterns and their changes. Our goal was to provide guidance and building blocks towards a cross-scale and cross-level monitoring framework supported by the integration of EO-based indicators and EO-fed models, to assist national and trans-national efforts related to the management and conservation of biodiversity.

The thesis includes three main sections: Introduction, Research papers, and General discussion and conclusions. Section I (*Introduction*) addresses the current challenges regarding the pressures and drivers of the global 'biodiversity crisis' in the Anthropocene era. A general contextualization and a broad overview of the 'multi-dimensional' concept of biodiversity and its impact on monitoring and assessment is presented. EO principles and data sources, as well as ecological models, are also introduced at this point. Finally, the overarching research objectives, strategy and development are described.

Section II (*Research papers*) includes six studies encompassing most of the scales, levels and facets that are intrinsic and relevant to biodiversity in terrestrial ecosystems. Three major topics were addressed in these studies: (i) the spatial and temporal components of functional connectivity (studies S1 to S3), (ii) habitat and ecosystem monitoring for protected area management (studies S4 and S5), and (iii) development of optimized methods for EO data processing for ecological change assessment.

In study S1 we used a comparative cross-scalar approach combining genetic tools, models, evolutionary algorithm-based optimization and EO data to investigate functional connectivity and gene flow in two Mediterranean amphibian pond-breeding species. The results clarify the effect of different landscape features on regional patterns

of population connectivity, gene flow and genetic differentiation in the two test species. Remarkable differences were found concerning the role of fine-scale patterns of vegetation cover, vegetation water content and its spatial heterogeneity in shaping patterns of regional genetic structure and gene flow for the two species. These differences in spatial heterogeneity were better portrayed by fine-scale remotely sensed spectral indices capturing land cover, vegetation and moisture in a continuous fashion. Our findings hold promising applications for addressing and evaluating functional connectivity in conservation and monitoring of vulnerable species.

In study S2, we investigated how EO-based variables related to ecosystem functioning could improve predictions and track short-term changes in habitat suitability for a vulnerable plant species. The results highlight the added value and the predictive ability of those EO-based functional variables, emphasizing their usefulness for species-level monitoring. EO time-series also contributed to clarifying the mechanisms underpinning species' temporal functional connectivity and responses to fluctuations in habitat suitability derived from multiple sources of disturbance. This holds promising applications of EO to monitor and anticipate shifts in ecosystems potentially impacting species persistence. Applications of this methodology include regional to local landscape species monitoring, management and reporting.

In study S3, we assessed the vulnerability to landscape fragmentation of reptile and amphibian species with low-dispersal abilities and facing climate and land use change. We combined Species Distribution Models (SDMs) and functional connectivity analyses to investigate the impact of fragmentation on the ability of species to track future climate change. Model projections show that environmental changes may cause severe contractions in suitable area for most test species. Moreover, connectivity analyses highlighted that potential migration corridors may be further impacted by the motorway network, making these species even more vulnerable to extinction or isolation. Contributions from this study span from methodological advances in synoptic analysis of functional connectivity up to regional and local climate change adaptation and monitoring.

Study S4 describes and tests a methodological approach for exploiting ultra-high resolution optical imagery and a digital surface model captured by an Unmanned Aerial Vehicle (UAV or ‘drone’) for fine-scale mapping of Natura 2000 priority habitats in a mountainous area under land use and rural abandonment. Our approach (based on supervised classification) obtained good overall accuracy for discriminating the target habitat types, which occur in small-scale, complex mosaics. It was also possible to

diagnose habitat quality and identify degraded patches of particular habitat types of high conservation priority. Overall, our results provide compelling indications that UAV imagery is suitable for mapping and monitoring Natura 2000 habitats, with application in protected area management and in habitat assessment and reporting on the Habitats Directive.

In study S5, we propose and evaluate an EO-based approach for measuring the performance of Protected Areas (PAs) to foster forest ecosystem stability. The approach is based on a time-series of MODIS Enhanced Vegetation Index (EVI), from which we calculated several stability metrics based on Ecosystem Functional Attributes, time-series decomposition and the non-linear Maximum Lyapunov Exponent. Then, we compared the distributions of stability metrics within and outside PAs (with similar environmental characteristics). We found a complex pattern of PA forest stability performance across the national network, both among and within PAs. Multi-model inference confirmed the pervasive negative effect of forest fires on stability, especially in mountainous PAs. Forest composition and structure also exerted a strong control over stability performance, with a positive signal related to coverage of broadleaf forests. PAs with taller and more vertically complex forest canopies, and with larger and more connected patches, were also more stable. We also found a strong positive effect of PA size, with larger parks generally holding greater stability. Potential applications of this approach are vast, spanning from PA adaptive management to disturbance control, monitoring and conservation.

In study S6, we aimed to contribute for improvement of methods in Geographic Object-based Image Analysis (GEOBIA), employed in processing (very-)high resolution EO data in ecological applications. We addressed this by optimizing the integration of two crucial steps in GEOBIA workflows: image segmentation, and classification. Genetic Algorithms were used to optimize image segmentation parameters, with synergistic benefits for both steps. A new open-source R package (*SegOptim*) was developed for implementing the proposed approach and dissemination. We tested this package in different settings, conditions and data sources. We found that no particular combination of an image segmentation and a classification algorithm is suited for all the tasks/objectives, suggesting an empirical verification of the "*no-free-lunch theorem*" for GEOBIA problems. Besides theoretical implications, this means that comparing and optimizing methods (for which *SegOptim* is well-tailored) is crucial to determine which ones are more suited to a particular objective. Contributions from this work span to all researchers/practitioners interested in applying GEOBIA methodologies, including ecologists, remote sensing specialists, cartographers, geographers, among others.

Finally, in Section III (*General discussion and conclusions*) we first summarize and link the main research contributions of each study to a broader overview around each major topic addressed in the thesis. We compare and integrate the three major approaches applied in this thesis for biodiversity monitoring and change assessment: detection, modelling, and combined. We discuss their advantages and shortcomings and provide guidelines to adopt each approach depending on the nature and objectives of global, continental (Europe) and national monitoring initiatives. We also provide a general summary of the impact and potential application of the research developed as well as possible paths to improve it. We close with a set of overarching remarks and an outlook focused on broad 'lessons learned', advances in the state of knowledge and methods, and a set of recommendations on operational challenges towards adopting a more "EO-based biodiversity monitoring" paradigm. Together with robust modelling frameworks, the plethora of EO data sources can (and already is) advancing the scientific knowledge regarding the causes underlying accelerated changes in biodiversity. Throughout this thesis, we supported this notion through a series of research papers that individually constitute building blocks to develop an EO-supported monitoring system. In its essence, that system could respond to the demands of national and international efforts aimed to track and halt biodiversity loss, by supporting meaningful sets of indicators to evaluate the implementation of conservation programs and policy instruments.

Resumo (PT)

As tecnologias de Observação Terrestre (OT) constituem uma poderosa ferramenta para monitorizar o estado e as alterações da biodiversidade, com uma vasta coleção de plataformas disponíveis com diferentes resoluções espaciais, espectrais e temporais. Esta variedade de fontes de dados de OT significa que é possível desenvolver sistemas de monitorização multinível (dos genes às paisagens), multi-escalares (local até global) e multifacetados (estrutura, composição e função) suportados pela integração de dados de OT e abordagens de modelação robustas. Com base numa moldura abrangente, que inclui as múltiplas dimensões da biodiversidade, o plano de investigação desta tese teve como objetivo contribuir para a investigação fundamental e aplicada em torno da análise, avaliação e monitorização dos padrões biodiversidade e da sua alteração. O objetivo foi providenciar linhas de orientação e os elementos constituintes para desenvolver molduras de monitorização cruzando diversas escalas e níveis e suportados pela integração de indicadores e modelos alimentados por dados de OT, e tendo como objetivo assistir os esforços nacionais e transnacionais relacionados com a gestão e conservação da biodiversidade.

A tese inclui três secções: Introdução, Artigos de investigação e Discussão e conclusões gerais. A Secção I (*Introdução*) aborda os atuais desafios relacionados com as pressões e os fatores de alteração da 'crise global da biodiversidade' no Antropoceno. Uma contextualização e uma visão panorâmica geral do conceito 'multidimensional' de biodiversidade e o impacto deste para a monitorização e avaliação é apresentado. Os princípios fundamentais e as fontes de dados de OT, assim como, os modelos ecológicos, são também introduzidos neste ponto. Para finalizar, são descritos os objetivos gerais de investigação, a estratégia e o seu desenvolvimento.

A Secção II (*Artigos de investigação*) inclui seis estudos que abarcam a maioria das escalas, níveis e facetas que são intrínsecas e relevantes para a biodiversidade nos ecossistemas terrestres. Três grandes tópicos são abordados nestes estudos: (i) as componentes espacial e temporal da conectividade funcional ao nível da espécie (estudos S1 a S3), (ii) a monitorização de habitats e ecossistemas para a gestão de áreas protegidas (estudos S4 e S5), e (iii) o desenvolvimento de métodos optimizados para a o processamento de dados de OT com aplicações na avaliação de alterações ecológicas.

No estudo S1 utilizámos uma abordagem trans-escalar combinando ferramentas genéticas, modelos, otimização baseada em algoritmos evolutivos e dados de OT para investigar a conectividade funcional e o fluxo genético em duas espécies Mediterrânicas de anfíbios que se reproduzem em charcos. Os resultados obtidos clarificam o efeito de diferentes estruturas da paisagem nos padrões regionais de conectividade populacional, fluxo genético e diferenciação genética nas duas espécies. Notáveis diferenças foram encontradas relativamente ao papel de aspetos finos dos padrões de coberto da vegetação, quantidade de água na vegetação e da heterogeneidade espacial destes nos padrões regionais da estrutura genética e fluxo genético para as duas espécies. As variações na heterogeneidade espacial foram melhor capturadas pela escala-fina dos índices espectrais derivados de deteção remota, capazes de capturar de forma contínua os padrões de coberto do solo, vegetação e humidade. Estes contributos evidenciam aplicações promissoras para abordar e avaliar a conectividade funcional na conservação e monitorização de espécies vulneráveis.

No estudo S2, investigámos o potencial de variáveis baseadas em OT relacionadas com o funcionamento dos ecossistemas para melhorar as previsões e detetar as alterações de curto-prazo na adequabilidade do habitat para espécies vulneráveis de plantas. Os resultados obtidos evidenciam as mais-valias e a capacidade preditiva das variáveis funcionais de OT, enfatizando a relevância destas para a monitorização ao nível da espécie. As séries-temporais de OT também contribuíram para clarificar os mecanismos subjacentes à componente temporal da conectividade funcional e a resposta a flutuações na adequabilidade do habitat derivadas de múltiplas fontes de perturbação. Estes resultados mostram aplicações relevantes da OT para monitorizar e antecipar alterações nos ecossistemas com potenciais impactos na persistência das espécies. As aplicações desta metodologia incluem a monitorização, gestão e o relato desde a escala local da paisagem até à regional.

No estudo S3, avaliámos a vulnerabilidade à fragmentação da paisagem de espécies de répteis e anfíbios com baixa capacidade dispersão e que atualmente enfrentam alterações climáticas e de uso do solo. Modelos de Distribuição de Espécies (SDMs) e análises de conectividade funcional foram combinados para investigar o impacto da fragmentação da paisagem na capacidade das espécies acompanharem futuras alterações do clima. As projeções dos modelos mostram que as alterações ambientais irão causar contrações severas na área adequada para a maioria das espécies testadas. Adicionalmente, as análises de conectividade mostram que os potenciais corredores de migração poderão ser adicionalmente impactados pela rede

de autoestradas, tornando estas espécies ainda mais vulneráveis à extinção ou isolamento. Os contributos deste estudo estendem-se desde avanços metodológicos na análise sinóptica da conectividade funcional até à adaptação e monitorização regional e local às alterações climáticas.

O estudo S4 descreve e avalia uma abordagem metodológica para explorar imagens óticas de resolução ultra-elevada e um modelo digital da superfície capturados por um Veículo Aéreo Não Tripulado (VANT, vulgo 'drone') para o mapeamento a fina-escala de habitats prioritários em contexto de áreas de montanha abrangidas na Rede Natura 2000, e submetidas a processos de abandono rural e de uso do solo. A abordagem (baseada em classificação supervisionada) obteve boa exatidão geral para discriminar os tipos de habitat alvo, que ocorrem em mosaicos complexos e escalarmente finos. Foi também possível diagnosticar a qualidade do habitat e identificar parcelas degradadas de tipos de habitat particulares de elevada prioridade para a conservação. Em termos gerais, os resultados providenciam uma convincente indicação que as imagens de UAV são adequadas para o mapeamento e monitorização de habitats Natura 2000, com aplicações na gestão de áreas protegidas e na avaliação do estado de habitats para efeitos de relato da Diretiva Habitats.

No estudo S5, foi proposta e avaliada uma abordagem baseada em OT para medir a performance de Áreas Protegidas (APs) para promover a estabilidade dos ecossistemas florestais. A abordagem é baseada numa série temporal da plataforma MODIS e do Índice de Vegetação Melhorado (IVM), a partir do qual foram calculadas várias métricas de estabilidade baseadas em Atributos Funcionais dos Ecossistemas, decomposição de séries temporais e em análise não-linear através do Expoente Máximo de Lyapunov. Em sequência, comparámos a distribuição dos indicadores de estabilidade calculados dentro e fora de APs (com base em área ambientalmente similares). Em termos gerais, encontramos um padrão complexo de estabilidade florestal ao longo da rede nacional de APs, tanto entre e dentro destas. Técnicas estatísticas de Inferência multi-modelo permitiram confirmar o efeito negativo generalizado que os fogos florestais exercem sobre a estabilidade florestal, especialmente em APs de montanha. A composição e estrutura da floresta também exerceram um elevado controlo sobre a performance da estabilidade, com um sinal positivo relacionado com a cobertura de floresta de folhosas. Adicionalmente, APs com dosséis florestais mais elevados e complexos, e com parcelas mais amplas e mais conectadas foram também consideradas mais estáveis. Também encontrámos um forte efeito positivo do tamanho da AP, com parques de maiores dimensões genericamente mais estáveis. As aplicações potenciais desta abordagem são vastas, compreendendo

desde a gestão adaptativa de APs ao controlo de fontes de perturbação, monitorização e conservação.

No estudo S6, tivemos como objetivo contribuir para a melhoria dos métodos de Análise Geográfica de Imagens Baseada em Objetos (GEOBIA), aplicada no processamento de dados de OT de (muito-)alta resolução para aplicações ecológicas. Abordamos este desafio através da otimização integrada de dois processos cruciais em fluxos de trabalho em GEOBIA: a segmentação de imagem e a classificação. Algoritmos Genéticos foram utilizados para otimizar os parâmetros da segmentação de imagem, com impactos sinergísticos em ambos os processos. Um novo pacote R *open-source* (denominado *SegOptim*) foi desenvolvido implementando a abordagem preconizada e para efeitos de disseminação. Este pacote foi testado em diferentes parametrizações, condições e com diferentes fontes de dados. Os resultados dos testes indicam que nenhuma combinação particular de um algoritmo de segmentação e classificação é adequada para todas as tarefas/objetivos, sugerindo uma verificação empírica do "*no-free-lunch theorem*" para problemas de GEOBIA. Para além das implicações teóricas, isto significa que comparar e otimizar métodos (objectivos para os quais o pacote *SegOptim* é perfeitamente adequado) é crucial para determinar quais são os algoritmos mais adequados para um objetivo particular. As contribuições deste trabalho estendem-se a todos os investigadores/técnicos interessados em aplicar metodologias de GEOBIA, incluindo ecólogos, especialistas em deteção remota, cartógrafos, geógrafos, entre outros.

Para finalizar, na Secção III (*Discussão geral e conclusões*) começamos por sumarizar e ligar os principais contributos de investigação de cada estudo a uma panorâmica mais geral em torno de cada tópico abordado na tese. Para este efeito, comparamos e integramos as três abordagens mais significativas aplicadas no desenvolvimento da tese aplicadas à monitorização da biodiversidade e avaliação de alterações: deteção, modelação e combinadas. Discutimos as vantagens e desvantagens e evidenciamos linhas orientadores para adotar cada uma destas abordagens em função da natureza e dos objetivos de iniciativas de monitorização globais, continentais (Europeias) e nacionais. Providenciámos também um sumário geral do impacto e das potenciais aplicações da investigação desenvolvida assim como possíveis caminhos para a sua melhoria. Fechamos com um conjunto de comentários abrangentes e um *outlook* focado em 'lições aprendidas', avanços no estado do conhecimento e métodos, e num conjunto de recomendações sobre desafios operacionais em direção à adoção de um paradigma de monitorização da biodiversidade

mais suportado por dados de OT. Em conjunto com abordagens de modelação robustas, a diversidade de fontes de dados de OT pode (e já está) a avançar o conhecimento científico em relação às causas da acelerada perda de biodiversidade. Ao longo desta tese, suportamos esta noção através de uma série de trabalhos de investigação que individualmente constituem os blocos elementares para desenvolver um sistema de monitorização suportado por OT. Na sua essência, um sistema destes poderá corresponder às exigências dos esforços nacionais e internacionais direcionados para deter a perda da biodiversidade, através do suporte à obtenção de conjuntos de indicadores para avaliar a implementação de programas de conservação e instrumentos políticos.

Index

List of figures 20
List of tables 24
List of abbreviations 27

SECTION I. Introduction 31
CHAPTER 1 - Ecological change: from theory to assessment 33
1.1. Ecological change across scales: drivers, pressures, tipping-points and responses 33
1.2. Scales, levels and 'facets' of biodiversity: implications for assessment and monitoring 38
References 42
CHAPTER 2 - Methods and tools for ecological change assessment 45
2.1. Earth observation systems for assessing and monitoring ecological change 45
2.1.1. Earth observation: principles, platforms and data 45
2.1.2. Applications on EO data in biodiversity science 51
2.2. Modelling tools for assessing change drivers and forecasting 55
2.2.1. Species Distribution Models (SDMs) 55
2.2.2. Ecological niche theory and SDM assumptions 57
2.2.3. Workflow and applications of SDMs 61
References 64
CHAPTER 3 - Research objectives and thesis structure 73
3.1. Research objectives 73
3.2. Research development and thesis structure 75

SECTION II. Research papers 81
Sub-section II.1. Gene level – Combining genetic and Earth Observation data for assessing gene flow and functional connectivity 83
Chapter 4 - Comparative landscape genetics of pond-breeding amphibians in Mediterranean temporal wetlands: the positive role of structural heterogeneity in promoting gene flow 83
DISCLAIMER 83
ABSTRACT 84

4.1. Introduction 85
4.2. Methods 87
4.3. Results 92
4.4. Discussion 99
References 103
Sub-section II.2. Species level – Model-based assessment of habitat suitability dynamics and vulnerability to global change 109
Chapter 5 - Exploring the spatiotemporal dynamics of habitat suitability to improve conservation management of a vulnerable plant species 109
DISCLAIMER 109
ABSTRACT 110
5.1. Introduction 111
5.2. Methods 113
5.3. Results 120
5.4. Discussion 128
References 133
Chapter 6 - A model-based framework for assessing the vulnerability of low dispersal vertebrates to landscape fragmentation under environmental change 139
DISCLAIMER 139
ABSTRACT 140
6.1. Introduction 141
6.2. Methods 143
6.3. Results 150
6.4. Discussion 157
References 162
Sub-section II.3. Habitat and ecosystem levels – Exploring Earth Observation data to assess extent, condition and stability 169
Chapter 7 – Evaluating an unmanned aerial vehicle-based approach for assessing habitat extent and condition in fine-scale early successional mountain mosaics 169
DISCLAIMER 169
ABSTRACT 170
7.1. Introduction 171
7.2. Methods 173
7.3. Results 180
7.4. Discussion 185
References 190

Chapter 8 – Assessing the effectiveness of Protected Areas in promoting forest stability – a methodological approach based on satellite time-series data and multi-model inference 195
DISCLAIMER 195
ABSTRACT 196
8.1. Introduction 197
8.2. Methods 201
8.3. Results 214
8.4. Discussion 223
References 229
Sub-section II.4. Developing novel tools for Geographic Object-based Image Analysis (GEOBIA) of high-spatial resolution EO imagery for ecological status and change assessment 235
Chapter 9 – *SegOptim* – a R package for optimizing segmentation parameters with genetic algorithms for supervised image classification .. 235
DISCLAIMER 235
ABSTRACT 236
9.1. Introduction 238
9.2. Methods 242
9.3. Results 255
9.4. Discussion 258
References 262

SECTION III. General discussion and conclusions 267

CHAPTER 10 – Combining EO and predictive models to improve the monitoring of biodiversity and ecological change 269
10.1. Species-level monitoring in Anthropocene landscapes: a focus on functional connectivity 270
10.2. Habitat and ecosystem monitoring for effective management of protected area networks 274
10.3. Improving GEOBIA methods for assessment of biodiversity and ecological change 277
10.4. Earth Observation detection and ecological modelling – combining approaches for improved biodiversity monitoring and assessment 279
CHAPTER 11 - Conclusions and outlook 287
11.1. Summary of contributions and future developments 287
11.2. Final remarks and outlook 294
References 298

SECTION IV. Appendices 305

Appendix I | Chapter 4 - Comparative landscape genetics of pond-breeding amphibians in Mediterranean temporal wetlands: the positive role of structural heterogeneity in promoting gene flow 305

Appendix II | Chapter 5 - Exploring the spatiotemporal dynamics of habitat suitability to improve conservation management of a vulnerable plant species..... 323

Appendix S1 – Description of the study area 323

Appendix S2 – Preliminary Maxent model used for sampling design 324

Appendix S3 – Competing hypotheses definition, justification and support . 327

Appendix S4 – Correlation matrix for predictor variables used in model fitting 330

Appendix S5 – Model diagnostics 331

Appendix S6 – Modified Corine Land Cover (CLC): methodological notes.. 332

Appendix S7 – Species response curves for predictors 337

References 344

Appendix III | Chapter 6 - A model-based framework for assessing the vulnerability of low dispersal vertebrates to landscape fragmentation under environmental change..... 347

Appendix S1 – Study-area description, species occurrence points and description of the test species..... 347

Appendix S2 – Results for the spatial filtering routine applied to occurrence records 350

Appendix S3 – List of available GCMs from WorldClim..... 351

Appendix S4 – Land-use categories used in DynaCLUE 2050 land-use change projections for Europe based on Corine Land Cover 352

Appendix S5 – Evaluation of species distribution dynamics and connectivity analyses (full methodological description)..... 353

Appendix S6 – Pearson correlation matrix for continuous predictor variables 357

Appendix S7 – Habitat suitability, stable habitat patches and landscape resistance by test species and scenario..... 358

Appendix S8 – Importance of predictor variables by species and modelling technique..... 362

Appendix S9 – Habitat suitability dynamics under projections of climate and land-use change 364

Appendix S10 – Connectivity metrics: summary statistics..... 365

References 367

Appendix IV | Chapter 7 – Evaluating an unmanned aerial vehicle-based approach for assessing habitat extent and condition in fine-scale early successional mountain mosaics 369
Appendix S1 – Test-site photographs recorded during in-field campaigns .. 369
Appendix S2 – Spectral sensitivity data for Canon cameras 372
Appendix S3 – Features used for supervised image classification 377
Appendix S4 – Preliminary cross-validation results 381
Appendix S5 – Overall classification performance measures 384
Appendix S6 – References used for comparing producer and user accuracy values 386
Appendix S7 – Confusion matrix calculated from validation/test set 1 389
References 390
Appendix V | Chapter 8 – Assessing the effectiveness of Protected Areas to ensure the stability of forests – a methodological approach employing MODIS EVI time-series data 393
Appendix S1 – List of selected Protected-areas in mainland Portugal 393
Appendix S2 – Demographic changes in selected protected areas 396
Appendix S3 – Description of common species in Corine Land cover forest classes 398
Appendix S4 – Details of smoothing algorithms 399
References 399
Appendix S5 – Search buffer distances by protected area 401
Appendix S7 – Area covered by different forest species according to 1995 forest inventory by PA and NPA 404
Appendix VI | Chapter 9 – *SegOptim* – a R package for optimizing image segmentation parameters with evolutionary algorithms in the context of supervised classification 405
Appendix S1 – List of reviewed papers in the context of OBIA and supervised classification 405
Appendix S2 – Ranges of image segmentation parameters by test site 411
Appendix S3 – List of land cover/use classes for multi-class test sites 412
Appendix S4 – Confusion matrices for multi-class tests 413
Appendix S5 – Full list of optimized parameters by test site and algorithm . 416

List of figures

(**Note**: figure numbering starts by the chapter numeral followed by figure numbers within that chapter)

Figure 1 - 1 – A representation of the proposed safe operating space for nine planetary systems (in green colour). The red wedges represent an estimate of the current position for each variable. The boundaries in three of these systems (rate of biodiversity loss, climate change and human interference with the nitrogen cycle), have already been exceeded. (reproduced from (Rockstrom et al. 2009)) 34
Figure 1 - 2 – Schematic representation of safe operating space with dynamic and interacting pressures at local scale (land use change, fragmentation, species introductions, etc.) with global scale stressors (related with climate change; source: (Scheffer et al. 2015)) 35
Figure 1 - 3 – GEO BON – The Group on Earth Observations Biodiversity Observation Network (source GEO BON, URL: http://geobon.org/about/vision-goals).). 37
Figure 1 - 4 – Space-time hierarchy diagram proposed by (Delcourt et al. 1982). Environmental disturbances regimes, biotic responses and vegetational patterns are shown in the context of space-time domains. The scale for each pattern or process reflects the spatiotemporal scale required to observe or analyse it. For vegetation patterns, the temporal scale represents the time needed to record their dynamics (reproduced from: (Turner and Gardner 2015)). 38
Figure 1 - 5 – Eight levels of biological and ecological organization with increasing degree of complexity and interactions from bottom to top (based on: (Solomon et al. 2008) and (Allen and Hoekstra 1990)). 39
Figure 1 - 6 – Compositional, structural and functional biodiversity shown as interconnected spheres along multiple levels of organization. (source: Noss (1990) and redrawn in Werner and Gallo-Orsi (2016)) 41

Figure 2 - 1 – The electromagnetic spectrum (source: https://sites.google.com/site/chempendix/em-spectrum; © Sapling Learning) 46
Figure 2 - 2 – Atmospheric absorption occurring along the EM spectrum (Source: CIMSS, URL: https://cimss.ssec.wisc.edu/sage/meteorology/lesson1/AtmAbsorbtion.htm) 48
Figure 2 - 3 – Reflectance profiles extracted from a hyperspectral sensor showing spectral differences between alien/invasive plant species of the *Acacia* genus (solid lines; *Acacia cyanophylla*, *A. karroo* and *A. longifolia*) and native species (dashed lines; *Corema album, Halimium halimifolium, Juniperus phoenica and Pinus pinaster*). Adapted and data compiled from Bradley, 2014; Lehmann et al., 2015; Mureriwa et al., 2016. Electromagnetic spectrum ranges: Vis – Visible (390 – 700nm); NIR – Near Infrared (700-1300nm); SWIR – Short-wave Infrared (1300 – 3000nm). 49
Figure 2 - 4 – (a) Spectral traits (ST) for quantifying biodiversity by EO techniques (source: simplified from original Lausch et al. (2016)) 52
Figure 2 - 5 - Quantification of spectral traits and their interactions with drivers and processes to discriminate and monitor plant species, populations, habitats, communities and biomes using EO (source Lausch et al. (2016)). 53
Figure 2 - 6 – A simplified scheme of a SDM input and output. 56
Figure 2 - 7 – (a) BAM diagram representing a species niche showing the effects of *biotic* (B), *abiotic* (A) and *mobility* (M) aspects [adapted from: Peterson et al. (2015)]; (b) representation of the ecological niche in a two-dimensional environmental space and its relationship to species' distribution in the geographical space (c,d). The grey area represents the *Grinnellian* fundamental niche (the cross sign indicates the niche optimum). Outside the niche envelope (bold line), growth is negative, decreasing until it reaches the lethal envelope (bold dashed line), beyond which the species cannot survive. The isolines, or envelopes, link all points of equal species per capita growth rate, *r*. (c) and (d) represent a spatial realization of the *Grinnellian* niche – or the 'potential' available habitat. A' (green areas) – represent occupied habitat with suitable A, B, and, M conditions i.e., *Hutchinson's* realized niche; B' (red area) – representation of suitable but unoccupied habitat due to inaccessible conditions and/or biotic constraints; A'' and B'' represented idealized predictions of a SDM with situations of correct, over- and under-prediction of the fundamental and/or realized niches where A'' areas (blue) have an 'admissible' extrapolation contrary to, B'' (yellow) showing a strong over-prediction of the realized niche but admissible prediction of the fundamental niche (for example, due to high environmental similarity with suitable locations sampled). Points show an idealized random sampling over the geographic area: black points are sample absence locations whereas green points are presence locations [adapted from Hirzel and Le Lay (2008)] 59
Figure 2 - 8 – Typical Species Distribution Modelling workflow. 63

Figure 3 - 1 – Cross-scale and cross-level complementarity between the six research studies conducted during this PhD. Here we do not address the 'conventional' levels of biotic organization (Figure 1 - 5; (Allen and Hoekstra 1990)) although the obvious overlap (exceptions to 'species' which relates to population level; or 'habitat' relating broadly to the community level). Instead, we prefer to address more directly to levels at which we analysed biodiversity status and change. 77

Figure 4 - 1 – Sampling locations for the two study species: *P. cultripes* (A) and *P. waltl* (B). Codes as in Table 4 - 1. Results of the optimal number of clusters for each species according to BAPS are also shown. 94
Figure 4 - 2 – Transformations applied to each variable (included in the most frequently selected models) to generate resistance surfaces for species *P. cultripes* (left-side) and *P. waltl* (right-side). Each curve represents a different transform parameterization optimized for D_{EST} (black color), F_{ST} (dark-grey) and G''_{ST} (light-grey). Original values are represented in the x-axis (including the full range of the variable) while transformed (resistance) values are shown in the y-axis and should be interpreted in relative fashion between variables. The dashed line shows the minimum resistance for the original values of each variable. The boxplot on top shows the distribution of the original untransformed variable (boxes are the 97
Figure 4 - 3 – Optimized resistance surfaces for *Pelobates cultripes (left-side)* and *Pleurodeles waltl (right-side)* based on the most frequently selected variables and considering F_{ST} genetic distances. For each species, on the left are maps showing the original continuous values for each variable; on the right, the resistance surface generated through optimization. Points represent sampling localities. 98

Figure 5 - 1 – Main features of the study-area (a) and its location in mainland Portugal (b) and in Europe (c). 114
Figure 5 - 2 – Flowchart representing model development to evaluate the spatiotemporal dynamics of habitat suitability and to address the added-value of multi-temporal data. 119
Figure 5 - 3 – (a) Number of suitable habitat predictions between 2001 and 2010 for each grid unit. Burned area is displayed in proportional circles for enabling the comparison of suitable areas against fire-prone locations; (b, c) study-area broader geographical context. 123
Figure 5 - 4 – Plot representing the inter-annual variation in total number of suitable areas predicted (black line), along with auxiliary data related to the total amount of burned area in the study-site (in hectares; orange line) and, the variation in total annual precipitation (blue line) showing three years with severe drought conditions: 2004, 2005 and 2007. 124
Figure 5 - 5 – Biplots displaying the association between anomalies (annual value minus the median for the whole studied period 2001-2010) in maximum value of the growing season (left column) or Actual Evapotranspiration (right column) and anomalies in total precipitation from the previous year (identified as lag+1yr ; first row) and average minimum temperature of the coldest month (second row) which show the effect of inter-annual variations in climatic conditions in remotely sensed indicators. Values for RS variables represent the anomaly in each year (from 2001-2010) in the median across the study-area, and considering only sites predicted as suitable at least one time in 2001-2010. Rsq – coefficient of determination for the regression line; Pearson cor. – Pearson correlation between variables. 125
Figure 5 - 6 – Boxplots showing the effect of motorways (constructed during 2002-2006; left-side of the panel) and wildfires (right-side) on the temporal variation of predictor variables: Seasonal Amplitude (AMPLT), Maximum Value of the growing season (MAXVL) and Actual Evapotranspiration (EVPTR) for the 2001-2010 period. Plotted locations only include areas that were at least one time predicted as suitable by the averaged model. Grey boxes represent affected areas (by motorways or wildfires) while white boxes represent control/unaffected areas by both types of disturbances. Outliers were represented as circles, i.e., values lying outside the box 1.5 times the inter-quartile range. 126
Figure 5 - 7 – Biplots showing the association between the number of suitable areas predicted per year (one point by year between 2001-2010) and anomalies (calculated as the annual value minus the median for the whole studied period 2001-2010) in the maximum value of the growing season (left), seasonal amplitude (center) and actual evapotranspiration (right). Values for RS variables represent the anomaly in each year (from 2001-2010) in the median across the study-area, and considering only sites predicted as suitable at least one time in 2001-2010. Rsq – coefficient of determination for the regression line; Pearson cor. – Pearson correlation between variables. 127

Figure 6 - 1 – Schematic representation of the methodological approach developed. 143
Figure 6 - 2 – Barplot displaying variable importance by species and averaged across all pseudo-absence sets, evaluation rounds and modelling algorithms. Error bars represent the standard-errors across modelling techniques. Species are *Anguis fragilis* (ANGFR), *Lacerta schreiberi* (LACSH), *Chioglossa lusitanica* (CHALU) and *Epidalea calamita* (EPCAL). 151

Figure 6 - 3 – Boxplot of the Mean Functional Distance index by species and scenario. The yy-axis was log transformed and outliers, *i.e.*, values 2 times the inter-quartile range outside the box, were represented as points. LES – low-emissions scenario (blue boxes); HES – high-emissions scenario (red boxes). 152
Figure 6 - 4 – Map representation of species distribution dynamics (a,d,g,j), connectivity between "lost" (source areas) and "kept" (target areas) using the Mean Functional Distance index (MFD, k=5; b,e,h,k), and the zonation of important areas for connectivity using the SPsum index (c,i,f,l) for each reptile species (*A. fragilis, L. schreiberi*) and scenario (low-emissions scenario and high-emissions scenario).....154
Figure 6 - 5 – Map representation of species distribution dynamics (a,d,g,j), connectivity between "lost" (source areas) and "kept" (target areas) using the Mean Functional Distance index (MFD, k=5; b,e,h,k), and the zonation of important areas for connectivity using the SPsum index (c,i,f,l) for each amphibian species (C. lusitanica, E. calamita) and scenario (low-emissions scenario and high-emissions scenario). 155
Figure 6 - 6 – Boxplot showing the distributions of *SPsum* values for all areas important for maintaining connectivity (i.e. with $SPsum \geq$; blue boxes) and those areas intersected by motorways (red boxes) across species and scenarios (LES – low-emissions scenario and HES – high-emissions scenario). The y-axis was log-transformed, and, outliers, *i.e.*, values lying outside the box 2 times the inter-quartile range were represented as points. 156

Figure 7 - 1 – Study-area location in the Iberian Peninsula and the NW region of Portugal. The test-site is fully included in the Natura 2000 "*Serra de Arga*" Site of Community Importance. 173
Figure 7 - 2 – The focal habitats as captured by the UAV platform. (a) wet heath, habitat type 4020*, in dense/large shrub formations in concave/wet areas; (b) habitat 4020* around a small pond; (c) continuous, species-rich *Nardus* grasslands, habitat type 6230*, with low shrub density; (d) 6230* habitat with bare soil, highlighting poor habitat condition; (e) dry heath, habitat type 4030, in mosaic with bare rock/soil areas; (f) heath (4030) encroachment on *Nardus* grassland denoting degradation due to decreased grazing pressure. 175
Figure 7 - 3 – Overview of the methodological approach tested. The scheme uses dashed boxes to denote processes (bold lettering signals important processing steps), grey boxes denote specific or detailed aspects for certain processes and blue boxes indicate data. 176
Figure 7 - 4 – Sample units (red quadrats) over the original colour image obtained with the UAV camera. The image evidences herbaceous (grassland) and woody (scrub) vegetation occurring in dense, complex mosaics as well as extensive rock outcrops and some linear elements such as water lines and tracks...177
Figure 7 - 5 – Example of colour and texture features for a sample unit. From left to right: original red colour channel, Haralick, Structural Feature Set (SFS) and Local Statistics texture features evidencing small-scale differences and fine discrimination of herbaceous (grassland), woody (scrub) vegetation and a pond.....178
Figure 7 - 6 – Boxplot containing the distribution of producer and user accuracy values collected from research articles on the subject of habitat classification for similar habitat types such as grasslands/meadows (62xx/ 64xx /65xx; n=15 articles, grey colour), and heathlands (40xx; n=8 articles, light grey). Boxes represent the 25, 50% and 75% quartiles and whiskers the minimum and maximum values. Overlapped points display producer and user accuracy values obtained from the tested UAV-based classification, for habitat type 6230* (squares), 4020* (circles) and 4030 (triangles). 181
Figure 7 - 7 – Density plots for some of the most important features (Table 7 - 3) used to calibrate the random forest classifiers showing the separation between the three habitat types in the study. (a) Surface elevation texture, Mean, 15×15; (b) R/B band ratio texture, Mean, 11×11; (c) Surface elevation texture, Standard-deviation, 15×15; (d) Structural Feature Set, Brightness band, WMean, Spectral threshold = 100. 183
Figure 7 - 8 – Map representation of the study-area displaying the coverage of different classes as predicted by the ensembling of RF classifiers. 185

Figure 8 - 1 – Schematic/conceptual representation of stability components in forest ecosystems as the relation between disturbance and response captured by a vegetation index time-series (VI; green line). The upper plot depicts VI annual/seasonal variation with two major abrupt changes (red arrows) showing disturbance frequency and the severity (black arrows). The lower plot depicts the post disturbance response as the return rate of the system towards the former steady state modulated by the systems' resilience. .201
Figure 8 - 2 – Schematic/conceptual representation of potential shifts happening in forest ecosystems as the result of interactive changes in disturbance regime components (frequency and severity) and resilience capacity [based on Pausas (2015) and Johnstone et al (2016)]. 202
Figure 8 - 3 – Workflow with the approach used to analyze ecosystem stability inside and outside PAs .203
Figure 8 - 4 – Map of the 25 selected protected areas in continental Portugal used in the study (1 - Montesinho, 2 - Corno do Bico, 3 - Peneda-Gerês, 4 - Albufeira do Azibo, 5 - Litoral Norte, 6 - Alvão, 7 - Douro Internacional, 8 - Dunas de São Jacinto, 9 - Serra da Estrela, 10 - Serra Malcata, 11 - Serra do Açor, 12 - Paul de Arzila, 13 - Tejo Internacional, 14 - Serras de Aire e Candeeiros, 15 - Serra de São Mamede, 16 - Serra de Montejunto, 17 - Açude do Monte da Barca, 18 - Sintra-Cascais, 19 - Arriba Fóssil da Costa da Caparica, 20 - Arrábida, 21 - Estuário do Sado, 22 - Lagoas de Santo André e Sancha, 23 - Vale do Guadiana, 24 - Sudoeste Alentejano e Costa Vicentina, 25 - Ria Formosa). 204

Figure 8 - 5 – Descriptive statistics for the 25 protected areas selected – (a) histogram of creation year; (b) histogram showing the distribution of size (in hectares; the x-axis is in log10 scale), lines show the 25% (left, dashed line), 50% (center, solid), and 75% quantiles (right, dashed); (c) histogram and density line depicting the distribution of elevation (meters a.s.l.) for the whole mainland Portugal (orange colour) vs. selected PAs (blue); and, (d) total area burnt per year (2000-2013) in selected protected areas in hectares. Values above each bar represent the percentage of the total burnt area in mainland Portugal that occurred inside all selected sites by year. 205
Figure 8 - 6 – Stability metrics represented for CLC 2000 forest areas in continental Portugal (colder/blue colors represent more stable areas whereas warmer/red colors correspond to less stable areas). All images were represented using intervals defined by the 1% and 99% quantiles (Note: Q95 was not presented here due to page space constraints) 215
Figure 8 - 7 – (a) Forest stability by indicator. Values show the percentage of Wilcoxon tests (n=1000) for which Protected Areas (PA) are relatively more stable than the surrounding non-protected area (NPA; only values greater than zero are shown). PAs are sorted in descendent order according to their overall stability ranking, obtained by summing the number of criteria that recorded a value greater than 50.0% (in bold). Each column represents a stability metric: inter-annual coefficient of variation of the annual 5% quantile (Q05), median (MED), 95% quantile (Q95), annual difference between 95 and 5% quantiles (DQT), and "summerness" (sine) transformation of the day of maximum (SMN). STL decomposition – trend component coefficient of variation (TRD) and maximum Lyapunov exponent (MLE); (b) Overall relative forest stability rank across the PA network. This ranking is based on counting the number of stability indicators that recorded a percentage higher than 50% (i.e., indicators for which PA is more stable than NPA). For PA names use Figure 8-4 caption..... 216
Figure 8 - 8 218
Figure 8 - 9 219

Figure 9 - 1 – The architecture of the software package *SegOptim*. 243
Figure 9 - 2 – Schematic representation of the fitness function. 246
Figure 9 - 3 – An example cross-tabulation by segment and land cover class (SID: segment unique identifier). 251
Figure 9 - 4 – Segmentation features and training data used for testing the GA-based approach in *SegOptim* package for single-class problems (detection of invasive species; E1, E3 and E5 pilot-test areas in top-two rows) and multi-class (habitat and land cover/use mapping; E2, E4 and E6 pilot-test areas in bottom-two rows). 254
Figure 9 - 5 – Classification outputs generated from the best GA-based solutions for each test-site. E1, E3 and E5 are single-class problems while the remaining E2, E4 and E6 are multi-class problems. E1 depicts the distribution of Carpobrotus sp. invasive species using SAGA GIS Simple Region Growing segmenter and GBM classifier; E2 maps different natural habitats using RSGISLib Shepherd iterative elimination segmenter and Random Forest (RF) classifier; E3 shows the distribution of *Acacia dealbata* invasive species (yellow patches) using TerraLib Baatz-Schäpe multi-resolution segmenter and RF classifier; E4 shows land cover/use classification using GRASS GIS region Growing segmenter and RF classifier; E5 shows the distribution of small patches of the invasive Acacia dealbata species across the landscape using TerraLib Mean Region Growing segmenter and RF classifier; and, E6 shows land cover/use mapped with OTB Mean-shift segmenter and RF classifier. 256
Figure 9 - 6 – GA optimization paths for three test sites with different convergence profiles in terms of speed: fast for E1, intermediate for E4, and slow for E5. These paths represent only the best performing solutions for each test site. The black line represents the average Kappa for all individuals (n=20) at each round of the GA optimizer while the red line shows the Kappa value of the best solution by round. 257

List of tables

(**Note**: table numbering starts by the chapter numeral followed by the table number within that chapter)

Table 2 - 1 – A non-exhaustive list of operating satellite platforms and sensors from moderate to 'ultra'-high spatial resolution used for ecological applications and spatiotemporal change analysis. (*) hyperspectral sensors (HS); the remaining are multispectral (MS). PAN – panchromatic band; B – band number. Blue lines represent the platforms//sensors used in this thesis. 50
Table 2 - 2 – Current adequacy of remote sensing to support tracking progress towards the Aichi Targets based on 3 broad categories: [●] Currently not observable by EO-based approach but some of the targets under this category maybe technically feasible in the future; [●] Could be partially derived from EO-based information or EO-based approaches currently in development; [●] Can be totally or partially derived from existing EO-based information. In some cases, only some of the corresponding operational indicators currently analysed fit the category. The attribution of each category is based on subjective estimates of adequacy based on the most recent information available to authors (source: Secades et al. (2014)). 54

Table 4 - 1 – Input variables by level and data source used to explain gene flow and calculate optimized resistance surfaces. Summary statistics in brackets: minimum (min), average (avg), maximum (max) and standard-deviation (std). 89
Table 4 - 2 – Locality information and genetic diversity estimates for sampled *Pelobates cultripes* (C) and *Pleurodeles waltl* (W) populations: *N* = sample size; N_C = sample size after exclusion of potential siblings from the sample; N_A = mean number of alleles per locus; H_O: observed heterozygosity; H_E = expected heterozygosity; F_{IS} = inbreeding coefficient..... 93
Table 4 - 3 – Model selection table for *P. cultripes* (left) and *P. waltl* (right). Models highlighted in bold attained the highest relative support and were included in the confidence set (ΔAICc≤4). AICc – Akaike Information Criterion value (with a correction for finite sample size), ΔAICc – delta AIC value, wi – Akaike weights. *IBD* – Isolation-by-distance model. *IntOnly* – Intercept-only/null model. 95

Table 5 - 1 – Predictor variables related to each hypothesis/model. Types of variables according to their spatiotemporal variability: DN – dynamic predictors, SD – semi-dynamic predictors and, ST – static predictors. 116
Table 5 - 2 – Model ranking and selection table; K – number of parameters (this value equals the sum of the degrees of freedom for each smoothing spline in the model plus the intercept term; the exception is M8 which has only one parameter), LogLik – log likelihood, AICc – Akaike's Information Criterion value (with finite sample size correction), ΔAICc – delta AICc, wi – Akaike weights, D2 – deviance, R2 – Nagelkerke's R-squared; AUC – Area Under the Receiver Operating Curve and, TSS –True-skill statistic calculated for the test set. With exception of ΔAICc and wi, all values in the table present the average across all 500 cross-validation rounds. 121
Table 5 - 3 – Evaluation statistics for the two types of model-averaged predictions (MAP): (i) single-year prediction (using only the calibration year of 2010), and, (ii) model-averaged predictions with the multi-temporal mean (average predictions for 2001-2010). Performance statistics: AUC – area under the receiver operating curve, and, TSS – true-skill statistic, were aggregated using the mean and standard-deviation across all 500-holdout cross-validation rounds. 122

Table 6 - 1 – Model performance statistics for biomod2 partial models and the final ensemble model ("Ensemble" column). Results were averaged across the test sets, pseudo-absence sets and model runs. Two evaluation measures were calculated: AUC (area under the curve), and TSS (true-skill statistic). Seven modelling techniques were used: GLM (Generalized Linear Model), GBM (Generalized Boosting Model), GAM (Generalized Additive Model), CTA (Classification Tree Analysis), FDA (Flexible Discriminant Analysis), RFO (Random Forests), and MAX (Maximum Entropy Model). Modelling techniques highlighted with an asterisk (*; i.e., the best five techniques by species considering the AUC values) were included in the final ensemble. Column "Cutoff" displays the value used to partition ensemble probability maps (ranging from 0 to 1000) into suitable/unsuitable areas; values inside parenthesis represent respectively the Sensitivity (or true positive rate) and Specificity (or true negative rate). Species are *Anguis fragilis* (ANGFR), *Lacerta schreiberi* (LACSH), *Chioglossa lusitanica* (CHALU) and *Epidalea calamita* (EPCAL). 150

Table 6 - 2 – Net variation in percentage ($\%nv = ((New + Kept)/(Kept + Lost) - 1) \times 100$) by species and scenario (2050 scenario: HES – high-emissions scenario; LES – low-emissions scenario) showing habitat area losses and gains, derived from the joint effects of climate and land use changes. Descriptive statistics (median) for the Mean Functional Distance index (MFD, k=5) by species and scenario. 153
Table 6 - 3 – Spatial intersection between important areas for connectivity (*i.e.,* with $SPsum \geq 1$) and the motorway network (considering a buffer of 500m around each road). HES – High-emissions scenario; LES – Low-emissions scenario. 156

Table 7 - 1 – Overall validation measures averaged across all 50 datasets. ACC – overall accuracy; HSS – Heidke skill score; PSS – Peirce skill score; GSS – Gerrity skill score. 180
Table 7 - 2 – Average producer and user accuracy values for each class. Values were aggregated using the mean and standard-deviation across the 50 validation datasets. 181
Table 7 - 3 – Average feature importance and overall ranking for calibrating the random forest-based classifiers. Results were aggregated across all training rounds. 182
Table 7 - 4 – Percentage cover and area (in hectares) of each class in the study-area. 184

Table 8 - 1 – CLC classes selected for assessment and PA vs. NPA comparison 207
Table 8 - 2 **–** Stability metrics calculated to compare PA and NPA (*n* equals the number of observations in the time-series). 210
Table 8 - 3 – List of explanatory variables (related to each hypotheses set) along with input datasets. 213
Table 8 - 4 – Results for AICc-based model ranking for each response stability metric including only selected models (i.e. ΔAICc<3): annual coefficient of variation of the annual 5% quantile (Q05), median (MED), 95% quantile (Q95), annual difference between 95 and 5% quantiles (DQT), and "summerness" (sine) transformation of the day of maximum (SMN). STL decomposition – trend component coefficient of variation (TRD), and maximum Lyapunov exponent (MLE). ΔAICc – Delta AIC (greater values translate lower model support; typically, values above 2 or 3 have relatively low support); w_i – Akaike weights (higher values represent greater relative model support within [0, 1]); and, D2 – explained deviance; symbols within parenthesis represent model significance: (***) p<0.001, (**) p<0.01, (*) p<0.05, (.) p<0.1; The : (colon) in model formula indicates an interaction between two variables. 221
Table 8 - 5 – Coefficient signs for models that were selected at least one time using the AICc-based ranking. The (↗) arrow represents a positive effect of a given predictor variable while (↙) is negative. The order of the arrows follows that of the predictor variables in each model represented in column two. The : (colon) in model formula indicates an interaction between two variables. 222

Table 9 - 1 – (a) GA parameters used for running the image segmentation tests as well as, (b) description of GA operators used. 247
Table 9 - 2 – List of software packages and algorithms for image segmentation currently available in *SegOptim*. (*1- OTB functionalities can be accessed through Monteverdi graphical interface; *2 - TerraLib functionalities can be accessed through TerraView 5 graphical interface). Also includes the list of currently optimizable parameters in *SegOptim.* 248
Table 9 - 3 - List of testing sites and description of testing objectives (UL – upper-left corner and LR – lower-right corner coordinates in WGS 1984 geographic). The six tests (E1-E6) are listed based on the spatial resolution of EO imagery. 250
Table 9 - 4 – Types of classification features used for each study area/experiment. NDI – Normalized Difference Index combinations based on any two different bands; HL – Haralick texture features; LS – Local Statistics features; SFS – Structural Feature Set texture features. (*) for the features in E6, two images (March/July 2016) were used to calculate classification features. 253
Table 9 - 5 – Results for 5-fold cross-validation using the Kappa Index to evaluate object-based classification performance based on *SegOptim*'s GA-optimized image segmentation for each of algorithm. Values highlighted in bold represent the best solutions for each test site. E1, E3 and E5 are single-class problems while the remaining E2, E4 and E6 are multi-class problems. 255

List of abbreviations

a.s.l.	Above sea level
ACC	Accuracy
AFN	*Autoridade Florestal Nacional* (prior forest autorithy to ICNF)
AIC	Akaike Information Criterion
AICc	Akaike Information Criterion (with a correction for finite sample size
ASTER	Advanced Spaceborne Thermal Emission and Reflection Radiometer
AUC	Area under the receiver operating curve (ROC)
BIO	Bioclimatic Indices from WorldClim global climatic dataset
BOA	Bottom-of-the-atmosphere
CAR	Catchment Area
CBD	Convention for Biological Diversity
CEAI	Clark-Evans aggregation index
CIBIO	*Centro de Investigação em Biodiversidade e Recursos Genéticos*
CLC	Corine Land Cover
CMIP	Coupled Model Intercomparison Project
CNIG	*Centro Nacional de Información Geográfica*
Csa	Hot-summer Mediterranean climate - Köppen-Geiger classification system
Csb	Warm-summer Mediterranean climate - Köppen-Geiger classification system
CTA	Classification Tree Analysis
D2, D^2	Deviance
DGPS	Differential Global Positioning System
DN	Digital number
DNA	Deoxyribonucleic acid
DSM	Digital Surface Model
Dyna-CLUE	Dynamic Conversion of Land Use and its Effects Model
ED2	Euclidean Distance 2
EEA	European Environmental Agency
EFA	Ecosystem Functional Attributes
EFI	European Forest Institute
EO	Earth Observation
E-OBS	E-OBS gridded climatic dataset from European Climate Assessment & Dataset project
EOLi-SA	Earth Observation Link - ESA client for EO Catalogue and Ordering Services
EROS	Earth Resources Observation and Science
ES	Ecosystem Services
ESA	European Space Agency
ESPA	EROS center science processing architecture
ESRI	Environmental Systems Research Institute
EU	European Union
EVI	Enhanced Vegetation Index
FAO	Food and Agriculture Organization
FDA	Flexible Discriminant Analysis

FIS	Inbreeding coefficient
FST	Fixation index
GA	Genetic Algorithms
GAM	Generalized Additive Models
GBM	Generalized Boosted Regression and Classification Model
GCMs	Global Circulation Models
GCP	Ground Control Points
GDEM	Global Digital Elevation Model
GEOBIA	Geographic Object-based Image Analysis
GIS	Geographic Information Systems
GLM	Generalized Linear Model
GPS	Global Positioning System
GRASS	Geographic Resources Analysis Support System
GSS	Gerrity skill score
HE	Expected heterozygosity
HL	Haralick texture features
HO	Observed heterozygosity
HSS	Heidke skill score
HWE	Hardy-Weinberg equilibrium
IBD	Isolation-by-distance
ICNF	*Instituto da Conservação da Natureza e Florestas*
InBIO	Research Network in Biodiversity and Evolutionary Biology
IPCC	Intergovernmental Panel on Climate Change
IPMA	*Instituto Português do Mar e da Atmosfera*
IUCN	International Union for Conservation of Nature
LD	Linkage disequilibrium
LEAF	Linking Landscape, Environment, Agriculture and Food
LiDAR	Light Detection and Ranging
LORACS	Landscape ORganization and Connectivity Survey
LS	Local Statistics texture features
LUC	Land use/cover
LULC	Land use/land cover
MAP	Model-averaged predictions
MAP-ST	Model-averaged predictions - multi-temporal mean
MAP-SY	Model-averaged predictions - single-year
MAX	Maximum Entropy model (for biomod2 R package)
MaxEnt	Maximum Entropy model
MD	Median
MFD	Mean Functional Distance index
MLE	Maximum Lyapunov exponent
MLPE	Maximum likelihood population effects
MMI	Multi-Model Inference
MODIS	MODerate Resolution Imaging Spectroradiometer
MP	Mega-pixel
MRT	MODIS Reprojection Tool

NA	Number of alleles
NDMI	Normalized Difference Moisture Index
NDVI	Normalized Difference Vegetation Index
NFLT	"No free-lunch theorem"
NIR	Near-infrared
NPA	Non-protected Area (i.e., all areas without protection status)
NT	Near Threatened (IUCN conservation status)
OBIA	Object-based Image Analysis
OTB	Orfeo Toolbox
PA	(Terrestrial) Protected Areas
PCR	Polymerase chain reaction
PSS	Peirce skill score
PWN	Pine Wilt Nematode
R2, R^2	Coefficient of determination
RADAR	Radio Detection And Ranging
RFO, RF	Random Forest model/classifier
RGB	Red, Blue, and Green channels of a true color image
RMSE	Root-mean-square error
ROC	Receiver Operating Curve
ROI	Region-of-interest
RS	Remote Sensing
RSGISLib	Remote Sensing and GIS Software Library
RTK	Real Time Kinematic (RTK) satellite navigation
SAGA	System for Automated Geoscientific Analyses (SAGA GIS)
SAR	Synthetic Aperture Radio Detection And Ranging
SD	Standard-deviation
SDM	Species Distribution Models
SFS	Structural Feature Set texture operators
SIOSE	*Sistema de Información sobre Ocupación del Suelo* for Spain
SP	Shortest-paths (in a graph structure between two nodes)
Spsum	Shortest-paths sum index
SRTM	Shuttle Radar Topography Mission
STL	Seasonal and Trend decomposition using Loess
SU	Sample unit
SVM	Support Vector Machines
TerraLib	Open source GIS software library
TIMESAT	Software package for analysing time-series of satellite sensor data
TM	Thematic Mapper
TOA	Top-of-the-atmosphere
TSS	True-skill statistic
TWI	Topographic Wetness Index
UAV	Unmanned Aerial Vehicle
UN	United Nations
UNEP	United Nations Environment Programme
USGS	United States Geological Survey
UTM	Universal Transverse Mercator coordinate system

VFD	Vegetation functioning dynamics
VI	(Spectral) vegetation Index
VIF	Variance Inflation Factors
VWC	Vegetation water content
WCMC	World Conservation Monitoring Centre
WGS	World Geodetic System

SECTION I. Introduction

CHAPTER 1 - Ecological change: from theory to assessment

1.1. Ecological change across scales: drivers, pressures, tipping-points and responses

Global biodiversity is currently undergoing fast changes marked by global declines in species distributions and populations combined with loss of large areas of natural habitat (e.g. (Butchart et al. 2010)). These widespread changes in biodiversity modify ecosystem processes and resilience, with consequences for the benefits that humans extract from these ecosystems (Chapin III et al. 2000). A new era – the *Anthropocene* (Crutzen 2002) – in which human actions are the main driver of global environmental change, is considered to have started in the late eighteenth century as a consequence of rising industrialization, agricultural intensification and fossil fuel consumption. A time which saw remarkable amounts of Earths' primary productivity being increasingly appropriated by humans and their client species (Haberl et al. 2007) – a strong fingerprint of the human domination of the biosphere. Also, an era marked by strong civilizational and technological developments that saw human activities push the planetary systems outside the Holocene stable environmental state the with detrimental and sometimes catastrophic consequences for large parts of the world (Rockstrom et al. 2009). To define and characterize the global challenges ahead of Humanity, the scientific community has proposed the concept of '*safe operating space',* which relies on the characterization and definition of 'planetary boundaries' with respect to fundamental biophysical subsystems or processes. If these thresholds or boundaries are crossed, then important Earth's subsystems can shift into a new state, with potentially disastrous consequences for humans (Rockstrom et al. 2009). For the same authors, three of nine interlinked planetary boundaries they proposed have already been surpassed (Figure 1 - 1). These include changes in the nitrogen cycle (amount of N_2 removed from the atmosphere for human use), climate change (atmospheric CO_2 concentration and changes in radiative forcing), along with the rate of biodiversity loss (Rockstrom et al. 2009).

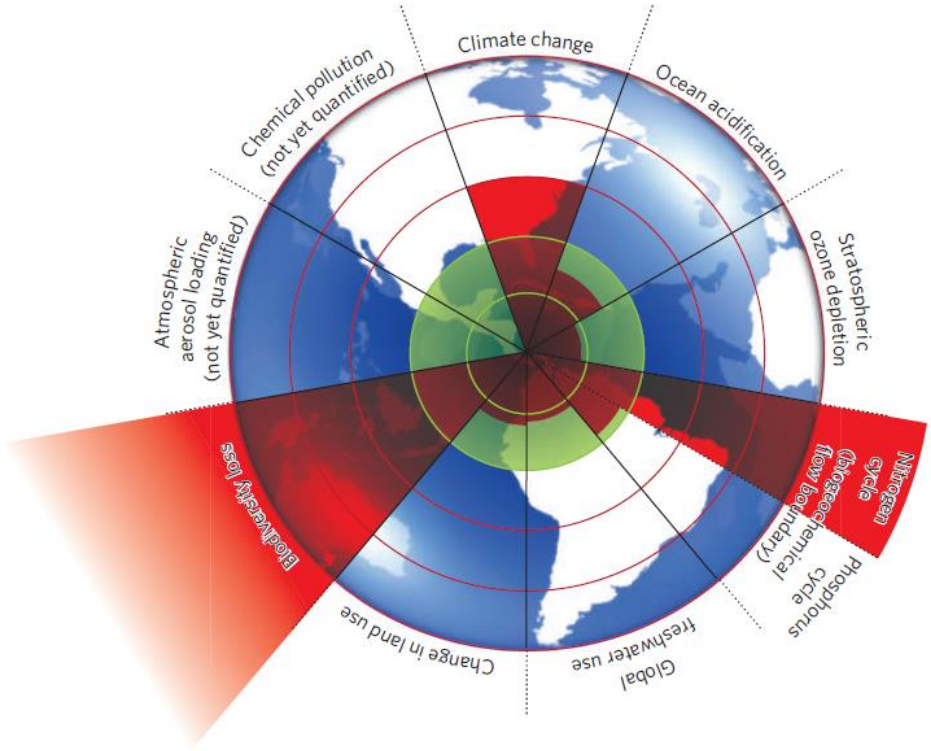

Figure 1 - 1 – A representation of the proposed safe operating space for nine planetary systems (in green colour). The red wedges represent an estimate of the current position for each variable. The boundaries in three of these systems (rate of biodiversity loss, climate change and human interference with the nitrogen cycle), have already been exceeded. (reproduced from (Rockstrom et al. 2009))

Although species extinction is a natural process that occurs without human intervention, the Anthropocene rate of biodiversity loss has risen tremendously and is estimated to be 100 to 1000 times higher than 'natural' baselines (Butchart et al. 2010, Pereira et al. 2010, Barnosky et al. 2011, Pimm et al. 2014, Ceballos et al. 2015)[1]. These glooming numbers have been related to a multitude of causes (often with synergistic effects). One major source of pressure is related to land use changes at local to regional scales. Those changes (e.g., deforestation, urbanization) include the loss, conversion, degradation and/or fragmentation of natural habitats which are needed for species survival; changes in the frequency, duration or magnitude of wildfires and similar disturbances; and the introduction of new (often invasive) species into land and freshwater environments (Sala et al. 2000, Pereira et al. 2010, CBD 2014). Besides the effects of local drivers of biodiversity change, there is increasing evidence that global climate changes will lead to a redistribution of species. Changes in species distributions

[1] See also Bull and Maron (2016) for a balanced discussion of human-mediated speciation and extinction processes.

will likely result in new interactions between species and often the disruption of current biotic interactions, novel communities and rapid changes in ecosystem functioning (Pecl et al. 2017). Increasing evidence is showing that biodiversity itself (or variety, as opposed to the presence of one or few species) is key for maintaining the productivity and stability of ecosystems across scales (Díaz et al. 2005, Hooper et al. 2005). Therefore, minimizing change or maintaining biodiversity is one strategic element for an adaptive response to global environmental change allowing to keep fundamental ecosystem functions and processes. Nonetheless, this is particularly challenging in a time of growing human population and demand, in which species redistribution may change the ability of ecosystems to deliver vital ecosystem services (Pecl et al. 2017).

In addition, although commonly assumed that ecosystems respond to gradual change in a smooth way, theory and accumulating empirical evidence show that regime shifts can abruptly happen, pushing systems into new stable states (Scheffer et al. 2001, Scheffer and Carpenter 2003, Folke et al. 2004). *Tipping points* define critical thresholds separating two states of a complex system. Some ecosystems show little response to environmental changes until a tipping point is reached and in that case a small perturbation can cause a sudden change into a new state from which recovery may be difficult to achieve (Scheffer et al. 2015). Such shifts imply new sets of conditions and the delivery of different ecosystem services with consequent impacts for humans (Folke et al. 2004).

For maintaining ecosystems, researchers must be aware that safe boundaries for local change processes (land use, wildfires, species invasion) may change due to interactions with global pressures coming from climate (Figure 1 - 2). Thus, decreasing local pressures may be crucial to maintain ecosystems functioning within their safe operating space under future climate (Scheffer et al. 2015). In a more general sense, combining efforts at multiple scales may be one of the most promising options to tackle the current biodiversity crisis.

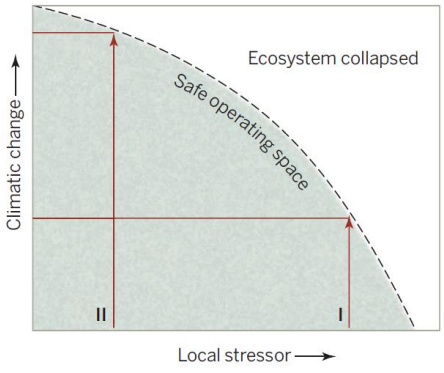

Figure 1 - 2 – Schematic representation of safe operating space with dynamic and interacting pressures at local scale (land use change, fragmentation, species introductions, etc.) with global scale stressors (related with climate change; source: (Scheffer et al. 2015))

In face of the previous diagnosis of current biodiversity trends and pervasive changes in Earth's ecosystems, there is a growing need of innovative and coordinate action and responses to halt or reverse the current *status quo*. For this intent, the *Convention on Biological Diversity* (CBD) to which 196 nations have commited, is leading the way and coordinating efforts to achieve a significant reduction in biodiversity loss. The CBD has devised a set of 20 targets (around five strategic goals; see Box 1 -1), known as the "*Aichi Biodiversity targets*" for 2011-2020 setting up an ambitious agenda to reduce the loss of species and natural habitats and safeguard ecosystem services, while simultaneously improving planning, financing schemes, knowledge transfer, capacity building and benefits from sustainable management (Johnson et al. 2017).

Strategic goal A: Address the underlying causes of biodiversity loss by mainstreaming biodiversity across government and society
Strategic goal B: Reduce the direct pressures on biodiversity and promote sustainable use
Strategic goal C: To improve the status of biodiversity by safeguarding ecosystems, species and genetic diversity
Strategic goal D: Enhance the benefits to all from biodiversity and ecosystem services
Strategic goal E: Enhance implementation through participatory planning, knowledge management and capacity building

Box 1 - 1 – Strategic goals defined by CBD's Aichi Biodiversity targets for 2011-2020 (source: https://www.cbd.int/sp/targets)

Among other aspects, "Strategic goal E" (see Box 1 - 1) encompasses the need of parties to devise their own National biodiversity strategies and action plans (Target 17; (CBD 2014)) aligned with the CBD's Strategic Plan for Biodiversity 2011-2020 and the *Aichi* Biodiversity Targets. In this respect, parties are also encouraged to devise their own targets with corresponding indicators as well as monitoring mechanisms to evaluate progress towards the defined objectives (CBD 2014). Portugal recently revised (June 2017) its *National Strategy for Nature and Biodiversity Conservation* for 2025 [ENCNB-2025; (Ministério-do-Ambiente 2017)], defining three strategic axes to halt the loss of natural capital (related to CBD's *Aichi* five strategic goals) (Ministério-do-Ambiente 2017). ENCNB-2025 however, lacks in proposing an approach and a set of indicators, to assess and monitor progress in the proposed strategy, although recognizing its need. This situation is common to other countries despite CBD's progresses in devising indicators to monitor the attainment of *Aichi* Targets (CBD 2014).

Information gaps for biodiversity management and conservation remain a constraint for better policy making as several assessments point out (Walpole et al. 2009). In addition, existing biodiversity monitoring often fail to fulfil these needs, due to the lack of detail in setting up goals and hypotheses, survey design, data quality and statistical power to measure trends (Legg and Nagy 2006). However, better information on biodiversity and ecosystem status and trends is crucial to halt its loss and achieve a sustainable planet. To this end, several hundred countries and organisations pooled their skills and knowledge to develop the *Group on Earth Observations* (GEO) (Walters and Scholes 2017) [URL: https://www.earthobservations.org]. GEO is a global partnership of more than 100 national governments and participating organizations that is promoting the use of coordinated, comprehensive and sustained Earth observations to improve decisions and actions for the benefit of humankind. GEO community is also responsible for the creation of a *Global Earth Observation System of Systems* (GEOSS) aiming to integrate observation systems and share data by linking the existing infrastructures. This includes more than 150 national and regional data providers such as NASA and ESA. One of GEO and GEOSS focal areas of concern is biodiversity, and the 'community of practice' that was developed to help implementing a global data sharing network on this subject is the Biodiversity Observation Network (BON) or GEO BON (Figure 1 - 3). Its ambitious mission is to: "improve the acquisition, coordination and delivery of biodiversity observations and related services to users including decision makers and the scientific community." and to contribute for "(…) effective management policies for the world's biodiversity and ecosystem services", articulated through a global biodiversity observation network (source: http://geobon.org/about/vision-goals).

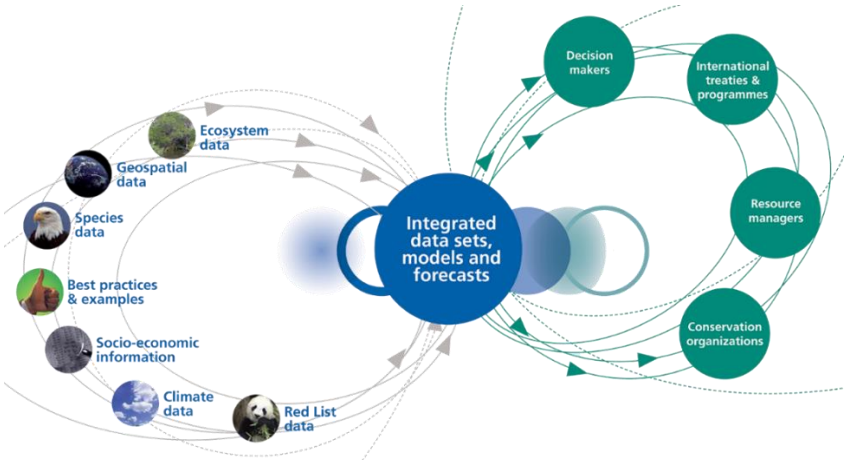

Figure 1 - 3 – GEO BON – The Group on Earth Observations Biodiversity Observation Network (source GEO BON, URL: http://geobon.org/about/vision-goals).).

Pooling global to national resources to monitor biodiversity status and change is promoting a pathway to identify its safe operational boundaries across multiple scales allowing to make better decisions and policy. International initiatives and networks such as CBD and GEO BON are paving the way to this endeavour.

1.2. Scales, levels and 'facets' of biodiversity: implications for assessment and monitoring

As mentioned before, climate and land use changes are two main drivers of change in the Anthropocene era, operating at distinct spatial (from global to local) and temporal scales (Figure 1 - 4), and impacting across the different levels of biodiversity (from genes to landscapes).

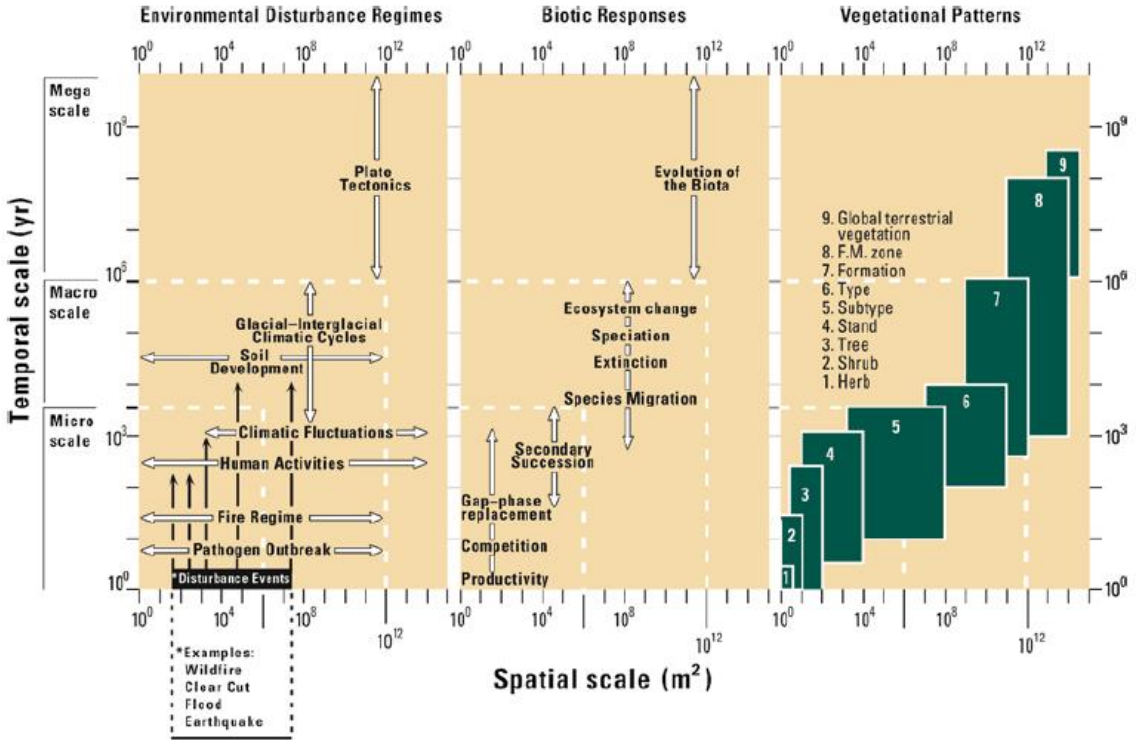

Figure 1 - 4 – Space-time hierarchy diagram proposed by (Delcourt et al. 1982). Environmental disturbances regimes, biotic responses and vegetational patterns are shown in the context of space-time domains. The scale for each pattern or process reflects the spatiotemporal scale required to observe or analyse it. For vegetation patterns, the temporal scale represents the time needed to record their dynamics (reproduced from: (Turner and Gardner 2015)).

'Scale' and 'level' are two key concepts in ecology (e.g. (Schneider 2001)) with great implications for the assessment and monitoring of biodiversity status and change (Noss 1990). As Levin (1992) noted: *"(…) the problem of pattern and scale is the central*

problem in ecology, unifying population biology and ecosystems science, and marrying basic and applied ecology.". Given the importance of scale-related terms it is imperative to define them at this stage to avoid ambiguity. For this matter, we adopt the definitions provided by Turner and Gardner (2015) who defined *scale* as the *"(…) spatial or temporal dimension of an object and process*". In a somewhat operational and spatial sense, scale is characterized by a certain *grain* and *extent*. Grain refers to the finest level of spatial resolution possible when using a dataset to investigate a process or pattern; while extent is simply the size of the study area or the temporal interval used for analysis. Scale needs to be carefully decided upon the nature of inquiry and according to the selected targets of monitoring or specific questions under investigation. While some problems may require a focus on an individual organism and its response to a local set of conditions (e.g. (Schreiber and Lloyd-Smith 2009)), others require a broader spatial scope to examine how (for example) species distributions change in space and time (Guisan and Thuiller 2005).

The concept of scale differs from that of *level of organization* (Figure 1 - 5), which defines the component or layer within a biotic hierarchy (Turner and Gardner 2015). These levels are not scale dependent (Allen and Hoekstra 1990) and, at each level, structure and function are precisely coordinated (Solomon et al. 2008). Each level also holds different attributes and is characterized by a set of processes that operate at specific spatiotemporal scales.

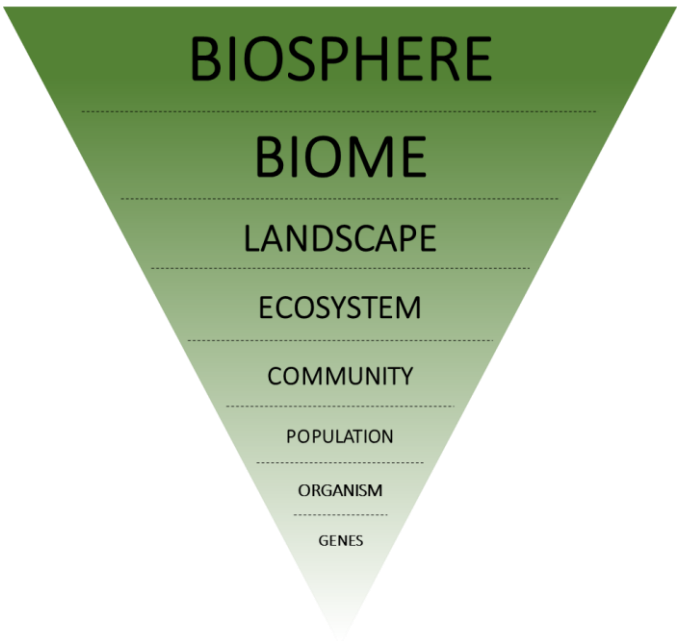

Figure 1 - 5 – Eight levels of biological and ecological organization with increasing degree of complexity and interactions from bottom to top (based on: (Solomon et al. 2008) and (Allen and Hoekstra 1990)).

Thus, a population of a given species may occupy a given space, move or disperse a certain distance, and reproduce within a given time interval. However, the community to which that species belongs is characterized by the different spatiotemporal scales of all populations composing that community (Turner and Gardner 2015).

Each organization level also has *emergent properties*, defining characteristics not found in the lower levels. For example, populations of organisms have emergent properties such as population density, age structure, birth and death rates which individuals composing that population do not have (Solomon et al. 2008). As we shift downward from ecosystems to individuals and finally to genes, the entities and processes addressed become more focussed and precise; however, there is an increasing loss of information regarding the interactions across levels and the emergent properties arising from these interactions (Walters and Scholes 2017). Ultimately, this choice is relevant for assessing and understanding biodiversity change and it depends on the scientific or management questions of interest and the type of entities selected for monitoring.

Based on the work of Franklin (1988), in which he recognized three primary attributes of ecosystems: *composition*, *structure* and *function*, and the hierarchical notion of biodiversity levels, Noss (1990) proposed a framework for devising and selecting sets of monitoring indicators (Figure 1 - 6). Composition addresses the variety of elements in a collection and may include allelic or genetic diversity, species lists for a certain region, or the set of different land cover and habitat types in a landscape. Structure (or configuration) is the physical organization, arrangement or pattern of a system. It relates to complexity and can be measured at the community level up to the spatial configuration (e.g., size, shape, isolation, connectivity) of different patches arranged in a landscape mosaic. Function relates to ecological and evolutionary processes occurring in a given system, including (among others) gene flow, disturbance (and the response that follows it), energy and matter flows, or nutrient cycling.

This framework links fundamental aspects of biodiversity (organization level) and allows for a more integrative view along three primary and complementary attributes of biodiversity. To understand the consequences of both climate and land use change requires to navigate its consequences both through the different hierarchical levels but also its effects on different structural, compositional and functional attributes (e.g., fragmentation of species populations' ranges, changes in community composition, alterations in ecosystems productivity or phenology).

The concept of 'biodiversity' is inherently a complex one, and for which multiple interconnected levels can be discerned, not only in relation to composition, structure and function (Noss 1990) but also to the several *facets* of biodiversity (taxonomic, functional, phylogenetic; (Jarzyna and Jetz 2016, Pollock et al. 2017)). In order to effectively measure and monitor biodiversity, its inherent complexity must be acknowledged as well as the cross-scale and cross-level interactions between different components. This requires ample, integrative and transdisciplinary approaches for bridging existing knowledge gaps.

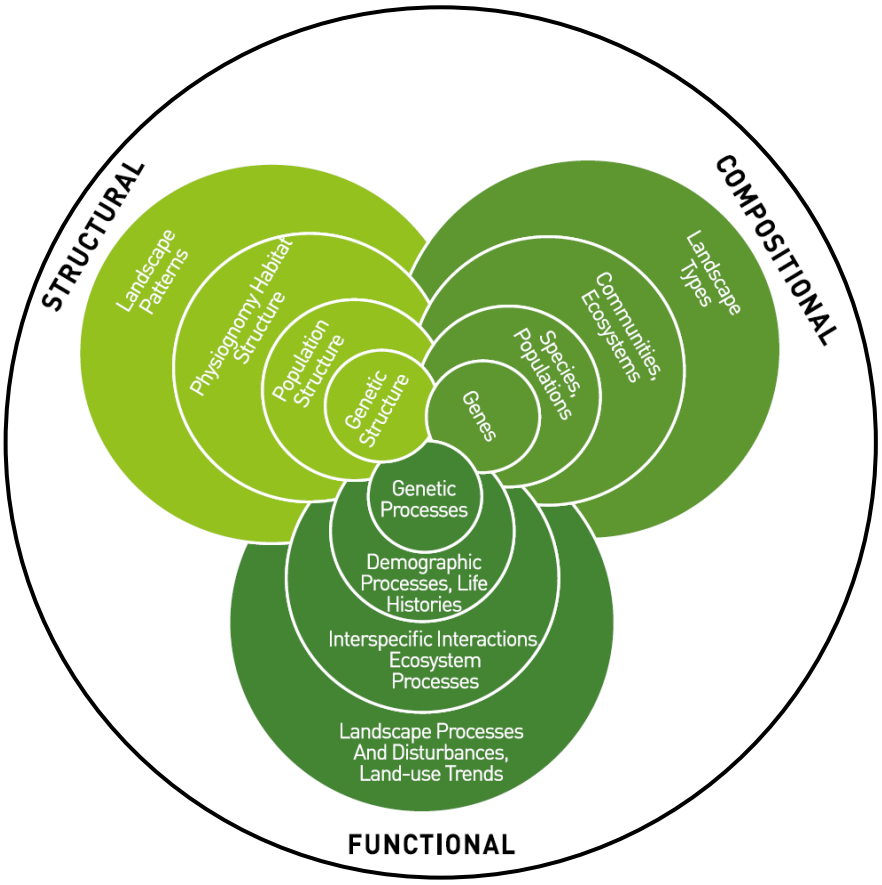

Figure 1 - 6 – Compositional, structural and functional biodiversity shown as interconnected spheres along multiple levels of organization. (source: Noss (1990) and redrawn in Werner and Gallo-Orsi (2016))

References

Allen, T. F. H., and T. W. Hoekstra. 1990. The confusion between scale-defined levels and conventional levels of organization in ecology. Journal of Vegetation Science 1:5-12.

Barnosky, A. D., N. Matzke, S. Tomiya, G. O. U. Wogan, B. Swartz, T. B. Quental, C. Marshall, J. L. McGuire, E. L. Lindsey, K. C. Maguire, B. Mersey, and E. A. Ferrer. 2011. Has the Earth/'s sixth mass extinction already arrived? Nature 471:51-57.

Bull, J. W., and M. Maron. 2016. How humans drive speciation as well as extinction. Proceedings of the Royal Society B: Biological Sciences 283:20160600.

Butchart, S. H. M., M. Walpole, B. Collen, A. v. Strien, J. P. W. Scharlemann, R. E. A. Almond, J. E. M. Baillie, B. Bomhard, C. Brown, J. Bruno, K. E. Carpenter, G. M. Carr, J. Chanson, A. M. Chenery, J. Csirke, N. C. Davidson, F. Dentener, M. Foster, A. Galli, J. N. Galloway, P. Genovesi, R. D. Gregory, M. Hockings, V. Kapos, J.-F. Lamarque, F. Leverington, J. Loh, M. A. McGeoch, L. McRae, A. Minasyan, M. H. Morcillo, T. E. E. Oldfield, D. Pauly, S. Quader, C. Revenga, J. R. Sauer, B. Skolnik, D. Spear, D. Stanwell-Smith, S. N. Stuart, A. Symes, M. Tierney, T. D. Tyrrell, J.-C. Vié, and R. Watson. 2010. Global Biodiversity: Indicators of Recent Declines. Science 328:1164-1168.

CBD. 2014. Global Biodiversity Outlook 4 - A mid-term assessment of progress towards the implementation of the Strategic Plan for Biodiversity 2011-2020. Secretariat of the Convention on Biological Diversity, Montréal, Quebec, Canada.

Ceballos, G., P. R. Ehrlich, A. D. Barnosky, A. García, R. M. Pringle, and T. M. Palmer. 2015. Accelerated modern human–induced species losses: Entering the sixth mass extinction. Science Advances 1.

Chapin III, F. S., E. S. Zavaleta, V. T. Eviner, R. L. Naylor, P. M. Vitousek, H. L. Reynolds, D. U. Hooper, S. Lavorel, O. E. Sala, S. E. Hobbie, M. C. Mack, and S. Diaz. 2000. Consequences of changing biodiversity. Nature 405:234-242.

Crutzen, P. J. 2002. Geology of mankind. Nature 415:23-23.

Delcourt, H. R., P. A. Delcourt, and T. Webb. 1982. Dynamic plant ecology: the spectrum of vegetational change in space and time. Quaternary Science Reviews 1:153-175.

Díaz, S., D. Tilman, J. Fargione, F. S. C. III, R. Dirzo, T. Kitzberger, B. Gemmill, Martin Zobel, M. Vilà, C. Mitchell, A. Wilby, G. C. Daily, M. Galetti, W. F. Laurance, J. Pretty, R. Naylor, A. Power, D. Harvell, S. Potts, C. Kremen, T. Griswold, and C. Eardley. 2005. Biodiversity regulation of ecosystem services. Pages 297-329 in R. Hassan, R. J. Scholes, and N. Ash, editors. Ecosystems and human wellbeing - Current state and trends: Findings of the condition and trends working group. Island Press, Washington D.C., USA.

Folke, C., S. Carpenter, B. Walker, M. Scheffer, T. Elmqvist, L. Gunderson, and C. S. Holling. 2004. Regime shifts, resilience, and biodiversity in ecosystem management. Annual Review of Ecology, Evolution, and Systematics 35:557-581.

Franklin, J. F. 1988. Structural and Functional Diversity in Temperate Forests. Pages 166-175 in E.O.Wilson and F. M. Peter, editors. Biodiversity. National Academy Press, Washington, D.C., USA.

Guisan, A., and W. Thuiller. 2005. Predicting species distribution: offering more than simple habitat models. Ecology Letters 8:993-1009.

Hooper, D. U., F. S. Chapin, J. J. Ewel, A. Hector, P. Inchausti, S. Lavorel, J. H. Lawton, D. M. Lodge, M. Loreau, S. Naeem, B. Schmid, H. Setälä, A. J. Symstad, J. Vandermeer, and D. A. Wardle. 2005. Effects of Biodiversity on Ecosystem

Functioning: A Consensus of Current Knowledge. Ecological Monographs 75:3-35.

Jarzyna, M. A., and W. Jetz. 2016. Detecting the Multiple Facets of Biodiversity. Trends in Ecology & Evolution 31:527-538.

Johnson, C. N., A. Balmford, B. W. Brook, J. C. Buettel, M. Galetti, L. Guangchun, and J. M. Wilmshurst. 2017. Biodiversity losses and conservation responses in the Anthropocene. Science 356:270-275.

Legg, C. J., and L. Nagy. 2006. Why most conservation monitoring is, but need not be, a waste of time. Journal of Environmental Management 78:194-199.

Levin, S. A. 1992. The Problem of Pattern and Scale in Ecology: The Robert H. MacArthur Award Lecture. Ecology 73:1943-1967.

Ministério-do-Ambiente. 2017. Estratégia Nacional de Conservação da Natureza e Biodiversidade - ENCNB 2025. Ministério do Ambiente - República Portuguesa, Lisboa, Portugal.

Noss, R. F. 1990. Indicators for Monitoring Biodiversity: A Hierarchical Approach. Conservation Biology 4:355-364.

Pecl, G. T., M. B. Araújo, J. D. Bell, J. Blanchard, T. C. Bonebrake, I.-C. Chen, T. D. Clark, R. K. Colwell, F. Danielsen, B. Evengård, L. Falconi, S. Ferrier, S. Frusher, R. A. Garcia, R. B. Griffis, A. J. Hobday, C. Janion-Scheepers, M. A. Jarzyna, S. Jennings, J. Lenoir, H. I. Linnetved, V. Y. Martin, P. C. McCormack, J. McDonald, N. J. Mitchell, T. Mustonen, J. M. Pandolfi, N. Pettorelli, E. Popova, S. A. Robinson, B. R. Scheffers, J. D. Shaw, C. J. B. Sorte, J. M. Strugnell, J. M. Sunday, M.-N. Tuanmu, A. Vergés, C. Villanueva, T. Wernberg, E. Wapstra, and S. E. Williams. 2017. Biodiversity redistribution under climate change: Impacts on ecosystems and human well-being. Science 355.

Pereira, H. M., P. W. Leadley, V. Proença, R. Alkemade, J. P. W. Scharlemann, J. F. Fernandez-Manjarrés, M. B. Araújo, P. Balvanera, R. Biggs, W. W. L. Cheung, L. Chini, H. D. Cooper, E. L. Gilman, S. Guénette, G. C. Hurtt, H. P. Huntington, G. M. Mace, T. Oberdorff, C. Revenga, P. Rodrigues, R. J. Scholes, U. R. Sumaila, and M. Walpole. 2010. Scenarios for Global Biodiversity in the 21st Century. Science 330:1496-1501.

Pimm, S. L., C. N. Jenkins, R. Abell, T. M. Brooks, J. L. Gittleman, L. N. Joppa, P. H. Raven, C. M. Roberts, and J. O. Sexton. 2014. The biodiversity of species and their rates of extinction, distribution, and protection. Science 344.

Pollock, L. J., W. Thuiller, and W. Jetz. 2017. Large conservation gains possible for global biodiversity facets. Nature 546:141-144.

Rockstrom, J., W. Steffen, K. Noone, A. Persson, F. S. Chapin, E. F. Lambin, T. M. Lenton, M. Scheffer, C. Folke, H. J. Schellnhuber, B. Nykvist, C. A. de Wit, T. Hughes, S. van der Leeuw, H. Rodhe, S. Sorlin, P. K. Snyder, R. Costanza, U. Svedin, M. Falkenmark, L. Karlberg, R. W. Corell, V. J. Fabry, J. Hansen, B. Walker, D. Liverman, K. Richardson, P. Crutzen, and J. A. Foley. 2009. A safe operating space for humanity. Nature 461:472-475.

Sala, O. E., F. Stuart Chapin III, J. J. Armesto, E. Berlow, J. Bloomfield, R. Dirzo, E. Huber-Sanwald, L. F. Huenneke, R. B. Jackson, A. Kinzig, R. Leemans, D. M. Lodge, H. A. Mooney, M. n. Oesterheld, N. L. Poff, M. T. Sykes, B. H. Walker, M. Walker, and D. H. Wall. 2000. Global Biodiversity Scenarios for the Year 2100. Science 287:1770-1774.

Scheffer, M., S. Barrett, S. R. Carpenter, C. Folke, A. J. Green, M. Holmgren, T. P. Hughes, S. Kosten, I. A. van de Leemput, D. C. Nepstad, E. H. van Nes, E. T. H. M. Peeters, and B. Walker. 2015. Creating a safe operating space for iconic ecosystems. Science 347:1317-1319.

Scheffer, M., S. Carpenter, J. A. Foley, C. Folke, and B. Walker. 2001. Catastrophic shifts in ecosystems. Nature 413:591-596.

Scheffer, M., and S. R. Carpenter. 2003. Catastrophic regime shifts in ecosystems: linking theory to observation. Trends in Ecology & Evolution 18:648-656.

Schneider, D. C. 2001. The Rise of the Concept of Scale in Ecology. BioScience 51:545-553.

Schreiber, Sebastian J., and James O. Lloyd-Smith. 2009. Invasion Dynamics in Spatially Heterogeneous Environments. The American Naturalist 174:490-505.

Solomon, E. P., L. R. Berg, and D. W. Martin. 2008. Biology. 8th edition. Thomson Higher Education, Belmont, CA, US.

Turner, M. G., and R. H. Gardner. 2015. Landscape Ecology in Theory and Practice - Pattern and Process. 2nd edition. Springer-Verlag, New York, USA.

Walpole, M., R. E. A. Almond, C. Besançon, S. H. M. Butchart, D. Campbell-Lendrum, G. M. Carr, B. Collen, L. Collette, N. C. Davidson, E. Dulloo, A. M. Fazel, J. N. Galloway, M. Gill, T. Goverse, M. Hockings, D. J. Leaman, D. H. W. Morgan, C. Revenga, C. J. Rickwood, F. Schutyser, S. Simons, A. J. Stattersfield, T. D. Tyrrell, J.-C. Vié, and M. Zimsky. 2009. Tracking Progress Toward the 2010 Biodiversity Target and Beyond. Science 325:1503-1504.

Walters, M., and R. J. Scholes. 2017. The GEO Handbook on Biodiversity Observation Networks. Springer, Switzerland.

Werner, F. A., and U. Gallo-Orsi. 2016. Biodiversity Monitoring For Natural Resource Management - An Introductory Manual. GIZ, Eschborn and Bonn, Germany. DOI: 10.13140/RG.2.1.3141.8488/1.

CHAPTER 2 - Methods and tools for ecological change assessment

2.1. Earth observation systems for assessing and monitoring ecological change

2.1.1. Earth observation: principles, platforms and data

In face of accelerated biodiversity changes, evaluating and monitoring the state and change of Earth's ecosystems is perhaps more crucial than ever. Complementarily, describing and understanding ecological patterns and processes and their spatiotemporal change is key to this effort and, to improve management and conservation strategies (Nagendra et al. 2013, Pettorelli et al. 2014, Mairota et al. 2015).

For these ambitious objectives, *Earth Observation* (EO) technologies are a powerful tool to monitor the status and change of multiple attributes and levels of biodiversity (Lausch et al. 2016), with a vast collection of available sensors and platforms (Petrou et al. 2015, Lausch et al. 2016). For avoiding ambiguity in the definition, for the purpose of this thesis, we refer to EO as the process of gathering information about planet Earth's biological, physical or chemical systems via *Remote Sensing* (RS) technologies, which include primarily sensors onboard satellite platforms (spaceborne) but also sensors onboard aerial platforms (airborne), such as aircrafts or unmanned aerial vehicles, UAVs (IJAEOG 2017). EO is commonly used to obtain information regarding the status, and changes, in the natural and the built-up environments. EO is commonly supplemented by *in situ* surveying techniques, that allow acquiring observational data intended to calibrate or evaluate classifiers or models that use EO data to obtain 'higher-level' and validated products (e.g., land cover, leaf area index, evapotranspiration, productivity, biomass). In this sense, EO observation capabilities can complement field surveys (related to species, habitats, or biophysical parameters of interest) by delivering a synoptic view and offering the opportunity to deliver consistent information in time and space (Vanden Borre et al. 2011).

EO works mainly by detecting the energy reflected or emitted from the Earth as electromagnetic (EM) radiation (Lavender and Lavender 2016) which is then measured by sensors onboard aircrafts, UAVs (suborbital) or orbital satellite platforms. The EM spectrum covers a large range of spectral domains (Figure 2 - 1), including the ultraviolet

radiation (lower wavelengths and higher frequency), visible, infrared, microwave, and radio waves (longer wavelengths and shorter frequency). The EM radiation in these wavelengths is absorbed and scattered differently both within the atmosphere and when interacting with the surface of an object or a region composed by certain surface types (e.g., forest, soil, water) (Lavender and Lavender 2016).

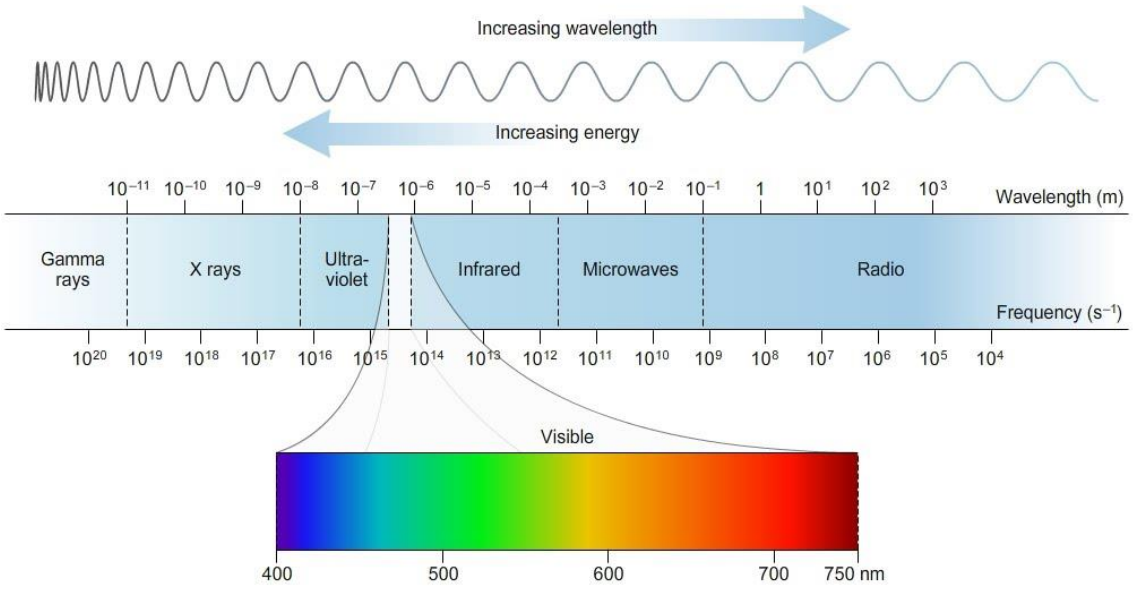

Figure 2 - 1 – The electromagnetic spectrum (source: https://sites.google.com/site/chempendix/em-spectrum; © Sapling Learning)

Two broad categories of EO sensors can be distinguished: '*active'* and '*passive'* sensors. Both types of sensors measure the intensity of a signal withiin a specific wavelength interval within the EM spectrum (commonly defined as a 'band' or 'channel') but operate differently.

Active sensors emit a pulse and later measure the energy returned, scattered or bounced back to a detector (e.g., SAR [2]or LiDAR[3]) (Turner et al. 2003). Therefore, these sensors do not depend on the sun's electromagnetic energy or thermal energy of the Earth (Jensen 2000). Both SAR and LiDAR have extensively been used for vegetation monitoring and conservation purposes [see the revision work by Nagendra et al. (2013)], however, for the purpose of this thesis, these sensors were not considered and therefore will not be further discussed.

[2] SAR – Synthetic Aperture Radio Detection and Ranging
[3] LiDAR - Light Detection And Ranging

Passive sensors (e.g., optical sensors[4]) measure the radiation that reaches a detector without the sensor first transmitting a pulse of radiation (Turner et al. 2003). These sensors use the incoming energy from the sun, which is emitted toward the Earth's surface (defined as *solar irradiance*) and then absorbed or scattered differently by diverse types of land or water surfaces. The amount of EM energy that is scattered or reemitted back up toward the detecting sensor is then measured and recorded. This quantity is defined as *radiance, i.e.*, the amount of radiation leaving a source for a given area that is captured from a narrow field of view (Jensen 2000). *Reflectance is* another important physical measure in this regard, and it is defined as the ratio between the EM energy coming down from the sun and the EM energy going back to the sensor (Lavender and Lavender 2016). This physical property can be used to discriminate different land cover and vegetation types, calculate spectral vegetation or water indices (i.e., numerical combinations of different spectral bands) or to estimate biophysical parameters of interest via empirical or process-based models.

In optical RS, the presence of a heterogeneous, dense and layered terrestrial atmosphere composed of water vapour, aerosols and gases (such as O2, O3, CO2 and CH4) disturbs the signal reaching EO sensors (Bakker et al. 2004). Particles and gases in the atmosphere can affect the incoming light and radiation by the mechanisms of *scattering* and *absorption*. Scattering occurs when particles or large gas molecules present in the atmosphere interact with and cause the EM radiation to be redirected from its original path. Absorption has more profound consequences for satellite-based EO. This happens because molecules in the atmosphere absorb energy in specific regions of the EM spectrum, thus limiting the 'usable' fraction of the spectrum for RS purposes and creating 'atmospheric windows' (non-shaded areas in Figure 2 - 2). Part of this 'window' coincides with high emission by the sun in the visible (390 – 700nm) and the near-infrared (NIR; 700 – 1300nm) regions which are particularly important for mapping vegetation and its condition [e.g., (Jobbágy et al. 2002, Pettorelli et al. 2005, Clerici et al. 2012)]. In the case of vegetation, plant's pigments (mainly chlorophyll) strongly absorb radiation in the visible region, while in the NIR the absorption by vegetation is low. The transition between the spectral response in the visible and NIR domains is considered an indicator of plants vigour, i.e., the larger the contrast between these two regions the larger the plant vigour. For example, the Normalized Difference Vegetation Index (NDVI), one of the most widely used indices in ecological applications (Pettorelli et al. 2014)), integrates the red (visible domain) and NIR bands in its calculation, and is

[4] Optical remote sensing makes use of visible, near infrared and short-wave infrared sensors

commonly associated with plant structural traits like biomass, vigour, and leaf area index. The heat energy emitted by the Earth also corresponds to a window around 10,000nm corresponding to the thermal infrared portion of the EM spectrum (Figure 2 - 2). Thermal bands also have important ecological applications such as to detect disturbance patterns at global scale (Mildrexler et al. 2009) by exploring the negative relationship between vegetation density and land surface temperatures (Duro et al. 2007) or using the Ts/VI space (surface temperature/vegetation index) for the retrieval of land surface energy fluxes and soil surface moisture (Petropoulos et al. 2009).

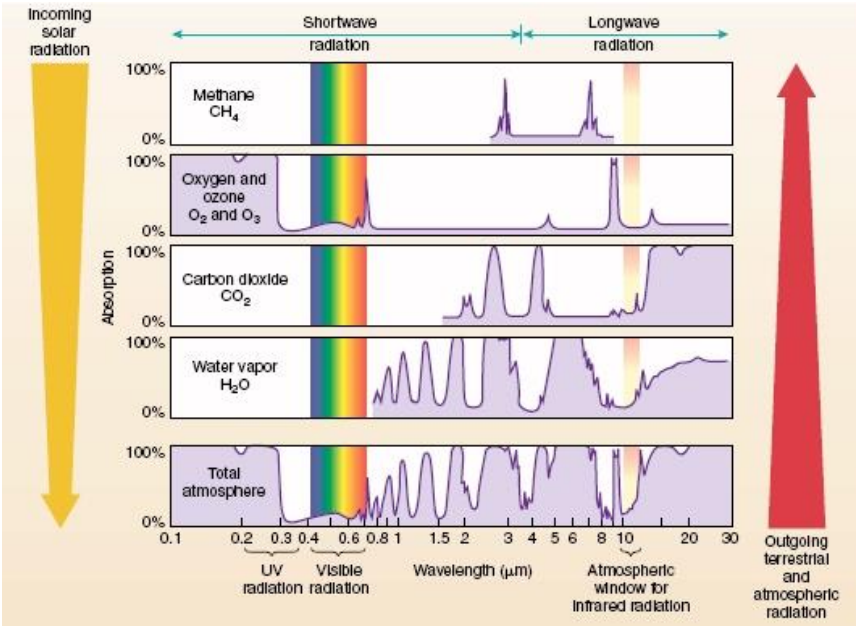

Figure 2 - 2 – Atmospheric absorption occurring along the EM spectrum (Source: CIMSS, URL: https://cimss.ssec.wisc.edu/sage/meteorology/lesson1/AtmAbsorbtion.htm)

In spaceborne RS, the sensor design and attributes as well as the orbital features (altitude, inclination angle, revisiting period, etc.) determine the image properties acquired by the EO platform. Image data characteristics (Jensen 2000, Bakker et al. 2004, Lavender and Lavender 2016), are defined (among other aspects) by:

- *Spatial resolution*: the size of the smallest object that can be recognized;
- *Spatial coverage*: the total area covered by one image proportional to the total field-of-view (FOV) of the instrument (for multispectral scanners);
- *Spectral resolution*: the number of bands within the EM spectrum that the sensor is capable of taking measurements;
- *Radiometric resolution*: the smallest difference in levels of energy that can be distinguished by the sensor (typically measured in *bit depth*);

- *Temporal resolution*: sometimes also referred as the *revisit time*, is defined as the amount of time (usually in hours or days) it takes for a satellite platform to return to collect data from exactly the same place on Earth.

Due to their importance for ecological applications and to the limitations imposed by these properties, spatial and spectral resolutions can be used to classify EO optical platforms (see Table 2 - 1). Regarding spatial resolution (mainly influencing the analysis scale) we can recognize five broad types: low (≥1000m), moderate (1000-30m), high (30m-5m), very-high (5m-1m), and (tentatively) 'ultra-high' (<1m) resolution. In terms of spectral resolution (mainly influencing the discrimination of different land cover or vegetation types), we recognize two broad categories: *multispectral* (sensors that take measures in a few relatively wide and non-contiguous spectral bands, typically less than 30-40 bands) and *hyperspectral* (sensors or imaging spectrometers that measure energy in many narrow, contiguous wavelengths often with as many as 200 bands or more). An example of the latter can be found in Figure 2 - 3, in which a hyperspectral instrument was used to collect reflectance profiles of several plant species allowing to discriminate them.

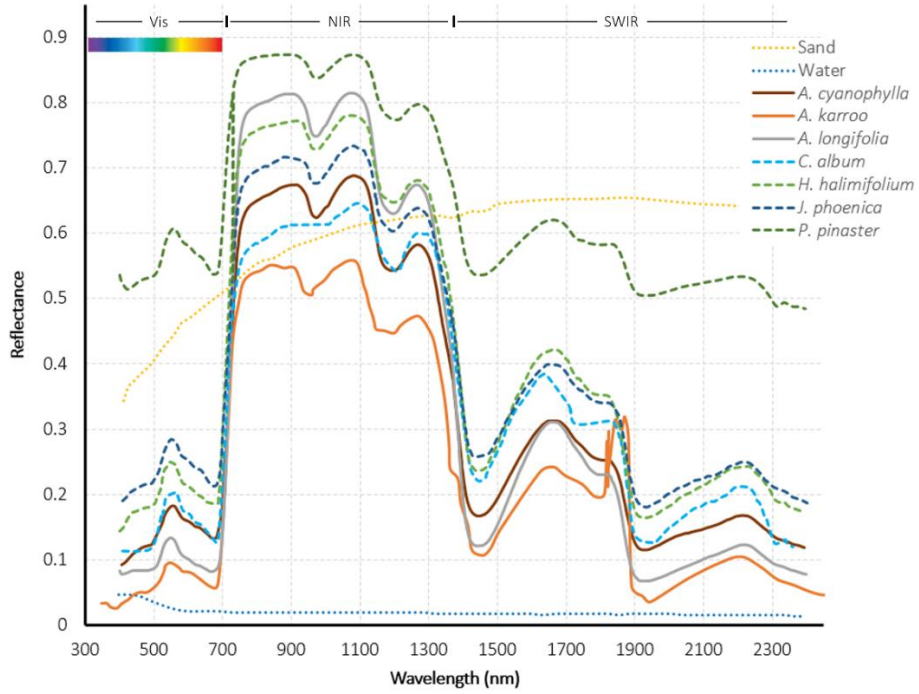

Figure 2 - 3 – Reflectance profiles extracted from a hyperspectral sensor showing spectral differences between alien/invasive plant species of the *Acacia* genus (solid lines; *Acacia cyanophylla*, *A. karroo* and *A. longifolia*) and native species (dashed lines; *Corema album, Halimium halimifolium, Juniperus phoenica and Pinus pinaster*). Adapted and data compiled from Bradley, 2014; Lehmann et al., 2015; Mureriwa et al., 2016. Electromagnetic spectrum ranges: Vis – Visible (390 – 700nm); NIR – Near Infrared (700-1300nm); SWIR – Short-wave Infrared (1300 – 3000nm).

Table 2 - 1 – A non-exhaustive list of operating satellite platforms and sensors from moderate to 'ultra'-high spatial resolution used for ecological applications and spatiotemporal change analysis. (*) hyperspectral sensors (HS); the remaining are multispectral (MS). PAN – panchromatic band; B – band number. Blue lines represent the platforms//sensors used in this thesis.

Satellite platform / sensor	Spatial resolution type	Start/end year	Orbital altitude (km)	# of bands	Spatial resolution (m)	Spectral range (µm)	Revisit period (days)
Proba-V / VGT-P	Moderate	2013	820	4	VIS/NIR: 300m, SWIR: 600m	0.438 - 0.914 µm, SWIR: 1.564 - 1.634µm	2
Terra (EOS AM-1) / MODIS	Moderate	1999	705	36	B1-B2: 250m, B3-B7: 500m, B8-B36: 1000m	0.4 µm - 14.4 µm	2
EO-1 / Hyperion	High	2000	705	200*	HS: 30m	0.4 - 2.5 µm	16
Proba-1 / CHRIS, HRC	High	2001	615	200*	HS: 18 m - 36 m, PAN : 5 m	0.415µm - 1.050µm	7
DEIMOS-1	High	2009	663	3	MS: 22 m	0.52 µm - 0.90 µm	2 - 3
FORMOSAT-2 / RSI, ISUAL	High	2004	888	4	PAN: 2m, MS: 8m	0.45 µm - 0.90 µm	1
IRS-P6 / LISS-III/IV, AWiFS	High	2003	817	5	LISS-IV: 5.8m, LISS-III: 23.5m, AWiFS: 56m	LISS-III/IV/AWiFS: 0.52-0.86 µm, LISS-III/AWiFS: SWIR: 1.55-1.70 µm	5
Landsat 5 / TM	High	1984	705	7	MS: 30m, TIR: 120m	0.45 - 0.90µm, SWIR:1.55 - 1.75µm, 2.08 - 2.35µm, TIR: 10.4 - 12.5 µm	16
Landsat 7 / ETM	High	1999	705	7	MS: 30m, PAN: 15m, TIR: 60m	0.45 - 0.90µm, SWIR: 1.55 - 2.35µm, TIR: 10.4 - 12.5 µm	16
Landsat 8 / OLI	High	2013	705	9	MS: 30m, PAN: 15m	0.43 - 0.88µm, Cirrus/SWIR:1.36 - 2.29µm	16
Sentinel-2	High	2015	786	13	MS: 10 - 20m	0.44 - 2190 µm	5
SPOT 4 / HRVIR	High	1998 - 2013	820	4	MS: 20 m	0.58 µm - 0.89 µm (SWIR: 1.58 - 1.75 µm)	26
GeoEye-1 / GIS-MS	Very-high	2008	681	4	PAN: 0.41m, MS: 1.65m	0.45 - 0.92 µm	2 - 8
IKONOS-2 / OSA	Very-high	1999	681 - 709	4	PAN: 1m, MS: 4m	0.45 - 0.9 µm	14
KOMPSAT-2 / MSC	Very-high	2006	685	4	MS: 4m, PAN: 1m	0.45 µm - 0.90 µm	14
KOMPSAT-3 / MSC	Very-high	2012	685	4	MS: 2.8m, PAN: 0.7m	0.45 µm - 0.90 µm	14
QuickBird	Very-high	2001	450	4	PAN: 0.61m, MS: 2.44m	0.45 µm - 0.90 µm	1 - 3.5
RapidEye / REIS	Very-high	2008	630	5	MS: 5 m	0.44 µm - 0.85 µm	5.5
SPOT 5 / HRG	Very-high	2002	832	4	PAN: 2.5 - 5m, MS: 10m, SW: 20m	0.48 - 0.9µm (SWIR: 1.58 - 1.75µm)	2 - 3
SPOT 6	Very-high	2012	694	4	PAN: 1.5m, MS: 6m	0.455 - 0.890 µm	1
WorldView-2	Very-high	2009	770	8	PAN: 0.5m, MS: 2m	0.45 - 1.05 µm	1.1
SenseFly UAV / Canon Ixus	'Ultra-high'	2014	<1	4	MS: 0.03 - 0.10	0.4 - 0.6 µm	-

Overall, the spatial, spectral, radiometric and temporal resolutions of image data strongly limit and determine the usefulness of the various EO platforms for analysing different levels or attributes of biodiversity as well as for setting the scale used to assess ecological processes. For example, a moderate resolution platform such as MODIS (250m-1000m) may not be able to discriminate certain specific types of land cover or vegetation however, very-high resolution satellites such as WorldView-2 (2m) are indeed capable of recognizing detailed aspects of Earth's surface related for example with habitat quality (Vaz et al. 2015) or the occurrence of invasive species at the landscape level (Monteiro et al. 2017). On the other hand, MODIS time-series, due to its high temporal resolution and coverage may be suited to measure functional aspects related to ecosystem level productivity and phenology (Alcaraz et al. 2006, Xiao et al. 2006, Alcaraz-Segura et al. 2008, Cabello et al. 2012, Sesnie et al. 2012), detect the occurrence and severity of fires (Giglio et al. 2003, Giglio et al. 2006, Veraverbeke et al. 2011) and vegetation recovery following it (Leon et al. 2012, Di Mauro et al. 2014, Caccamo et al. 2015).

2.1.2. Applications on EO data in biodiversity science

As new EO imagery and related products become available, this opens new possibilities, in conjunction with ecological models, to answer fundamental questions about biodiversity (Turner et al. 2003). In addition, the variety of EO sensors and data sources currently available allows to evaluate multiple features of ecosystems and to deliver meaningful information for management and conservation (Kuenzer et al. 2014). Such variability may help in the process of selecting the sensors and platforms that are particularly suited for addressing biodiversity at specific scales (local to global), levels (species populations to ecosystems) or dimensions (composition, structure and functions) and in relation to specific questions or hypotheses.

In a review of EO methods in biodiversity, Lausch et al. (2016) stress that these offer an affordable, repeatable and comparable set of data and techniques to measure, describe and model taxonomic (or compositional), structural and functional diversity. The same authors, refer, in an analogy to the concept of plant traits', that EO as a physical system based mostly on measuring spectral reflectance, can directly or indirectly record "Spectral traits" (ST). This includes the detection capability of all spectral data recorded from optical, thermal or radar EO technologies. In addition, the author supports that STs can be measured and quantified across biodiversity hierarchy levels (species to ecosystems) and attributes (composition, structure and function; see Figure 2 - 4). By

recording changes in ST's – termed "Spectral Trait variations" (STV), EO is also capable of detecting alterations in biodiversity as a result of change processes and drivers that affect traits or lead to trait variations in populations, communities and ecosystems throughout space and time (Figure 2 - 5). The concepts of ST and STV provide a comprehensive basis for selecting EO-based indicators for ecological monitoring and thereby operationalize EO-based monitoring systems.

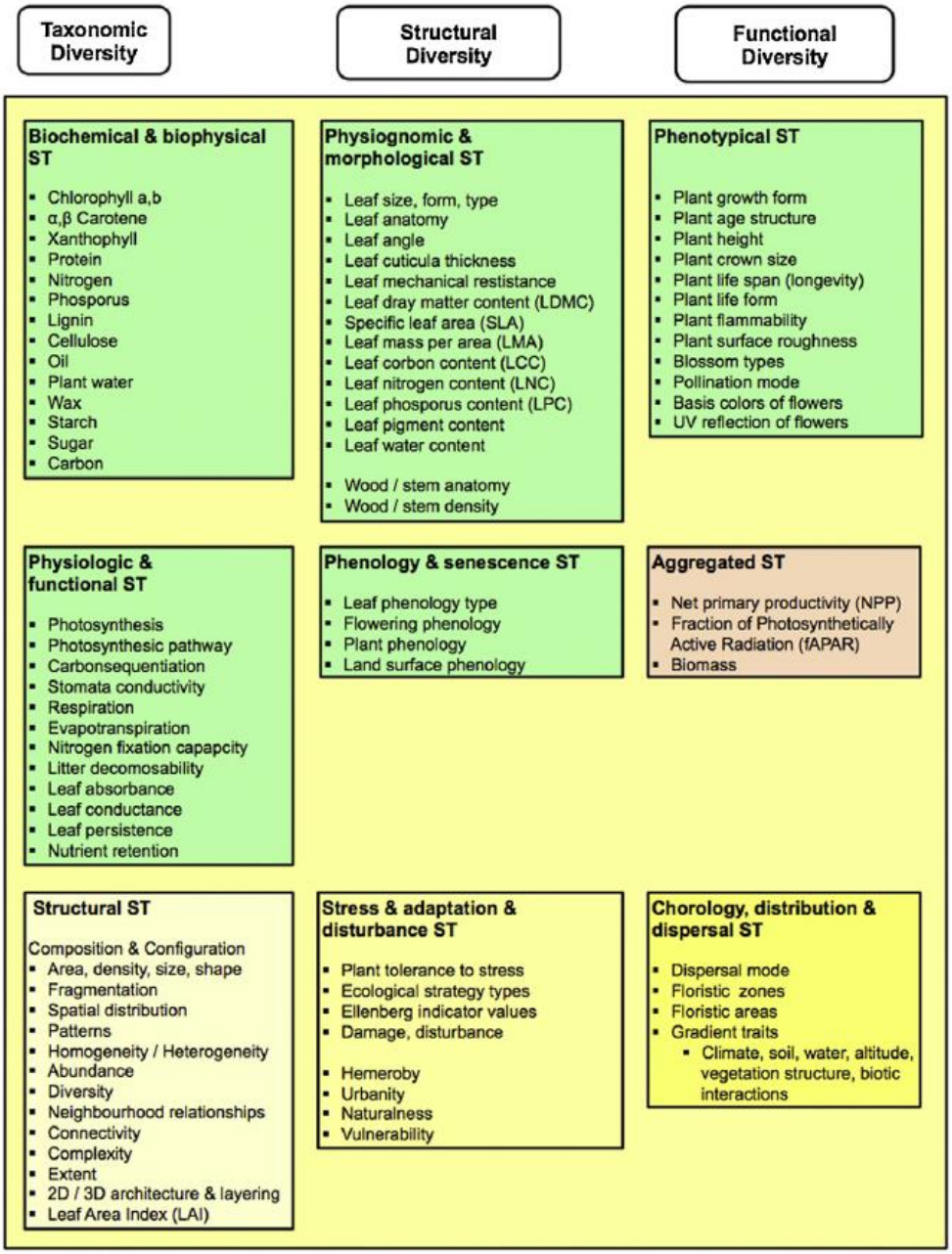

Figure 2 - 4 – (a) Spectral traits (ST) for quantifying biodiversity by EO techniques (source: simplified from original Lausch et al. (2016)).

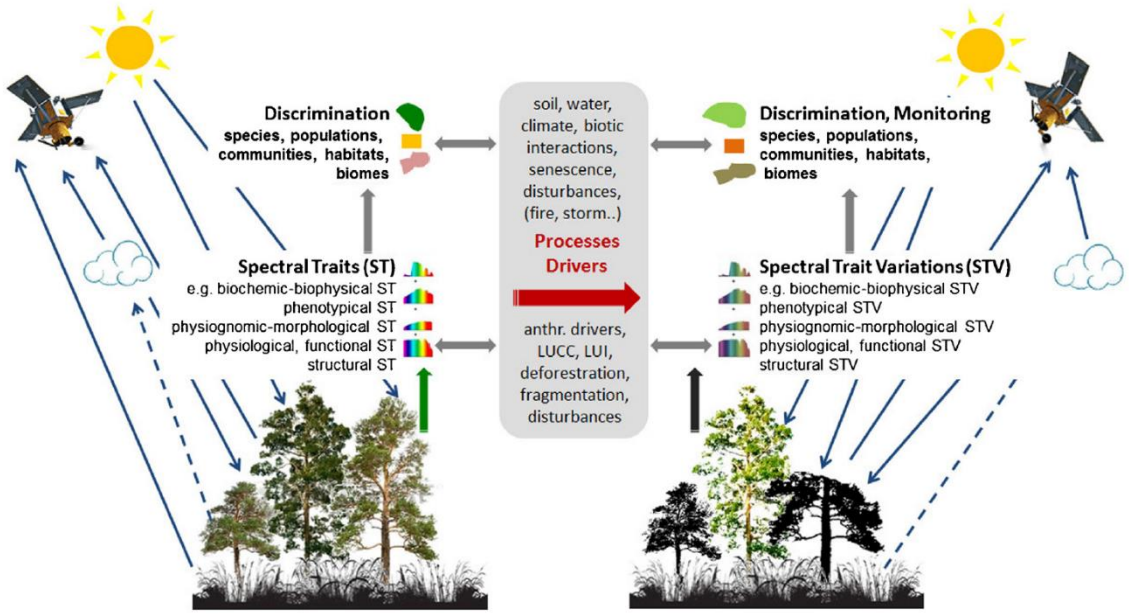

Figure 2 - 5 - Quantification of spectral traits and their interactions with drivers and processes to discriminate and monitor plant species, populations, habitats, communities and biomes using EO (source Lausch et al. (2016)).

Due to its versatility, EO has increasingly been used to support the assessment of biodiversity-related characteristics and functions (Kuenzer et al. 2014, Petrou et al. 2015, Lausch et al. 2016). Nonetheless, its systematic and operational use for monitoring widely adopted CBD biodiversity indicators and *Aichi* targets is still limited (Petrou et al. 2015). Most EO applications in biodiversity focus on specific aspects and applications tend to have a relatively narrow context. However, the scientific community is proposing a synthesis of current knowledge in order to overcome these limitations and to streamline the adoption of EO-based assessment of conservation targets. In fact, EO existing and emerging technologies can strongly contribute or support the evaluation and monitoring of progress towards several *Aichi* Biodiversity Targets (Secades et al. 2014, O'Connor et al. 2015, Petrou et al. 2015). This includes, among other features, the development of EO-based spatiotemporal analysis of land cover/use change, the evaluation of habitat connectivity/fragmentation and quality, or the assessment of land surface and ecosystem functioning properties related to vegetation productivity dynamics and phenology (Secades et al. 2014). Modelling is also an emerging area of interest for which EO data and products can contribute either as input variables or as a way to constrain models. In particular, Species Distribution Models (SDMs) can benefit with integrating EO data (e.g., He et al. 2011, Rocchini et al. 2016). Table 2 - 2 presents a synthesis of current findings based on Secades et al. (2014) defining which strategic areas within *Aichi* targets can EO-based technologies support.

Table 2 - 2 – Current adequacy of remote sensing to support tracking progress towards the Aichi Targets based on 3 broad categories: [●] Currently not observable by EO-based approach but some of the targets under this category maybe technically feasible in the future; [●] Could be partially derived from EO-based information or EO-based approaches currently in development; [●] Can be totally or partially derived from existing EO-based information. In some cases, only some of the corresponding operational indicators currently analysed fit the category. The attribution of each category is based on subjective estimates of adequacy based on the most recent information available to authors (source: Secades et al. (2014)).

Strategic Goal	Aichi Biodiversity Target	Current remote sensing adequacy		
A	1. Awareness of biodiversity values	●		
	2. Integration of biodiversity values	●		
	3. Incentives	●		
	4. Sustainable production and consumption		●	
B	5. Habitat loss, fragmentation and degradation			●
	6. Sustainable exploitation of marine resources		●	
	7.Biodiversity-friendly agriculture, forestry and aquaculture		●	
	8. Pollution reduction			●
	9. Control of invasive alien species		●	
	10. Coral reefs and other vulnerable ecosystems		●	
C	11. Protected areas			●
	12. Prevented extinction of threatened species		●	
	13. Genetic diversity of socio-economically and culturally valuable species	●		
D	14. Ecosystem services			●
	15. Ecosystem resilience		●	
	16. Access and benefit sharing	●		
E	17. NBSAPs	●		
	18. Traditional Knowledge and customary use	●		
	19. Biodiversity knowledge improvement and transfer	●		
	20. Resource mobilisation	●		

Despite impressive advances, many challenges still lie ahead in the way to streamline the adoption of EO-based methods for biodiversity assessment and monitoring (Secades et al. 2014, O'Connor et al. 2015, Petrou et al. 2015, Skidmore et al. 2015). Improving the communication between EO-specialists and ecologists is one important point in the agenda. Convincing and engaging stakeholders and national agencies about the value of EO technologies for assessing Earth's dynamics in multiple domains such as biodiversity, forestry, agriculture, water management, risk evaluation and disaster control is also an important task. In this regard, GEOSS and GEO BON are

also making valuable efforts to implement their EO-supported programs with potential benefits for addressing the core issues in their agendas.

For progressing further, we need multi-disciplinary syntheses and approaches to understand ecological patterns and processes and their spatiotemporal change. The same applies to EO technologies, as to truly profit from them will require conjugating efforts and research from various scientific disciplines as well as developing a common language. Moreover, upcoming developments in EO platforms (such as spaceborne LiDAR – *LIST* (Yu et al. 2010) or hyperspectral sensor – *EnMap* (Guanter et al. 2015)) are opening new possibilities to track biodiversity from space, in all its facets and with greater detail. The novel augmented and faster ways to process large volumes of data using cloud-based infrastructures (such as *Google Earth Engine*, *Descartes Labs* or *Raster Foundry*) are also creating the conditions to truly harness the power of Earth Observation.

2.2. Modelling tools for assessing change drivers and forecasting

2.2.1. Species Distribution Models (SDMs)

In Ecology, a large plethora of models is currently available to analyse ecological phenomena (Jørgensen 2008) from different epistemological perspectives, approaches and toolsets. From a hierarchical and non-exhaustive perspective, we can find: (i) *Species Distribution Models*, correlative models used to investigate species ranges and ecological responses to environmental determinants (Elith and Leathwick 2009a, Elith et al. 2010), (ii) *Population Dynamic Models*, mainly based on differential equations, these models explain changes in the number of individuals based on population parameters (Jørgensen 2016), (iii) *Individual Based Models*, used to simulate populations and communities by following individuals, their properties and interactions (DeAngelis and Grimm 2014), (iv) *Landscape Dynamics Simulation models*, used to forecast and simulate landscape change (Daniel et al. 2016), and highly complex Dynamic Global Vegetation Models, allowing to project past, current and future vegetation patterns and associated biogeochemical cycles at a global scale; (Bonan et al. 2003). Three broad model categories can tentatively be discriminated: (i) mechanistic, (ii) process-based and, (iii) correlative (Peterson et al. 2015). Mechanistic models use biophysical modelling approaches incorporating physiological processes that limit species distributions and abundance; i.e., these models aim to understand the physiologically based environmental constraints that influence species distribution and abundance (Kearney et

al. 2010). Similarly, process-based models explicitly include the processes that describe the distribution of species and biodiversity (Dormann et al. 2012). Both mechanistic and process-based models demand a large number of input parameters, which are often not available at adequate spatiotemporal resolution, thus limiting their application (Dormann et al. 2012). On the other hand, correlative approaches describe the patterns, not the mechanisms, associated to species distribution and biodiversity by exploring the statistical relationship between spatial environmental data and occurrence records (Kearney et al. 2010, Dormann et al. 2012). Our focus will be in describing the latter approach and to explore its procedure for ecological applications.

Thoroughly describing, categorizing or classifying the existing diversity of ecological models is a challenging task, which, however, falls outside the scope of this thesis introduction (but, see some classification proposals in, e.g., (Gertsev and Gertseva 2004, Jørgensen 2008)). Instead, we will focus our attention in a particular type of correlative models defined above – *Species Distribution Models* (SDM; Figure 2 - 6) – and describe some of its properties. We will also provide a brief description of its underlying assumptions and connections to ecological theory.

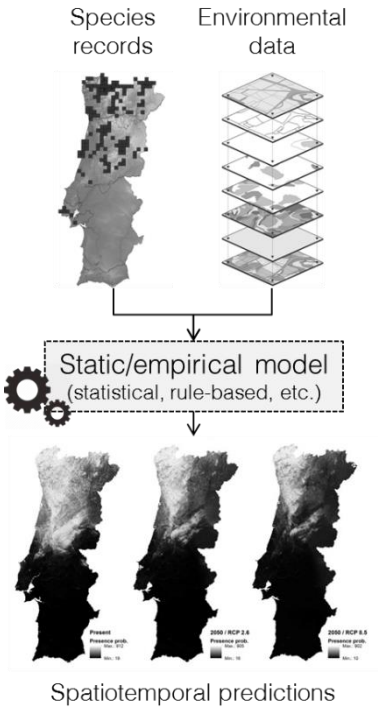

Figure 2 - 6 – A simplified scheme of a SDM input and output.

In a broad sense, *Species Distribution Models* (SDMs) and their output habitat suitability maps (Guisan and Thuiller 2005) allow combining observations of species occurrence or abundance with the spatial representation and characterization of environmental factors of those locations, to investigate and/or to obtain spatiotemporal predictions of species distributions (Figure 2 - 6) (Guisan and Zimmerman 2000, Elith and Leathwick 2009a). Several characteristics of SDMs determine their scientific scope and applications, namely:

- Correlative and empirical approach: this means that observed species presence/absence or abundance is related to environmental data through a 'learning' algorithm which can assume many forms: statistical-based, tree-based, neural-network based, etc capturing linear and/or non-linear aspects of species relations to their environmental determinants. The calibrated model

is then used to make predictions to the whole geographic and environmental space of interest (Elith and Leathwick 2009b, Elith et al. 2010);

- Single-entity: in SDMs only a one entity (typically a species but also a species-group or community) is used as response variable and modelled. Consequently, this implies that species interactions are not accounted nor explicitly modelled (thus excluding inter- or intra-specific biotic interactions and other ecological processes);
- Spatially defined – SDMs allow to obtain spatial predictions of species occurrence or abundance across the geographic space of interest or to make inferences about spatial features of distributions. However, this is not accomplished directly or explicitly, but through a linkage with the environmental space used for model calibration. By definition, SDMs are 'spatially implicit' which means that spatial information is not directly accounted in model structure and that spatially interactive ecological dynamics or processes [expressed in biotic interactions (see for example (Araújo and Luoto 2007)) or ecological processes such as dispersal] are not modelled;
- Static – SDMs are calibrated for a specific time or interval and thus, temporal dynamics are not explicitly accounted nor modelled. Still, SDMs can be used to make predictions in the temporal domain. For example, when calibrated for current conditions, SDMs are able to forecast species distributions to past (Nogués-Bravo 2009) or future (Thuiller et al. 2011) times usually including climate reconstructions or projections. However, this is accomplished by holding some 'strong' assumptions related to temporal and spatial transferability and 'niche conservatism'[5] (Pearman et al. 2008, Elith et al. 2010).

2.2.2. Ecological niche theory and SDM assumptions

At this stage, already knowing some of the most relevant features of SDMs, is important to establish a connection with ecological niche theory. For this reason, SDMs have also been called *Ecological Niche Models* (ENMs) however, for this thesis purpose, we adopt the former name. In another hand, frequently the names SDM and ENM have often been confused or synonymized thus obscuring their meaning and use.

[5] According to Pearman et al. (2008), niche conservatism is the tendency for related species to have similar fundamental and/or realized niches; also, the tendency for the niche of a species to be little changed over time (i.e. to exhibit temporal autocorrelation).

The many and diverse concepts related with the term 'niche' have long been central in ecological theory (Chase and Leibold 2003). In addition, many authors have delved into this subject (with different and sometimes conflicting views) making it difficult to produce a synthesis of current theory. However, for this purpose, we follow the explanations of (Soberon and Nakamura 2009, Peterson et al. 2011, Peterson and Soberón 2012, Peterson et al. 2015). A niche can be defined as a multidimensional object (or 'hypervolume') enclosing the set of environmental conditions that a species requires for reproduction and survival i.e., with positive growth rate, r (Hutchinson 1957).

At least three types of niches can be distinguished: (i) *Grinnell's fundamental niche,* which includes only species requirements to maintain positive population growth rates regardless of biotic interactions and dispersal, (ii) the *Hutchinson's realised* niche, a modification of the fundamental niche to include the effects of biotic interactions and dispersal, and (iii) an intermediate entity termed as the '*existing'* niche, defined as a subset of the fundamental niche conditions that is actually represented on the geographical space relevant to the species [also known as the 'potential niche' by (Jackson and Overpeck 2000) but renamed after (Peterson et al. 2011)].

Biotic-Abiotic-Movement (BAM) diagrams (Peterson et al. 2011) allow to more rigorously examine and explore the joint effects of biotic (B), abiotic (A) and movement (dispersal) considerations surrounding the niche concept (Figure 2 - 7a). BAM diagrams can also ease the inclusion of geographic space into the definition of niches and to translate between organismal characteristics related to physiological tolerances and responses operating at the microscale into the larger macroscale related to species distributions. When integrating the geographic space, Peterson et al. (2011) propose that the fundamental niche can then be conceived as a scaled translation (onto the geographical space) of physiological tolerances and responses within which a species is capable of maintaining viable populations without emigration subsidy (Figure 2 - 7a,b,c). On the geographic space, we consider that regions of the world (hereafter, $\boldsymbol{G}$) exist where the physiological requirements of a species are fulfilled (hereafter $\boldsymbol{A}$) hence, $\boldsymbol{A}$ can be regarded as the spatial expression of the fundamental niche ($\boldsymbol{N_F}$). Regions where the biotic conditions are suitable for the species are called $\boldsymbol{B}$. Regions accessible by dispersal to the species over relevant time periods are called $\boldsymbol{M}$ (for mobility).

The intersection of these three areas, and defined as the *occupied distribution* ($\boldsymbol{G_O}$), is the area in which viable populations of a species can potentially persist, and may be found.

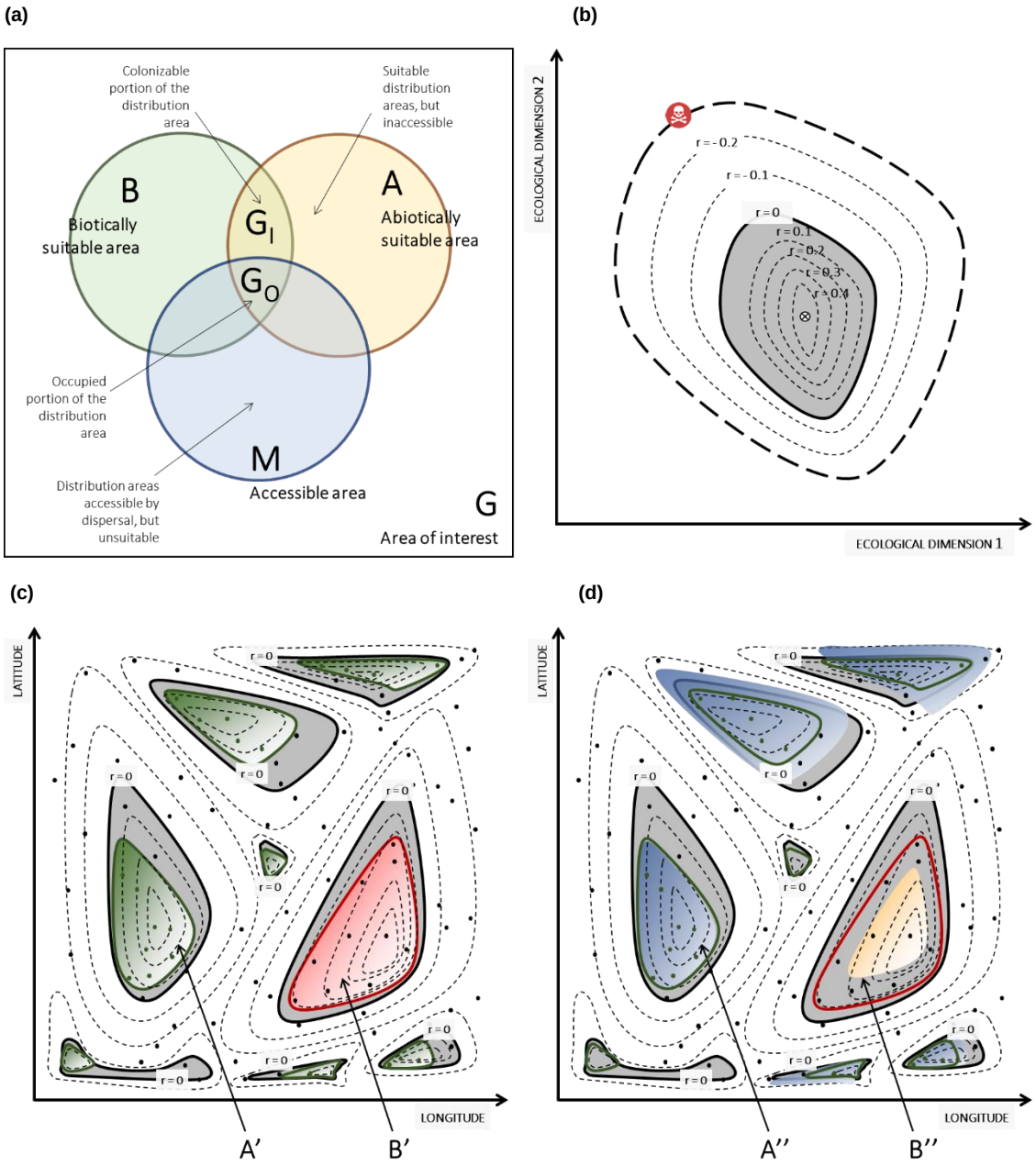

Figure 2 - 7 – (a) BAM diagram representing a species niche showing the effects of *biotic* (B), *abiotic* (A) and *mobility* (M) aspects [adapted from: Peterson et al. (2015)]; (b) representation of the ecological niche in a two-dimensional environmental space and its relationship to species' distribution in the geographical space (c,d). The grey area represents the *Grinnellian* fundamental niche (the cross sign indicates the niche optimum). Outside the niche envelope (bold line), growth is negative, decreasing until it reaches the lethal envelope (bold dashed line), beyond which the species cannot survive. The isolines, or envelopes, link all points of equal species per capita growth rate, *r*. (c) and (d) represent a spatial realization of the *Grinnellian* niche – or the 'potential' available habitat. A' (green areas) – represent occupied habitat with suitable A, B, and, M conditions i.e., *Hutchinson's* realized niche; B' (red area) – representation of suitable but unoccupied habitat due to inaccessible conditions and/or biotic constraints; A'' and B'' represented idealized predictions of a SDM with situations of correct, over- and under-prediction of the fundamental and/or realized niches where A'' areas (blue) have an 'admissible' extrapolation contrary to, B'' (yellow) showing a strong over-prediction of the realized niche but admissible prediction of the fundamental niche (for example, due to high environmental similarity with suitable locations sampled). Points show an idealized random sampling over the geographic area: black points are sample absence locations whereas green points are presence locations [adapted from Hirzel and Le Lay (2008)].

The fundamental niche, $\boldsymbol{N_F}$, is solely defined in the environmental space (Figure 2 - 7b) but it can be mapped into the geographic (Figure 2 - 7c). We can further reduce $\boldsymbol{N_F}$ by intersecting it with the set of environments represented within the accessible area for the species ($\boldsymbol{M}$) at a given time, thus obtaining a subset of environments that is termed the existing niche, which in notation yields: $\boldsymbol{N_{F*}} = \boldsymbol{N_F} \cap \eta(\boldsymbol{M})$ [where $\eta(X)$ is 'the environments associated with X'']. The realized niche ($\boldsymbol{N_R}$) can then be noted as: $\boldsymbol{N_R} = \boldsymbol{N_F} \cap \eta(\boldsymbol{M}) \cap \eta(\boldsymbol{B})$ or simply $\boldsymbol{N_R} = \boldsymbol{N_{F*}} \cap \eta(\boldsymbol{B})$ thus also including the effects of biotic interactions as well Figure 2 - 7c – A'.

By these definitions, some authors argue that correlative approaches used in SDMs actually estimate a 'niche' that is almost certainly a hybrid between the realized and the fundamental niches (Lobo et al. 2010), but its actual position is rather poorly defined (Peterson et al. 2015). In fact, due to sampling or modelling features/deficiencies and to the characteristics of species records (Figure 2 - 7b,c,d), SDMs can actually produce correct, over- or under-predictions of species fundamental or realized niches as we tried to demonstrate in Figure 2 - 7d. SDMs can (and often do) predict suitable locations in inaccessible places to species due to environmentally similarities to actually occupied sampled sites (hence sometimes addressing SDM outcomes as 'potential' habitat suitability). This way, SDMs may project portions of the realized niche environmental space into the geographic space. In turn, these projections may constitute a subset of the fundamental niche (as illustrated in Figure 2 - 7d – B''). In any case, as advised by (Peterson and Soberón 2012) modelers should be cautious when actually addressing to SDM outputs as (actual) species distributions and, if possible, they should provide means to refine their predictions by accounting to dispersal and/or biotic constraints. Ultimately, the complexity surrounding the niche concept and its connection to SDMs is important to bear in mind when interpreting models. It is crucial to establish a guiding rationale and to interpret results accordingly and cautiously. BAM diagrams can be used for this purpose. Given the heightened interest of SDMs for forecasting species range shifts (due to climate and land use changes), being aware of model limitations and interpretation in the light of niche theory is even more important. Communicating uncertainty related to model forecasts is also crucial to make informed decisions and provide guidance to stakeholders.

Besides niche concepts and terminology which form the basis of 'SDM theory', these also have several assumptions that are important to be aware when developing models. The first is that species should be in *equilibrium* with current environmental conditions and abundance is indicative of environmental tolerances and resource

requirements. This assumption holds important consequence when predicting species in space and time. If this assumption is not met, models that fit the observed distribution too narrowly might underestimate the true potential range of the species (Guisan and Thuiller 2005). In particular, many invasive species are not in equilibrium in the invaded range and therefore its native range distribution might be used to obtain model predictions (Peterson 2003, Elith 2015).

Another important assumption for SDMs is *niche conservatism* (already introduced above) i.e., the postulate that the niche remains unchanged through time (Guisan and Thuiller 2005). This is particularly important for SDMs when used to obtain spatiotemporal predictions and responses of biodiversity in presence of climate or other environmental changes. When niche shifts occur, models can under- or over-predict species ranges with consequences for the usefulness and uncertainty of model outcomes. The issue of time scale is also important in this regard. Although sometimes acceptable to assume that some species might conserve their niches over short time periods (decade) it might not be the case in larger time intervals (centuries or millennia) (see e.g., (Wiens and Graham 2005, Wiens et al. 2010, Peterson 2011) for a detailed discussion of this topics).

Independence of species records is also an important prerequisite for most statistical-based models (although machine-learning algorithms are relatively less affected by this problem). Structure, clustering or any form of spatial dependence and auto-correlation may violate this assumption and weaken model inference. However, spatial dependence of true biological origin (generated by dispersal, demography or behaviour mechanisms) is commonly observed in ecological data (Guisan and Thuiller 2005). Some potential solutions include adding a spatial autocorrelation term until no more spatial structure is detected in model residuals (Lichstein et al. 2002) or (re)sampling plots at sufficient spatial distance to decrease or avoid autocorrelation (Guisan and Theurillat 2000).

2.2.3. Workflow and applications of SDMs

The development of SDMs encompasses several steps (Figure 2 - 8). This usually starts by screening the relevant bibliography and establishing the ecological hypotheses that will be analysed (Franklin 2010). Then, describing the target species (autoecology, ecological requirements) and defining which environmental variables are expected to be important for understanding and predicting its distribution. Typically, some form of preliminary statistical analysis is performed to screen the distribution of each variable

and inspect for potential sources of multicollinearity (which can potentially hamper the estimation of coefficients during calibration stage and weaken inference; see (Zuur et al. 2010)). Ideally, the spatial resolution of environmental data should be adequate to model the target species at the scale selected thus avoiding potential mismatches that may fail to evidence the importance of a certain environmental factor (e.g., Guisan and Thuiller 2005, Seo et al. 2009, Mitchell et al. 2017). At the same (or posterior) stage, presence/absence, presence-only (more frequently) or abundance data are collected. This can be performed through a specifically tailored sampling design (e.g., stratified, random, two-stage, see, for example (Gruijter et al. 2006)) allowing to collect *in situ* species data[6]. Often, data collection is performed in natural museum collections, herbaria or through large database facilities such as GBIF (URL: http://www.gbif.org). Data cleaning and validity checks are usually performed before model calibration to avoid erroneous results. After tidying input data, a statistical, machine learning, or other type of model/learning algorithm is used to describe the relationship between species occurrence and environmental data. Usually, cross-validation (CV; bootsrap, 10-fold CV, holdout CV) is employed to perform an assessment of model performance by splitting the input data into two separate sets: train (used for model calibration) and test (used for evaluation). Several metrics can be used to evaluate model performance on the test set(s): the area under the receiver operating curve (but see, (Lobo et al. 2008)), the true-skill statistic and Cohen's Kappa are some of the most commonly used (Thuiller et al. 2009). Finally, after calibrating model parameters or response functions, output coefficients or decision rules are then applied to environmental maps yielding spatial predictions of species distribution or habitat suitability (Franklin 2010).

Although somewhat reductionist in their intrinsic nature (as defined above), SDMs are profoundly useful tools to investigate a large set of ecological questions and answer to several applied management, conservation or monitoring challenges (Guisan et al. 2013, Honrado et al. 2016). SDMs are widely used to describe patterns, deliver spatiotemporal predictions at several scales (Elith and Leathwick 2009a) and to address fundamental questions in Ecology such as the 'niche shift *vs*. conservatism' debate (Pearman et al. 2008, Rödder and Lötters 2009, Guisan et al. 2014, Fernández and Hamilton 2015) or, applied questions related to the assessment of ecological impacts of

[6] In fact, SDMs themselves can be used to guide sampling design and surveillance efforts, which has showed to be useful for rare or low-detectability species. See for example: (Guisan et al. 2006, Williams et al. 2009, Le Lay et al. 2010)

climate and land-use changes (Broennimann et al. 2006, de Chazal and Rounsevell 2009, Pecl et al. 2017).

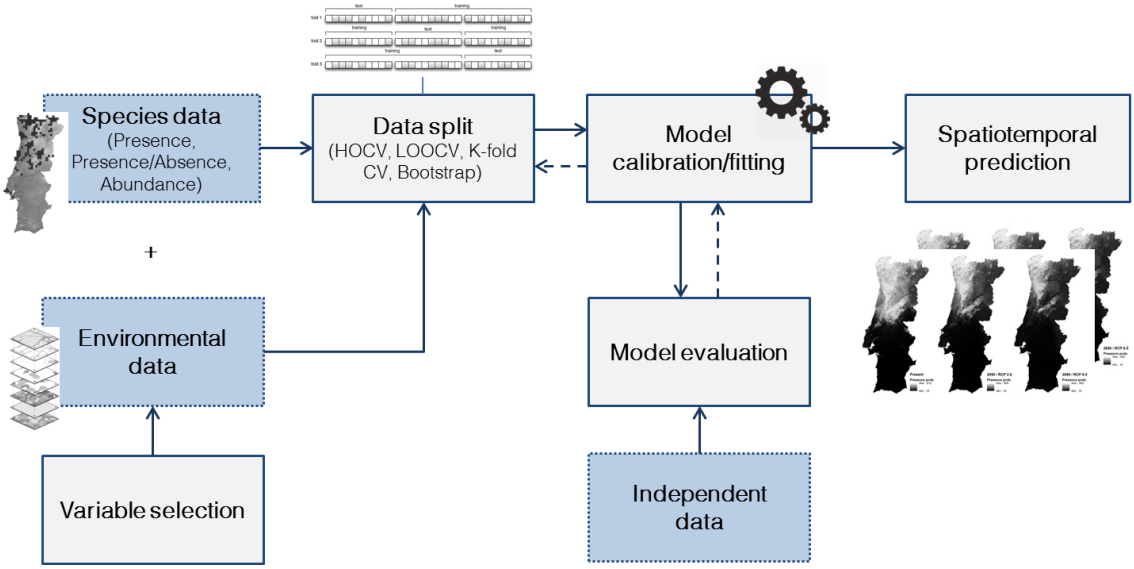

Figure 2 - 8 – Typical Species Distribution Modelling workflow.

Investigating species responses as consequence of a changing climate has been perhaps one of the most active areas of research where SDMs have been applied. Bellard et al. (2012) noted that species can respond to climate change by shifting their climatic niche along three non-exclusive axes: time (e.g. phenology), space (e.g. range) and self (e.g. physiology). In this sense, SDMs, due to the spatial nature of its predictions, are particularly well equipped to investigate shifts in species ranges. As an example, SDMs were used by (Thuiller et al. 2011) to estimate the consequences of climate change on the phylogenetic diversities of plant, bird and mammal assemblages across Europe. By combining climate projections with land cover/use scenarios in SDMs, researchers were able to investigate the conjugate and often synergistic effects of expected future changes in bird (Regos et al. 2015) and amphibian species (Hof et al. 2011). Besides these applications, SDMs have also been used for addressing other topics in applied ecological research, such as: conservation planning and reserve design selection (Esselman and Allan 2011, Zhang et al. 2012, Cuesta et al. 2017), impact assessment and resource management (Clauzel et al. 2013, Girardet et al. 2013, Makki et al. 2013), habitat restoration and reintroduction (Olsson and Rogers 2009, Frick et al. 2014, Angelieri et al. 2016), invasive species risk assessment (Vicente et al. 2010, Vicente et al. 2011, Vicente et al. 2013, Vicente et al. 2014), improve species surveying (especially for rare species) and monitoring network design (Amorim et al. 2014, Carvalho et al. 2015).

SDMs have benefited from the integration with other disciplines and fields including statistics, machine-learning, economics and information theory (among other). One particularly innovative aspect for SDMs, that benefited from the integration of trans-disciplinary innovations and concepts, is the notion of ensemble modelling (or ensemble forecasting) (Araújo and New 2006). It is based on the realization that individual models tend to give different results and generate varying predictions from equal initial conditions and input data, potentially compromising their usefulness for guiding policy decisions (Araújo and New 2006). In case of SDMs, this happens due to the differences in the correlative process which links input species records with the multivariate environmental space. To avoid this, software packages such as *biomod2 (Thuiller et al. 2009, Thuiller et al. 2014)* allow to model species distributions with several algorithms and to combine model predictions generated by those techniques through several ensembling techniques. This way, consensus predictions are obtained allowing to improve model forecasts and to assess model uncertainty.

Another innovative aspect is the integration with EO-based data. Satellite or airborne-based EO platforms are currently making available large quantities of data across several aspects of the Earth surface that are useful for SDMs. By measuring Earth surface's 'spectral traits' and their spatiotemporal variations at several levels (Lausch et al. 2016), EO-based variables can be used to understand properties related with species habitat and map their distribution. In this context, EO-based spectral indices as well as topographic datasets and 'high-level' products (e.g., evapotranspiration, LAI, GPP, NPP) have strongly contributed to improve biodiversity monitoring as well as the development of SDMs (Bradley and Fleishman 2008, Nagendra et al. 2013, He et al. 2015, Skidmore et al. 2015). By providing repeated and synoptic measures of the Earth surface, EO offers a cost-effective approach to measure biodiversity and predict changes in species composition (Rocchini et al. 2016). EO data products, available at multiple spatial and temporal resolutions, from multi- or hyperspectral sensors, as well as, LiDAR (Light Detection and Ranging) and RADAR missions can further improve SDM performance and form the backbone for 'next-generation' SDMs (He et al. 2015).

References

Alcaraz-Segura, D., J. Cabello, J. M. Paruelo, and M. Delibes. 2008. Trends in the surface vegetation dynamics of the national parks of Spain as observed by satellite sensors. Applied Vegetation Science 11:431-440.

Alcaraz, D., J. Paruelo, and J. Cabello. 2006. Identification of current ecosystem functional types in the Iberian Peninsula. Global Ecology and Biogeography 15:200-212.

Amorim, F., S. B. Carvalho, J. Honrado, and H. Rebelo. 2014. Designing Optimized Multi-Species Monitoring Networks to Detect Range Shifts Driven by Climate Change: A Case Study with Bats in the North of Portugal. PLoS ONE 9:e87291.

Angelieri, C. C. S., C. Adams-Hosking, K. M. P. M. d. B. Ferraz, M. P. de Souza, and C. A. McAlpine. 2016. Using Species Distribution Models to Predict Potential Landscape Restoration Effects on Puma Conservation. PLoS ONE 11:1-18.

Araújo, M. B., and M. Luoto. 2007. The importance of biotic interactions for modelling species distributions under climate change. Global Ecology and Biogeography 16:743-753.

Araújo, M. B., and M. New. 2006. Ensemble forecasting of species distributions. Trends in Ecology & Evolution 22:42-47.

Bakker, W. H., A. S. M. Gieske, B. G. H. Gorte, K. A. Grabmaier, C. A. Hecker, J. A. Horn, G. C. Huurneman, L. L. F. Janssen, N. Kerle, F. D. v. d. Meer, G. N. Parodi, C. Pohl, A. Prakash, C. V. Reeves, F. J. v. Ruitenbeek, K. Tempfli, M. J. C. Weir, and T. Woldai. 2004. Principles of Remote Sensing - An introductory textbook. Page 540 *in* N. Kerle, L. L. F. Janssen, and G. C. Huurneman, editors. International Institute for Geo-Information Science and Earth Observation, Enschede, Netherlands.

Bellard, C., C. Bertelsmeier, P. Leadley, W. Thuiller, and F. Courchamp. 2012. Impacts of climate change on the future of biodiversity. Ecology Letters 15:365-377.

Bonan, G. B., S. Levis, S. Sitch, M. Vertenstein, and K. W. Oleson. 2003. A dynamic global vegetation model for use with climate models: concepts and description of simulated vegetation dynamics. Global Change Biology 9:1543-1566.

Bradley, B. A., and E. Fleishman. 2008. Can remote sensing of land cover improve species distribution modelling? Journal of Biogeography 35:1158-1159.

Broennimann, O., W. Thuiller, G. Hughes, G. F. Midgley, J. M. R. Alkemade, and A. Guisan. 2006. Do geographic distribution, niche property and life form explain plants' vulnerability to global change? Global Change Biology 12:1079-1093.

Cabello, J., N. Fernández, D. Alcaraz-Segura, C. Oyonarte, G. Piñeiro, A. Altesor, M. Delibes, and J. Paruelo. 2012. The ecosystem functioning dimension in conservation: insights from remote sensing. Biodiversity and Conservation 21:3287-3305.

Caccamo, G., R. Bradstock, L. Collins, T. Penman, and P. Watson. 2015. Using MODIS data to analyse post-fire vegetation recovery in Australian eucalypt forests. Journal of Spatial Science 60:341-352.

Carvalho, S. B., J. Gonçalves, A. Guisan, and J. P. Honrado. 2015. Systematic site selection for multispecies monitoring networks. Journal of Applied Ecology:n/a-n/a.

Chase, J. M., and M. A. Leibold. 2003. Ecological Niches: Linking Classical and Contemporary Approaches (Interspecific Interactions). 1st edition. University of Chicago Press.

Clauzel, C., X. Girardet, and J. C. Foltete. 2013. Impact assessment of a high-speed railway line on species distribution: Application to the European tree frog (Hyla arborea) in Franche-Comte. Journal of Environmental Management 127:125-134.

Clerici, N., C. J. Weissteiner, and F. Gerard. 2012. Exploring the Use of MODIS NDVI-Based Phenology Indicators for Classifying Forest General Habitat Categories. Remote Sensing 4:1781-1803.

Cuesta, F., M. Peralvo, A. Merino-Viteri, M. Bustamante, F. Baquero, J. F. Freile, P. Muriel, and O. Torres-Carvajal. 2017. Priority areas for biodiversity conservation in mainland Ecuador. Neotropical Biodiversity 3:93-106.

Daniel, C. J., L. Frid, B. M. Sleeter, and M.-J. Fortin. 2016. State-and-transition simulation models: a framework for forecasting landscape change. Methods in Ecology and Evolution 7:1413-1423.

de Chazal, J., and M. D. A. Rounsevell. 2009. Land-use and climate change within assessments of biodiversity change: A review. Global Environmental Change 19:306-315.

DeAngelis, D. L., and V. Grimm. 2014. Individual-based models in ecology after four decades. F1000Prime Reports 6:39.

Di Mauro, B., F. Fava, L. Busetto, G. F. Crosta, and R. Colombo. 2014. Post-fire resilience in the Alpine region estimated from MODIS satellite multispectral data. International Journal of Applied Earth Observation and Geoinformation 32:163-172.

Dormann, C. F., S. J. Schymanski, J. Cabral, I. Chuine, C. Graham, F. Hartig, M. Kearney, X. Morin, C. Römermann, B. Schröder, and A. Singer. 2012. Correlation and process in species distribution models: bridging a dichotomy. Journal of Biogeography 39:2119-2131.

Duro, D. C., N. C. Coops, M. A. Wulder, and T. Han. 2007. Development of a large area biodiversity monitoring system driven by remote sensing. Progress in Physical Geography 31:235-260.

Elith, J. 2015. Predicting distributions of invasive species. ArXiv.org arXiv:1312.0851 (v2).

Elith, J., M. Kearney, and S. Phillips. 2010. The art of modelling range-shifting species. Methods in Ecology and Evolution 1:330-342.

Elith, J., and J. Leathwick. 2009a. Species Distribution Models: Ecological Explanation and Prediction Across Space and Time. Annual Review of Ecology, Evolution, and Systematics 40:677-697.

Elith, J., and J. R. Leathwick. 2009b. Species Distribution Models: Ecological Explanation and Prediction Across Space and Time. Annual Review of Ecology, Evolution, and Systematics 40:677-697.

Esselman, P. C., and J. D. Allan. 2011. Application of species distribution models and conservation planning software to the design of a reserve network for the riverine fishes of northeastern Mesoamerica. Freshwater Biology 56:71-88.

Fernández, M., and H. Hamilton. 2015. Ecological Niche Transferability Using Invasive Species as a Case Study. PLoS ONE 10:e0119891.

Franklin, J. 2010. Mapping Species Distributions: Spatial Inference and Prediction. Cambridge, University Press.

Frick, A., F. Tanneberger, and J. Bellebaum. 2014. Model-Based Selection of Areas for the Restoration of Acrocephalus paludicola Habitats in NE Germany. Environmental Management 53:728-738.

Gertsev, V. I., and V. V. Gertseva. 2004. Classification of mathematical models in ecology. Ecological Modelling 178:329-334.

Giglio, L., I. Csiszar, and C. O. Justice. 2006. Global distribution and seasonality of active fires as observed with the Terra and Aqua Moderate Resolution Imaging Spectroradiometer (MODIS) sensors. Journal of Geophysical Research: Biogeosciences 111:n/a-n/a.

Giglio, L., J. Descloitres, C. O. Justice, and Y. J. Kaufman. 2003. An Enhanced Contextual Fire Detection Algorithm for MODIS. Remote Sensing of Environment 87:273-282.

Girardet, X., J.-C. Foltête, and C. Clauzel. 2013. Designing a graph-based approach to landscape ecological assessment of linear infrastructures. Environmental Impact Assessment Review 42:10-17.

Gruijter, J. d., D. Brus, M. Bierkens, and M. Knotters. 2006. Sampling for Natural Resource Monitoring. Springer-Verlag, Berlin Heidelberg.

Guanter, L., H. Kaufmann, K. Segl, S. Foerster, C. Rogass, S. Chabrillat, T. Kuester, A. Hollstein, G. Rossner, C. Chlebek, C. Straif, S. Fischer, S. Schrader, T. Storch, U. Heiden, A. Mueller, M. Bachmann, H. Mühle, R. Müller, M. Habermeyer, A. Ohndorf, J. Hill, H. Buddenbaum, P. Hostert, S. van der Linden, P. Leitão, A. Rabe, R. Doerffer, H. Krasemann, H. Xi, W. Mauser, T. Hank, M. Locherer, M. Rast, K. Staenz, and B. Sang. 2015. The EnMAP Spaceborne Imaging Spectroscopy Mission for Earth Observation. Remote Sensing 7:8830.

Guisan, A., O. Broennimann, R. Engler, M. Vust, N. G. Yoccoz, A. Lehmann, and N. E. Zimmermann. 2006. Using Niche-Based Models to Improve the Sampling of Rare Species. Conservation Biology 20:501-511.

Guisan, A., B. Petitpierre, O. Broennimann, C. Daehler, and C. Kueffer. 2014. Unifying niche shift studies: insights from biological invasions. Trends in Ecology & Evolution 29:260-269.

Guisan, A., and J.-P. Theurillat. 2000. Equilibrium modeling of alpine plant distribution: how far can we go? Phytocoenologia 30:353 - 384.

Guisan, A., and W. Thuiller. 2005. Predicting species distribution: offering more than simple habitat models. Ecology Letters 8:993-1009.

Guisan, A., R. Tingley, J. B. Baumgartner, I. Naujokaitis-Lewis, P. R. Sutcliffe, A. I. T. Tulloch, T. J. Regan, L. Brotons, E. McDonald-Madden, C. Mantyka-Pringle, T. G. Martin, J. R. Rhodes, R. Maggini, S. A. Setterfield, J. Elith, M. W. Schwartz, B. A. Wintle, O. Broennimann, M. Austin, S. Ferrier, M. R. Kearney, H. P. Possingham, and Y. M. Buckley. 2013. Predicting species distributions for conservation decisions. Ecology Letters 16:1424-1435.

Guisan, A., and N. E. Zimmerman. 2000. Predictive habitat distribution models in ecology. Ecological Modelling 135:147–186.

He, K. S., B. A. Bradley, A. F. Cord, D. Rocchini, M.-N. Tuanmu, S. Schmidtlein, W. Turner, M. Wegmann, N. Pettorelli, H. Nagendra, and N. Horning. 2015. Will remote sensing shape the next generation of species distribution models? Remote Sensing in Ecology and Conservation 1:4-18.

He, K. S., D. Rocchini, M. Neteler, and H. Nagendra. 2011. Benefits of hyperspectral remote sensing for tracking plant invasions. Diversity and Distributions 17:381-392.

Hirzel, A. H., and G. Le Lay. 2008. Habitat suitability modelling and niche theory. Journal of Applied Ecology 45:1372-1381.

Hof, C., M. B. Araujo, W. Jetz, and C. Rahbek. 2011. Additive threats from pathogens, climate and land-use change for global amphibian diversity. Nature 480:516-519.

Honrado, J. P., H. M. Pereira, and A. Guisan. 2016. Fostering integration between biodiversity monitoring and modelling. Journal of Applied Ecology 53:1299-1304.

IJAEOG. 2017. Aims and Scope (URL: https://www.journals.elsevier.com/international-journal-of-applied-earth-observation-and-geoinformation/; visited in 23/06/2017). Elsevier.

Jackson, S. T., and J. T. Overpeck. 2000. Responses of plant populations and communities to environmental changes of the late Quaternary. Paleobiology 26:194-220.

Jensen, J. R. 2000. Remote sensing of the environment: an earth resource perspective. Prentice-Hall, NJ, USA.

Jobbágy, E. G., O. E. Sala, and J. M. Paruelo. 2002. Patterns and controls of primary productivity in the Patagonian steppe: a remote sensing approach. Ecology 83:307-319.

Jørgensen, S. E. 2008. Overview of the model types available for development of ecological models. Ecological Modelling 215:3-9.

Jørgensen, S. E. 2016. Ecological Model Types. 1st edition. Elsevier.

Kearney, M. R., B. A. Wintle, and W. P. Porter. 2010. Correlative and mechanistic models of species distribution provide congruent forecasts under climate change. Conservation Letters 3:203-213.

Kuenzer, C., M. Ottinger, M. Wegmann, H. Guo, C. Wang, J. Zhang, S. Dech, and M. Wikelski. 2014. Earth observation satellite sensors for biodiversity monitoring: potentials and bottlenecks. International Journal of Remote Sensing 35:6599-6647.

Lausch, A., L. Bannehr, M. Beckmann, C. Boehm, H. Feilhauer, J. M. Hacker, M. Heurich, A. Jung, R. Klenke, C. Neumann, M. Pause, D. Rocchini, M. E. Schaepman, S. Schmidtlein, K. Schulz, P. Selsam, J. Settele, A. K. Skidmore, and A. F. Cord. 2016. Linking Earth Observation and taxonomic, structural and functional biodiversity: Local to ecosystem perspectives. Ecological Indicators 70:317-339.

Lavender, S., and A. Lavender. 2016. Practical Handbookof Remote Sensing. 1st edition. CRC Press, FL, USA.

Le Lay, G., R. Engler, E. Franc, and A. Guisan. 2010. Prospective sampling based on model ensembles improves the detection of rare species. Ecography 33:1015-1027.

Leon, J. R. R., W. J. D. van Leeuwen, and G. M. Casady. 2012. Using MODIS-NDVI for the Modeling of Post-Wildfire Vegetation Response as a Function of Environmental Conditions and Pre-Fire Restoration Treatments. Remote Sensing 4:598-621.

Lichstein, J. W., T. R. Simons, S. A. Shriner, and K. E. Franzreb. 2002. Spatial Autocorrelation and Autoregressive Models in Ecology. Ecological Monographs 72:445-463.

Lobo, J. M., A. Jiménez-Valverde, and J. Hortal. 2010. The uncertain nature of absences and their importance in species distribution modelling. Ecography 33:103-114.

Lobo, J. M., A. Jiménez-Valverde, and R. Real. 2008. AUC: a misleading measure of the performance of predictive distribution models. Global Ecology and Biogeography 17:145-151.

Mairota, P., B. Cafarelli, R. K. Didham, F. P. Lovergine, R. M. Lucas, H. Nagendra, D. Rocchini, and C. Tarantino. 2015. Challenges and opportunities in harnessing satellite remote-sensing for biodiversity monitoring. Ecological Informatics 30:207-214.

Makki, T., S. Fakheran, H. Moradi, M. Iravani, and J. Senn. 2013. Landscape-scale impacts of transportation infrastructure on spatial dynamics of two vulnerable ungulate species in Ghamishloo Wildlife Refuge, Iran. Ecological Indicators 31:6-14.

Mildrexler, D. J., M. Zhao, and S. W. Running. 2009. Testing a MODIS Global Disturbance Index across North America. Remote Sensing of Environment 113:2103-2117.

Mitchell, P. J., J. Monk, and L. Laurenson. 2017. Sensitivity of fine-scale species distribution models to locational uncertainty in occurrence data across multiple sample sizes. Methods in Ecology and Evolution 8:12-21.

Monteiro, A., J. Gonçalves, R. Fernandes, S. Alves, B. Marcos, R. Lucas, A. Teodoro, and J. Honrado. 2017. Estimating Invasion Success by Non-Native Trees in a National Park Combining WorldView-2 Very High Resolution Satellite Data and Species Distribution Models. Diversity 9:6.

Nagendra, H., R. Lucas, J. P. Honrado, R. H. G. Jongman, C. Tarantino, M. Adamo, and P. Mairota. 2013. Remote sensing for conservation monitoring: Assessing protected areas, habitat extent, habitat condition, species diversity, and threats. Ecological Indicators 33:45-59.

Nogués-Bravo, D. 2009. Predicting the past distribution of species climatic niches. Global Ecology and Biogeography 18:521-531.

O'Connor, B., C. Secades, J. Penner, R. Sonnenschein, A. Skidmore, N. D. Burgess, and J. M. Hutton. 2015. Earth observation as a tool for tracking progress towards the Aichi Biodiversity Targets. Remote Sensing in Ecology and Conservation 1:19-28.

Olsson, O., and D. J. Rogers. 2009. Predicting the distribution of a suitable habitat for the white stork in Southern Sweden: identifying priority areas for reintroduction and habitat restoration. Animal Conservation 12:62-70.

Pearman, P. B., A. Guisan, O. Broennimann, and C. F. Randin. 2008. Niche dynamics in space and time. Trends in Ecology & Evolution 23:149-158.

Pecl, G. T., M. B. Araújo, J. D. Bell, J. Blanchard, T. C. Bonebrake, I.-C. Chen, T. D. Clark, R. K. Colwell, F. Danielsen, B. Evengård, L. Falconi, S. Ferrier, S. Frusher, R. A. Garcia, R. B. Griffis, A. J. Hobday, C. Janion-Scheepers, M. A. Jarzyna, S. Jennings, J. Lenoir, H. I. Linnetved, V. Y. Martin, P. C. McCormack, J. McDonald, N. J. Mitchell, T. Mustonen, J. M. Pandolfi, N. Pettorelli, E. Popova, S. A. Robinson, B. R. Scheffers, J. D. Shaw, C. J. B. Sorte, J. M. Strugnell, J. M. Sunday, M.-N. Tuanmu, A. Vergés, C. Villanueva, T. Wernberg, E. Wapstra, and S. E. Williams. 2017. Biodiversity redistribution under climate change: Impacts on ecosystems and human well-being. Science 355.

Peterson, A. T. 2003. Predicting the Geography of Species' Invasions via Ecological Niche Modeling. The Quarterly Review of Biology 78:419-433.

Peterson, A. T. 2011. Ecological niche conservatism: a time-structured review of evidence. Journal of Biogeography 38:817-827.

Peterson, A. T., M. Papeş, and J. Soberón. 2015. Mechanistic and Correlative Models of Ecological Niches. Pages 28-38 European Journal of Ecology.

Peterson, A. T., and J. Soberón. 2012. Species Distribution Modeling and Ecological Niche Modeling: Getting the Concepts Right. Natureza & Conservação 10:102-107.

Peterson, A. T., J. Soberón, R. G. Pearson, R. P. Anderson, E. Martínez-Meyer, M. Nakamura, and M. B. Araújo. 2011. Ecological Niches and Geographic Distributions. Princeton University Press.

Petropoulos, G., T. N. Carlson, M. J. Wooster, and S. Islam. 2009. A review of Ts/VI remote sensing based methods for the retrieval of land surface energy fluxes and soil surface moisture. Progress in Physical Geography 33:224-250.

Petrou, Z. I., I. Manakos, and T. Stathaki. 2015. Remote sensing for biodiversity monitoring: a review of methods for biodiversity indicator extraction and assessment of progress towards international targets. Biodiversity and Conservation 24:2333-2363.

Pettorelli, N., W. F. Laurance, T. G. O'Brien, M. Wegmann, H. Nagendra, and W. Turner. 2014. Satellite remote sensing for applied ecologists: opportunities and challenges. Journal of Applied Ecology 51:839-848.

Pettorelli, N., J. O. Vik, A. Mysterud, J.-M. Gaillard, C. J. Tucker, and N. C. Stenseth. 2005. Using the satellite-derived NDVI to assess ecological responses to environmental change. Trends in Ecology & Evolution 20:503-510.

Regos, A., M. D'Amen, N. Titeux, S. Herrando, A. Guisan, L. Brotons, and E. Di Minin. 2015. Predicting the future effectiveness of protected areas for bird conservation in Mediterranean ecosystems under climate change and novel fire regime scenarios. Diversity and Distributions:n/a-n/a.

Rocchini, D., D. S. Boyd, J.-B. Féret, G. M. Foody, K. S. He, A. Lausch, H. Nagendra, M. Wegmann, and N. Pettorelli. 2016. Satellite remote sensing to monitor species diversity: potential and pitfalls. Remote Sensing in Ecology and Conservation 2:25-36.

Rödder, D., and S. Lötters. 2009. Niche shift versus niche conservatism? Climatic characteristics of the native and invasive ranges of the Mediterranean house gecko (Hemidactylus turcicus). Global Ecology and Biogeography 18:674-687.

Secades, C., B. O'Connor, C. Brown, and M. Walpole. 2014. Earth Observation for Biodiversity Monitoring: A review of current approaches and future opportunities for tracking progress towards the Aichi Biodiversity Targets - Technical Series No. 72. Secretariat of the Convention on Biological Diversity, Montréal, Canada.

Seo, C., J. H. Thorne, L. Hannah, and W. Thuiller. 2009. Scale effects in species distribution models: implications for conservation planning under climate change. Biology Letters 5:39-43.

Sesnie, S. E., B. G. Dickson, S. S. Rosenstock, and J. M. Rundall. 2012. A comparison of Landsat TM and MODIS vegetation indices for estimating forage phenology in desert bighorn sheep (Ovis canadensis nelsoni) habitat in the Sonoran Desert, USA. International Journal of Remote Sensing 33:276-286.

Skidmore, A. K., N. Pettorelli, N. C. Coops, G. N. Geller, M. Hansen, R. Lucas, C. A. Mücher, B. O'Connor, M. Paganini, H. M. Pereira, M. E. Schaepman, W. Turner, T. Wang, and M. Wegmann. 2015. Agree on biodiversity metrics to track from space. Nature 523.

Soberon, J., and M. Nakamura. 2009. Niches and distributional areas: concepts, methods, and assumptions. Proc Natl Acad Sci U S A 106 Suppl 2:19644-19650.

Thuiller, W., D. Georges, and R. Engler. 2014. biomod2: Ensemble platform for species distribution modeling, R package version 3.1-48, URL: http://CRAN.R-project.org/package=biomod2.

Thuiller, W., B. Lafourcade, R. Engler, and M. B. Araújo. 2009. BIOMOD – a platform for ensemble forecasting of species distributions. Ecography 32:369-373.

Thuiller, W., S. Lavergne, C. Roquet, I. Boulangeat, B. Lafourcade, and M. B. Araujo. 2011. Consequences of climate change on the tree of life in Europe. Nature 470:531-534.

Turner, W., S. Spector, N. Gardiner, M. Fladeland, E. Sterling, and M. Steininger. 2003. Remote sensing for biodiversity science and conservation. Trends in Ecology & Evolution 18:306-314.

Vanden Borre, J., D. Paelinckx, C. A. Mücher, L. Kooistra, B. Haest, G. De Blust, and A. M. Schmidt. 2011. Integrating remote sensing in Natura 2000 habitat monitoring: Prospects on the way forward. Journal for Nature Conservation 19:116-125.

Vaz, A. S., B. Marcos, J. Gonçalves, A. Monteiro, P. Alves, E. Civantos, R. Lucas, P. Mairota, J. Garcia-Robles, J. Alonso, P. Blonda, A. Lomba, and J. P. Honrado. 2015. Can we predict habitat quality from space? A multi-indicator assessment based on an automated knowledge-driven system. International Journal of Applied Earth Observation and Geoinformation 37:106-113.

Veraverbeke, S., S. Lhermitte, W. W. Verstraeten, and R. Goossens. 2011. A time-integrated MODIS burn severity assessment using the multi-temporal differenced normalized burn ratio (dNBRMT). International Journal of Applied Earth Observation and Geoinformation 13:52-58.

Vicente, J., P. Alves, C. Randin, A. Guisan, and J. Honrado. 2010. What drives invasibility? A multi-model inference test and spatial modelling of alien plant species richness patterns in northern Portugal. Ecography 33:1081-1092.

Vicente, J., C. Randin, J. Gonçalves, M. Metzger, Â. Lomba, J. Honrado, and A. Guisan. 2011. Where will conflicts between alien and rare species occur after climate and land-use change? A test with a novel combined modelling approach. Biological Invasions 13:1209-1227.

Vicente, J. R., R. F. Fernandes, C. F. Randin, O. Broennimann, J. Gonçalves, B. Marcos, I. Pôças, P. Alves, A. Guisan, and J. P. Honrado. 2013. Will climate change drive alien invasive plants into areas of high protection value? An improved model-

based regional assessment to prioritise the management of invasions. Journal of Environmental Management 131:185-195.

Vicente, J. R., H. M. Pereira, C. F. Randin, J. Gonçalves, A. Lomba, P. Alves, J. Metzger, M. Cezar, A. Guisan, and J. Honrado. 2014. Environment and dispersal paths override life strategies and residence time in determining regional patterns of invasion by alien plants. Perspectives in Plant Ecology, Evolution and Systematics 16:1-10.

Wiens, J. J., D. D. Ackerly, A. P. Allen, B. L. Anacker, L. B. Buckley, H. V. Cornell, E. I. Damschen, T. Jonathan Davies, J. A. Grytnes, S. P. Harrison, B. A. Hawkins, R. D. Holt, C. M. McCain, and P. R. Stephens. 2010. Niche conservatism as an emerging principle in ecology and conservation biology. Ecol Lett 13:1310-1324.

Wiens, J. J., and C. H. Graham. 2005. Niche Conservatism: Integrating Evolution, Ecology, and Conservation Biology. Annual Review of Ecology, Evolution, and Systematics 36:519-539.

Williams, J. N., C. Seo, J. Thorne, J. K. Nelson, S. Erwin, J. M. O'Brien, and M. W. Schwartz. 2009. Using species distribution models to predict new occurrences for rare plants. Diversity and Distributions 15:565-576.

Xiao, X., S. Hagen, Q. Zhang, M. Keller, and B. Moore. 2006. Detecting leaf phenology of seasonally moist tropical forests in South America with multi-temporal MODIS images. Remote Sensing of Environment 103:465-473.

Yu, A. W., M. A. Krainak, D. J. Harding, J. B. Abshire, and X. Sun. 2010. A spaceborne lidar for high-resolution topographic mapping of the Earth's surface. SPIE SPIE Newsroom.

Zhang, M.-G., Z.-K. Zhou, W.-Y. Chen, J. W. F. Slik, C. H. Cannon, and N. Raes. 2012. Using species distribution modeling to improve conservation and land use planning of Yunnan, China. Biological Conservation 153:257-264.

Zuur, A. F., E. N. Ieno, and C. S. Elphick. 2010. A protocol for data exploration to avoid common statistical problems. Methods in Ecology and Evolution 1:3-14.

CHAPTER 3 - Research objectives and thesis structure

3.1. Research objectives

In the scope of the theoretical and methodological challenges described in Chapters 1 and 2, the research developed for this thesis involved a set of six studies aimed to contribute to improving the analysis, assessment and monitoring of biodiversity status and trends. Those studies focused on evaluating the current condition and dynamics at several scales, levels and facets which underpin the major dimensions of biodiversity in terrestrial ecosystems.

The research plan was especially aimed at exploring the potential of modelling tools and Earth Observation data sources and methodologies to map, analyse and forecast contemporary changes in biodiversity patterns, and to improve the current knowledge regarding the main driving factors underlying observed (i.e., detected) or modelled alterations (e.g., employing climate and/or land cover/use scenarios). In this context, our ultimate goal was to provide guidance and some of the fundamental building blocks of a cross-scalar and cross-level monitoring framework supported by the integration of EO-based indicators and EO-fed models to assist national and trans-national efforts related to the management and conservation of biodiversity.

The specific objectives underlying the research developed for the thesis can be divided into two main groups: (i) assessment of biodiversity patterns at the various scales and levels; and (ii) development and testing of improved methods and tools for biodiversity assessment.

In biodiversity assessment of current status and change, the following specific objectives were outlined:

- Compare and assess the factors underlying functional connectivity, gene flow and genetic structuring in species of conservation interest as well as potential sources of habitat fragmentation;
- Analyse the spatiotemporal dynamics of habitat suitability of vulnerable species and explore the underlying factors related to the identified dynamics;
- Assess and forecast the vulnerability of low dispersal species to landscape fragmentation in relation to multi-scalar environmental changes;

- Assess the extent and condition of fine-scale mountain habitat mosaics undergoing rapid land use changes, by exploring the opportunities provided by unmanned aerial vehicles; and
- Assess the effectiveness of a national network of protected areas in promoting ecosystem stability and evaluate the factors underlying differences in protection success related to socio-ecological drivers and disturbance dynamics.

In the development of new improved methods and tools, the following specific objectives were outlined:

- Foster the integration between EO data and modelling and develop improved methodologies to harness the potential of such combination;
- Develop spatial metrics and a framework to assess landscape fragmentation effects in the context of species range shifts caused by environmental changes;
- Test and develop indicators related to Earth's ecosystem functional dynamics to support the analysis of multi-scalar and multi-level biodiversity status and changes and its identify main driving factors;
- Test and develop EO-based multi-temporal indicators that address the challenging quantification of ecosystem stability through a time-continuous integration of disturbance and responses mediated by ecosystem resilience;
- Provide a systematic, integrative and model-based approach to assess the effectiveness of Protected Areas supported by EO data;
- Develop novel methods and a software solution (*R* package) to improve the exploitation of EO data through Geographic Object-based Image Analysis (GEOBIA) for supporting the evaluation of biodiversity across different scales.

From a more strategic, applied perspective, the assessment of biodiversity and the development of new methods and tools were aimed to contribute to more powerful and effective management of biodiversity across scales and levels, namely by:

- Testing and identifying useful data sources and indicators based on different EO platforms capable of informing the progress of ongoing conservation initiatives, programmes or policies; and

- Evaluating the added-value of predictive models and their integration with EO products, as well as state-of-the-art spatial analysis methods, for informing and evaluating policy and management decisions.

3.2. Research development and thesis structure

Adopting a multidimensional, multi-scalar and multi-level approach to biodiversity assessment and monitoring is crucial to analyse current trends, investigate factors underlying patterns and changes, and ultimately provide meaningful measures and indicators capable of informing about progress in the achievement of conservation targets. We followed these premises to setting the research objectives, as described in the previous section, and to devise the scientific program that was developed.

The close integration between biodiversity theory, predictive modelling and Earth Observation was explored throughout the thesis, which is organized in three broad sections: a general introduction (Section I); the six research papers (Section II); and finally, a general discussion and conclusions. The three sections encompass a total of 11 chapters as described next.

Section I describes the broad theoretical and methodological context and rationale under which the research was developed. This section includes Chapters 1 to 3. In Chapter 1 of this thesis, we outlined current threats, pressures and challenges that biodiversity is currently facing due to ongoing changes in Earth's ecosystems derived from global alterations in climate, to local pressures related to land use change. In face of these problems, several parties have taken action to halt this biodiversity crisis. We have also provided a summary synthesis of how biodiversity is structured at multiple scales, hierarchical levels and facets. Such characterization helped to describe biodiversity in its highly complex and multidimensional nature. In order to assess and monitor biodiversity, we must recognize this complexity and address it properly.

In Chapter 2 we have delved into Earth Observation (EO) as a fundamental source of data and tools to assess and monitor Earth's surface. We provided a brief summary of EO concepts and available platforms that can be used to track biodiversity changes through space and time. International organisms such as UN's CBD are progressively implementing EO as a way to track progress towards international biodiversity conservation targets and to devise sets of monitoring indicators based on

EO capabilities. Finally, we described how Species Distribution Models can be used for modelling the responses of biodiversity to environmental change and evaluate shifts in species distributions. We provided a description of elementary concepts that build up the theoretical basis of SDMs, its workflow and novel methods that are enhancing the applicability of these models. In particular, the integration and assimilation of EO data into SDMs is providing new and still un- or under-explored opportunities to cover gaps in both fundamental and applied biodiversity research. In this thesis, we addressed some of these opportunities and challenges. Finally, in Chapter 3 (*i.q.*) we have outlined the research objectives and the approach to research development, and described the structure of the thesis.

In **Section II** (Chapters 4 to 9) we present the research papers that compose the core of the thesis and materialize the goals and the research program defined. More specifically, and to address the overarching objectives proposed in the thesis, six non-overlapping, non-sequential and complementary research papers were developed. The organization, complementarity and interactions between these studies across scales and levels of biodiversity are shown in Figure 3 - 1.

In Sub-section II.1 we present one research paper (Chapter 4) that investigates and compares the factors underlying functional connectivity, gene flow and genetic structuring of two pond-breeding, syntopic, and low-dispersal ability amphibian species (*Pleurodeles waltl* and *Pelobates cultripes*) inhabiting Mediterranean habitats currently threatened by land use and global climate alterations. In this study, a multi-level structuring of environmental factors was explored partially based on EO data to reveal fine-scale or detailed aspects controlling genetic structuring and gene flow between the species evaluated.

In Sub-section II.2 we present two research papers addressing challenges related to biodiversity assessment, monitoring and forecasting at the species-level. In Chapter 5, we explored how EO time-series related to ecosystem functioning attributes could be used to exploit the spatiotemporal dynamics of habitat suitability. We tested this rationale with a rare plant species that is currently targeted for conservation under European and national laws, *Veronica micrantha*. We also addressed how multi-temporal time-series could be used to understand temporal dynamics and produce improved models of species distributions and habitat suitability. Finally, the possible factors underlying spatiotemporal habitat suitability changes were investigated. In Chapter 6, a series of methodological developments (spatial connectivity metrics and

modelling integration) were developed and implemented to analyse the vulnerability to landscape fragmentation of two reptile (*Lacerta schreiberi and Anguis fragilis*) and two amphibian species (*Epidalea calamita* and *Chioglossa lusitanica*), all with low dispersal abilities. We investigated how climate and land use changes could expose these species to increased risks by being unable to track environmental changes via range shift adaption.

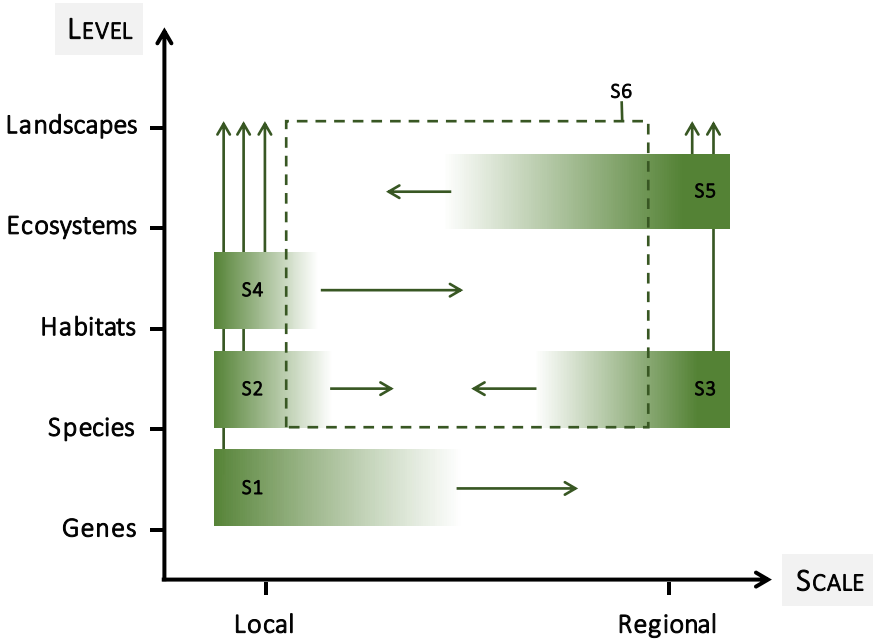

S1: Comparative landscape genetics of pond-breeding amphibians in Mediterranean temporal wetlands: the positive role of structural heterogeneity in promoting gene flow

S2: Exploring the spatiotemporal dynamics of habitat suitability to improve conservation management of a vulnerable plant species

S3: A model-based framework for assessing the vulnerability of low dispersal vertebrates to landscape fragmentation under environmental change

S4: Evaluating an unmanned aerial vehicle-based approach for assessing habitat extent and condition in fine-scale early successional mountain mosaics

S5: Assessing the effectiveness of Protected Areas in promoting forest stability – a methodological approach based on satellite time-series data and multi-model inference

S6: *SegOptim* – a R package for optimizing segmentation parameters with genetic algorithms for supervised image classification

Figure 3 - 1 – Cross-scale and cross-level complementarity between the six research studies conducted during this PhD. Here we do not address the 'conventional' levels of biotic organization (Figure 1 - 5; (Allen and Hoekstra 1990)) although the obvious overlap (exceptions to 'species' which relates to population level; or 'habitat' relating broadly to the community level). Instead, we prefer to address more directly to levels at which we analysed biodiversity status and change.

In Sub-section II.3, we present two research papers that address challenges in habitat mapping and ecosystem stability analysis. In Chapter 7, we used an innovative, sub-orbital and lightweight EO platform – a SenseFly® Swinglet Cam UAV - to test an approach, based on supervised image classification, to map habitat extent and condition in a rather challenging and dynamic fine-scale early successional mountain mosaic. This study assessed how low-spectral but 'ultra-high' spatial resolution imagery can be used to discriminate fine spatial details of natural habitats protected under national and European law. In Chapter 8, we explored a robust time-series of a spectral vegetation index (EVI) from the MODIS platform to evaluate multi-temporal (2000-2017) forest ecosystem stability through a series of functional indicators related to three major dimensions: productivity, seasonality and phenology. We provided an innovative and systematic approach to evaluate and rank the effectiveness of Protected Areas (PA) to ensure the stability of forest ecosystems by looking into the disturbance and response dynamics mediated by resilience. We also provided an analysis of factors underlying our effectiveness ranking, related to several components from socio-ecological conditions, forest composition and structure to disturbance regime.

In Sub-section II.4, we present a single research paper (Chapter 9) making a contribution to advance the methods of Geographic Object-based Image Analysis (GEOBIA) of EO data in the context of ecological applications such as the production of habitat or land use/cover maps and invasive species detection. In this research paper, we explored how genetic algorithms can be used to improve the process of defining parameters of image segmentation with benefits for improved detection of natural resources. We evaluated and tested the added value of such approach in a range of different sensors, scales and application contexts in ecology domain. We also provided an open-source R package which implements the proposed methods.

Finally, in **Section III** (Chapters 10 and 11) we first provided an integrative discussion of the main results and contributions from the six research papers (Chapter 10), bearing in mind the cross-scale and cross-level scheme outlined in Figure 3.1. The advantages and limitations of integrating EO data, resulting from different platforms and with different spatial, temporal and spectral resolutions, with species distribution were analysed and discussed according to the scales, levels and facets of biodiversity under study. Moreover, the overall potential of such integration of data and modelling tools for supporting operational biodiversity conservation actions in international and national programmes is also discussed. We close the thesis by providing some general and

overarching conclusions and with an outlook on applications and future developments (Chapter 11).

References

Allen, T. F. H., and T. W. Hoekstra. 1990. The confusion between scale-defined levels and conventional levels of organization in ecology. Journal of Vegetation Science 1:5-12.

SECTION II. Research papers

Sub-section II.1. Gene level – Combining genetic and Earth Observation data for assessing gene flow and functional connectivity

CHAPTER 4 - Comparative landscape genetics of pond-breeding amphibians in Mediterranean temporal wetlands: the positive role of structural heterogeneity in promoting gene flow

Author list: J. Gutiérrez-Rodríguez (1), **J. Gonçalves** (2), E. Civantos (1,2) and I. Martínez-Solano (1,2,3,4)

(1) Museo Nacional de Ciencias Naturales, CSIC, c/ José Gutiérrez Abascal, 2, 28006 Madrid, Spain
(2) CIBIO/InBIO, Centro de Investigacão em Biodiversidade e Recursos Genéticos da Universidade do Porto, InBIO, Campus Agrário de Vairão, 4485-661 Vairão, Portugal
(3) Instituto de Investigación en Recursos Cinegéticos (IREC-CSIC-UCLM-JCCM), Ronda de Toledo, s/n, 13071 Ciudad Real, Spain
(4) Ecology, Evolution, and Development Group, Department of Wetland Ecology, Doñana Biological Station, CSIC, c/ Américo Vespucio, s/n, 41092 Seville, Spain

DISCLAIMER

This work is an original contribution also included in Gutiérrez-Rodríguez, J. (lead author) PhD dissertation and published in Molecular Ecology journal under the same title. Gonçalves, J., (second author) contributed extensively to this manuscript by developing analysis of landscape functional connectivity, modelling, integration of Earth Observation technologies as well as to the discussion of results and manuscript writing.

ABSTRACT

Comparative landscape genetics studies can provide key information to implement cost-effective conservation measures favoring a broad set of taxa. These studies are scarce, particularly in Mediterranean areas, which include diverse but threatened biological communities. Here we focus on Mediterranean wetlands in central Iberia and perform a multi-level, comparative study of two endemic pond-breeding amphibians, a salamander (*Pleurodeles waltl*) and a toad (*Pelobates cultripes*). We genotyped 411 salamanders from 20 populations and 306 toads from 16 populations at 18 and 16 microsatellite loci, respectively, and identified major factors associated with population connectivity through the analysis of three sets of variables potentially affecting gene flow at increasingly finer levels of spatial resolution. Topographic, land use/cover, and remotely sensed vegetation/moisture indices were used to derive optimized resistance surfaces for the two species. We found contrasting patterns of genetic structure, with stronger, finer-scale genetic differentiation in *Pleurodeles waltl*, and notable differences in the role of fine-scale patterns of heterogeneity in vegetation cover and water content in shaping patterns of regional genetic structure in the two species. Overall, our results suggest a positive role of structural heterogeneity in population connectivity in pond-breeding amphibians, with habitat patches of Mediterranean scrubland and open oak woodlands (“dehesas”) facilitating gene flow. Our study highlights the usefulness of remotely sensed continuous variables of land cover, vegetation and water content (e.g., NDVI, NDMI) in conservation-oriented studies aimed at identifying major drivers of population connectivity.

Keywords: Population connectivity, gene flow, NDVI, NDMI, Iberian Peninsula, Conservation

4.1. Introduction

Comparative landscape genetics studies on co-distributed species have great potential to design cost-effective conservation plans focusing on measures favoring a wider set of taxa, but are still relatively scarce. So far, comparative studies have focused primarily on vertebrates, including amphibians (Richardson 2012; Zancolli et al. 2014; Coster et al. 2015), mammals (Muscarella et al. 2011; Frantz et al. 2012; Dudaniec et al. 2016), and fishes (Olsen et al. 2011), and more occasionally on invertebrates (Engler et al. 2014; Ortego et al. 2015; Phillipsen et al. 2015). These multi-species studies may allow identifying inter-specific differences in the way landscape features influence connectivity and gene flow and provide general guidelines for land management programs aimed at protecting biological communities or ecosystems (Nicholson & Possingham 2006; Goldberg & Waits 2010a; Schwenk & Donovan 2011; Keller et al. 2014). Additionally, by comparing spatial genetic patterns across syntopic species in a shared landscape, important yet often obscure aspects about species life-history traits can be inferred (Steele et al. 2009; Goldberg & Waits 2010a; Richardson 2012; Igawa et al. 2013; Kurz et al. 2014; Coster et al. 2015).

Pond-breeding amphibians are a good study system for comparative landscape genetics studies because they form communities including species that use to different extents both terrestrial and aquatic habitats. Due to their low dispersal abilities (Bowne & Bowers 2004; Graeter et al. 2008), small effective population sizes (Funk et al. 1999), and the discontinuous distribution of their preferred breeding habitats (Jehle et al. 2005) they tend to form “patchy” breeding assemblages. Dispersal and the maintenance of gene flow between breeding ponds depends on the composition and configuration of the landscape (Coster et al. 2015), and studies focusing on functional connectivity have described different species responses to landscape features such as differences in soil moisture, clear-cut habitats, agriculture lands, riparian network, as well as differences in metamorphosis, philopatry, dispersal, selection of breeding sites, and post-breeding behavior (Steele et al. 2009; Goldberg & Waits 2010a; Richardson 2012; Coster et al. 2015; Peterman et al. 2015). Identification of the factors promoting or reducing gene flow is key to prevent local and regional extinctions in the long-term and to inform conservation management.

Most comparative amphibian landscape genetic studies have focused on North American communities with continental (Goldberg & Waits 2010a; Richardson 2012; Coster et al. 2015), temperate (Steele et al. 2009) or humid subtropical climates (Peterman et al. 2015), but little is known about factors shaping regional patterns of gene

flow across taxa in Mediterranean wetlands, which are diverse and highly threatened ecosystems (Blondel & Aronson 1999; Beja & Alcazar 2003). The effects of unpredictability in hydroperiod, coupled with a continued decline in the number and extent of these wetlands (Doulgeris et al. 2015), challenge the survival of their rich biotic communities (Green et al. 2016). Assessing comparative patterns of regional gene flow can help in developing integrative management practices that preserve pond-breeding communities with explicit consideration of functional connectivity.

Landscape analysis methods allow simultaneously testing for the relative influence of different factors acting as potential barriers to dispersal at different spatial scales, at an increasingly finer resolution (Wulder et al. 2004; Greenberg et al. 2005). This allows linking genetic data with different potential response variables and explicitly quantifying the effects of landscape composition, configuration and matrix quality on gene flow and spatial genetic variation (Storfer et al. 2007). Here we perform a multi-level, comparative study focusing on two endemic pond-breeding amphibian species that are characteristic of Mediterranean wetlands in the Iberian Peninsula, *Pleurodeles waltl* Michahelles, 1830 and *Pelobates cultripes* (Cuvier, 1829). Both are usually syntopic but probably differ in their use of the available terrestrial and aquatic habitats, although much of their life-history remains little studied. In addition, both are facing a slow but continued decline mostly associated with habitat loss, invasive species and road mortality, and as a consequence they are listed with 'Near Threatened' (NT) status by the IUCN (Beja et al. 2009; Beja et al. 2016). We compared patterns of genetic diversity and structure and identified the key factors associated with gene flow and population connectivity in both species through the analysis of genotypic data from a suite of highly polymorphic microsatellites in a large sample of individuals of both species in a shared geographic setting.

We explored the relative contribution of landscape features in shaping regional patterns of genetic structure in the two species. We anticipated land cover-related variables to have a strong impact on population genetic structure in both species, since the study region (near the city of Madrid, central Spain) has experienced major land use changes in the last century (Hewitt & Escobar 2011). Thus, to derive optimized resistance surfaces, besides maps with discrete land use/cover categories, we incorporated continuous remotely sensed vegetation/moisture indices which allow for detailed characterization of components of terrestrial habitats at scales relevant for low-dispersing taxa. A model ranking approach was then used to identify variables with greater influence on regional patterns of genetic structure.

4.2. Methods

Study-area and sampling

The study area is bounded by -4.136º to -3.296º longitude and 40.131º to 41.416º latitude (Figure 4 - 1). Elevation ranges from 482 m up to 2403 m a.s.l. The two species are widely distributed in the study area, but their populations are fragmented due to the continued loss of terrestrial and aquatic habitats (Martínez-Solano 2006).

We sampled 306 individuals of *P. cultripes* and 411 of *P. waltl* at 16 and 20 ponds, respectively (Figure 4 - 1 and Table 4 - 2). Average geographic distances between populations for both species were similar and ranged from 0.7 to 40 km between the closest sampled populations (Figure 4 - 1; Appendix I, Suppl. Table 4 - 1 and Table 4 - 2). The scale of analysis reflects uncertainty about actual dispersal potential in both species but includes minimum estimates of adult dispersal (700 meters) based on capture-mark-recapture studies (Gutiérrez-Rodríguez et al. 2017a). Tissues were obtained from tail tips of larvae (most samples) and toe clips of adults (only the *P. waltl* samples from populations W4 and W17). All sampled individuals were released back in their place of capture after sample collection.

Genetic analyses

Genomic DNA was extracted using NucleoSpin Tissue-Kits (Macherey-Nagel). A total of 16 previously characterized microsatellite markers for *P. cultripes* were amplified following the PCR conditions described in Gutiérrez-Rodríguez and Martínez-Solano (2013). For *P. waltl*, 18 previously published loci (Van de Vliet et al. 2009; Gutiérrez-Rodríguez et al. 2014) were grouped into six multiplex reactions (multiplex 1: Pleu2.3, Pleu2.19, Pleu2.34; multiplex 2: Pleu2.16, Pleu2.31, Pleu3.2; multiplex 3: Pleu3.5, Pleu4.1; multiplex 4: Ppl2, Ppl3, Ppl5; multiplex 5: Ppl1, Ppl12, Ppl13, Ppl14; and multiplex 6: Ppl6, Ppl7, Ppl10). PCR conditions and genotype calling followed Gutiérrez-Rodríguez et al. (2014).

We tested for the presence of possible null alleles, stuttering and large allele dropout in microsatellite markers using MICROCHECKER v2.2.3 (Van Oosterhout et al. 2004). Since including sibs and half sibs in population samples can introduce undesired biases in the analyses (Goldberg & Waits 2010b), we conducted genetic parentage analyses with software COLONY v2.0.5.1 (Jones & Wang 2010), assuming a monogamous mating system for both sexes, with the full-likelihood method (Wang 2004). Analyses consisted of ten independent runs, with medium-length likelihood precision and

updated allele frequencies, and individuals identified as full-siblings with a probability of 0.8 or higher were discarded from subsequent analyses.

We tested for deviations from Hardy-Weinberg equilibrium (HWE) and evidence of linkage disequilibrium (LD) with the software GENEPOP (Raymond & Rousset 1995; Rousset 2008), applying the sequential Bonferroni correction (Rice 1989) to adjust significance values for multiple tests. We calculated different estimates of genetic diversity for each population using GENALEX v6.5b5 (Peakall & Smouse 2012), 2012), including the number of alleles (NA), observed (HO) and expected heterozygosity (HE). We also calculated the inbreeding coefficient (F_{IS}) because it is an indirect measure of philopatry (more philopatric species will in principle have higher F_{IS} values).

We used BAPS v6 (Corander et al. 2008; Cheng et al. 2013) to characterize population genetic structure for both species datasets. We ran spatial genetic mixture analyses, with ten independent runs and a maximum number of groups equal to the number of sampled localities. We compared clusters resulting from each replicate run based on their likelihood score and identified the optimal clustering level based on a stochastic optimization algorithm (Corander et al. 2008).

We calculated three estimates of genetic differentiation between populations, F_{ST} (Weir & Cockerham 1984), G''_{ST} (Meirmans & Hedrick 2011) and D_{EST} (Jost, 2008) using Genepop, GENODIVE v2.0b23 (Meirmans & Van Tienderen 2004) and SMOGD v1.2.5 (Crawford 2010), respectively, to compare patterns of regional genetic structure across species and characterize genetic differentiation between populations. We used software CODIDI v1.0 (Wang 2015) (100,000 permutations) to determine if G''_{ST} provides an accurate estimate of genetic differentiation in the two species. We also estimated recent migration rates between localities using the software BAYESASS v3.0 (Wilson & Rannala 2003). We ran three different replicates for each species with 50,000,000 iterations, a burn-in period of 2,000,000 and sampling frequency each 2000. We assessed convergence of results across runs and used those with the best likelihood in subsequent analyses.

Input data used for resistance surfaces and pre-processing

During pre-processing we aggregated all raster variables to a spatial resolution of 100m to make the optimization of resistance surfaces tractable and with the same raster support characteristics. We obtained elevation data from ASTER Global Digital Elevation Model (GDEM v2; Tachikawa et al. 2011) with a spatial resolution of 30m later resampled to 100m (bilinear method). Then, from elevation data we calculated percent slope,

describing surface roughness, and the Topographic Wetness Index (TWI) describing the tendency of a cell to accumulate water (Quinn et al. 1995). We hypothesized elevation, slope and TWI as potential factors for explaining gene flow and genetic differences between sampled populations at a coarser regional scale (see Table 4 - 1 listing all factors).

Table 4 - 1 – Input variables by level and data source used to explain gene flow and calculate optimized resistance surfaces. Summary statistics in brackets: minimum (min), average (avg), maximum (max) and standard-deviation (std).

Level	Variable	Description	Source
Regional	*elev*	Elevation (meters a.s.l; min:482.0, avg:935.0, max:2403.0, std:326.1)	USGS/ASTER GDEM
	slope	Slope (%; min:0.0, avg:9.4, max:121.2, std:10.4)	
	twi	Topographic wetness index (unitless; min:2.9, avg:7.0, max:12.6, std:1.2)	
Local	*clc06*	Corine Land Cover class for year 2006 (15 classes)	EEA
	siose05	SIOSE 2005 Land cover class (resistance weights, unitless; min:0.0, avg:12.7, max:100.0, std:26.3)	CNIG/Spain
	rdens	Road density (m/ha; min:0, avg:27.5, max:1272.5,	
Habitat	*ndvi_avg*	Normalized Difference Vegetation Index (spatial average from 30m to 100m; vegetation biomass/greenness amount; $\times 10^{-4}$, unitless, min:-3013, avg:3652, max:8971,	Landsat 5 TM USGS/ESPA
	ndvi_std	Normalized Difference Vegetation Index (spatial standard-deviation from 30m to 100m; vegetation heterogeneity; $\times 10^{-4}$, unitless, min:0, avg:429, max:5503, std:310)	
	ndmi_avg	Normalized Difference Moisture Index (spatial average from 30m to 100m; vegetation water content; $\times 10^{-4}$, unitless, min:-4976, avg:-335, max:5613, std:1413)	
	ndmi_std	Normalized Difference Moisture Index (spatial standard-deviation from 30m to 100m; vegetation water content heterogeneity; $\times 10^{-4}$, unitless, min:10, avg:385, max:3862, std:277)	

Land use/cover (LUC) considering both composition (the amount of certain land cover categories) and configuration (referring mainly to the spatial distribution and diversity of land cover types) have been hypothesized to impact connectivity, species movements and gene flow (Pérez-Espona et al. 2008) at the landscape level. To assess this, we used two land use/cover datasets to derive resistance surfaces and test the effect of landscape matrix composition. We used the first dataset, Corine Land Cover (CLC) (spatial resolution: 100m), as a categorical map in optimization procedures to derive a resistance surface accounting for the different resistance of each land cover category. Then we reclassified this dataset into a lower number of categories (Appendix I – Supp. Table 3) to make it tractable by the *ResistanceGA* package (Peterman 2014; Peterman et al. 2014. We also used a second fine-scale LUC dataset (SIOSE) for deriving a continuous resistance surface. Due to the large number of initial classes in the dataset a reclassification was also necessary (Appendix I – Supp. Table 4). We initially attributed an aprioristic resistance weight to each class reflecting the increased resistance to amphibian movement and higher mortality rates associated with artificial (urban habitats, roads) vs natural land cover/use classes observed in our study area; these weights were subsequently optimized (see initial weights in Appendix I – Supplemental Table 5).

Roads have also been linked to species mortality, movements and gene flow (Pérez-Espona et al. 2008). Considering this, we obtained linear road data by Spanish Provinces from the Centro Nacional de Información Geográfica (CNIG; URL: http://centrodedescargas.cnig.es) to calculate total road density for each 100m pixel (m/ha) in the study-area.

Finally, we hypothesized that the amount and spatial heterogeneity of vegetation cover and vegetation water content (VWC) might also affect genetic differentiation. We downloaded pre-processed remote sensing image data for the Landsat 5 TM sensor, with a spatial resolution of 30m, from the USGS/ESPA service (URL: http://espa.cr.usgs.gov/). We used one scene for each month of June, August and September 2009, coinciding with field surveys, to generate a single average composite image. The Normalized Difference Vegetation Index (NDVI), extensively used in ecological applications (Turner et al. 2003; Nagendra et al. 2013) provides a continuous measure related to vegetation canopy characteristics such as biomass, leaf area index and percentage of vegetation cover. This index varies from -1 (non-vegetated/artificial surfaces) to 1 (densely vegetated areas). Complementarily, we employed the Normalized Difference Moisture Index (NDMI) to characterize vegetation water content

(VWC; Gao 1996). NDMI also varies from -1 (indicative of low VWC) to 1 (high VWC). Image data was aggregated to 100m to match the same spatial resolution of topographic and land cover data using the average (defining the amount of vegetation cover and VWC) and the standard deviation (translating the spatial heterogeneity of vegetation cover and VWC).

Statistical modelling and resistance surface optimization

To assess the relative support of each variable to explain differences in patterns of genetic structure between sampled populations of *P. cultripes* and *P. waltl* we used the *ResistanceGA* package in R v3.0.3 (R Core Team 2014). This package implements a genetic algorithm that optimizes a set of equation parameters used to transform the initial values of each variable into resistance surfaces. This optimized surface is then used to calculate cost-based distances between sampled locations through least-cost path analyses using the *gdistance* package (Van Etten 2015). We used a linear mixed effects model with the maximum likelihood population effects (MLPE) parameterization (Clarke et al. 2002) to relate the genetic and the cost-based distance matrices and to calculate the model Akaike Information Criterion (with a correction for finite sample size; AICc). The AICc value is the fitness function output used for iteratively improving the genetic algorithm. The MLPE allows accounting for the non-independence of values within pairwise distance matrices (Clarke et al. 2002; Van Strien et al. 2012) and was fitted by maximum likelihood using R package LME4 (Bates et al. 2014).

We used pairwise genetic distances (measured by F_{ST}, G''_{ST}, and D_{EST}), as well as migration rates between populations as the response variable, while scaled and centered effective cost-based resistance distances between populations were considered the independent variable. The genetic algorithm to determine the best set of parameters for optimizing the resistance surfaces used a maximum number of 250 rounds, or 20 rounds without performance improvement.

To evaluate model performance, we compared AICc values between models generated with each optimized resistance surface to two baseline null-models: one based on a single intercept-term (*IntOnly*) and other including only Isolation-by-distance (IBD) effects. Then we ranked each model based on delta AICc values (ΔAICc) considering the confidence set determined by models with substantial or good support, i.e. with $\Delta AICc \leq 4$. We calculated Akaike weights (w_i) to quantitatively represent the strength of evidence or support of each tested model.

4.3. Results

We amplified genotypes with a success rate of >99% for both species. Based on MICROCHECKER results, we discarded two microsatellite loci (Pc4.7 and Pc4.11) in *P. cultripes*, because of the possible presence of null alleles. In *P. waltl*, locus Pleu2.3 was monomorphic in all samples analyzed and was thus discarded. Sibship analyses in COLONY detected a low proportion of full-sibs in both species (see Table 4 - 1), which were subsequently removed from the dataset, leaving one representative per sibship group. We did not detect significant deviations from HWE and LD, except in locus Pleu3.5 in Pop14 (Brunete) in *P. waltl*, which showed evidence of heterozygote deficit.

Descriptive statistics of genetic diversity for *P. cultripes* and *P. waltl* are presented in Table 4 - 1. Estimates of genetic diversity were slightly higher in *P. waltl.* The mean number of alleles per population ranged from 1.43 (Pop3) to 4.14 (Pop16) in *P. cultripes* and from 2.06 (Pop18) to 5.12 (Pop5) in *P. waltl*. The observed heterozygosity ranged from 0.19 (Pop3) to 0.55 (Pop16) in *P. cultripes*, and from 0.35 (Pop18) to 0.65 (Pop10) in *P. waltl*. Average population inbreeding coefficients (F_{IS}) were higher in *P. waltl* (0.01) than in *P. cultripes* (0.004).

The results of BAPS analyses supported optimal clustering levels at K=13 and K=7 for *P. waltl* and *P. cultripes*, respectively (Figure 4 - 1). The number of clusters was consistent across replicate runs. In *P. waltl*, inferred clusters included geographically close sampling locations, such as clusters (W2+W3), (W4+W10+W11), (W7+W8+W9), and (W16+W17+W19), whereas in *P. cultripes* some clusters included larger groups of populations, especially one cluster including locations:
(C2+C4+C5+C6+C7+C8+C9+C11), distributed across medium elevations at the foothills of Sierra de *Guadarrama*, and the cluster (C13+C14+C16) in the south of our study area. This is consistent with resistance surfaces, where these areas generally show low resistance / higher connectivity (see below). Overall, there are clear differences between species, with a stronger signal of geographic structure in *P. waltl* (Figure 4 - 1).

Pairwise estimates of F_{ST}, G''_{ST}, and D_{EST} between populations of each species are presented in Appendix I – Supp. Tables 6-11. Lower average values, indicating greater population connectivity, were found in *P. cultripes* (F_{ST} = 0.117; G''_{ST} = 0.192; D_{EST} = 0.044) than in *P. waltl* (F_{ST} = 0.187; G''_{ST} = 0.402; D_{EST} = 0.184). Analyses with CODIDI did not detect significant negative correlations between diversity (*Hs*) and G''_{ST} in either species (*P. cultripes*: r = 0.20, p = 0.73; *P. waltl*: r = -0.21, p = 0.21), indicating G''_{ST} estimates accurately describe population differentiation and are comparable across

species. BAYESASS results indicate low migration rates across sites, except among geographically close localities (Appendix I – Supp. Tables 12 and 13), with higher average migration rates between populations of *P. cultripes* (mean = 0.0179) than in populations of *P. waltl* (mean = 0.0126).

Table 4 - 2 – Locality information and genetic diversity estimates for sampled *Pelobates cultripes* (C) and *Pleurodeles waltl* (W) populations: *N* = sample size; N_C = sample size after exclusion of potential siblings from the sample; N_A = mean number of alleles per locus; H_O: observed heterozygosity; H_E = expected heterozygosity; F_{IS} = inbreeding coefficient.

ID	Locality	Longitude	Latitude	*N*	N_C	N_A	H_O	H_E	F_{IS}
C1	Segovia, Boceguillas	-3.618	41.330	10	9	2.857	0.341	0.364	0.121
C2	Madrid, Buitrago de Lozoya	-3.644	40.974	20	16	2.857	0.341	0.362	0.088
C3	Madrid, Canencia, Prado Toril	-3.800	40.859	20	12	1.429	0.190	0.159	-0.154
C4	Madrid, Valdemanco	-3.645	40.853	19	18	3.786	0.437	0.460	0.080
C5	Guadalajara, El Cubillo de Uceda	-3.451	40.795	19	13	3.571	0.455	0.419	-0.043
C6	Madrid, El Vellón	-3.586	40.773	20	18	3.714	0.452	0.447	0.017
C7	Madrid, Guadalix de la Sierra, Medianillos	-3.676	40.756	20	15	3.786	0.367	0.380	0.070
C8	Madrid, Algete, Salomón	-3.561	40.648	18	14	3.286	0.436	0.410	-0.027
C9	Madrid, Colmenar Viejo	-3.786	40.628	20	14	3.857	0.413	0.407	0.021
C10	Madrid, Hoyo de Manzanares	-3.916	40.613	20	14	1.786	0.352	0.296	-0.151
C11	Madrid, Las Rozas	-3.923	40.509	20	16	3.786	0.424	0.427	0.039
C12	Madrid, Getafe, Camino de Preresa	-3.596	40.303	20	14	2.643	0.352	0.358	0.054
C13	Madrid, Fuenlabrada, Valdehondillo	-3.801	40.261	20	16	3.714	0.531	0.493	-0.045
C14	Madrid, Fuenlabrada, Camino de las Panaderas	-3.800	40.255	20	17	3.643	0.492	0.480	0.006
C15	Madrid, Batres, Soto del Endrinal	-3.950	40.238	20	16	2.286	0.330	0.323	0.009
C16	Madrid, Griñon, Cerro del Rayo	-3.821	40.223	20	18	4.143	0.552	0.526	-0.020
W1	Segovia, Santo Tomé del Puerto	-3.589	41.200	20	20	2.824	0.476	0.478	0.028
W2	Madrid, Gascones	-3.651	41.012	20	20	3.235	0.529	0.518	0.003
W3	Madrid, Buitrago de Lozoya	-3.644	40.975	20	9	2.941	0.458	0.439	0.017
W4	Madrid, Bustarviejo, Fuente del Collado	-3.724	40.855	20	17	3.765	0.550	0.517	-0.034
W5	Madrid, Valdemanco	-3.645	40.853	33	28	5.118	0.610	0.583	-0.028
W6	Madrid, Torrelaguna	-3.573	40.830	20	12	2.647	0.490	0.456	-0.030
W7	Guadalajara, El Cubillo de Uceda	-3.451	40.795	20	17	4.059	0.578	0.596	0.060
W8	Madrid, El Vellón, Cotos de Monterrey	-3.603	40.786	20	14	4.059	0.558	0.595	0.101
W9	Madrid, El Vellón	-3.586	40.773	20	16	3.765	0.563	0.547	0.004
W10	Madrid, Guadalix de la Sierra, Medianillos	-3.676	40.756	18	16	4.588	0.652	0.593	-0.067
W11	Madrid, Colmenar Viejo	-3.786	40.628	20	17	4.353	0.612	0.603	0.015
W12	Madrid, Hoyo de Manzanares, La Berzosa	-3.928	40.603	20	18	4.471	0.592	0.573	-0.004
W13	Madrid, Las Rozas	-3.923	40.509	20	18	3.824	0.526	0.526	0.028
W14	Madrid, Brunete	-4.000	40.413	20	16	3.765	0.500	0.533	0.094
W15	Madrid, San Fernando de Henares, La Guindalera	-3.504	40.409	20	17	3.059	0.554	0.504	-0.068
W16	Madrid, Fuenlabrada, Valdehondillo	-3.801	40.261	20	17	3.941	0.522	0.542	0.067
W17	Madrid, Fuenlabrada, Camino de las Panaderas	-3.800	40.255	20	19	4.000	0.563	0.560	0.021
W18	Madrid, Morata de Tajuña	-3.408	40.241	20	17	2.059	0.353	0.320	-0.066
W19	Madrid, Parla, Sancha Barca	-3.793	40.239	20	19	4.235	0.554	0.569	0.052
W20	Madrid, Griñon, Cerro del Rayo	-3.821	40.223	20	19	3.353	0.495	0.489	0.013

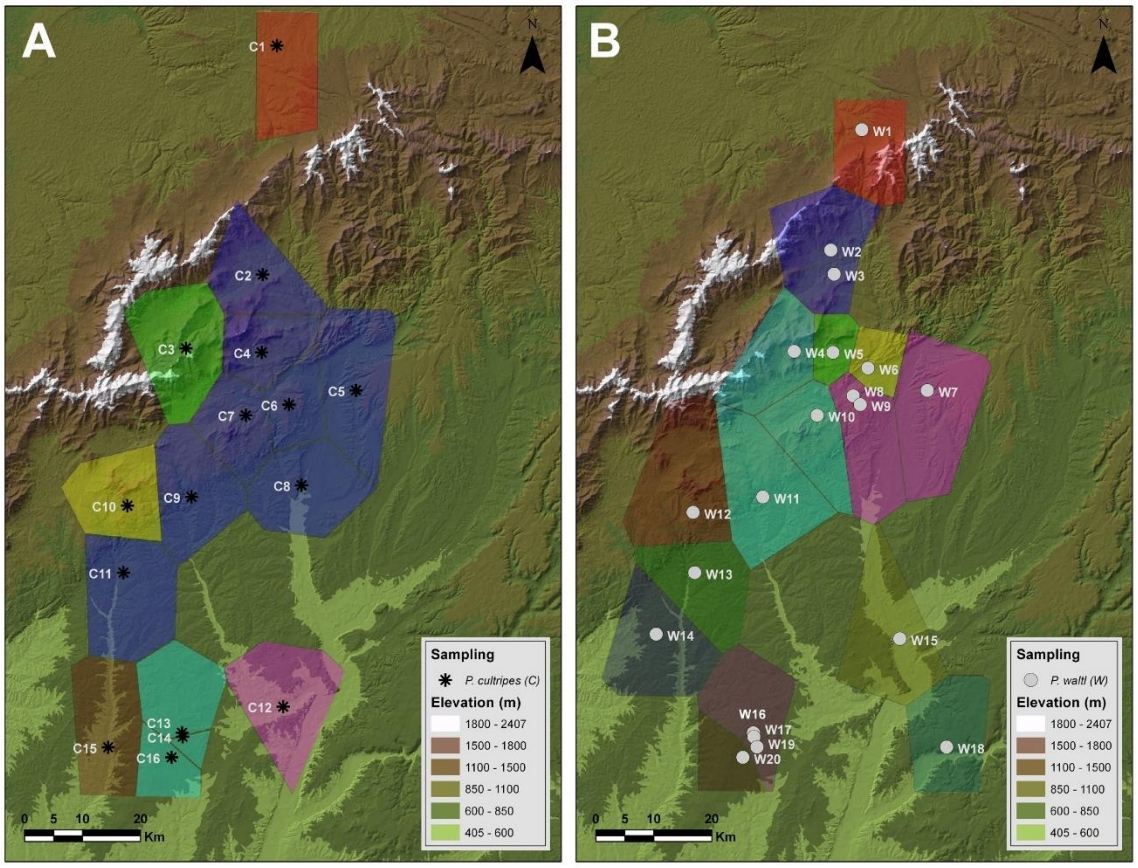

Figure 4 - 1 – Sampling locations for the two study species: *P. cultripes* (A) and *P. waltl* (B). Codes as in Table 4 - 1. Results of the optimal number of clusters for each species according to BAPS are also shown.

Multi-model selection and ranking

For *P. cultripes* optimization and model selection showed similar and congruent results with low model uncertainty when comparing rankings obtained for distance matrices based on D_{EST}, F_{ST} and G''_{ST} (Table 4 - 3). For this species, average NDVI (related to vegetation amount) was the most frequently selected variable for all distance measures. Topographic variables related to elevation (selected for D_{EST}) and slope (selected for F_{ST} and G''_{ST}) were also important to explain genetic differentiation in *P. cultripes*.

For *P. waltl* model selection also showed similar and coherent results with low model uncertainty across different genetic distances. For this species, spatial heterogeneity of vegetation (ndvi_std) and spatial heterogeneity in vegetation water content (ndmi_std), were the most frequently selected variables. These attained very high model support being selected for all genetic distances (Table 4 - 3). Topographic resistance surfaces related to elevation (selected for D_{EST} and F_{ST}) and slope (selected for F_{ST}) were also important to explain genetic differentiation for *P. waltl*.

Table 4 - 3 – Model selection table for *P. cultripes* (left) and *P. waltl* (right). Models highlighted in bold attained the highest relative support and were included in the confidence set (ΔAICc≤4). AICc – Akaike Information Criterion value (with a correction for finite sample size), ΔAICc – delta AIC value, wi – Akaike weights. *IBD* – Isolation-by-distance model. *IntOnly* – Intercept-only/null model.

Genetic distance metric	*Pelobates cultripes*				*Pleurodeles waltl*			
	Variable	**AICc**	**ΔAIC**	**wi**	**Variable**	**AICc**	**ΔAIC**	**wi**
D_{EST}	***elev***	**-578.90**	**0.00**	**0.47**	***ndvi_std***	**-522.71**	**0.00**	**0.52**
	ndvi_avg	**-578.72**	**0.18**	**0.43**	***elev***	**-521.95**	**0.75**	**0.36**
	ndmi_avg	-573.38	5.52	0.03	***ndmi_std***	**-519.76**	**2.95**	**0.12**
	slope	-573.37	5.54	0.03	*rdens*	-511.89	10.81	0.00
	twi	-570.84	8.06	0.01	*slope*	-511.23	11.47	0.00
	ndmi_std	-570.48	8.43	0.01	*twi*	-509.96	12.74	0.00
	ndvi_std	-570.09	8.82	0.01	*ndvi_avg*	-508.57	14.14	0.00
	siose05	-569.66	9.24	0.00	*siose05*	-502.84	19.87	0.00
	rdens	-569.58	9.33	0.00	*IBD*	-502.24	20.46	0.00
	IntOnly	-569.46	9.44	0.00	*ndmi_avg*	-502.09	20.62	0.00
	clc06	-568.84	10.06	0.00	*clc06*	-488.00	34.70	0.00
	IBD	-567.70	11.20	0.00	*IntOnly*	-387.81	134.90	0.00
F_{ST}	***ndvi_avg***	**-495.08**	**0.00**	**0.59**	***ndvi_std***	**-646.58**	**0.00**	**0.63**
	slope	**-492.48**	**2.60**	**0.16**	***slope***	**-643.24**	**3.35**	**0.12**
	twi	-490.29	4.79	0.05	***ndmi_std***	**-642.69**	**3.89**	**0.09**
	siose05	-490.29	4.80	0.05	***elev***	**-642.45**	**4.14**	**0.08**
	elev	-489.90	5.18	0.04	*rdens*	-641.74	4.84	0.06
	ndmi_std	-489.85	5.23	0.04	*twi*	-638.87	7.72	0.01
	rdens	-488.20	6.88	0.02	*ndvi_avg*	-638.44	8.14	0.01
	ndvi_std	-488.10	6.98	0.02	*siose05*	-636.99	9.60	0.01
	ndmi_avg	-487.73	7.35	0.01	*clc06*	-629.92	16.66	0.00
	IBD	-484.04	11.04	0.00	*ndmi_avg*	-624.61	21.98	0.00
	IntOnly	-482.72	12.36	0.00	*IBD*	-624.42	22.16	0.00
	clc06	-479.98	15.10	0.00	*IntOnly*	-516.03	130.55	0.00
G''_{ST}	***ndvi_avg***	**-383.78**	**0.00**	**0.77**	***ndvi_std***	**-364.56**	**0.00**	**0.74**
	slope	**-381.21**	**2.57**	**0.21**	***ndmi_std***	**-361.18**	**3.38**	**0.14**
	twi	-375.35	8.44	0.01	*rdens*	-358.92	5.64	0.04
	ndmi_std	-372.81	10.97	0.00	*slope*	-358.32	6.24	0.03
	elev	-372.58	11.20	0.00	*elev*	-357.48	7.08	0.02
	ndvi_std	-372.54	11.24	0.00	*twi*	-355.91	8.64	0.01
	ndmi_avg	-371.50	12.28	0.00	*siose05*	-355.15	9.41	0.01
	rdens	-369.93	13.85	0.00	*ndvi_avg*	-354.98	9.58	0.01
	siose05	-368.80	14.98	0.00	*IBD*	-343.12	21.44	0.00
	IBD	-364.43	19.35	0.00	*ndmi_avg*	-342.98	21.58	0.00
	clc06	-363.11	20.67	0.00	*clc06*	-340.58	23.98	0.00
	IntOnly	-360.67	23.11	0.00	*IntOnly*	-230.69	133.86	0.00

For both species models related to landscape composition and structure (siose05) or road density showed very little to no support in explaining genetic differentiation (
Table 4 - 3). Overall, for both species and considering all genetic distance matrices, the IBD and the intercept-only models attained no relative support, showing a good relative performance of resistance surfaces to explain gene flow patterns.

Resistance surfaces

Resistance surface optimization revealed several non-linearities regarding the way landscape features influence gene flow (Figure 4 - 2). Also, when considering model-selected variables (Table 4 - 3), the transformations used for generating optimized resistance surfaces showed a very strong similarity of responses across different genetic distances translating a certain degree of stability between optimization rounds.

For P. cultripes we found lower resistance areas for below median elevations (with a minimum resistance around 870m) and moderate slopes (minimum 11.4%) corresponding to low- and midland areas. Vegetated areas with above median NDVI values had low resistance (minimum around 0.42; Figure 4 - 3) showing both an avoidance for artificial areas (e.g., urban settlements, roads; typically, with very low or negative NDVI values) and strongly vegetated areas mostly related to elevated mountainous zones with forest cover.

For P. waltl we found two different (and complementary) transformations for elevation. When considering FST and G''ST, the relationship was almost linear, i.e., with increasing resistance following the increase in altitude (Figure 4 - 3), while for DEST, strong resistance values were related to lowland areas. In addition, low resistance landscapes had very-high NDVI / NDMI standard deviation, corresponding to highly heterogeneous and moderately disturbed areas with natural and/or semi-natural vegetation, frequently with water surfaces or lines.

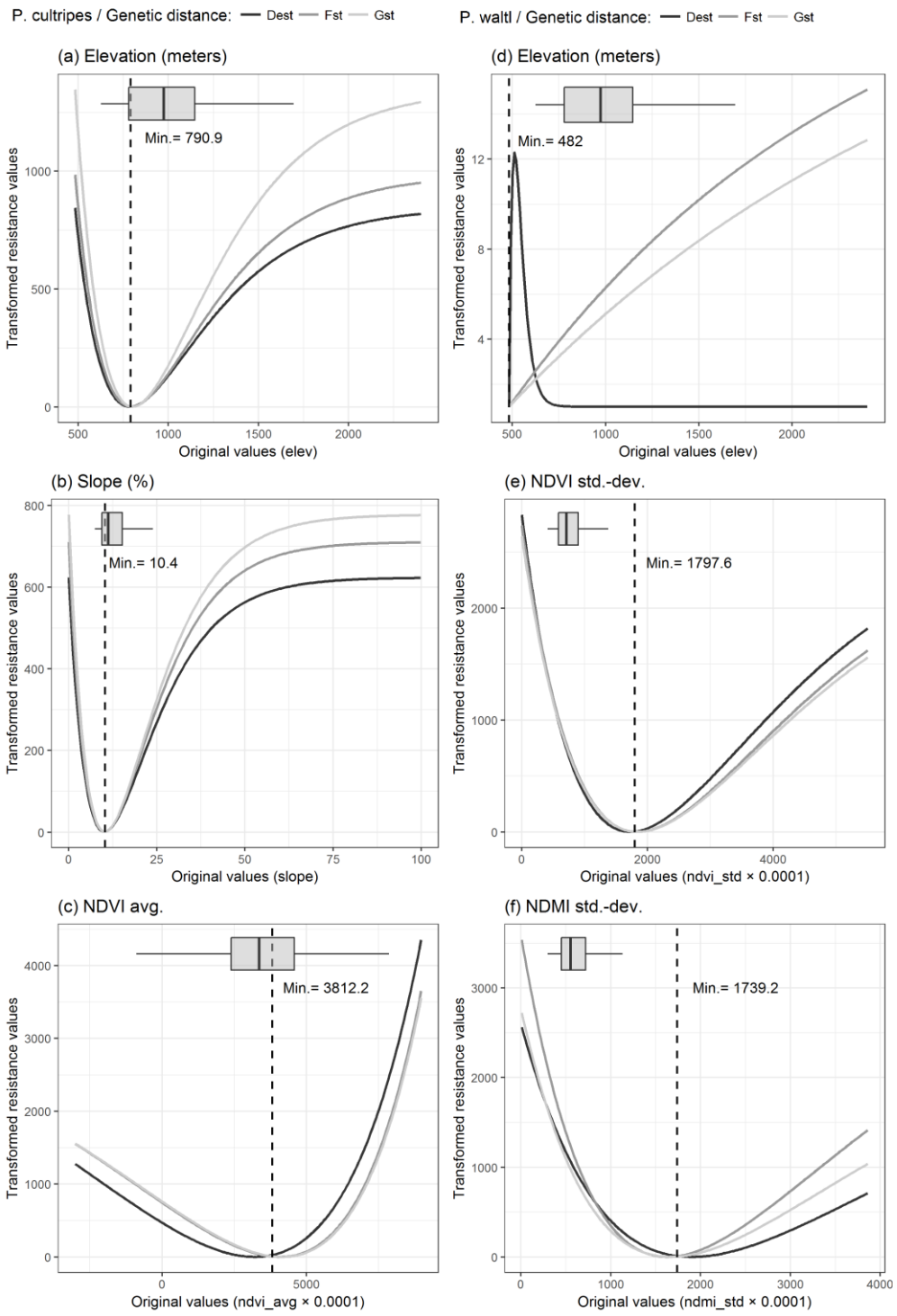

Figure 4 - 2 – Transformations applied to each variable (included in the most frequently selected models) to generate resistance surfaces for species *P. cultripes* (left-side) and *P. waltl* (right-side). Each curve represents a different transform parameterization optimized for D_{EST} (black color), F_{ST} (dark-grey) and G''_{ST} (light-grey). Original values are represented in the x-axis (including the full range of the variable) while transformed (resistance) values are shown in the y-axis and should be interpreted in relative fashion between variables. The dashed line shows the minimum resistance for the original values of each variable. The boxplot on top shows the distribution of the original untransformed variable (boxes are the Figure 2. 25%, 50% and 75% quartiles and whiskers show the smallest/largest observation greater/less than or equal to lower hinge -/+ 1.5 times the inter-quartile range). NDVI and NDMI values have a 10^{-4} scale factor.

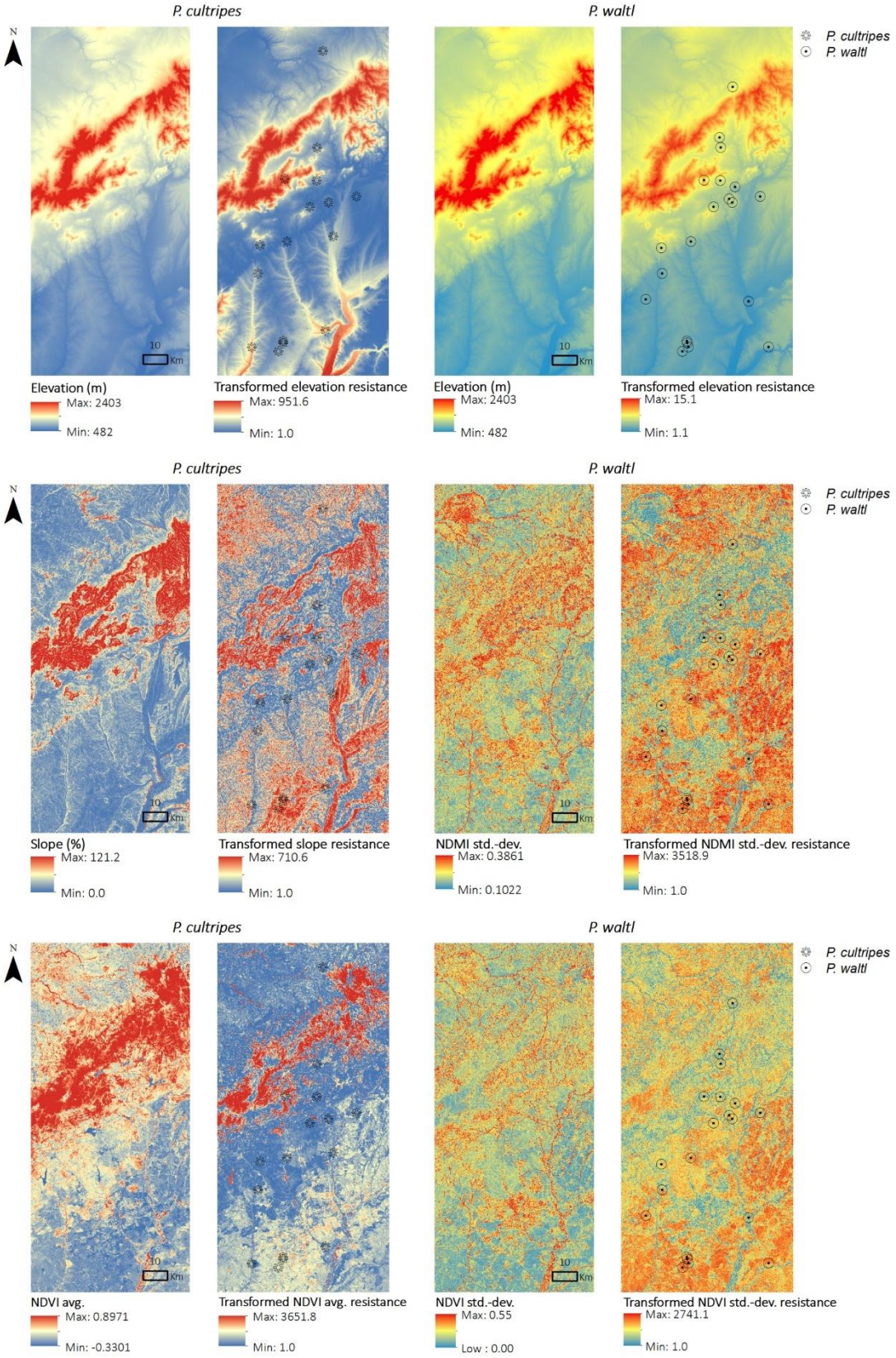

Figure 4 - 3 – Optimized resistance surfaces for *Pelobates cultripes (left-side)* and *Pleurodeles waltl (right-side)* based on the most frequently selected variables and considering F_{ST} genetic distances. For each species, on the left are maps showing the original continuous values for each variable; on the right, the resistance surface generated through optimization. Points represent sampling localities.

4.4. Discussion

Comparative studies based on molecular approaches hold great potential to improve our understanding on the effect of different landscape features on regional patterns of population connectivity across taxa. Here we anticipated land cover-related variables to have the most impact on genetic structure, and hypothesized remotely sensed data would provide a more accurate description of terrestrial habitats at the relevant spatial scale for low dispersing organisms than other traditionally used discrete categories of land use/cover. Our results support this notion, with genetic differentiation in the two species mainly associated to environmental factors related to land and vegetation cover. Our comparative study revealed contrasting patterns of genetic structure in the two species, with stronger, finer-scale genetic differentiation in *P. waltl* (see Figure 4 - 1). This difference can be associated to demographic (especially differences in dispersal rates) and life-history traits, or divergent terrestrial habitat preferences. These factors are not mutually exclusive, and our resistance surfaces provide some keys to sort out their relative effects. Leaving aside the common effect of topography on both species (see below), land-cover related categorical variables did not have an important role in shaping genetic structure. Some studies have previously reported negative effects of roads on gene flow in anurans (Richardson 2012) and salamanders (Coster et al. 2015). Nevertheless, models including road density as a variable were not well supported in either species (Table 4 - 3). Instead, we found remarkable differences associated to the role of fine-scale patterns of vegetation cover, vegetation water content and their spatial heterogeneity in shaping patterns of regional genetic structure for the two species. These differences were better captured by fine-scale remotely sensed spectral indices (NDVI/NDMI) portraying land cover, vegetation and moisture in a continuous fashion, highlighting their value in landscape genetics studies.

For *P. cultripes*, genetic differentiation increased with both high and low values of vegetation coverage (NDVI avg.), with medium values in this variable associated with reduced resistance to gene flow (Table 4 - 3). Patches with high resistance are typically related to urban/artificial areas and roads (low NDVI values) or high altitude forested areas (high values; Figure 4 - 3). Habitats with mid-range canopy cover have been reported as areas preferentially selected during dispersal in other species of anurans, such as *Bufo boreas* (Bartelt et al. 2004). In *P. waltl,* high or very high values in variables related to the spatial heterogeneity of vegetation cover (NDVI and NDVI std.-dev.), and the spatial heterogeneity in vegetation water content (NDMI std.-dev.), were associated with higher connectivity between populations. These values correspond to

heterogeneous and moderately disturbed areas with different types of natural and/or semi-natural vegetation frequently linked to water surfaces or lines (Table 4 - 3 and Figure 4 - 3). Thus, our results suggest a positive role of structural heterogeneity in population connectivity for the two species, with habitat patches of Mediterranean scrubland and open oak woodlands ("*dehesas*") facilitating gene flow.

Fine-scale aspects of the landscape, described by remotely sensed data, strongly influenced gene flow in both species, as anticipated. However, different variables were more important in shaping patterns of gene flow between species. This is surprising in view of the extensive overlap in their geographic ranges, probably reflecting similar ecological requirements at the macro (bioclimatic) scale (Sillero et al. 2009). Regionally, vegetation amount played a key role in *P. cultripes*, whereas in *P. waltl* the spatial heterogeneity in vegetation coverage and water content / water stress were more important. Since NDMI is an indicator of water stress, its presence in models for *P. waltl* may indicate that this species is more sensitive to drought conditions. With potential alterations in hydrologic regimes derived from climate change (affecting wetlands and ponds through changes in hydroperiod) this has important consequences for connectivity and conservation assessments. Also, low-resistance areas (with importance for connectivity) are less common in the landscape for *P. waltl* than for *P. cultripes* (notice the difference in resistance curves in Figure 4 - 2; in *P.* waltl, low-resistance conditions are pushed to the right-side, close to extreme data values; while in *P. cultripes* they are closer to the median). This observation, in conjunction with the inferred lower dispersal ability in Pleurodeles, probably make this species more vulnerable to the effects of fragmentation, whereas Pelobates could be considered more of a generalist species, in the sense that it benefits from a higher availability of favorable areas for dispersal in the study area.

In addition to variables related with land and vegetation cover, our results also showed some effect of topography on regional patterns of genetic structure. Variables related to topography have been previously shown to explain genetic differentiation in a wide range of taxa (for examples in amphibians, see Funk et al. 2005; Giordano et al. 2007; Savage et al. 2010; Igawa et al. 2013; Zancolli et al. 2014; Funk et al. 2016). In our study area, we also found that neither elevation nor slope favor gene flow in the two species studied (Table 4 - 3). Both are typical inhabitants of Mediterranean habitats at low and medium elevations, with upper altitudinal limits of up to 1480 meters in *P. waltl* and 1770 meters in *P. cultripes* (Cejudo 1990; Montori et al. 2002; Tejedo & Reques 2002; García-París et al. 2004). Restrictions to population connectivity imposed by elevation and slope

probably operate on deeper time scales than those related to land use/cover. Recent phylogeographic studies have shown that the Iberian Central System has acted as an historical barrier to gene flow in the two species, separating different evolutionary groups north and south of this mountain range (Gutiérrez-Rodríguez et al. 2017b,c). These groups would have experienced limited connectivity during the Last Glacial Maximum (21 ka), since glacial areas occupied lower altitudes around 1350 m in the study area (Bullón 2016). In contrast, vegetation dynamics in the Central System mountains have been constantly changing during the Holocene due to human activities (López-Sáez et al. 2014). In addition, large water surfaces and rivers are also associated to potential barrier effects in areas of low elevation and slope.

Demographic and life history traits, such as dispersal, philopatry, population effective size, generation time, clutch size and larval phenology have been described as promoters of genetic differentiation in amphibians (Richardson 2012; Whiteley et al. 2014; Nowakowski et al. 2015). One of the most important biological traits affecting the genetic structure of populations is dispersal capacity, which is fundamental to maintain gene flow between populations. Amphibians generally present limited dispersal and significant differences have been observed between anurans and salamanders (Smith & Green 2005). In the case of *P. cultripes* and P. waltl, there is no published information about dispersal distance or home range. Nonetheless, our analyses suggest low migration rates in both species (Appendix I – Supplementary Tables 12-13). While these values may underestimate actual migration rates because of our sampling strategy (mostly larvae, which cannot be migrants) and other factors, like the potential presence of unsampled ponds that could act as stepping-stones, low rates are consistent with our own field data. Over an 8-year period, we recorded 0.5% vs 1.2% dispersal event rates involving distances over 250 meters of marked adult individuals of Pleurodeles (6 dispersal events per 1172 recaptures) and Pelobates (16 dispersal events per 1293 recaptures), respectively (Gutiérrez-Rodríguez et al. 2017a). The lower frequency of dispersal events in P. waltl is in agreement with the observed higher population genetic differentiation as compared to Pelobates. Other indirect evidence, like higher frequency of road-kills in *P. cultripes* in areas where the two species co-occur (D'Amico et al. 2015) also suggest more dispersal capacity and propensity in Pelobates, in line with previous studies documenting higher migration potential in anurans compared to urodeles. Another life history trait linked to dispersal and population structure is breeding site philopatry, with the species with higher philopatry showing increased population genetic differentiation. Here, we inferred philopatry based on the comparison of inbreeding coefficients (F_{IS}), with results in agreement with dispersal estimates: mean values of F_{IS}

in P. waltl (0.010) doubled those in *P. cultripes* (0.004), suggesting a more philopatric behavior of the former species.

Our study represents a valuable contribution to the knowledge on the functioning and conservation of Mediterranean habitats, including the finding of a positive role of structural heterogeneity on gene flow in pond-breeding amphibians. More generally, it illustrates how remotely-sensed continuous variables of vegetation cover and water content (e.g., NDVI, NDMI) have great potential to offer relevant insights about major drivers of population connectivity in landscape genetics studies. In our study area, variables associated to fine-scale structural habitat heterogeneity/complexity proved to have a major impact on regional patterns of genetic differentiation in two syntopic pond breeding amphibians. This heterogeneity is a characteristic of Mediterranean landscapes with low/ medium elevations, which include extensively managed areas together with natural and/or semi-natural habitats. While it remains to be seen whether our results are generalizable to other taxa, the differences observed in our comparison regarding two taxonomically and ecologically similar taxa highlight the conservation value of these areas and point to the need of considering species individually when identifying and designing corridors connecting local populations in Mediterranean habitats.

Acknowledgements

We thank Agentes Forestales de la Comunidad de Madrid and G. Astudillo, C. Grande, J.L. Gutiérrez, A. López, J.A. Lucas, L. Martín, B. Paños, R. Pereira, E. Recuero and G. Sánchez Montes for help in sampling and T. Cuartero and V. González (Laboratorio de Biogeografía Informática, MNCN-CSIC) for support with spatial data. JGR was supported by the Consejo Superior de Investigaciones Científicas of Spain (CSIC) and the European Social Fund (ESF) (JAE-pre PhD fellowship). JG was financially supported by FCT (Portuguese Foundation for Science and Technology) through PhD grant SFRH/BD/90112/2012 funded by POPH-QREN (2007-2013). EC was also supported by FCT through Postdoctoral Grant SFRH/BPD/109182/2015 funded by CSF (2014-2020). This research was funded by grants CGL2008-04271-C02-01/BOS, and CGL2011-28300 (Ministerio de Ciencia e Innovación -MICINN-), Ministerio de Economía y Competitividad -MEC-, Spain, and FEDER) to IMS, who was also supported by funding from the Spanish Severo Ochoa Program (SEV-2012-0262).

Author contributions

Author name	Study conception and design	Sampling design, infield surveys and/or data collection	Data processing, analysis and/or modelling	Manuscript writing	Manuscript revision
J. Gutierrez	☑	☑	☑	☑	☑
J. Gonçalves	☑		☑	☑	☑
E. Civantos	☑		☑	☑	☑
I. Martínez-Solano	☑	☑		☑	☑

References

Bartelt PE, Peterson CR, Klaver RW (2004) Sexual differences in the post-breeding movements and habitats selected by western toads (*Bufo boreas*) in southeastern Idaho. *Herpetologica* **60**, 455-467.

Bates D, Maechler M, Bolker B, Walker S (2014) lme4: Linear mixed-effects models using Eigen and S4. R package version 1.1-7.

Beja P, Alcazar R (2003) Conservation of Mediterranean temporary ponds under agricultural intensification: an evaluation using amphibians. *Biological Conservation* **114**, 317-326.

Beja P, Bosch J, Tejedo M *et al.* (2009) *Pleurodeles waltl*. The IUCN Red List of Threatened Species 2009.

Beja P, Bosch J, Tejedo M *et al.* (2016) *Pelobates cultripes*. The IUCN Red List of Threatened Species 2016.

Blondel J, Aronson J (1999) *Biology and wildlife of the Mediterranean region* Oxford University Press, USA.

Bowne DR, Bowers MA (2004) Interpatch movements in spatially structured populations: a literature review. *Landscape Ecology* **19**, 1-20.

Bullón T (2016) The upper Pleistocene on the northern face of the Guadarrama Mountains (central Spain): Palaeoclimatic phases and glacial activity. *Geomorphology* **268**, 233-245.

Cejudo D (1990) Nueva altitud máxima para Pelobates cultripes. Boletín de la Asociación Herpetológica Española **1**, 20.

Cheng L, Connor TR, Sirén J, Aanensen DM, Corander J (2013) Hierarchical and Spatially Explicit Clustering of DNA Sequences with BAPS Software. *Molecular Biology and Evolution* **30**, 1224-1228.

Clarke RT, Rothery P, Raybould AF (2002) Confidence limits for regression relationships between distance matrices: Estimating gene flow with distance. *Journal of Agricultural, Biological, and Environmental Statistics* **7**, 361-372.

Corander J, Sirén J, Arjas E (2008) Bayesian spatial modeling of genetic population structure. *Computational Statistics* **23**, 111-129.

Coster SS, Babbitt KJ, Cooper A, Kovach AI (2015) Limited influence of local and landscape factors on finescale gene flow in two pond-breeding amphibians. *Molecular Ecology* **24**, 742-758.

Crawford NG (2010) SMOGD: software for the measurement of genetic diversity. *Molecular Ecology Resources* **10**, 556-557.

D'Amico M, Román J, de los Reyes L, Revilla E (2015) Vertebrate road-kill patterns in Mediterranean habitats: Who, when and where. *Biological Conservation* **191**, 234-242.

Doulgeris C, Papadimos D, Kapsomenakis J (2015) Impacts of climate change on the hydrology of two Natura 2000 sites in Northern Greece. *Regional Environmental Change*, 1-10.

Dudaniec RY, Worthington Wilmer J, Hanson JO *et al.* (2016) Dealing with uncertainty in landscape genetic resistance models: a case of three co-occurring marsupials. *Molecular Ecology* **25**, 470-486.

Engler JO, Balkenhol N, Filz KJ, Habel JC, Rödder D (2014) Comparative Landscape Genetics of Three Closely Related Sympatric Hesperid Butterflies with Diverging Ecological Traits. *PLoS ONE* **9**, e106526.

Frantz AC, Bertouille S, Eloy MC *et al.* (2012) Comparative landscape genetic analyses show a Belgian motorway to be a gene flow barrier for red deer (*Cervus elaphus*), but not wild boars (*Sus scrofa*). *Molecular Ecology* **21**, 3445-3457.

Funk WC, Blouin MS, Corn PS *et al.* (2005) Population structure of Columbia spotted frogs (*Rana luteiventris*) is strongly affected by the landscape. *Molecular Ecology* **14**, 483-496.

Funk WC, Murphy MA, Hoke KL *et al.* (2016) Elevational speciation in action? Restricted gene flow associated with adaptive divergence across an altitudinal gradient. *Journal of Evolutionary Biology* **29**, 241-252.

Funk WC, Tallmon DA, Allendorf FW (1999) Small effective population size in the long-toed salamander. *Molecular Ecology* **8**, 1633-1640.

Gao B-C (1996) NDWI—A normalized difference water index for remote sensing of vegetation liquid water from space. *Remote Sensing of Environment* **58**, 257-266.

García-París M, Montori A, Herrero P (2004) *Fauna Iberica. Vol. 24. Amphibia: Lissamphibia* Museo Nacional de Ciencias Naturales, Consejo Superior de Investigaciones Cientificas.

Giordano AR, Ridenhour BJ, Storfer A (2007) The influence of altitude and topography on genetic structure in the long-toed salamander (*Ambystoma macrodactulym*). *Molecular Ecology* **16**, 1625-1637.

Goldberg CS, Waits LP (2010a) Comparative landscape genetics of two pond-breeding amphibian species in a highly modified agricultural landscape. *Mol Ecol* **19**, 3650-3663.

Goldberg CS, Waits LP (2010b) Quantification and reduction of bias from sampling larvae to infer population and landscape genetic structure. *Molecular Ecology Resources* **10**, 304-313.

Graeter GJ, Rothermel BB, Gibbons JW (2008) Habitat Selection and Movement of Pond-Breeding Amphibians in Experimentally Fragmented Pine Forests. *The Journal of Wildlife Management* **72**, 473-482.

Green AJ, Bustamante J, Janss GFE, Fernández-Zamudio R, Díaz Paniagua C. (2016) Doñana Wetlands (Spain). In: *The Wetland Book* (Eds. Finlayson CM, Milton GR, Prentice RC, Davidson NC). Springer, Dordrecht.

Greenberg JA, Dobrowski SZ, Ustin SL (2005) Shadow allometry: Estimating tree structural parameters using hyperspatial image analysis. *Remote Sensing of Environment* **97**, 15-25.

Gutiérrez-Rodríguez J, Martínez-Solano Í (2013) Isolation and characterization of sixteen polymorphic microsatellite loci in the Western Spadefoot, Pelobates cultripes (Anura: Pelobatidae) via 454 pyrosequencing. *Conservation Genetics Resources* **5**, 981-984.

Gutiérrez-Rodríguez J, Gonzalez EG, Martínez-Solano Í (2014) Development and characterization of twelve new polymorphic microsatellite loci in the Iberian ribbed

newt, (Caudata: Salamandridae), with data on cross-amplification in *P. nebulosus*. *Amphibia-Reptilia* **35**, 129-134.

Gutiérrez-Rodríguez J, Sánchez-Montes G, Martínez-Solano Í. (2017a) Effective to census population size ratios in two Near Threatened Mediterranean amphibians: *Pleurodeles waltl* and *Pelobates cultripes. Conservation Genetics.* In press.

Gutiérrez-Rodríguez J, Barbosa AM, Martínez-Solano Í. (2017b) Present and past climatic effects on the current distribution and genetic diversity of the Iberian spadefoot toad (*Pelobates cultripes*): an integrative approach. *Journal of Biogeography* **44**, 245-258.

Gutiérrez-Rodríguez J, Barbosa AM, Martínez-Solano Í. (2017c) The relative importance of deep vs recent population history in shaping contemporary patterns of genetic diversity: an integrative study on the Ibero-Maghrebian endemic *Pleurodeles waltl* (Salamandridae). *Molecular Phylogenetics and Evolution.* Under Review.

Hewitt R, Escobar F (2011) The territorial dynamics of fast-growing regions: Unsustainable land use change and future policy challenges in Madrid, Spain. *Applied Geography* **31**, 650-667.

Igawa T, Oumi S, Katsuren S, Sumida M (2013) Population structure and landscape genetics of two endangered frog species of genus *Odorrana*: different scenarios on two islands. *Heredity* **110**, 46-56.

Jehle R, Burke T, Arntzen JW (2005) Delineating fine-scale genetic units in amphibians: probing the primacy of ponds. *Conservation Genetics* **6**, 227-234.

Jones OR, Wang J (2010) Molecular marker-based pedigrees for animal conservation biologists. *Animal Conservation* **13**, 26-34.

Jost L (2008) GST and its relatives do not measure differentiation. *Molecular Ecology* **17**, 4015-4026.

Keller D, Holderegger R, Strien MJ, Bolliger J (2014) How to make landscape genetics beneficial for conservation management? *Conservation Genetics* **16**, 503-512.

Kurz DJ, Nowakowski AJ, Tingley MW, Donnelly MA, Wilcove DS (2014) Forest-land use complementarity modifies community structure of a tropical herpetofauna. *Biological Conservation* **170**, 246-255.

López-Sáez JA, Abel-Schaad D, Pérez-Díaz S *et al.* (2014) Vegetation history, climate and human impact in the Spanish Central System over the last 9000 years. *Quaternary International* **353**, 98-122.

Martínez-Solano Í (2006) Atlas de distribución y estado de conservación de los anfibios de la Comunidad de Madrid. *Graellsia* **62**, 253-291.

Meirmans PG, Van Tienderen PH (2004) genotype and genodive: two programs for the analysis of genetic diversity of asexual organisms. *Molecular Ecology Notes* **4**, 792-794.

Meirmans PG, Hedrick PW (2011) Assessing population structure: F_{ST} and related measures. *Molecular Ecology Resources* **11**, 5-18.

Montori A, Llorente GA, Santos X, Carretero MA (2002) *Pleurodeles waltl* Michahelles, 1830. Gallipato. In: *Atlas y libro rojo de los anfibios y reptiles de España* (eds. Pleguezuelos JM, Márquez R, Lizana M), pp. 51-54. Dirección General de Conservación de la Naturalez-Asociación Herpetológica Española, Madrid.

Muscarella RA, Murray KL, Ortt D, Russell AL, Fleming TH (2011) Exploring Demographic, Physical, and Historical Explanations for the Genetic Structure of Two Lineages of Greater Antillean Bats. *PLoS ONE* **6**, e17704.

Nagendra H, Lucas R, Honrado JP *et al.* (2013) Remote sensing for conservation monitoring: Assessing protected areas, habitat extent, habitat condition, species diversity, and threats. *Ecological Indicators* **33**, 45-59.

Nicholson E, Possingham HP (2006) Objectives for Multiple-Species Conservation Planning. *Conservation Biology* **20**, 871-881.

Nowakowski AJ, DeWoody JA, Fagan ME, Willoughby JR, Donnelly MA (2015) Mechanistic insights into landscape genetic structure of two tropical amphibians using field-derived resistance surfaces. *Molecular Ecology* **24**, 580-595.

Olsen J, Crane P, Flannery B *et al.* (2011) Comparative landscape genetic analysis of three Pacific salmon species from subarctic North America. *Conservation Genetics* **12**, 223-241.

Ortego J, García-Navas V, Noguerales V, Cordero PJ (2015) Discordant patterns of genetic and phenotypic differentiation in five grasshopper species codistributed across a microreserve network. *Molecular Ecology* **24**, 5796-5812.

Peakall R, Smouse PE (2012) GenAlEx 6.5: genetic analysis in Excel. Population genetic software for teaching and research—an update. *Bioinformatics* **28**, 2537-2539.

Pérez-Espona S, Pérez-Barbería FJ, McLeod JE *et al.* (2008) Landscape features affect gene flow of Scottish Highland red deer (*Cervus elaphus*). *Molecular Ecology* **17**, 981-996.

Peterman W, Anderson T, Ousterhout B *et al.* (2015) Differential dispersal shapes population structure and patterns of genetic differentiation in two sympatric pond breeding salamanders. *Conservation Genetics* **16**, 59-69.

Peterman WE (2014) ResistanceGA: An R package for the optimization of resistance surfaces using genetic algorithms. *bioRxiv*. doi: http://dx.doi.org/10.1101/007575

Peterman WE, Connette GM, Semlitsch RD, Eggert LS (2014) Ecological resistance surfaces predict fine-scale genetic differentiation in a terrestrial woodland salamander. *Molecular Ecology* **23**, 2402-2413.

Phillipsen IC, Kirk EH, Bogan MT *et al.* (2015) Dispersal ability and habitat requirements determine landscape-level genetic patterns in desert aquatic insects. *Molecular Ecology* **24**, 54-69.

Quinn PF, Beven KJ, Lamb R (1995) The in(a/tan/β) index: How to calculate it and how to use it within the topmodel framework. *Hydrological Processes* **9**, 161-182.

R Core Team (2014) R: A language and environment for statistical computing. R Foundation for Statistical Computing, Vienna, Austria.

Raymond M, Rousset F (1995) GENEPOP (Version 1.2): Population Genetics Software for Exact Tests and Ecumenicism. *Journal of Heredity* **86**, 248-249.

Rice WR (1989) Analyzing Tables of Statistical Tests. *Evolution* **43**, 223-225.

Richardson JL (2012) Divergent landscape effects on population connectivity in two co-occurring amphibian species. *Molecular Ecology* **21**, 4437-4451.

Rousset F (2008) genepop'007: a complete re-implementation of the genepop software for Windows and Linux. *Molecular Ecology Resources* **8**, 103-106.

Savage WK, Fremier AK, Bradley Shaffer H (2010) Landscape genetics of alpine Sierra Nevada salamanders reveal extreme population subdivision in space and time. *Molecular Ecology* **19**, 3301-3314.

Schwenk WS, Donovan TM (2011) A Multispecies Framework for Landscape Conservation Planning. *Conservation Biology* **25**, 1010-1021.

Sillero N, Brito JC, Skidmore AK, Toxopeus AG (2009) Biogeographical patterns derived from remote sensing variables: the amphibians and reptiles of the Iberian Peninsula. *Amphibia Reptilia* **30**, 185-206.

Smith MA, Green DM (2005) Dispersal and the metapopulation paradigm in amphibian ecology and conservation: are all amphibian populations metapopulations? *Ecography* **28**, 110-128.

Steele CA, Baumsteiger J, Storfer A (2009) Influence of life-history variation on the genetic structure of two sympatric salamander taxa. *Molecular Ecology* **18**, 1629-1639.

Storfer A, Murphy MA, Evans JS *et al.* (2007) Putting the "landscape" in landscape genetics. *Heredity* **98**, 128-142.

Tachikawa T, Hato M, Kaku M, Iwasaki A (2011) Characteristics of ASTER GDEM version 2, 3657-3660.

Tejedo M, Reques R (2002) *Pelobates cultripes* (Cuvier, 1829). Sapo de espuelas. In: *Atlas y libro rojo de los anfibios y reptiles de España* (eds. Pleguezuelos JM, Márquez R, Lizana M), pp. 94-96. Dirección General de Conservación de la Naturaleza-Asociación Herpetológica Española, Madrid.

Turner W, Spector S, Gardiner N *et al.* (2003) Remote sensing for biodiversity science and conservation. *Trends in Ecology & Evolution* **18**, 306-314.

Van de Vliet MS, Diekmann OE, Serrão EA, Beja P (2009) Isolation of highly polymorphic microsatellite loci for a species with a large genome size: sharp-ribbed salamander (*Pleurodeles waltl*). *Molecular Ecology Resources* **9**, 425-428.

Van Etten J (2015) gdistance: distances and routes on geographical grids. R package version 1.1-7.

Van Oosterhout C, Hutchinson WF, Wills DPM, Shipley P (2004) MICRO-CHECKER: software for identifying and correcting genotyping errors in microsatellite data. *Molecular Ecology Notes* **4**, 535-538.

Van Strien MJ, Keller D, Holderegger R (2012) A new analytical approach to landscape genetic modelling: least-cost transect analysis and linear mixed models. *Molecular Ecology* **21**, 4010-4023.

Wang J (2004) Sibship Reconstruction From Genetic Data With Typing Errors. *Genetics* **166**, 1963-1979.

Wang J (2015) Does GST underestimate genetic differentiation from marker data? *Molecular Ecology* **24**, 3546-3558.

Weir BS, Cockerham CC (1984) Estimating F-statistics for the analysis of population structure. *Evolution*, 1358-1370.

Whiteley A, McGarigal K, Schwartz M (2014) Pronounced differences in genetic structure despite overall ecological similarity for two *Ambystoma* salamanders in the same landscape. *Conservation Genetics* **15**, 573-591.

Wilson GA, Rannala B (2003) Bayesian inference of recent migration rates using multilocus genotypes. *Genetics* **163**, 1177-1191.

Wulder MA, Hall RJ, Coops NC, Franklin SE (2004) High Spatial Resolution Remotely Sensed Data for Ecosystem Characterization. *BioScience* **54**, 511-521.

Zancolli G, Rödel M-O, Steffan-Dewenter I, Storfer A (2014) Comparative landscape genetics of two river frog species occurring at different elevations on Mount Kilimanjaro. *Molecular Ecology* **23**, 4989-5002.

Sub-section II.2. Species level – Model-based assessment of habitat suitability dynamics and vulnerability to global change

Chapter 5 - Exploring the spatiotemporal dynamics of habitat suitability to improve conservation management of a vulnerable plant species

Author list: **João Gonçalves** (1), Paulo Alves (1), Isabel Pôças (2), Bruno Marcos (1), Rita Sousa-Silva (3), Ângela Lomba (1), João Pradinho Honrado (1,4)

(1) InBIO/CIBIO-Centro de Investigação em Biodiversidade e Recursos Genéticos, Campus Agrário de Vairão, Universidade do Porto, 4485-601 Vairão, Portugal
(2) LEAF – Linking Landscape, Environment, Agriculture and Food, Instituto Superior de Agronomia, Universidade de Lisboa, Tapada da Ajuda, 1349-017 Lisboa, Portugal; Centro de Investigação em Ciências Geo-Espaciais, Universidade do Porto, Portugal
(3) Division of Forest, Nature and Landscape, Department of Earth and Environmental Sciences, KU Leuven – University of Leuven, BE-3001 Leuven, Belgium
(4) Faculdade de Ciências da Universidade do Porto, Edifício FC4 (Biologia), Rua do Campo Alegre, s/n, 4169-007 Porto, Portugal

DISCLAIMER

This manuscript is an original contribution of this thesis published in *Biodiversity and Conservation* journal under the same title. Gonçalves, J., lead the work with contributions from all co-authors.

ABSTRACT

Ongoing declines in biodiversity caused by global environmental changes call for adaptive conservation management, including the assessment of habitat suitability spatiotemporal dynamics potentially affecting species persistence. Remote Sensing (RS) provides a wide-range of satellite-based environmental variables that can be fed into Species Distribution Models (SDMs) to investigate species-environment relations and forecast responses to change.

We address the spatiotemporal dynamics of species' habitat suitability at the landscape level by combining multi-temporal RS data with SDMs for analysing inter-annual habitat suitability dynamics.

We implemented this framework with a vulnerable plant species (*Veronica micrantha*), by combining SDMs with a time-series of RS-based metrics of vegetation functioning related to primary productivity, seasonality, phenology and actual evapotranspiration. Besides RS variables, predictors related to landscape structure, soils and wildfires were ranked and combined through Multi-Model Inference (MMI). To assess recent dynamics, a habitat suitability time-series was generated through model hindcasting.

MMI highlighted the strong predictive ability of RS variables related to primary productivity and water availability for explaining the test-species distribution, along with soil, wildfire regime and landscape composition. The habitat suitability time-series revealed the effects of short-term land cover changes and inter-annual variability in climatic conditions. Multi-temporal SDMs further improved predictions, benefiting from RS time-series.

Overall, results emphasize the integration of landscape attributes related to function, composition and spatial configuration for improving the explanation of ecological patterns. Moreover, coupling SDMs with RS functional metrics may provide early-warnings of future environmental changes potentially impacting habitat suitability. Applications discussed include the improvement of biodiversity monitoring and conservation strategies.

5.1. Introduction

Despite the increasing number of conservation initiatives, the rate of biodiversity loss does not appear to be diminishing, nor do the pressures upon species and their habitats (Butchart et al. 2010). Recent quantitative scenarios of biodiversity change consistently indicate that this decline will continue throughout the 21st century, with global environmental changes and land-use shifts driving alterations in terrestrial ecosystems (Pereira et al. 2010). As a response, the Aichi Biodiversity Targets for 2011–2020 were devised by parties of the Convention for Biological Diversity (CBD 2010) and supported the definition of new conservation targets for 2020 in Europe (European Union 2011). Measuring progress towards these goals is therefore crucial and requires robust and long-term monitoring data on status and trends to assess habitat changes potentially impacting biodiversity (Magurran et al. 2010).

Effective local-scale conservation requires an accurate identification of habitat areas supporting species at higher risk of decline, as well as an assessment of how land management constrains or contributes to maintain viable populations of wild species (Prendergast et al. 1999). As such, identifying the drivers determining species distributions is at the core of applied ecological research aimed to prevent further loss of biodiversity (Butchart et al. 2010). Species Distribution Models (SDMs) combine observations of species occurrence or abundance with the spatial representation of environmental factors to predict species distributions (Guisan and Zimmerman 2000, Elith and Leathwick 2009). They are widely used to describe patterns, to deliver spatiotemporal predictions at several scales (Elith and Leathwick 2009) and to address fundamental questions such as the ecological impacts of climate and land-use changes (Broennimann et al. 2006). SDMs have also shown their potential for management and conservation of vulnerable and rare species, for which distribution data are often scarce, biased and/or incomplete (Guisan et al. 2006, Lomba et al. 2010, Gogol-Prokurat 2011, Sousa-Silva et al. 2014).

Remote Sensing (RS) has strongly contributed to improve ecosystems and biodiversity monitoring as well as the development of SDMs (Bradley and Fleishman 2008, Nagendra et al. 2013, He et al. 2015, Skidmore et al. 2015). By providing repeated and synoptic measures of the Earth surface, RS offers a cost-effective approach to measure biodiversity and predict changes in species composition (Rocchini et al. 2016). Technologies based on RS can also provide data on habitat quantity and quality, with positive feedbacks for conservation management (Mairota et al. 2015, Vaz et al. 2015). RS data products, available at multiple spatial and temporal resolutions, from multi- or

hyperspectral sensors, as well as, LiDAR (Light Detection and Ranging) and RADAR missions can further improve SDM performance and form the backbone for next-generation SDMs (He et al. 2015). Often, satellite data are used in the form of spectral vegetation indices, which are mathematical combinations of two or more spectral bands selected to describe the biophysical parameters of interest (Jones and Vaughan 2010). The Normalised Difference Vegetation Index (NDVI) is one of the most widely used vegetation indices in ecological applications (Pettorelli et al. 2014). NDVI is regarded as a proxy of chlorophyll content in plants, or vegetation vigour, and indirectly of aboveground net primary production, absorbed photosynthetically active radiation (Kerr and Ostrovsky 2003) and leaf area index (Wang et al. 2005).

Currently available time-series of satellite data with high-temporal resolutions (such as those available from the MODerate Resolution Imaging Spectroradiometer, MODIS) greatly enhance the ability to assess and monitor both inter-annual (e.g. trends, landscape change) and intra-annual (e.g. seasonal changes, phenology) aspects of vegetation and ecosystem dynamics (Heumann et al. 2007, Cabello et al. 2012, Pettorelli et al. 2014). Various metrics of vegetation functioning, either related with overall productivity/biomass (e.g., maximum annual value, relative range) or with phenology (e.g., dates of the start, end and peak of the growing-season), can be derived from NDVI time-series (Jönsson and Eklundh 2004, Alcaraz et al. 2006). These metrics were successfully used, for example, to model tree species distribution (Cord et al. 2014), to assess phenological changes (Jönsson et al. 2010), and to predict breeding bird species richness (Coops et al. 2009). Besides vegetation indices, other RS-based variables have been used for characterizing vegetation response, such as evapotranspiration (Pôças et al. 2013). MODIS products currently available also include an actual evapotranspiration dataset (Mu et al. 2011) with high-temporal resolution, which can also be used in SDM applications.

RS ability to inform on ecosystem and landscape dynamics is a valuable asset to anticipate changes in the status of threatened species and habitats (Cabello et al. 2012). For vulnerable species, integrative approaches combining RS and SDM can improve inference and prediction at the landscape level (Parviainen et al. 2013). Although much effort has been employed in developing methods to spatially predict habitat suitability for vulnerable and/or rare plant species at multiple spatial scales (Lomba et al. 2010, Gogol-Prokurat 2011), the effects of short-term environmental fluctuations on habitat suitability, distribution and abundance of those species are seldom addressed.

Here we describe a framework combining SDMs, landscape structural metrics and a time-series of remotely-sensed proxies of vegetation functioning to predict inter-annual variations in habitat suitability at the landscape level. The approach was implemented with *Veronica micrantha,* an Iberian endemic plant species with "vulnerable" conservation status and protected under European and National law. Our overarching goals were: i) to assess and rank the predictive ability of RS variables related to vegetation functioning and actual evapotranspiration, as well as of variables related to landscape structural features, fire regime and soils to explain the distribution of the test-species, and to combined them through model-averaging; ii) to evaluate temporal variations in habitat suitability by performing model hindcasting and thereby generating a time-series of habitat suitability; iii) to assess the added-value of this time-series of habitat suitability by comparing the model performance of single-year vs. multi-temporal averaged predictions; and iv) to explore potential causes for inter-annual changes in habitat suitability related to alterations in precipitation, temperature, and land cover/use. Finally, we discuss the potential of our framework to improve the monitoring of vulnerable species and to support local conservation planning and management, while discussing potential caveats and perspectives for future developments and applications.

5.2. Methods

Study area and test-species distribution

The study area is located in northern Portugal bounded by 7.785°W to 7.471°W longitude and 41.391°N to 41.640°N latitude. It comprises the full extent of *Vila Pouca de Aguiar* municipality with an area of roughly 437 km^2 (Figure 5 - 1). The elevation ranges from 225m a.s.l. in the valley areas to 1200m in the mountain tops (Appendix II – S1).

Veronica micrantha Hoffmanns & Link (Scrophulariaceae; hereafter *V. micrantha*) is a perennial herbaceous plant with flowering typically occurring from May to July. Pollination is commonly entomophilous and the plant does not display a specific strategy for seed dispersal. It is an endemic species which distribution is restricted to the central- and north-western Iberian Peninsula (Sousa-Silva et al. 2014). In Portugal it occurs in the northern and centre regions, with approximately 500 reported individuals (CEC 2009). Our study-area encompasses some of the most central and large populations, hence its significance for the conservation of the species. The species has been reported to occur in open-spaces of deciduous woodland landscape matrices, heaths and herbaceous communities of forest fringes and riparian galleries, preferring shaded biotopes with humid soils (Peraza Zurita 2011, Sousa-Silva et al. 2014). Under the rainier

conditions of the temperate Atlantic climate, *V. micrantha* also occurs in ruderal areas along rural tracks with forb vegetation.

Listed in the Habitats Directive (92/43/EEC of 21 May 1999, Annex II), *V. micrantha* is considered an important asset by both European and National laws. However, due to low number of individuals, fragmented subpopulations, and recorded decreasing trends in population size, *V. micrantha* is listed as *Vulnerable* in the 2011 IUCN Red List of Vascular Plants, with forest exploitation and conversion, and roads highlighted as main threats (Bilz et al. 2011, Peraza Zurita 2011).

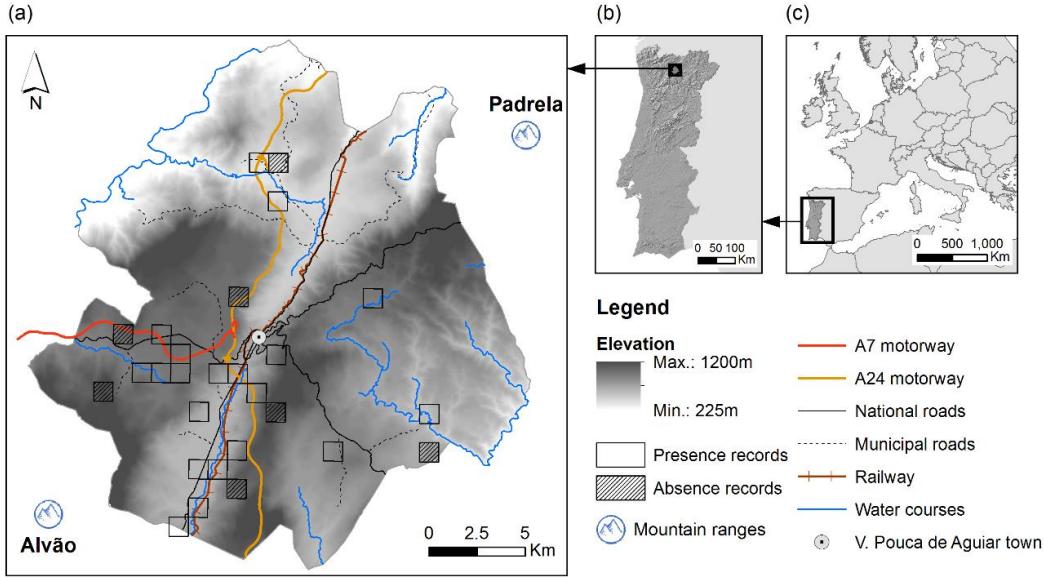

Figure 5 - 1 – Main features of the study-area (a) and its location in mainland Portugal (b) and in Europe (c).

Field data collection and sampling

SDMs were used to increase sampling efficiency and detectability as suggested by recent research (Guisan et al. 2006, Le Lay et al. 2010). Pre-existing *V. micrantha* distribution data for northern Portugal, collected mostly from herbaria sources, totalling 38 presence records represented in a 1km^2 regular grid, were used to develop a preliminary presence-only MaxEnt model (Phillips and Dudík 2008). A good predictive accuracy was obtained with the preliminary model (AUC=0.81; Appendix II – S2). This model was spatially projected and used to select 32 sampling locations in the study-area, with selection probabilities proportional to habitat suitability which allowed maximizing detection probability.

Field campaigns to collect new data were performed during Spring and early Summer of 2011. An approximately linear transect along each 1km^2 quadrat diagonal was followed with controlled time for standardizing surveying effort proportionally to the

landscape heterogeneity. Different land cover categories, occurring throughout the transect path, were surveyed to maximize the coverage of different vegetation and environmental conditions. When required, specific locations/habitats outside the diagonal where surveyed if the probability of occurrence was presumably high, following the assessment by experienced field botanists and supported by ancillary GIS data for the study-area. During fieldwork, five locations which were considered inaccessible for complete surveying were discarded. A total of 27 records were available after field surveys including 20 presence records and 7 absences.

Multi-model inference – hypothesis definition and variable selection

Multi-model inference (MMI), based on measures such as the Akaike Information Criterion (AIC), enables comparing and ranking multiple competing models (Burnham and Anderson 2002, Burnham et al. 2011, Symonds and Moussalli 2011). MMI requires an *a priori* definition of multiple competing hypotheses, ideally fewer than the sample size (Burnham et al. 2011). In this study, competing hypotheses were supported by previous research, literature review (Table 5 - 1 and, Appendix II – S3 for further details), expert-knowledge, as well as observations during in-field surveys regarding *V. micrantha* ecological requirements and distribution.

Predictor variables used in model development

The selection of predictor variables focused on landscape level ecological determinants of the test-species distribution related to vegetation functioning dynamics (VFD), landscape composition (percentage cover of certain land cover types) and configuration (spatial arrangement of landscape elements), water availability, soil types, and fire regime (Table 5 - 1). Modelling procedures were performed on a regular grid with 1km^2 units, following the available resolution for some of the predictor variables as well as for *V. micrantha* records. To examine multicollinearity effects, predictors were tested for pair-wise correlations using Spearman's correlation coefficient and Variance Inflation Factors (VIF; Appendix II – S4 and S5). All pairwise correlations had an absolute value below 0.6 and thus predictors were all kept for subsequent analyses. In addition, no $\sqrt{VIF} > 2$ was found in competing models signalling low to moderate multicollinearity.

Table 5 - 1 – Predictor variables related to each hypothesis/model. Types of variables according to their spatiotemporal variability: DN – dynamic predictors, SD – semi-dynamic predictors and, ST – static predictors.

Hypothesis/ Model	Predictors	Rationale	References
M1: Vegetation functioning dynamics – productivity	MAXVL (DN) AMPLT (DN)	The properties of annual NDVI time-series can be summarized in a set of metrics with the ability to dynamically and synoptically capture changes in phenology and productivity of earth ecosystems and provide insights about habitat quality. These metrics were divided in two types of measures: (i) productivity (M1; MAXVL – peak value; AMPLT – seasonal amplitude), and, (ii) phenology (M2; MIDSN – mid of growing season, in days; START – start of season, in days)	Zimmermann et al. (2007) Bradley and Fleishman (2008) Ivits *et al.* (2011) Cord *et al.* (2014)
M2: Vegetation functioning dynamics – phenology	MIDSN (DN) START (DN)		
M3: Landscape composition	PAGFO (SD) PURBD (SD)	Several studies have shown the importance of landscape pattern, in particular of landscape composition and configuration for predicting the distribution, relative abundance, and richness of different species. Given this we considered two models related to: (i) landscape composition (M3; PAGFO - % covered by agroforestry; PURBD - % covered by discontinuous low-density urban-rural areas) and spatial configuration (M4; MEDPS – median patch size in m^2; TEDGE – Total patch edge, in meters considering all land cover categories)	Lomba *et al.* (2010) Thornton *et al.* (2011) Sousa-Silva et al. (2014)
M4: Landscape configuration	MEDPS (SD) TEDGE (SD)		
M5: Soil type	PCAMB (ST)	Recent works using SDMs have shown the relevance of predictor variables related to soil type or soil attributes to enhance rare species predictions at a local scale. Soil related variables (e.g., % cover of cambisols; PCAMB) were included in M5.	Wiser *et al.* (1998) Lomba *et al.* (2010) Gogol-Prokurat (2011)
M6: Water availability	EVPTR (DN) RDENS (ST)	Actual evapotranspiration (EVPTR) is an important element of energy and water balance conveying important constraints on water availability at the land surface. Therefore, EVPTR influences ecosystem parameters and processes such as soil moisture content, vegetation productivity, water balance, and ecosystem nutrient, highlighting the interactions between EVPTR and several other earth-system processes (M6). River density in each grid unit (RDENS, in $m.km^{-2}$) was also used as a proxy for water availability and soil moisture.	Hawkins *et al.* (2003) Wever *et al.* Fisher *et al.* (2011)
M7: Fire regime	ABURN (ST) BTRND (ST)	The effects of wildfires are of particular importance in Mediterranean landscapes where they exert a strong influence on its structure, functioning and dynamics. Fire regime components (frequency, season, intensity) significantly influence the composition and diversity of plant communities at the local scale. This effect was considered in M7 (ABURN – average burned area between 2001 and 2010; BTRND – burned area trend for the same period).	Bowman and Murphy Gogol-Prokurat (2011) Reside *et al.* (2012)
M8: Intercept-only		This model including a single intercept-term was used as a baseline comparison for model fitting.	-

Predictor variables were categorized into three groups: static, semi-dynamic, and dynamic. In the static group (Table 5 - 1), we considered those that either varied over geologic time (soil types, river density) or that were based on the analysis of a fixed time period (e.g., fire regime). In both cases, only a single block was used to cover the entire time-frame being analysed. For the distribution of soil types, the percentage cover of cambisols for each grid unit was calculated (PCAMB). To capture the indirect proximal effects of rivers on soil moisture and nutrient content levels we calculated the density of main rivers (RDENS, in $m.km^{-2}$). To analyse fire regime effects, data from the National Forest Fires Database (AFN 2011) was used to calculate the average area burned per year, between 2000 and 2009, for each grid unit (ABURN, in m^2). Finally, to portray the temporal tendency of burned area, we used the trend slope (BTRND, in $m^2.year^{-1}$) for the same period using Sen-Theil's method (Sen 1968).

Dynamic variables tend to display moderate to strong temporal fluctuations, as in the case of variables related to VFD and evapotranspiration. For dynamic variables, we considered a number of blocks equal to the number of time-steps, totalling 10 years for the interval 2001-2010. VFD metrics, calculated from NDVI time-series, were used as proxy measures of vegetation properties related to productivity (e.g., maximum or mean annual value), seasonality (e.g., intra-annual range) and phenology (e.g., start or end of the growing-season) potentially related to *V. micrantha* habitat requirements at the landscape level. The computation of VFD metrics was based on Jönsson and Eklundh (2004), using free and open-access products derived from MODIS satellite data. Composites of 16-days of MODIS NDVI (MOD13Q1 product), with spatial resolution of 250m, were used for each year of the 2001-2010 studied period. The double-logistic function-fitting method was applied to reduce noise effects on data, generating a smoothed NDVI curve for each year which was used to calculate VFD metrics (Heumann et al. 2007, Eklundh and Jönsson 2010). These two procedures were performed using the TIMESAT software (Jönsson and Eklundh 2004). Based on their intrinsic ecological properties and on exploratory statistical analysis (not shown), four VFD metrics were selected as predictor variables. All metrics were multiplied by 10^4 and used as integers in modelling procedures. The maximum value for the fitted function during the growing season (MAXVL) and seasonal amplitude (AMPLT) were selected to represent primary productivity. The time for the start of the growing-season (START, in days) and the time for the mid of the growing-season (zonal maximum; MIDSN, in days) were selected to represent phenology. All VFD variables were up-scaled to the same spatial resolution of species records (1000m) using the mean (for AMPLT and START) or the maximum (for MAXVL and MIDSN). Finally, to characterize water availability we used the MODIS

MOD16A3 actual evapotranspiration (EVPTR in $mm.year^{-1}$) product, computed according to Mu et al. (2011) with a spatial resolution of 1000m comprising the studied period between 2001 and 2010.

Semi-dynamic variables comprised that exhibiting low to moderate temporal variability or which are unavailable for all the time-steps used for modelling (e.g., land cover). In this case, two blocks covering the periods 2001-2005 and 2006-2010 were considered. To analyse the effects of landscape structure on the test-species distribution, several landscape pattern statistics were calculated for each grid unit. A modified version of Corine Land Cover (Appendix II – S6) available for mainland Portugal for years 2000 and 2006 was used. For landscape composition, we calculated the percentages covered by agroforestry mosaics (PAGFO) and discontinuous low-density urban-rural areas (PURBD). For capturing landscape spatial configuration, median patch size (MEDPS, in m^2) and the total length of patch edges (TEDGE, in m) were used.

For each previously specified hypotheses we devised a single model (Table 5 - 1 and Appendix II – S3) as recommended in Burnham et al. (2011). In this step, we also linked each predictor variable to its corresponding hypothesis/model thus providing a basis for model fitting procedures. For baseline comparison purposes, we used an intercept-only model (M8).

Model development

Species occurrence (presence/absence) was related to predictor variables for the reference year of 2010 (Figure 5 - 2) using Generalized Additive Models (GAMs). GAMs are an extension of generalized linear models recognized as a powerful and versatile method (Guisan and Zimmerman 2000, Guisan et al. 2002) due to their ability to include non-linear and asymmetric responses in species-environment relations. For this purpose, we used the R package *mgcv* (Wood 2006), which includes a penalized regression spline approach with automatic smoothness selection (Wood 2004), to reduce overfitting problems. A maximum basis dimension equal to 2 was set for smooth terms, and bivariate models were combined through multi-model averaging, as described Lomba et al. (2010) to further prevent overfitting.

For model comparison and ranking we used Akaike Information Criterion with a correction for finite sample size (AICc), following Symonds and Moussalli (2011). In order to rank competing models, ΔAICc was calculated to build four groups discriminated by their support to explain *V. micrantha* distribution patterns *viz.*, substantial support: $\Delta AICc \leq 2$; some support: $2 < \Delta AICc \leq 7$; little support: $7 < \Delta AICc \leq 10$; no support: $\Delta AICc > 10$

(Burnham and Anderson 2002). Multi-model averaging was performed using the "*natural averaging*" procedure (sensu Burnham and Anderson 2002) combining all models within the confidence set, *i.e.,* for which ΔAICc<2 through a weighted-average using Akaike weights.

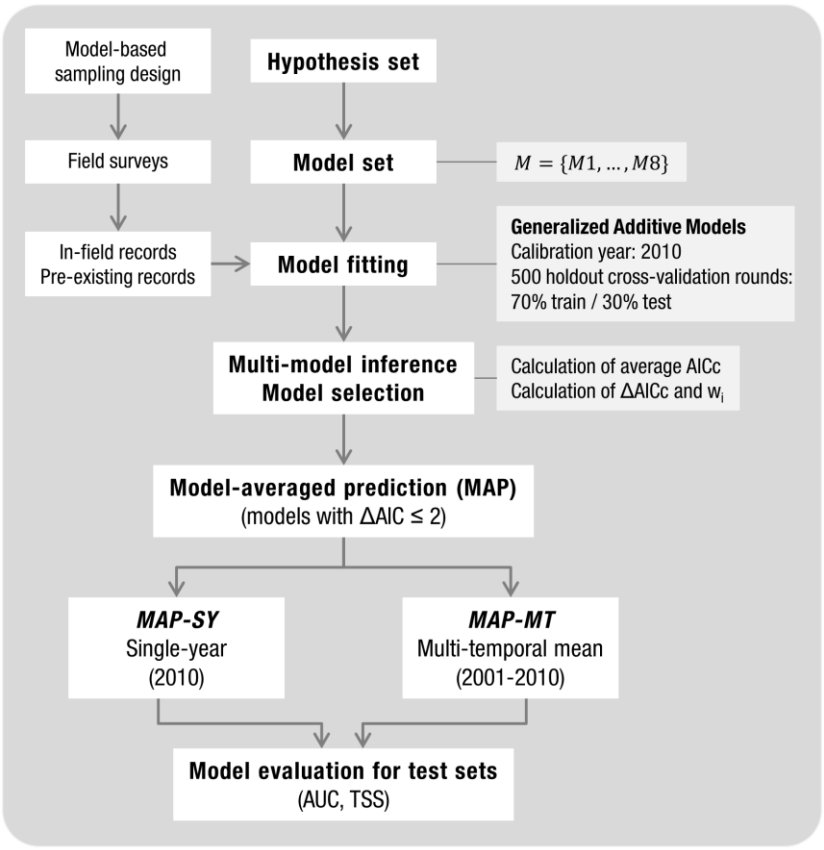

Figure 5 - 2 – Flowchart representing model development to evaluate the spatiotemporal dynamics of habitat suitability and to address the added-value of multi-temporal data.

In order to fully evaluate the competing models as well as the averaged-model, MMI procedures were integrated with holdout cross-validation (Figure 5 - 2). To perform the holdout cross-validation, 500 evaluation rounds were implemented with a data split of 70% for model training and 30% for testing, and balancing the number of presences and absences. After these rounds, we estimated the AICc using the mean (across all rounds) and from this other MMI parameters were calculated, namely: ΔAICc and the Akaike weights (w_i).

Competing models goodness-of-fit was assessed through Nagelkerke's generalized coefficient of determination (R^2) and deviance (D^2) averaged across all holdout cross-validation rounds.

To assess performance of competing and averaged models, the Area Under the Receiver Operating Curve (AUC) and the True-skill statistic (TSS) were calculated for the test set.

In order to transform predicted probabilities into suitable/unsuitable areas we used a threshold minimizing the straight-line distance between the receiver operating curve plot and the upper-left corner of the unit square (Freeman and Moisen 2008).

Inter-annual analysis of habitat suitability

To assess the added-value of including multi-temporal RS variables with SDM, two types of model-averaged predictions (MAP) were tested: (i) single-year predictions using data solely for the calibration year of 2010; and, (ii) a multi-temporal mean, by model hindcasting and then averaging predictions across the entire 2001-2010 time-series. This was accomplished by replacing dynamic and semi-dynamic predictors at each time-step (Table 5 - 1 and Figure 5 - 2). These two types of MAPs were then evaluated and compared through holdout cross-validation for the same test sets used for assessing competing models.

Considering all areas predicted as suitable at least one time between 2001 and 2010, linear regression and Pearson's pairwise correlation (ρ) were used to investigate the association between inter-annual anomalies in RS variables (MAXVL, EVPTR) and anomalies in average temperature of the coldest month and total annual precipitation (collected from E-OBS, www.ecad.eu/E-OBS/; and IPMA, https://www.ipma.pt; visited Dec-2014). We also analyzed the relation between anomalies in RS variables (MAXVL, AMPLT and EVPTR) on the amount of area predicted as suitable for each year. Anomalies were calculated by subtracting the median value (between 2001-2010) to annual values. The effect of disturbances, such as motorway construction and wildfires, on VFD metrics and actual evapotranspiration was also evaluated by comparing areas that were either affected or unaffected by those disturbances.

5.3. Results

Performance of competing models

As measured by Deviance (D^2) and R-squared (R^2) statistics, which yielded very similar results, individual competing models explained variation in sample data reasonably well, with models M1 (D^2 and R^2 of 0.55 and 0.66, respectively), M6 (0.51, 0.65) and M7 (0.53, 0.66) obtaining the best scores (Table 5 - 2). These results were generally consistent

with the AICc ranking, with exceptions for M5 (0.29, 0.55) and M3 (0.44, 0.62), although comparisons must be restricted due to the different degrees of freedom in competing models. The AUC evaluation (average value across all test sets) displayed relatively similar results, with competing models' performance going from fair (M2, M3, M4, M5, M7, AUC=0.74 to 0.79) to good (M1, AUC=0.81 and M6, AUC=0.85). The intercept-only model (M8) revealed no predictive ability regardless of the performance statistic.

Multi-model inference: model ranking and averaging

MMI results (Table 5 - 2) revealed high uncertainty from competing models, thus supporting the use of model-averaging procedures with Akaike weights [w_i=(0, 1)] defining the relative contribution of each competing model to averaged predictions. In decreasing order of support, competing models M1 (VFD-Productivity; ΔAICc=0.00, w_i=0.25), M6 (Water availability; ΔAICc=0.42, w_i=0.20), M5 (Soils; ΔAICc=0.61, w_i=0.18), M7 (Fire disturbance; ΔAICc=1.25, w_i=0.13) and M3 (Landscape composition; ΔAICc=1.59, w_i=0.11) obtained substantial support and were thus included in the confidence set, later used for multi-model averaging. Competing models M2 (VFD-Phenology; ΔAICc=2.76, w_i=0.06) and M4 (Landscape configuration; ΔAICc=3.50, w_i=0.04) obtained comparatively much less support. The intercept-only model (M8) obtained the lowest support (ΔAICc=4.53, w_i=0.03).

Table 5 - 2 – Model ranking and selection table; K – number of parameters (this value equals the sum of the degrees of freedom for each smoothing spline in the model plus the intercept term; the exception is M8 which has only one parameter), LogLik – log likelihood, AICc – Akaike's Information Criterion value (with finite sample size correction), ΔAICc – delta AICc, wi – Akaike weights, D2 – deviance, R2 – Nagelkerke's R-squared; AUC – Area Under the Receiver Operating Curve and, TSS –True-skill statistic calculated for the test set. With exception of ΔAICc and wi, all values in the table present the average across all 500 cross-validation rounds.

Model code	Model hypothesis	K	LogLik	AICc	ΔAICc	w_i	D^2	R^2	AUC	TSS
M1	VFD (productivity)	3.66	-4.94	19.61	0.00	0.25	0.55	0.66	0.81	0.67
M6	Water availability	3.50	-5.42	20.02	0.42	0.20	0.51	0.65	0.85	0.78
M5	Soils	2.00	-7.73	20.22	0.61	0.18	0.29	0.55	0.76	0.70
M7	Fire disturbance	3.92	-5.11	20.86	1.25	0.13	0.53	0.66	0.79	0.57
M3	Landscape composition	3.39	-6.17	21.19	1.59	0.11	0.44	0.62	0.75	0.62
M2	VFD (phenology)	3.19	-7.07	22.36	2.76	0.06	0.35	0.58	0.76	0.66
M4	Landscape configuration	3.07	-7.64	23.11	3.50	0.04	0.30	0.55	0.74	0.59
M8	Intercept-only	1.00	-10.95	24.14	4.53	0.03	0.00	0.38	0.50	0.00

Regarding the model-averaged predictions, although good results were attained for single-year predictions (AUC=0.88, TSS=0.82), the inclusion of RS data in multi-temporal predictions further increased model accuracy (AUC=0.95, TSS=0.92) (Table 5 - 3).

Table 5 - 3 – Evaluation statistics for the two types of model-averaged predictions (MAP): (i) single-year prediction (using only the calibration year of 2010), and, (ii) model-averaged predictions with the multi-temporal mean (average predictions for 2001-2010). Performance statistics: AUC – area under the receiver operating curve, and, TSS – true-skill statistic, were aggregated using the mean and standard-deviation across all 500-holdout cross-validation rounds.

Test of MAP	Evaluation metric	Average	Standard-deviation
Single-year	AUC	0.88	0.16
	TSS	0.82	0.22
Multi-temporal mean	AUC	0.95	0.08
	TSS	0.92	0.14

Determinants and inter-annual fluctuations of habitat suitability at the landscape level

A substantial portion of the study-area was considered suitable for the test species, at least at one time-step of the focal period (63%). However, when focusing on areas most often predicted, this area decreased considerably (only 21% for the entire focal period), as well as the spatial contiguity of suitable habitat (Figure 5 - 3). Suitable areas are generally distributed along low-elevation areas and valleys, often close to rivers or areas with high water availability, and locations with high productivity and seasonality dynamics. Suitable areas are also related to agroforestry mosaics (with dispersed and intermixed agricultural and forest patches) and discontinuous urban-rural elements with edge and ruderal habitats (Table 5 - 2; Appendix II – S7). In addition, a negative association was detected between average burned area and habitat suitability (Figure 5 - 3, Figure 5 - 4 and, Appendix II – S7).

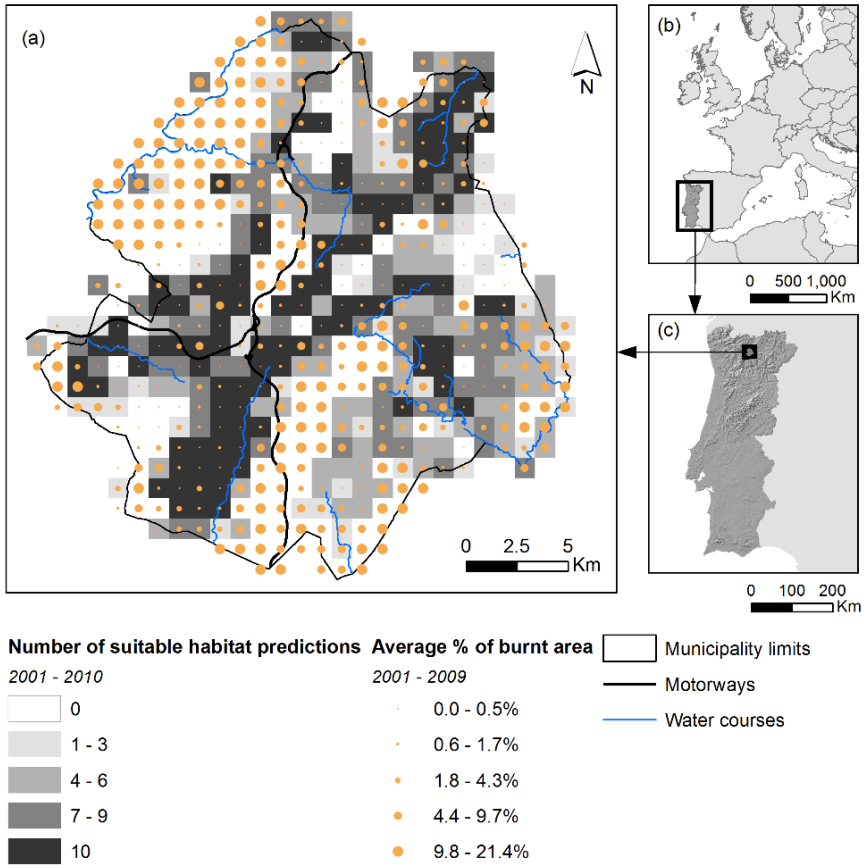

Figure 5 - 3 – (a) Number of suitable habitat predictions between 2001 and 2010 for each grid unit. Burned area is displayed in proportional circles for enabling the comparison of suitable areas against fire-prone locations; (b, c) study-area broader geographical context.

During the studied time-frame (2001-2010) a large decrease in habitat suitability or in the amount of suitable areas was recorded for years 2005 and 2006, related to the severe drought of 2004-2005 and with the high-incidence of wildfires in 2005 (Figure 5 - 4). Following this period, a partial recovery of habitat suitability was observed in 2007, followed by a new decrease towards 2009, an apparent lag response to the 2007 drought conditions.

Effects of inter-annual changes in climate and land cover on habitat suitability dynamics

Overall, inter-annual anomalies (Figure 5 - 3) in remotely-sensed variables of vegetation functioning (MAXVL) and evapotranspiration (EVPTR) were positively related to anomalies in annual precipitation (MAXVL: R^2=0.63, ρ=0.79; EVPTR: R^2=0.23, ρ=0.48) and average minimum temperature of the coldest month (MAXVL: R^2=0.38, ρ=0.62; EVPTR: R^2=0.49, ρ=0.70).

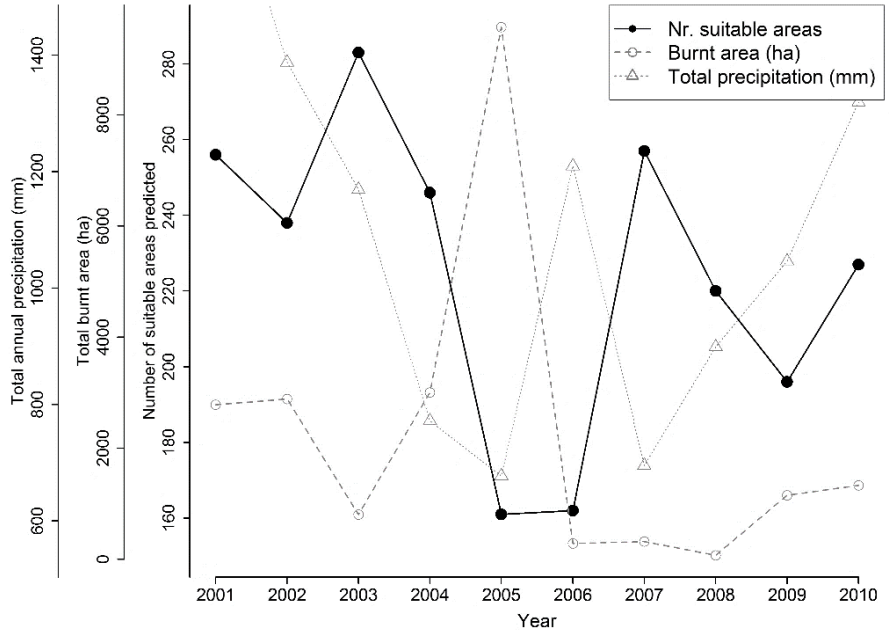

Figure 5 - 4 – Plot representing the inter-annual variation in total number of suitable areas predicted (black line), along with auxiliary data related to the total amount of burned area in the study-site (in hectares; orange line) and, the variation in total annual precipitation (blue line) showing three years with severe drought conditions: 2004, 2005 and 2007.

When comparing areas affected and unaffected by changes in land cover, derived from the construction of new motorways during 2002-2006 or from wildfires, inter-annual (i.e., non-seasonal) variation in remote-sensing variables (MAXVL, AMPLT and EVPTR) showed that these variables were sensitive to changes (Figure 5 - 6). Both types of disturbances caused strong decreases in vegetation functioning variables (MAXVL, AMPLT; Figure 5 - 6 - a,b,c,d), especially during the period 2002-2007 (*i.e.,* throughout the motorways construction period) followed by some recovery towards 2008. For wildfires, declines were mostly observed in 2004-2006, during and after large fire events occurring in 2004 and, especially, 2005. Actual evapotranspiration (EVPTR; Figure 5 - 6 - e,f) was overall less sensitive to changes induced by motorway construction and more sensitive to wildfires and drought conditions (especially in the period 2004-2005, followed by a slow recovery after these years). In turn, anomalies in number of predicted suitable areas by year recorded strong positive associations to RS variables (Figure 5 - 7; MAXVL: R^2=0.93, ρ=0.97; AMPLT: R^2=0.51, ρ=0.72; EVPTR: R^2=0.66, ρ=0.81).

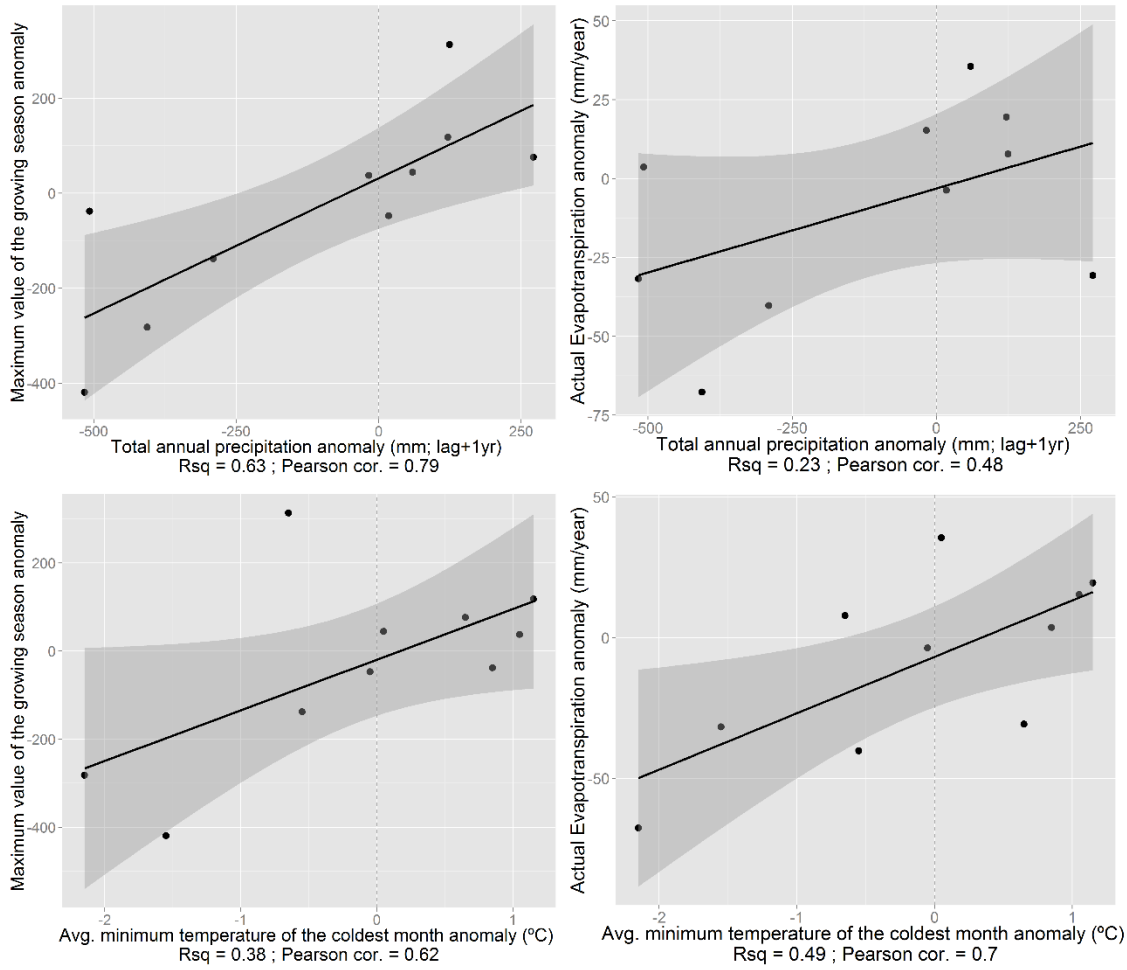

Figure 5 - 5 – Biplots displaying the association between anomalies (annual value minus the median for the whole studied period 2001-2010) in maximum value of the growing season (left column) or Actual Evapotranspiration (right column) and anomalies in total precipitation from the previous year (identified as lag+1yr ; first row) and average minimum temperature of the coldest month (second row) which show the effect of inter-annual variations in climatic conditions in remotely sensed indicators. Values for RS variables represent the anomaly in each year (from 2001-2010) in the median across the study-area, and considering only sites predicted as suitable at least one time in 2001-2010. Rsq – coefficient of determination for the regression line; Pearson cor. – Pearson correlation between variables.

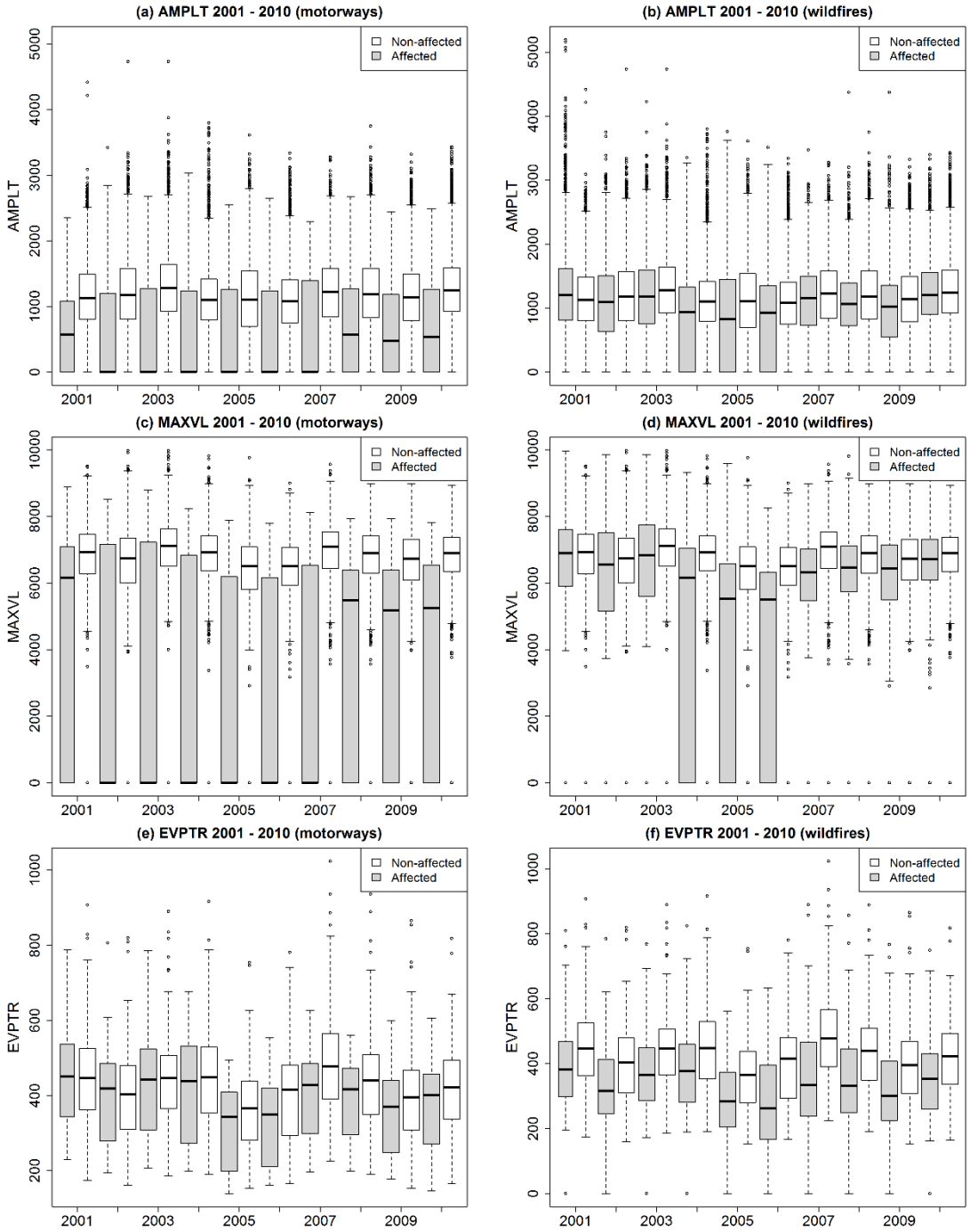

Figure 5 - 6 – Boxplots showing the effect of motorways (constructed during 2002-2006; left-side of the panel) and wildfires (right-side) on the temporal variation of predictor variables: Seasonal Amplitude (AMPLT), Maximum Value of the growing season (MAXVL) and Actual Evapotranspiration (EVPTR) for the 2001-2010 period. Plotted locations only include areas that were at least one time predicted as suitable by the averaged model. Grey boxes represent affected areas (by motorways or wildfires) while white boxes represent control/unaffected areas by both types of disturbances. Outliers were represented as circles, i.e., values lying outside the box 1.5 times the inter-quartile range.

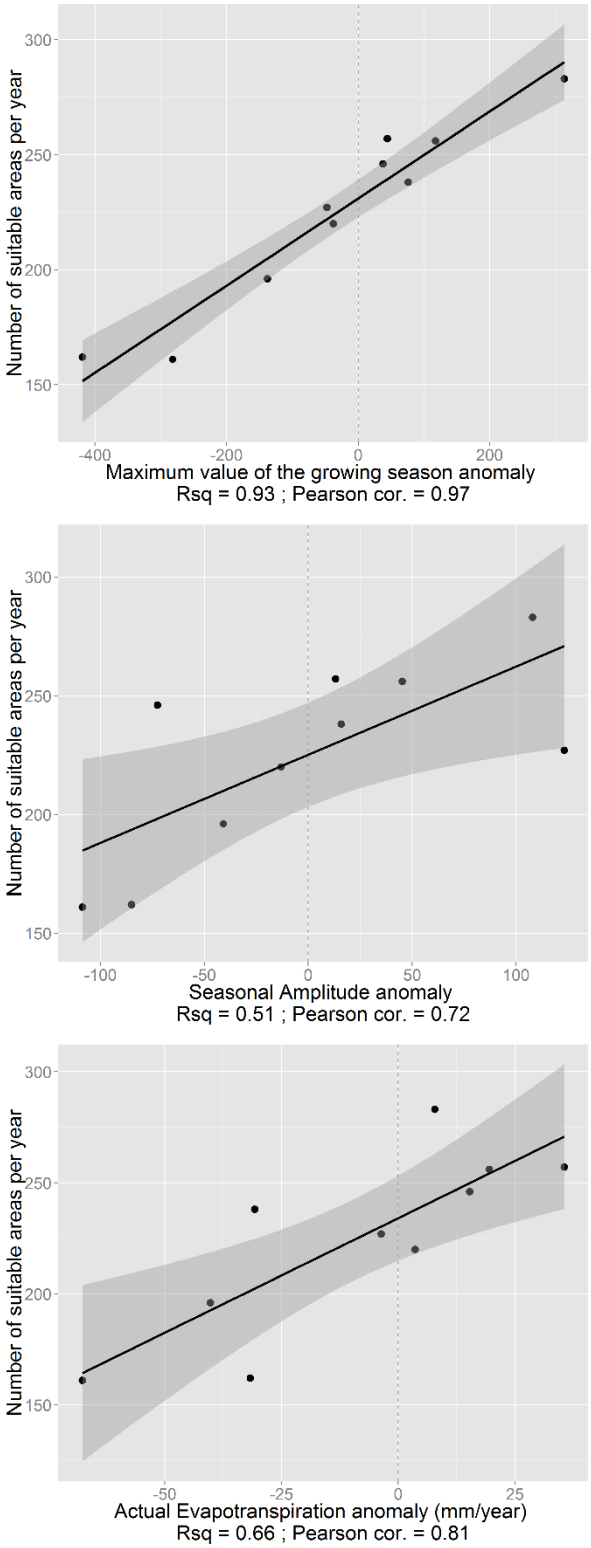

Figure 5 - 7 – Biplots showing the association between the number of suitable areas predicted per year (one point by year between 2001-2010) and anomalies (calculated as the annual value minus the median for the whole studied period 2001-2010) in the maximum value of the growing season (left), seasonal amplitude (center) and actual evapotranspiration (right). Values for RS variables represent the anomaly in each year (from 2001-2010) in the median across the study-area, and considering only sites predicted as suitable at least one time in 2001-2010. Rsq – coefficient of determination for the regression line; Pearson cor. – Pearson correlation between variables.

5.4. Discussion

Combining structural and functional determinants for better predictions of habitat suitability

Multi-model inference results emphasized the strong predictive ability of RS variables related to vegetation functioning dynamics (VFD; Table 5 - 2), highlighting their usefulness for developing robust SDMs and habitat suitability predictions (Zimmermann et al. 2007, Bradley and Fleishman 2008, Cord et al. 2014). Water availability, quantified from the MODIS actual evapotranspiration product, also contributed to explain landscape patterns of habitat suitability (Table 5 - 2), confirming its importance for SDMs and other ecological assessments (Hawkins et al. 2003, Fisher et al. 2011). Our results suggest that, despite the relatively coarse spatial resolution considered in the study, RS-based variables were capable of capturing vegetation functional attributes and the heterogeneity of landscape mosaics that are linked with *V. micrantha* suitable habitat. Typically, the species occurs in landscapes with high levels of productivity, seasonality and water availability (Appendix II – S7). High levels of productivity have been positively related to diversity (e.g., Bai et al. 2007), which matches our observations that the species is often found in species-rich and heterogeneous mosaics.

Additionally, we found a clear negative association between habitat suitability for *V. micrantha* and fire occurrence (average burned area per year, and its trend; see Appendix II – S7), another result with important consequences for conservation management (Driscoll et al. 2010, Gogol-Prokurat 2011).

Although with comparatively less relevance, features related to soils and to landscape composition and configuration yielded additional (and partially interrelated) contributions to explain habitat suitability (see Table 5 - 2). The distribution of agroforestry mosaics, low-density discontinuous urban-rural areas, and edge habitats were particularly relevant for *V. micrantha*, highlighting the importance of small-scale heterogeneous landscapes for conservation (Thornton et al. 2011). Phenological attributes of vegetation attained considerably less support for explaining the distribution of the test species (see Table 5 - 2), apparently contradicting results from other studies (e.g., Ivits et al. 2011, Cord et al. 2014) in which phenology attained higher predictive importance. To a certain extent, comparisons are hindered due to differences in the species tested. Still, this may reflect the fact that *V. micrantha* is associated to different vegetation types (e.g., deciduous woodlands fringes, heathlands and herbaceous communities) with a wide spectrum of vegetation phenologies', which hampers the model

ability to discriminate between suitable and unsuitable locations. Such limitations may be overcome through the inclusion of phenology metrics within modelling procedures to characterize the heterogeneity of flowering periods or different durations of the growing-season in a given landscape. Another approach would be to combine continuous vegetation functioning metrics into a discrete map of ecosystem functional types at the landscape level (Alcaraz et al. 2006). Such data could then be used to quantify landscape heterogeneity and analyse spatial patterns.

Overall, our results strongly emphasize the importance of simultaneously considering landscape attributes related to function, composition and spatial configuration to improve the explanation of ecological patterns (Vaz et al. 2015).

Habitat suitability dynamics and the conservation of vulnerable species

Based on multi-temporal remote-sensing data, our approach allowed exploring the effects of short-term fluctuations in environmental conditions on the spatiotemporal dynamics of landscape level of habitat suitability for our test-species (see Figure 5 - 4 and Figure 5 - 5). Thus, it contributes to clarify the mechanisms underpinning species' responses to fluctuations in habitat suitability derived from multiple and often overlapping sources of disturbance, such as land cover changes and wildfires, but also to strong inter-annual climatic variability (such as drought conditions; see Figure 5 - 5 and Figure 5 - 7). This is especially useful since these fluctuations may pose additional threats to vulnerable species with already small and highly fragmented populations and hence higher extinction risk (Bilz et al. 2011, Peraza Zurita 2011). Such added-value may be particularly useful when conservation plans are based on adaptive management strategies focused on maintaining key ecosystem processes and functions (Haney and Power 1996). In addition, by focusing on the landscape level, our approach presents several advantages for the focal species conservation namely because local and regional management frequently target this scale for planning and are typically multi-objective (e.g., Sayer et al. 2013), and also because, from a monitoring perspective, it allows to identify and assess landscape change processes and dynamics (Nagendra et al. 2013, Mairota et al. 2015) affecting habitat suitability and biodiversity.

Habitat suitability time-series can also provide useful inputs for systematic conservation planning (Pressey et al. 2007), allowing to assess and rank suitable habitat areas according to their relative stability in time. By identifying locations that have lost their suitability in a recent past due to environmental changes, our approach may help to spatially prioritize habitat protection and restoration actions with higher benefits for species persistence (Renton et al. 2012). Among other aspects, RS data could be used

for monitoring the dynamics and the temporal stability of suitable locations and their habitat quality (Mairota et al. 2015, Vaz et al. 2015) and serve as early-warning system helping to identify critical changes in essential variables (Skidmore et al. 2015).

Contributions of the framework to improve the monitoring of vulnerable species

Incorporating high-temporal resolution data related to landscape-level vegetation functioning and evapotranspiration in SDMs conveyed better predictions and the ability to evaluate spatiotemporal habitat suitability dynamics. This has several obvious implications for improving the effectiveness of biodiversity monitoring (Kerr and Ostrovsky 2003, Pettorelli et al. 2014, Skidmore et al. 2015). First, this may provide some evidence that RS-based functional metrics could provide early-warnings of changes in ecosystem processes affecting habitat suitability, well before assessments based on structural metrics such as those derived from land cover maps (Bradley and Fleishman 2008, Cabello et al. 2012, Cord et al. 2014). Second, since the later typically have lower update frequencies and higher production costs (especially for moderate or high spatial resolution products such as those used here), a RS-based functional approach using freely accessible data (e.g., MODIS, Landsat, Sentinel-2) could also potentially improve the cost-efficiency of vulnerable species monitoring. Third, the spatiotemporal dynamics of habitat suitability and the RS variables used in SDMs can be employed by regional or local authorities to devise monitoring schemes to develop useful vegetation or ecosystem functioning indicators aimed to track (or even anticipate) shifts in biodiversity (Cabello et al. 2012, Nagendra et al. 2013, Pettorelli et al. 2014). Fourth, reporting on threatened species (such as *V. micrantha*), with periodical information requests on their conservation status (Sousa-Silva et al. 2014), could potentially benefit from the proposed framework to develop comprehensive indicators based on species' spatiotemporal dynamics and to detail pressures affecting them. Finally, by taking advantage of an iterative and model-based design (as implemented in this study), existing data on species occurrence can be used to improve species detectability and cover data gaps especially for vulnerable and/or rare species (Guisan et al. 2006, Le Lay et al. 2010).

Using this approach, improved monitoring can also be achieved in cases where small-scale landscapes are prone to frequent and various disturbances, especially those related to fire occurrence, or then submitted to drastic changes in land cover/use (e.g., large infrastructures). In this sense, landscape-level vegetation functioning attributes derived from spectral vegetation indices time-series (e.g., NDVI) have proved useful for their capacity to provide a synthetic overview of ecosystem changes caused by multiple

drivers (Brook et al. 2008). Moreover, our results show that, as expected, RS variables were sensitive to inter-annual variations in temperature and precipitation (Figure 5 - 5 and Figure 5 - 6). The tested multi-temporal mean approach (Figure 5 - 2 and Table 5 - 3) can be used to generate improved predictions by averaging habitat suitability time-series and thereby capturing long-term trends. Moreover, analysing or aggregating multi-temporal predictions (using the mean as in this case, or other statistical measures), instead of relying on a preliminary multi-temporal aggregation of RS variables (e.g., Coops et al. 2009, Cord et al. 2014), can provide a more robust framework to evaluate shifts and trends in suitable habitat dynamics and to assess pressures affecting it (Figure 5 - 5 and Figure 5 - 7).

Limitations, sources of uncertainty, and future prospects

As in any practical application of models in conservation and management, uncertainties underlying models and their predictions should be carefully handled and efficiently communicated to stakeholders (Guisan et al. 2013). These uncertainties mainly derive from caveats that vulnerable and rare species distributions pose to model development, due to the frequently small occurrence datasets (Wiser et al. 1998, Lomba et al. 2010). Overfitting may also be an issue, however model-averaging parsimonious bivariate models in a MMI framework, similarly to Lomba et al. (2010), may prove beneficial.

Temporal (Tuanmu et al. 2011) as well as spatial transferability (Randin et al. 2006) also pose some limitations that require careful inspection. Here, given the short time-span of this study, niche conservatism was assumed. In a recent review, Peterson (2011) found that ecological niche characteristics are strongly preserved over short to moderate time-frames. However, to fully evaluate temporal transferability, historical time-series on species occurrence would be required (not available in our case) coupled with appropriate methods (e.g., Rapacciuolo et al. 2014). Given the relatively small extent of the study-area (compared to the full species range in Iberia (Sousa-Silva et al. 2014)), spatial transferability may be more problematic, reducing model forecast ability for other regions (Randin et al. 2006). As such, our results for *V. micrantha* are mostly applicable to the test-area, but the framework can be easily generalized to its whole range as more data becomes available to fully encompass the species environmental niche.

Remote sensing based variables also pose some challenges in a modelling context due to various ‘noise’ sources (Jönsson and Eklundh 2004, Hird and McDermid 2009). However, appropriate pre-processing methods – such as geometric, atmospheric, as well as smoothing/filtering routines (Jönsson and Eklundh 2004, Hird and McDermid 2009) – can be used to minimize those problems. Therefore, the selection of an

appropriate algorithm for time-series smoothing and its parameterization are crucial aspects to adequately fill data gaps and filter noise from undetected clouds or poor atmospheric conditions (Kandasamy et al. 2013).

Additional tests implementing the approach presented here are required, including other species with different life-history traits, ranges and habitat attributes, involving sensitivity analyses as well as methods to cope with model uncertainties. Besides species presence/absence, other parameters could also be modelled with remote sensing multi-temporal indices, such as abundance, habitat quality or population fitness. This will further improve the integration of multi-temporal remote sensing data in species distribution models as a way to inform and advance biodiversity monitoring and conservation.

Acknowledgements

J. Gonçalves was financially supported by FCT (Portuguese Science Foundation) through PhD grant SFRH/BD/90112/2012. I. Pôças was supported by FCT through postdoctoral grant SFRH/BPD/79767/2011. B. Marcos was supported by FCT and FEDER/COMPETE (project IND_CHANGE; PTDC/AAG-MAA/4539/2012; FCOMP-01-0124-FEDER-027863). R. Sousa-Silva was supported by a PhD grant in the framework of the FORBIO Climate project, financed by BRAIN.be. A. Lomba was supported by FCT through postdoctoral grant SFRH/BPD/80747/2011.

Author contributions

Author name	Study conception and design	Sampling design, infield surveys and/or data collection	Data processing, analysis and/or modelling	Manuscript writing	Manuscript revision
João Gonçalves	☑	☑	☑	☑	☑
Paulo Alves		☑		☑	☑
Isabel Pôças			☑	☑	☑
Bruno Marcos			☑	☑	☑
Rita Sousa-Silva				☑	☑
Ângela Lomba				☑	☑
João P Honrado				☑	☑

References

AFN. 2011. Cartografia nacional de áreas ardidas (national mapping of burnt areas), URL: http://www.afn.min-agricultura.pt/portal/dudf/cartografia/cartograf-areas-ardidas-1990-2009, accessed on 10-01-2011. Autoridade Florestal Nacional (National Forestry Authority).

Alcaraz, D., J. Paruelo, and J. Cabello. 2006. Identification of current ecosystem functional types in the Iberian Peninsula. Global Ecology and Biogeography 15:200-212.

Bai, Y., J. Wu, Q. Pan, J. Huang, Q. Wang, F. Li, A. Buyantuyev, and X. Han. 2007. Positive linear relationship between productivity and diversity: evidence from the Eurasian Steppe. Journal of Applied Ecology 44:1023-1034.

Bilz, M., S. P. Kell, N. Maxted, and R. V. Lansdown. 2011. European Red List of Vascular Plants. Luxembourg.

Bradley, B. A., and E. Fleishman. 2008. Can remote sensing of land cover improve species distribution modelling? Journal of Biogeography 35:1158-1159.

Broennimann, O., W. Thuiller, G. Hughes, G. F. Midgley, J. M. R. Alkemade, and A. Guisan. 2006. Do geographic distribution, niche property and life form explain plants' vulnerability to global change? Global Change Biology 12:1079-1093.

Brook, B. W., N. S. Sodhi, and C. J. A. Bradshaw. 2008. Synergies among extinction drivers under global change. Trends in Ecology & Evolution 23:453-460.

Burnham, K., D. Anderson, and K. Huyvaert. 2011. AIC model selection and multimodel inference in behavioral ecology: some background, observations, and comparisons. Behavioral Ecology and Sociobiology 65:23-35.

Burnham, K. P., and D. R. Anderson. 2002. Model Selection and Multi-Model Inference: A Practical Information-Theoretic Approach. 2nd edition. Springer-Verlag, New York.

Butchart, S. H. M., M. Walpole, B. Collen, A. van Strien, J. P. W. Scharlemann, R. E. A. Almond, J. E. M. Baillie, B. Bomhard, C. Brown, J. Bruno, K. E. Carpenter, G. M. Carr, J. Chanson, A. M. Chenery, J. Csirke, N. C. Davidson, F. Dentener, M. Foster, A. Galli, J. N. Galloway, P. Genovesi, R. D. Gregory, M. Hockings, V. Kapos, J.-F. Lamarque, F. Leverington, J. Loh, M. A. McGeoch, L. McRae, A. Minasyan, M. H. Morcillo, T. E. E. Oldfield, D. Pauly, S. Quader, C. Revenga, J. R. Sauer, B. Skolnik, D. Spear, D. Stanwell-Smith, S. N. Stuart, A. Symes, M. Tierney, T. D. Tyrrell, J.-C. Vié, and R. Watson. 2010. Global Biodiversity: Indicators of Recent Declines. Science 328:1164-1168.

Cabello, J., N. Fernández, D. Alcaraz-Segura, C. Oyonarte, G. Piñeiro, A. Altesor, M. Delibes, and J. Paruelo. 2012. The ecosystem functioning dimension in conservation: insights from remote sensing. Biodiversity and Conservation 21:3287-3305.

CBD. 2010. Strategic Plan for Biodiversity 2011–2020 and the Aichi Targets. CBD, Montreal, Quebec, Canada.

CEC. 2009. Composite Report on the Conservation Status of Habitat Types and Species as required under Article 17 of the Habitats Directive, COM(2009) 358 final. Commission of European Communities, EU, Brussels.

Coops, N. C., M. A. Wulder, and D. Iwanicka. 2009. Exploring the relative importance of satellite-derived descriptors of production, topography and land cover for predicting breeding bird species richness over Ontario, Canada. Remote Sensing of Environment 113:668-679.

Cord, A. F., D. Klein, F. Mora, and S. Dech. 2014. Comparing the suitability of classified land cover data and remote sensing variables for modeling distribution patterns of plants. Ecological Modelling 272:129-140.

Driscoll, D. A., D. B. Lindenmayer, A. F. Bennett, M. Bode, R. A. Bradstock, G. J. Cary, M. F. Clarke, N. Dexter, R. Fensham, G. Friend, M. Gill, S. James, G. Kay, D. A. Keith, C. MacGregor, J. Russell-Smith, D. Salt, J. E. M. Watson, R. J. Williams, and A. York. 2010. Fire management for biodiversity conservation: Key research questions and our capacity to answer them. Biological Conservation 143:1928-1939.

Eklundh, L., and P. Jönsson. 2010. TIMESAT 3.0. Software Manual. Page 74. Lund University, Lund, Sweden.

Elith, J., and J. Leathwick. 2009. Species Distribution Models: Ecological Explanation and Prediction Across Space and Time. Annual Review of Ecology, Evolution, and Systematics 40:677-697.

European Union. 2011. The EU Biodiversity Strategy to 2020. European Union, Belgium.

Fisher, J. B., R. J. Whittaker, and Y. Malhi. 2011. ET come home: potential evapotranspiration in geographical ecology. Global Ecology and Biogeography 20:1-18.

Freeman, E. A., and G. G. Moisen. 2008. A comparison of the performance of threshold criteria for binary classification in terms of predicted prevalence and kappa. Ecological Modelling 217:48-58.

Gogol-Prokurat, M. 2011. Predicting habitat suitability for rare plants at local spatial scales using a species distribution model. Ecological Applications 21:33-47.

Guisan, A., O. Broennimann, R. Engler, M. Vust, N. G. Yoccoz, A. Lehmann, and N. E. Zimmermann. 2006. Using Niche-Based Models to Improve the Sampling of Rare Species. Conservation Biology 20:501-511.

Guisan, A., T. C. Edwards Jr, and T. Hastie. 2002. Generalized linear and generalized additive models in studies of species distributions: setting the scene. Ecological Modelling 157:89-100.

Guisan, A., R. Tingley, J. B. Baumgartner, I. Naujokaitis-Lewis, P. R. Sutcliffe, A. I. T. Tulloch, T. J. Regan, L. Brotons, E. McDonald-Madden, C. Mantyka-Pringle, T. G. Martin, J. R. Rhodes, R. Maggini, S. A. Setterfield, J. Elith, M. W. Schwartz, B. A. Wintle, O. Broennimann, M. Austin, S. Ferrier, M. R. Kearney, H. P. Possingham, and Y. M. Buckley. 2013. Predicting species distributions for conservation decisions. Ecology Letters 16:1424-1435.

Guisan, A., and N. E. Zimmerman. 2000. Predictive habitat distribution models in ecology. Ecological Modelling 135:147–186.

Haney, A., and R. Power. 1996. Adaptive management for sound ecosystem management. Environmental Management 20:879-886.

Hawkins, B. A., R. Field, H. V. Cornell, D. J. Currie, J.-F. Guégan, D. M. Kaufman, J. T. Kerr, G. G. Mittelbach, T. Oberdorff, E. M. O'Brien, E. E. Porter, and J. R. G. Turner. 2003. Energy, water, and broadscale geographic patterns of species richness. Ecology 84:3105-3117.

He, K. S., B. A. Bradley, A. F. Cord, D. Rocchini, M.-N. Tuanmu, S. Schmidtlein, W. Turner, M. Wegmann, N. Pettorelli, H. Nagendra, and N. Horning. 2015. Will remote sensing shape the next generation of species distribution models? Remote Sensing in Ecology and Conservation 1:4-18.

Heumann, B. W., J. W. Seaquist, L. Eklundh, and P. Jönsson. 2007. AVHRR derived phenological change in the Sahel and Soudan, Africa, 1982–2005. Remote Sensing of Environment 108:385-392.

Hird, J. N., and G. J. McDermid. 2009. Noise reduction of NDVI time series: An empirical comparison of selected techniques. Remote Sensing of Environment 113:248-258.

Ivits, E., G. Buchanan, L. Olsvig-Whittaker, and M. Cherlet. 2011. European Farmland Bird Distribution Explained by Remotely Sensed Phenological Indices. Environmental Modeling and Assessment 16:385-399.

Jones, H. G., and R. A. Vaughan. 2010. Remote sensing of vegetation. Principles, techniques, and applications. 1st edition. Oxford University Press, Oxford.

Jönsson, A. M., L. Eklundh, M. Hellström, L. Bärring, and P. Jönsson. 2010. Annual changes in MODIS vegetation indices of Swedish coniferous forests in relation to snow dynamics and tree phenology. Remote Sensing of Environment 114:2719-2730.

Jönsson, P., and L. Eklundh. 2004. TIMESAT - a program for analyzing time-series of satellite sensor data. Computers & Geosciences 30:833-845.

Kandasamy, S., F. Baret, A. Verger, P. Neveux, and M. Weiss. 2013. A comparison of methods for smoothing and gap filling time series of remote sensing observations - application to MODIS LAI products. Biogeosciences 10:4055-4071.

Kerr, J. T., and M. Ostrovsky. 2003. From space to species: ecological applications for remote sensing. Trends in Ecology & Evolution 18:299-305.

Le Lay, G., R. Engler, E. Franc, and A. Guisan. 2010. Prospective sampling based on model ensembles improves the detection of rare species. Ecography 33:1015-1027.

Lomba, A., L. Pellissier, C. Randin, J. Vicente, F. Moreira, J. Honrado, and A. Guisan. 2010. Overcoming the rare species modelling paradox: A novel hierarchical framework applied to an Iberian endemic plant. Biological Conservation 143:2647-2657.

Magurran, A. E., S. R. Baillie, S. T. Buckland, J. M. Dick, D. A. Elston, E. M. Scott, R. I. Smith, P. J. Somerfield, and A. D. Watt. 2010. Long-term datasets in biodiversity research and monitoring: assessing change in ecological communities through time. Trends in Ecology & Evolution 25:574-582.

Mairota, P., B. Cafarelli, R. K. Didham, F. P. Lovergine, R. M. Lucas, H. Nagendra, D. Rocchini, and C. Tarantino. 2015. Challenges and opportunities in harnessing satellite remote-sensing for biodiversity monitoring. Ecological Informatics 30:207-214.

Mu, Q., M. Zhao, and S. W. Running. 2011. Improvements to a MODIS global terrestrial evapotranspiration algorithm. Remote Sensing of Environment 115:1781-1800.

Nagendra, H., R. Lucas, J. P. Honrado, R. H. G. Jongman, C. Tarantino, M. Adamo, and P. Mairota. 2013. Remote sensing for conservation monitoring: Assessing protected areas, habitat extent, habitat condition, species diversity, and threats. Ecological Indicators 33:45-59.

Parviainen, M., N. E. Zimmermann, R. K. Heikkinen, and M. Luoto. 2013. Using unclassified continuous remote sensing data to improve distribution models of red-listed plant species. Biodiversity and Conservation 22:1731-1754.

Peraza Zurita, M. D. 2011. *Veronica micrantha*. IUCN Red List of Threatened Species. Version 2011.2 [URL: http://www.iucnredlist.org/apps/redlist/details/162008/0]. IUCN.

Pereira, H. M., P. W. Leadley, V. Proença, R. Alkemade, J. P. W. Scharlemann, J. F. Fernandez-Manjarrés, M. B. Araújo, P. Balvanera, R. Biggs, W. W. L. Cheung, L. Chini, H. D. Cooper, E. L. Gilman, S. Guénette, G. C. Hurtt, H. P. Huntington, G. M. Mace, T. Oberdorff, C. Revenga, P. Rodrigues, R. J. Scholes, U. R. Sumaila, and M. Walpole. 2010. Scenarios for Global Biodiversity in the 21st Century. Science 330:1496-1501.

Peterson, A. T. 2011. Ecological niche conservatism: a time-structured review of evidence. Journal of Biogeography 38:817-827.

Pettorelli, N., W. F. Laurance, T. G. O'Brien, M. Wegmann, H. Nagendra, and W. Turner. 2014. Satellite remote sensing for applied ecologists: opportunities and challenges. Journal of Applied Ecology 51:839-848.

Phillips, S. J., and M. Dudík. 2008. Modeling of species distributions with Maxent: new extensions and a comprehensive evaluation. Ecography 31:161-175.

Pôças, I., M. Cunha, L. S. Pereira, and R. G. Allen. 2013. Using remote sensing energy balance and evapotranspiration to characterize montane landscape vegetation with focus on grass and pasture lands. International Journal of Applied Earth Observation and Geoinformation 21:159-172.

Prendergast, J. R., R. M. Quinn, and J. H. Lawton. 1999. The Gaps between Theory and Practice in Selecting Nature Reserves. Conservation Biology 13:484-492.

Pressey, R. L., M. Cabeza, M. E. Watts, R. M. Cowling, and K. A. Wilson. 2007. Conservation planning in a changing world. Trends in Ecology & Evolution 22:583-592.

Randin, C. F., T. Dirnböck, S. Dullinger, N. E. Zimmermann, M. Zappa, and A. Guisan. 2006. Are niche-based species distribution models transferable in space? Journal of Biogeography 33:1689-1703.

Rapacciuolo, G., D. B. Roy, S. Gillings, and A. Purvis. 2014. Temporal validation plots: quantifying how well correlative species distribution models predict species' range changes over time. Methods in Ecology and Evolution 5:407-420.

Renton, M., N. Shackelford, and R. J. Standish. 2012. Habitat restoration will help some functional plant types persist under climate change in fragmented landscapes. Global Change Biology 18:2057-2070.

Reside, A. E., J. VanDerWal, A. Kutt, I. Watson, and S. Williams. 2012. Fire regime shifts affect bird species distributions. Diversity and Distributions 18:213-225.

Rocchini, D., D. S. Boyd, J.-B. Féret, G. M. Foody, K. S. He, A. Lausch, H. Nagendra, M. Wegmann, and N. Pettorelli. 2016. Satellite remote sensing to monitor species diversity: potential and pitfalls. Remote Sensing in Ecology and Conservation 2:25-36.

Sayer, J., T. Sunderland, J. Ghazoul, J.-L. Pfund, D. Sheil, E. Meijaard, M. Venter, A. K. Boedhihartono, M. Day, C. Garcia, C. van Oosten, and L. E. Buck. 2013. Ten principles for a landscape approach to reconciling agriculture, conservation, and other competing land uses. Proceedings of the National Academy of Sciences 110:8349-8356.

Sen, P. K. 1968. Estimates of the Regression Coefficient Based on Kendall's Tau. Journal of the American Statistical Association 63:1379-1389.

Skidmore, A. K., N. Pettorelli, N. C. Coops, G. N. Geller, M. Hansen, R. Lucas, C. A. Mücher, B. O'Connor, M. Paganini, H. M. Pereira, M. E. Schaepman, W. Turner, T. Wang, and M. Wegmann. 2015. Agree on biodiversity metrics to track from space. Nature 523.

Sousa-Silva, R., P. Alves, J. Honrado, and A. Lomba. 2014. Improving the assessment and reporting on rare and endangered species through species distribution models. Global Ecology and Conservation 2:226-237.

Symonds, M., and A. Moussalli. 2011. A brief guide to model selection, multimodel inference and model averaging in behavioural ecology using Akaike's information criterion. Behavioral Ecology and Sociobiology 65:13-21.

Thornton, D., L. Branch, and M. Sunquist. 2011. The influence of landscape, patch, and within-patch factors on species presence and abundance: a review of focal patch studies. Landscape Ecology 26:7-18.

Tuanmu, M.-N., A. Viña, G. J. Roloff, W. Liu, Z. Ouyang, H. Zhang, and J. Liu. 2011. Temporal transferability of wildlife habitat models: implications for habitat monitoring. Journal of Biogeography 38:1510-1523.

Vaz, A. S., B. Marcos, J. Gonçalves, A. Monteiro, P. Alves, E. Civantos, R. Lucas, P. Mairota, J. Garcia-Robles, J. Alonso, P. Blonda, A. Lomba, and J. P. Honrado. 2015. Can we predict habitat quality from space? A multi-indicator assessment

based on an automated knowledge-driven system. International Journal of Applied Earth Observation and Geoinformation 37:106-113.

Wang, Q., S. Adiku, J. Tenhunen, and A. Granier. 2005. On the relationship of NDVI with leaf area index in a deciduous forest site. Remote Sensing of Environment 94:244-255.

Wiser, S. K., R. K. Peet, and P. S. White. 1998. Prediction of rare-plant occurrence: A southern Appalachian example. Ecological Applications 8:909-920.

Wood, S. 2006. Generalized additive models: an introduction with R. 1st ed. edition. Chapman and Hall/CRC.

Wood, S. N. 2004. Stable and Efficient Multiple Smoothing Parameter Estimation for Generalized Additive Models. Journal of the American Statistical Association 99:673-686.

Zimmermann, N. E., T. C. Edwards, G. G. Moisen, T. S. Frescino, and J. A. Blackard. 2007. Remote sensing-based predictors improve distribution models of rare, early successional and broadleaf tree species in Utah. Journal of Applied Ecology 44:1057-1067.

Chapter 6 - A model-based framework for assessing the vulnerability of low dispersal vertebrates to landscape fragmentation under environmental change

Author list: **João Gonçalves** (1,2), João P. Honrado (1,2), Joana R. Vicente (1,2), Emilio Civantos (1,3*)

(1) InBIO/CIBIO - Research Centre in Biodiversity and Genetic Resources – University of Porto. Campus Agrário de Vairão, Rua Padre Armando Quintas, nr. 7, 4485-661 Vairão, Portugal
(2) Faculdade de Ciências, Universidade do Porto, Rua do Campo Alegre, FC4 building, 4169-007 Porto, Portugal
(3) Instituto de Investigación en Recursos Cinegéticos (IREC), CSIC. Ronda de Toledo, s/n. 13071 Ciudad Real. Spain.

DISCLAIMER

This manuscript is an original contribution of this thesis published in *Ecological Complexity* journal under the same title. Gonçalves, J., lead the work with contributions from all co-authors.

ABSTRACT

Environmental changes are driving rapid geographic shifts of suitable environmental conditions for species. These might survive by tracking those shifts, however successful responses will depend on the spatial distribution of suitable habitats (current and future) and on their connectivity. Most herptiles (i.e. amphibians and reptiles) have low dispersal abilities, and therefore herptiles are among the most vulnerable groups to environmental changes. Here we assessed the vulnerability of herptile species to future climate and land use changes in fragmented landscapes. We developed and tested a methodological approach combining the strengths of Species Distribution Models (SDMs) and of functional connectivity analysis. First, using SDMs we forecasted current and future distributions of potential suitable areas as well as range dynamics for four herptile species in Portugal. SDM forecasts for 2050 were obtained under two contrasting emission scenarios, translated into moderate (low-emissions scenario) or large (high-emissions scenario) changes in climate and land use conditions. Then, we calculated and analysed functional connectivity from areas projected to lose environmental suitability towards areas keeping suitable conditions. Landscape matrix resistance and barrier effects of the national motorway network were incorporated as the main sources of fragmentation. Potential suitable area was projected to decrease under future conditions for most test species, with the high-emissions scenario amplifying the losses or gains. Spatiotemporal patterns of connectivity between potentially suitable areas signalled the most important locations for maintaining linkages and migration corridors, as well as potential conflicts due to overlaps with the current motorway network. By integrating SDM projections with functional connectivity analysis, we were able to assess and map the vulnerability of distinct herptile species to isolation or extinction under environmental change scenarios. Our framework provides valuable information, with fairly low data requirements, for optimizing biodiversity management and mitigation efforts, aiming to reduce the complex and often synergistic negative impacts of multiple environmental change drivers. Implications for conservation planning and management are discussed from a global change adaptation perspective.

6.1. Introduction

Climate and land use changes are topics of scientific and political concern, especially when focusing on their potential impacts on biodiversity as well as on ecosystem processes and services upon which human well-being is closely dependent (Thomas et al. 2004, Thuiller et al. 2011). Climate change and habitat loss due to land use change are thus among the most important threats to terrestrial biodiversity (Sala et al. 2000, Jetz et al. 2007), fostering modifications of key ecosystem functions, and often the depletion of essential ecosystem services (Bellard et al. 2012). Habitat loss, degradation and fragmentation, well-known threats to global biodiversity (IUCN 2014), have been shown to be more important than climate change at regional and local scales (Dirnböck et al. 2003). Moreover, their effects are likely to be intensified under climate change (Brook et al. 2008, Bellard et al. 2012). These synergistic interactions between climate, land use and other habitat changes pose constant challenges for species to cope with, and they can produce unexpected responses that might go undetected using conventional monitoring schemes, therefore raising the issue of timely adaption (e.g., migration) (Pullin et al. 2013).

Climate and land use changes are resulting in the geographic shifting of species' suitable conditions (Chen et al. 2011), to which only some organisms can adapt, either via phenotypic or ecological plasticity and/or evolutionary changes (Williams et al. 2008). When suitable conditions change rapidly many species may not have enough time to adapt locally, hence their survival will depend on their capacity to track suitable environmental conditions and habitats at novel locations (Pearson 2006). Thereby, extinctions may occur if populations cannot migrate or adapt fast enough (Williams et al. 2008).

In this context, landscape fragmentation is a determinant factor of species survival by potentially decreasing the connectivity between source areas and other patches with suitable conditions for the species (Taylor et al. 1993). In fact, habitat connectivity is recognized as one of the most important factors for maintaining biological diversity (Taylor et al. 1993, Hodgson et al. 2009), because gene flow is essential for genetic fitness and adaptation to environmental changes (Hanski 1998). To minimise the threats associated with fragmentation, landscape connectivity should be enhanced, for example, by protecting linkages between suitable areas (Fahrig and Merriam 1994), and by building efficient ecological networks to facilitate the movement of species under future environmental conditions (Devictor et al. 2007). This may be particularly important

in the context of climate change were enhancing connectivity has been defined as an important strategy (among others) for adaptation (Heller and Zavaleta 2009).

Functional connectivity, *i.e.*, the degree to which the landscape promotes or hinders movements among resource patches for a given species (Taylor et al. 1993), is a major determinant of processes such as dispersion or gene flow, and includes species-specific aspects and their interaction with landscape structures (Taylor et al. 2006). Functional connectivity is therefore essential to support many conservation decisions and actions (Luque et al. 2012). In contrast, structural connectivity refers to the landscape elements that are physically or spatially connected through, for example, corridors (Taylor et al. 1993), regardless of specific interactions. Developing methods to effectively identify common landscape linkages for multiple species with conservation concern is a major challenge in conservation and landscape ecology (Beier et al. 2011). However, creating a standard approach is challenging due to the plethora of methods for quantifying connectivity and to the distinct ecological requirements of the different species (Luque et al. 2012). Thus, managers often focus on improving the structural connectivity of the landscape (which it is not species-specific), for example by establishing connections among forest patches, assuming an *ad hoc* equivalence with functional connectivity (Ribeiro et al. 2011). Furthermore, connectivity can be increased by conserving or restoring the habitat lying between current and future suitable areas for selected species (Akçakaya et al. 2007). Such an approach can reduce local extinctions by facilitating the 'rescue effect' of colonization, and also increase the rate of re-colonization after a local extinction (Rudnick et al. 2010).

This study aimed to incorporate the effects of functional landscape connectivity in predictions of species' responses to climate and land use changes in order to improve the design of ecological networks by identifying potential barriers to species movement; and, to prioritize areas for monitoring the responses of vulnerable species. For illustration purposes, we selected reptiles and amphibians as they are among those groups potentially more affected by ongoing and future environmental changes due to their low dispersal capacity (Gibbons et al. 2000, Blaustein et al. 2001). Using Species Distribution Models, we assessed whether the extent of potential suitable habitat is projected to increase or decrease under future environmental conditions. For each test species, we analysed functional connectivity from areas projected to lose environmental suitability to areas expected to maintain suitable environmental conditions by including species-specific landscape resistance effects. This approach also allowed the identification and evaluation of multiple least-cost paths (Pinto and Keitt 2009) potentially establishing

dispersal corridors under climate and land use changes in mainland Portugal. Finally, by forecasting how multiple environmental changes may affect the distribution of species under future conditions, our approach also allowed assessing species vulnerability to regional extinction and/or isolation. We concluded by discussing the value of our framework to inform authorities and managers about upcoming conservation priorities and mitigation actions, and to guide the set-up of efficient monitoring schemes to track biodiversity responses to multiple (and interacting) environmental change processes.

6.2. Methods

Analytical framework

The analytical approach (Figure 6 - 1) encompassed three main steps. In the first step, we obtained spatial predictions on the distribution of current and future suitable areas using Species Distribution Models (SDM). In the second step, we combined current and future projections to obtain maps of species distribution dynamics informing about potential range shifts and changes in the distribution of suitable areas under future scenarios of climate and land use change. Finally, in the third step, we evaluated connectivity from areas projected to lose environmental suitability to areas projected to maintain suitable conditions. Connectivity analyses emphasized the assessment of potential barrier effects induced by the Portuguese motorway network.

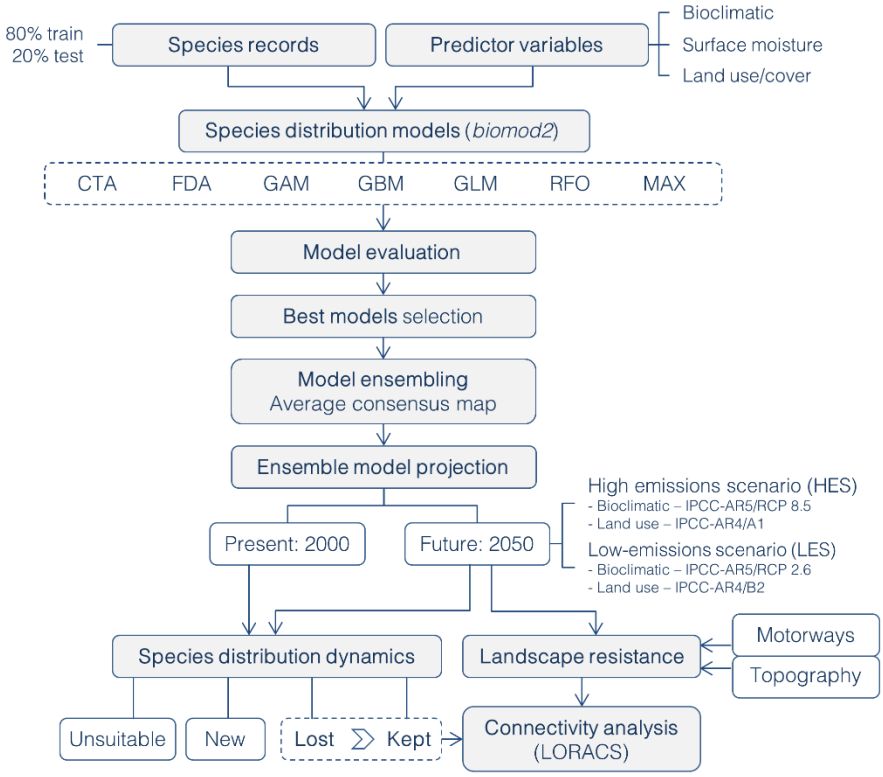

Figure 6 - 1 – Schematic representation of the methodological approach developed.

Study area

The study area comprises mainland Portugal, southwest Europe, with an area of approximately 89 100km^2. Elevation ranges from 0 to 1993 meters a.s.l. with the mountain areas occurring mainly in the northern half of the territory. The climate ranges from temperate Atlantic in the northwest to dry Mediterranean in the southernmost areas (for more details see Appendix III – S1).

Test species and distribution data

The test species were two amphibian and two reptile species occurring in the study area. Due to their biological characteristics, these two groups of vertebrates are very sensitive to environmental changes, particularly climate change (Araújo et al. 2006) and also, to fragmentation and degradation of habitats by action of human activities (Bennett and Saunders 2010). In addition, with few exceptions, herptiles have poor dispersal ability (Blaustein et al. 2001), therefore their capacity to move to new suitable habitats is limited in comparison to endotherms. Moreover, during their migration events herptiles are very sensitive to unsuitable conditions being more exposed to predation, desiccation and human barriers. Specifically, large roads have been identified as major barriers for amphibians and reptiles with profound negative impacts on dispersal (Andrews et al. 2008).

Species data included occurrence records for two amphibian and two reptile species distributed in Portugal: *Epidalea calamita* (Laurenti, 1768), *Chioglossa lusitanica* (Bocage, 1864), *Lacerta schreiberi* (Bedriaga, 1878), and *Anguis fragilis* (Linnaeus, 1758). These species were selected due to their differences in terms of current distribution, range, IUCN conservation status and dispersal abilities (see Appendix III – S1). We collected occurrence data from the Portuguese Atlas of Amphibians and Reptiles (Loureiro et al. 2008), based on a 1000×1000m square grid (European Datum 1950 – UTM 29N coordinate reference system). We verified and harmonized all available records. In order to remove duplicates and decrease spatial sampling bias and autocorrelation in presence records we used a spatial filtering routine (Boria et al. 2014). To achieve this goal, we filtered records by imposing a minimum pairwise distance between neighbouring points (optimized for each species) corresponding to a Clark-Evans aggregation index (CEAI; Clark and Evans 1954) between [0.9, 1.0] (see Appendix III – Appendix S2) allowing to decrease spatial clustering, while maintaining an appropriated number of records for model fitting. Afterwards, 191 presence-only records

were available for *E. calamita*, 112 for *C. lusitanica*, 133 for *L. schreiberi*, and 178 for *A. fragilis* (see also Appendix III – S2).

Climatic data and scenarios

The biology and ecology of amphibians and reptiles are tightly related to temperature and moisture (Duellman and Trueb 1986, Angilletta Jr et al. 2002), which thus constitute important limiting factors for the distribution of these species (Tingley and Herman 2009). In order to relate these two factors with current species records applying a SDM framework, we used the following five bioclimatic variables for model fitting (available in the *WorldClim* database; (Hijmans et al. 2005)): mean diurnal range (*BIO_02*), temperature seasonality (*BIO_04*), maximum temperature of warmest month (*BIO_05*), minimum temperature of the coldest month (*BIO_06*), and precipitation of the driest month (*BIO_14*). The climatic data for current conditions consists of an average for the period 1950–2000 with a spatial resolution of 30 arc-second (*c.a.* 900m at the equator), resampled to 1000×1000m (using bilinear interpolation) and registered in the same coordinate reference system as the species' presence records (see Appendix III – S3 for a numeric description of these variables).

To forecast the distribution of suitable areas, we used climate projections for the reference year of 2050 (average for the period 2041–2060) for two contrasting emission scenarios (IPCC 2014), namely: i) IPCC AR-CMIP 5/RCP 8.5 (*i.e.* maximum energy requirements, emissions balanced between fossil and non-fossil sources) and, ii) IPCC AR-CMIP 5/RCP 2.6 (lower energy requirements and thus lower emissions than RCP 8.5). Since uncertainty in forecasting future distributions is partly related to global circulation models (GCMs; see Buisson et al. (2010)), we combined twelve different GCMs to produce an ensemble average of projections (see the full list of ensemble GCMs in Appendix III – S4).

Topographic data

Topographic indices representing surface moisture gradients and water flow/drainage patterns have been used to explain the distribution of herptile species (Blank and Blaustein 2012). To introduce such effects in the SDMs, we used elevation data from the Shuttle Radar Topography Mission database (SRTM version-4; Jarvis et al. (2008); with a spatial resolution of 90×90m) to calculate the Catchment Area (CAR), and the Topographic Wetness Index (TWI). While CAR provides a measure of catchment area and hydrological flow accumulation (Gruber and Peckham 2008), TWI describes the tendency of a cell to accumulate water (Quinn et al. 1995). In order to match the spatial

resolution of species and climatic data, we up-scaled TWI and CAR from the 90×90m spatial resolution of SRTM data to 1000×1000m, using the median (*TWI_MD*, *CAR_MD*) and standard-deviation (*TWI_SD*, *CAR_SD*) as aggregation functions (see also Appendix III – S3 for a numeric description of these variables).

Land use data and scenarios

Land use has been previously related to herptile species richness and distribution (Martins et al. 2014, Trimble and van Aarde 2014). In addition, land use change has also been linked to herptile community composition and diversity (Wanger et al. 2010, Trimble and van Aarde 2014). Following this rationale, we considered land use data with a spatial resolution of 1km as a categorical predictor in the models (hereafter termed *LULC_CL*). These data were available from the EURURALIS project (Eickhout and Prins 2008), providing current land use information at European level as well as scenarios for future land use change. Scenario data for land use were obtained by the Dynamic Conversion of Land Use and its Effects Model (Dyna-CLUE) software, which integrates demand-driven changes in land area with locally determined conversion processes, thus allowing an exploration of the future dynamics of European land use and landscapes (Verburg and Overmars 2009). We applied the model on pre-existing land use data for Europe based on a reclassified version of Corine Land Cover (EEA 2007) which included a total of 16 land use types with eight types represented in the study-area (see complete list in Appendix III – S5, and also the area coverage for each land use class, relative frequencies, and transition matrices between present and future scenarios). The most updated version of the land use projections dataset (for year 2050) was available for IPCC4 storylines A1 and B2, which was used for forecasting the test species distributions.

Model development: fitting, evaluation and projection

Before model fitting, we tested potential multicollinearity effects in the selected spatial covariates by calculating Pearson correlation (see Appendix III – S6). Since all absolute pairwise correlations were below 0.75 we kept all ten initially selected variables for model fitting.

Model development used the *biomod2* platform (Thuiller et al. 2009). Seven modelling techniques were employed and combined with model parameters set to default: (1) generalized linear model (GLM); (2) generalized additive model (GAM); (3) generalized boosted models (GBM); (4) classification tree analysis (CTA); (5) flexible

discriminant analysis (FDA); (6) random forests (RFO); and (7) maximum entropy (MAX). Since true absence data were unavailable, we generated 30 sets of randomly selected pseudo-absences, keeping an equal number of presences and pseudo-absences for each set. We calibrated the models with 80% of the data selected at random, and then evaluated the predictive performance of each model on the remaining 20% with two evaluation metrics: the area under the Receiver Operating Characteristic (ROC) curve (AUC; Fielding and Bell (1997); but see Lobo et al. (2008)) and the maximum true-skill statistic (TSS; Jolliffe and Stephenson (2003)). Although TSS is a threshold-dependent measure, *biomod2* tests multiple sequenced values, bounded within the prediction probability interval: [0, 1000], to determine the threshold maximizing TSS. We performed holdout cross-validation for 10 rounds and then averaged the evaluation results across all rounds. We calculated variable importance by *biomod2* without accounting for interactions, and finally we averaged it for pseudo-absence sets, evaluation rounds, and modelling algorithms.

In order to produce robust forecasts for the test species distribution, we obtained an ensemble forecast combining the five best (out of seven) modelling techniques for each species. Then, for each technique we selected the upper 2.5% quantile of the best performing models as ranked by AUC. Model predictions from the selected models were then averaged to produce the final ensemble.

Using the ensemble model calibrated for current conditions, we projected the future distribution of the selected species using two sets of conditions for the reference year of 2050: (i) a low-emissions scenario (LES) combining climatic projections for IPCC-AR5/RCP 2.6 and land use projections for the IPCC-AR4/B2 scenario, and, (ii) a high-emissions scenario (HES) combining climatic projections for IPCC-AR5/RCP 8.5 and land use projections for the IPCC-AR4/A1 scenario. We partitioned ensemble probability maps for current and projected future conditions into binary maps of suitable/unsuitable areas by choosing the probability threshold (ranging from 0 to 1000) that minimized the distance between the ROC curve and the (0, 1) point (Liu et al. 2005); see also Table 1).

Species distribution dynamics

Model projections for current and future conditions allowed quantifying changes in suitable area distribution, therefore, allowing to define four distinct types of dynamics: (i) ”unsuitable”, areas currently predicted as unsuitable that will remain unsuitable in future projections; (ii) “lost”, areas currently predicted as suitable that will lose suitability in the future; (iii) ”kept”, areas that are currently predicted as suitable that will remain with

suitable conditions in the future, and (iv) ”new”, areas that are currently predicted as unsuitable that may become suitable in the future.

In this analysis, we assumed that populations affected by loss of environmental suitability (*i.e.*, in areas identified as “lost”), due to combined effects of climate and land use changes, will be forced to migrate to stable areas that remain suitable under the future conditions (identified as “kept”). Thus, we analysed the likelihood of potential migrations from “lost” to “kept” areas by quantifying the functional connectivity between these two instances, measured as the degree to which the landscape facilitates or hinders the movement of each test species; the analysis was therefore both species and landscape-specific (Taylor et al. 1993, Watts et al. 2010). It would also be possible to study the potential colonization of projected new suitable areas by analysing connectivity between “kept” and/or “lost” areas to “new” areas. Nonetheless, in this test we focused our attention on how species will respond to loss of conditions by reaching stable areas, and thus on the likelihood of potential migrations from “lost” to “kept” areas.

Connectivity analyses

We performed connectivity analyses with LORACS software (Pinto and Keitt 2009, Pinto et al. 2012) implementing a graph-theoretical approach to calculate corridor redundancy, while accounting for landscape matrix resistance. This procedure allowed evaluating multiple shortest-paths (SP) from “lost” to “kept” areas, assumed to represent potential dispersal corridors.

The parameterization of LORACS was set to a corridor width of 30% (which defines corridor breadth size) and 10 different SPs were calculated between each “lost” cell, hereafter denoted as a source area, $s_i, i \in \{1, \dots, m\}$, and the closest target “kept” area, denoted as $t_j, j \in \{1, \dots, n\}$ measured by the Euclidean distance between the two sites. We then aggregated the results for the 10 simulated SPs to the average cost distance, denoted as $c(s_i, t_j)$. In order to simulate variability in potential migration routes, we calculated the average cost distance between a source area and multiple k neighbouring target areas, residing in different and spatially disjoint “kept” habitat patches, $P_u, u \in \{1, \dots, p\}$ and $t \subset P$ (see Appendix III – S5 and S7). We computed connectivity to the five nearest-neighbours and averaged to calculate the Mean Functional Distance index (MFD; Equation 1), given by:

$$MFD_i = \frac{1}{\mathrm{k}} \sum^{\mathrm{k}} c(s_i, t_j) \qquad \text{(Equation 1)}$$

This index represents a cost-based distance metric of functional connectivity which explicitly uses a cost-surface defining landscape matrix resistance (including, in this study: habitat suitability, topographical complexity and road effects). MFD calculation is based on the assessment of multiple least-cost paths (within a predefined corridor breathe) thus allowing to analyse linkage redundancy and variability. The MFD index varies from > 0 to an undefined upper bound and is measured on "resistance" units since it depends on the spatial configuration of source/target areas and the spatial patterning of landscape resistance values. Overall, higher values of MFD signal lower connectivity. LORACS software calculates multiple SPs enabling to compute the number of times that a given area is redundantly selected for the pathway of a given shortest-path, noted as $a(s_i, t_j) \in [0, 10]$ (with the maximum value equal to the number of simulated SPs). Calculating the total summation of $a(s_i, t_j)$ across all source areas (Equation 2), and k neighbours, we obtained a zonation of areas important for maintaining connectivity, as well as, potential migration corridors, defined as:

$$SPsum = \sum^{\mathrm{m}} \sum^{\mathrm{k}} a(s_i, t_j) \qquad \text{(Equation 2)}$$

This index assumes integer-only values and varies from 0 to an undefined upper bound. In general, a higher amount of source areas increases the upper limit of $SPsum$, which means that particular areas are selected more frequently in least-cost pathways. For this index, higher values correlate to areas that are relatively more important for maintaining connectivity or potential corridors.

By mapping the $SPsum$ index, we further analysed the intersection between important areas for connectivity (for which: $SPsum \geq 1$) and the national motorway network (considering a buffer of 500m around each road) in order to evaluate conflicts for each species.

In order to determine shortest-paths, LORACS uses a cost-surface defining landscape matrix resistance to movement. In this study, the cost-surface included three main components hypothesized to affect movement or dispersal probabilities for each test species, thus affecting functional connectivity (Spear et al. 2010). These components were related to: (i) projected habitat suitability for each species, (ii) linear structures inducing barrier or high-resistance effects, and (iii) topographic roughness/heterogeneity. The total landscape resistance cost was obtained by a weighted sum of each rescaled partial component (see details in Appendix III – S7). We

implemented the connectivity analyses and spatial indices as a distributable R package (available by contacting the corresponding author).

6.3. Results

Model performance

Cross-validation tests indicated that overall model performance ranged from excellent to good considering AUC (0.94 to 0.83), while in general, TSS recorded more conservative performance ranging from good to moderate (0.80 to 0.52; Table 6 - 1). In a decreasing order, *C. lusitanica* recorded the best test results (0.94 - AUC; 0.80 - TSS) followed by *A. fragilis* (0.90 - AUC; 0.68 - TSS), *L. schreiberi* (0.88 - AUC; 0.61 - TSS), and *E. calamita* (0.83 - AUC; 0.52 - TSS). Overall, results also indicated that applying ensemble forecast techniques increased the model performance (see "*Ensemble*" column, Table 6 - 1). When comparing different modelling algorithms, GAM was the best performing technique for all species, followed by GBM, Random Forests, and Maxent.

Table 6 - 1 – Model performance statistics for biomod2 partial models and the final ensemble model ("Ensemble" column). Results were averaged across the test sets, pseudo-absence sets and model runs. Two evaluation measures were calculated: AUC (area under the curve), and TSS (true-skill statistic). Seven modelling techniques were used: GLM (Generalized Linear Model), GBM (Generalized Boosting Model), GAM (Generalized Additive Model), CTA (Classification Tree Analysis), FDA (Flexible Discriminant Analysis), RFO (Random Forests), and MAX (Maximum Entropy Model). Modelling techniques highlighted with an asterisk (*; i.e., the best five techniques by species considering the AUC values) were included in the final ensemble. Column "Cutoff" displays the value used to partition ensemble probability maps (ranging from 0 to 1000) into suitable/unsuitable areas; values inside parenthesis represent respectively the Sensitivity (or true positive rate) and Specificity (or true negative rate). Species are *Anguis fragilis* (ANGFR), *Lacerta schreiberi* (LACSH), *Chioglossa lusitanica* (CHALU) and *Epidalea calamita* (EPCAL).

Species	Eval. measure	GLM	GBM	GAM	CTA	FDA	RFO	MAX	Ensemble	Cutoff (Sens. /spec.)
ANGFR	AUC	0.82*	0.82*	0.87*	0.77	0.81	0.82*	0.82*	0.90	559.5 (0.93; 0.75)
	TSS	0.56	0.58	0.65	0.52	0.56	0.58	0.57	0.68	
LACSH	AUC	0.73	0.75*	0.86*	0.67	0.74*	0.76*	0.76*	0.88	629.5 (0.84; 0.77)
	TSS	0.45	0.48	0.62	0.35	0.44	0.48	0.48	0.61	
CHALU	AUC	0.88	0.90*	0.95*	0.82	0.89*	0.89*	0.89*	0.94	505.5 (1.00; 0.80)
	TSS	0.71	0.74	0.83	0.63	0.74	0.74	0.73	0.80	
EPCAL	AUC	0.67*	0.68*	0.76*	0.60	0.66*	0.67*	0.66	0.83	502.5 (0.87; 0.65)
	TSS	0.33	0.34	0.44	0.22	0.31	0.34	0.31	0.52	

Species distribution dynamics under climate and land use changes

The distribution of potential suitable areas based on ensemble forecasting presented a diverse array of spatial responses to environmental changes across scenarios (Figure 6 - 3, Figure 6 - 4, and Figure 6 - 5; see also, Appendix III – S8 and S9). The test species were overall more sensitive to climatic (especially BIO_14, BIO_04 and BIO_05) and topographic (mainly TWI_MD) than to land use variables (see Figure 6 - 2 and Appendix III – S10 for more details).

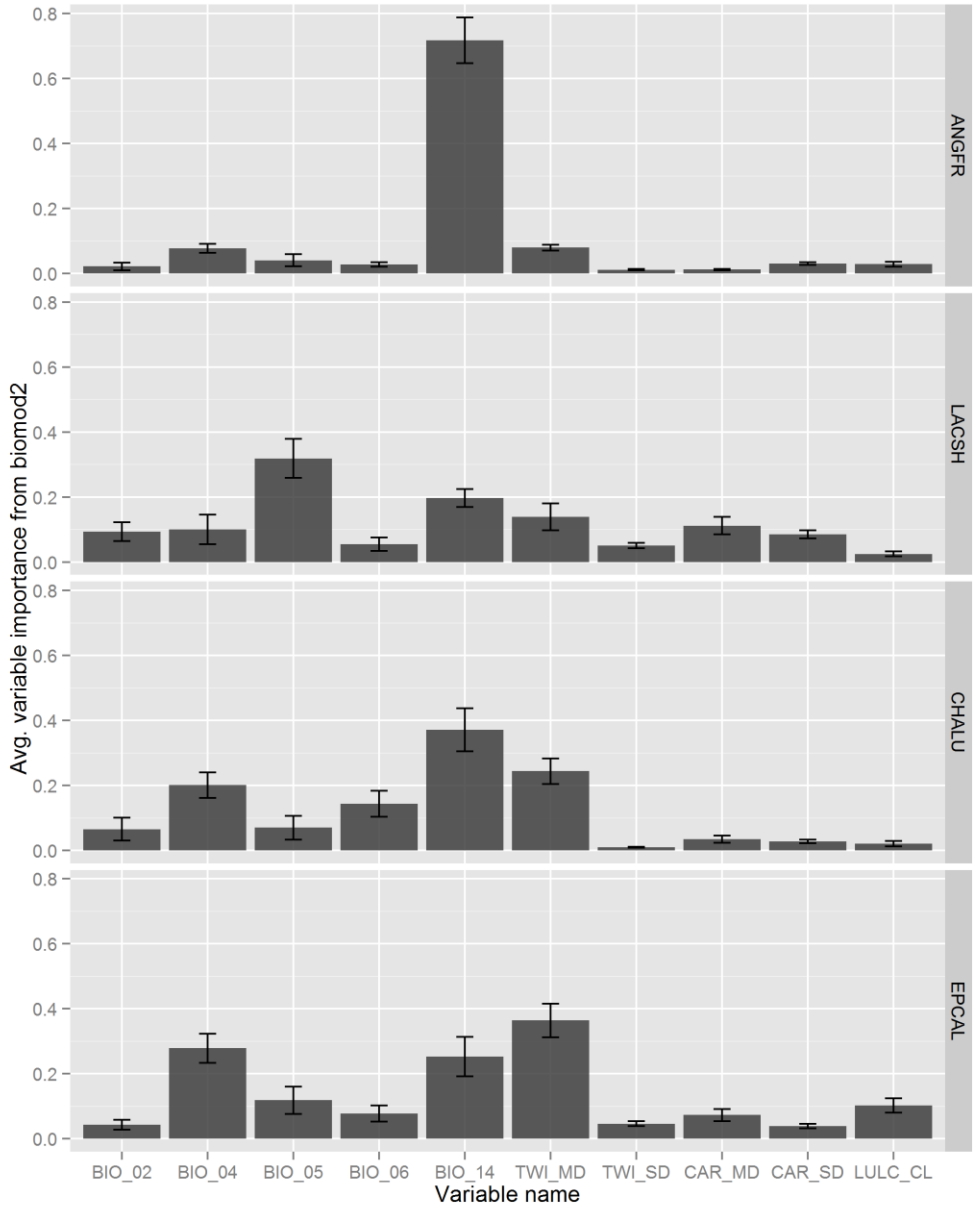

Figure 6 - 2 – Barplot displaying variable importance by species and averaged across all pseudo-absence sets, evaluation rounds and modelling algorithms. Error bars represent the standard-errors across modelling techniques. Species are *Anguis fragilis* (ANGFR), *Lacerta schreiberi* (LACSH), *Chioglossa lusitanica* (CHALU) and *Epidalea calamita* (EPCAL).

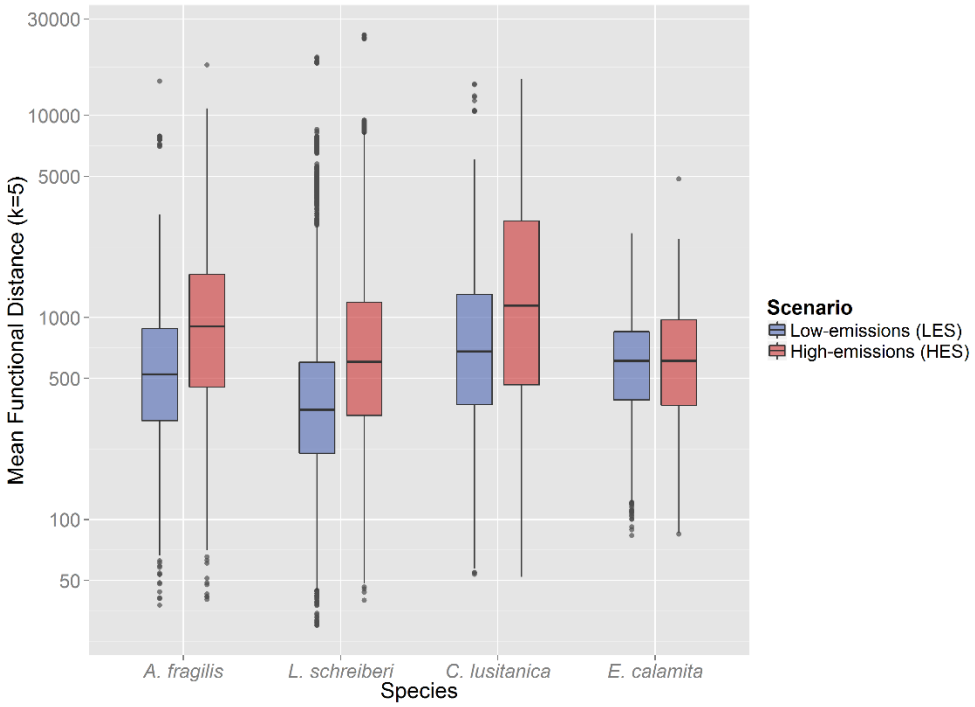

Figure 6 - 3 – Boxplot of the Mean Functional Distance index by species and scenario. The yy-axis was log transformed and outliers, *i.e.*, values 2 times the inter-quartile range outside the box, were represented as points. LES – low-emissions scenario (blue boxes); HES – high-emissions scenario (red boxes).

For three of the four species, a substantial decrease of their current distribution was projected for 2050 (-44.6% to -73.5%, Table 6 - 2) considering both scenarios, although range contraction was higher under the high-emissions scenario (HES). The net variation percentage (Table 6 - 2), balancing losses and gains of suitable area, was negative for the majority of species: *L. schreiberi* (LES: -61.2%, HES: -73.5%), *C. lusitanica* (LES: -54.1%, HES: -71.3%) and *A. fragilis* (LES: -44.6%, HES: -60.7%), but positive for *E. calamita*, the single species for which gains of suitable space were clearly higher than losses (LES: 51.9%, HES: 66.5%). Major losses were observed for areas exhibiting less pronounced or transitional Atlantic climatic characteristics. These areas are mostly distributed along the north and central-eastern inland regions of Portugal, the main mountain areas in the central region, and the north-east mountains (Figure 6 - 4 - a,d,g,j and Figure 6 - 5 - a,d). Contrastingly, *E. calamita* major gains were projected for the eastern Mediterranean climatic regions and the centre south-western coast of Portugal (Figure 6 - 5 - g,j).

Table 6 - 2 – Net variation in percentage ($\%nv = ((New + Kept)/(Kept + Lost) - 1) \times 100$) by species and scenario (2050 scenario: HES – high-emissions scenario; LES – low-emissions scenario) showing habitat area losses and gains, derived from the joint effects of climate and land use changes. Descriptive statistics (median) for the Mean Functional Distance index (MFD, k=5) by species and scenario.

Species	2050 scenario	$\%nv$	Median MFD (k=5)
A. fragilis	LES	-44.6%	522.7
	HES	-60.7%	902.3
L. schreiberi	LES	-61.2%	350.2
	HES	-73.5%	602.6
C. lusitanica	LES	-54.1%	678.4
	HES	-71.3%	1143.2
E. calamita	LES	51.9%	611.0
	HES	66.5%	611.2

Effects of landscape fragmentation on regional connectivity

Connectivity results obtained for the Mean Functional Distance index (MFD, see Table 6 - 2, and Appendix III – S11), considering the low-emissions scenario, revealed that *C. lusitanica* obtained the lowest connectivity, corresponding to the highest median value (678.4), followed by *E. calamita* (611.0), *A. fragilis* (522.7) and *L. schreiberi* (350.2). For the high-emissions scenario, *C. lusitanica* (1143.2) also presented the lowest connectivity, followed by *A. fragilis* (902.3), *E. calamita* (611.2) and *L. schreiberi* (602.6). Higher geographical distance between areas projected to lose environmental suitability and areas expected to maintain it in the future, combined with the conditions for higher landscape fragmentation and resistance to dispersal conduced invariably to the lowest connectivity values.

The *SPsum* index presented similar patterns for *A. fragilis* and *C. lusitanica* under both scenarios (Figure 6 - 4 - c,f and Figure 6 - 5 - c,f) with important areas for connectivity stretching from north to the centre of the country in the interior region of Portugal. For *E. calamita* important connectivity areas were mainly located in the upper NW part of the country (Figure 6 - 5 - i,l). Finally, *L. schreiberi* presented a more complex spatial patterning, with the most important areas occurring in the central part of the country (Figure 6 - 4 - i,l). The spatial intersection of motorways and important areas for connectivity presented similar values across all species and scenarios, varying from approximately 5 to 7% (Table 6 - 3), with *C. lusitanica* showing the highest values (LES: 7.10% and HES: 6.89%), followed by *L. schreiberi* (6.48% and 6.67%), *A. fragilis* (6.04% and 6.27%) and *E. calamita* (4.86% and 4.71%). Although spatial intersection presented relatively low values (Table 6 - 3), in many cases motorways have intersected areas with high values for the *SPsum* index, which represent an overlap with areas extremely important for maintaining connectivity in potential migration corridors (Figure 6 - 6).

Figure 6 - 4 – Map representation of species distribution dynamics (a,d,g,j), connectivity between "lost" (source areas) and "kept" (target areas) using the Mean Functional Distance index (MFD, k=5; b,e,h,k), and the zonation of important areas for connectivity using the SPsum index (c,i,f,l) for each reptile species (*A. fragilis, L. schreiberi*) and scenario (low-emissions scenario and high-emissions scenario)

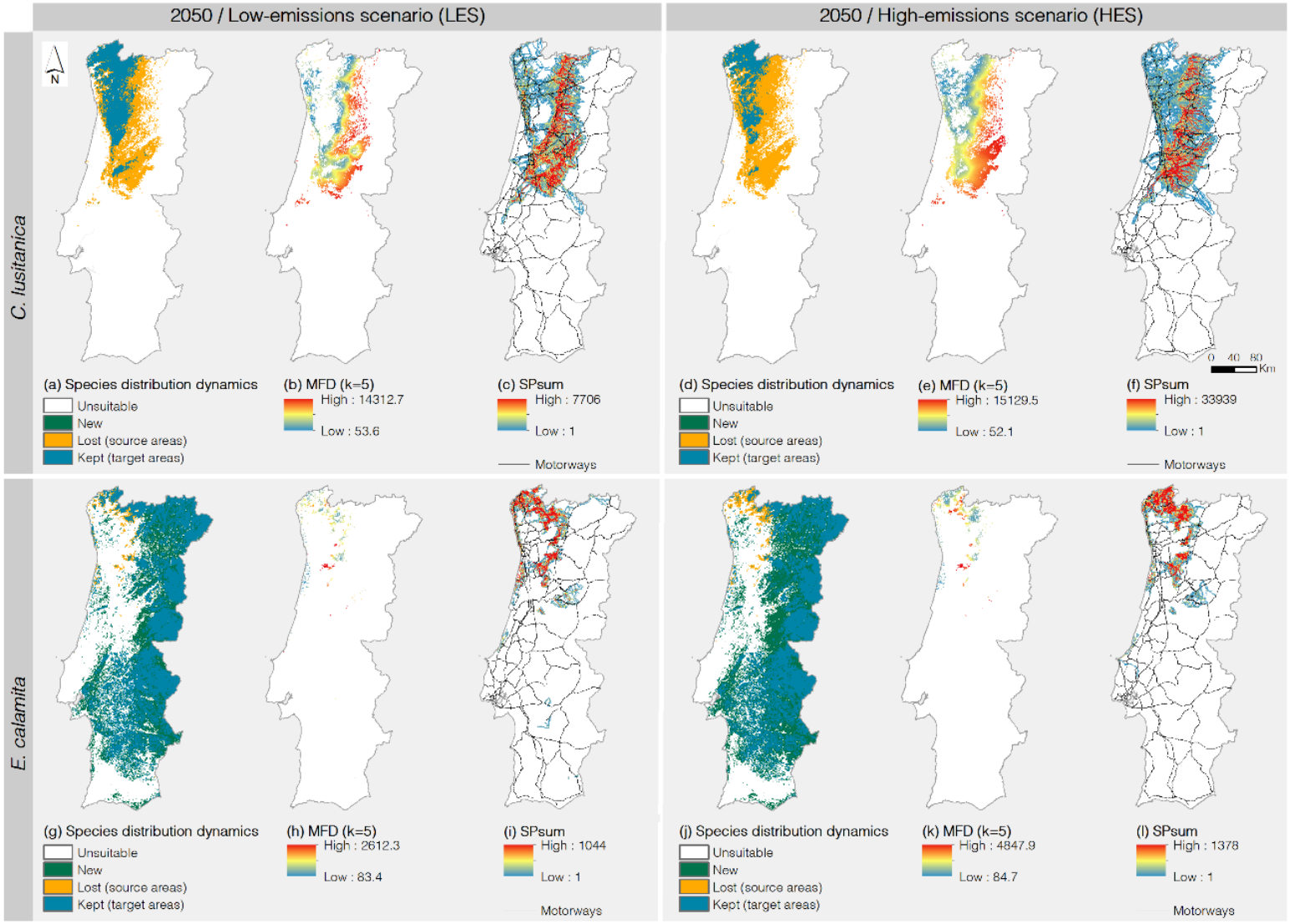

Figure 6 - 5 – Map representation of species distribution dynamics (a,d,g,j), connectivity between "lost" (source areas) and "kept" (target areas) using the Mean Functional Distance index (MFD, k=5; b,e,h,k), and the zonation of important areas for connectivity using the SPsum index (c,i,f,l) for each amphibian species (C. lusitanica, E. calamita) and scenario (low-emissions scenario and high-emissions scenario).

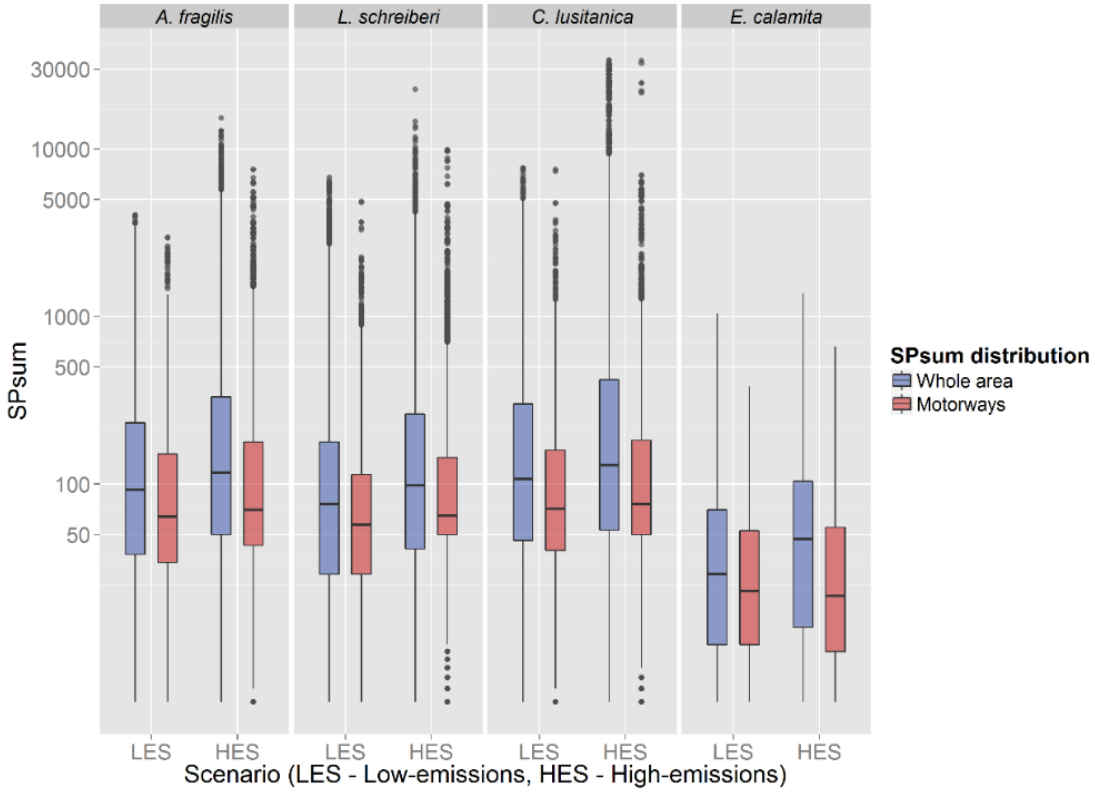

Figure 6 - 6 – Boxplot showing the distributions of *SPsum* values for all areas important for maintaining connectivity (i.e. with $SPsum \geq$; blue boxes) and those areas intersected by motorways (red boxes) across species and scenarios (LES – low-emissions scenario and HES – high-emissions scenario). The y-axis was log-transformed, and, outliers, *i.e.*, values lying outside the box 2 times the inter-quartile range were represented as points.

Table 6 - 3 – Spatial intersection between important areas for connectivity (*i.e.,* with $SPsum \geq 1$) and the motorway network (considering a buffer of 500m around each road). HES – High-emissions scenario; LES – Low-emissions scenario.

Species	**% intersected by motorway network**	
	LES	**HES**
A. fragilis	6.04%	6.27%
L. schreiberi	6.48%	6.67%
C. lusitanica	7.10%	6.89%
E. calamita	4.86%	4.71%

6.4. Discussion

Species distribution drivers, projections and uncertainty

Ecological and biogeographic theory establishes that species distributions are determined by processes acting at multiple spatial and temporal scales (Lomolino et al. 2006, Vicente et al. 2014). In this study at a regional scale, climatic and topographic variables were comparatively more important than land use variables for predicting the test-species distributions, as previously observed in similar studies (Luoto et al. 2007, Martin et al. 2013, Sohl 2014). Projected range shifts for our test-species were also more affected by changes in climate than in land use. These results may confirm that climate is known to determine species distributions at broader spatial scales (*i.e.* regional to global, e.g., (Pearson and Dawson 2003, Luoto et al. 2007)). They may also reflect the relatively coarse resolution of the land use dataset used (1000×1000m), potentially generating a scale mismatch for estimating species-environment relations (Wiens et al. 2009).

Climate change scenarios have been extensively used to forecast potential changes of species distributions (Thuiller et al. 2005, Araújo et al. 2006). Land use and its dynamics are also used for modelling species distributions at local and regional scales (Dirnböck et al. 2003), but less often applied to forecast future distributions, probably due to the lack of publicly available post-processed products (Barbet-Massin et al. 2012). Although we found that in our study land use had relatively less predictive power, we incorporated future scenarios for this variable since it is well known that land use changes may cause habitat destruction, degradation and fragmentation, imposing severe pressures on species (Pimm and Raven 2000, Sala et al. 2000) and further limiting their ability to cope with other environmental changes (Barbet-Massin et al. 2012). Interactions among different anthropogenic pressures may cause severe challenges for species and originate unforeseen responses (Jetz et al. 2007, Brook et al. 2008). Therefore, we stress that for adequately analysing these synergies improved and readily available land use/cover datasets are required for current conditions as well as for future scenarios (Tingley and Herman 2009, Martin et al. 2013).

Our approach is not exempt of the uncertainties inherent to using SDMs (Schwartz 2012, Guisan et al. 2013) resulting, among others, from forecasting species' distributions into non-analogous climates (Fitzpatrick and Hargrove 2009), from using different climatic projections, and/or from the modelling algorithms themselves (Buisson et al. 2010). To partially overcome some uncertainties associated with SDMs, we applied

an ensemble forecasting approach combining several modelling algorithms (Thuiller et al. 2009). Still, further enhancements could be achieved by integrating correlative and mechanistic models (Buckley et al. 2010, Ceia-Hasse et al. 2014). Moreover, SDMs assume niche conservatism (broadly defined as the tendency of species to retain ancestral ecological characteristics; Wiens and Graham (2005)) affecting spatial and temporal model projections. Although caution should be taken assuming such assumption, recent studies have found evidence of niche conservatism for amphibians (Olalla-Tárraga et al. 2011), reptiles (Morales-Castilla et al. 2011) and other groups in a wider-breath review by Peterson (2011).

The usual lack of fine-scale resolution environmental data (e.g., on climate or land use) adds further limitations and uncertainty to model calibration (Wiens et al. 2009). Updated and fine-resolution occurrence data for herptiles is also still limited for Europe, which further imposes limitations to the development of SDMs and the robust assessment of species range shifts. Improving data quality is thus essential to produce better and more accurate assessments and model projections (Pôças et al. 2014, Vicente et al. 2014).

Assessing species vulnerability to climate and landscape changes

We proposed a three-step approach to assess the vulnerability of species to several environmental change processes, combining species distribution dynamics with functional connectivity. The approach relies on predictors related to climate, land use, and topography, delivering range shift projections based on future climate and land use dynamics. By integrating the statistical robustness and projections of SDMs (by applying ensemble forecasting) with functional connectivity analysis, we were able to obtain realistic projections for future dynamics of target species under contrasting scenarios. This integrative approach provides valuable insights considering the vulnerability of multiple species to isolation and ultimately to extinction under rapid environmental changes.

Determining the degree to which a given landscape facilitates or hinders the movement of species among suitable habitat or resource patches is essential for conservation and management of wildlife populations (Taylor et al. 1993, Hamer and McDonnell 2008). We assessed broad scale habitat connectivity using a cost surface defining the resistance of the landscape matrix to species' movement, confirming the utility of raster-based models to investigate barriers or facilitators to connectivity, such as roads and/or topography (Cushman et al. 2006). Connectivity analyses allowed the

identification and evaluation of migration corridors, based on a graph-theoretical approach explicitly accounting for species-specific landscape matrix resistance, an analytical approach holding wide breadth and acceptance (Minor and Urban 2008, Pascual-Hortal and Saura 2008, Decout et al. 2012). Our proposed approach allowed to quantify connectivity and assess potential migration corridors with a relatively small amount of input data compared to other widely used approaches, *e.g.* agent-based models (ABM) such as implemented in *MigClim* (Engler and Guisan 2009) or coupled population dynamics-dispersal (CPDD) models such as *RangeShifter* (Bocedi et al. 2014). This data-related advantage makes our framework more generalizable and thus potentially more suited for assessing multiple species.

The proposed framework assumes some simplifications, *e.g.* by not including population or dispersal parameters, a clear advantage in the many cases where such information is simply not available (as in this study). In addition, species' movement responses are strongly dependent on landscape structure and matrix resistance. As a consequence, dispersal may vary heterogeneously throughout the landscape and may be different across regions for the same species (Taylor et al. 2006) thus presenting many challenges for measurement and direct estimation (Jacobson and Peres-Neto 2010). Although for example, dispersal parameters may be available for some species, frequently they are biased towards some specific landscapes or regions.

Complementarily, using the *MFD* or *SPsum* indices for comparing the full spectrum of connectivity values across a study area between different species will provide a preliminary regional-scale synoptic overview of connectivity patterns. This will allow comparing different regions, identifying critical situations and selecting a subset of relevant areas to develop detailed studies, *e.g.* by implementing ABM or CPDD models for assessing changes derived from climate and land use change (Engler and Guisan 2009, Bocedi et al. 2014).

Vulnerability of low dispersal vertebrates

Our results for two contrasting scenarios showed that, within a relatively short time-frame, environmental changes may cause severe impacts on the test species, with strong contractions in suitable area for most of them. Our findings are consistent with previous studies reporting substantial range contractions for herptile species in the Iberian Peninsula under future environmental changes (Araújo et al. 2006, Carvalho et al. 2010). The study species presenting current small ranges in Portugal (*i.e.*, *C. lusitanica, A. fragilis* and *L. schreiberi*) will potentially suffer an important loss of suitable areas. Moreover, *C. lusitanica* and *L. schreiberi* are threatened by other pressures too

(IUCN 2014), exacerbating the synergistic effect of environmental changes. Conversely, *E. calamita*, with a widespread range and higher dispersal capacity, is projected to maintain or even expand its potential suitable area. However, projections of extensive geographic shifts in environmental conditions do not necessarily mean that species distributions will change likewise, as individuals will be able to move and survive in new areas as a function of their dispersal capacity and presence of adequate pathways connecting current and future suitable areas (Baguette et al. 2013). Yet, for less mobile species, such as amphibians and reptiles, projections of large range contractions may suggest higher risk of population isolation under future conditions (McLaughlin et al. 2002).

Connectivity analyses highlighted an overall pattern widely dependent on the complex interplay between the spatial configuration of source/target areas (*i.e.* respectively, areas with projected conservation or loss of environmental suitability in the future) and landscape elements increasing landscape resistance (such as motorways, future habitat suitability decrease, or higher topographic complexity). The complex local patterns of connectivity obtained were particularly evident in areas with similar Euclidean distance between source and target areas but contrasting functional connectivity distances. Additionally, species experiencing a higher contraction of suitable areas clearly showed lower connectivity due to an increase in landscape resistance and geographic distance between “lost” and “kept” areas. The stability and integrity of migration corridors for these species may be further impacted by the presence of motorways (Andrews et al. 2008), making these species even more vulnerable to extinction or isolation under future environmental changes.

Applications in conservation planning and management

The multispecies approach described here provides useful information for conservation and management, by anticipating the ecological effects of rapid environmental changes. On the one hand, it allows the identification of priority areas for conservation together with a deeper understanding of how landscape resistance will promote or hinder species movements. On the other hand, connectivity analyses improve the identification of potential migration corridors, essential when designing appropriate conservation or protection measures for multi-objective environmental planning (Dennis et al. 2013, Nunez et al. 2013). More broadly, our approach can be used to define ecological networks for long-term metapopulation persistence, and to assess the impacts of infrastructures on species movements.

Likewise, our approach can be used to design management interventions and set priorities aiming to increase landscape connectivity, thereby contributing to climate change adaptation for multiple species (Heller and Zavaleta 2009, Krosby et al. 2010) by facilitating dispersal and mitigating the impacts of land use dynamics. Previous studies have shown that habitat restoration along model-informed landscape corridors is a better promoter of metapopulation persistence, compared to expert-informed habitat restoration (Hodgson et al. 2011). In fact, the importance of considering landscape connectivity when selecting and designing habitat reserves has been widely acknowledged in the literature (e.g., (Minor and Urban 2008, Alagador et al. 2012)).
The design of impact mitigation actions can also be improved using the approach described here. Mapping the intersections between key migration corridors and motorways can guide managers and planners in determining which motorway segments will most likely act as barriers, thus having the greatest impact on wildlife movement (McRae et al. 2012). This information can be used to plan and implement conservation measures intended to mitigate fragmentation effects, for example, specific road-crossing structures.

Finally, the application of our framework can improve the effectiveness of monitoring schemes, a main component of adaptive conservation management under global change (Lindenmayer and Likens 2009), specifically by guiding the design of efficient observation networks. This corroborates the increasing application of SDMs for ecological monitoring and conservation, with successful examples for different taxa in different ecosystems (e.g., (Carvalho et al. 2015, Vicente et al. 2016)). Moreover, by integrating landscape corridors in the design of monitoring networks, valuable ecological information can be collected to explain and predict species movements under environmental change. This may be essential for species of high-conservation concern and with low dispersal capacity, such as amphibians and reptiles, for which patches playing an important connectivity role must be identified and highlighted as of conservation and/or monitoring priority (e.g., (Minor and Urban 2008, Pascual-Hortal and Saura 2008)). More broadly, the identification of potential dispersal corridors or areas of the landscape promoting dispersal is crucial for effectively long-term monitoring and adaptive management of the wildlife populations (Bennett and Saunders 2010).

Acknowledgments

João Gonçalves is financially supported by FCT (Portuguese Science Foundation) through PhD grant SFRH/BD/90112/2012. J.R. Vicente received support from the Portuguese Ministry of Education and Science and the European Social Fund, though the Portuguese Foundation of Science and Technology (FCT), under POPH - QREN - Typology 4.1. J. Honrado was supported by FCT and FEDER/COMPETE through project MOBIA (PTDC/AAC-AMB/114522/2009). Emilio Civantos was supported by Project "Biodiversity, Ecology and Global Change" co-financed by North Portugal Regional Operational Programme 2007/2013 (ON.2 – O Novo Norte), under the National Strategic Reference Framework (NSRF), through the European Regional Development Fund (ERDF).

Author contributions

Author name	Study conception and design	Data processing, analysis and/or modelling	Manuscript writing	Manuscript revision
João Gonçalves	☑	☑	☑	☑
João Honrado	☑		☑	☑
Joana R. Vicente			☑	☑
Emilio Civantos	☑		☑	☑

References

Akçakaya, H. R., G. Mills, and C. P. Doncaster. 2007. The role of metapopulations in conservation. Pages 64-84 *in* D. W. Macdonald and K. Service, editors. Key Topics in Conservation Biology. Blackwell Publishing.

Alagador, D., M. Triviño, J. O. Cerdeira, R. Brás, M. Cabeza, and M. B. Araújo. 2012. Linking like with like: optimising connectivity between environmentally-similar habitats. Landscape Ecology 27:291-301.

Andrews, K. M., J. W. Gibbons, and D. M. Jochimsen. 2008. Ecological effects of roads on amphibians and reptiles: a literature review. Pages 121-143 *in* J. C. Mitchell, R. E. J. Brown, and B. Bartholomew, editors. Urban Herpetology. Society for the Study of Amphibians & Reptiles, Salt Lake City, UT.

Angilletta Jr, M. J., P. H. Niewiarowski, and C. A. Navas. 2002. The evolution of thermal physiology in ectotherms. Journal of Thermal Biology 27:249-268.

Araújo, M. B., W. Thuiller, and R. G. Pearson. 2006. Climate warming and the decline of amphibians and reptiles in Europe. Journal of Biogeography 33:1712-1728.

Baguette, M., S. Blanchet, D. Legrand, V. M. Stevens, and C. Turlure. 2013. Individual dispersal, landscape connectivity and ecological networks. Biological Reviews 88:310-326.

Barbet-Massin, M., W. Thuiller, and F. Jiguet. 2012. The fate of European breeding birds under climate, land-use and dispersal scenarios. Global Change Biology 18:881-890.

Beier, P., W. Spencer, R. F. Baldwin, and B. H. McRae. 2011. Toward best practices for developing regional connectivity maps. Conserv Biol 25:879-892.

Bellard, C., C. Bertelsmeier, P. Leadley, W. Thuiller, and F. Courchamp. 2012. Impacts of climate change on the future of biodiversity. Ecology Letters 15:365-377.

Bennett, A. F., and D. A. Saunders. 2010. Habitat fragmentation and landscape change. Pages 88-106 *in* N. S. Sodhi and P. R. Ehrlich, editors. Conservation Biology for All. Oxford University Press, New York, US.

Blank, L., and L. Blaustein. 2012. Using ecological niche modeling to predict the distributions of two endangered amphibian species in aquatic breeding sites. Hydrobiologia 693:157-167.

Blaustein, A. R., L. K. Belden, D. H. Olson, D. M. Green, T. L. Root, and J. M. Kiesecker. 2001. Amphibian Breeding and Climate Change. Conservation Biology 15:1804-1809.

Bocedi, G., S. C. F. Palmer, G. Pe'er, R. K. Heikkinen, Y. G. Matsinos, K. Watts, J. M. J. Travis, and R. Freckleton. 2014. RangeShifter: a platform for modelling spatial eco-evolutionary dynamics and species' responses to environmental changes. Methods in Ecology and Evolution 5:388-396.

Boria, R. A., L. E. Olson, S. M. Goodman, and R. P. Anderson. 2014. Spatial filtering to reduce sampling bias can improve the performance of ecological niche models. Ecological Modelling 275:73-77.

Brook, B. W., N. S. Sodhi, and C. J. A. Bradshaw. 2008. Synergies among extinction drivers under global change. Trends in Ecology & Evolution 23:453-460.

Buckley, L. B., M. C. Urban, M. J. Angilletta, L. G. Crozier, L. J. Rissler, and M. W. Sears. 2010. Can mechanism inform species' distribution models? Ecol Lett 13:1041-1054.

Buisson, L., W. Thuiller, N. Casajus, S. Lek, and G. Grenouillet. 2010. Uncertainty in ensemble forecasting of species distribution. Global Change Biology 16:1145-1157.

Carvalho, S. B., J. C. Brito, E. J. Crespo, and H. P. Possingham. 2010. From climate change predictions to actions - conserving vulnerable animal groups in hotspots at a regional scale. Global Change Biology 16:3257-3270.

Carvalho, S. B., J. Gonçalves, A. Guisan, and J. P. Honrado. 2015. Systematic site selection for multispecies monitoring networks. Journal of Applied Ecology:n/a-n/a.

Ceia-Hasse, A., B. Sinervo, L. Vicente, and H. M. Pereira. 2014. Integrating ecophysiological models into species distribution projections of European reptile range shifts in response to climate change. Ecography 37:679-688.

Chen, I.-C., J. K. Hill, R. Ohlemüller, D. B. Roy, and C. D. Thomas. 2011. Rapid Range Shifts of Species Associated with High Levels of Climate Warming. Science 333:1024-1026.

Clark, P. J., and F. C. Evans. 1954. Distance to Nearest Neighbor as a Measure of Spatial Relationships in Populations. Ecology 35:445-453.

Cushman, S. A., K. S. McKelvey, J. Hayden, and M. K. Schwartz. 2006. Gene flow in complex landscapes: testing multiple hypotheses with causal modeling. Am Nat 168:486-499.

Decout, S., S. Manel, C. Miaud, and S. Luque. 2012. Integrative approach for landscape-based graph connectivity analysis: a case study with the common frog (Rana temporaria) in human-dominated landscapes. Landscape Ecology 27:267-279.

Dennis, R. L. H., L. Dapporto, J. W. Dover, and T. G. Shreeve. 2013. Corridors and barriers in biodiversity conservation: a novel resource-based habitat perspective for butterflies. Biodiversity and Conservation 22:2709-2734.

Devictor, V., L. Godet, R. Julliard, D. Couvet, and F. Jiguet. 2007. Can common species benefit from protected areas? Biological Conservation 139:29-36.

Dirnböck, T., S. Dullinger, and G. Grabherr. 2003. A regional impact assessment of climate and land-use change on alpine vegetation. Journal of Biogeography 30:401-417.

Duellman, W. E., and L. Trueb. 1986. Biology of Amphibians. McGraw Hill, New York.

EEA. 2007. CLC2006 technical guidelines. Page 70. Office for Official Publications of the European Communities, Luxembourg.

Eickhout, B., and A. G. Prins. 2008. Eururalis 2.0 - Technical background and indicator documentation. Wageningen UR and Netherlands Environmental Assessment Agency (MNP) Bilthoven, The Netherlands.

Engler, R., and A. Guisan. 2009. MigClim: Predicting plant distribution and dispersal in a changing climate. Diversity and Distributions 15:590-601.

Fahrig, L., and G. Merriam. 1994. Conservation of Fragmented Populations. Conservation Biology 8:50-59.

Fielding, A. H., and J. F. Bell. 1997. A review of methods for the assessment of prediction errors in conservation presence/absence models. Environmental Conservation 24:38-49.

Fitzpatrick, M. C., and W. W. Hargrove. 2009. The projection of species distribution models and the problem of non-analog climate. Biodiversity and Conservation 18:2255-2261.

Gibbons, J. W., D. E. Scott, T. J. Ryan, K. A. Buhlmann, T. D. Tuberville, B. S. Metts, J. L. Greene, T. Mills, Y. Leiden, S. Poppy, and C. T. Winne. 2000. The Global Decline of Reptiles, Déjà Vu Amphibians. BioScience 50:653.

Gruber, S., and S. Peckham. 2008. Land-Surface Parameters and Objects in Hydrology.*in* T. Hengl and H. I. Reuter, editors. Geomorphometry: Concepts, Software, Applications - Developments in Soil Science. Elsevier.

Guisan, A., R. Tingley, J. B. Baumgartner, I. Naujokaitis-Lewis, P. R. Sutcliffe, A. I. T. Tulloch, T. J. Regan, L. Brotons, E. McDonald-Madden, C. Mantyka-Pringle, T. G. Martin, J. R. Rhodes, R. Maggini, S. A. Setterfield, J. Elith, M. W. Schwartz, B. A. Wintle, O. Broennimann, M. Austin, S. Ferrier, M. R. Kearney, H. P. Possingham, and Y. M. Buckley. 2013. Predicting species distributions for conservation decisions. Ecology Letters 16:1424-1435.

Hamer, A. J., and M. J. McDonnell. 2008. Amphibian ecology and conservation in the urbanising world: A review. Biological Conservation 141:2432-2449.

Hanski, I. 1998. Metapopulation dynamics. Nature 396:41-49.

Heller, N. E., and E. S. Zavaleta. 2009. Biodiversity management in the face of climate change: A review of 22 years of recommendations. Biological Conservation 142:14-32.

Hijmans, R. J., S. E. Cameron, J. L. Parra, P. G. Jones, and A. Jarvis. 2005. Very high resolution interpolated climate surfaces for global land areas. Pages 1965-1978. John Wiley & Sons, Ltd.

Hodgson, J. A., A. Moilanen, B. A. Wintle, and C. D. Thomas. 2011. Habitat area, quality and connectivity: striking the balance for efficient conservation. Journal of Applied Ecology 48:148-152.

Hodgson, J. A., C. D. Thomas, B. A. Wintle, and A. Moilanen. 2009. Climate change, connectivity and conservation decision making: back to basics. Journal of Applied Ecology 46:964-969.

IPCC. 2014. Climate Change 2014 - Synthesis Report (Longer Report), Fifth Assessment Synthesis Report.

IUCN. 2014. The IUCN Red List of Threatened Species. Version 2014.3.

Jacobson, B., and P. R. Peres-Neto. 2010. Quantifying and disentangling dispersal in metacommunities: how close have we come? How far is there to go? Landscape Ecology 25:495-507.

Jarvis, A., H. I. Reuter, A. Nelson, and E. Guevara. 2008. Hole-filled SRTM for the globe Version 4, available from the CGIAR-CSI SRTM 90m Database (http://srtm.csi.cgiar.org).

Jetz, W., D. S. Wilcove, and A. P. Dobson. 2007. Projected Impacts of Climate and Land-Use Change on the Global Diversity of Birds. PLoS Biol 5:e157.

Jolliffe, I. T., and D. B. Stephenson. 2003. Forecast Verification - A Practitioner's Guide in Atmospheric Science. 1st Ed. edition. John Wiley & Sons, Chichester, West Sussex, England.

Krosby, M., J. Tewksbury, N. M. Haddad, and J. Hoekstra. 2010. Ecological connectivity for a changing climate. Conserv Biol 24:1686-1689.

Lindenmayer, D. B., and G. E. Likens. 2009. Adaptive monitoring: a new paradigm for long-term research and monitoring. Trends in Ecology & Evolution 24:482-486.

Liu, C., P. M. Berry, T. P. Dawson, and R. G. Pearson. 2005. Selecting thresholds of occurrence in the prediction of species distributions. Ecography 28:385-393.

Lobo, J. M., A. Jiménez-Valverde, and R. Real. 2008. AUC: a misleading measure of the performance of predictive distribution models. Global Ecology and Biogeography 17:145-151.

Lomolino, M. V., B. R. Riddle, and J. H. Brown. 2006. Biogeography. 3rd edition. Sinauer Associates, Sunderland, MA.

Loureiro, A., N. Ferrand de Almeida, M. A. Carretero, and O. S. Paulo. 2008. Atlas dos Anfíbios e Répteis de Portugal. 1st Ed. edition. Instituto da Conservação da Natureza, Lisboa.

Luoto, M., R. Virkkala, and R. K. Heikkinen. 2007. The role of land cover in bioclimatic models depends on spatial resolution. Global Ecology and Biogeography 16:34-42.

Luque, S., S. Saura, and M.-J. Fortin. 2012. Landscape connectivity analysis for conservation: insights from combining new methods with ecological and genetic data. Landscape Ecology 27:153-157.

Martin, Y., H. Van Dyck, N. Dendoncker, and N. Titeux. 2013. Testing instead of assuming the importance of land use change scenarios to model species distributions under climate change. Global Ecology and Biogeography 22:1204-1216.

Martins, I. S., V. Proença, and H. M. Pereira. 2014. The unusual suspect: Land use is a key predictor of biodiversity patterns in the Iberian Peninsula. Acta Oecologica 61:41-50.

McLaughlin, J. F., J. J. Hellmann, C. L. Boggs, and P. R. Ehrlich. 2002. Climate change hastens population extinctions. Proceedings of the National Academy of Sciences 99:6070-6074.

McRae, B. H., S. A. Hall, P. Beier, and D. M. Theobald. 2012. Where to restore ecological connectivity? Detecting barriers and quantifying restoration benefits. PLoS One 7:e52604.

Minor, E. S., and D. L. Urban. 2008. A graph-theory framework for evaluating landscape connectivity and conservation planning. Conserv Biol 22:297-307.

Morales-Castilla, I., M. Á. Olalla-TÁRraga, L. M. Bini, P. De Marco Jr, B. A. Hawkins, and M. Á. RodrÍGuez. 2011. Niche conservatism and species richness patterns of squamate reptiles in eastern and southern Africa. Austral Ecology 36:550-558.

Nunez, T. A., J. J. Lawler, B. H. McRae, D. J. Pierce, M. B. Krosby, D. M. Kavanagh, P. H. Singleton, and J. J. Tewksbury. 2013. Connectivity planning to address climate change. Conserv Biol 27:407-416.

Olalla-Tárraga, M. Á., L. McInnes, L. M. Bini, J. A. F. Diniz-Filho, S. A. Fritz, B. A. Hawkins, J. Hortal, C. D. L. Orme, C. Rahbek, M. Á. Rodríguez, and A. Purvis. 2011. Climatic niche conservatism and the evolutionary dynamics in species range boundaries: global congruence across mammals and amphibians. Journal of Biogeography 38:2237-2247.

Pascual-Hortal, L., and S. Saura. 2008. Integrating landscape connectivity in broad-scale forest planning through a new graph-based habitat availability methodology: application to capercaillie (Tetrao urogallus) in Catalonia (NE Spain). European Journal of Forest Research 127:23-31.

Pearson, R. G. 2006. Climate change and the migration capacity of species. Trends Ecol Evol 21:111-113.

Pearson, R. G., and T. P. Dawson. 2003. Predicting the impacts of climate change on the distribution of species: are bioclimate envelope models useful? Global Ecology and Biogeography 12:361-371.

Peterson, A. T. 2011. Ecological niche conservatism: a time-structured review of evidence. Journal of Biogeography 38:817-827.

Pimm, S. L., and P. Raven. 2000. Biodiversity: Extinction by numbers. Nature 403:843-845.

Pinto, N., and T. Keitt. 2009. Beyond the least-cost path: evaluating corridor redundancy using a graph-theoretic approach. Landscape Ecology 24:253-266.

Pinto, N., T. H. Keitt, and M. Wainright. 2012. LORACS: JAVA software for modeling landscape connectivity and matrix permeability. Ecography 35:388-392.

Pôças, I., J. Gonçalves, B. Marcos, J. Alonso, P. Castro, and J. P. Honrado. 2014. Evaluating the fitness for use of spatial data sets to promote quality in ecological assessment and monitoring. International Journal of Geographical Information Science 28:2356-2371.

Pullin, A. S., W. Sutherland, T. Gardner, V. Kapos, and J. E. Fa. 2013. Conservation priorities: identifying need, taking action and evaluating success. Pages 3-22 *in* D. W. Macdonald and K. J. Willis, editors. Key Topics in Conservation Biology. John Wiley & Sons.

Quinn, P. F., K. J. Beven, and R. Lamb. 1995. The ln(a/tan beta) index: how to calculate it and how to use it within the TOPMODEL framework. Hydrol. Process. 9:161182.

Ribeiro, R., M. Carretero, N. Sillero, G. Alarcos, M. Ortiz-Santaliestra, M. Lizana, and G. Llorente. 2011. The pond network: can structural connectivity reflect on (amphibian) biodiversity patterns? Landscape Ecology 26:673-682.

Rudnick, D. A., S. J. Ryan, P. Beier, S. A. Cushman, F. Dieffenbach, C. W. Epps, L. R. Gerber, J. Hartter, J. S. Jenness, J. Kintsch, A. M. Merenlender, R. M. Perkl, D. V. Preziosi, and Trombulak.S.C. 2010. The role of landscape connectivity in planning and implementing conservation and restoration priorities. Issues in Ecology 16.

Sala, O. E., F. Stuart Chapin III, J. J. Armesto, E. Berlow, J. Bloomfield, R. Dirzo, E. Huber-Sanwald, L. F. Huenneke, R. B. Jackson, A. Kinzig, R. Leemans, D. M. Lodge, H. A. Mooney, M. n. Oesterheld, N. L. Poff, M. T. Sykes, B. H. Walker, M. Walker, and D. H. Wall. 2000. Global Biodiversity Scenarios for the Year 2100. Science 287:1770-1774.

Schwartz, M. W. 2012. Using niche models with climate projections to inform conservation management decisions. Biological Conservation 155:149-156.

Sohl, T. L. 2014. The Relative Impacts of Climate and Land-Use Change on Conterminous United States Bird Species from 2001 to 2075. PLoS ONE 9:e112251.

Spear, S. F., N. Balkenhol, M.-J. Fortin, B. H. McRae, and K. I. M. Scribner. 2010. Use of resistance surfaces for landscape genetic studies: considerations for parameterization and analysis. Molecular Ecology 19:3576-3591.

Taylor, P. D., L. Fahrig, K. Henein, and G. Merriam. 1993. Connectivity Is a Vital Element of Landscape Structure. Oikos 68:571-573.

Taylor, P. D., L. Fahrig, and K. A. With. 2006. Landscape connectivity: a return to the basics *in* K. R. Crooks and M. Sanjayan, editors. Connectivity Conservation. Cambridge University Press, New York, USA.

Thomas, C. D., A. Cameron, R. E. Green, M. Bakkenes, L. J. Beaumont, Y. C. Collingham, B. F. N. Erasmus, M. F. de Siqueira, A. Grainger, L. Hannah, L. Hughes, B. Huntley, A. S. van Jaarsveld, G. F. Midgley, L. Miles, M. A. Ortega-Huerta, A. Townsend Peterson, O. L. Phillips, and S. E. Williams. 2004. Extinction risk from climate change. Nature 427:145-148.

Thuiller, W., B. Lafourcade, R. Engler, and M. B. Araújo. 2009. BIOMOD – a platform for ensemble forecasting of species distributions. Ecography 32:369-373.

Thuiller, W., S. Lavergne, C. Roquet, I. Boulangeat, B. Lafourcade, and M. B. Araujo. 2011. Consequences of climate change on the tree of life in Europe. Nature 470:531-534.

Thuiller, W., S. Lavorel, M. B. Araújo, M. T. Sykes, and I. C. Prentice. 2005. Climate change threats to plant diversity in Europe. Proceedings of the National Academy of Sciences of the United States of America 102:8245-8250.

Tingley, R., and T. B. Herman. 2009. Land-cover data improve bioclimatic models for anurans and turtles at a regional scale. Journal of Biogeography 36:1656-1672.

Trimble, M. J., and R. J. van Aarde. 2014. Amphibian and reptile communities and functional groups over a land-use gradient in a coastal tropical forest landscape of high richness and endemicity. Animal Conservation 17:441-453.

Verburg, P., and K. Overmars. 2009. Combining top-down and bottom-up dynamics in land use modeling: exploring the future of abandoned farmlands in Europe with the Dyna-CLUE model. Landscape Ecology 24:1167-1181.

Vicente, J. R., D. Alagador, C. Guerra, J. M. Alonso, C. Kueffer, A. S. Vaz, R. F. Fernandes, J. A. Cabral, M. B. Araújo, and J. P. Honrado. 2016. Cost-effective monitoring of biological invasions under global change: a model-based framework. Journal of Applied Ecology:n/a-n/a.

Vicente, J. R., J. Gonçalves, J. P. Honrado, C. F. Randin, J. Pottier, O. Broennimann, A. Lomba, and A. Guisan. 2014. A framework for assessing the scale of influence of environmental factors on ecological patterns. Ecological Complexity 20:151-156.

Wanger, T. C., D. T. Iskandar, I. Motzke, B. W. Brook, N. S. Sodhi, Y. Clough, and T. Tscharntke. 2010. Effects of Land-Use Change on Community Composition of Tropical Amphibians and Reptiles in Sulawesi, Indonesia

Efectos del Cambio de Uso de Suelo sobre la Composición de la Comunidad de Anfibios y Reptiles en Sulawesi, Indonesia. Conservation Biology 24:795-802.

Watts, K., A. Eycott, P. Handley, D. Ray, J. Humphrey, and C. Quine. 2010. Targeting and evaluating biodiversity conservation action within fragmented landscapes: an approach based on generic focal species and least-cost networks. Landscape Ecology 25:1305-1318.

Wiens, J. A., D. Stralberg, D. Jongsomjit, C. A. Howell, and M. A. Snyder. 2009. Niches, models, and climate change: assessing the assumptions and uncertainties. Proc Natl Acad Sci U S A 106 Suppl 2:19729-19736.

Wiens, J. J., and C. H. Graham. 2005. Niche Conservatism: Integrating Evolution, Ecology, and Conservation Biology. Annual Review of Ecology, Evolution, and Systematics 36:519-539.

Williams, S. E., L. P. Shoo, J. L. Isaac, A. A. Hoffmann, and G. Langham. 2008. Towards an Integrated Framework for Assessing the Vulnerability of Species to Climate Change. PLoS Biol 6:e325.

Sub-section II.3. Habitat and ecosystem levels – Exploring Earth Observation data to assess extent, condition and stability

Chapter 7 – Evaluating an unmanned aerial vehicle-based approach for assessing habitat extent and condition in fine-scale early successional mountain mosaics

Author list: **João Gonçalves** (1,2), Renato Henriques, (3), Paulo Alves (1), Rita Sousa-Silva (4), António T. Monteiro (1), Ângela Lomba (1), Bruno Marcos (1), João Honrado (1,2)

(1) InBIO, Research Network in Biodiversity and Evolutionary Biology Associate Laboratory, CIBIO, Research Center in Biodiversity and Genetic Resources, Predictive Ecology Group, Vila do Conde, Portugal
(2) Faculty of Sciences, University of Porto, Porto, Portugal
(3) Institute of Earth Sciences (ICT/University of Minho/CCT), Portugal
(4) Division Forest Nature and Landscape, Department of Earth and Environmental Sciences, Katholieke Universiteit Leuven, Leuven, Belgium

DISCLAIMER

This manuscript is an original contribution of this thesis published in *Applied Vegetation Science* journal under the same title. Gonçalves, J., lead the work with contributions from all co-authors.

ABSTRACT

Question. Can very-high resolution colour orthophotography and digital surface models (DSMs) from an unmanned aerial vehicle (UAV) be effectively used for assessment of habitat extent and condition in fine-scale disturbance-dependent mosaics?

Location. The study-area is located in the *Serra de Arga* mountain range, a *Natura 2000* protected site in the NW region of Portugal where drastic changes in pastoral activities have occurred over recent decades.

Methods. An UAV platform was used to collect very-high resolution (6cm) images and to produce a DSM (10cm). From these data, several features were extracted related to colour, band ratios, as well as, texture features calculated from colour imagery and surface elevation. Based on a systematic sampling design, field data were collected for both training and validation of a supervised classifier. Extracted features and ground-truth training data were combined to calibrate a pixel-based *Random Forest* classifier with the purpose of devising a habitat map for the entire study-area. Map validation was performed to assess classification accuracy, and feature importance metrics were calculated.

Results. Validation results revealed a good mean overall accuracy (0.89), with some performance decrease in situations of high interspersion of habitat types. The priority habitat type 6230* (*Nardus* grasslands), defining the vegetation matrix of the test-site, obtained 0.96 and 0.91 considering, respectively, producer and user accuracy. In turn, priority habitat type 4020* (Atlantic wet heathlands) recorded 0.68 and 0.77. The obtained habitat map allowed measuring the extent, describe the spatial arrangement and provide an indication on the conservation condition of target habitat types. Test results regarding the discrimination ability of different features highlighted the importance of surface elevation textures derived from the DSM, followed by band ratios textures, as well as other more complex texture features calculated from colour imagery.

Conclusions. Overall the developed methodology showed promising results for assessing the extent and condition of habitats of high conservation priority in fine-scale, dynamic vegetation mosaics. Future advances in the use of UAV platforms may play an important role for monitoring protected sites and fulfil legal reporting obligations of EU member-states while reducing the costs associated with intensive in-field assessments.

7.1. Introduction

The continuous monitoring of species and habitats of high conservation value across *Natura 2000* protected areas is an obligation established under the Habitats Directive across European Union (European Commission 1992). It is also a requirement in order to tackle human-driven land-use changes, which severely impact terrestrial biodiversity, and are expected to affect it considerably throughout the next 100 years (Sala et al. 2000; Waldhardt et al. 2004). A large extent of these protected areas are located in mountainous regions, including marginal Mediterranean mountains currently affected by socio-economic changes (Bolliger et al. 2007). These cultural landscapes, frequently exhibiting high levels of biological diversity (Bielsa et al. 2005; Brown et al. 2011), currently face shifts on agricultural practices and human inputs, varying from partial abandonment of some parcels originating a landscape mosaic of unused and cropped areas (Bielsa *et al*., 2005), to total abandonment of agriculture (and pastoralism) and a progressive transformation into uncultivated land (MacDonald et al. 2000). This usually leads to an increase of the area occupied by semi-natural vegetation like scrubland and woodland (Bielsa et al. 2005) and a gradual colonization by non-crop species, initially with annual herbaceous plants (mainly ruderal species) which are gradually replaced by perennial herbs and low shrubs creating the conditions for the development of taller woody species which ultimately cause the loss of open habitats (Plieninger 2006).

In such context, the *Natura 2000* network represents a key instrument to preserve the high-nature value occurring on small-scale and actively managed habitats under threat due to abandonment of farming and grazing activities. However, monitoring the extent and condition of disturbance-dependent habitat types is particularly challenging as they often occur in fine-grained, highly dynamic mosaics maintained through extensive farming and/or moderate grazing pressure (Halada et al. 2011). Monitoring strategies are even more challenging under a scenario of widespread abandonment of husbandry in marginal rural areas since these habitats will have their occupancy area reduced due to successional evolution towards scrub or woodland, especially in regions where the wild herbivore fauna has been depleted by centuries of human land management (Goodall & Perry 2009). In addition, changes in fire regimes triggered by shrub encroachment and fuel biomass accumulation are another threat to these habitats (Burkinshaw & Bork 2009).

Currently national and regional authorities liable to provide an assessment on the distribution and extent of Annex I habitats are faced with urgent data needs yet with

limited means to acquire it (Weiers et al. 2004; Vanden Borre et al. 2011; Spanhove et al. 2012). As financial resources are limited, the monitoring approaches need to be as cost-effective and consistent as possible. As such, remote sensing techniques have emerged as a powerful tool for habitat mapping and monitoring (Weiers et al. 2004; Vanden Borre et al. 2011; Nagendra et al. 2013; Corbane et al. 2015).The analysis of high spatial resolution aerial photography is commonly used for vegetation classification and species identification (González-Orozco et al. 2010) however the resolution of these image sensors is usually insufficient to provide accurate quantifications of small-scale and complex habitats thus forcing the need to use more advanced systems (Gross et al. 2009; Vanden Borre et al. 2011). Recent advances in the use of very-high spatial resolution satellite imagery (e.g., RapidEye, QuickBird) have proven highly useful for mapping Natura 2000 habitat types, such as grasslands (Hernando et al. 2012; Schmidt et al. 2014; Buck et al. 2015) and heathlands (Förster et al. 2008). In addition, developments in unmanned aerial vehicles (UAVs) for environmental remote sensing purposes have provided the means for achieving accuracies that meet or exceed traditional aerial photointerpretation techniques (Knoth et al. 2013; Husson et al. 2014). The low flight altitude relatively to other aircrafts and satellites, the reduced or absent cloud contamination, as well as their fine resolution and flexible scheduling of flight missions allows UAVs to provide visual imagery at a more localized and biologically distinguishable level, thus bridging the gap between ground-based observations and lower resolution remotely sensed data (Laliberte & Rango 2008; Getzin et al. 2012). Moreover, UAV platforms allow obtaining information in problematic areas in terms of accessibility, such as bogs or cliffs (Knoth et al. 2013), riverine or lake ecosystems (Husson et al. 2014).

Despite all advantages, major challenges still exist on data processing, namely on image classification procedures (Huang et al. 2007) due to the large amount of data that is stored during flight missions (Permuter et al. 2006). Automated or semi-automated classification methods are therefore crucial for UAV applications in ecology and other fields. In this respect, a plethora of classification methods have been developed with *Random Forest* (hereafter RF; Breiman (2001)), a powerful machine learning technique, becoming increasingly popular in remote sensing applications (Pal 2005; Immitzer et al. 2012; Rodriguez-Galiano et al. 2012). Several studies have shown that RF performs better in comparison to other classification algorithms (Rodriguez-Galiano & Chica-Rivas 2012; Rodriguez-Galiano et al. 2012; Zhang & Xie 2013) with a strong ability to handle high-dimensional datasets making it attractive for processing high spatial resolution data.

In this study, focused on disturbance-dependent habitat mosaics in a Natura 2000 site, we tested an UAV-based methodology for assessing complex, dynamic vegetation mosaics composed of several EU habitat types of high conservation value, including two considered of high priority (Atlantic wet heath and *Nardus* grasslands). We discuss the classification performance and the suitability of this approach to support the assessment and monitoring of habitat types with high conservation value with a reduction in running costs and operational complexity of image acquisition with UAV technologies.

7.2. Methods

Study-area and focal habitat mosaic

The study-area is located in the *Serra de Arga* mountain range (Figure 7 - 1), a *Natura 2000* site located in the northwest region of Portugal (longitude: 8º42'39.662"W, latitude: 41º49'13.890"N) comprising a total area of 9.72ha. Elevation ranges from 747m to 781m a.s.l. and the climate is "cool-summer" Mediterranean type Csb according to the Köppen-Geiger classification system (Peel et al. 2007). Total annual precipitation equals 1510mm and minimum, average and maximum annual temperatures equal, respectively: 6.1ºC, 11.7ºC, and 17.4ºC (Ninyerola et al. 2005).

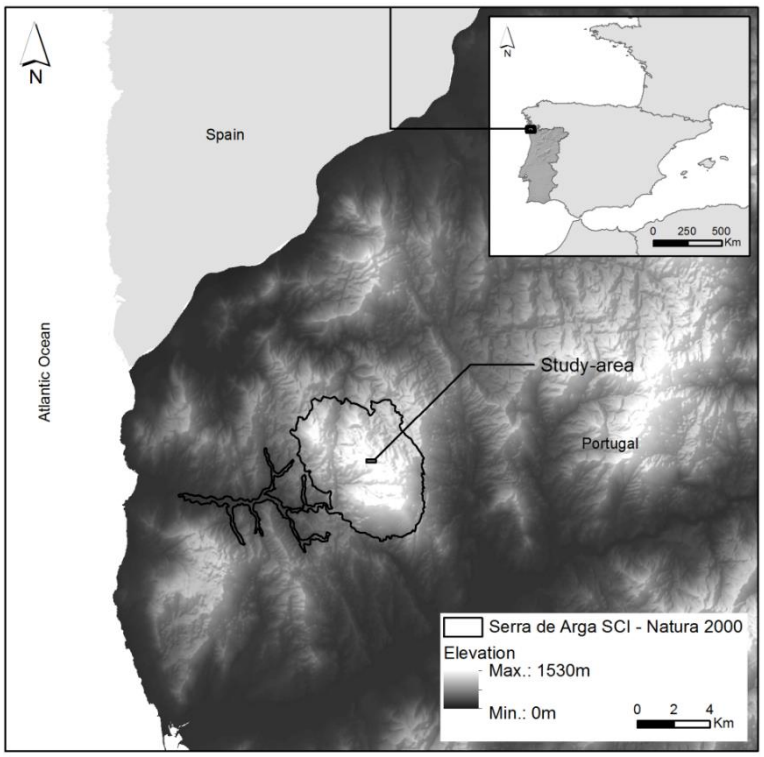

Figure 7 - 1 – Study-area location in the Iberian Peninsula and the NW region of Portugal. The test-site is fully included in the Natura 2000 "*Serra de Arga*" Site of Community Importance.

This area is characterized by a mosaic dominated by two different types of vegetation, corresponding to two priority habitat types listed in Annex I of the EU Habitats Directive (see Figure 7 - 2 and Appendix IV – S5): Atlantic wet heathlands (habitat 4020*) and *Nardus* grasslands (habitat 6230*). Habitat type 4020* (Temperate Atlantic wet heaths with *Erica ciliaris* and *Erica tetralix*) corresponds to dense formations on wet acid soils, dominated by different species of heather (*Erica ciliaris*, *E. tetralix*, *Calluna vulgaris*) and gorse (*Ulex minor*) and hygrophilous species of genus *Genista* (*G. anglica*, *G. micrantha*). This habitat type may include various densities of grasses and occasional bare soil depending on local conditions and disturbances. Habitat type 6230* (Species-rich *Nardus* grassland, on siliceous substrates in mountain areas and sub-mountain areas in continental Europe) is dominated by perennial grasses and rushes (*Nardus stricta*, *Danthonia decumbens*, *Juncus squarrosus*, *Agrostis hesperica*), usually accompanied by several small-sized forbs (*Serratula tinctoria* subsp. *seoanei*, *Polygala serpyllifolia*, *Galium saxatile*). Heath shrubs may occur as scattered plants or small patches, but the grassland component is typically dominant except in degraded forms of the habitat. In this case, shrubs and bare soil will become more abundant and the typical vegetation structure and species assembly will be depleted. In this southern limit of their distribution, these two habitat types occur in dense, dynamic mosaics on wet oligotrophic soils, usually on high plains and near springs. Small ponds or streams, dry heath (habitat 4030) and areas of bare ground (soil or rock) are other, less frequent components of the mosaic.

The composition and conservation value of the mosaic depends on the disturbance regime, especially on grazing pressure. Thus, low levels of grazing will favour wet heath, which becomes the vegetation habitat type. Conversely, high levels of grazing will favour *Nardus* grasslands, however intensive grazing will reduce their species diversity and their conservation value, and may even trigger its replacement by other vegetation types more adapted to heavy loads of grazing, such as species-poor grasslands dominated by *Agrostis capillaris*. On the other hand, no grazing or even very-low pressure will allow scrub encroachment and a decrease in the extent of both habitat types. The fact that this and other mountainous areas in the region have been undergoing changes in pastoral activities (namely abandonment of husbandry and local concentration of grazing pressure) over recent decades justifies our option for this site for testing the methodology.

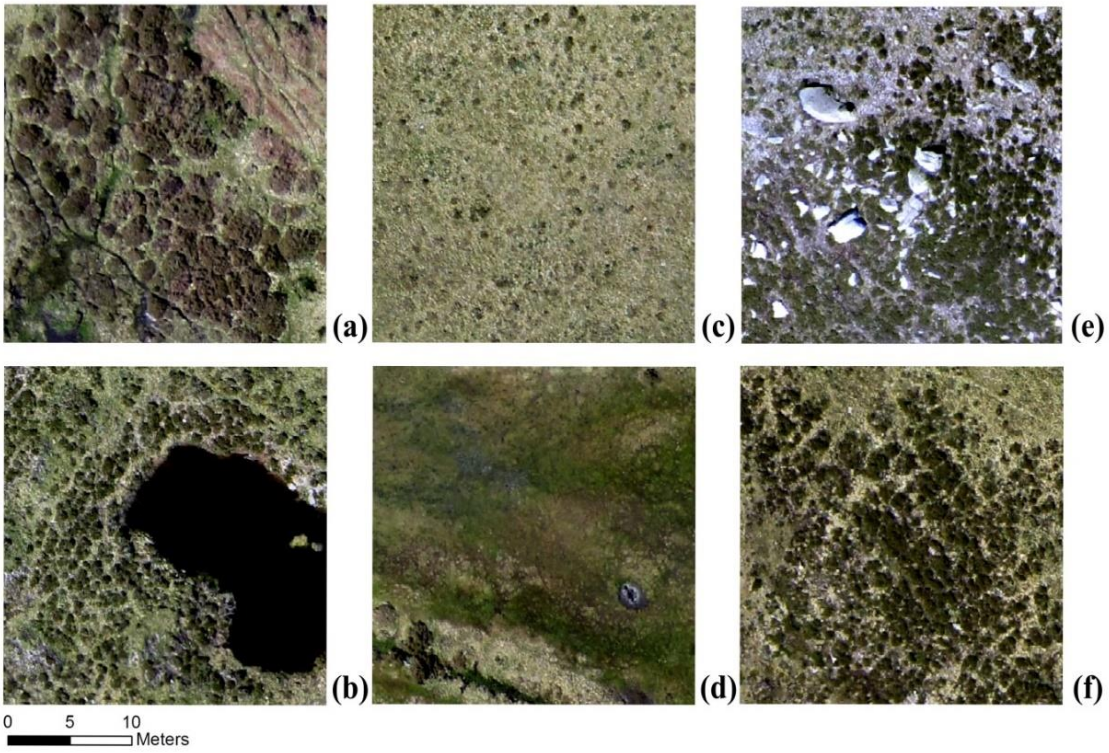

Figure 7 - 2 – The focal habitats as captured by the UAV platform. (a) wet heath, habitat type 4020*, in dense/large shrub formations in concave/wet areas; (b) habitat 4020* around a small pond; (c) continuous, species-rich *Nardus* grasslands, habitat type 6230*, with low shrub density; (d) 6230* habitat with bare soil, highlighting poor habitat condition; (e) dry heath, habitat type 4030, in mosaic with bare rock/soil areas; (f) heath (4030) encroachment on *Nardus* grassland denoting degradation due to decreased grazing pressure.

Aerial imagery and surface elevation data acquisition and pre-processing

The general workflow of the tested methodology is illustrated in Figure 7 - 3 and included several steps regarding imagery acquisition, post-processing, feature extraction and selection, sampling design and field surveying and finally image classification and validation.

The workflow started by the acquisition of very high-resolution aerial images (6cm.pixel^{-1}) at the beginning of spring 2013 (April 17th) using a SenseFly-SwingletCAM UAV platform equipped with a Canon Ixus 220 HS digital camera with 12MP sensor (4000×3000 pixels). Although spectral sensitivity data for this camera were unavailable from the UAV manufacturer, we compared it to twelve Canon models and calculated the average band centres (and standard-errors) for the red, green and blue bands (see Appendix IV – S7 for more details). These were located respectively at: 594±2nm, 527±2nm and 462±2nm; overall the green band exhibited higher relative spectral sensitivity, a common feature in commercial digital sensors (Campbell & Wynne 2011). The flight was performed at 3:00PM under clear sky conditions at an altitude of approximately 940m. Additional flight parameters, such as image overlap (set to 60 and

70% in the X and Y directions respectively), study-area limits and spatial resolution were set and uploaded to the device internal memory.

Before the flight, the terrain was prepared with visible targets later used as ground control points (GCP) for georeferencing the aerial photographs and the digital surface model (DSM). GCP positioning was collected by a Trimble 5800 RTK dual-frequency DGPS with a positional error below 20mm.

The photogrammetric processing, orthorectification and mosaicking were performed with the PhotoScan software (Agisoft 2012) allowing to obtain a very-high resolution DSM with 10cm.pixel^{-1} and a orthorectified image with a RMSE equal to 0.628 pixel^{-1} in GeoTIFF format and using the WGS1984 geographic coordinate system.

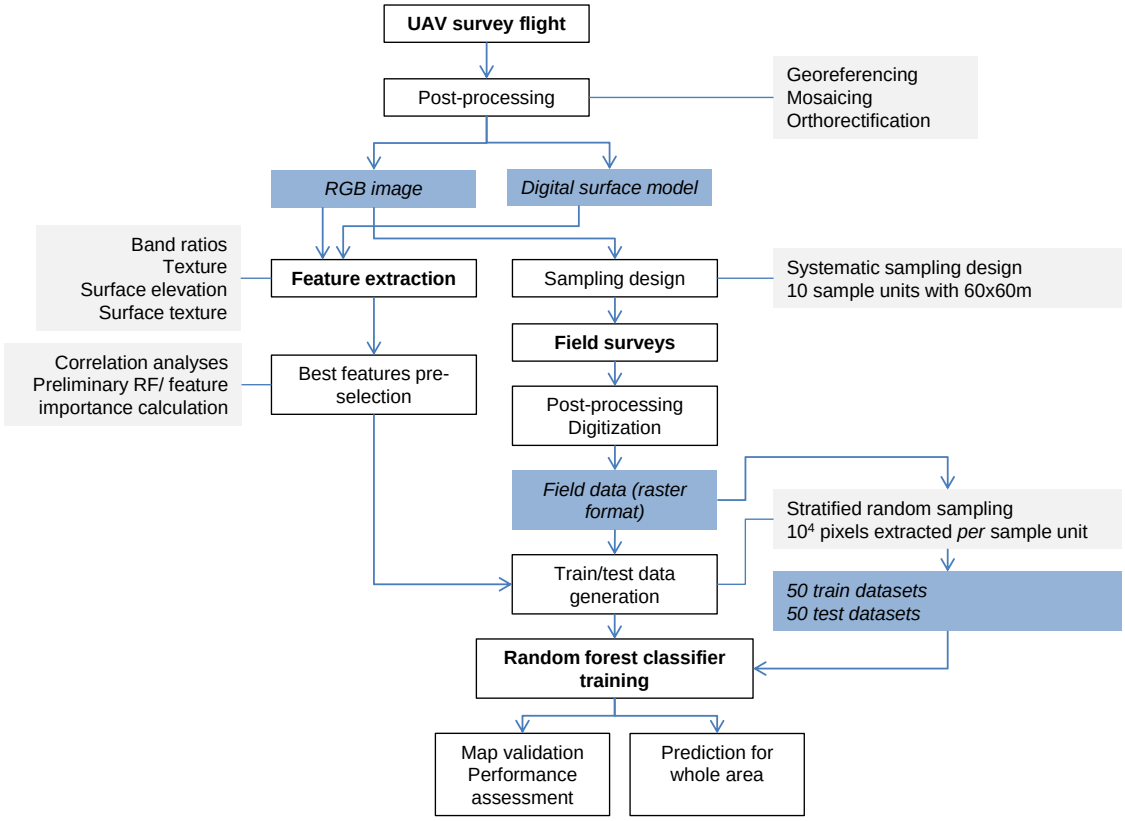

Figure 7 - 3 – Overview of the methodological approach tested. The scheme uses dashed boxes to denote processes (bold lettering signals important processing steps), grey boxes denote specific or detailed aspects for certain processes and blue boxes indicate data.

Sampling design and in-field data collection for training and validation

Training data is required for calibrating supervised classification algorithms such as *Random Forests*. In order to obtain this data, we employed a design-based systematic sampling strategy (Gruijter et al. 2006) with ten regularly spaced sample units with 60×60m covering approximately 37% of the study-area (Figure 7 - 4). Systematic

sampling allows for a uniform coverage with generally more efficient and accurate results than simple random sampling, and it also presents operational advantages since regularity of the grid decreased the time required to locate and move between consecutive plots during fieldwork (Gruijter et al. 2006; Köhl et al. 2006). Field surveys were used to collect ground-truth train/validation data and started after defining a suitable map legend including all observable classes in the previously obtained UAV colour image. The implemented protocol was based on a fine-scale in-field photo-interpretation (over the UAV colour images) of each sample unit by delineating each homogeneous patch pertaining to a given dominant class. The minimum mapping unit was set to 0.36m^2 due to the very-high spatial resolution of the obtained orthophotos (6cm.pixel^{-1}) and to the fine-scale patchiness of vegetation. This field mapping procedure was supported by previously defined spatial and thematic criteria thus standardizing collection processes. Field collected data was later digitized and corrected in a GIS environment.

Figure 7 - 4 – Sample units (red quadrats) over the original colour image obtained with the UAV camera. The image evidences herbaceous (grassland) and woody (scrub) vegetation occurring in dense, complex mosaics as well as extensive rock outcrops and some linear elements such as water lines and tracks.

Feature extraction

In order to test the usefulness of colour imagery and the DSM obtained from the UAV platform, we calculated several colour, band ratios and texture, as well as, surface elevation, curvature and surface texture features from this data. A total of 176 features were obtained (see examples in Figure 7 - 5; the complete list of features is presented in Appendix IV – S1). Colour features were obtained directly from digital number values for the Red (R), Green (G) and Blue (B) channels. Texture features using individual R, G and B channels were extracted by calculating the mean, variance, skewness and kurtosis for three different kernel sizes: 3×3, 5×5 and 9×9 pixels. Kernel sizes were selected based on a preliminary visual inspection of image patterns, balancing the ability

to identify different vegetation/habitat types (and their edges) with the loss of detail when increasing kernel size.

Additionally, band ratios were calculated by performing simple algebraic operations based on combinations of colour channels, *e.g.*: R/G, R/B, R/(G+B), R/(R+G+B). Using each calculated band ratio, texture features were also extracted by calculating the mean and variance for two different kernel sizes: 5×5 and 11×11.

The calculation of texture features was also based on co-occurrence matrices using Haralick indices (Haralick 1979) for two different kernel sizes: 3×3 and 9×9 and using as input a brightness transform of the original RGB image calculated as: $BRG = [(299 \times R) + (587 \times G) + (114 \times B)]/1000$. Texture measures based on Structural Feature Set (Xin et al. 2007) were also calculated using the same brightness transformation. Both Haralick and SFS features were calculated using Orfeo Toolbox (CNES 2014).

Additionally, a set of surface elevation features were obtained from the DSM by calculating the mean and standard-deviation for three different kernel sizes: 5×5, 9×9 and 15×15 representing surface ruggedness. Surface curvature measures were also calculated to highlight surface convexity or concavity (Jenness 2013).

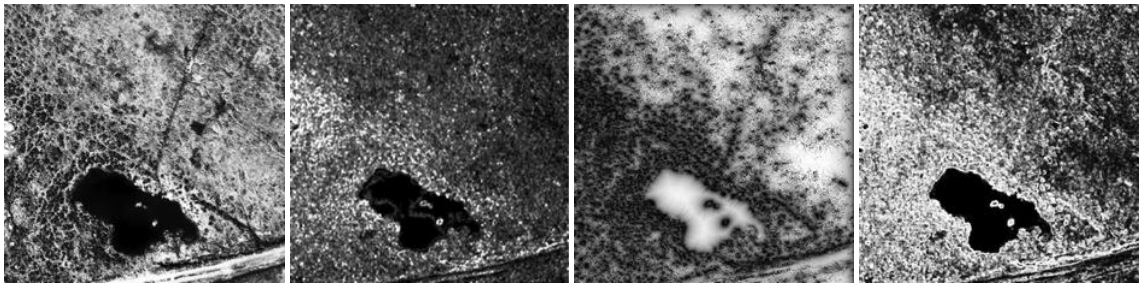

Figure 7 - 5 – Example of colour and texture features for a sample unit. From left to right: original red colour channel, Haralick, Structural Feature Set (SFS) and Local Statistics texture features evidencing small-scale differences and fine discrimination of herbaceous (grassland), woody (scrub) vegetation and a pond.

Random Forest classifier training and validation

In this test, a pixel-based supervised classification framework was employed by combining ground-truth training data with several colour, texture and surface features to produce an ensemble *RF* classifier (Breiman 2001). This algorithm was selected after a preliminary performance comparison between several other classification methods, including Support Vector Machines, Neural Networks, k-Nearest Neighbour, Generalized Boosted Model, and C5.0. In this test, RF attained the largest accuracy and Kappa values (see detailed information in Appendix IV – S4) and for that reason it was the one

selected to conduct the study. The *R* software package (R-Core-Team 2014; URL: http://www.r-project.org) was used for developing all image classification routines, in particular with the *randomForest* library (Liaw & Wiener 2002).

This stage started by generating 50 train and 50 validation datasets each containing a stratified random draw of 10^5 pixels sampled from each digitized field-surveyed sample unit (SU). For each SU, 10^4 pixels were sampled with proportional to stratum area allocation, using the previously defined classes as strata and ensuring that train pixels were not included in test sets. Due to the relatively large number of features and to decrease multicollinearity and enhance processing speed, Spearman nonparametric correlation analysis was performed and features with very-high correlation ($\rho \geq 0.9$) were initially discarded. Following this step, a preliminary RF classifier was devised and feature importance measures were calculated. After some testing, only the 20 best features (see Table 7 - 3) were kept thus greatly reducing computation time and increasing classifier performance (not shown).

Using solely the selected features, the final RF classifiers were developed for the previously generated train datasets. Using each trained RF classifier, we predicted the target classes for the entire area and ensembled the results through majority voting (*i.e.*, for each pixel the class most often predicted was maintained in the final map). Feature importance values were calculated and averaged across all training datasets using the total decrease in node impurities measured by the Gini index (Liaw & Wiener 2002).

To evaluate classification performance, we used the validation datasets and calculated several classification performance indices (Jolliffe & Stephenson 2003): overall accuracy, Heidke skill score, Peirce skill score, Gerrity skill core (see Appendix IV – S2 for more details). To evaluate classification performances at class level, both producer and user accuracies were calculated.

We also compared producer and user accuracy values obtained by our UAV-based methodology to values collected from a semi-systematic literature review on the state-of-the-art of habitat classification and mapping in the context of Natura 2000 (25 articles were reviewed and two discarded for comparison purposes; see Figure 7 - 6). To allow a meaningful comparison, this compilation focused only on habitat types similar to those analysed in this study, such as grasslands/meadows (62xx /64xx /65xx; 15 articles) and heathlands (40xx; 8 articles). See also Appendix IV – S6 for detailed information.

7.3. Results

Performance of the classification approach

Test results revealed a fairly good mean overall accuracy equal to 0.89 (Table 7 - 1). Complementarily, other performance metrics also recorded an overall good agreement between the predicted classes and validation data with Gerrity skill score recording the highest value (0.86), followed similarly by the Peirce skill score (0.86) and finally, recording a lower performance, the Heidke skill score (0.84). In general, as shown by standard-deviation values, overall classification performance measures displayed low variability across validation sets.

Table 7 - 1 – Overall validation measures averaged across all 50 datasets. ACC – overall accuracy; HSS – Heidke skill score; PSS – Peirce skill score; GSS – Gerrity skill score.

	Average	Standard-deviation
ACC	0.89	0.0010
HSS	0.84	0.0014
PSS	0.86	0.0015
GSS	0.86	0.0018

High values of producer and user accuracy were obtained for habitat type 6230*, as well as for bare rock and for ponds (Table 7 - 2; see also Appendix IV – S3). Other water surfaces/lines, such as temporary streams, drainage channels or small puddles, occurring mostly in the west side of the area, obtained good accuracy values. Habitat type 4020* and bare soil attained moderate producer accuracy values (respectively 0.68 and 0.65) and slightly better accuracy at user level (0.77 and 0.80). Degraded versions of some habitat types, such as 6230*, were also discriminated with fairly good accuracy. Isolated patches of habitat type 4030 as well as patches of this habitat interspersed with bare rock, in poor conservation state, obtained good discrimination accuracy in the test. Results from the analysis of standard-deviation values showed low variability in producer and user accuracy across validation sets.

Table 7 - 2 – Average producer and user accuracy values for each class. Values were aggregated using the mean and standard-deviation across the 50 validation datasets.

	4020*	4030	6230*	6230* degraded	Bare rock	Bare rock / 4030 degraded	Bare soil	Tracks	Water surfaces / water lines	Ponds
Average prod. acc.	0.68	0.84	0.96	0.87	0.94	0.80	0.65	0.90	0.77	0.97
Prod. acc. standard-dev.	0.0079	0.0053	0.0013	0.0037	0.0023	0.0074	0.0072	0.0063	0.0198	0.0082
Average user acc.	0.77	0.82	0.91	0.94	0.95	0.82	0.80	0.91	0.83	0.97
User acc. standard-dev.	0.0070	0.0056	0.0015	0.0031	0.0026	0.0055	0.0060	0.0067	0.0133	0.0080

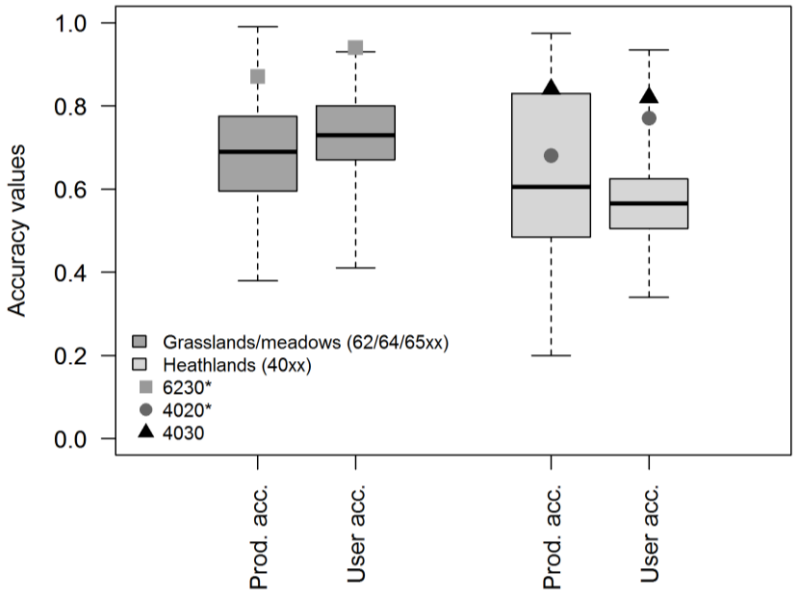

Figure 7 - 6 – Boxplot containing the distribution of producer and user accuracy values collected from research articles on the subject of habitat classification for similar habitat types such as grasslands/meadows (62xx/ 64xx /65xx; n=15 articles, grey colour), and heathlands (40xx; n=8 articles, light grey). Boxes represent the 25, 50% and 75% quartiles and whiskers the minimum and maximum values. Overlapped points display producer and user accuracy values obtained from the tested UAV-based classification, for habitat type 6230* (squares), 4020* (circles) and 4030 (triangles).

Feature importance ranking for habitat classification

Importance metrics calculated from the RF algorithm allowed ranking features according to their relative contribution for classification (Table 7 - 3). The ranking clearly highlighted the importance of surface elevation textures calculated with different kernel sizes. These features show the complex patterning of vegetation types occurring with varying densities at different elevations in the test area (Figure 7 - 7a). Lower roughness/variability in surface values occurred (as expected) for the herbaceous habitat

type 6230* increasing up to tall shrub habitat type 4030 (Figure 7 - 7c). Band ratio textures, especially the B/R ratio, also recorded high importance thus greatly contributing to discriminate classes. The B/R ratio texture displayed a fairly good separation between habitat type 4030 and habitat types 4020*/6230* both exhibiting in average higher values for this variable (Figure 7 - 7b). Ranking also shown that multiple band ratios based on several band combinations were useful for developing the RF classifier.

Table 7 - 3 – Average feature importance and overall ranking for calibrating the random forest-based classifiers. Results were aggregated across all training rounds.

Rank	Mean Decrease Gini	Feature acronym	Feature description	Input and texture parameters
1	6573.2	DSM_SurfElevation_MN_R15	Surface elevation texture	DSM, mean, 15×15
2	6399.5	DSM_SurfElevation_MN_R9	Surface elevation texture	DSM, mean, 9×9
3	6328.4	DSM_SurfElevation_MN_R5	Surface elevation texture	DSM, mean, 5×5
4	4961.3	BR_Ratio_AVG_k11	Band ratio texture	B/R ratio, mean, 11×11
5	4695.5	SFS_WMean_LT100	Structural Feature Set	Brightness transform, WMean, Spectral threshold = 100
6	4451.2	LS_Mean_CH1_RD9	Local statistics	R band, mean, 9×9
7	4014.1	LS_Var_CH3_RD9	Local statistics	B band, variance, 9×9
8	3896.3	LS_Mean_CH2_RD9	Local statistics	G band, mean, 9×9
9	3800.2	RB_Ratio_AVG_k11	Band ratio texture	R/B ratio, mean, 11×11
10	3486.8	LS_Mean_CH3_RD9	Local statistics	B band, mean, 9×9
11	3439.3	B_BGR_Ratio_AVG_k11	Band ratio texture	B/(B+R+G) ratio, mean, 11×11
12	3210.1	HC_HG_LGRE_XR9_YR9	Haralick texture	Brightness transform, Low Grey-Level Run Emphasis, 9×9
13	3047.1	HC_HG_SRLGE_XR9_YR9	Haralick texture	Brightness transform, Short Run Low Grey-Level Emphasis, 9×9
14	2895.9	DSM_SurfElevation_SD_R15	Surface elevation texture	DSM, standard-deviation, 15×15
15	2817.1	BG_Ratio_AVG_k11	Band ratio texture	B/G ratio, mean, 11×11
16	2495.9	R_RGB_Ratio_AVG_k11	Band ratio texture	R/(R+G+B) ratio, mean, 11×11
17	2246.9	R_BG_Ratio_AVG_k11	Band ratio texture	R/(B+G) ratio, mean, 11×11
18	2217.7	DSM_SurfElevation_SD_R9	Surface elevation texture	DSM, standard-deviation, 9×9
19	2213.4	GB_Ratio_AVG_k11	Band ratio texture	G/B ratio, mean, 11×11
20	1963.9	BR_Ratio_AVG_k5	Band ratio texture	B/R ratio, mean, 5×5

Also, ranking in the top five is the SFS WMean feature showing that this type of texture descriptor was rather important for classification purposes. Average values for this texture descriptor showed a moderate differentiation considering habitat types 4020* (with lowest WMean values), 4030 up to 6230 (recording the highest WMean values among these classes; Figure 7 - 7d). Although with less relative contribution, local statistics calculated from raw colour channels using the mean and the variance as texture descriptors were included within the top ten of the ranking.

Haralick texture metrics ranked the lowest scores displaying relatively less contribution to discriminate classes. Overall in this test, larger kernel sizes used to calculate texture features such as 9×9, 11×11 up to 15×15 (when compared to 3×3 or 5×5 sizes), as well as the mean used as an aggregate function were considered the most important.

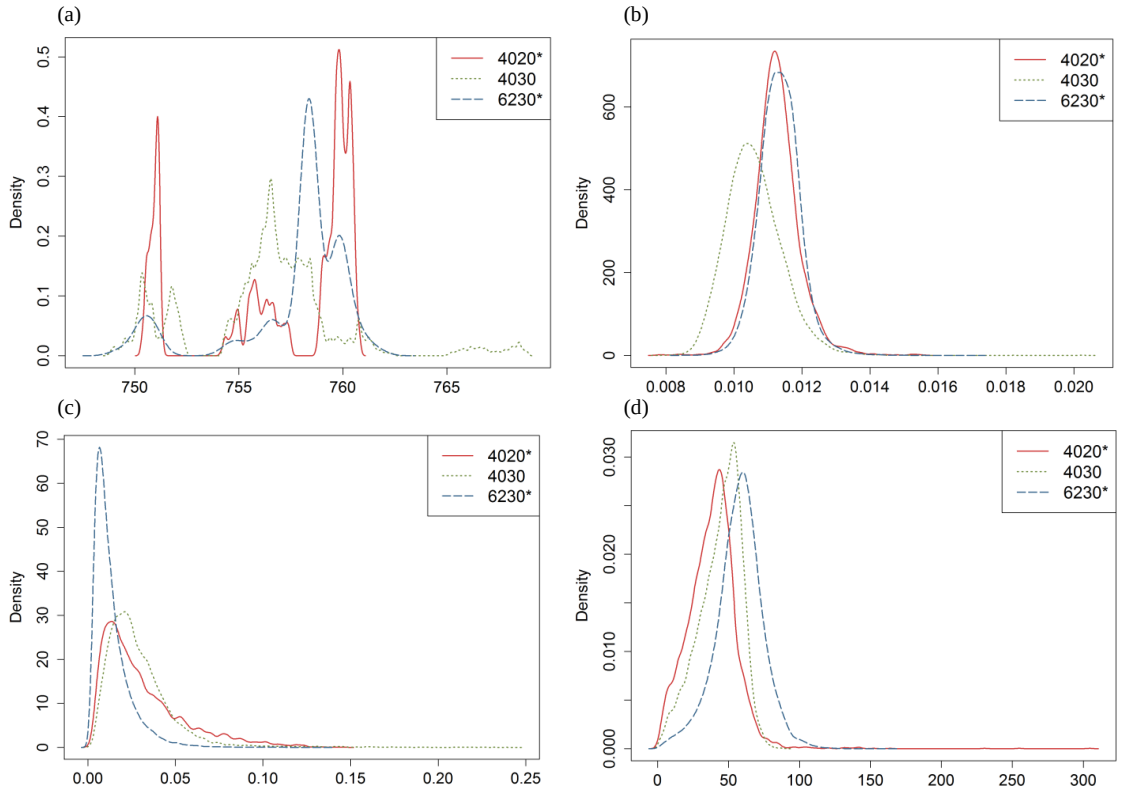

Figure 7 - 7 – Density plots for some of the most important features (Table 7 - 3) used to calibrate the random forest classifiers showing the separation between the three habitat types in the study. (a) Surface elevation texture, Mean, 15×15; (b) R/B band ratio texture, Mean, 11×11; (c) Surface elevation texture, Standard-deviation, 15×15; (d) Structural Feature Set, Brightness band, WMean, Spectral threshold = 100.

Distribution and extent of habitat types in the study-area

The distribution and spatial arrangement of the several classes in the test area are illustrated in Figure 7 - 7. From the classified image, it is possible to visualize that the western portion of the study-area is by far more complex, with a reticulated vegetation patterning intercalated with bare soil and shallow water puddles in concave areas, or with bare rock in upper areas with higher slopes. Habitat type 6230* is by far the predominant class, covering an estimated area of 5.88ha which comprises 60.63% of the test site (Table 7 - 4) and represents the matrix of the mosaic.

Table 7 - 4 – Percentage cover and area (in hectares) of each class in the study-area.

Class	% cover	Area (ha)
4020*	5.41	0.53
4030	8.50	0.82
6230*	60.63	5.88
6230* degraded / bare soil	4.26	0.41
Bare rock	7.01	0.68
Bare rock / 4030 degraded	5.16	0.50
Bare soil	4.87	0.47
Tracks	1.94	0.19
Water surfaces / water lines	1.96	0.19
Ponds	0.25	0.02

A degraded version of this habitat type, with a less favourable habitat condition (0.41ha, or 4.26% of the study-area), occurs mostly in a single large patch located in southwest portion of the site. Habitat type 4020* and all the other classes occur scattered in this matrix, occupying less than 10% of the area individually. Small mosaics of drier areas, dominated by bare rock, bare soil and dry heath are easily distinguished from wet areas with the focal priority habitat types and small water surfaces (Figure 7 - 2 and Figure 7 - 8). Overall, these results are consistent with the high grazing pressure observed in the field and possibly related with the concentration of pastoral activities in these highly productive mosaics.

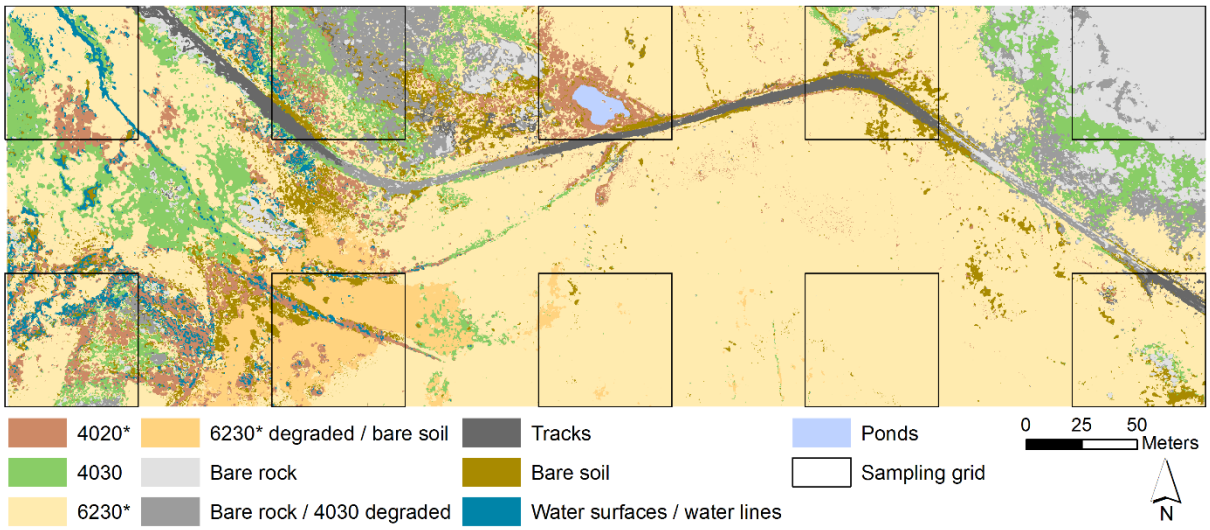

Figure 7 - 8 – Map representation of the study-area displaying the coverage of different classes as predicted by the ensembling of RF classifiers.

7.4. Discussion

Strengths and caveats of the methodology

Developing methods for fine-scale mapping of valuable habitats based on UAV imagery represents a step forward in ecological assessments (Anderson & Gaston 2013). These images allow capturing a high level of detail and to portray the 2D and 3D structure of vegetation from digital surface elevation models. In this test, we developed a UAV-based assessment methodology to map the extent of Natura 2000 priority habitats, obtaining good overall accuracy, in spite of some decrease in classification performance in situations of high interspersion of vegetation types. However, comparisons with officially reported national statistics of habitat extent and distribution could not be performed due to the lack of updated information and to the coarseness of existing databases.

At the class level, grasslands (habitat type 6230*), which are the vegetation matrix in the test-site, attained better results, while wet heath (4020*) obtained only moderate accuracy values as evaluated by test data. Misclassification of habitat type 4020* may be due to some degree of generalization in the definition of complex training areas, to the patchiness of vegetation patterns in the study-area, and to the tendency of this habitat type to occur in intricate mosaics with different species becoming locally dominant, thus hampering its correct identification and delineation both in the field and for classification purposes. Moreover, there were some difficulties distinguishing dominant species of each type of vegetation with similar life forms. One such example is *Ulex europaeus* (subsp. *latebracteatus*) and *Ulex minor*, the first being dominant in

habitat type 4030 (European dry heathlands) and the second dominating much of the patches of habitat type 4020* (temperate wet heath). Other problematic example is distinguishing among species of perennial grasses, such as *Agrostis capillaris*, *Agrostis hesperica* or *Nardus stricta*. *Agrostis capillaris* can be found in a great diversity of habitats and it is dominant in the degraded versions of habitat type 6230* (*Nardus* grasslands) and in other types of grasslands not corresponding to any particular Annex I habitat type.

In further fine-tuning of the methodology, most of these problems could potentially be resolved using contextual information, for example, the percentage of rocks in the neighbouring areas may be a helpful indicator to determine the species of *Ulex*, and consequently the particular Annex I habitat type. Regarding the discrimination of perennial grasses, the coexistence with other ubiquitous mesophytic species, such as *Pteridium aquilinum*, may also be a valuable indicator.

When compared to reference producer and user accuracy values collected from literature (Figure 7 - 6), our UAV-based approach presents above-median performance for both grassland and heathland habitats (in most cases above the 75% quartile, with the exception of producer accuracy for habitat type 4020*). Nevertheless, these comparisons must be interpreted only as an indirect baseline since no directly comparable results (i.e., applications using UAV imagery for similar or the same habitat types) were found in the literature, and also due to differences in input remote sensing data (e.g., RapidEye, QuickBird, Landsat, LiDAR), classification approach (pixel vs. object-based) and classification algorithms (e.g., Support Vector Machines, Maximum Likelihood, Nearest Neighbour; see Appendix IV – S6 for more details). Comparison results suggest that UAV low-spectral resolution may be partially compensated by its very-high, sub-decimetre spatial resolution. They also highlight the cost-efficiency of UAV-based methodologies, since most habitat classification approaches currently employ very-high resolution satellite imagery (e.g., Buck et al. (2015), Förster et al. (2008), Hernando et al. (2012)) with comparatively higher acquisition costs.

This methodology also allowed distinguishing several meaningful classes as well as some degraded patches of particular habitat types in a quite challenging, dynamic and dense vegetation mosaic. In some cases, we are able to detect the presence of dry heathland, bare soil patches or shallow water puddles neighbouring habitat type 4020*, possibly identifying situations where the habitat occurs in less favourable conservation conditions, likely due to over-grazing and localized used of fire. We were also able to identify patches of habitat type 6230* exhibiting a less favourable habitat condition,

related to visible changes in the typical vegetation structure and species-assembly (as verified during in-field surveys) and identifiable in UAV imagery by higher textural heterogeneity or chromatic alterations due to higher shrub density (or encroachment) and presence of open soil (see Figure 7 - 2 and Figure 7 - 4). This type of information may prove useful for management and conservation of the focal habitats, and it is still poorly explored in ecological applications (with exceptions, e.g., Spanhove et al. (2012)) of UAV imagery.

Test results also highlighted the adequacy of the RF algorithm to produce a classifier capable of coping both with the large amount and the high-dimensionality of imagery data (see also Appendix IV – S4). Additionally, low variability of validation metrics across test datasets further showed the high generalization ability of this algorithm. Using sampling strategies to generate train/test data such as those developed in our methodology and performing an initial selection of best features allowed improving classification accuracy and reducing computation time.

Our results strongly emphasized the usefulness of features derived from photogrammetric digital surface models, as well as different texture features calculated from colour imagery as observed in previous UAV applications (e.g., Laliberte & Rango 2008; Laliberte & Rango 2009). These features allowed including useful vicinal and context information in the classification for identifying different vegetation/habitat types and their edges. Computationally inexpensive texture features such as those based on the calculation of local statistics (e.g., mean, variance) for various kernel sizes obtained better results in comparison, for example, with Haralick features which require much longer computation time and resources. Band-ratios, previously highlighted as important in the context of UAV habitat/species classification (e.g., Dunford et al. 2009; Laliberte & Rango 2011), also obtained better results when compared to raw input data. This may be due to the ability of band-ratios removing much of the effect of illumination and enhancing (or revealing) latent information when there is an inverse relationship between two spectral responses to the same biophysical phenomenon (Campbell & Wynne 2011). Moreover, the use of near-infrared images (not available in our UAV platform) could be used to allow the calculation of vegetation indices (Anderson & Gaston 2013; Knoth et al. 2013; Calviño-Cancela et al. 2014) and improve the assessment of habitat extent and condition. These data, combined with a 3D representation of vegetation obtained through a canopy height model (Dandois & Ellis 2013), could potentially contribute to further enhance classification accuracy and the ability to diagnose the condition of some habitat types in fine-scale mosaics.

Applications in the monitoring of small-scale habitat mosaics and future directions

The results obtained in this test, employing UAV-based colour imagery and a DSM for the classification of a complex and dynamic habitat mosaic, revealed that the methodology can successfully discriminate a relatively large number of classes with high to very-high levels of accuracy. This suggests that it can provide robust estimates of class/habitat diversity as well as of the extent of each habitat type, which in turn may be particularly useful for supporting mandatory Natura 2000 reporting obligations (Vanden Borre et al. 2011), especially in member-states currently lacking detailed assessments and/or standardized procedures for such task. UAV-based assessments show a large potential to complement previous research in the detection and mapping of Natura 2000 habitats currently employing satellite imagery from moderate spatial resolution (Díaz Varela et al. 2008) to very-high spatial resolution (Förster et al. 2008; Hernando et al. 2012; Schmidt et al. 2014; Buck et al. 2015), hyperspectral sensors (Haest et al. 2010; Chan et al. 2012; Spanhove et al. 2012), radar satellite data (Schuster et al. 2011; Schuster et al. 2015) and LiDAR (Bässler et al. 2011; Zlinszky et al. 2014). We argue that well planned, standardized and systematic UAV surveying over a statistically sound selection of sites could help to develop a monitoring system that could inform on the extent, connectivity, habitat condition and trends of Natura 2000 habitats in a reproducible fashion and allowing a reduction in running costs and operational complexity of image acquisition (Anderson & Gaston 2013; Mancini et al. 2013; Calviño-Cancela et al. 2014). This would require the definition of highly standardized field methods incorporating botanical, vegetation and remote sensing expertise as a crucial step to bridge gaps between field and UAV-based remote sensing methods.

Covering much wider areas (by a factor of 10 or 100) than the one used in this pilot-test (with roughly 10ha) would be perfectly accomplishable by adapting flight parameters, by performing multiple flights, and/or by employing UAV platforms with higher operating ranges and autonomy (Anderson & Gaston 2013). Due to the diversity and adaptability of existing UAV platforms it would be possible to extend surveying to other different small-scale habitat mosaics such as dunes (Mancini et al. 2013), wetlands (Ishihama et al. 2012) or riparian ecosystems (Dunford et al. 2009). In order to adequately accomplish this, nature protection agencies and/or they partner stakeholders should acquire suitable UAV equipment, train their staff in using this type of technology and to develop semi-automated procedures for image post-processing and classification thus making it easier and faster to analyse UAV data. In turn, long-term advantages of

UAV-based ecological monitoring related to flexible flight scheduling, prompt availability of very-high resolution images, reduced acquisition costs, low or absent cloud contamination (Getzin et al. 2012; Anderson & Gaston 2013) along with other factors could provide a cost-effective solution for conservation agencies.

Acknowledgements

This study was developed as part of the LIFE+ project “Higro” (Demonstrative Actions for the Conservation of Priority Habitats in Northern Mountain Areas in Portugal; LIFE09NAT/PT/000043).

João Gonçalves was supported by the Portuguese Foundation for Science and Technology (FCT) by PhD grant nr. SFRH/BD/90112/2012. Rita Sousa-Silva is supported by a PhD grant of KU Leuven in the framework of the FORBIO Climate project, financed by BRAIN.be, Belgian Research Action through INterdisciplinary research. António T. Monteiro is supported through the Project “Biodiversity, Ecology and Global Change” co-financed by North Portugal Regional Operational Programme 2007/2013 (ON.2 – O Novo Norte), under the National Strategic Reference Framework (NSRF), through the European Regional Development Fund (ERDF). A. Lomba is supported by the PFST through Post-Doctoral Fellowhip SFRH/BPD/80747/2011. Bruno Marcos received support from FEDER/COMPETE and FCT through project grant “IND_CHANGE” (PTDC/AAG-MAA/4539/2012 – FCOMP-01-0124-FEDER-027863).

Author contributions

Author name	Study conception and design	Sampling design, infield surveys and/or data collection	Data processing, analysis and/or modelling	Manuscript writing	Manuscript revision
João Gonçalves	☑	☑	☑	☑	☑
Renato Henriques		☑	☑	☑	☑
Paulo Alves		☑		☑	☑
Rita Sousa-Silva				☑	☑
António Monteiro				☑	☑
Ângela Lomba				☑	☑
Bruno Marcos				☑	☑
João Honrado				☑	☑

References

Agisoft 2012. Agisoft Photoscan User Manual, Professional Edition, Version 0.9.0. In.

Anderson, K. & Gaston, K.J. 2013. Lightweight unmanned aerial vehicles will revolutionize spatial ecology. *Frontiers in Ecology and the Environment* 11: 138-146.

Bässler, C., Stadler, J., Müller, J., Förster, B., Göttlein, A. & Brandl, R. 2011. LiDAR as a rapid tool to predict forest habitat types in Natura 2000 networks. *Biodiversity and Conservation* 20: 465-481.

Bielsa, I., Pons, X. & Bunce, B. 2005. Agricultural Abandonment in the North Eastern Iberian Peninsula: The Use of Basic Landscape Metrics to Support Planning. *Journal of Environmental Planning and Management* 48: 85-102.

Bolliger, J., Kienast, F., Soliva, R. & Rutherford, G. 2007. Spatial sensitivity of species habitat patterns to scenarios of land use change (Switzerland). *Landscape Ecology* 22: 773-789.

Breiman, L. 2001. Random forests. *Machine Learning* 45: 5-32.

Brown, J., Kothari, A., Brown, J. & Kothari, A. 2011. Traditional agricultural landscapes and community conserved areas: an overview. *Management of Environmental Quality: An International Journal* 22: 139-153.

Buck, O., Millán, V.E.G., Klink, A. & Pakzad, K. 2015. Using information layers for mapping grassland habitat distribution at local to regional scales. *International Journal of Applied Earth Observation and Geoinformation* 37: 83-89.

Burkinshaw, A. & Bork, E. 2009. Shrub Encroachment Impacts the Potential for Multiple Use Conflicts on Public Land. *Environmental Management* 44: 493-504.

Calviño-Cancela, M., Méndez-Rial, R., Reguera-Salgado, J. & Martín-Herrero, J. 2014. Alien Plant Monitoring with Ultralight Airborne Imaging Spectroscopy. *PLoS ONE* 9: e102381.

Campbell, J.B. & Wynne, R.H. 2011. *Introduction to remote sensing*. 5th Ed. Guilford Press, New York.

Castroviejo, S. 1986-2013. *Flora iberica, vols. 1-8, 10-15, 17-18, 21*. Real Jardín Botánico, CSIC, Madrid, Spain.

Chan, J.C.-W., Beckers, P., Spanhove, T. & Borre, J.V. 2012. An evaluation of ensemble classifiers for mapping Natura 2000 heathland in Belgium using spaceborne angular hyperspectral (CHRIS/Proba) imagery. *International Journal of Applied Earth Observation and Geoinformation* 18: 13-22.

CNES 2014. The ORFEO Tool Box Software Guide - Updated for OTB-4.0. In.

Corbane, C., Lang, S., Pipkins, K., Alleaume, S., Deshayes, M., García Millán, V.E., Strasser, T., Vanden Borre, J., Toon, S. & Michael, F. 2015. Remote sensing for mapping natural habitats and their conservation status – New opportunities and challenges. *International Journal of Applied Earth Observation and Geoinformation* 37: 7-16.

Dandois, J.P. & Ellis, E.C. 2013. High spatial resolution three-dimensional mapping of vegetation spectral dynamics using computer vision. *Remote Sensing of Environment* 136: 259-276.

Díaz Varela, R.A., Ramil Rego, P., Calvo Iglesias, S. & Muñoz Sobrino, C. 2008. Automatic habitat classification methods based on satellite images: A practical assessment in the NW Iberia coastal mountains. *Environmental Monitoring and Assessment* 144: 229-250.

Dunford, R., Michel, K., Gagnage, M., Piégay, H. & Trémelo, M.L. 2009. Potential and constraints of Unmanned Aerial Vehicle technology for the characterization of Mediterranean riparian forest. *International Journal of Remote Sensing* 30: 4915-4935.

European Commission 1992. Council Directive 92/43/EEC of 21 May 1992 on the conservation of natural habitats and of wild fauna and flora, 1992L0043. In: The Council of the European Communities (ed.) Brussels, Belgium.

Förster, M., Frick, A., Walentowski, H. & Kleinschmit, B. 2008. Approaches to utilising QuickBird data for the monitoring of NATURA 2000 habitats. *Community Ecology* 9: 155-168.

Franco, J.A. 1984. Nova Flora de Portugal (Continente e Açores). Vol. II, Clethraceae-Compositae. Author's edition. Lisbon, Portugal.

Franco, J.A. & Afonso, M.R. 1998. Nova Flora de Portugal (Continente e Açores). Vol. III (Fasc. II), Gramineae. Lisbon, Portugal.

Getzin, S., Wiegand, K. & Schöning, I. 2012. Assessing biodiversity in forests using very high-resolution images and unmanned aerial vehicles. *Methods in Ecology and Evolution* 3: 397-404.

González-Orozco, C.E., Mulligan, M., Trichon, V. & Jarvis, A. 2010. Taxonomic identification of Amazonian tree crowns from aerial photography. *Applied Vegetation Science* 13: 510-519.

Goodall, D.W. & Perry, R.A. 2009. Arid Land Ecosystems: Volume 2, Structure, Functioning and Management. 1st. Cambridge University Press.

Gross, J.E., Goetz, S.J. & Cihlar, J. 2009. Application of remote sensing to parks and protected area monitoring: Introduction to the special issue. *Remote Sensing of Environment* 113: 1343-1345.

Gruijter, J.d., Brus, D., Bierkens, M. & Knotters, M. 2006. *Sampling for Natural Resource Monitoring*. Springer-Verlag, Berlin Heidelberg.

Haest, B., Thoonen, G., Borre, J.V., Spanhove, T., Delalieux, S., Bertels, L., Kooistra, L., Mücher, C.A. & Scheunders, P. 2010. An object-based approach to quantity and quality assessment of heathland habitats in the framework of Natura 2000 using hyperspectral airborne images. In: Addink, E.A. & Coillie, F.M.B.V. (eds.) *GEOBIA 2010: Geographic Object-Based Image Analysis*, pp. 6. Ghent, Belgium.

Halada, L., Evans, D., Romão, C. & Petersen, J.-E. 2011. Which habitats of European importance depend on agricultural practices? *Biodiversity and Conservation* 20: 2365-2378.

Haralick, R.M. 1979. Statistical and structural approaches to texture. *Proceedings of the IEEE* 67: 786-804.

Hernando, A., Arroyo, L.A., Velázquez, J. & Tejera, R. 2012. Objects-based Image Analysis for Mapping Natura 2000 Habitats to Improve Forest Management. *Photogrammetric Engineering & Remote Sensing* 78: 991-999.

Huang, X., Zhang, L. & Li, P. 2007. Classification and extraction of spatial features in urban areas using high-resolution multispectral imagery. *Geoscience and Remote Sensing Letters, IEEE* 4: 260-264.

Husson, E., Hagner, O. & Ecke, F. 2014. Unmanned aircraft systems help to map aquatic vegetation. *Applied Vegetation Science* 17: 567-577.

Immitzer, M., Atzberger, C. & Koukal, T. 2012. Tree species classification with Random forest using very high spatial resolution 8-band worldView-2 satellite data. *Remote Sensing* 4: 2661-2693.

Ishihama, F., Watabe, Y. & Oguma, H. 2012. Validation of a high-resolution, remotely operated aerial remote-sensing system for the identification of herbaceous plant species. *Applied Vegetation Science* 15: 383-389.

Jenness, J. 2013. DEM Surface Tools for ArcGIS (surface_area.exe). Jenness Enterprises.

Jolliffe, I.T. & Stephenson, D.B. 2003. *Forecast Verification - A Practitioner's Guide in Atmospheric Science*. 1st Ed. John Wiley & Sons, Chichester, West Sussex, England.

Knoth, C., Klein, B., Prinz, T. & Kleinebecker, T. 2013. Unmanned aerial vehicles as innovative remote sensing platforms for high-resolution infrared imagery to

support restoration monitoring in cut-over bogs. *Applied Vegetation Science* 16: 509-517.

Köhl, M., Magnussen, S. & M., M. 2006. *Sampling Methods, Remote Sensing and GIS Multiresource Forest Inventory*. Springer-Verlag, Berlin Heidelberg.

Laliberte, A. & Rango, A. 2008. Incorporation of texture, intensity, hue, and saturation for rangeland monitoring with unmanned aircraft imagery. In: *GEOBIA Proceedings*, pp. 4/C1. Calgary, Canada.

Laliberte, A.S. & Rango, A. 2011. Image Processing and Classification Procedures for Analysis of Sub-decimeter Imagery Acquired with an Unmanned Aircraft over Arid Rangelands. *GIScience & Remote Sensing* 48: 4-23.

Laliberte, A.S. & Rango, A. 2009. Texture and Scale in Object-Based Analysis of Subdecimeter Resolution Unmanned Aerial Vehicle (UAV) Imagery. *Geoscience and Remote Sensing, IEEE Transactions on* 47: 761-770.

Liaw, A. & Wiener, M. 2002. Classification and Regression by randomForest. *R News* 2: 18-22.

MacDonald, D., Crabtree, J.R., Wiesinger, G., Dax, T., Stamou, N., Fleury, P., Gutierrez Lazpita, J. & Gibon, A. 2000. Agricultural abandonment in mountain areas of Europe: Environmental consequences and policy response. *Journal of Environmental Management* 59: 47-69.

Mancini, F., Dubbini, M., Gattelli, M., Stecchi, F., Fabbri, S. & Gabbianelli, G. 2013. Using Unmanned Aerial Vehicles (UAV) for High-Resolution Reconstruction of Topography: The Structure from Motion Approach on Coastal Environments. *Remote Sensing* 5: 6880-6898.

Nagendra, H., Lucas, R., Honrado, J.P., Jongman, R.H.G., Tarantino, C., Adamo, M. & Mairota, P. 2013. Remote sensing for conservation monitoring: Assessing protected areas, habitat extent, habitat condition, species diversity, and threats. *Ecological Indicators* 33: 45-59.

Ninyerola, M., Pons, X. & Roure, J.M. 2005. Atlas Climático Digital de la Península Ibérica. Metodología y aplicaciones en bioclimatología y geobotánica. ISBN 932860-8-7. In: Universidad Autónoma de Barcelona, Bellaterra.

Pal, M. 2005. Random forest classifier for remote sensing classification. *International Journal of Remote Sensing* 26: 217-222.

Peel, M.C., Finlayson, B.L. & McMahon, T.A. 2007. Updated world map of the Köppen-Geiger climate classification. *Hydrol. Earth Syst. Sci.* 11: 1633-1644.

Permuter, H., Francos, J. & Jermyn, I. 2006. A study of Gaussian mixture models of color and texture features for image classification and segmentation. *Pattern Recognition* 39: 695-706.

Plieninger, T. 2006. Habitat loss, Fragmentation, and Alteration – Quantifying the Impactof Land-use Changes on a Spanish Dehesa Landscape by Use of Aerial Photography and GIS. *Landscape Ecology* 21: 91-105.

R-Core-Team 2014. R: A Language and Environment for Statistical Computing, version 3.0.3. R Foundation for Statistical Computing, Vienna, Austria.

Rodriguez-Galiano, V.F. & Chica-Rivas, M. 2012. Evaluation of different machine learning methods for land cover mapping of a Mediterranean area using multi-seasonal Landsat images and Digital Terrain Models. *International Journal of Digital Earth* 1-18.

Rodriguez-Galiano, V.F., Ghimire, B., Rogan, J., Chica-Olmo, M. & Rigol-Sanchez, J.P. 2012. An assessment of the effectiveness of a random forest classifier for land-cover classification. *ISPRS Journal of Photogrammetry and Remote Sensing* 67: 93-104.

Romero García, A.T., Blanca López, G. & Morales Torres, C. 1988. Revisión del género Agrostis L.(Poaceae) en la península ibérica. *Ruizia* 7: 1-160.

Sala, O.E., Stuart Chapin , F., III, Armesto, J.J., Berlow, E., Bloomfield, J., Dirzo, R., Huber-Sanwald, E., Huenneke, L.F., Jackson, R.B., Kinzig, A., Leemans, R., Lodge, D.M., Mooney, H.A., Oesterheld, M.n., Poff, N.L., Sykes, M.T., Walker, B.H., Walker, M. & Wall, D.H. 2000. Global Biodiversity Scenarios for the Year 2100. *Science* 287: 1770-1774.

Schmidt, T., Schuster, C., Kleinschmit, B. & Forster, M. 2014. Evaluating an Intra-Annual Time Series for Grassland Classification - How Many Acquisitions and What Seasonal Origin Are Optimal? *Selected Topics in Applied Earth Observations and Remote Sensing, IEEE Journal of* 7: 3428-3439.

Schuster, C., Ali, I., Lohmann, P., Frick, A., Förster, M. & Kleinschmit, B. 2011. Towards Detecting Swath Events in TerraSAR-X Time Series to Establish NATURA 2000 Grassland Habitat Swath Management as Monitoring Parameter. *Remote Sensing* 3: 1308-1322.

Schuster, C., Schmidt, T., Conrad, C., Kleinschmit, B. & Förster, M. 2015. Grassland habitat mapping by intra-annual time series analysis – Comparison of RapidEye and TerraSAR-X satellite data. *International Journal of Applied Earth Observation and Geoinformation* 34: 25-34.

Spanhove, T., Vanden Borre, J., Delalieux, S., Haest, B. & Paelinckx, D. 2012. Can remote sensing estimate fine-scale quality indicators of natural habitats? *Ecological Indicators* 18: 403-412.

Vanden Borre, J., Paelinckx, D., Mücher, C.A., Kooistra, L., Haest, B., De Blust, G. & Schmidt, A.M. 2011. Integrating remote sensing in Natura 2000 habitat monitoring: Prospects on the way forward. *Journal for Nature Conservation* 19: 116-125.

Waldhardt, R., Simmering, D. & Otte, A. 2004. Estimation and prediction of plant species richness in a mosaic landscape. *Landscape Ecology* 19: 211-226.

Weiers, S., Bock, M., Wissen, M. & Rossner, G. 2004. Mapping and indicator approaches for the assessment of habitats at different scales using remote sensing and GIS methods. *Landscape and Urban Planning* 67: 43-65.

Xin, H., Liangpei, Z. & Pingxiang, L. 2007. Classification and Extraction of Spatial Features in Urban Areas Using High-Resolution Multispectral Imagery. *Geoscience and Remote Sensing Letters, IEEE* 4: 260-264.

Zhang, C. & Xie, Z. 2013. Object-based vegetation mapping in the Kissimmee River watershed using HyMap data and machine learning techniques. *Wetlands* 1-12.

Zlinszky, A., Schroiff, A., Kania, A., Deák, B., Mücke, W., Vári, Á., Székely, B. & Pfeifer, N. 2014. Categorizing Grassland Vegetation with Full-Waveform Airborne Laser Scanning: A Feasibility Study for Detecting Natura 2000 Habitat Types. *Remote Sensing* 6: 8056-8087.

Chapter 8 – Assessing the effectiveness of Protected Areas in promoting forest stability – a methodological approach based on satellite time-series data and multi-model inference

Author list: **João Gonçalves** (1,2), Isabel Pôças (3,4), Bruno Marcos (1,2), António T. Monteiro (1), Alfredo Huete (5), Domingo Alcaraz-Segura (6), C. A. Mücher (7), João Honrado (1,2)

(1) CIBIO – Research Center in Biodiversity and Genetic Resources / InBIO – Research Network in Biodiversity and Evolutionary Biology, Associate Laboratory; Campus Agrário de Vairão, Universidade do Porto, 4485-601 Vairão, Portugal
(2) Faculty of Sciences – University of Porto (FCUP); Edifício FC4 (Biologia), Rua do Campo Alegre, s/n, 4169-007 Porto, Portugal
(3) Linking Landscape, Environment, Agriculture and Food, Instituto Superior de Agronomia, Universidade de Lisboa, Lisboa 1349-017, Portugal; Isabel.pocas@fc.up.pt
(4) Geo-Space Sciences Research Centre, Universidade do Porto, Porto 4169-007, Portugal
(5) University of Technology Sydney, Plant Functional Biology and Climate Change Cluster (C3), Sydney, NSW, Australia
(6) Department of Botany, Facultad de Ciencias, Planta 6 Sección de Biología. Campus Universitario de Fuentenueva. Universidad de Granada. 18071. Granada. Spain
(7) Wageningen Environmental Research (Alterra), Earth Informatics subdivision, Wageningen University, Droevendaalsesteeg 3 6708PB Wageningen, Netherlands

DISCLAIMER

This manuscript is an original contribution of this thesis currently *in prep*. Gonçalves, J., lead the work with contributions from all co-authors.

ABSTRACT

The establishment of Protected Areas (PAs) is an important strategy to promote the conservation of natural heritage as well as ecosystem stability in face of global change. In particular, forest ecosystems in Mediterranean countries are undergoing alterations derived from land use changes, wildfires, pathogens and invasive species. Diminishing the current frequency and severity of disturbances and promoting resilient forest systems is thus paramount for ensuring that PAs fulfil their role. However, a systematic evaluation of PA effectiveness for maintaining stable forest ecosystems applicable at country (or continental) level is still lacking. Such assessment of PA effectiveness must take into account the 'natural' seasonal dynamics of ecosystems, thus allowing a more thorough characterization of disturbance or change.

Here we present an approach that uses a 250m Enhanced Vegetation Index (EVI) time-series (2000-2016) from MODIS platform, to evaluate the effectiveness of a national (Portugal) network of PAs for ensuring forest ecosystem stability. Forest ecosystem stability is described as the capacity to maintain key ecosystem functioning properties and is measured continuously using time-series as the dynamic relation between disturbance (modulated by frequency and severity) and response (modulated by resilience). Several stability metrics were calculated based on Ecosystem Functioning Attributes, STL time-series decomposition and the Maximum Lyapunov exponent. Using these metrics, statistical resampling and a corrected multi-testing approach were employed to compare the distributions of stability metrics between PA and non-PA locations, while maintaining similar environmental conditions and land cover composition and minimizing the geographic distance. Statistical models (based on Generalized Linear Models, GLM) were developed and ranked through a multi-model inference framework to investigate the drivers involved in different stability performance across PAs for each metric calculated.

Results showed that most PAs effectively promoted higher relative forest stability in comparison to surrounding non-protected areas between 2000 and 2016. However, we found strongly different performances across PAs and among stability metrics. Inside PAs we also observed widely heterogeneous stability patterns between forest patches. Model results showed a positive effect on stability of PA size and amount of broadleaf forest, and a negative effect of the interaction between forest fires and PA average altitude. A structural component was also found, since PAs with taller forests, higher vertical complexity, larger mean forest patch size and higher connectivity presented

higher relative stability. A negative effect of the interaction between area affected by pathogen pine wilt nematode and coniferous cover was also found. Inter-annual precipitation variability was found to have only a weak negative effect while temperature (minima and maxima) had no effect. We found only a weak positive effect regarding the overlap of PAs with the Natura 2000 conservation network, and (somewhat surprisingly) no effect regarding PA age. We argue that multitemporal metrics derived from VI time-series can be used to measure conservation efficiency and ecosystem dynamics. We also discuss the advantages, pitfalls and potential sources of uncertainty in our approach.

8.1. Introduction

Terrestrial Protected Areas (PAs) represent 14.8% of total land area (UNEP-WCMC and IUCN 2016) and are an important part of global and regional efforts towards the conservation of biodiversity (Watson et al. 2014) as well as to ensure the stable and sustainable delivery of ecosystem services (ES) in face of fast paced environmental changes.

Forest ecosystems hold an invaluable planetary importance in this regard (Bonan 2008), as they support and deliver a diversity of services of high importance for human well-being (Mori et al. 2017). These range from provisioning of goods (e.g., wood and non-wood products) to regulating services (e.g., climate regulation, carbon sequestration and storage, erosion control, water regulation) and cultural services (e.g., recreation and health, tourism) (EEA 2016). Biodiverse forest ecosystems (i.e., with higher number of tree species) usually ensure higher functionality (Díaz and Cabido 2001) and provide higher levels of multiple ecosystem services (Gamfeldt et al. 2013) highlighting the importance of adequately preserving and managing biodiverse forest ecosystems.

The effective support of forests to the provision of those ES strongly relies on ecosystem stability, including the response of forests to disturbances and their adaptation to a changing climate. Assessing the effectiveness of PAs in promoting forest stability is therefore paramount to measure the degree of achievement of PA objectives and to devise or adapt management plans. This task is particularly relevant considering the global expansion of PAs over the past century as well as the pressures upon them (Watson et al. 2014). In addition, PAs play an important role in worldwide maintenance and conservation of forests (Morales-Hidalgo et al. 2015). Still, despite management and conservation efforts at several levels, the FAO 2016 report on the State of World's Forest (FAO 2016) shows marked differences across worldwide forest condition. In the tropical

domain, net annual loss of forest area from 2000 to 2010 was about 7 million ha/year, mainly due to large-scale commercial and subsistence agriculture demands. In contrast, Europe, North America and Northeast Asia recorded net gains in forest and net losses in agricultural area, as a result of reduced pressure on forests, declining rural populations or improved agricultural productivity, and forest expansion policies.

In Europe, forests are now the largest land cover type, covering approximately 43% of the surface area of the continent (EEA 2016). Although several European countries recorded an increase in forest area, some countries exhibited an opposite trend. Portugal, for instance, recorded a loss of forested land of 3% between 1990 and 2015 (FAO/World-Bank (2016) and of 5% between 1995 and 2010 according to national statistics (ICNF 2013). A strong contribution for this trend has come from the large amount of forest fires that stroke the country in the last decades. Portugal is currently the most affected European country in terms of burnt forest area and number of forest fires (FAO and EFI 2015, EEA 2016). Moreover, emerging pathogens such as the North American pine wilt nematode caused severe damages, structural and functional forest changes and loss of natural capital (Proença et al. 2017).

Given this state of affairs, robust methods and indicators are vital to effectively monitor the current status and trends in forest ecosystems, as well as to provide a better understanding of the role that PAs are playing in promoting forest stability. For these objectives, Earth Observation (EO) technologies currently provide a vast array of data products at different spatial and temporal resolutions, which strongly contribute to improve the assessment and monitoring of biodiversity, ecosystems and pressures (Nagendra et al. 2013, Nagendra et al. 2015, Skidmore et al. 2015). In fact, EO data has also been used for evaluating PA effectiveness (e.g., Wegmann et al. 2014, Hughes et al. 2016) and, more broadly, EO platforms have been suggested as an important data source to monitor ecosystem services (Cord et al. 2017) and to track the progress towards international strategic goals such as CBD's Aichi Biodiversity Targets (O'Connor et al. 2015).

By providing repeated and synoptic measures of the Earth surface, EO offers a cost-effective approach to assess land cover/vegetation state and changes. Available time-series of satellite data with high-temporal resolution greatly enhance the ability to assess and monitor both inter-annual (e.g. trends, landscape change) and intra-annual (e.g. seasonal changes, phenology) features of vegetation and ecosystem dynamics (Heumann et al. 2007, Cabello et al. 2012, Pettorelli et al. 2014). Time-series of spectral vegetation indices (VI; (Huete et al. 2002), such as the Normalized Difference Vegetation

Index (NDVI) or the Enhanced Vegetation Index (EVI), which are regarded as proxies of chlorophyll content in plants, of vegetation vigor, and indirectly also of aboveground net primary production, absorbed photosynthetically active radiation (Kerr and Ostrovsky 2003) and leaf area index (Wang et al. 2005), are frequently considered in studies of forest condition and dynamics (e.g., Gond et al. 2013).

Due to their continuous nature, VI time-series allow to measure and analyse two key facets that shape ecosystem stability: *disturbance regime* and *post-disturbance response* (Donohue et al. 2016). Disturbances may be defined as events or any abiotic, biotic, natural or man-made process that disrupt any ecological level, environmental component, the organizational status of a biological cycle of organisms, as well as change resources, substrate availability, or physical environment (Pickett and White 1985, Pickett et al. 1989, Hobbs and Huenneke 1992). The disturbance regime is mainly shaped by the duration and frequency of events and by their severity. The duration and frequency can be represented by the timing and number of abrupt changes in a VI time-series (Verbesselt et al. 2010a, Verbesselt et al. 2010b), while severity is represented by the amount of change produced by each disturbance event (Veraverbeke et al. 2011). In turn, post-disturbance response is greatly determined by the resilience capacity of ecosystems. Holling (1996) proposed a separation between "engineering resilience", defined as a "*measure of the rate at which a system approaches steady state after a perturbation*", in other words, the speed of return to equilibrium (inverse of the return time); and "ecological resilience", defined more broadly as the "*capacity of a system to absorb disturbance and reorganize while undergoing change so as to still retain essentially the same function, structure, identity and feedbacks…"* (Walker et al. 2004).

An integrative approach to stability, as allowed by EO VI time-series, must include the dynamic, interactive and continuous relation between disturbance and the response that follows it. Several measures of vegetation functioning, either related with overall productivity/biomass (e.g., maximum annual value, annual mean), seasonality (e.g., annual range) or phenology (e.g., dates of the start, end and peak of the growing-season), can be derived from EO VI time-series (Jönsson and Eklundh 2004, Alcaraz et al. 2006). These integrative measures can be used for assessing ecosystem dynamics and stability and for investigating the relative effectiveness of PAs with advantages over traditional land cover-based structural metrics, typically with lower spatiotemporal coverage and/or update frequency (Paruelo et al. 2001, Alcaraz-Segura et al. 2008, Cabello et al. 2012). Examples of applications of EO VI time-series for assessing functional ecosystem changes, trends, stability and resilience are vast, including: (i) using Ecosystem Functional Attributes (EFAs; derived from a NDVI time-series) for

monitoring and assessing trends in ecosystem productivity, seasonality and phenology in National Park networks (Alcaraz-Segura et al. (2009); (ii) classifying biomes and monitor global changes over a 30-year period (Higgins et al. (2016); (iii) assessing the reliability of global ecosystem stability metrics (De Keersmaecker et al. 2014); (iv) investigating the role of plant species diversity in ecosystem stability (van Rooijen et al. 2015); (v) evaluating ecosystem stability following drought events (Ivits et al. 2016); (vi) quantifying post-fire resilience in forests as well as phenological changes (Di Mauro et al. 2014); (vii) monitoring the resilience of tropical forests and its possible determinants; (vii) investigating multiple ecosystem stable states and regime shifts in coastal wetland systems (Moffett et al. (2015); and (viii) anticipating species range shifts under climate change (Alcaraz-Segura et al. 2017).

As noted above, EO VI time-series hold great value for studying ecosystem functioning dynamics and stability with an increasing body of literature supporting it. However, to date, most PA effectiveness assessments based on EO data have focused on specific processes (e.g., deforestation or more broadly land use/cover changes) (e.g., Nelson and Chomitz 2009, Rogers 2011, Rodríguez et al. 2012), therefore neglecting a more holistic and integrative ecosystem functioning perspective (but see, Alcaraz-Segura et al. 2009, Cabello et al. 2012). Moreover, a systematic evaluation of PA effectiveness, applicable at the country- (or continental-) level is lacking, with ample room for improving EO-based methodologies. Hence, in this study we present and test a framework for an integrative assessment of forest stability, applicable to PA effectiveness assessments and based on a set of metrics extracted from EO VI time-series. This ecosystem functioning approach to forest stability was tested in the PA National Network of continental Portugal. A MODIS EVI time-series was used to calculate a set of indicators related to the stability of forest ecosystems across the 2000–2016 period. Statistical comparisons using those indicators allowed ranking PAs and comparing the stability dynamics between inside and outside PAs. We furthered this assessment by analyzing potential driving factors behind the observed dynamics, related to PA environmental attributes, forest structural features, and global to regional sources of disturbance and pressure. The implications of our results for management of PAs and forest conservation are finally discussed.

8.2. Methods

Proposed approach and workflow

Grounded on the disturbance-response binomial for stability assessment (Figure 8 - 1), we aimed to compare forest ecosystem stability inside vs. outside a national network of PAs. Our approach encompassed those two broad components (disturbance regime and resilience modulated responses) to deliver a measure of the systems' likelihood to preserve its current stable state in terms of structure and functioning (i.e., a forest-like state; Figure 8 - 2), or to undergo a regime shift (Pausas 2015, Johnstone et al. 2016). This comparison also accounted for the 'natural' seasonal dynamics of ecosystems, thus allowing to evidence 'true' disturbance or change situations (Figure 8 - 1).

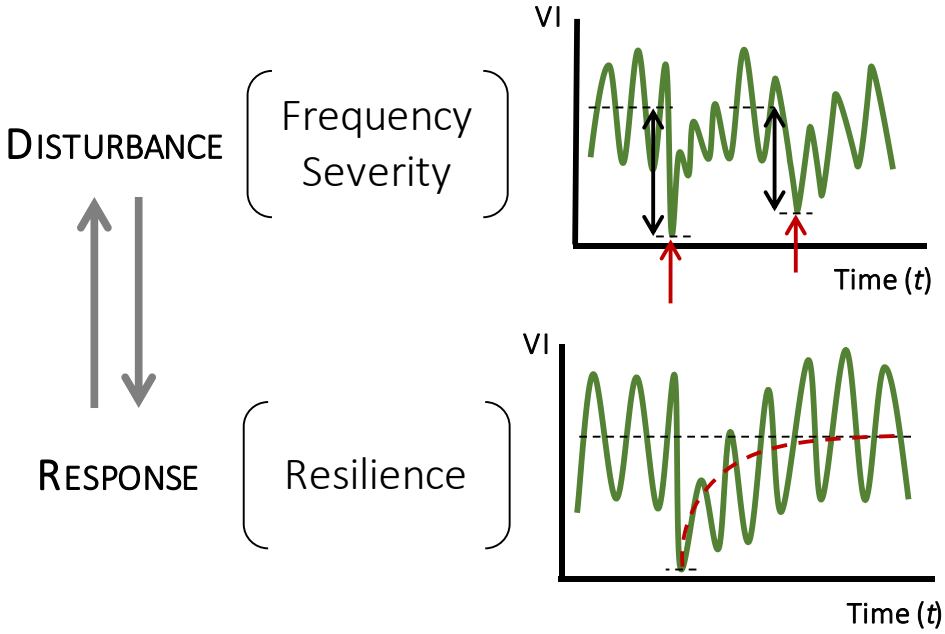

Figure 8 - 1 – Schematic/conceptual representation of stability components in forest ecosystems as the relation between disturbance and response captured by a vegetation index time-series (VI; green line). The upper plot depicts VI annual/seasonal variation with two major abrupt changes (red arrows) showing disturbance frequency and the severity (black arrows). The lower plot depicts the post disturbance response as the return rate of the system towards the former steady state modulated by the systems' resilience.

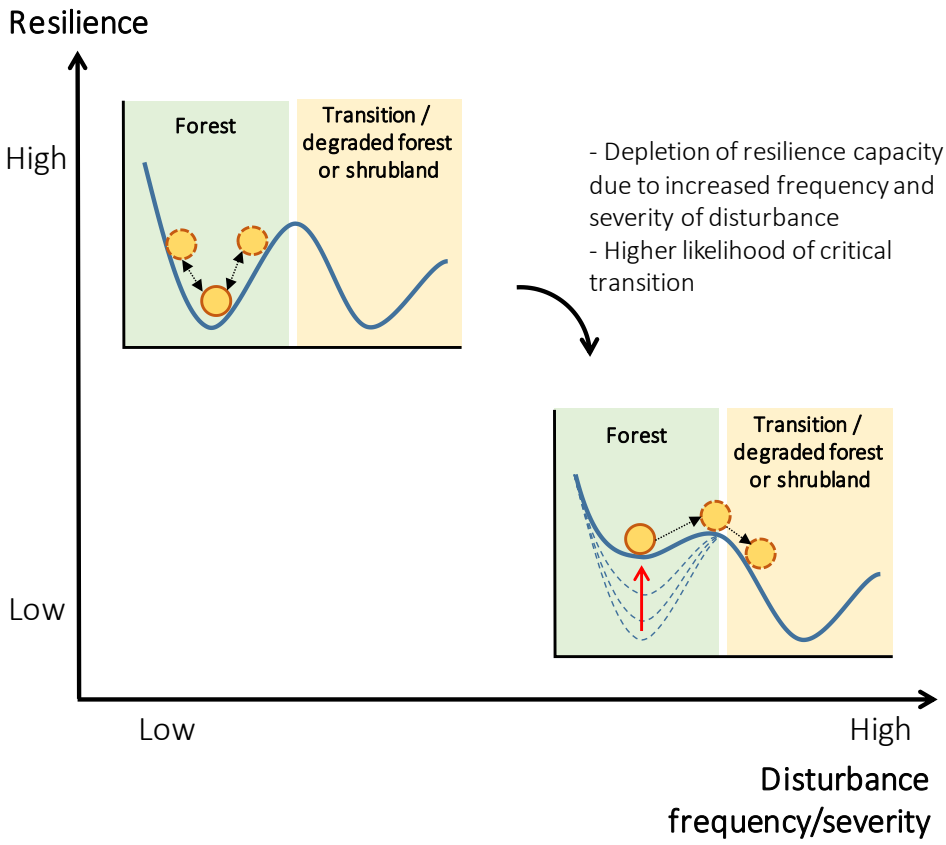

Figure 8 - 2 – Schematic/conceptual representation of potential shifts happening in forest ecosystems as the result of interactive changes in disturbance regime components (frequency and severity) and resilience capacity [based on Pausas (2015) and Johnstone et al (2016)].

Our workflow was devised to address two sequential objectives: (i) to rank and determine which PAs performed better in maintaining stable forest ecosystems during the focal period; and (ii) to identify the drivers of relative stability performance across PAs. To address the first objective, we calculated several indicators of stability based on MODIS EVI time-series grounded on the following analyses: (i) inter-annual variability of ecosystem functioning attributes; (ii) additive time-series decomposition (focusing on the inter-annual fluctuations of the trend component); and, (iii) Lyapunov exponent (a general measure of stability in non-linear systems). These indicators did not focus on particular disturbance events or specific periods but rather on the complete length of the time-series (from 2000 to 2016), thus allowing a broader view of the system's behavior.

Based on these EO indicators of forest stability, we compared forest areas using a spatial referential: inside PAs vs. outside PA (non-PA, hereafter NPA) with the purpose of analyzing and differentiating the dynamics of PA sites *vs*. NPA and to identify the potential factors driving those dynamics. Comparisons used the same forest amount and composition and similar environmental features by minimizing the geographic distance

between PA and NPA (see below). For the second objective, explanatory models were developed based on a set of *a priori* hypotheses (see below), to explore possible factors explaining the observed differences in stability performance among PAs.

The analytical workflow thus consisted of four main steps: i) MODIS MOD13Q1 EVI data download and pre-processing (filtering and smoothing); ii) calculation of stability metrics; iii) comparison between PA and NPA areas; and iv) development, implementation and evaluation of explanatory models (Figure 8 - 3).

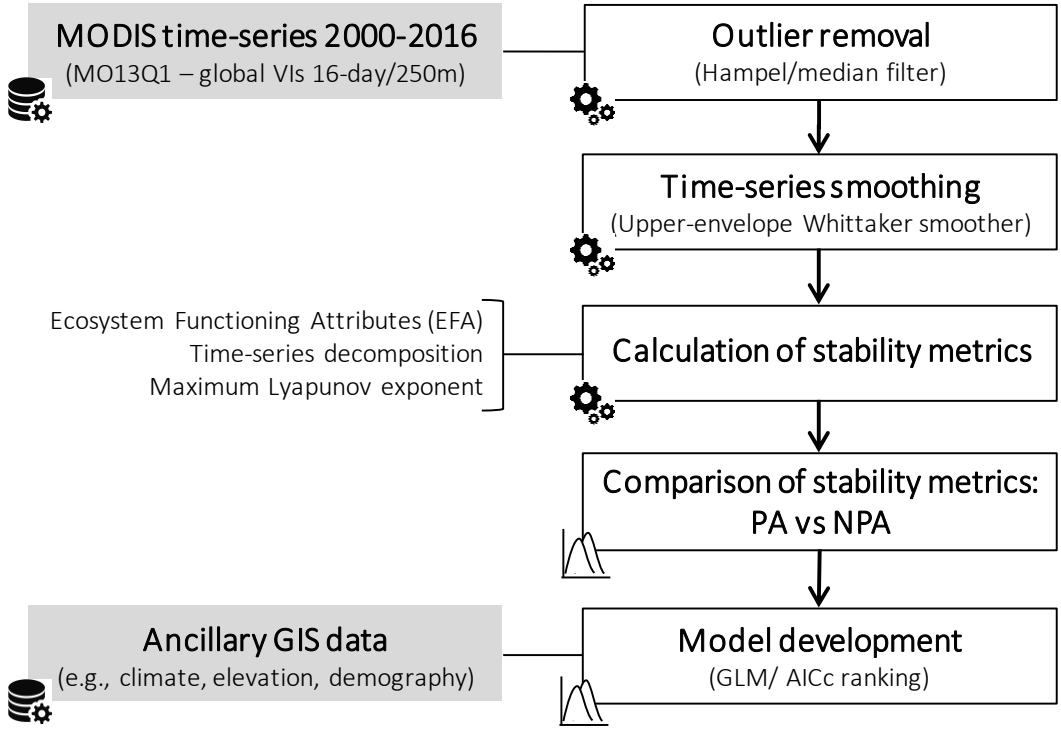

Figure 8 - 3 – Workflow with the approach used to analyze ecosystem stability inside and outside PAs

Selection of Protected Areas

A set of 25 PAs was selected for the analysis out of 43 candidate PAs included in the Portuguese National Network of Protected Areas in year 2016 (Figure 8 - 4; see also Appendix V – S1 for the full list). The selected PAs included those that were designated before or in year 2000 and with a forest area equal or larger than 200ha (≥32 pixels with 250×250m) to improve the sample size. The selected 25 sites correspond to 7.65% (681 501ha) of the surface area of continental Portugal.

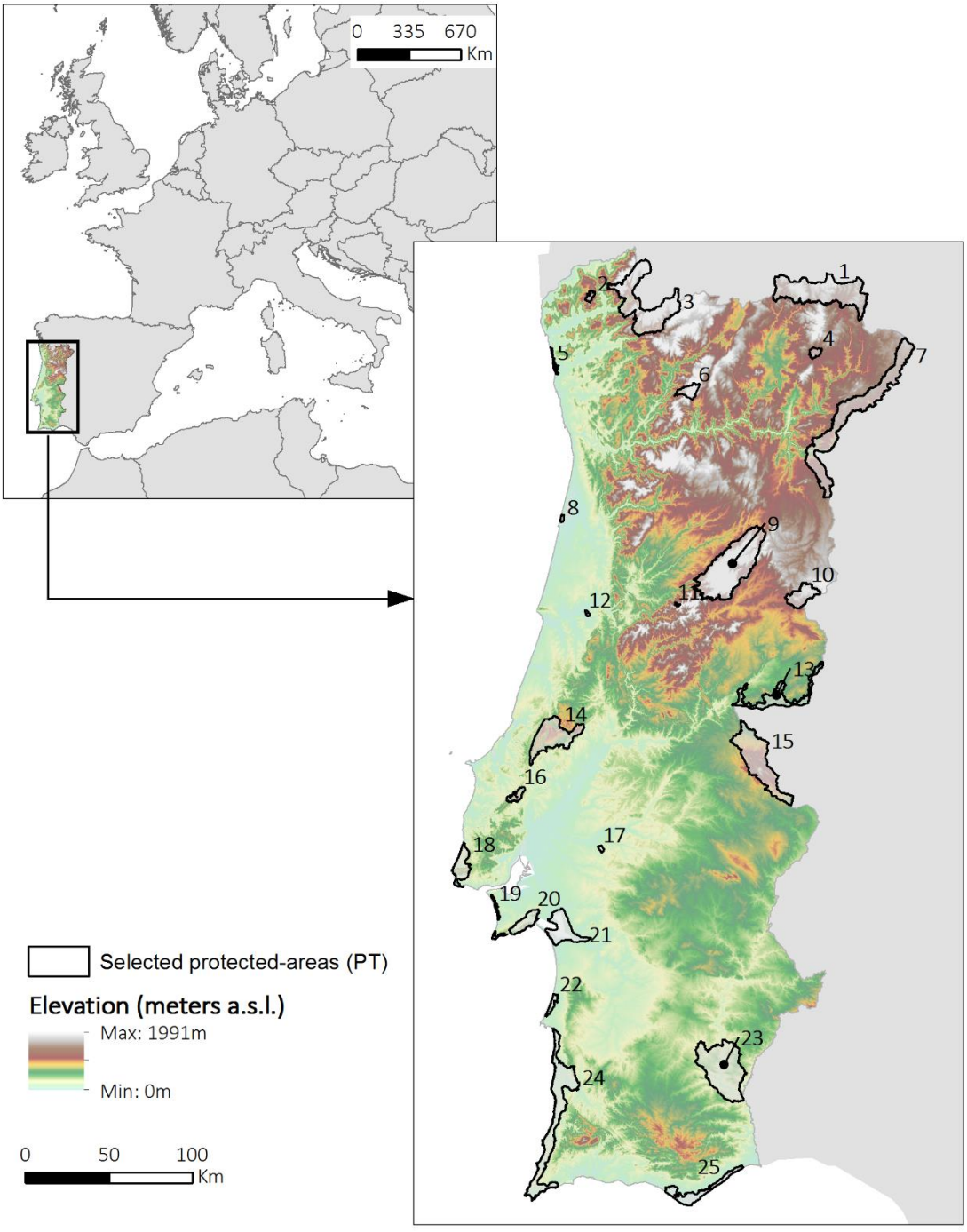

Figure 8 - 4 – Map of the 25 selected protected areas in continental Portugal used in the study (1 - Montesinho, 2 - Corno do Bico, 3 - Peneda-Gerês, 4 - Albufeira do Azibo, 5 - Litoral Norte, 6 - Alvão, 7 - Douro Internacional, 8 - Dunas de São Jacinto, 9 - Serra da Estrela, 10 - Serra Malcata, 11 - Serra do Açor, 12 - Paul de Arzila, 13 - Tejo Internacional, 14 - Serras de Aire e Candeeiros, 15 - Serra de São Mamede, 16 - Serra de Montejunto, 17 - Açude do Monte da Barca, 18 - Sintra-Cascais, 19 - Arriba Fóssil da Costa da Caparica, 20 - Arrábida, 21 - Estuário do Sado, 22 - Lagoas de Santo André e Sancha, 23 - Vale do Guadiana, 24 - Sudoeste Alentejano e Costa Vicentina, 25 - Ria Formosa).

The first PA designated in Portugal was *'Peneda-Gerês'* (the only PA with 'National Park' status) in year 1971, with three periods of the XX-XXIth centuries marking the designation of several other sites (Figure 8 - 5a): late 1970's/early-1980's (most PAs were defined in this period), late-1980's/early-1990's, and more recently in late-1990's/early-2000's. In terms of area (size), the selected sites range from 373ha up to 89 089ha (Figure 8 - 5b). These PAs can be grouped in three broad ecological types: 6 near-coastal/estuarine sites (below 50m), 10 lowland/mid-elevation sites (between 50 and 500m), and 9 highland/mountain sites (above 500m; Figure 8 - 5c).

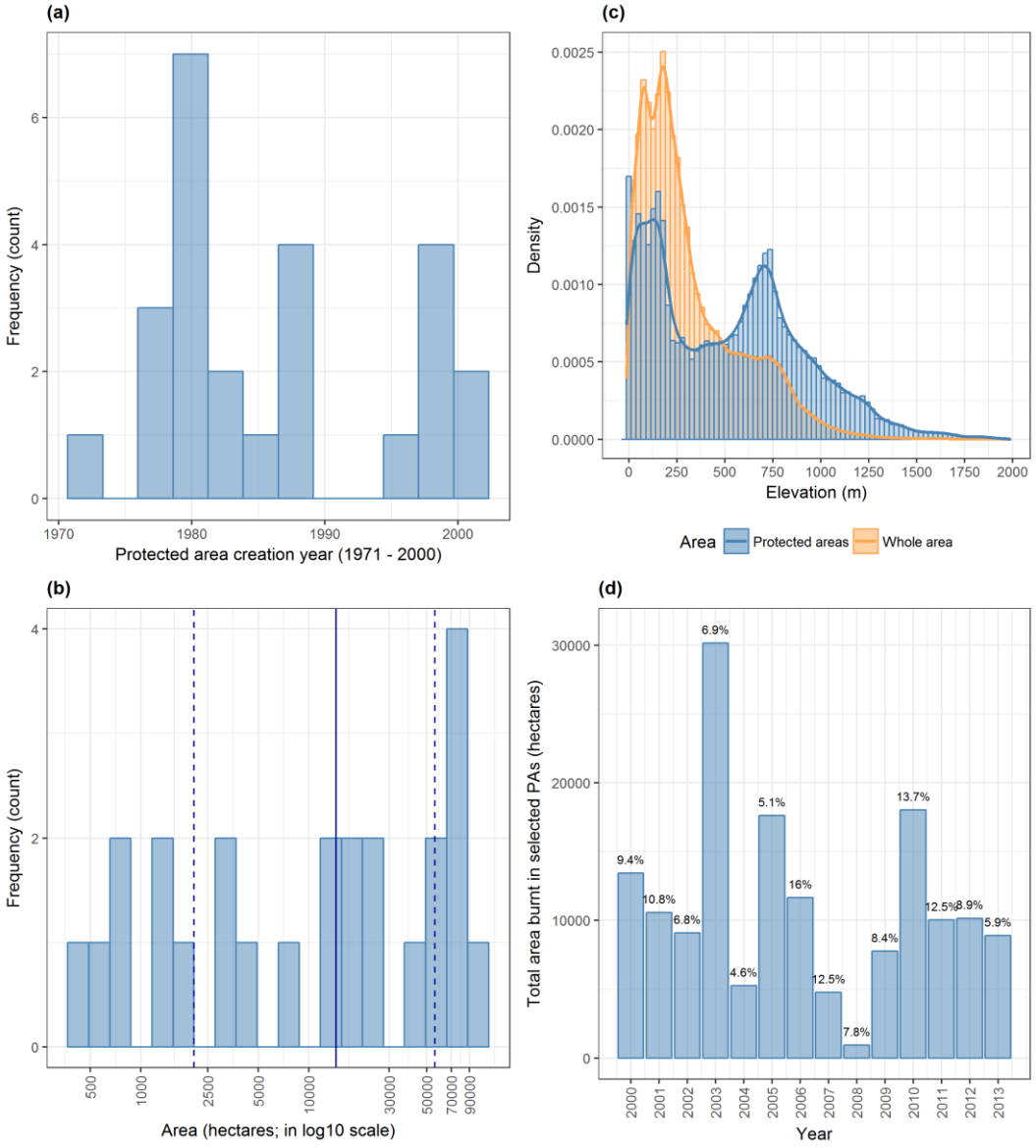

Figure 8 - 5 – Descriptive statistics for the 25 protected areas selected – (a) histogram of creation year; (b) histogram showing the distribution of size (in hectares; the x-axis is in log10 scale), lines show the 25% (left, dashed line), 50% (center, solid), and 75% quantiles (right, dashed); (c) histogram and density line depicting the distribution of elevation (meters a.s.l.) for the whole mainland Portugal (orange colour) vs. selected PAs (blue); and, (d) total area burnt per year (2000-2013) in selected protected areas in hectares. Values above each bar represent the percentage of the total burnt area in mainland Portugal that occurred inside all selected sites by year.

The selected PAs cover the main climatic gradients in continental Portugal, spanning from a wet Atlantic type of climate (in the NW mountains) to a dry Mediterranean type of climate (NE valleys and southern plains) (Mesquita and Sousa 2009).

Wildfires represent a major threat to ecosystem stability in Portuguese PAs. According to official data (ICNF 2016), approximately 11 313 ha were burned on average per year between 2000 and 2013 inside the selected PAs, with critical years in 2003 (30 147ha), 2005 (17 545ha), and 2010 (18 029ha). For the same period, on average, 9.2% of the total burnt area in mainland Portugal occurred inside the selected PAs, reaching 16.0% in year 2006 (Figure 8 - 5d).

Based on official data (INE 2011), a strong demographic dynamics has recently occurred in the selected PAs, which hosted 422 289 inhabitants in 1991, but only 391 153 in 2011, representing a total loss of 7.4% in only two decades. Still, these demographic trends were strongly heterogeneous across the selected PAs, with 17 (out of 25) recording depopulation dynamics whereas in 8 PAs the population has actually increased in the same period. In general, inland and mountainous PAs displayed most population losses, while PAs in lowlands and near the coastline recorded population increase (see Appendix V – S2).

Selection and description of forest areas

Comparisons between PAs and NPAs focused on forest ecosystems. We used the Corine Land Cover (CLC) raster dataset (250m spatial resolution) for year 2000 (the start of the period under analysis) to select forest areas. CLC provides wall-to-wall coverage of Europe's land cover and is considered a reference dataset for environmental assessment purposes and policy making (EEA 1999, 2007). All three CLC forest classes were targeted for assessment (Table 8 - 1), and only MODIS 250m pixels intersecting these areas were selected for comparisons. We considered the entire area of mainland Portugal and a 50km buffer extending to Spain. A description of common species in CLC forest classes is presented in Appendix V – S3. Due to the characteristics of the CLC dataset, in the analyses no distinction could be made between native and exotic species, nor between evergreen and deciduous trees (namely in the case of broad-leaved forests).

Table 8 - 1 – CLC classes selected for assessment and PA vs. NPA comparison

Class	Description
Broad-leaved forests (CLC 311)	Vegetation formations composed mainly of trees, including shrub and bush understory, where broad-leaved species predominate (> 75 % of the area);
Coniferous forests (CLC 312)	Vegetation formation composed principally of trees, including shrub and bush understory, where coniferous species predominate (> 75 % of the area);
Mixed forests (CLC 313)	Vegetation formation composed principally of trees, including shrub and bush understory, where neither broad-leaved nor coniferous species predominate. The share of coniferous or broad-leaved species does not exceed 25% in the canopy closure.

Input data and pre-processing

The MODerate Resolution Imaging Spectroradiometer (MODIS) MOD13Q1 (version 6) product provides 16-day composite VIs at 250m spatial resolution, making available consistent, spatial and temporal time-series of global vegetation conditions that can be used to monitor terrestrial photosynthetic vegetation activity as well as seasonal and inter-annual changes in ecosystems. Two VIs are available from MOD13Q1 product, namely NDVI and EVI. Only the latter was used in this study since it provides improved sensitivity over high-biomass regions and greater vegetation monitoring ability through the decoupling of the canopy background signal and a reduction in atmosphere influences (Huete et al. 2002, Didan et al. 2015).

The original data were downloaded from the *EarthData* platform (URL: https://search.earthdata.nasa.gov/) and then mosaicked, subset and re-projected to the WGS 1984 – UTM 29N coordinate system using the MODIS Reprojection Tool (MRT release 4.1, 2011, URL: https://lpdaac.usgs.gov/tools/modis_reprojection_tool).

For improving the retrieval of meaningful information from the EVI time-series, and increase the signal-to-noise ratio, two procedures were used in tandem, combining robust outlier detection/removal and time-series smoothing: the Hampel filter (Hampel 1974, Davies and Gather 1993) and the Whittaker-Henderson smoother [attributed to Whittaker (1923)] (see also Appendix V – S4 for more details).

Calculation of stability indicators

Annual indices of ecosystem functioning

Several annual indices can be computed from an EVI time-series and serve as proxy measures of the flows of matter and energy in ecosystems (Paruelo et al. 2001, Alcaraz et al. 2006, Cabello et al. 2012). These indices allow to characterize three broad

ecosystem functional dimensions related to: (i) productivity (linked to the amount of biomass or vegetation cover), (ii) seasonality (the intra-annual range or difference), and (iii) phenology (timing of certain events in the annual vegetative cycle; e.g., day of growing-season peak).

To capture productivity, we considered the annual median, $MED_y = median(x_i)$, with x_i equal to an EVI value in a given 16-day period $i = \{1, \dots, 23\}$; in total, a year y has a maximum of 23 values. Other data quantiles were also considered for quantifying low annual values (5% quantile: $Q05_y = quantile(x_i, p = 0.05)$) and high annual values (95% quantile: $Q95_y = quantile(x_i, p = 0.95)$). To evaluate seasonality, we calculated the difference between the 95% and 5% quantiles as: $DQT = Q95 - Q05$. Robust non-parametric measures (median and quantiles) were selected to further avoid potential outliers in annual time-series. For portraying phenology, and taking into account the cyclical properties of this variable, we calculated the sine ('*summerness*'; SMN) transformation of the day of maximum value recorded annually during the growing season, as given by: $D_{max} = DOY(\arg_{max}\{x_i\})$; where DOY is a function that gives the day-of-the-year for a certain value (in this case the maximum value recorded in a year): $SMN_y = \sin(D_{max}/365 \times \pi)$. SMN ranges between 0 and 1, with higher values corresponding to ecosystems that have their peak around the summer season.

To analyse the inter-annual stability of ecosystem functioning metrics, we calculated the coefficient of variation, commonly used in this type of application (De Keersmaecker et al. 2014, van Rooijen et al. 2015), $CV = SD/MN$, with SD and MN respectively equal to the intra-annual standard-deviation and mean of an annual metric. Only complete years were considered (i.e., $y = \{2001, \dots, 2015\}$), to avoid biasing annual values. All calculated indices were based on the smoothed EVI time-series to avoid spurious values and to reduce errors.

Time-series decomposition

The temporal fluctuation of a VI time-series typically contains three components: (i) a seasonal component (due to phenological cycles), (ii) a trend component (e.g., due to gradual vegetation changes or sensor degradation), and (iii) a remainder component. Changes in the usual fluctuation patterns of a time-series typically occur due to 'natural' environmental factors (e.g., inter-annual climatic variation – 'climatic year') and/or 'extreme' perturbations such as wildfires or land use/cover changes (e.g., harvesting). Trends can be considered to represent medium or long-term changes in the equilibrium state of vegetation, such as the drop and recovery from a fire disturbance or severe

drought conditions. Overall, higher fluctuations in the trend component of a time-series may be indicative of lower stability.

STL (*Seasonal* and *Trend* decomposition using *Loess*) is a filtering procedure for decomposing a seasonal time-series into three components: trend, seasonal, and remainder (Cleveland et al. 1990). STL has a simple design that consists of a sequence of applications of the loess smoother to extract these three components. Suppose the data, the trend component, the seasonal component, and the remainder component are denoted by Y_i, T_i, S_i, and R_i, respectively, for $i = 1$ to N observations. Then STL assumes these components are additive: $Y_i = T_i + S_i + R_i$. We used the STL routines implemented in R statistical software with *stats* package (R Development Core Team 2017), with parameter *s.window* = 7 (*s.window* controls how rapidly the seasonal component can change) to extract each component based on the original non-smoothed data. After decomposing the series, we calculated the coefficient of variation for the trend component, as: $CV_{T_i} = mean\{T_i\}/sd\{T_i\}$.

Maximum Lyapunov exponent

The Maximum Lyapunov exponent (MLE) determines a notion of predictability for a dynamic system. A positive MLE is usually taken as an indication that the system is chaotic (provided some other conditions are met). There are several ways to calculate MLE and we followed the method described in Hegger et al. (1999).

Consider the time-series as a trajectory of the values in the embedding space and assume that you observe a very close return $s_{n'}$ to a previously visited point in that series denoted as s_n. From this, we can consider the distance: $\Delta_0 = s_n - s_{n'}$ as a small perturbation, which expectedly should grow exponentially as time progresses. If this holds, then future values can be calculated from the time-series as: $\Delta_l = s_{n+l} - s_{n'+l}$. If one finds that: $|\Delta_l| \approx \Delta_0 e^{\lambda l}$, then λ is the MLE. In practice, there will be many fluctuations due to several effects but this can be used to derive a robust and unbiased estimator the MLE. To achieve this, we can compute:

$$S(\epsilon, m, t) = \langle ln\left(\frac{1}{|\mathcal{U}_n|}\sum_{s_{n'}}|s_{n+t} - s_{n'+t}|\right)\rangle_n$$

If $S(\epsilon, m, t)$ exhibits a linear increase with identical slope for all m (embedding dimension) larger than some m_0 and for a reasonable range of ϵ (radius to find nearest-neighbor points), then this slope can be taken as an estimate of the maximal exponent λ_1. This algorithm is implemented in function *lyap_k* included in *tseriesChaos* R package (Narzo 2013). After some experimentation, we set the function parameters to: *m=2*

(embedding dimension), d=2 (time delay), s=50 (iterations along which follow the neighbours of each point), t=20 (Theiler window), ref=80 (number of points to take into account), k=1 (number of considered neighbours – default value), eps=4 (radius where to find nearest neighbours). MLE was calculated from the smoothed time-series to reduce potential estimation errors.

A summary of the stability metrics computed in this study is presented in Table 8 - 2.

Table 8 - 2 **–** Stability metrics calculated to compare PA and NPA (*n* equals the number of observations in the time-series).

Temporal resolution / interval	**Approach**	**Metric**
Aggregated annual values / 2001-2015 (*n*=15)	Variability in annual metrics of ecosystem functioning – productivity	Inter-annual coefficient of variation of annual medians (MED)
		Inter-annual coefficient of variation of annual 5% quantiles (Q05)
		Inter-annual coefficient of variation of annual 95% quantiles (Q95)
	Variability in annual metrics of ecosystem functioning – seasonality (intra-annual variation)	Inter-annual coefficient of variation of annual differences between 95 and 5% quantiles (DQT)
	Annual metrics of ecosystem functioning – phenology (timing of growing season events)	Inter-annual coefficient of variation of "summerness" (sine) transformations of the day of maximum (SMN)
Full time-series with 16-day values / 2000-2016 (*n*=381)	Fluctuation in trend component	Trend component coefficient of variation (TRD)
	System dynamics	Maximum Lyapunov exponent (MLE)

Comparisons between PA and NPA

Comparison between protected and non-protected areas for each PA used only the broadleaved, coniferous and mixed forest pixels of the CLC dataset (see Table 8 - 1). The first stage of the comparison consisted in determining the buffer distance from the PA border required to include, in the NPA space, an area of each forest class corresponding to twice the area of that class recorded inside the PA (see Appendix V – S5 for calculated buffer distances). This procedure minimized environmental dissimilarities between PA and NPA (induced by increasing geographical distance) while simultaneously allowing some variability in forest conditions in the NPA space. If the NPA buffer covered Portuguese or Spanish pixels pertaining to other PAs, those were excluded from the analyses.

In a second stage, we compared the distribution of values of each stability indicator between PAs and NPAs. To do so, we used the entire set of values for the PA

and draw a random distribution of values in the NPA space constrained by the buffer distance and maintaining the same amount and proportion of forest types between PA and NPA samples. Then, we compared these two distributions with the non-parametric Wilcoxon signed rank test. We set the test always to be "one-sided", since we assumed PAs to be more stable (in median) than NPAs. Hence, the alternative hypothesis was set as PA < NPA [i.e., the inter-annual coefficient of variation of the annual medians (MED) is lower in PAs than NPAs]. This comparison/testing procedure was repeated 1000 times for different NPA random draws.

Since multiple comparison tests were performed, we adjusted the test *p*-values using the Benjamini and Hochberg (1995) correction, which controls the false discovery rate (the expected proportion of false discoveries amongst the rejected hypotheses). The false discovery rate is generally a less stringent condition than the family-wise error rate, so this method is potentially more powerful than others (such as the Bonferroni correction).

We considered a PA to be relatively more stable than its NPA counterpart if, for a given stability indicator (Table 8 - 2), 50% or more of the tests rejected the null-hypothesis at a significance level of $\alpha = 0.05$. This allowed to convert the comparisons made for each stability metric into a binomial/dichotomic variable: stable (value: 1) and unstable (value: 0). This transformation was considered the response/dependent variable later used for model development.

Model development for observed stability patterns

Generalized Linear Models (GLM) with a Binomial distribution of errors were used to explain the stability of PAs vs. NPAs. Several hypotheses, related to seven groups of explanatory variables, were considered to explain the observed differences in stability performance across PAs. Those hypotheses were formulated based on prior knowledge regarding the PA dynamics, preliminary data analyses (e.g., demography, fire regime), national and international reports on forest ecosystems, and current literature. Explanatory variables (linked to each model/hypothesis) and input data are listed in Table 8 - 3. Lack of data or inadequate data granularity regarding land use, land management, monetary investment or expenditure in PAs, forest management, fire suppression, detailed structural and compositional forest description or other relevant factors to explain forest stability dynamics prevented us to consider those hypotheses although we a priori recognized their potential explanatory power. For each hypothesis, we defined the corresponding models and explanatory variables (see Table 8 - 3 with

variables description and Table 8 - 4 with model structures and combinations of variables).

The first set of hypotheses was linked to climatic anomalies in temperature and precipitation (set I) defined as: $anom = avg(Y_i) - Y_i$, with Y_i equal to annual average temperatures (minimum, maximum or mean; °C) or total precipitation (mm/year). To capture the inter-annual fluctuation in climatic anomalies across PAs, we used the standard-deviation. Protected Area attributes (set II) included variables related to PA size (hectares; log10 transform), spatial elongation/compactness, average elevation (meters a.s.l.), age (years), and the percentage of the PA area overlapped with the Natura 2000 conservation network. Human pressure (set III) included population density (inhabitants/sq.km), population change (% between 1990-2011), and road density (m/km2). Forest and landscape composition (set IV) contained variables related to the fractional cover of each forest type and to total land cover diversity (Simpson diversity index). Landscape pattern metrics were calculated using FragStats software (McGarigal et al. 2002). Forest structural attributes (set V) were also considered relevant for explaining PA stability, and included forest patch area, connectivity [measured by the cohesion index (McGarigal et al. 2002)], as well as forest canopy average height and variability to portray vertical structure. Forest disturbance factors were also included (set VI) by considering the average percentage of burnt PA area (2000-2013, last year available in official databases), average percentage of burnt forest area, and percentage of PA area affected (or in risk) by the pine wilt nematode. Finally, to portray the complexity and potential interaction effects between different hypotheses, we included models combining explanatory variables from the above groups (set VII).

Models were then compared and ranked through a multi-model inference framework using the Akaike Information Criterion (with a correction for small sample size; AICc) for evaluation, following Symonds and Moussalli (2011). In addition, to display the amount of variation explained by each model we calculated the Deviance measure (D2). The Chi-squared test was used to evaluate model significance. Multicollinearity (simply denoted by high correlation among explanatory variables in a model) was diagnosed using Variance Inflation Factors (VIF). Typically, if one or more model terms have $\sqrt{VIF} > 2$ then the model has high collinearity. In these cases, we removed such models from further evaluation. To avoid overfitting and overcomplexity given the relatively low sample size (n=25), individual models were fit with a maximum of three explanatory variables.

Table 8 - 3 – List of explanatory variables (related to each hypotheses set) along with input datasets.

Hypotheses set	Acronym	Variables	Datasets
I. Climatic anomalies	**PREC_ANOM**	Average climatic anomaly variation in annual precipitation 2000-2015 (mm/year)	ECA&D - E-OBS Ensembles climatic data for Europe (daily/1995-2016) URL: http://www.ecad.eu
	TMIN_ANOM	Average climatic anomaly variation in minimum temperature 2000-2015 (°C)	
	TMAX_ANOM	Average climatic anomaly variation in maximum temperature 2000-2015 (°C)	
II. PA attributes	**PA_SIZE**	Protected area size (log10 transform)	ICNF Portuguese Network of Protected Areas (boundaries and creation year) URL: http://www.icnf.pt/portal/naturaclas/cart
	PA_AGE	Protected area age (years)	
	PA_CIRC	Protected area shape - circle index	
	PA_ELEV	Protected area average elevation (meters a.s.l.)	SRTM v4 elevation data (90m) URL: http://www.cgiar-csi.org/data/srtm-90m-digital-elevation-database-v4-1
	PA_SAC	% of PA area that is overlapped by Natura 2000 SAC	Natura 2000 Special Areas of Conservation (SAC) and Special Protection Areas (SPA) URL: http://www.eea.europa.eu/ds_resolveuid/DAT-68-en
	PA_SPA	% of PA area that is overlapped by Natura 2000 SPA	
III. Human pressure	**POP_DENS**	Population density in year 2001 (inhabitants/km2)	Portuguese National Census database - INE URL: https://www.ine.pt
	POP_CHANGE	% change in resident population between years 2001 and 2011	
	ROAD_DENS	Road density (m/km^2)	OpenStreetMap road data for Portugal URL: http://download.geofabrik.de/europe/portugal.html
IV. Forest and landscape composition	**LC_BRLF**	% of PA covered by broadleaf forests	EEA Corine Land Cover 2000 (250m; 44 classes) URL: http://www.eea.europa.eu/ds_resolveuid/DAT-79-en
	LC_CONF	% of PA covered by coniferous forests	
	LC_MIXF	% of PA covered by mixed forests	
	LC_SIDI	PA landscape Simpson Diversity Index	
V. Forest structure	**FOR_AREA**	Average forest patch area (hectares)	
	FOR_COHES	Forest cohesion index	
	FCH_AVG	Forest canopy height average (meters)	Global Forest Canopy Height (1000m) from (Simard et al., 2011) / SDAT/ORNL DAAC URL: http://webmap.ornl.gov/wcsdown/dataset.jsp?ds_id=10023
	FCH_STD	Forest canopy height standard-deviation (meters)	
VI. Forest disturbances	**BURN_PA**	Average % of total burnt area inside PA between 2000 and 2013	ICNF National database of burnt areas from 1990 to 2013 (MMU 1ha) URL: http://www.icnf.pt/portal/florestas/dfci/inc/info-geo
	BURN_FOR	Average % of burnt forest area inside PA between 2000 and 2013	
	PWN_PERC	% of PA area already affected or in risk by pine wilt nematode	Pine Wilt Nematode areas (May-2016) URL: http://www.icnf.pt/portal/florestas/prag-doe/ag-bn/nmp/infgeo

8.3. Results

Spatial patterns of forest stability

Overall, the spatial distribution of forest stability indicators (Figure 8 - 6) shows a very complex pattern across the country with strong local variation and no particular zonation in terms of geographic, elevation or climatic gradients. Some relatively larger and often continuous areas, located in the centre and south of the country, show focal spots were strong forest instability occurred throughout the study period. Overall, we also found a strong spatial coherence among forest stability indicators, especially for MED, TRD and MLE which signal similar patterns of 'hot' and 'cold' spots of forest stability. SMN was the most dissimilar indicator in terms of overall spatial pattern, signalling less unstable areas in the northern portion of the country in contrast to southern forest areas.

Performance of the national Protected Area network

The comparison of stability values between PA and neighbouring NPA locations allowed to rank PAs according to their relative forest stability performance (Figure 8 - 7). This ranking reveal that 28% of PAs (7 of the 25 selected PAs) were more stable than their NPA counterparts for six or even all seven indicators; 20% (5 PAs) are more stable for 4 to 5 indicators; and 28% (7 PAs) are more stable than their NPA according to 1 to 3 indicators. For 24% (6 PAs), none of the stability indicators found PAs to be more stable than their NPA counterparts.

Forest stability scores exhibit a complex geographic distribution across the PA network, without evident observable patterns, structures or clusters (Figure 8 - 7). Still, there is a higher prevalence of PAs with moderate (PA IDs: 2, 8, 9 and 12) to no indication of higher relative stability (PA IDs: 3, 4, 5 and 6) in the north portion of the PA network. The most consistently stable PAs are located (with several exceptions, e.g. PA ID: 1) along the coastal and near-coastal areas in the centre and south of the country, as well as near the border in the centre part of the country (PA IDs: 13 and 15).

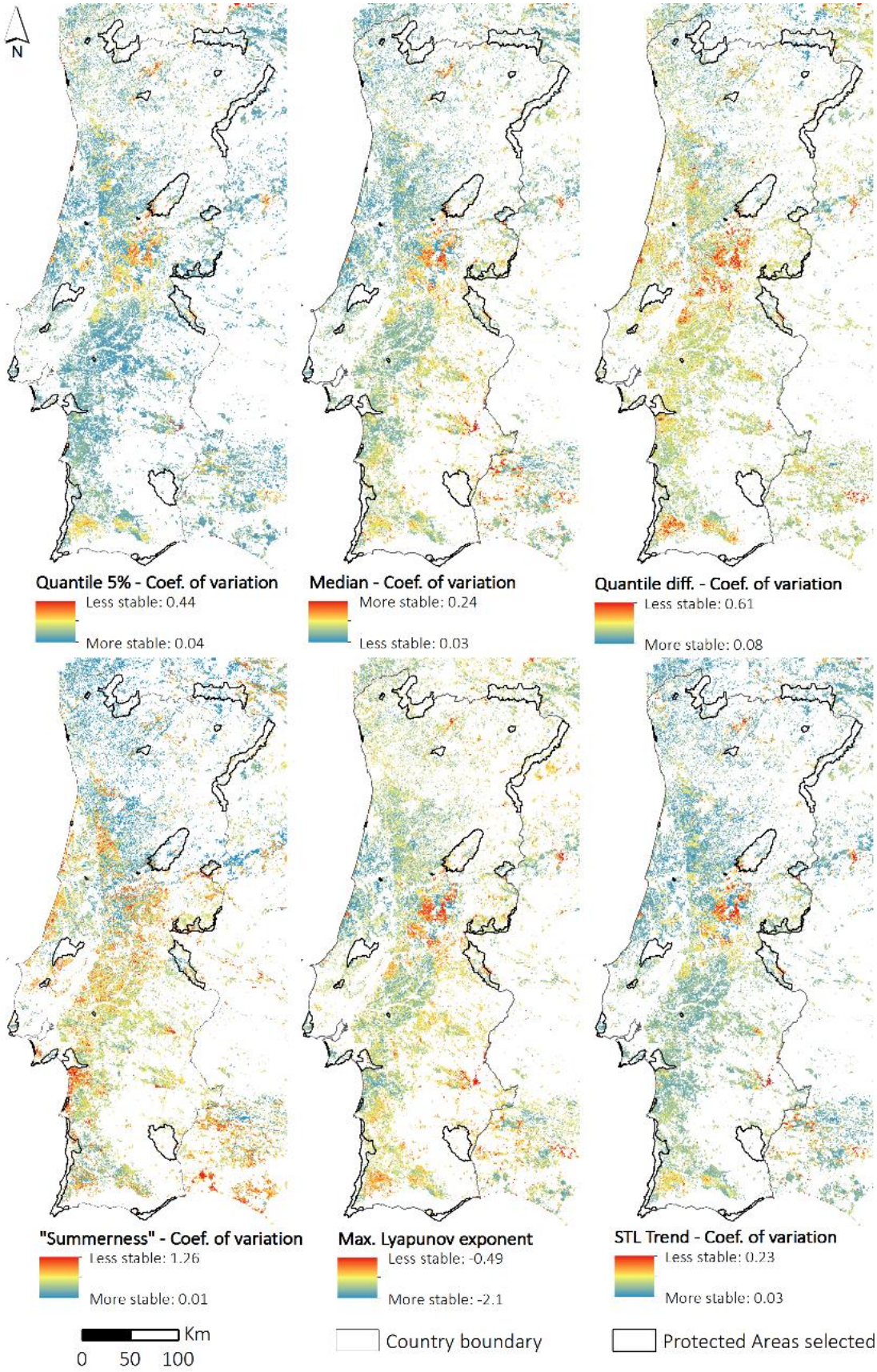

Figure 8 - 6 – Stability metrics represented for CLC 2000 forest areas in continental Portugal (colder/blue colors represent more stable areas whereas warmer/red colors correspond to less stable areas). All images were represented using intervals defined by the 1% and 99% quantiles (Note: Q95 was not presented here due to page space constraints)

(a)

ID	Q05	MED	Q95	DQT	SMN	TRD	MLE
1	**100.0**	**100.0**	**100.0**	**100.0**	**96.7**	**100.0**	**99.9**
18	**100.0**	**100.0**	**100.0**	**54.9**	**100.0**	**100.0**	**100.0**
20		**100.0**	**100.0**	**100.0**	**100.0**	**100.0**	**100.0**
15		**100.0**	**100.0**	**100.0**	**100.0**	**100.0**	**100.0**
11		**85.7**	**99.9**	**100.0**	**99.9**	**100.0**	**69.4**
13	**99.8**	**100.0**	**100.0**	**100.0**		**100.0**	**100.0**
24	**100.0**	**99.9**	**100.0**	**100.0**		**100.0**	
7		**100.0**	**100.0**			**81.0**	**100.0**
21	**100.0**	**100.0**	**96.3**			**100.0**	
10		**100.0**	**100.0**		26.3	**100.0**	**100.0**
14		**96.2**	**100.0**	**99.8**	**100.0**	41.1	
12			**62.1**	**100.0**	**100.0**		
2	**100.0**			**99.9**		33.9	
9				**100.0**	**100.0**		
16			**94.5**		**100.0**		
19					**99.7**		
8					**98.6**		
25							**98.2**
23					**99.9**		
17							
4							
6							
22							
5							
3							

(b)

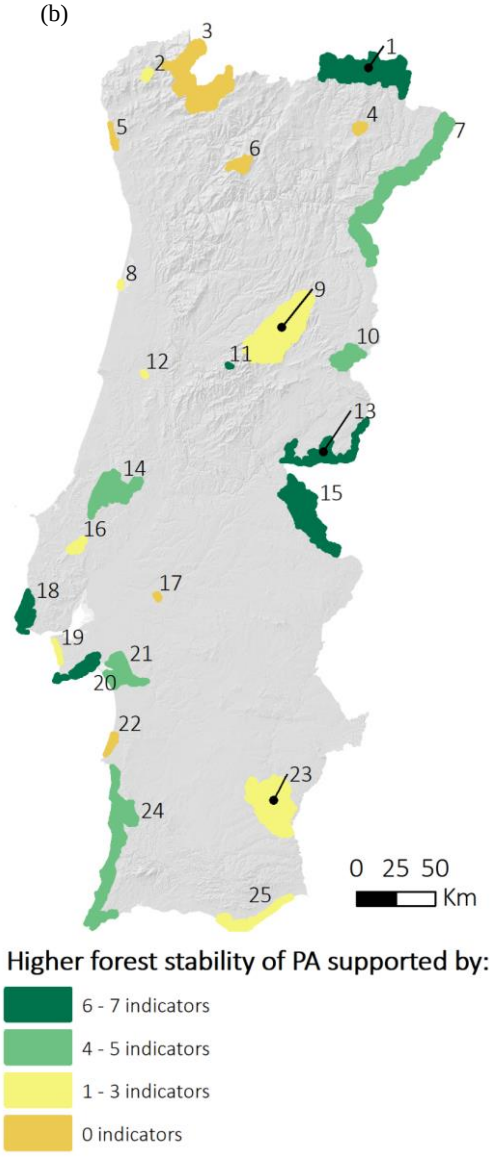

Figure 8 - 7 – (a) Forest stability by indicator. Values show the percentage of Wilcoxon tests (n=1000) for which Protected Areas (PA) are relatively more stable than the surrounding non-protected area (NPA; only values greater than zero are shown). PAs are sorted in descendent order according to their overall stability ranking, obtained by summing the number of criteria that recorded a value greater than 50.0% (in bold). Each column represents a stability metric: inter-annual coefficient of variation of the annual 5% quantile (Q05), median (MED), 95% quantile (Q95), annual difference between 95 and 5% quantiles (DQT), and "summerness" (sine) transformation of the day of maximum (SMN). STL decomposition – trend component coefficient of variation (TRD) and maximum Lyapunov exponent (MLE); (b) Overall relative forest stability rank across the PA network. This ranking is based on counting the number of stability indicators that recorded a percentage higher than 50% (i.e., indicators for which PA is more stable than NPA). For PA names use Figure 8-4 caption.

A strong spatial variation in forest stability was also found inside each PA for the various indicators. For example, in "*Serra da Estrela*" Natural Park (PA 9), forest areas in the SW section of the park and closer to this PA border are considerably less stable than those in the NE interior part of this site. The same happens for "*Peneda-Gerês*" National Park (PA 3), where some particular areas recorded very low stability scores,

whereas others attained very-high stability. For these two PAs, examples of unstable locations are presented in Figure 8 - 8. For these illustrative locations, EVI time-series depict disturbance events (possibly related to wildfires and/or vegetation clearing), with strong breaks in vegetation cover and productivity followed by a recovery period. These time series and associated image data also flag alterations in vegetation cover and seasonal amplitude as well as potential changes in vegetation composition. In contrast, illustrative locations with highly stable dynamics were selected from "*Montesinho*" (PA 1) and "*Sintra-Cascais*" Natural Parks. For the first PA 1, we can see a forest area with a strong recovery response following the 2004-2005 drought (notice the decrease in seasonal amplitude for that year; Figure 8 - 9 – Panel I). The example from the "*Sintra-Cascais*" PA depicts very stable dynamics with a long-term increasing trend. Also, we noticed alterations in the seasonal component (see STL decomposition plots) in unstable locations (Figure 8 - 8b) in comparison to steady seasonal dynamics observed in stable locations (Figure 8 - 9b).

Drivers of Protected Area stability performance

Binomial GLM results allowed to explore the driving factors behind PA forest stability scores for each indicator. In terms of overall model fitting performance (evaluated by deviance, D2) we found very different results across forest stability indicators. The best fitting models for TRD, MED and Q95 attained the highest performance (D2=0.59 to 0.48). For DQT, Q05 and MLE, the best fitting performances were lower (D2=0.34 to 0.29). SMN recorded the lowest fitting performance overall (best model with D2=0.19). All best fitting models were statistically significant for α=0.05 (Table 8 - 4). The VIF test signalled low collinearity for all bivariate or multivariate models and so none were removed from subsequent analyses (see Appendix V – S6).

We used a multi-model inference framework, with AICc as a criterion for model ranking, and considered that models with a ΔAICc < 3 ('confidence set') had a good support to explain forest stability scores (Table 8 - 4; see Appendix V – S6 with all models). Lower ΔAICc and higher wi convey models with stronger support. In general, we found a coherent and strong evidence for set VII across forest stability indicators (Table 8 - 4). This set combines several hypothesized components related to protected area attributes but mostly from landscape and forest composition, forest structure, and disturbance (and interactions between some of these components).

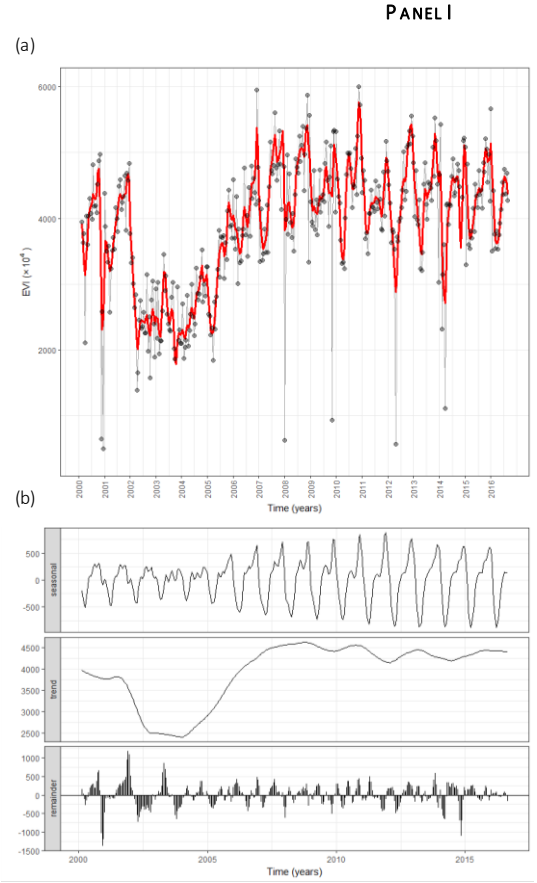

Figure 8 - 8

Panel I (top) – representation of vegetation changes (encroachment and *Acacia dealbata* invasion) following fire/clearing disturbance in 2002 in 'Caldas do Gerês' – *Peneda-Gerês* National Park. Plot (a) depicts the original (points/grey line) and filtered/smoothed (red line) MODIS EVI time-series. Plot (b) depicts the STL decomposition of the series showing the alterations in the seasonal (upper), trend (middle) and remainder (bottom) components. Notice the increased annual median value and larger seasonal amplitude.

Panel II (bottom) – vegetation changes following the 2005 fire in 'Aguincho/Fontão' – *Serra da Estrela* Natural Park. In the aerial photos, it is possible to observe large forest losses followed by partial recovery, shrub encroachment (broom or gorse) and species invasion (*Acacia* spp.) in the valley areas (yellow tones). Notice the large drop and recovery in EVI values (a) and the alterations in STL components (b) such as larger seasonal amplitude. All aerial photos were extracted from the available catalog in ©Google Earth (Dec-2016).

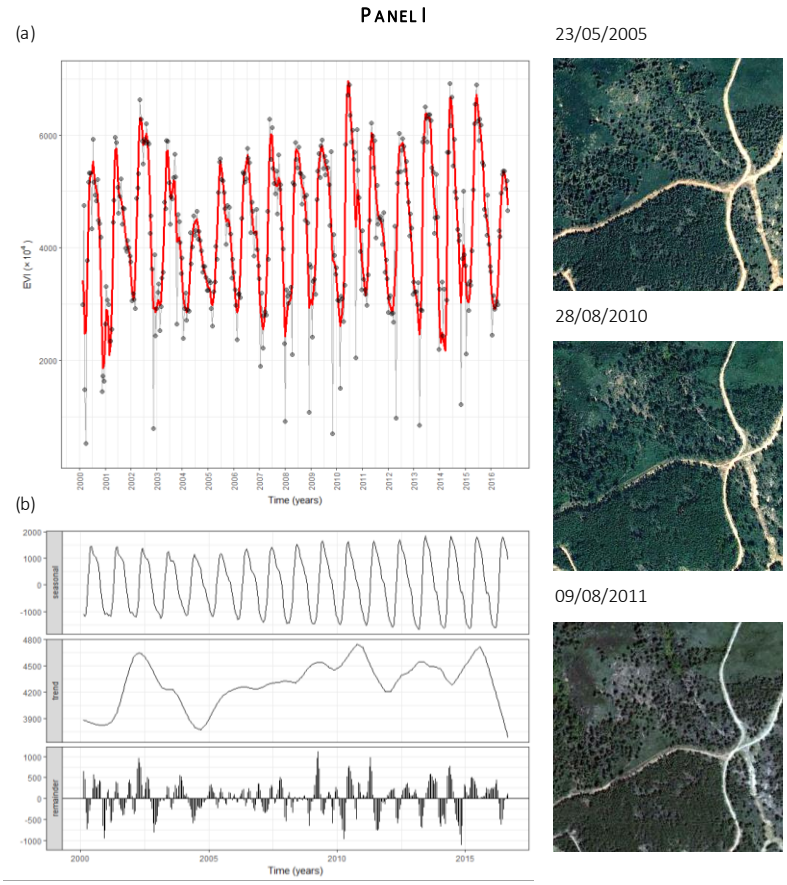

Figure 8 - 9

Panel I (top) – EVI time-series of a stable forest area near *'Deilão'* – *Montesinho* Natural Park. Plot (a) depicts the original (points/grey line) and filtered/smoothed (red line) series. Plot (b) depicts the STL decomposition with a small increase in seasonal amplitude. Year 2004-2005 recorded a strong drought followed by a resilient response in the following years.

Panel II (bottom) – depicts also a stable forest area close to *'São Pedro de Penaferrim'* (near *'Pena'* National Palace heritage site) – *Sintra-Cascais* Natural Park. STL decomposition shows a stable seasonal dynamic with a slightly increasing trend. All aerial photos were extracted from the available catalog in ©Google Earth (Dec-2016).

For Q05, several models composed the confidence set. For this indicator, models including the % cover of broadleaf forest, PA size, burnt forest area and structural aspects related to canopy height heterogeneity and forest patch connectivity attained the highest support for explaining PA stability scores. For MED and TRD we found that combined models including the % of broadleaf forest, PA size and the interaction between burnt forest area and PA average elevation recorded stronger explanatory support. For Q95, only a single model was selected, with a strong signal related to the effect of the % of PA area impacted by pine wilt nematode pathogen and its interaction with the % of coniferous forest cover in the PA. For DQT, the compositional features of the forest related to the % cover of broadleaf or coniferous forest, but also the structural aspects of canopy height and its variability, obtained stronger weight of evidence to explain PA scores for this indicator.

Regarding MLE, several models were selected thus evidencing higher model uncertainty. Models including compositional features related to the total % of forest area and the % of broadleaf as well as structural aspects such as canopy height, its variability and the connectivity of forest patches, all attained a strong support. MLE was also the only indicator to detect a signal in PA forest stability scores related to precipitation anomalies. Models including both the effect of PA size and shape, as well as disturbance features related to burnt forest area or PWN, either in combined or partial models also showed a strong weight of evidence to explain this stability indicator. As for SMN, only a single model was selected, including the effect of road density (but with relatively low model fitting quality).

Table 8 - 4 – Results for AICc-based model ranking for each response stability metric including only selected models (i.e. ΔAICc<3): annual coefficient of variation of the annual 5% quantile (Q05), median (MED), 95% quantile (Q95), annual difference between 95 and 5% quantiles (DQT), and "summerness" (sine) transformation of the day of maximum (SMN). STL decomposition – trend component coefficient of variation (TRD), and maximum Lyapunov exponent (MLE). ΔAICc – Delta AIC (greater values translate lower model support; typically, values above 2 or 3 have relatively low support); w_i – Akaike weights (higher values represent greater relative model support within [0, 1]); and, D2 – explained deviance; symbols within parenthesis represent model significance: (***) p<0.001, (**) p<0.01, (*) p<0.05, (.) p<0.1; The : (colon) in model formula indicates an interaction between two variables.

Hypothesis set	Model code / predictor variables	ΔAICc	w_i	D2
Q05				
IV. Landscape and forest composition	M4.2 = LC_BRLF	0.00	0.12	0.13 (.)
VII. 'Combined' models	M7.1 = LC_BRLF + PA_SIZE	0.04	0.12	0.23 (*)
VII. 'Combined' models	M7.2 = PA_SIZE + LC_BRLF + BURN_FOR:PA_ELEV	1.10	0.07	0.29 (*)
V. Forest structure	M5.5 = FCH_STD	1.38	0.06	0.08
VI. Forest disturbance	M6.2 = BURN_FOR	1.91	0.05	0.07
II. Protected area attributes	M2.1 = PA_SIZE	1.96	0.04	0.06
V. Forest structure	M5.2 = FOR_COHES	1.99	0.04	0.06
II. Protected area attributes	M2.6 = PA_SPA	2.11	0.04	0.06
IV. Landscape and forest composition	M4.3 = LC_CONF	2.11	0.04	0.06
VII. 'Combined' models	M7.4 = BURN_FOR + PA_SIZE + FCH_AVG	2.46	0.03	0.24 (.)
MED				
VII. 'Combined' models	M7.2 = PA_SIZE + LC_BRLF + BURN_FOR:PA_ELEV	0.00	0.58	0.57 (***)
VII. 'Combined' models	M7.1 = LC_BRLF + PA_SIZE	3.17	0.12	0.40 (**)
Q95				
VII. 'Combined' models	M7.6 = PWN_PERC + PWN_PERC:LC_CON	0.00	0.74	0.48 (***)
DQT				
VII. 'Combined' models	M7.5 = LC_BRLF + FCH_AVG + FCH_STD	0.00	0.17	0.34 (**)
V. Forest structure	M5.6 = FCH_AVG + FCH_STD	0.20	0.16	0.25 (*)
V. Forest structure	M5.5 = FCH_STD	0.48	0.14	0.16 (*)
IV. Landscape and forest composition	M4.2 = LC_BRLF	1.23	0.09	0.14 (*)
IV. Landscape and forest composition	M4.3 = LC_CONF	1.94	0.07	0.12 (*)
VII. 'Combined' models	M7.6 = PWN_PERC + PWN_PERC:LC_CON	2.69	0.05	0.17 (.)
VII. 'Combined' models	M7.1 = LC_BRLF + PA_SIZE	3.02	0.04	0.16 (.)
SMN				
III. Human pressure	M3.3 = ROAD_DENS	0.00	0.46	0.19 (*)
MLE				
V. Forest structure	M5.1 = FOR_AREA	0.00	0.14	0.17 (*)
I. Climatic anomalies	M1.1 = PREC_ANOM	0.53	0.11	0.15 (*)
VII. 'Combined' models	M7.1 = LC_BRLF + PA_SIZE	1.18	0.08	0.21 (*)
IV. Landscape and forest composition	M4.2 = LC_BRLF	1.26	0.08	0.13 (*)
VII. 'Combined' models	M7.2 = PA_SIZE + LC_BRLF + BURN_FOR:PA_ELEV	1.59	0.07	0.29 (*)
VII. 'Combined' models	M7.6 = PWN_PERC + PWN_PERC:LC_CON	1.68	0.06	0.2 (*)
II. Protected area attributes	M2.4 = PA_CIRC	1.82	0.06	0.11 (.)
V. Forest structure	M5.5 = FCH_STD	1.83	0.06	0.11 (.)
V. Forest structure	M5.2 = FOR_COHES	3.01	0.03	0.08
VII. 'Combined' models	M7.5 = LC_BRLF + FCH_AVG + FCH_STD	3.34	0.03	0.23 (.)
TRD				
VII. 'Combined' models	M7.2 = PA_SIZE + LC_BRLF + BURN_FOR:PA_ELEV	0.00	0.60	0.59 (***)
VII. 'Combined' models	M7.1 = LC_BRLF + PA_SIZE	2.64	0.16	0.43 (***)

Model coefficient signs allow to diagnose if a certain variable has a positive or negative effect on PA stability scores. Overall, we found coefficient signs highly consistent across tested models and also across stability indicators (Table 8 - 5).

Table 8 - 5 – Coefficient signs for models that were selected at least one time using the AICc-based ranking. The (↗) arrow represents a positive effect of a given predictor variable while (↙) is negative. The order of the arrows follows that of the predictor variables in each model represented in column two. The : (colon) in model formula indicates an interaction between two variables.

Hypothesis set	Model code / predictor variables	Q05	MED	Q95	DQT	SMN	MLE	TRD
I. Climatic anomalies	M1.1 = PREC_ANOM						↙	
II. Protected area attributes	M2.1 = PA_SIZE	↗						
	M2.4 = PA_CIRC						↙	
	M2.6 = PA_SPA	↗						
III. Human pressure	M3.3 = ROAD_DENS					↗		
IV. Landscape and forest composition	M4.2 = LC_BRLF	↗			↗		↗	
	M4.3 = LC_CONF	↙			↙			
V. Forest structure	M5.1 = FOR_AREA						↗	
	M5.2 = FOR_COHES	↗					↗	
	M5.5 = FCH_STD	↗			↗		↗	
	M5.6 = FCH_AVG + FCH_STD				↗↗			
VI. Forest disturbance	M6.2 = BURN_FOR	↙						
VII. 'Combined' models	M7.1 = LC_BRLF + PA_SIZE	↗↗	↗↗		↗↗		↗↗	↗↗
	M7.2 = PA_SIZE + LC_BRLF + BURN_FOR:PA_ELEV	↗↗↙	↗↗↙				↗↗↙	↗↗↙
	M7.4 = BURN_FOR + PA_SIZE + FCH_AVG	↙↗↗						
	M7.5 = LC_BRLF + FCH_AVG + FCH_STD				↗↗↗		↗↗↗	
	M7.6 = PWN_PERC + PWN_PERC:LC_CON			↗↙	↗↙		↗↙	

For hypothesized climatic effects, precipitation anomalies (related to inter-annual fluctuations) had a negative effect. Protected area attributes related to size and overlap with Natura 2000 recorded a positive effect, while for PA shape, forests were generally more stable in bulkier (or less elongated) sites. Road coverage recorded a positive effect on relative stability.

In terms of forest features, we recorded a strong positive effect of broadleaf forests and a negative effect of coniferous forests. PAs with higher total forest cover, higher connectivity between forest patches and with taller canopy and higher vertical complexity generally presented higher stability. Finally, we found a strong negative effect of forest fires (with interactions with PA average elevation) as well as negative effects

related to the interaction between PWN affected area and the coverage of coniferous forest (the type of forest affected by this pathogen).

8.4. Discussion

A functional approach to forest stability and Protected Area performance

In this study, we propose and test an approach to measure forest ecosystem stability and PAs performance, based on indicators calculated from EO VI time-series. These indicators capture, in an integrative fashion, several facets of ecosystem functioning dynamics related to the flow of matter and energy in ecosystems. Our approach builds on the perspective that forest stability dynamics relies on the interactive and continuous relation between disturbance and the response that follows it (see Figure 8 - 1).

We also advocate that EO VI time-series, due to their high-temporal resolution, are capable of capturing this disturbance-response binomial, thus allowing to evaluate and quantify ecosystem stability over time. Building on results from previous research (Alcaraz-Segura et al. 2008, Alcaraz-Segura et al. 2009, Cabello et al. 2012), we argue that this integrated, functional approach has several advantages over structural approaches, which are typically based on land cover/use datasets and target focal processes such as deforestation or wildfires. In addition, with this functional approach we were able to account for the seasonal variation of ecosystems by using STL decomposition or EFA-based indices, and thereby evidence the signal related to disturbances and other non-seasonal ecosystem changes.

Our approach and the proposed indicators were also useful to assess the performance and effectiveness of PAs to promote forest stability. In this study, we addressed this challenge by statistically comparing the distribution of stability indicators inside vs. outside PAs, using a spatial referential that allowed minimizing environmental dissimilarity (and maximizing comparability) between the PA and NPA spaces. This statistical multi-testing assessment of relative stability provides a novel and systematic way to rank PAs, according to their ability to promote stability in forest ecosystems submitted to pressures acting in their broader regional context (see Figure 8 - 7a). Although the neighboring NPA space may provide a valid referential for comparison (previously used in similar studies; e.g., (Mas 2005)), it does hold some limitations. In fact, a PA may be undergoing unstable conditions and still, if the dynamics observed outside is comparatively worse, that PA would be considered “relatively stable”. Nonetheless, if PAs are supposed to buffer or counteract local negative dynamics,

having relatively more stable (or less unstable) conditions does fulfill one of its main goals.

In addition, EO-based maps of stability indicators (Figure 8 - 6) allow to identify specific locations inside PAs with different stability dynamics and to perform an in-depth examination of potential causes for application in conservation management. From our analyses, we have provided illustrative and contrasting examples ranging from unstable to stable forest ecosystems (see Figure 8 - 8 and Figure 8 - 9). Since many PAs are large enough to cover distinct social-ecological contexts, this additional output from our approach can support the development of tailored management strategies aimed at promoting forest stability in contrasting settings.

Patterns and drivers of forest stability

We found a complex pattern in terms of PA forest stability performance across the national network, both among and within PAs. This may reflect spatial differences in disturbance regimes, in the occurrence of stochastic events, but also contrasting land cover patterns, landscape structure and land use dynamics. To investigate the potential factors underlying forest stability patterns across the network of selected PAs, we applied a multi-model inference framework based on a set of plausible hypotheses (see Table 8 - 3).

The most striking, while expectable, result was related to forest fires, which revealed a clear negative effect on stability. We also found an interaction between forest fires and PA elevation which may be related to different fire regimes occurring on lowland vs. mountainous PAs. Despite the substantial national efforts and monetary investment allocated to fight and suppress wildfires, Portugal remains the European country with highest incidence rates and burnt area in Europe. PAs are not an exception to this situation. In fact, *Peneda-Gerês* National Park (the oldest and the only park with such classification in the country) holds an average burnt area (1990 – 2013) of around 3%/year (in 2010, 11% of this PA was affected by fire). Although wildfire damage is shared between forests and other vegetation types, forests are being cumulatively affected by frequent fires with impacts on their resilience. Pausas (2015) found that changes in fire regime and climatic conditions in Patagonia can cause abrupt shifts from cold temperature *Nothofagus* forests into pyrophilic shrublands. Satellite data was previously used to show decreasing resilience in Mediterranean plant communities following recurrent wildfires (Díaz-Delgado et al. 2002), potentially triggering state changes due to a ‘resilience debt’ (Johnstone et al. 2016) (see Figure 8 - 2 for a

conceptual diagram of such dynamics). Increased wildfire frequency may also promote invasion by non-native plants, leading to biodiversity loss, changes in community composition and decreased supply of ecosystem services. Invasive species may further change the fire regime of invaded ecosystems (Strayer et al. 2006), their function and structure, thus potentially generating new and 'unknown' system states (including 'novel ecosystems'). In a recent report (FAO and EFI 2015), Portugal was identified as the sixth European country (out of 31 analyzed) with the highest share of forest area dominated by introduced (often invasive) species.

Forest composition and structure were also found to have a strong control over stability performance across the PA network. Contrary to forest fires, which strongly drive the disturbance regime, forest composition and structure play a stronger role in post-disturbance response. We found a strong positive signal in stability related to the fraction cover of broadleaf forests. This may be explained by the fact that PAs usually hold a greater proportion of native deciduous broadleaf species (*Quercus* spp.) in comparison to NPA (Appendix V – S7). Previous studies showed that native broadleaf species are more resistant to fire and/or capable of recovering shortly after fire (Proença et al. 2010). The effect of these less fire-prone trees is especially important in mountain PAs. For example, "*Montesinho*" Natural Park, considered one of the most stable PAs in our ranking (see Figure 8 - 7), holds some of the largest extensions of native forests of Pyrenean oak (*Quercus pyrenaica*).

Contrarily, we found some evidence that coniferous forests have a negative effect on stability. This may be explained by the high incidence rate of fires in this forest type, typically with higher severity and lower resilience capacity (longer recovery times) (Proença et al. 2010). Coniferous forests dominated by maritime pine (*Pinus pinaster*), by far the most widespread conifer in continental Portugal, have also been strongly affected by the pine wilt nematode (PWN), especially in the south and center parts of the country. Interestingly, PWN effects on stability seem to be more evident in indicators related to annual maximum (Q95) and seasonality (DQT; Table 8 - 5). An explanation may be related to a slow and partial decay in greenness levels and productivity observable in PWN affected forests.

Forest structure, and particularly vertical structure (assessed through an EO-based global forest canopy height dataset), was found to have a strong effect on stability. Specifically, PAs hosting forest areas with taller forest canopies and higher vertical complexity/variability were found to be more stable (see Table 8 - 4). These structural features, in combination with forest composition, may discriminate older and more complex or diverse forests that tend to have more stable dynamics. (Musavi et al. 2017)

found that older and more biodiverse forests are capable of dampening the effects of inter-annual climate variability on the carbon cycle regardless of the forest type. In fact, older or mature forests are (unequally) distributed throughout the PA network and are one the major conservation targets of PAs. As evidenced here, they also contribute to overall forest stability.

Although with less model support, we also found positive effects of total forest area and connectivity between forest patches on stability. In fact, PAs with higher forest cover and higher connectivity between forest areas are relatively more stable. This may be due to positive effects of propagule sources and their connectivity on resilience and especially on recovery capacity. Connectivity is known to hold important contributions to ecosystem functioning and biodiversity, but also negative effects related to the spread of disturbances such as fire, invasive species and pathogen outbreaks. Unfortunately, due to the lack of fine-scale data it was impossible to disentangle fine structural effects of connectivity in our focal PA network.

As for PA attributes, we found a strong positive effect of PA size, with larger parks having a higher stability performance. This may be explained by the fact that larger PAs are more effective in buffering sources of disturbances and pressures, and in promoting better conservation or recovery of forest areas. Allocation of resources (both monetary and human) may also be a cause for this finding as larger areas usually have more available resources. A (weak) positive effect of the overlap with Natura 2000 Special Protection Areas was also found, suggesting that overlapping protection regimes may further reinforce conservation policies and strengthen land use constraints and management rules that buffer landscape change pressures. We could not find evidence for an expectable effect of PA age on relative forest stability, which may be partially explained by the disturbance regime (namely involving wildfires) observed in some of the 'older' PAs.

The effects of these several factors on forest stability should not be seen in isolation as they are, in fact, welded together in a non-linear and complex socio-ecological web. One factor or one model alone is not capable of explaining why a PA is stable or not. The fact that the more complex models (set VII; Table 8 - 4) have in general performed better is likely a reflection of complex interactions between different factors. This may also explain why some models performed relatively poorly for some stability indicators. Absent data on other crucial aspects related to forest management, land use, detailed structural and compositional forest attributes, monetary expenditure in PAs, among others, may account for other part of unexplained variance.

Outlook: from stability assessment to Protected Area management

Stability is a key property of ecosystems, which are complex adaptive systems (Levin 1999) characterized by historical dependency, non-linear dynamics and thresholds between different stable states (Folke et al. 2004). In some cases, regime shifts can cause drastic changes from one stable state to another (Scheffer et al. 2001, Folke et al. 2004). These new stable states are characterized by a different set of ecosystem functions and feedbacks that may be either positive or negative for humans, and may hold lower or higher resilience in relation to the former state (Folke et al. 2004, Gunderson et al. 2010). By using a functionally oriented approach, we believe that it is possible to assess and monitor how forest ecosystems absorb disturbance regimes and to characterize their resilience capacity. In turn, stabilizing dynamics will translate into a higher likelihood of natural systems keeping their current stable state, in this case a forest-type structural and functional dynamics (see Figure 8 - 2) (Johnstone et al. 2016).

Stable forest ecosystems do not mean “crystalized” or “non-dynamical” ecosystems. In fact, disturbance-free systems are hardly possible or even desirable management-wise. Forest fires, for example, promote the creation of landscape heterogeneity and of spatial discontinuities that may be beneficial for biodiversity or limit the spread of other disturbances. However, highly frequent and/or severe fires may push stability limits to unknown boundaries and trigger shifts into undesirable states by means of a ‘resilience-debt’ (Johnstone et al. 2016).

We argue that adopting our EO-based functional framework to assess and monitor the disturbance - response binomial of stability (Figure 8 - 2) will hold advantages for forest management and conservation planning. Current and future management goals for PAs should embrace both ends of the equation, namely by fostering a ‘smart’ disturbance regime (Fernandes 2013) while simultaneously promoting forest resilience and adaptive capacity to minimize the risks related to potential regime shifts (which increase uncertainty and vulnerability). Using this approach to stability, combined with explanatory models, we were able to uncover several aspects of stability dynamics in the Portuguese PA network providing insight into the definition of management goals.

Forest fires were highlighted as one of the major sources of disturbance and instability in forests. To address this problem, better forest planning and management looking at the causes and drivers of fire regimes (current and future) may boost adaptation and resilience under global change (Fernandes 2013). Still, no ‘magical’ solution exists to this complex socio-ecological issue that requires robust planning and decisive actions in multiple fronts, from policy and prevention to fire suppression

strategies. Our results suggest that increasing the use of native broadleaf species for plantation, reforestation or through the promotion of natural regeneration may contribute to effective fire management and yield good results for enhancing stability overall. Allowing these areas to mature in a connected web of highly resilient patches may further its benefits for biodiversity and ecosystem functioning. Still, for addressing connectivity the PA level may not be enough to guarantee positive returns. Measures directed to the promotion of forest stability should be fostered not only by PAs but through integrative regional plans promoting PA connectivity through the non-protected matrix. This multifunctional perspective would allow balancing conservation and production functions and diversifying the provision of vital ecosystem services at the regional level.

According to our results, increasing the size of current PAs and/or opting for the new designation of large areas, in detriment of smaller ones, may be more beneficial in terms of ecosystem stability. However, our analysis lacks in assessing the contribution of smaller areas to the overall connectivity of the PA network. These smaller sites may act as potential corridors or stepping stones with benefits for biodiversity, ecosystem functioning and ecological processes such as dispersal. Diversifying strategies and balancing network design between large and small PAs (with an emphasis on larger areas) may be key in this regard. More research is necessary to understand these effects and provide optimized solutions.

Improving conservation measures in PA networks will require addressing the several components of disturbance regimes and recognizing their multi-scalar socio-ecological ramifications. Disturbances generate biological legacies that interact with environmental conditions shaping ecosystem recovery (Franklin et al. 2000). Currently, global changes involving climate, land use, and biological invasions are rapidly altering disturbance regimes and legacies as well as the context in which ecosystems recover from damaging events (Trumbore et al. 2015). This may trigger abrupt shifts between different states (Frelich 2002; Hughes et al. 2013) and even originate novel environments and ecosystems (Williams and Jackson 2007). Following a transition, alternate states may be maintained by new sets of legacies and reinforcing feedbacks (Scheffer et al. 2001; Bowman et al. 2015). In face of this, managers and stakeholders must take into account the non-linear and complex dynamics of ecosystems and the potential occurrence of regime shifts that may drive ecosystems into undesired (or less desirable) states. As a consequence, it is crucial to look both to the disturbance regime and the ecosystem state and conditions that support recovery. For this endeavour, we showed that EO platforms provide useful data to support ecosystem monitoring with high

temporal coverage and update frequency, thus providing a deeper understanding of systems' dynamics. As more data becomes available to feed robust modelling frameworks, from specialists and sensors on the field up to satellites on orbit, this new paradigm opens up new and unforeseen opportunities to develop better tools to support decision making and conservation policies.

Author contributions

Author name	Study conception and design	Sampling design, infield surveys and/or data collection	Data processing, analysis and/or modelling	Manuscript writing	Manuscript revision
João Gonçalves	☑	☑	☑	☑	☑
Bruno Marcos				☑	☑
Isabel Pôças		☑	☑	☑	☑
A. T. Monteiro				☑	☑
C.S. Mücher				☑	☑
Alfredo Huete				☑	☑
D.Alcaraz-Segura				☑	☑
João Honrado				☑	☑

References

Alcaraz-Segura, D., J. Cabello, J. Paruelo, and M. Delibes. 2009. Use of Descriptors of Ecosystem Functioning for Monitoring a National Park Network: A Remote Sensing Approach. Environmental Management 43:38-48.

Alcaraz-Segura, D., J. Cabello, J. M. Paruelo, and M. Delibes. 2008. Trends in the surface vegetation dynamics of the national parks of Spain as observed by satellite sensors. Applied Vegetation Science 11:431-440.

Alcaraz-Segura, D., A. Lomba, R. Sousa-Silva, D. Nieto-Lugilde, P. Alves, D. Georges, J. R. Vicente, and J. P. Honrado. 2017. Potential of satellite-derived ecosystem functional attributes to anticipate species range shifts. International Journal of Applied Earth Observation and Geoinformation 57:86-92.

Alcaraz, D., J. Paruelo, and J. Cabello. 2006. Identification of current ecosystem functional types in the Iberian Peninsula. Global Ecology and Biogeography 15:200-212.

Benjamini, Y., and Y. Hochberg. 1995. Controlling the False Discovery Rate: A Practical and Powerful Approach to Multiple Testing. Journal of the Royal Statistical Society. Series B (Methodological) 57:289-300.

Bonan, G. B. 2008. Forests and Climate Change: Forcings, Feedbacks, and the Climate Benefits of Forests. Science 320:1444-1449.

Cabello, J., N. Fernández, D. Alcaraz-Segura, C. Oyonarte, G. Piñeiro, A. Altesor, M. Delibes, and J. Paruelo. 2012. The ecosystem functioning dimension in conservation: insights from remote sensing. Biodiversity and Conservation 21:3287-3305.

Cleveland, R. B., W. S. Cleveland, J. E. McRae, and I. Terpenning. 1990. STL: A Seasonal-Trend Decomposition Procedure Based on Loess. Journal of Official Statistics 6:3-73.

Cord, A. F., K. A. Brauman, R. Chaplin-Kramer, A. Huth, G. Ziv, and R. Seppelt. 2017. Priorities to Advance Monitoring of Ecosystem Services Using Earth Observation. Trends in Ecology & Evolution 32:416-428.

Davies, L., and U. Gather. 1993. The Identification of Multiple Outliers. Journal of the American Statistical Association 88:782-792.

De Keersmaecker, W., S. Lhermitte, O. Honnay, J. Farifteh, B. Somers, and P. Coppin. 2014. How to measure ecosystem stability? An evaluation of the reliability of stability metrics based on remote sensing time series across the major global ecosystems. Global Change Biology 20:2149-2161.

Di Mauro, B., F. Fava, L. Busetto, G. F. Crosta, and R. Colombo. 2014. Post-fire resilience in the Alpine region estimated from MODIS satellite multispectral data. International Journal of Applied Earth Observation and Geoinformation 32:163-172.

Díaz-Delgado, R., F. Lloret, X. Pons, and J. Terradas. 2002. Satellite evidence of decreasing resilience in Mediterranean plant communities after recurrent wildfires. Ecology 83:2293-2303.

Díaz, S., and M. Cabido. 2001. Vive la différence: plant functional diversity matters to ecosystem processes. Trends in Ecology & Evolution 16:646-655.

Didan, K., A. B. Munoz, R. Solano, and A. Huete. 2015. MODIS Vegetation Index User's Guide (MOD13 Series) - version 3.00, June 2015 (Collection 6). University of Arizona, Vegetation Index and Phenology Lab.

Donohue, I., H. Hillebrand, J. M. Montoya, O. L. Petchey, S. L. Pimm, M. S. Fowler, K. Healy, A. L. Jackson, M. Lurgi, D. McClean, N. E. O'Connor, E. J. O'Gorman, and Q. Yang. 2016. Navigating the complexity of ecological stability. Ecology Letters 19:1172-1185.

EEA. 1999. CORINE Land Cover - A key database for European integrated environmental assessment.

EEA. 2007. CLC2006 technical guidelines. Page 70. Office for Official Publications of the European Communities, Luxembourg.

EEA. 2016. European forest ecosystems - State and trends (EEA Report No 5/2016). European Environment Agency, Luxembourg.

FAO. 2016. State of the World's Forests 2016. Forests and agriculture: land-use challenges and opportunities. Food and Agriculture Organization of the United Nations, Rome.

FAO, and EFI. 2015. State of Europe's Forests 2015. Ministerial Conference on the Protection of Forests in Europe, Madrid.

FAO/World-Bank. 2016. Forest area (% of land area) by year 1990-2015.

Folke, C., S. Carpenter, B. Walker, M. Scheffer, T. Elmqvist, L. Gunderson, and C. S. Holling. 2004. Regime shifts, resilience, and biodiversity in ecosystem management. Annual Review of Ecology, Evolution, and Systematics 35:557-581.

Gamfeldt, L., T. Snäll, R. Bagchi, M. Jonsson, L. Gustafsson, P. Kjellander, M. C. Ruiz-Jaen, M. Fröberg, J. Stendahl, C. D. Philipson, G. Mikusiński, E. Andersson, B. Westerlund, H. Andrén, F. Moberg, J. Moen, and J. Bengtsson. 2013. Higher

levels of multiple ecosystem services are found in forests with more tree species. Nature Communications 4:1340.

Gond, V., A. Fayolle, A. Pennec, G. Cornu, P. Mayaux, P. Camberlin, C. Doumenge, N. Fauvet, and S. Gourlet-Fleury. 2013. Vegetation structure and greenness in Central Africa from Modis multi-temporal data. Philosophical Transactions of the Royal Society B: Biological Sciences 368:20120309.

Gunderson, L. H., C. R. Allen, and C. S. Holling. 2010. Foundations of Ecological Resilience. Island Press, Washington DC, USA.

Hampel, F. R. 1974. The Influence Curve and Its Role in Robust Estimation. Journal of the American Statistical Association 69:383-393.

Hegger, R., H. Kantz, and T. Schreiber. 1999. Practical implementation of nonlinear time series methods: The TISEAN package. Chaos 9:413-435.

Heumann, B. W., J. W. Seaquist, L. Eklundh, and P. Jönsson. 2007. AVHRR derived phenological change in the Sahel and Soudan, Africa, 1982–2005. Remote Sensing of Environment 108:385-392.

Higgins, S. I., R. Buitenwerf, and G. R. Moncrieff. 2016. Defining functional biomes and monitoring their change globally. Glob Chang Biol 22:3583-3593.

Hobbs, R. J., and L. F. Huenneke. 1992. Disturbance, Diversity, and Invasion: Implications for Conservation. Conservation Biology 6:324-337.

Holling, C. S. 1996. Engineering Resilience versus Ecological Resilience.*in* P. C. Schulze, editor. Engineering Within Ecological Constraints. National Academy Press, Washington, D.C.

Huete, A., K. Didan, T. Miura, E. P. Rodriguez, X. Gao, and L. G. Ferreira. 2002. Overview of the radiometric and biophysical performance of the MODIS vegetation indices. Remote Sensing of Environment 83:195-213.

Hughes, K. A., L. C. Ireland, P. Convey, and A. H. Fleming. 2016. Assessing the effectiveness of specially protected areas for conservation of Antarctica's botanical diversity. Conservation Biology 30:113-120.

ICNF. 2013. 6.º Inventário Florestal Nacional - Resultados preliminares (v1.1). Instituto da Conservação da Natureza e das Florestas, Lisboa.

ICNF. 2016. National burnt area database (1990-2013) - URL: http://www.icnf.pt/portal/florestas/dfci/inc/info-geo (last visited Nov-2016).*in* ICNF, editor., Lisboa, PT.

INE. 2011. Censos 1991, 2001 and 2011 at BGRI level. Instituto Nacional de Estatística (Portugal).

Ivits, E., S. Horion, M. Erhard, and R. Fensholt. 2016. Assessing European ecosystem stability to drought in the vegetation growing season. Global Ecology and Biogeography 25:1131-1143.

Johnstone, J. F., C. D. Allen, J. F. Franklin, L. E. Frelich, B. J. Harvey, P. E. Higuera, M. C. Mack, R. K. Meentemeyer, M. R. Metz, G. L. W. Perry, T. Schoennagel, and M. G. Turner. 2016. Changing disturbance regimes, ecological memory, and forest resilience. Frontiers in Ecology and the Environment 14:369-378.

Jönsson, P., and L. Eklundh. 2004. TIMESAT - a program for analyzing time-series of satellite sensor data. Computers & Geosciences 30:833-845.

Kerr, J. T., and M. Ostrovsky. 2003. From space to species: ecological applications for remote sensing. Trends in Ecology & Evolution 18:299-305.

Levin, S. 1999. Fragile Dominion: Complexity and the Commons. Perseus Books, Cambridge, MA.

Mas, J.-F. 2005. Assessing protected area effectiveness using surrounding (buffer) areas environmentally similar to the target area. Environmental Monitoring and Assessment 105:69-80.

McGarigal, K., S. Cushman, M. C. Neel, and E. Ene. 2002. FRAGSTATS: Spatial Pattern Analysis Program for Categorical Maps. Computer software program produced

by the authors at the University of Massachusetts, Amherst., http://www.umass.edu/landeco/research/fragstats/fragstats.html.

Mesquita, S., and A. J. Sousa. 2009. Bioclimatic mapping using geostatistical approaches: application to mainland Portugal. International Journal of Climatology 29:2156–2170.

Moffett, K., W. Nardin, S. Silvestri, C. Wang, and S. Temmerman. 2015. Multiple Stable States and Catastrophic Shifts in Coastal Wetlands: Progress, Challenges, and Opportunities in Validating Theory Using Remote Sensing and Other Methods. Remote Sensing 7:10184.

Morales-Hidalgo, D., S. N. Oswalt, and E. Somanathan. 2015. Status and trends in global primary forest, protected areas, and areas designated for conservation of biodiversity from the Global Forest Resources Assessment 2015. Forest Ecology and Management 352:68-77.

Mori, A. S., K. P. Lertzman, and L. Gustafsson. 2017. Biodiversity and ecosystem services in forest ecosystems: a research agenda for applied forest ecology. Journal of Applied Ecology 54:12-27.

Musavi, T., M. Migliavacca, M. Reichstein, J. Kattge, C. Wirth, T. A. Black, I. Janssens, A. Knohl, D. Loustau, O. Roupsard, A. Varlagin, S. Rambal, A. Cescatti, D. Gianelle, H. Kondo, R. Tamrakar, and M. D. Mahecha. 2017. Stand age and species richness dampen interannual variation of ecosystem-level photosynthetic capacity. 1:0048.

Nagendra, H., R. Lucas, J. P. Honrado, R. H. G. Jongman, C. Tarantino, M. Adamo, and P. Mairota. 2013. Remote sensing for conservation monitoring: Assessing protected areas, habitat extent, habitat condition, species diversity, and threats. Ecological Indicators 33:45-59.

Nagendra, H., P. Mairota, C. Marangi, R. Lucas, P. Dimopoulos, J. P. Honrado, M. Niphadkar, C. A. Mücher, V. Tomaselli, M. Panitsa, C. Tarantino, I. Manakos, and P. Blonda. 2015. Satellite Earth observation data to identify anthropogenic pressures in selected protected areas. International Journal of Applied Earth Observation and Geoinformation.

Narzo, A. F. D. 2013. tseriesChaos: Analysis of nonlinear time series (R package version 0.1-13, URL: https://CRAN.R-project.org/package=tseriesChaos).

Nelson, A., and K. M. Chomitz. 2009. Protected Area Effectiveness in Reducing Tropical Deforestation - A Global Analysis of the Impact of Protection Status. World Bank, Washington, D.C., US.

O'Connor, B., C. Secades, J. Penner, R. Sonnenschein, A. Skidmore, N. D. Burgess, and J. M. Hutton. 2015. Earth observation as a tool for tracking progress towards the Aichi Biodiversity Targets. Remote Sensing in Ecology and Conservation 1:19-28.

Paruelo, J. M., E. G. Jobbágy, and O. E. Sala. 2001. Current Distribution of Ecosystem Functional Types in Temperate South America. Ecosystems 4:683-698.

Pausas, J. G. 2015. Alternative fire-driven vegetation states. Journal of Vegetation Science 26:4-6.

Pettorelli, N., W. F. Laurance, T. G. O'Brien, M. Wegmann, H. Nagendra, and W. Turner. 2014. Satellite remote sensing for applied ecologists: opportunities and challenges. Journal of Applied Ecology 51:839-848.

Pickett, S. T., and P. S. White. 1985. Natural Disturbance and Patch Dynamics: An Introduction. Pages 3-13 *in* S. T. Pickett and P. S. White, editors. The Ecology of Natural Disturbance and Patch Dynamics. Academic Press, Inc., Orlando, Florida.

Pickett, S. T. A., J. Kolasa, J. J. Armesto, and S. L. Collins. 1989. The Ecological Concept of Disturbance and Its Expression at Various Hierarchical Levels. Oikos 54:129-136.

Proença, D. N., G. Grass, and P. V. Morais. 2017. Understanding pine wilt disease: roles of the pine endophytic bacteria and of the bacteria carried by the disease-causing pinewood nematode. MicrobiologyOpen 6:e00415-n/a.

Proença, V., H. M. Pereira, and L. Vicente. 2010. Resistance to wildfire and early regeneration in natural broadleaved forest and pine plantation. Acta Oecologica 36:626-633.

R Development Core Team. 2017. R: A Language and Environment for Statistical Computing; URL: https://www.R-project.org/. R Foundation for Statistical Computing, Vienna, Austria.

Rodríguez, N., D. Armenteras, and J. Retana. 2012. Effectiveness of protected areas in the Colombian Andes: deforestation, fire and land-use changes. Regional Environmental Change 13:423-435.

Rogers, J. 2011. The Effectiveness of Protected Areas in Central Africa: A Remotely Sensed Measure of Deforestation and Access. Columbia University.

Scheffer, M., S. Carpenter, J. A. Foley, C. Folke, and B. Walker. 2001. Catastrophic shifts in ecosystems. Nature 413:591-596.

Skidmore, A. K., N. Pettorelli, N. C. Coops, G. N. Geller, M. Hansen, R. Lucas, C. A. Mücher, B. O'Connor, M. Paganini, H. M. Pereira, M. E. Schaepman, W. Turner, T. Wang, and M. Wegmann. 2015. Agree on biodiversity metrics to track from space. Nature 523.

Strayer, D. L., V. T. Eviner, J. M. Jeschke, and M. L. Pace. 2006. Understanding the long-term effects of species invasions. Trends in Ecology & Evolution 21:645-651.

Symonds, M., and A. Moussalli. 2011. A brief guide to model selection, multimodel inference and model averaging in behavioural ecology using Akaike's information criterion. Behavioral Ecology and Sociobiology 65:13-21.

UNEP-WCMC, and IUCN. 2016. Protected Planet Report 2016 - Update on global statistics December 2016, CBD COP13. Cambridge, UK
Gland, Switzerland.

van Rooijen, N. M., W. de Keersmaecker, W. A. Ozinga, P. Coppin, S. M. Hennekens, J. H. J. Schaminée, B. Somers, and O. Honnay. 2015. Plant Species Diversity Mediates Ecosystem Stability of Natural Dune Grasslands in Response to Drought. Ecosystems 18:1383-1394.

Veraverbeke, S., S. Lhermitte, W. W. Verstraeten, and R. Goossens. 2011. A time-integrated MODIS burn severity assessment using the multi-temporal differenced normalized burn ratio (dNBRMT). International Journal of Applied Earth Observation and Geoinformation 13:52-58.

Verbesselt, J., R. Hyndman, G. Newnham, and D. Culvenor. 2010a. Detecting trend and seasonal changes in satellite image time series. Remote Sensing of Environment 114:106-115.

Verbesselt, J., R. Hyndman, A. Zeileis, and D. Culvenor. 2010b. Phenological change detection while accounting for abrupt and gradual trends in satellite image time series. Remote Sensing of Environment 114:2970-2980.

Walker, B., C. S. Holling, S. R. Carpenter, and A. Kinzig. 2004. Resilience, adaptability and transformability in social–ecological systems. Ecology and Society 9(2):5. [online] URL: http://www.ecologyandsociety.org/vol9/iss2/art5/.

Wang, Q., S. Adiku, J. Tenhunen, and A. Granier. 2005. On the relationship of NDVI with leaf area index in a deciduous forest site. Remote Sensing of Environment 94:244-255.

Watson, J. E., N. Dudley, D. B. Segan, and M. Hockings. 2014. The performance and potential of protected areas. Nature 515:67-73.

Wegmann, M., L. Santini, B. Leutner, K. Safi, D. Rocchini, M. Bevanda, H. Latifi, S. Dech, and C. Rondinini. 2014. Role of African protected areas in maintaining

connectivity for large mammals. Philosophical Transactions of the Royal Society B: Biological Sciences 369:20130193.

Whittaker, E. T. 1923. On a new method of graduation. Proc. Edinburgh Math. Soc. 41:63–75.

Sub-section II.4. Developing novel tools for Geographic Object-based Image Analysis (GEOBIA) of high-spatial resolution EO imagery for ecological status and change assessment

Chapter 9 – *SegOptim* – a R package for optimizing segmentation parameters with genetic algorithms for supervised image classification

Author list: **João Gonçalves** (1,2), Isabel Pôças (3,4), Bruno Marcos (1,2), Sander Mücher (4), João Honrado (1,2)

(1) CIBIO – Research Center in Biodiversity and Genetic Resources / InBIO – Research Network in Biodiversity and Evolutionary Biology, Associate Laboratory; Campus Agrário de Vairão, Universidade do Porto, 4485-601 Vairão, Portugal
(2) Faculty of Sciences – University of Porto (FCUP); Edifício FC4 (Biologia), Rua do Campo Alegre, s/n, 4169-007 Porto, Portugal
(3) Linking Landscape, Environment, Agriculture and Food, Instituto Superior de Agronomia, Universidade de Lisboa, Lisboa 1349-017, Portugal
(4) Geo-Space Sciences Research Centre, Universidade do Porto, Porto 4169-007, Portugal
(5) Wageningen Environmental Research (Alterra), Earth Informatics subdivision, Wageningen University, Droevendaalsesteeg 3 6708PB Wageningen, Netherlands

DISCLAIMER

This manuscript is an original contribution of this thesis, submitted and under evaluation in the *International Journal of Applied Earth Observation and Geoinformation*. Gonçalves, J., lead the work with contributions from all co-authors.

ABSTRACT

Geographic Object-based Image Analysis (GEOBIA) paradigm is gaining more traction for processing high spatial resolution imagery with many ecological applications ranging from species to land cover mapping and, with several algorithms and software developed in recent years. Object identification and, therefore image segmentation plays a key role in GEOBIA workflows, allowing to partition images into a set of homogenous and mutually exclusive regions. However, segmentation techniques require a meaningful parameterization to achieve the best results. Frequently, inappropriate parameterization leads to sub-optimal results and difficulties for comparing distinct methods.

In this work, we present an approach based on Genetic Algorithms (GA) to iteratively optimize image segmentation parameters by using the cross-validation performance results from classification as the output value of GA fitness function. This way we assess the goodness of a segmented image in relation to the classification problem. This approach was implemented in a new R package called *SegOptim*. From this, several image segmentation algorithms are interfaced mostly focusing on open-source software: *SAGA GIS* – simple region-growing, *TerraLib* – Baatz-Schäpe multiresolution and mean region-growing, *GRASS GIS* – region-growing, *Orfeo Toolbox* – large-scale mean-shift and, *RSGISLib* – Shepherd k-means iterative elimination; but, also from proprietary software: *ESRI ArcGIS* – mean-shift. Our implementation also provides access to several machine-learning classification algorithms currently available in R, including: Gradient Boosted Modelling, Support Vector Machines, and Random Forest.

We tested our approach using very-high to high spatial resolution images collected from an Unmanned Aerial Vehicle (0.03 – 0.10m), WorldView-2 (2m), RapidEye (5m) as well as Sentinel-2 (10 – 20m) in six different test sites located in northern Portugal with varying environmental conditions and landscape patterns/dynamics and for different purposes.

Results provide a novel comparison of several state-of-the-art image segmentation and classification algorithms focused on the processing of Earth Observation (EO) data. Overall classification performances (assessed through cross-validation with the Kappa index) ranged from 0.85 to 1.00. Tests show that our GA-based approach is capable of providing sound results for optimizing the parameters of different

image segmentation algorithms with benefits for improving classification and comparisons between different techniques.

We also found that no particular combination of an image segmentation and a classification algorithm is suited for all the tasks/objectives. We argue that this may be an empirical verification of the "*no free-lunch theorem*" (NFLT) for GEOBIA problems which implies that learning algorithms "cannot be universally good" across all problems and domains. As a consequence, it is crucial to compare and optimize available methods to understand which one is more suited for a certain objective. *SegOptim* package provides the required functionalities for this purpose. Although GA-based optimization may help to improve object-based analyses, it is still crucial that the human operator carefully defines every input and monitors the optimization process.

By providing a closer integration between the segmentation and classification stages, typical in GEOBIA workflows, we show that this may have some advantages for comparing and optimizing both processes. We also discuss some limitations and potential solutions of *SegOptim* approach as well as a future roadmap to expand its current functionalities.

9.1. Introduction

Geographic Object-based Image Analysis (GEOBIA) is a recent sub-discipline of Geographic Information Systems (GIS) Science that according to Hay and Castilla (2008) is *" (…) devoted to developing automated methods to partition remote sensing imagery into meaningful image-objects, and assessing their characteristics through spatial, spectral and temporal scales, so as to generate new geographic information in GIS-ready format.".* GEOBIA is also the object-based analysis of Earth Observation (EO) data allowing to describe the imaged reality using spectral, textural, spatial, contextual and topological features (Lang 2008) in a multi-scalar and integrated fashion. GEOBIA benefitted from the availability of (very-)high spatial resolution imagery, from vast progresses in image segmentation (not only from the Remote Sensing (RS) community but from others, such as Computer Vision or Medical Imaging) as well as software that bridge image processing and GIS functionalities in an object-based environment ready for exploration and analysis (Blaschke 2010). All of these factors contributed to form this new subdiscipline of *GIScience* that has been gaining momentum since the last decade.

GEOBIA concepts and methods have been used in several ecological, nature management and conservation contexts such as: mapping the invasion success of non-native tree species (Monteiro et al. 2017)[7], determining habitat quality (Vaz et al. 2015)[8], describing landscape resources for wildlife research (Recio et al. 2013), characterizing protected areas (Martínez-López et al. 2016) and pressures upon them (Nagendra et al. 2015), assessing land cover change (Lu et al. 2016) or monitoring habitats (Mücher et al. 2013, Lucas et al. 2015, Mücher et al. 2015) to name a few.

Image segmentation plays an important role in GEOBIA (Lang 2008, Blaschke 2010). Independently of the method used, segmentation provides the elementary blocks used for object-based image analysis (Blaschke 2010), interpretation, classification and modelling. Segmentation involves the partitioning of an image into a set of jointly exhaustive and mutually disjoint regions (a.k.a. segments, composed by multiple image pixels), that are internally more homogeneous and similar, compared to adjacent ones. Image segments are then related to geographic objects of interest (e.g., forests, agricultural or urban areas) through some form of object-based classification (Castilla and Hay 2008). Image segments are created on the basis of one or more homogeneity

[7] This paper is a collaborative contribution developed during this PhD thesis
[8] *idem*

(and merging) criteria in one or more dimensions of a feature space (Blaschke 2010). As such, these segments have additional information related to the properties and moments of the distribution of spectral data from each individual contained pixel as well as contextual, morphological and spatial information (distances, neighbourhoods, shape, topologies, etc.) (Hay and Castilla 2008, van der Werff and van der Meer 2008, Blaschke 2010). Overall, the image segmentation process by decreasing the level of detail and reducing image complexity makes image data easier to process and classify in subsequent steps (Lang 2008). However, image segments should be meaningful in respect to a particular task and their properties should allow to convert them into useful geographic objects. This is challenging because widely different segmentation results can be obtained by varying parameters values (Liu et al. 2012, Dragut et al. 2014). Defining objective criteria is thus needed to address this problem as this would allow to understand and compare which image segmentation algorithms and parameterization may provide optimal solutions.

In order to better understand how image segmentation parameters are typically defined by users/researchers, we performed a semi-systematic, sample-based review of the current literature (see methodological details in Appendix VI – S1). We found that 44% of 72 randomly selected papers (out of 1067 retrieved in our search) did not explicitly mentioned how image segmentation parameters were defined or tuned (Appendix VI – Figure S1 – 1a). From publications that did mentioned this, 28% corresponded to specific procedures (e.g., geostatistical analysis, inter-/intra-segment variance comparison, segmentation goodness/discrepancy measures), 19% used a visual interpretation/trial-and-error approach and 9% the ESP tool (Dragut et al. 2014) available for *eCognition* multi-resolution segmentation (Baatz and Schape 2000). Only very few examples (ca. 7%) explicitly integrated both image segmentation and classification steps for improving or optimizing results.

Although we found that a large percentage of works currently did not documented the procedure used to define and/or tune image segmentation parameters, or simply applied a trial-and-error approach, there are more rigorous alternatives to perform this task. For example, ESP is an automatic tool developed for *eCogniton*® software capable of determining a set of suitable 'scale' parameters for multi-resolution image segmentation (Dragut et al. 2014). This unsupervised approach uses changes in local variance to detect scale transitions in spatial data.

Other works have employed a supervised approach to this problem. Clinton et al. (2010) proposed several discrepancy measures to assess segmentation quality based on area, location, or the combination of both aspects. Based on this work, Liu et al. (2012)

devised a supervised discrepancy measure named *Euclidean Distance 2* (ED2) to evaluate segmentation quality based on geometric and arithmetic similarity and used it to define the best parameters for segmentation (Liu et al. 2012, Novelli et al. 2017). Similarly, Montaghi et al. (2013) used a set of topological and geometric similarity measures and tested these for optimizing multi-resolution segmentation of WorldView-2 images for land parcel identification. Despite the different methods and measures, Räsänen et al. (2013) compared several of them for mapping boreal forest habitats and concluded that it is crucial to state the objectives of image segmentation and that discrepancy evaluation measures should be used with care. In addition, some of the above methods are software or algorithm-specific, typically focus on geometric, positional or areal similarity between segments and reference data and are not integrated with classification procedures.

In order to overcome some of these limitations and to generalize the process of comparing and optimizing different image segmentation parameters in a context of supervised classification we developed and propose a solution that integrates both processing steps (segmentation and classification) in a single and unified workflow that uses Genetic Algorithms (GA) to optimize image segmentation parameters.

Genetic Algorithms are broadly included in the class of evolutionary algorithms and constitute a type of computational search method used to find exact and approximate solutions to a given optimization problem (Scrucca 2013). In comparison to derivative-based methods which use the numerical gradient of the problem to be optimized, or computationally expensive enumerative methods which fail when the search space is large, GA allow for a general-purpose and flexible approach that can be applied to many types of problems (Rothlauf 2011). Broadly described, GA are a stochastic search technique that are able to solve optimization problems both for continuous and discrete functions and are based on the biological principles of evolution and natural selection (Haupt and Haupt 2004, Scrucca 2013).

Among many other optimization techniques, GA have gained more attention in recent years in several fields such as image processing, pattern recognition, machine learning, and artificial intelligence (Rothlauf 2011). Among other, GA provide several advantages such as: (i) allow optimizing continuous or discrete variables; (ii) do not require derivative information; (iii) allow to simultaneously search from a wide sample portion of the cost surface; (iv) allow dealing with a large number of variables; (v) parallelized computation is possible; and, (vi) allow optimizing variables with extremely

complex and sometimes noisy cost surfaces with the ability to jump out from local minima (Haupt and Haupt 2004).

Here we describe and test a new approach to iteratively optimize image segmentation parameters, implemented in a novel R package we have called *SegOptim*. Given the aforementioned advantages, we selected GA as a suitable optimization method to improve and tune image segmentation parameters in the context of supervised classification of EO images.

We also provide results from a set of tests using high (10-20m), very-high (2-5m) and 'ultra'-high (0.03-0.10m) spatial resolution images, collected from distinct EO platforms in six test sites in northern Portugal with different environmental and landscape conditions, and in which image segmentation was used for different purposes.

GA algorithms have been used before to optimize image segmentation parameters or results (e.g., Bhanu et al. 1995, Costa et al. 2008, Freddrich and Feitosa 2008, Ribeiro et al. 2011, Nikfar et al. 2012), and these examples would constitute a solid basis for our exploration. However, such applications typically presented a narrow context (e.g., targeted very specific problems such as urban areas classification) and did not explicitly integrate both image segmentation and supervised classification tasks.

Thus, integrating image segmentation and classification into a single and unified workflow suitable for optimization is a crucial feature of our proposed approach. As referred by Baatz et al. (2008) there is a mutual dependency between image segmentation and classification stages in the GEOBIA paradigm and object attributes (and their intrinsic quality) used to evaluate and classify image objects directly depend on the process generating those objects. Therefore, our aim was to optimize and fine-tune segmentation parameters allowing to generate image-objects that maximize the thematic accuracy of supervised classification as assessed via cross-validation through performance metrics summarizing confusion matrices (e.g., Kappa, accuracy). Our main motivation was to provide a generic approach to compare different algorithms based on optimized solutions. It was not our goal to show that our approach yields better results than others aiming at similar purposes but using widely different criteria and techniques for tuning image segmentation (e.g., ESP, discrepancy measures).

In addition, none of the above-mentioned works provided completely free/open-source tools to explore different algorithms for EO imagery object-based classification. In fact, from our literature review, only 12% of the cases used open-source software for image segmentation considering the pool of articles that explicitly documented this information (Appendix VI – Figure S1 - 1b). Hence, for addressing some of the challenges elicited above related to image segmentation, we developed *SegOptim – a*

R package directed towards non-specialized users interested in applying, comparing and optimizing object-based approaches to image segmentation and classification of EO data. We provide access to the package source code through a *Bitbucket* repository: https://bitbucket.org/joao_goncalves/segoptim, and a tutorial describing the package functionalities: https://segoptim.bitbucket.io/docs/ (*in prep*).

9.2. Methods

The proposed optimization approach

Implementing the optimization approach in R

The R environment and language for statistical computing (R Development Core Team 2017), as well as its packaging and documentation system, provided the backbone to implement *SegOptim* – the R package responsible for implementing the GA optimized approach to multi-technique image segmentation and GEOBIA supervised classification.

R has been gaining more popularity among the RS, EO and GIS communities due to its ability to handle raster datasets (*raster* package (Hijmans 2016)), perform (pre-) processing steps on EO data (e.g., cloud masking, co-registration, radiometric calibration, pan-sharpening – included in packages such as *RStoolbox* (Leutner and Horning 2017), *landsat* (Goslee 2011) or *satellite* (Nauss et al. 2015)), and to perform supervised classification with numerous methods available on data from these domains (e.g., package *rasclass* (Wiesmann and Quinn 2016) or *RStoolbox*).

However, currently there is no R extension providing access to image segmentation functionalities specifically for EO data. That is partly due to the inherent complexity of these algorithms and their implementations as well as constraints imposed by the type, formats and size of the data used. One way to circumvent this limitation, and the strategy adopted here, is to use 3rd party (or external) software to perform the image segmentation stage (check bellow details on software used for this stage). The segmented image outputted by an algorithm (in raster format) is then pushed into R for further analysis. While external software is used for image segmentation, R is responsible for the remaining processing and analysis tasks. R is especially well tailored for running the classification stage since it has a large number of available algorithms for this end.

Using this architecture, R acts as an interface between 3rd party programs used for image segmentation, centralizing all data and metadata required for performing the comparison and optimization of object-based classification in a GEOBIA context.
The package accesses 3rd party software either via command-line interface (CLI; namely: *GRASS*, *OTB*, *SAGA GIS* and *TerraLib*; see next sub-section on available software for image segmentation) or through the available *Python* programming interface (for *ArcGIS* and *RSGISLib*). Segmentation results are then loaded into R through the *raster* package (Hijmans 2016) which provided the basic structures to handle this type of data (Figure 9 - 1).

SegOptim is capable of handling both *single-class* problems (defined as a type of supervised classification problem with only one class with two mutually exclusive levels, e.g., species presence / absence, burned / unburned, cut / uncut forest) as well as *multi-class* (defined as a type of supervised classification problem with multiple, n≥2, mutually exclusive classes). The last is typically used when mapping a whole region into discrete land cover classes (e.g., forest, agriculture, urban).

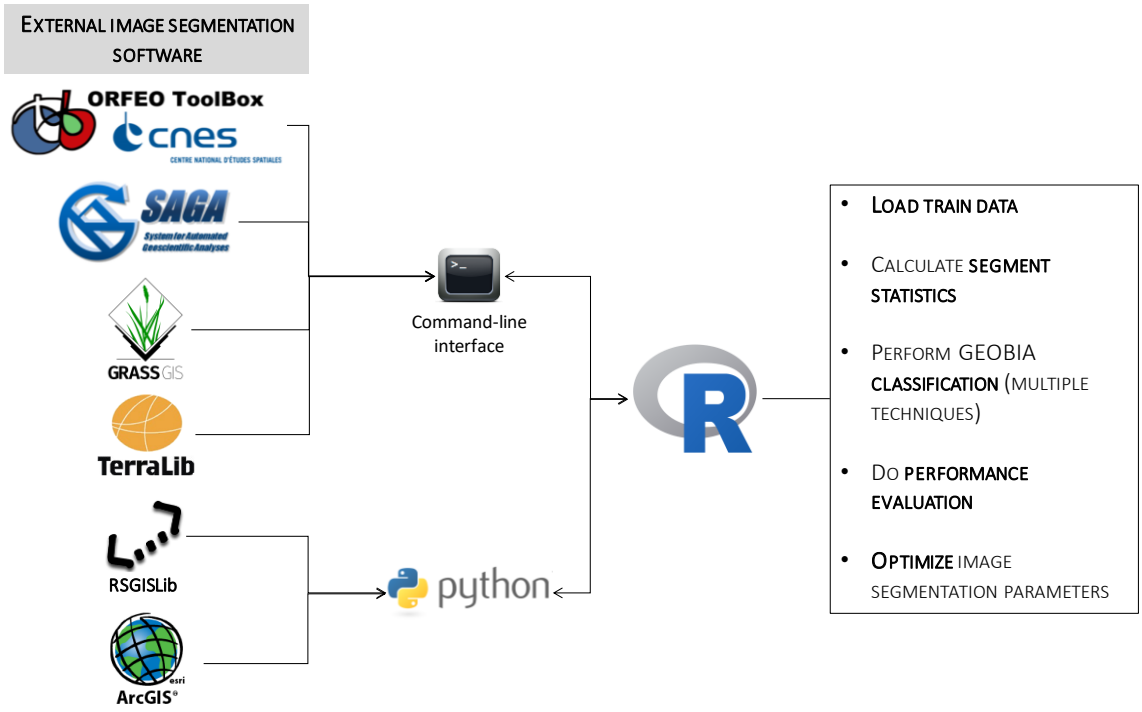

Figure 9 - 1 – The architecture of the software package *SegOptim*.

Genetic Algorithms: fitness function definition

In GA computation, at a certain stage of evolution, a population is composed by a number of individuals each representing a possible solution to the problem. Individuals are composed of several units (such as genes) which control the inheritance and passing of information between individuals. The capacity of individuals to solve a certain problem is determined by the *fitness function* and only the fittest individuals reproduce and pass their genetic information to their offspring. GA evolutionary strategy replicates the behaviour of natural organisms in a competitive environment where at each generation the less fit individuals (or solutions) are discarded and new ones are generated by the reproduction of the fittest (Scrucca 2013). This is accomplished by several genetic operators in two complementary stages: *exploration* and *exploitation*. The first aims at exploring the search space and is performed by operators such as *crossover* (which forms new offspring by combining parts of the genetic information from two parent individuals) and *mutation* (which randomly alters the values of genes in parents). Complementarily, exploitation, aims to reduce the diversity in the populations and focus on higher quality solutions. For this matter a *selection* strategy is employed thus allowing the fittest individuals to persist (Rothlauf 2011), commonly using an *elitist* strategy. The GA evolution process is stopped if some convergence criteria is attained. This can be: (i) reaching a pre-defined maximum number of generations; (ii) when a given number of iterations has passed without improving the best fitness value; or, (iii) achieving the maximum bound defined for the fitness value.

GA such as those implemented in R's '*GA'* package, require the definition of a *fitness function* (also defined as objective or cost function in optimization terminology). This function provides a single score ranking the "merit" of each solution and summarising how close it is to the established set of goals. The fitness function is the 'core' component of *SegOptim* package around each other part connects to. In this particular case, the target of GA optimization, expressed in the fitness function, is to devise a segmented image that maximizes the thematic accuracy of the supervised classification based on a predefined set of image inputs such as labelled train input data, a set of classification features and finally, control parameters (Figure 9 - 2). GA is then responsible for iteratively modifying the segmentation algorithm arguments in order to improve classification accuracy for the specific task at hands. For implementing the fitness function, a sequence of processing steps presented in Box 1 was implemented.

1. Run the image segmentation;
2. Load training data into the segmented image;
3. Calculate segment statistics (e.g., mean, standard-deviation) for classification features;
4. Merge training and segment statistics data (steps 2-3);
5. Do train/test data partitions (e.g., 5-fold cross-validation);
6. For each train/test set:
    a. Train the supervised classifier;
    b. Evaluate results for the test set;
7. Return the average evaluation score across all train/test rounds (fitness value);

Box 1 – Pseudo-code describing the workflow for the proposed GA fitness function.

For evaluating the merit of each solution, *SegOptim* uses either 5-fold, 10-fold or holdout cross-validation. Depending if the problem is single- or multi-class, it is possible to calculate several metrics that summarise the confusion matrix generated at each evaluation split and focus on assessing the thematic accuracy of each solution generated. For single-class problems, the Area Under the Receiver Operating Curve (AUC), Cohen Kappa, Peirce Skill score (or true-skill score; PSS) and the Gerrity skill score (GSS) are available, while for multi-class, accuracy, Kappa, PSS and GSS can be used. For testing purposes, we selected Kappa as the fitness value.

Genetic Algorithm parameterization and setup

Running the GA also requires the setup of several parameters responsible for controlling the initial population and the exploration / exploitation stages using the three basic operators of *selection*, *cross-over* and *mutation*. We used the parameters in Table 9 - 1(a) to run the GA responsible for optimizing image segmentation parameters.

Given the complexity of the fitness function and the time required to generate a single solution, the parameters controlling GA were setup in a ‘conservative fashion’ meaning that population size was relatively low (but enough to generate diverse solutions in the exploration stage). This parameterization was suited to find an approximate solution with a relatively small population size and a relatively low number of iterations

and simultaneously it allowed to decrease computation time and keep processes tractable.

The '*GA*' package also includes several different operators for controlling the way *selection*, *cross-over* and *mutation* work. Providing an in-depth description of these operators is outside the scope of this work, but details can be found in (Bäck et al. 2000a, b) and Yu and Gen (2010). Selected GA operators are defined in Table 9 - 1(b).

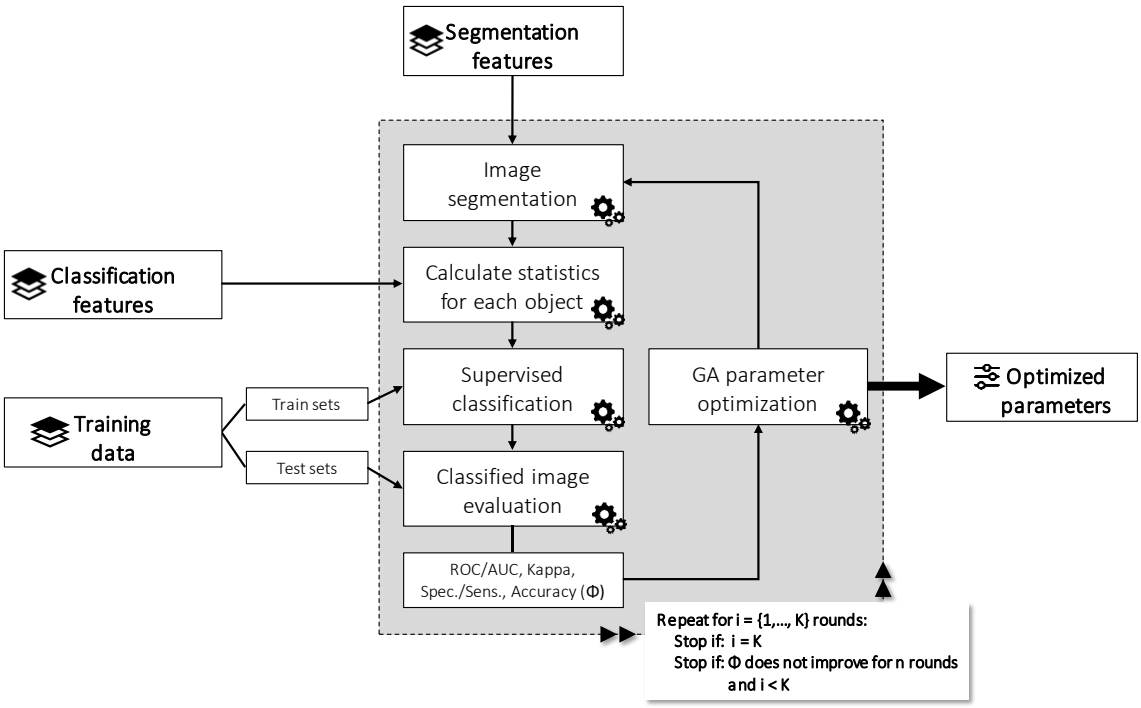

Figure 9 - 2 – Schematic representation of the fitness function.

Finally, besides other parameter inputs, GA also requires the search space to be constrained and therefore the user must define the min-max boundaries of each image segmentation parameter for each algorithm. This is critical to achieve good results as well as to avoid parameter combinations that may give rise to useless solutions thus increasing computing time. This requires some degree of knowledge and experience about the problem context and the specific aspects of each algorithm and its software implementation. Therefore, min-max boundaries were set specifically for each test set and image segmentation algorithm (see details in Appendix VI – S2).

Table 9 - 1 – (a) GA parameters used for running the image segmentation tests as well as, (b) description of GA operators used.

(a)

GA acronym	**Definition**	**Value**
popSize	The population size (number of individuals or solutions) generated at each round.	**20**
pcrossover	The probability of crossover between pairs of chromosomes. Typically defined as a large value close to 1.	**0.8**
pmutation	The probability of mutation in a parent chromosome. Usually mutation occurs with a small probability.	**0.2**
elitism	The number of best fitness individuals to survive at each round.	**1**
maxiter	The maximum number of iterations to run before the GA search is halted.	**100**
run	The number of consecutive generations without any improvement in the best fitness value before the GA is stopped.	**20**

(b)

Operator name	**Description**
gareal_Population	Generate a random (uniform) population of real values bounded by the user-provided range for each parameter
gareal_lsSelection	Selection probability is proportional to fitness value with fitness linear scaling
gareal_laCrossover	Local arithmetic crossover
gareal_raMutation	Uniform random mutation

Image segmentation algorithms available in the package

SegOptim currently interfaces with six external state-of-the-art programs responsible for performing the image segmentation stage (Table 9 - 2). From these, a total of seven image segmentation algorithms are available. Four types of algorithms can be identified (based on similar characteristics) albeit differences in their computational implementations: (i) mean-shift (*ESRI ArcGIS* and *OTB*) (Comaniciu and Meer 2002, Michel et al. 2015); (ii) region growing and merging (*GRASS GIS*, *SAGA GIS* and *TerraLib*) (Adams and Bischof 1994, Tremeau and Borel 1997, Hojjatoleslami and Kittler 1998, Bechtel et al. 2008); (iii) Shepherd k-means iterative elimination (*RSGISLib*)

(Clewley et al. 2014); and, (iv) Multi-resolution image segmentation (also in *TerraLib*) (Baatz and Schape 2000).

Table 9 - 2 – List of software packages and algorithms for image segmentation currently available in *SegOptim*. (*1- OTB functionalities can be accessed through Monteverdi graphical interface; *2 - TerraLib functionalities can be accessed through TerraView 5 graphical interface). Also includes the list of currently optimizable parameters in *SegOptim.*

Software / package	Version	Algorithm(s) / optimizable parameters
ESRI ArcGIS	10.3.0	Mean-shift (optimizable parameters: spatial detail, spectral detail, minimum segment size)
GRASS GIS	7.2	Region growing (optimizable parameters: merge threshold, minimum segment size)
Orfeo Toolbox (OTB *[1])	6.0.0	Large-scale mean-shift (optimizable parameters: spatial detail, spectral detail, minimum segment size)
RSGISLib	3.2	Shepherd k-means iterative elimination (optimizable parameters: number of clusters, spectral threshold, minimum segment size)
SAGA GIS	4.0	Simple region growing (optimizable parameters: bandwidth, Gaussian weighting bandwidth, variance in feature space, variance in position space)
TerraLib (*[2])	5.2.1	Mean region growing (optimizable parameters: merge threshold, minimum segment size) Multi-resolution image segmentation (optimizable parameters: compactness weight, colour weight, minimum segment size, merging threshold)

Supervised classification algorithms

Currently, *SegOptim* package offers several machine-learning classification algorithms which can be used to perform GEOBIA classification stage, these are: (i) Gradient Boosted Regression and Classification (GBM) available through *gbm* package (Ridgeway 2017); (ii) Random Forests (RF) accessible in R through *randomForest* package (Liaw and Wiener 2002); and (iii) Support Vector Machines (SVM) available via *e1071* package (Meyer et al. 2017). These techniques (along with available segmentation methods) were used and compared through a series of tests for several distinct sites and image classification problems. The default parameterization for each method was used.

Input data

Briefly described, the *SegOptim* package relies on three basic data inputs used to perform image segmentation and object-based classification (Figure 9 - 2). These are:

- Training data: a single-layer raster dataset containing user-labelled samples for training a classifier. The class labels were coded as integers $\{0, 1\}$ for single-class problems, or $\{1, 2, \ldots, n\}$ for multi-class problems. Training data is independent of any segmentation solution but it is contingent on the features used for segmentation and/or classification, i.e., the delineation of input training objects is based (but not exclusively) on image features used to segment and classify them. Training objects are delineated as far as possible to be spatially consistent, comprehensive, and its borders representative of 'real-life' objects of each target class.
- Segmentation features: a multi-layer raster dataset with features used only for the segmentation stage (e.g., spectral bands);
- Classification features: a multi-layer raster dataset with features used for classification (e.g., spectral data, band ratios, spectral vegetation or water indices, texture features, topographic or surface data). The classification feature space is commonly wider than the segmentation feature space. Classification features were selected due to their ability to differentiate the distinct target classes. Preliminary classifiers were trained and inspected to assess which features attained the highest discriminative importance thus allowing to reduce this feature space complexity and improve computation.

Carefully defining these inputs is key to ensure that results are meaningful and classification achieves good performance. In the same sense, optimized results are always conditioned upon data defined in these three inputs.

Testing the optimized approach

Input training data

Six sites located in northern Portugal were used to conduct image segmentation optimization tests comprising three single-class and three multi-class problems. These tests represent a diverse array of ecological applications and domains (e.g., land use/cover mapping, habitat conservation, invasive species management) as well as of

environmental conditions, ranging from coastal, lowlands up to mountainous areas and different levels of landscape heterogeneity (Table 9 - 3).

The first set (single-class tests; Table 9 - 3) targeted the detection of invasive species associated to sand dune environments (Carpobrotus spp.; E1) or forest areas (Acacia spp.; E3 and E5). In the second set (multi-class tests; Table 9 - 3), we used SegOptim to improve segmentation parameters for producing maps of natural habitats (E2; Gonçalves et al. (2016)) or land use/cover maps (E4 and E6; the target classes are listed in Appendix VI – S3).

Table 9 - 3 - List of testing sites and description of testing objectives (UL – upper-left corner and LR – lower-right corner coordinates in WGS 1984 geographic). The six tests (E1-E6) are listed based on the spatial resolution of EO imagery.

Site code	**Site name and description**	**Problem type**	**Classification task / context**	**EO platform**	**Spatial resolution**	**Spectral / radiometric resolution**	**Test area size** (pixels)
E1	*Mindelo/Árvore, V. Conde* UL: (41°19'42.39"N, 8°44'14.4"W) LR: (41°19'41.42"N, 8°44'13.11"W) Elevation: 8-10m	Single-class	*Carpobrotus spp.* invasive species mapping (2 levels: invaded/non-invaded)	SenseFly UAV	0.06 - 0.10m	4 bands (VIS, NIR); 8-bit	1000 × 1000
E2	*Serra d'Arga* mountain range, Caminha UL: (41°49'16.93"N, 8°42'51.53"W) LR: (41°49'14.98"N, 8°42'48.95"W) Elevation: 741-787m	Multi-class	Natural habitats mapping (9 target classes)	SenseFly UAV	0.03m	3 bands (VIS); 8-bit	1000 × 1000
E3	*Vilar da Veiga, Peneda-Gêres* National Park UL: (41°44'14.11"N, 8°10'53.58"W) LR: (41°43'8.65"N, 8°9'27.89"W) Elevation: 290-957m	Single-class	*Acacia spp.* invasive species mapping (2 levels: invaded/non-invaded)	WorldView-2	2m	8 bands (VIS, NIR); 11-bit	1000 × 1000
E4	Viana do Castelo city UL: (41°42'51.48"N, 8°51'53.13"W) LR: (41°40'9.05"N, 8°48'17.26"W) Elevation: 0-70m.	Multi-class	Land cover/use mapping (9 target classes)	RapidEye	5m	5 bands (VIS, NIR); 12-bit	1000 × 1000
E5	*Caminha/V. Castelo* municipalities UL: (41°49'53.78"N, 8°51'25.79"W) LR: (41°41'46.51"N, 8°43'9.37"W) Elevation: 5-742m.	Single-class	*Acacia dealbata* invasive species mapping (2 levels: invaded/non-invaded)	Sentinel-2a	10m	4 bands (VIS, NIR); 12-bit	1150 × 1500
E6	*Vez* river watershed, *Arcos de Valdevez* municipality UL: (42°1'3.7"N, 8°31'31.62"W) LR: (41°48'16.6"N, 8°15'22.24"W) Elevation: 13-1419m	Multi-class	Land cover/use mapping (10 target classes)	Sentinel-2a	10/20m	10 bands (VIS, NIR, SWIR); 12-bit	2250 × 2350

Regarding the collection and/or digitization of training data, for test-sites E1 (sample size, n=80) and E2 (n=25) we followed a systematic sampling approach using a regular sampling grid to select sample locations later used in the field to collect ground-truth data. In site E3 we used purposive sampling (n=40) to locate the target species in the field complemented with locations digitized from *GoogleEarth* imagery (Monteiro et al. 2017). In site E4 we used a systematic sampling approach (n=271) for digitizing training locations based on *GoogleEarth* imagery. For site E5 we followed a purposive sampling scheme for locating patches of *Acacia dealbata (n=108)* complemented with a set of random samples for the species absence digitized from *GoogleEarth* imagery. In site E6 we used a stratified random sampling approach with strata defined through clustering of several layers related to topography, soils and other datasets (Bastos et al. 2016) for collecting training samples (n=1545) based on ground-truth data, ancillary land cover data and *GoogleEarth* imagery.

SegOptim uses a simple threshold rule for performing the conversion of user-defined training samples or areas (in a raster representation) into training segments. This uses a threshold value ($t =]0, 1]$) defined by the user and the areal proportion ($a_c = [0, 1]$) of the segment covered by each class $c = \{0, 1\}$ (plus the background or *NoData* class). Then, the following rule is applied for single-class problems:

$$\begin{cases} 1, if\ a_{c=1} \geq t \\ 0, if\ a_{c=0} = 0 \\ Null, otherwise \end{cases}$$

For multi-class problems, this threshold rule operates in a slightly different manner. First, a cross-tabulation matrix is generated by calculating the proportion of each segment covered by each land cover class (Figure 9 - 3).

SID	Class_1	Class_2	Class_3	…	Class_n	Majority_class
1	0.2	0.8	0.0	…	0.0	2
2	0.5	0.2	0.1	…	0.2	1
3	0.2	0.2	0.2	…	0.4	n
…	…	…	…	…	…	…
N	0.0	0.0	1.0	…	0.0	3

Figure 9 - 3 – An example cross-tabulation by segment and land cover class (SID: segment unique identifier).

After determining the majority class (i.e., the class with higher areal coverage) the train function verifies if that class coverage is above or equal to t, if not, the segment is removed from the training set. In the example (Figure 9 - 3), if $t = 0.5$, then segments with identifiers: $SID = \{1,2,N\}$ would be kept while $SID = \{3\}$ would be removed. Overall, the higher the value of the threshold, t, the 'purer' the training segments will be. Hence, this value reflects the degree to which 'class-mixing' at segment-level is admissible for classification.

Image data pre-processing and segmentation features

Input imagery used for *SegOptim* testing was selected to cover a diverse set of spatial resolutions (from high at 20m to 'ultra'-high at 0.03m), different EO platforms (from airborne: SenseFly UAV, to spaceborne: WorldView-2, RapidEye and Sentinel-2a) and different spectral resolutions (from 3 up to 10 bands; Table 9 - 3 and Figure 9 - 4).

Image data from a SenseFly UAV were acquired and pre-processed according to Gonçalves et al. (2016) for site E1 on 2013-03-17, and for site E2 on 2014-11-20. Raw digital number (DN) values were used for image segmentation and classification. For site E3, one WorldView-2 image for 2013-06-23 was pre-processed and orthorectified according to Monteiro et al. (2017). For E4, one RapidEye image for 2014-10-29 (not previously used) was freely available from ESA's EOLi-SA Catalogue and Ordering Service and the Copernicus Urban Atlas initiative. We pre-processed image data and radiometrically calibrated to top-of-the-atmosphere (TOA) reflectance using at-sensor metadata. As for sites E5 and E6, Sentinel-2a data (also not previously used) was collected from ESA's Sentinel DataHub (URL: https://scihub.copernicus.eu) for two different dates: 2016-03-14 and 2016-07-19 and processed to bottom-of-the-atmosphere (BOA) reflectance (level L2A) using SNAP with *sen2cor* atmospheric correction plugin (Mueller-Wilm et al. 2016). Segmentation features mainly coincide with spectral bands used as ancillary information to acquire ground-truth data in the field or for manually digitizing training samples. The segmentation feature space encompassed less dimensions (in comparison to the classification feature space) to allow fast processing needed to run segmentation. For E1, E2, E3 and, E4 the Red (R), Green (G) and Blue (B) bands were employed while for E5 and E6 we used the R, G, B bands plus the Near-infrared (NIR). In particular, for site E6 we used these four bands for the two available dates (March/July-2016) to improve segmentation results and capture seasonal differences.

Classification features

Classification features were used to extract signatures related to each class of interest. This data enables the classifier to learn from class attributes and later use those signatures to label each object in the image. For each test site, several types of classification features were used (see Table 9 - 4), namely: (a) spectral data – reflectance values or raw DN values in case of UAV images; (b) alternative colour spaces (other than RGB but with better separability between components; e.g., XYZ, YUV); (c) multiple combinations of band ratios in the form: $BR = b_i \,/\, b_j$ where b_i and b_j are any two different spectral bands centred at a given wavelength; (d) vegetation and/or water indices (e.g., NDVI, EVI); (e) multiple combinations of Normalized Difference Indices (NDI) in the form $NDI = (b_i - b_j)/(b_i + b_j)$; (f) texture operators such as Haralick (Haralick 1979) (HL; e.g., energy, entropy, correlation, inertia), Local Statistics (LS; mean, variance, skewness and kurtosis) or Structural Feature Set (Huang et al. 2007) (SFS; e.g., Length, Width, PSI, W-Mean) based on different kernel sizes and parameterizations; and, (g) topographic features (e.g., elevation, slope, curvature) or surface elevation.

Table 9 - 4 – Types of classification features used for each study area/experiment. NDI – Normalized Difference Index combinations based on any two different bands; HL – Haralick texture features; LS – Local Statistics features; SFS – Structural Feature Set texture features. (*) for the features in E6, two images (March/July 2016) were used to calculate classification features.

Test site	**Classification features**								
	Spectral data	Alternative colour spaces	Band ratios	Vegetation / water indices	NDI combinations	Texture operators			Topographic / surface
						HL	LS	SFS	
E1	✓	✓	✓	✓	✓	✓	✓	✓	✓
E2	✓	✓	✓	✓	✓		✓		✓
E3	✓			✓	✓				
E4	✓			✓	✓				
E5	✓				✓				
E6	✓*				✓*				✓

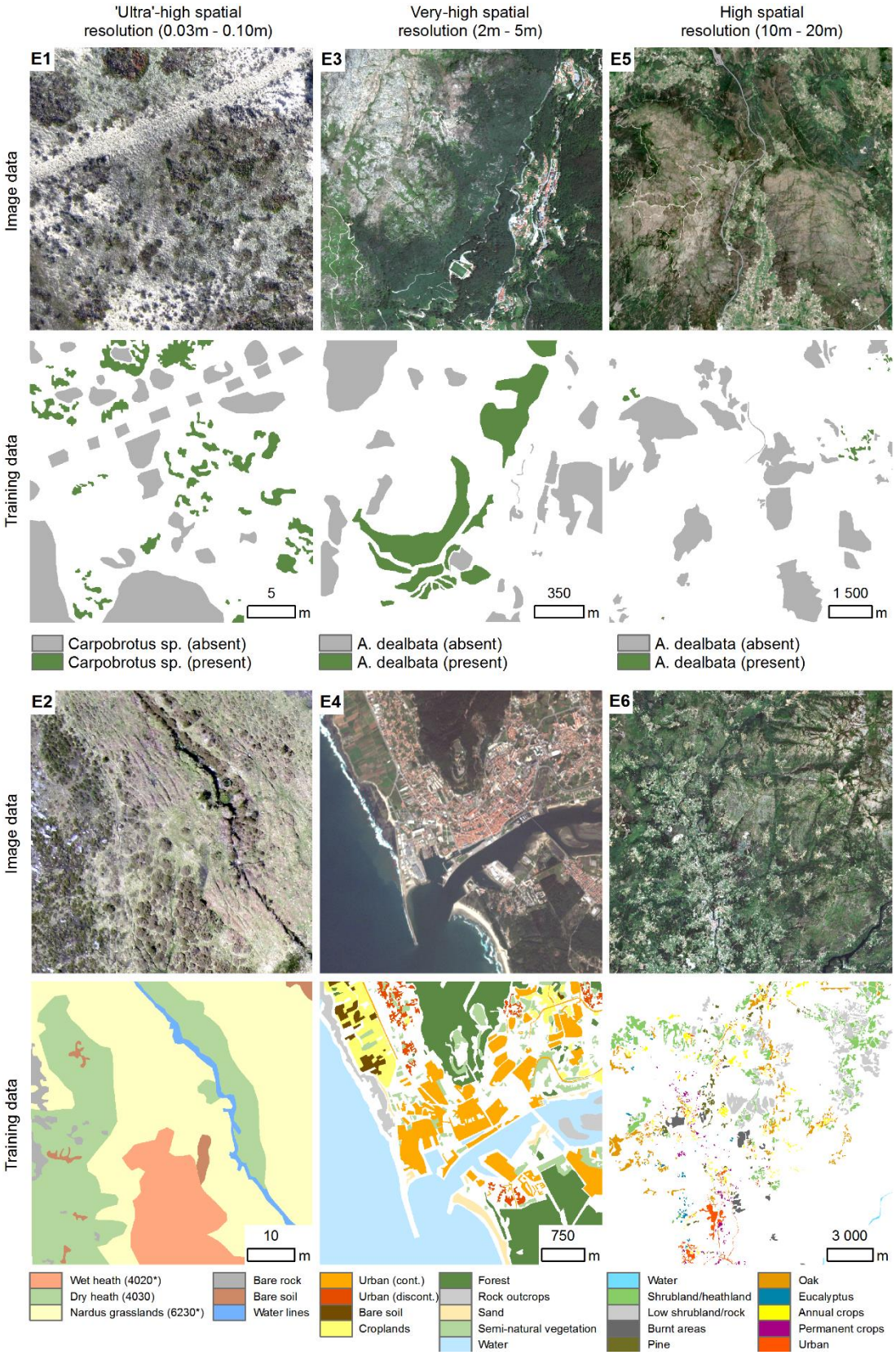

Figure 9 - 4 – Segmentation features and training data used for testing the GA-based approach in *SegOptim* package for single-class problems (detection of invasive species; E1, E3 and E5 pilot-test areas in top-two rows) and multi-class (habitat and land cover/use mapping; E2, E4 and E6 pilot-test areas in bottom-two rows).

9.3. Results

General performance across test sites

Supervised classification performance for 5-fold cross-validation, based on optimized image segmentation, attained very good to excellent results across the six test sites (see Table 9 - 5 and Figure 9 - 5). Kappa values ranged from 0.96 (E1) to 1.00 (E3) for single-class tests and, between 0.85 (E2) to 0.94 (E6) for multi-class tests (see also Appendix VI – S4 with confusion matrices and producer/user accuracies).

Overall, no particular image segmentation algorithm outperformed its competitors in our test. Still, TerraLib and SAGA region growing-based algorithms were selected twice. In contrast, for classification methods, the RF algorithm has shown very good overall performance being selected five out of six times as the best performing classification algorithm (in some instances tied with other algorithms, E3 and E6).

Table 9 - 5 – Results for 5-fold cross-validation using the Kappa Index to evaluate object-based classification performance based on *SegOptim*'s GA-optimized image segmentation for each of algorithm. Values highlighted in bold represent the best solutions for each test site. E1, E3 and E5 are single-class problems while the remaining E2, E4 and E6 are multi-class problems.

Segmentation software / algorithm	Classification method	Test sites / experiences					
		E1	E2	E3	E4	E5	E6
ESRI ArcGIS – Mean-shift	RF	0.96	0.78	0.77	0.86	0.91	0.92
	SVM	0.90	0.74	0.78	0.83	0.94	0.93
	GBM	0.95	0.59	0.84	0.83	0.82	0.87
GRASS GIS – Region Growing	RF	0.87	0.79	0.97	**0.92**	0.95	0.91
	SVM	0.88	0.73	0.94	0.70	0.93	0.93
	GBM	0.90	0.62	0.95	0.85	0.87	0.81
SAGA GIS – Simple Region Growing	RF	0.93	0.79	**1.00**	0.88	0.91	0.93
	SVM	0.84	0.76	**1.00**	0.87	0.87	0.92
	GBM	**0.96**	0.66	**1.00**	0.84	0.82	0.86
OTB – Large Scale Mean-shift	RF	0.89	0.80	0.92	0.88	0.94	**0.94**
	SVM	0.86	0.73	0.90	0.86	0.90	**0.94**
	GBM	0.89	0.61	0.83	0.84	0.78	0.87
RSGISLib – Shepherd Iterative Elimination	RF	0.79	**0.85**	0.99	0.81	0.86	0.86
	SVM	0.75	0.74	0.99	0.79	0.87	0.86
	GBM	0.75	0.61	0.99	0.76	0.71	0.76
TerraLib – Mean Region Growing	RF	0.92	0.80	**1.00**	0.69	**0.97**	0.90
	SVM	0.94	0.72	**1.00**	0.66	0.97	0.73
	GBM	0.88	0.61	0.92	0.60	0.84	0.81
TerraLib – Multiresolution Baatz-Schäpe	RF	0.79	0.81	**1.00**	0.88	0.92	0.93
	SVM	0.93	0.74	**1.00**	0.87	0.93	0.93
	GBM	0.88	0.63	**1.00**	0.85	0.86	0.85

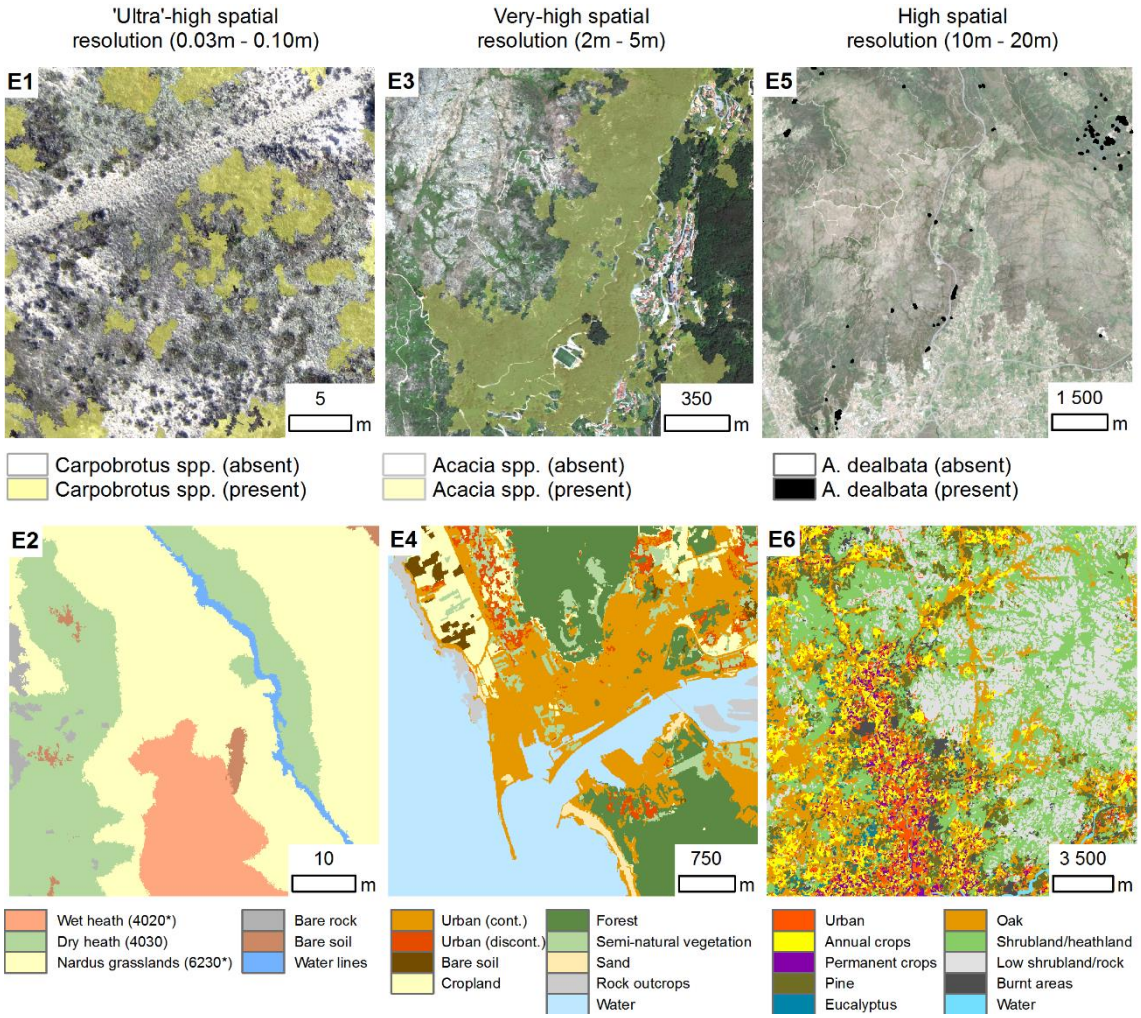

Figure 9 - 5 – Classification outputs generated from the best GA-based solutions for each test-site. E1, E3 and E5 are single-class problems while the remaining E2, E4 and E6 are multi-class problems. E1 depicts the distribution of Carpobrotus sp. invasive species using SAGA GIS Simple Region Growing segmenter and GBM classifier; E2 maps different natural habitats using RSGISLib Shepherd iterative elimination segmenter and Random Forest (RF) classifier; E3 shows the distribution of *Acacia dealbata* invasive species (yellow patches) using TerraLib Baatz-Schäpe multi-resolution segmenter and RF classifier; E4 shows land cover/use classification using GRASS GIS region Growing segmenter and RF classifier; E5 shows the distribution of small patches of the invasive Acacia dealbata species across the landscape using TerraLib Mean Region Growing segmenter and RF classifier; and, E6 shows land cover/use mapped with OTB Mean-shift segmenter and RF classifier.

Performance differences and optimization results per test site

When analysing the distribution of paired absolute differences of performance (Kappa index) for each test site across segmentation algorithms (median = 0.03) and across classification algorithms (for the same segmentation method; median = 0.06) we found a significant difference (**)[9] with larger performance differences arising from the

[9] Wilcoxon signed-rank test, alternative hypothesis: “greater”: (***) p<0.001, (**) p<0.01, (*) p<0.05, (.) p<0.1, NS non-significant

classification algorithm used, rather than the type of segmentation method. However, when looking at disaggregated differences per test site, in fact, for half of the situations we found greater differences originated by the segmentation algorithm [although not all were significant, E1: NS, E3: (**) and E4: (.)] and half otherwise [E2: (***), E5: (**) and E6: (**)].

Results also showed a large difference, equal to 0.25 (in average), between the best and worst performer combination of segmentation/classification algorithms for each test site although these comparisons are always based on optimized setups (Table 9 - 5).

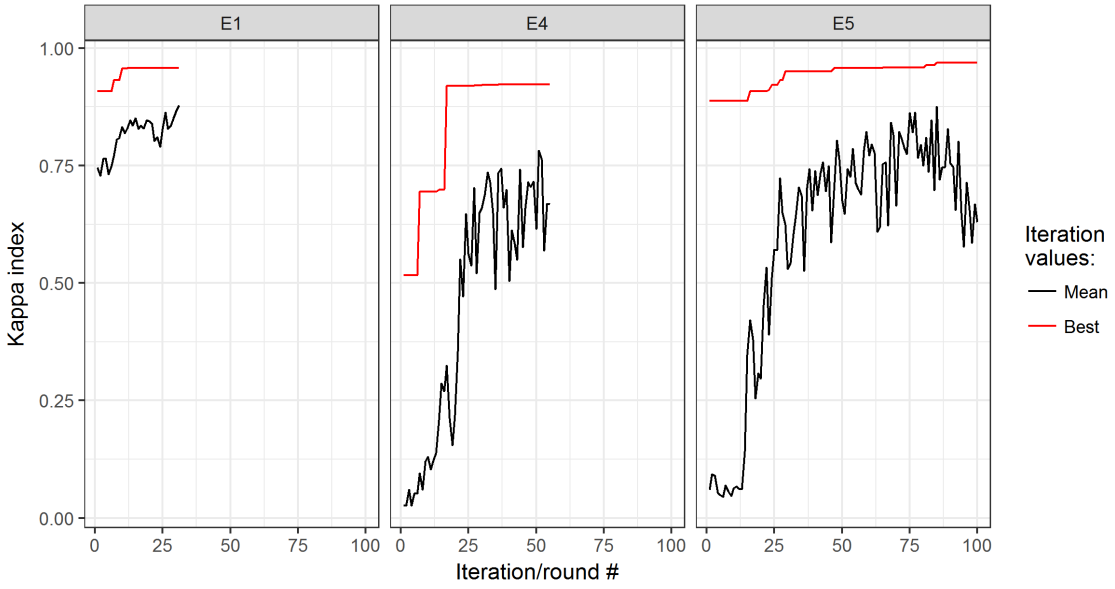

Figure 9 - 6 – GA optimization paths for three test sites with different convergence profiles in terms of speed: fast for E1, intermediate for E4, and slow for E5. These paths represent only the best performing solutions for each test site. The black line represents the average Kappa for all individuals (n=20) at each round of the GA optimizer while the red line shows the Kappa value of the best solution by round.

Best segmentation parameters per test site were the following: for E1, SAGA GIS Simple Region Growing: bandwidth = 25.75, Gaussian weighting bandwidth = 6.32, variance in feature space = 0.76, variance in position space = 0.76; for test site E2, RSGISLib Shepherd iterative elimination: number of clusters = 10, minimum segment size = 20, spectral threshold = 20.56); in test site E3, multiple segmentation algorithms were selected but, for example, TerraLib Baatz-Schäpe multi-resolution (for RF) used: compactness weight = 0.79, spectral weight = 0.73, threshold = 0.12, minimum segment size = 17); for test site E4, GRASS GIS region growing: merging threshold = 0.06, minimum segment size = 5; for test site E5, TerraLib Mean Region Growing: merging threshold = 0.01, minimum segment size = 4) and, for test site E6, OTB Mean-shift:

spectral range = 10.03, spatial range = 11.87, minimum segment size = 50. The complete set of all optimized parameters can be found in Appendix VI – S5.

For the best performing combinations of algorithms, and considering the stopping conditions maxiter = 100, run = 20 (see Table 9 - 1), in average the GA optimization took 45 rounds to converge. Different GA optimization paths were observed (Figure 9 - 6) in terms of speed of convergence, varying from relatively fast (low number of iterations required, e.g., E1: #iterations=31) to slow (stopping caused by hitting the maximum number of iterations defined, e.g., E5: #iterations=100). We could not perform a comparison of execution times because tests were performed in three different machines (with dissimilar computational resources/architectures). In terms of improvement degree due to GA parameter optimization, we also recorded widely different results across tests varying from relatively low (E1) to high improvement (E4; Figure 9 - 6).

9.4. Discussion

Main contributions to improve GEOBIA workflow

In this study we developed a generic approach to object-based analysis comparison and optimization which integrates two crucial steps in GEOBIA workflows typically exhibiting mutual dependencies: image segmentation and classification (Baatz et al. 2008). Due to their flexibility and power, we selected Genetic Algorithms as a suitable method to optimize and fine-tune segmentation parameters. Overall, the use of GA for optimizing image segmentation parameters with the aim of maximizing the thematic accuracy of supervised classification, together with the comparison of multiple techniques, represents a significant advancement in GEOBIA workflows.

A new open-source R package (*SegOptim*) implements the proposed approach with a rich set of features for testing, comparing and optimizing different image segmentation and classification algorithms within the R environment and computing language (R Development Core Team 2017). This package is available through Bitbucket hosting service with Git serving as version control system. The several tests performed for this study strongly suggest that *SegOptim* provides a novel and robust comparison of several state-of-the-art algorithms and software focused on the object-based analysis of EO data for different application contexts [see also, e.g., (Meinel and Neubert 2004, Marpu et al. 2010, Li et al. 2016, Teodoro and Araújo 2016)].

Performance comparison and best option selection

Given their wide accessibility for users, we focused comparisons on specialized open-source software for GIS and RS. GA-optimized results for image segmentation and object-based classification allowed to identify which algorithms performed best for each situation. Tests encompassed a wide range of sites across northern Portugal from coastal beach environments or urban settlements up to complex mosaic landscapes in mountainous areas covering distinct environmental conditions, landscape patterns and dynamics. Different input EO imagery was also tested, ranging from 'ultra'-high resolution UAV data (0.03 - 0.10m), very-high resolution (WorldView2, 2m to RapidEye, 5m) to high resolution Sentinel-2a (10 - 20m) multi-temporal images. Calibration conditions for image segmentation, classification and optimization were also diverse encompassing a wide range of problems and objectives from single-class (aiming to identify and map the distribution of invasive species) to multi-class problems (with the objective of discriminating and mapping natural habitats or land cover/use classes).

Our results highlight that no particular combination of an image segmentation and a classification algorithm is suited for all the tasks/objectives, an empirical verification of the "*no free-lunch theorem*" (NFLT; (Wolpert 1996, Wolpert and Macready 1997)) for object-based image classification problems. Broadly described, the NFLT (which, among other, applies to machine-learning and optimization problems) implies that learning algorithms "cannot be universally good" across all problems and domains (Magdon-Ismail 2000). This seems to apply also in our particular case and especially for image segmentation algorithms. Besides theoretical implications, this means that comparing and optimizing methods procedures is crucial for determining which ones are more suited for a particular objective. *SegOptim* provides the required functionalities for this purpose. Despite these results, the RF classifier has shown good overall performance across tests, which is coherent with previous findings (Fernández-Delgado et al. 2014). However, this may be a consequence of this algorithm requiring much less fine-tuning in comparison to other techniques such as SVM (Breiman 2001).

The results from our tests also showed that, depending on the specific problem under consideration, either segmentation algorithms produce greater differences in object-based analyses or (more likely) different classifiers will generate stronger differences. Still, most studies focus only on comparing performances between different classification algorithms (e.g., (Li et al. 2016)). In addition, comparisons may be of particular importance given that we found strong differences between "best" and "worst" performers for the same task/objective, which may imply that the probability of obtaining

sub-optimal results without comparing available methods and/or optimizing its parameters is fairly high.

Besides the "*best solution*" (i.e., the one with best performance), other solutions may also be visually inspected because these may also provide good results worth to consider. Lang (2008) considers that human perception or cognition skills required to evaluate the delineated and classified objects is still the "ultimate benchmark" for assessment. In the same sense, user control and expert decision are still required to assess situations of potential under- or over-segmentation, and to make informed choices, similarly to what Grybas et al. (2017) found for unsupervised segmentation parameter optimization.

An alternative to selecting the "best solution" could be to ensemble multiple solutions (a.k.a. "classifier stacking" or "decision fusion"). Although we could not find any examples combining different segmentation methods, 'fusing' multiple classifiers is often performed with gains in terms of accuracy (Oza and Tumer 2008, Clinton et al. 2015, Löw et al. 2015).

A general framework for GEOBIA optimization

GEOBIA has become a popular toolset for performing land cover classification. However, the critical step of defining the best segmentation parameters remains problematic. Several works proposed different unsupervised (Dragut et al. 2014, Grybas et al. 2017) or supervised methods (Clinton et al. 2010, Liu et al. 2012, Montaghi et al. 2013) for this purpose, with both groups of methods holding advantages and caveats.

Our supervised approach however, differs from what we found in the literature, since previous approaches typically measure the geometric, arithmetic, topological or spectral discrepancy between a reference dataset and image segments. Instead, the cornerstone of our approach is the close integration between both the image segmentation and the classification steps common in GEOBIA workflows (Baatz et al. 2008, Lang 2008, Blaschke 2010). Hence, the objective was to use GA for optimizing image segmentation parameters with the aim of maximizing the thematic accuracy of supervised classification. This way we provide a relatively simple and generalizable approach for optimizing object-based image analysis and compare multiple techniques. From our tests, we observed that this approach allows to define segmentation parameters which balance between the over- and under-segmentation spectrum across all target classes, without a relevant loss in overall classification performance.

Although GA-based optimization may help to improve object-based analyses, it is still crucial that the human operator carefully defines every input and monitors the optimization process. More specifically, in some preliminary runs we found that GA can provide useless or low performance results if (for example) segmentation parameter bounds are defined too broadly. It is up to the user to rectify those kinds of situations. To profit from GA-based optimization, and to avoid high computational costs, the user must carefully set up its parameters.

Future developments and outlook

The volume of data has grown immensely in recent years due to high- and very-high spatial resolution EO platforms and sensors. “Big data” poses several problems and challenges for processing, and not all available GEOBIA algorithms and software are up to the task (but see, e.g., Michel et al. (2015) or Happ et al. (2016)). The *SegOptim* package by performing complex analyses in a desktop-based environment is therefore limited to the available resources in terms of RAM, CPU power and disk space/speed. One way to circumvent this problem, and still optimize object-based analysis, is to extract smaller regions-of-interest (ROI) preferentially through an adequate spatial sampling design (e.g., Köhl et al. 2006) and process each ROI independently. By inspecting the distribution properties of the target segmentation parameters for all ROI’s it is still possible to obtain useful information without having to use a complete scene.

Another possible limitation of our GEOBIA optimization approach, is the fact that GA may require long computing time. From our tests, we observed a wide variation in the number of rounds required to achieve convergence conditions, depending on input data and parameterization (Figure 9 - 6). A possible solution to this, allowing to speed-up computations, is to use parallel processing already implemented in the ‘GA’ package (Scrucca 2013). As mentioned earlier, another possible solution is to provide a thoughtful configuration of GA optimization parameters (among other) leading to faster and more meaningful results.

Besides these computational limitations, our proposed approach focuses on devising a non-hierarchical, single-level classification for the area of interest, thus inherently simplifying some aspects, and making it less applicable to some settings or goals. Still, users interested in performing an object-based land cover/use classification may find this classification approach easier to use and more flexibly adaptable to their particular case.

In fact, *SegOptim* open-source R package offers users the possibility to test, compare and optimize different GEOBIA methods related to image segmentation and

classification with benefits for producing thematic maps for land cover characterization or mapping specific classes, species or processes based on EO image data. Besides these features, this package also offers the possibility to use several unsupervised classification methods and compare different solutions through cluster validity indices. Exploring the latter in detail is, however, outside the scope of this study. By providing free access to *SegOptim* we aim to overcome limitations for accessing methods that may be useful for all users interested in applying these techniques.

Still, *SegOptim* is only giving its first steps as a computational solution for such a complex problem. The roadmap of future developments includes (among others) user-defined fitness functions based on cross-validation results, integrating and testing more algorithms already available (for segmentation but mostly for classification), multi-classifier stacking/fusion, calculation of shape and context metrics for segments, the possibility of evaluating and performing optimization through supervised discrepancy measures or even unsupervised techniques. We are hopeful that researchers and practitioners may find the package useful for their activities and research, allowing to test, adjust and improve its functionalities over time.

Author contributions

Author name	Study conception and design	Sampling design, infield surveys and/or data collection	Data processing, analysis and/or modelling	Manuscript writing	Manuscript revision
João Gonçalves	☑		☑	☑	☑
Isabel Pôças	☑			☑	☑
Bruno Marcos			☑	☑	☑
Sander Mücher					☑
João Honrado				☑	☑

References

Adams, R., and L. Bischof. 1994. Seeded region growing. IEEE Transactions on Pattern Analysis and Machine Intelligence 16:641-647.

Baatz, M., C. Hoffmann, and G. Willhauck. 2008. Progressing from object-based to object-oriented image analysis.*in* T. Blaschke, S. Lang, and G. J. Hay, editors.

Object-Based Image Analysis - Spatial Concepts for Knowledge-Driven Remote Sensing Applications. Springer-Verlag, Berlin.

Baatz, M., and A. Schape. 2000. Multiresolution Segmentation: An Optimization Approach for High Quality Multi-Scale Image Segmentation. Pages 12-23 *in* Angewandte Geographische Informations-Verarbeitung, XII, Wichmann Verlag, Karlsruhe, Germany.

Bäck, T., D. B. Fogel, and Z. Michalewicz. 2000a. Evolutionary Computation 1: Basic Algorithms and Operators. 1st edition. IOP Publishing, Bristol, UK and Philadelphia, USA.

Bäck, T., D. B. Fogel, and Z. Michalewicz. 2000b. Evolutionary Computation 2: Advanced Algorithms and Operators. 1st edition. IOP Publishing, Bristol, UK and Philadelphia, USA.

Bastos, R., M. D'Amen, J. Vicente, M. Santos, H. Yu, D. Eitelberg, J. Gonçalves, E. Civantos, J. Honrado, and J. A. Cabral. 2016. A multi-scale looping approach to predict spatially dynamic patterns of functional species richness in changing landscapes. Ecological Indicators 64:92-104.

Bechtel, B., A. Ringeler, and J. Boehner. 2008. Segmentation for Object Extraction of Trees using MATLAB and SAGA. Pages 59-70 *in* J. Boehner, T. Blaschke, and L. Montanarella, editors. SAGA - Seconds Out. Hamburger Beitraege zur Physischen Geographie und Landschaftsoekologie.

Bhanu, B., S. Lee, and J. Ming. 1995. Adaptive image segmentation using a genetic algorithm IEEE Transactions on Systems, Man, and Cybernetics 25:1543 - 1567.

Blaschke, T. 2010. Object based image analysis for remote sensing. ISPRS Journal of Photogrammetry and Remote Sensing 65:2-16.

Breiman, L. 2001. Random Forests. Machine Learning 45:5-32.

Castilla, G., and G. J. Hay. 2008. Image objects and geographic objects.*in* T. Blaschke, S. Lang, and G. J. Hay, editors. Object-Based Image Analysis - Spatial Concepts for Knowledge-Driven Remote Sensing Applications. Springer-Verlag, Berlin.

Clewley, D., P. Bunting, J. Shepherd, S. Gillingham, N. Flood, J. Dymond, R. Lucas, J. Armston, and M. Moghaddam. 2014. A Python-Based Open Source System for Geographic Object-Based Image Analysis (GEOBIA) Utilizing Raster Attribute Tables. Remote Sensing 6:6111.

Clinton, N., A. Holt, J. Scarborough, L. Yan, and P. Gong. 2010. Accuracy Assessment Measures for Object-based Image Segmentation Goodness. Photogrammetric Engineering & Remote Sensing 76:289-299.

Clinton, N., L. Yu, and P. Gong. 2015. Geographic stacking: Decision fusion to increase global land cover map accuracy. ISPRS Journal of Photogrammetry and Remote Sensing 103:57-65.

Comaniciu, D., and P. Meer. 2002. Mean shift: a robust approach toward feature space analysis. IEEE Transactions on Pattern Analysis and Machine Intelligence 24:603-619.

Costa, G. A. O. P., R. Q. Feitosa, T. B. Cazes, and B. Feijó. 2008. Genetic adaptation of segmentation parameters.*in* T. Blaschke, S. Lang, and G. J. Hay, editors. Object-Based Image Analysis - Spatial Concepts for Knowledge-Driven Remote Sensing Applications. Springer-Verlag, Berlin.

Dragut, L., O. Csillik, C. Eisank, and D. Tiede. 2014. Automated parameterisation for multi-scale image segmentation on multiple layers. ISPRS J Photogramm Remote Sens 88:119-127.

Fernández-Delgado, M., E. Cernadas, and S. Barro. 2014. Do we Need Hundreds of Classifiers to Solve Real World Classification Problems? Journal of Machine Learning Research 15:3133-3181.

Freddrich, C. M. B., and R. Q. Feitosa. 2008. Automatic Adaptation of Segmentation Parameters Applied to Non-homogeneous Object Detection.*in* GEOBIA 2008 –

Pixels, Objects, Intelligence: GEOgraphic Object-Based Image Analysis for the 21St Century, Calgary, Alberta, Canada

Gonçalves, J., R. Henriques, P. Alves, R. Sousa-Silva, A. T. Monteiro, Â. Lomba, B. Marcos, and J. Honrado. 2016. Evaluating an unmanned aerial vehicle-based approach for assessing habitat extent and condition in fine-scale early successional mountain mosaics. Applied Vegetation Science 19:132-146.

Goslee, S. C. 2011. Analyzing Remote Sensing Data in R: The landsat Package. 2011 43:25.

Grybas, H., L. Melendy, and R. G. Congalton. 2017. A comparison of unsupervised segmentation parameter optimization approaches using moderate- and high-resolution imagery. GIScience & Remote Sensing 54:515-533.

Happ, P. N., R. S. Ferreira, G. A. O. P. Costa, R. Q. Feitosa, C. Bentes, R. Farias, and P. M. Achanccaray. 2016. Interseg: a distributed image segmentation tool.

Haralick, R. M. 1979. Statistical and structural approaches to texture. Proceedings of the IEEE 67:786-804.

Haupt, R. L., and S. E. Haupt. 2004. Practical Genetic Algorithms. 2nd Ed. edition. John Wiley & Sons, Hoboken, New Jersey.

Hay, G. J., and G. Castilla. 2008. Geographic Object-Based Image Analysis (GEOBIA): A new name for a new discipline.*in* T. Blaschke, S. Lang, and G. J. Hay, editors. Object-Based Image Analysis - Spatial Concepts for Knowledge-Driven Remote Sensing Applications. Springer-Verlag, Berlin.

Hijmans, R. J. 2016. raster: Geographic Data Analysis and Modeling. R package version 2.5-8. URL: https://CRAN.R-project.org/package=raster.

Hojjatoleslami, S. A., and J. Kittler. 1998. Region growing: a new approach. IEEE Transactions on Image Processing 7:1079-1084.

Huang, X., L. Zhang, and P. Li. 2007. Classification and Extraction of Spatial Features in Urban Areas Using High-Resolution Multispectral Imagery. IEEE Geoscience and Remote Sensing Letters 4:260-264.

Köhl, M., S. Magnussen, and M. M. 2006. Sampling Methods, Remote Sensing and GIS Multiresource Forest Inventory. Springer-Verlag, Berlin Heidelberg.

Lang, S. 2008. Object-based image analysis for remote sensing applications: modeling reality – dealing with complexity.*in* T. Blaschke, S. Lang, and G. J. Hay, editors. Object-Based Image Analysis - Spatial Concepts for Knowledge-Driven Remote Sensing Applications. Springer-Verlag, Berlin.

Leutner, B., and N. Horning. 2017. RStoolbox: Tools for Remote Sensing Data Analysis. http://bleutner.github.io/RStoolbox, https://github.com/bleutner/RStoolbox.

Li, M., L. Ma, T. Blaschke, L. Cheng, and D. Tiede. 2016. A systematic comparison of different object-based classification techniques using high spatial resolution imagery in agricultural environments. International Journal of Applied Earth Observation and Geoinformation 49:87-98.

Liaw, A., and M. Wiener. 2002. Classification and Regression by randomForest. R News 2:18-22.

Liu, Y., L. Bian, Y. Meng, H. Wang, S. Zhang, Y. Yang, X. Shao, and B. Wang. 2012. Discrepancy measures for selecting optimal combination of parameter values in object-based image analysis. ISPRS Journal of Photogrammetry and Remote Sensing 68:144-156.

Löw, F., C. Conrad, and U. Michel. 2015. Decision fusion and non-parametric classifiers for land use mapping using multi-temporal RapidEye data. ISPRS Journal of Photogrammetry and Remote Sensing 108:191-204.

Lu, M., J. Chen, H. Tang, Y. Rao, P. Yang, and W. Wu. 2016. Land cover change detection by integrating object-based data blending model of Landsat and MODIS. Remote Sensing of Environment 184:374-386.

Lucas, R., P. Blonda, P. Bunting, G. Jones, J. Inglada, M. Arias, V. Kosmidou, Z. I. Petrou, I. Manakos, M. Adamo, R. Charnock, C. Tarantino, C. A. Mücher, R. H. G. Jongman, H. Kramer, D. Arvor, J. P. Honrado, and P. Mairota. 2015. The Earth Observation Data for Habitat Monitoring (EODHaM) system. International Journal of Applied Earth Observation and Geoinformation 37:17-28.

Magdon-Ismail, M. 2000. No Free Lunch for Noise Prediction. Neural Computation 12:547-564.

Marpu, P. R., M. Neubert, H. Herold, and I. Niemeyer. 2010. Enhanced evaluation of image segmentation results. Journal of Spatial Science 55:55-68.

Martínez-López, J., B. Bertzky, F. Bonet-García, L. Bastin, and G. Dubois. 2016. Biophysical Characterization of Protected Areas Globally through Optimized Image Segmentation and Classification. Remote Sensing 8:780.

Meinel, G., and M. Neubert. 2004. A comparison of segmentation programs for high resolution remote sensing data. International Archives of the Photogrammetry, Remote Sensing and Spatial Information Sciences 35:1097-1105.

Meyer, D., E. Dimitriadou, K. Hornik, A. Weingessel, and F. Leisch. 2017. e1071: Misc Functions of the Department of Statistics, Probability Theory Group (Formerly: E1071), TU Wien. R package version 1.6-8. https://CRAN.R-project.org/package=e1071.

Michel, J., D. Youssefi, and M. Grizonnet. 2015. Stable Mean-Shift Algorithm and Its Application to the Segmentation of Arbitrarily Large Remote Sensing Images. IEEE TRANSACTIONS ON GEOSCIENCE AND REMOTE SENSING 53:952-964.

Montaghi, A., R. Larsen, and M. H. Greve. 2013. Accuracy assessment measures for image segmentation goodness of the Land Parcel Identification System (LPIS) in Denmark. Remote Sensing Letters 4:946-955.

Monteiro, A., J. Gonçalves, R. Fernandes, S. Alves, B. Marcos, R. Lucas, A. Teodoro, and J. Honrado. 2017. Estimating Invasion Success by Non-Native Trees in a National Park Combining WorldView-2 Very High Resolution Satellite Data and Species Distribution Models. Diversity 9:6.

Mücher, C. A., L. Kooistra, M. Vermeulen, J. V. Borre, B. Haest, and R. Haveman. 2013. Quantifying structure of Natura 2000 heathland habitats using spectral mixture analysis and segmentation techniques on hyperspectral imagery. Ecological Indicators 33:71-81.

Mücher, C. A., L. Roupioz, H. Kramer, M. M. B. Bogers, R. H. G. Jongman, R. M. Lucas, V. E. Kosmidou, Z. Petrou, I. Manakos, E. Padoa-Schioppa, M. Adamo, and P. Blonda. 2015. Synergy of airborne LiDAR and Worldview-2 satellite imagery for land cover and habitat mapping: A BIO_SOS-EODHaM case study for the Netherlands. International Journal of Applied Earth Observation and Geoinformation 37:48-55.

Mueller-Wilm, U., O. Devignot, and L. Pessiot. 2016. S2 MPC: Sen2Cor Configuration and User Manual (S2-PDGS-MPC-L2A-SUM-v2.3). ESA.

Nagendra, H., P. Mairota, C. Marangi, R. Lucas, P. Dimopoulos, J. P. Honrado, M. Niphadkar, C. A. Mücher, V. Tomaselli, M. Panitsa, C. Tarantino, I. Manakos, and P. Blonda. 2015. Satellite Earth observation data to identify anthropogenic pressures in selected protected areas. International Journal of Applied Earth Observation and Geoinformation.

Nauss, T., H. Meyer, F. Detsch, and T. Appelhans. 2015. Manipulating satellite data with satellite (R-package version 0.2.0; URL: https://cran.r-project.org/web/packages/satellite).

Nikfar, M., M. J. V. Zoej, A. Mohammadzadeh, M. Mokhtarzade, and A. Navabi. 2012. Optimization of multiresolution segmentation by using a genetic algorithm. Journal of Applied Remote Sensing 6:1-18.

Novelli, A., M. Aguilar, F. Aguilar, A. Nemmaoui, and E. Tarantino. 2017. AssesSeg—A Command Line Tool to Quantify Image Segmentation Quality: A Test Carried Out in Southern Spain from Satellite Imagery. Remote Sensing 9:40.

Oza, N. C., and K. Tumer. 2008. Classifier ensembles: Select real-world applications. Information Fusion 9:4-20.

R Development Core Team. 2017. R: A Language and Environment for Statistical Computing; URL: https://www.R-project.org/. R Foundation for Statistical Computing, Vienna, Austria.

Räsänen, A., A. Rusanen, M. Kuitunen, and A. Lensu. 2013. What makes segmentation good? A case study in boreal forest habitat mapping. International Journal of Remote Sensing 34:8603-8627.

Recio, M. R., R. Mathieu, G. B. Hall, A. B. Moore, and P. J. Seddon. 2013. Landscape resource mapping for wildlife research using very high resolution satellite imagery. Methods in Ecology and Evolution 4:982-992.

Ribeiro, A., J. Ranz, X. P. Burgos-Artizzu, G. Pajares, M. J. del Arco, and L. Navarrete. 2011. An image segmentation based on a genetic algorithm for determining soil coverage by crop residues. Sensors (Basel) 11:6480-6492.

Ridgeway, G. 2017. gbm: Generalized Boosted Regression Models. R package version 2.1.3. https://CRAN.R-project.org/package=gbm.

Rothlauf, F. 2011. Optimization Methods. Design of Modern Heuristics. Springer-Verlag, Berlin, Heidelberg.

Scrucca, L. 2013. GA: A Package for Genetic Algorithms in R. Journal of Statistical Software 53:1-37.

Teodoro, A. C., and R. Araújo. 2016. Comparison of performance of object-based image analysis techniques available in open source software (Spring and Orfeo Toolbox/Monteverdi) considering very high spatial resolution data. Journal of Applied Remote Sensing 10:1-22.

Tremeau, A., and N. Borel. 1997. A region growing and merging algorithm to color segmentation. Pattern Recognition 30:1191-1203.

van der Werff, H. M. A., and F. D. van der Meer. 2008. Shape-based classification of spectrally identical objects. ISPRS Journal of Photogrammetry and Remote Sensing 63:251-258.

Vaz, A. S., B. Marcos, J. Gonçalves, A. Monteiro, P. Alves, E. Civantos, R. Lucas, P. Mairota, J. Garcia-Robles, J. Alonso, P. Blonda, A. Lomba, and J. P. Honrado. 2015. Can we predict habitat quality from space? A multi-indicator assessment based on an automated knowledge-driven system. International Journal of Applied Earth Observation and Geoinformation 37:106-113.

Wiesmann, D., and D. Quinn. 2016. rasclass: Supervised Raster Image Classification. R package version 0.2.2. https://CRAN.R-project.org/package=rasclass.

Wolpert, D. H. 1996. The Lack of A Priori Distinctions Between Learning Algorithms. Neural Computation 8:1341-1390.

Wolpert, D. H., and W. G. Macready. 1997. No free lunch theorems for optimization. IEEE Transactions on Evolutionary Computation 1:67-82.

Yu, X., and M. Gen. 2010. Introduction to Evolutionary Algorithms. 1st edition. Springer-Verlag, London, UK.

SECTION III. General discussion and conclusions

CHAPTER 10 – Combining EO and predictive models to improve the monitoring of biodiversity and ecological change

The research developed in this thesis involved a set of six studies (Figure 10 - 1) aimed to contribute to fundamental and applied research around the analysis, assessment and monitoring of biodiversity patterns and trends. These complementary studies encompassed most of the scales, levels and facets that are intrinsic and relevant to biodiversity in terrestrial ecosystems. Although there are certain specificities pertaining to each study, the research plan also addressed cross-scale and/or cross-level dependencies, allowing (for example) to link species-specific aspects to more 'holistic' landscape pattern and dynamics.

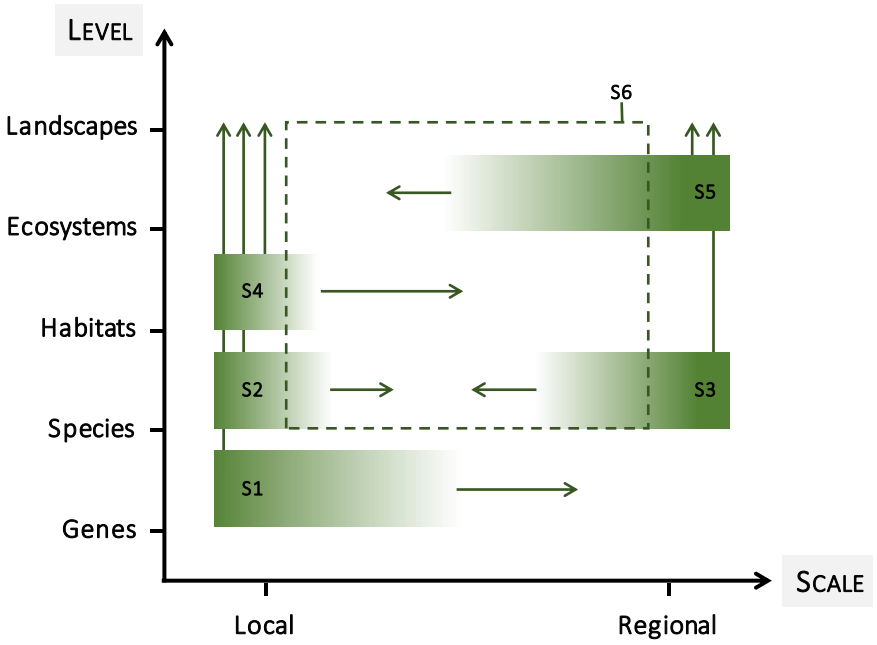

Figure 10 - 1 – Cross-scale and cross-level complementarity between the six research studies. Here we do not address the 'conventional' levels of biotic organization (Figure 1 - 5; (Allen and Hoekstra 1990)) although the obvious overlap (exceptions to 'species' which relates to population level; or 'habitat' relating broadly to the community level). Instead, we prefer to address more directly to the levels at which we analysed biodiversity status and change.

The research plan also aimed to exploring the potential and complementarities of modelling tools and Earth Observation (EO) data sources and methodologies to map, analyse and predict contemporary changes in biodiversity patterns, and to improve the current knowledge regarding the main driving factors underlying the observed (i.e., detected) or modelled alterations (e.g., employing climate and/or land cover/use

scenarios). In this context, our ultimate goal was to provide guidance and some of the fundamental building blocks of a cross-scalar and cross-level monitoring framework supported by the integration of EO-based indicators and EO-fed models to assist national and trans-national efforts related to the management and conservation of biodiversity.

This section presents a summary of research contributions from the several studies developed (S1 to S6), followed by a broader synthesis with recommendations for guiding the development of biodiversity assessments and monitoring schemes with different but complementary approaches: detection, modelling or the combination of both.

10.1. Species-level monitoring in Anthropocene landscapes: a focus on functional connectivity

In general terms, landscape connectivity can be defined from two distinct perspectives: (i) *structural connectivity* (which mainly relates to the spatial composition and configuration of landscape patches, such as the presence of barriers in the landscape matrix), and (ii) *functional connectivity* (which depicts how the behaviour of a dispersing organism is affected by landscape composition and spatial configuration) (Baguette and Van Dyck 2007). Thus, functional connectivity incorporates, either directly or indirectly, species-specific aspects (e.g., dispersal ability, habitat suitability and resistance to movement) and their interaction with landscape structure. As such, functional connectivity can be regarded as 'actual connectivity' from a species' perspective. The importance of landscape connectivity is vast as it is a crucial driving factor of the amount of dispersal among resource patches in fragmented landscapes, thus influencing gene flow, local adaptation, extinction risk, colonization probability, demographic rescue and the potential for organisms to move as a way to cope with climate change (Hodgson et al. 2009, Hodgson et al. 2012, McRae et al. 2012). Functional connectivity can further be defined and computed considering a *spatial component* (related to spatial patterns) and a *temporal component* (linking to the persistence of species in time, in a given location) (Auffret et al. 2015).

Given the importance of functional connectivity, in this thesis, we explicitly dedicated two studies (S1 and S3) to the improvement of methods regarding its analysis and quantification thus contributing for the assessment of fragmentation effects in gene flow or the ability to track climate change in presence of accelerated land use modifications. Moreover, in study S2 we addressed inter-annual fluctuations of predicted

habitat suitability, which may be an important filter to species persistence, thereby approaching the concept of 'temporal functional connectivity' (Auffret et al. 2015).

The comparative analysis performed in **study S1** allowed to clarify the effect of different landscape features on regional patterns of population connectivity and gene flow in two syntopic and pond-breeding amphibian species. Results from this study support that genetic differentiation in the test species tested is linked to environmental factors related to land and vegetation cover and revealed contrasting patterns of genetic structure in the two species, with stronger, finer-scale genetic differentiation in *Pleurodeles waltl*. Besides a common effect of topography for both species, we found that strictly compositional land-cover features did not play an important role in shaping genetic structure. Instead, we found remarkable differences associated to the role of fine-scale patterns of vegetation cover, vegetation water content and their spatial heterogeneity in shaping patterns of regional genetic structure for the two species. These differences were better captured by fine-scale remotely sensed spectral indices (NDVI and NDMI) portraying land cover, vegetation and moisture in a continuous fashion. These findings highlight the value of such indices in landscape genetics studies and provide support for the gradient continuous model of landscape representation (Cushman et al. 2010) instead of the 'classical' patch-corridor-matrix discrete model (Forman and Wilson 1995).

Another interesting outcome of this study was that different EO-based variables and different aspects of their spatial structuring (quantity or variation) were most important in shaping patterns of gene flow for the two species. This is surprising considering the strong overlap in their geographic ranges, probably reflecting similar ecological requirements at the macro (bioclimatic) scale (Sillero et al. 2009). However, at a regional scale, vegetation amount played a key role in *Pelobates cultripes*, whereas in *P. waltl* the spatial heterogeneity in vegetation coverage and water content were more important. This may also indicate that *P. waltl* is more sensitive to drought conditions and that climate change may further imperil this species. In addition, model results also suggest that low-resistance areas (with importance for connectivity) are less common in the landscape for *P. waltl* than for *P. cultripes.* This observation, in conjunction with the inferred lower dispersal ability in *Pleurodeles*, probably make this species more vulnerable to the effects of fragmentation.

In **study S3**, we performed an assessment of the vulnerability response to landscape fragmentation of reptile and amphibian species (characterized by low-

dispersal abilities) in the presence of accelerated changes in both global climate and local land use. To assess this, we evaluated current distributions of the test species and projected distribution shifts triggered by future environmental changes. This was accomplished by combining SDMs with functional connectivity analysis.

The results from this study revealed that, within a relatively short time-frame, environmental changes may cause severe impacts on the test species, with strong contractions in suitable area for most of them. Our findings are consistent with previous studies reporting substantial range contractions for herptile species in the Iberian Peninsula under future environmental changes (Araújo et al. 2006, Carvalho et al. 2010). The study species presenting current small ranges in Portugal (*i.e.*, *Chioglossa lusitanica, Anguis fragilis* and *Lacerta schreiberi*) will potentially suffer an important loss of suitable areas. Moreover, *C. lusitanica* and *L. schreiberi* are threatened by other pressures too (IUCN 2014), exacerbating the synergistic effect of environmental changes. Conversely, *Epidalea calamita*, with a widespread range and higher dispersal capacity, is projected to maintain or even expand its potential suitable area.

Overall, connectivity analyses highlighted an overall pattern widely dependent on the complex interplay between the spatial configuration of source/target areas (*i.e.* respectively, areas with projected conservation or loss of environmental suitability in the future) and landscape elements increasing landscape resistance (such as motorways). Species experiencing a higher contraction of suitable areas clearly showed lower connectivity due to an increase in landscape resistance and geographic distance between “lost” and “kept” areas. The stability and integrity of migration corridors for these species may be further impacted by the presence of motorways (Andrews et al. 2008), making them even more vulnerable to extinction or isolation.

Contributions of study S3 also extend to methodological improvements, as we proposed a three-step approach to assess the vulnerability of species to several environmental change processes, combining species distribution dynamics with functional connectivity. Connectivity analyses allowed the identification and evaluation of migration corridors, based on a graph-theoretical approach explicitly accounting for species-specific landscape matrix resistance, an analytical approach holding wide breadth and acceptance (Minor and Urban 2008, Pascual-Hortal and Saura 2008, Decout et al. 2012). This approach is characterized by its low data requirements potentially making it more generalizable and thus potentially more suited for assessing multiple species. Complementarily, using the proposed *MFD* or *SPsum* indices for comparing the full spectrum of connectivity values across a study area between different

species provides a preliminary regional-scale synoptic overview of connectivity patterns. This allows comparing different regions, identifying critical situations and selecting a subset of relevant areas to develop detailed studies.

Analysing shifts in species distributions and habitat suitability conditions, with resulting alterations in biotic communities' and ecosystem functioning (Pecl et al. 2017), is at the core of applied ecological research allowing to investigate the joint effects of 'extreme' disturbance events (e.g., wildfires, droughts), land use alterations and climate change. The development of SDMs along with the availability of current data and future projections on climate and land use paved the way to forecast future biodiversity changes (Guisan and Thuiller 2005). In parallel, the increasing availability and diversity of EO platforms currently provide unparalleled data on the Earth surface biophysical properties and 'spectral traits', their spatiotemporal variation and change at several levels and scales (Lausch et al. 2016). Together, these innovations call for innovative ways of combining concepts, methodologies and datasets from both fields for improving biodiversity monitoring.

In **study S2**, we addressed the above challenge by investigating how EO-based variables related to ecosystem functioning can be used to improve predictions and to track short-term changes in habitat suitability of a vulnerable plant species (*V. micrantha*) protected under national and European laws. Our results highlight the added value and the predictive ability of EO-based variables, related to ecosystem functioning, emphasizing their usefulness for developing robust habitat suitability predictions (Zimmermann et al. 2007, Bradley and Fleishman 2008, Cord et al. 2014). In particular, water availability (from MODIS actual evapotranspiration product) largely contributed to explain landscape patterns of habitat suitability (Hawkins et al. 2003, Fisher et al. 2011) by capturing vegetation functional attributes and the heterogeneity of landscape mosaics. From EO-based variables, we also found that the target species was associated to landscapes with high levels of productivity, seasonality (intra-annual variation) and water availability. In turn, high levels of productivity have been positively related to species diversity (e.g., Bai et al. 2007), which matches our observations that the species is often found in species-rich and heterogeneous landscape mosaics. Such assessment was possible due to the inclusion of EO-based predictors, otherwise it would be difficult to characterize these functional dimensions of the species habitat. Although with comparatively less importance, structural features related to soils and to landscape composition and configuration yielded additional contributions to explain habitat suitability. Overall, these findings emphasize the importance of simultaneously

considering landscape attributes related to function, composition and spatial configuration to improve the explanation of ecological patterns (Vaz et al. 2015).

Based on a yearly time-series for EO-based predictors, we also explored the effects of short-term fluctuations in environmental conditions on the spatiotemporal dynamics of habitat suitability. Results from this study contributed to clarify the mechanisms underpinning species' responses to fluctuations in habitat suitability derived from multiple and often overlapping sources of disturbance, such as land cover changes and wildfires, but also due to inter-annual climatic variability. By focusing on the landscape level (as an integrative level for performing analysis), our approach presents several advantages for the focal species conservation, namely since local and regional management frequently target this scale for planning (e.g., Sayer et al. 2013). From a monitoring perspective, this allows to identify and assess landscape change processes and dynamics (Nagendra et al. 2013, Mairota et al. 2015) affecting habitat suitability and biodiversity change.

Overall, we propose that species-level habitat suitability time-series can provide useful inputs for monitoring and, hence for the conservation of species by allowing to assess and rank suitable habitat areas according to their relative stability through time and thus to the potential persistence of species (temporal functional connectivity *sensu* (Auffret et al. 2015)). Among other aspects, EO data could be used for monitoring the dynamics and the temporal stability of suitable locations and their habitat quality (Mairota et al. 2015, Vaz et al. 2015) and serve as an early-warning system helping to identify critical changes in essential variables (Skidmore et al. 2015).

10.2. Habitat and ecosystem monitoring for effective management of protected area networks

Networks of protected or otherwise classified areas (PA's), have grown globally during the last decades (UNEP-WCMC and IUCN 2016) and remain as one of the most important strategies for nature conservation, to halt the loss of biodiversity and to promote high levels of ecosystem services supply. In this context, multi-scalar monitoring of PA's (from local to regional scales) is especially important given their vulnerability to anthropogenic pressures (e.g., land use and climatic changes) as well as to assess the effectiveness of PA's in fulfilling national and international nature conservation agendas (Nagendra et al. 2013).

Although most monitoring efforts until now have relied on field surveys, Remote Sensing/Earth Observation (RS/EO) data can play a key role in defining baselines of the extent and condition of habitats of conservation interest, in tracking the actual distribution of species or their habitat suitability conditions and assess species diversity patterns and their changes. Furthermore, EO can be used to identify disturbances, land degradation or recovery paths following specific events or processes (e.g., wildfires) (Nagendra et al. 2013). Among other aspects, EO data provide additional and complementary inputs and data to support a systematic, repeatable and (in some cases, depending on the platform/sensor used) synoptic coverage of Earth ecosystems. To further explore this potential of RS/EO for protected areas monitoring, we developed two studies aimed to improve the monitoring of focal mountain habitat types in Natura 2000 sites (study S4) or of forest ecosystem stability in the National Network of Protected Areas (study S5).

Thus, in **study S4** we developed and tested methods for fine-scale mapping of small habitat areas based on UAV imagery. For testing purposes, we mapped the extent of several Natura 2000 priority habitats in a mountainous area under land use and rural abandonment. We found that our proposed approach based on supervised classification and supported by UAV optical imagery obtained good overall accuracy, despite some decrease in classification performance in situations of high interspersion of vegetation/habitat types. At the class level, grasslands (habitat type 6230*), which form the vegetation matrix in the test-site, attained better results, while wet heathland (4020*) obtained only moderate accuracy values as evaluated by test data.

Overall, a comparison to reference producer and user accuracy values collected from literature revealed that our UAV-based approach presented above-median performance for both grassland and heathland habitats (in most cases above the 75% quartile, with the exception of producer accuracy for habitat type 4020*). These results suggest that the low spectral resolution of UAV imagery may be partially compensated by its very-high, sub-decimetre spatial resolution, and thus provide accurate discrimination via textural descriptors calculated with different kernels. They also highlight the cost-efficiency of UAV-based methodologies, since most similar habitat classification approaches currently employ very-high resolution imagery from commercial satellite platforms such as IKONOS, QuickBird or WorldView (e.g., Buck et al. (2015), Förster et al. (2008), Hernando et al. (2012)) with comparatively much higher acquisition costs.

This methodology also allowed distinguishing several degraded patches of particular habitat types in a quite challenging, dynamic and dense vegetation mosaic. In some cases, we are able to detect the presence of dry heathland, bare soil patches or

shallow water puddles neighbouring habitat type 4020*, possibly identifying situations where the habitat occurs in less favourable conservation conditions, likely due to over-grazing and localized used of fire. We were also able to identify patches of habitat type 6230* exhibiting a less favourable habitat condition, related to visible changes in the typical vegetation structure and species-assembly. Such information may prove useful for management and conservation of the focal habitats, and it is still poorly explored in ecological applications of UAV imagery (with exceptions, e.g., Spanhove et al. (2012)).

Our results strongly emphasized the usefulness of features derived from photogrammetric digital surface models, as well as different texture features calculated from colour imagery as observed in previous UAV applications (e.g., Laliberte & Rango 2008; Laliberte & Rango 2009). These features included useful vicinal and context information in the classification pipeline for identifying different vegetation/habitat types and their edges. Computationally inexpensive texture features such as those based on the calculation of local statistics (e.g., mean, variance) for various kernel sizes obtained better results in comparison, for example, with Haralick features (which comparably require much longer computation time and resources). Band-ratios, previously highlighted as important in the context of UAV image classification (e.g., Dunford et al. 2009; Laliberte & Rango 2011), also obtained better results when compared to raw input data.

In **study S5**, we proposed and tested an approach to measure forest ecosystem stability and PAs performance based on indicators calculated from an EO time-series of a spectral vegetation index (VI) – MODIS MOD13Q1 Enhanced Vegetation Index (EVI). Our approach builds on the perspective that forest stability dynamics relies on the interactive and continuous relation between disturbance and the response that follows it. In turn, EO VI time-series, due to their high-temporal resolution and coverage, are suitable for capturing this disturbance-response binomial thus allowing to quantify ecosystem stability.

In this study, we also addressed the challenge of assessing PA forest stability performance by statistically comparing the distribution of stability indicators inside vs. outside PAs. This relative assessment of stability provides a novel and systematic way to rank PAs performance submitted to pressures acting in a broader regional context.

Results show a complex pattern in terms of PA forest stability performance across the national network, both among and within PAs possibly reflecting spatial differences in disturbance regimes, in the occurrence of stochastic events, but also contrasting land cover patterns and land use dynamics.

To investigate the potential factors underlying forest stability across selected PAs, we applied a multi-model inference framework based on a set of plausible hypotheses.

From models we found that the most striking (although expectable) effect was related to forest fires, with a clear negative effect. We also found an interaction between forest fires and PA elevation which may be related to different fire regimes occurring on lowland *vs*. mountainous PA. Forest composition and structure were also found to have a strong control over stability performance across the PA network. Contrary to forest fires, which strongly drive the disturbance regime, forest composition and structure play a stronger role in post-disturbance response. We found a strong positive signal in stability related to the fraction cover of broadleaf forests. Contrarily, we found some evidence that coniferous forests have a negative effect on stability. Forest structure, and particularly vertical structure, was found to have a strong effect on stability. Specifically, PAs hosting forest areas with taller forest canopies and higher vertical complexity/variability were found to be more stable. These structural features, in combination with forest composition, may discriminate older and more diverse forests that tend to have more stable dynamics.

We also found positive effects of total forest area and connectivity between forest patches on stability. In fact, PAs with higher forest cover and higher connectivity between forest areas are relatively more stable. As for PA attributes, we found a strong positive effect of PA size, with larger parks having a higher stability performance. We could not find evidence for an expectable effect of PA age on relative forest stability, which may be partially explained by the disturbance regime (namely involving wildfires) observed in some of the 'older' PAs.

Overall, these multiple effects should not be seen in isolation as they are, in fact, welded together in a non-linear and complex socio-ecological web.

10.3. Improving GEOBIA methods for assessment of biodiversity and ecological change

Efficient mapping and detection of ecological change requires the application of high-performance algorithms for EO imagery processing pipelines. In this sense, GEOBIA methods have strongly contributed to the ability of analysing high- and very-high spatial resolution EO imagery by enhancing the available toolset and introducing new concepts in this domain (Hay and Castilla 2008, Blaschke 2010). Albeit their undisputable usefulness for biodiversity research and monitoring (e.g., Mücher et al. 2013, Lucas et

al. 2015, Mücher et al. 2015), GEOBIA methods remain difficult to set up and compare, especially image segmentation algorithms.

In **study S6** we addressed this challenge by developing a generic approach to object-based analysis comparison and optimization which integrates two crucial steps in GEOBIA workflows typically exhibiting mutual dependencies: image segmentation, and classification (Baatz et al. 2008). Due to their flexibility and power, we selected Genetic Algorithms as a suitable method to optimize and fine-tune segmentation parameters. Overall, the use of GA for optimizing image segmentation parameters with the aim of maximizing the thematic accuracy of supervised classification, together with the comparison of multiple techniques, represents a significant advancement in GEOBIA workflows.

A new open-source R package (*SegOptim*) implements the proposed approach with a large set of features for testing, comparing and optimizing different image segmentation and classification algorithms within the R environment and computing language (R Development Core Team 2017). The several tests performed for this study strongly suggest that *SegOptim* provides a novel and robust comparison of several state-of-the-art algorithms and software focused on the object-based analysis of EO data for different application contexts [see also, e.g., (Meinel and Neubert 2004, Marpu et al. 2010, Li et al. 2016, Teodoro and Araújo 2016)].

The tests performed to evaluate our GA-based method covered a wide range of EO images and environmental conditions. Results show that no particular combination of an image segmentation and a classification algorithm is suited for all the tasks/objectives suggesting an empirical verification of the "*no free-lunch theorem*" (NFLT; (Wolpert 1996, Wolpert and Macready 1997)) for object-based image classification problems. Besides theoretical implications, this means that comparing and optimizing methods procedures is crucial for determining which ones are more suited for a particular objective or task. For this purpose, *SegOptim* provides the required functionalities.

The results from our tests also showed that, depending on the specific problem under consideration, either segmentation algorithms produce greater differences in object-based analyses or (more likely) different classifiers will generate stronger differences. In addition, comparisons may be of particular importance given that we found strong differences between "best" and "worst" performers for the same task/objective, which may imply that the probability of obtaining sub-optimal results without comparing available methods and/or optimizing its parameters is fairly high.

Thus, our new approach, by optimizing and comparing distinct image segmentation and classification algorithms, can contribute to improve GEOBIA workflows with benefits for land cover mapping, detecting target species or habitat types of conservation interest or concern and thus provide better estimates of ecosystem patterns (e.g., patch size distribution, connectivity), ecosystem processes (e.g., colonization, invasion, succession), ecosystem functions (e.g., primary production) and its services.

10.4. Earth Observation detection and ecological modelling – combining approaches for improved biodiversity monitoring and assessment

In broad strokes, regarding the use of EO data and ecological models, **three distinct approaches** were used in the development of this thesis research plan: (i) detection (studies S4 and S6; and partially, S5), modelling (study S3), and a combination of both approaches (studies S1, S2; and partially S5). These approaches have different characteristics, workflows and processing pipelines, and answer to different problems regarding the overarching thesis objectives, generally linked to the assessment and monitoring of biodiversity and ecological change.

Detection-based approaches typically refer to the mapping or geographical representation of the actual (physical) distribution of the entities of interest (or their properties) using EO data. These entities can be species, habitats, communities, land cover types or ecosystems that are of interest for management, conservation or monitoring. This approach is similar to what Turner et al. (2003) define as the 'direct' remote sensing of organisms, species assemblages or communities, made possible due to very-high spatial and hyperspectral space or airborne sensors (among other). Commercial very-high spatial resolution spaceborne sensors such as IKONOS, QuickBird, GeoEye, OrbView, RapidEye or WorldView-2 (the latter two explored in study S6; see also Table 2 - 1) greatly increase the accuracy of detection, identification and representation of small objects at spatial scales only previously available from airborne platforms (Wang et al. 2010). Moreover, novel platforms such as lightweight Unmanned Aerial Vehicles (UAV) currently provide highly detailed and scale-appropriate measurements of ecological phenomena with exciting opportunities for detection-based approaches to biodiversity assessment (Anderson and Gaston 2013), some of which already explored in this thesis (studies S4 and S6).

Detection-based approaches require that the 'spectral traits' of the monitoring targets (*sensu* Lausch et al. (2016); including optical, thermal or radar spectra) can be

directly measured by the sensor with adequate spectral, spatial and/or temporal resolutions. In this case, typically some kind of statistical or machine-learning algorithm is employed to 'learn' the spectral, textural or contextual properties of each entity and map them across space and time. GEOBIA methods, such as those explored and developed in this thesis (study S6), are a particular toolkit employed in detection-based approaches. Besides these empirical or correlative approaches, process-based eco-physiological or radiative-transfer models can be coupled with EO measurements to estimate certain biophysical variables of interest (e.g., LAI, GPP, NPP, canopy structure, biomass, carbon storage and sequestration, leaf chlorophyll) (e.g., Lu et al. 2017, Zhang et al. 2017). Despite the undisputable usefulness of such approach, process-based models were not explored in this thesis.

By employing methods of temporal comparison between different time-slices of processed or classified EO spectral data (current vs. past status; e.g., delta calculations, change vector analysis, confusion matrices) or using time-series analysis (e.g., trend analysis, time-series decomposition) we are able to detect actual/observed changes (either gradual or abrupt) or to obtain a diagnosis of temporal fluctuations and trends. However, due to their 'data-driven' nature, detection-based approaches are limited by the amount of historical/archive data, the temporal resolution of EO imagery, the existence of data gaps (caused by, for example, cloud or snow cover) as well as the continuity of EO missions and the coherence in the design of sensor technologies which affect data homogeneity (although this last can be overcome with some data integration and fusion techniques). Nonetheless, with the current increase in amount and diversity of EO sources and platforms (with varying spectral, spatial and temporal resolutions), EO data availability has been growing along with the usefulness and adequacy of detection-based approaches in ecological and biodiversity applications (Figure 10 - 2).

Model-based approaches provide a set of robust and powerful concepts and tools to understand ecological patterns and their changes. In a broad sense, ecological models are conceptual and mathematical constructs, either analytic or simulation-based, that can be used to study complex ecological patterns and processes and predict how populations or ecosystems might change. Quantitative models can thus translate ecological hypotheses into predictions that can be evaluated with existing or new data (Jackson et al. 2000). Given their importance for conducting the research plan, we emphasize in this sub-section models based on empirical/correlative approaches supported by statistical (e.g., GLM, GAM, mixed models) or machine-learning (e.g., Random Forests, Neural Networks) techniques. These models can be further subdivided

into *predictive* or *explanatory*, depending if the core objective is (respectively) to obtain spatiotemporal predictions (as in studies S2, or S3), or to answer some fundamental question regarding the causal or driving factors underlying some phenomena (studies S1 and S5). In several cases, these objectives can be mixed if, for example, there is an interest in simultaneously testing some specific hypothesis and obtaining spatiotemporal predictions that can be used in subsequent analyses (e.g., connectivity between suitable habitat patches).

Species Distribution Models (SDMs; which are of particular importance to the core research developed during this thesis) can be defined by this 'hybrid' nature (mostly predictive but also used for explanatory purposes). In a nutshell, SDMs are correlative models used to investigate species ranges and ecological responses to environmental determinants (Elith and Leathwick 2009, Elith et al. 2010). The increasing amount of spatial thematic data (e.g., climate, topography, land cover, vegetation) and the availability of global-scale bioinformatic databases facilitated the development and the widespread use of SDMs for answering many of the pressing challenges in ecology, biogeography and biodiversity management and conservation (despite the few 'real' operational applications in conservation and decision-making; e.g., (Guisan et al. 2013)). Moreover, SDMs excel at making spatiotemporal predictions (Figure 10 - 2) and their growing application can also be attributed to this powerful ability. Thanks to this, SDMs have been amply used to investigate biogeographic hypothesis regarding species distributions, (re-)colonization pathways and past refugia during glaciations (using model hindcasts based on past climate reconstructions) or to investigate species range shifts as a consequence of climate change (using model forecasts based on future climate projections). For these assessments, climate is considered the main driving factor (and perhaps the focus of most publications to date), allowing to obtain projections at large temporal and spatial scales. In contrast, 'data-driven' detection-based approaches, which rely on observed remotely sensed spectral data, cannot be used to investigate past dynamics beyond the platform/sensor data archive, nor to forecast future outcomes. For such objective (among others) one must consider the combined use of EO data and models.

By combining the strengths of both models and EO data (either as time-slices or time-series of continuous or discrete variables), applications to biodiversity monitoring and ecological change assessment broaden tremendously. **Combined approaches** allow to use EO-fed models to analyse and quantify certain aspects of species or assemblages (most often), such as their habitat suitability, abundance or diversity, even when these entities are 'invisible' to EO-sensors. Frequently, this avenue of enquiry is

the only one viable, if and when the biological entities of interest are not 'large' enough to affect the signal captured by the sensor (i.e., spatial resolution is not fine enough) or because spectral separability is not possible making them undetectable. Therefore, 'indirect' remote sensing of biodiversity based on coupling models with EO-based environmental variables as proxies can overcome certain limitations and still provide meaningful outputs. For example, many species are restricted to (or strongly associated to) certain discrete habitats, such as woodlands, grasslands, or seagrass beds, that can be identified by EO techniques (Turner et al. 2003). Moreover, due to EO's ability to capture multiple environmental aspects, EO-fed models can test hypotheses and assess the effect of different habitat and ecosystem dimensions (including structure, composition and/or function) on species habitat suitability, distribution, abundance or diversity. In particular, ecosystem functional attributes (such as those addressed in studies S2 or S5) may provide an additional dimension seldom addressed in ecological studies to date. Complementarily to optical platforms, features derived from radar, LiDAR and hyperspectral sources currently provide additional variables to characterize spectral and spatial heterogeneity, habitat structure and its complexity or species-specific requirements, with benefits for obtaining model-based predictions of species habitat suitability or species diversity (He et al. 2011, Colgan et al. 2012, Simonson et al. 2012, Rocchini et al. 2016, Betbeder et al. 2017).

Combined approaches are especially well-suited for providing model-based projections of change, if and when multiple time-slices or time-series of EO data are available. These issues were developed in studies S2 and S5, respectively to evaluate short-term changes in habitat suitability at species-level, and to assess ecosystem-level stability and the factors driving it. As another example, simulation models (based on agent-based or cellular automata approaches) can be used to provide future land cover projections (Almeida et al. 2005), which in turn can be fed into SDMs to make predictions about species habitat suitability or to obtain species diversity projections. This way, we extend the ability of EO-based data (in particular, land cover products) not only to hindcast or predict current biodiversity status and trends (based on EO data archives) but also to forecast future pathways based on scenario projections (Bastos et al. 2016). As discussed above, due to the versatility of combined approaches, besides employing EO data archives to provide actual estimates of biodiversity, this approach can also couple with simulation-based or process-based models to make projections of future outcomes (Figure 10 - 2). This way, a large spectrum of contemporary challenges in

applied ecology, could (and already is) being addressed by a combination of models and EO data.

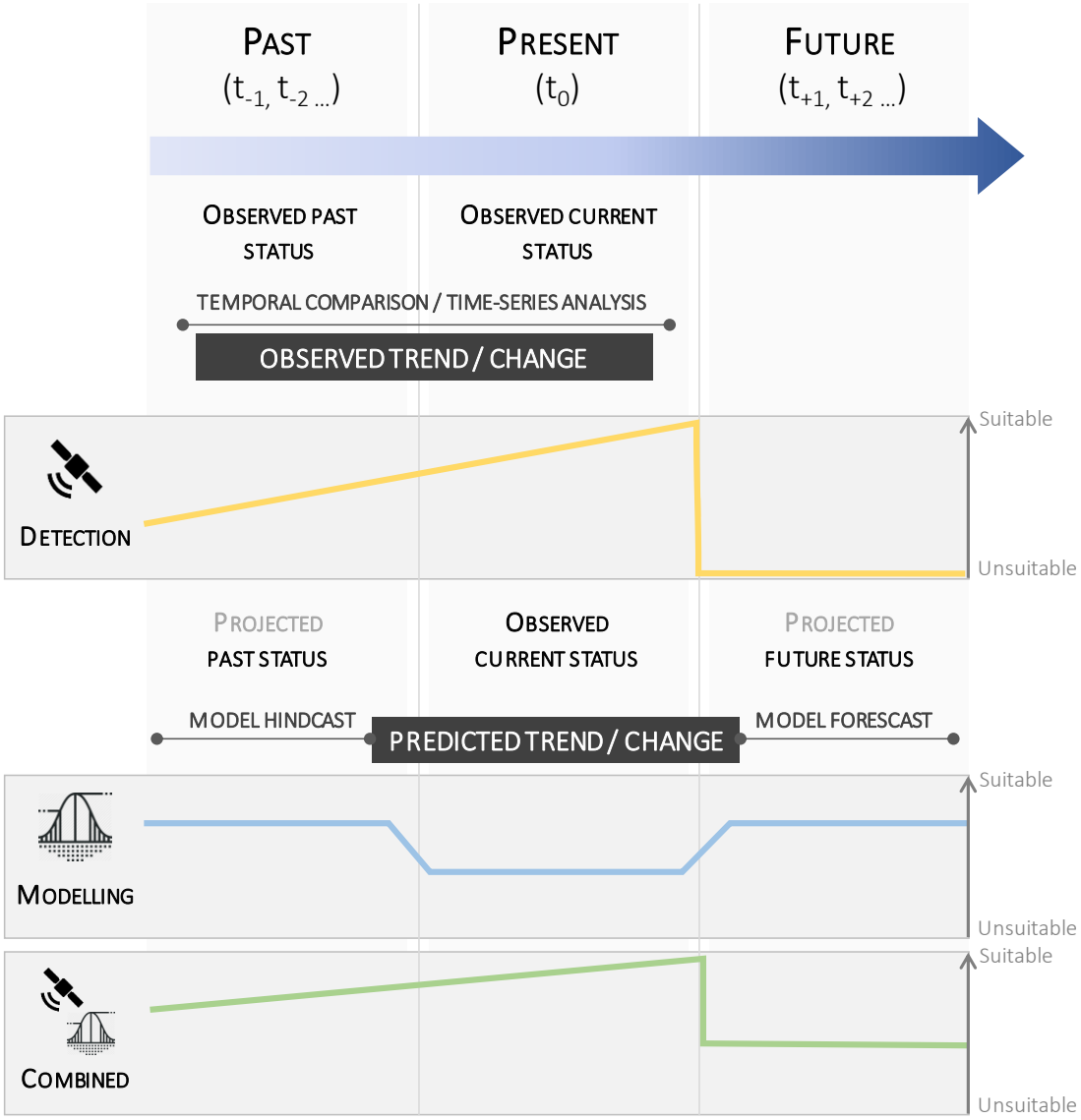

Figure 10 - 2 – Relative adequacy/suitability of: (i) detection, (ii) modelling, or, (iii) combined approaches for biodiversity monitoring and assessment based on each approach characteristics (pros and cons') and using time as an integrator. The 'observed status' here refers to (for example) the actual distribution of a species or natural habitat when using a detection approach, and the 'projected status', to its modelled 'potential' distribution when using a modelling or combined approach.

Despite the usefulness and potential of these combined approaches, pitfalls do exist. Depending on the scale of analysis, the characteristics of species or assemblages, and the spatial resolution of EO data, some caution is required to not mistaken detection ('direct') and combined ('indirect') approaches, thus potentially introducing some biases. Such problems may occur when including continuous remote sensing variables that could inadvertently describe the actual species distribution instead of its habitat

suitability. This is largely due to unique spectral or temporal characteristics of the target entities as captured by EO sensors (Bradley et al. 2012). Similarly, scale, sampling and ecological requirements should be accounted for when linking land cover-based discrete variables to species habitat suitability. Moreover, as uncertainties arise from both components (EO data and models), error and uncertainty propagation should be carefully considered, handled and communicated to better profit from the integration of both parts. For example, different levels of spatial accuracy and uncertainty exist when dealing with the actual (detected) distribution of a species in comparison to its (modelled) potential distribution. Depending on the specific objectives, one approach may be more suited than the other. Thus, a project aiming to eradicate or control an invasive tree species may find more useful a detection-based approach, due to its ability of very accurately track the progress of eradication actions. However, if the objective is to understand key driving factors behind invasion pathways, describe or map regional distribution patterns or forecast its potential expansion in face of land use or climate change, then model-based or combined approaches will provide more suited concepts and tools.

Overall, and most importantly, combined approaches can synergistically leverage the potential of SDMs (or other sorts of ecological models) and EO products by amplifying the applicability of both, providing new research avenues and answering to important challenges in biodiversity management and conservation in the Anthropocene era. Upcoming developments in both fields, and new ways to integrate both components, will certainly push the envelope even further.

Taking into consideration the scope, goals and focal biodiversity components of representative Global, Continental (European) and National observation/monitoring programmes, initiatives, networks, or policy instruments, in Table 10 - 1 we provide a **tentative synthesis** of adequacy for each of the different three approaches: detection, modelling or combined. This exercise builds on the characteristics (‘pros and cons’) of each approach described above, to assess their relevance and ability to fulfil the main requirements and objectives in terms of biodiversity assessment or monitoring that have been set in each instance. This evaluation is based on the best knowledge and most updated literature concerning each case; still, there may be some degree of subjectivity in the attribution of adequacy categories.

Several initiatives (listed in Table 10 - 1) already use detection-based or EO-fed modelling methodologies (e.g., CBD, ECOPOTENTIAL, SWOS), however, in some other

instances, well-integrated and well-formulated combined approaches could greatly enhance the existing ability to provide meaningful indicators for monitoring the progress and attainment of conservation objectives. For example, Natura 2000 reporting (regarding the extent and condition of habitat types) or SEBI indicators, which pertain to the European sphere (but extend to the national level of each member state), would surely benefit from well-designed detection and/or combined approaches to provide more systematic and temporally-homogeneous indicators for assessing the conservation status of natural and semi-natural habitat types. Still, commonly agreed methodologies and supporting data sources for addressing such challenge are still a distant mirage. Addressing the issues of method transferability by employing more generalizable approaches fed by free EO data sources (e.g., Copernicus' Sentinel platforms), limiting ground-data dependence and making code and image processing/analysis pipelines readily and openly available may help to overcome some of the currently identified operational shortcomings (Vanden Borre et al. 2017).

At the national level (more specifically in the Portuguese case), many opportunities also exist to implement detection-based or combined approaches to design biodiversity monitoring structures. In combination with distributed infrastructures for biodiversity data management and sharing, such processing pipelines would benefit the implementation and evaluation of conservation policies, the assessment of short and long-term impacts of infrastructures (e.g., transportation, energy production) and the regional and local adaptation to global environmental change. Moreover, connecting citizen-based field monitoring programmes (such as the Annual Census of Common Birds from SPEA[10]) to EO time-series of environmental data, also holds promising opportunities to investigate changes and trends in species diversity and community assemblages and to devise indicator-based early-warning systems.

[10] SPEA is the Portuguese Society for the Study of Birds, "*an environmental non-profit organization whose mission is to support research and conservation of wild birds and their habitats, by promoting sustainable development for the benefit of future generations*" (http://www.spea.pt/en/).

Table 10 - 1 – Current adequacy of each approach (detection, modelling or combined) to support the objectives of the listed policies, observation networks, initiatives or projects: [●] totally suitable for most of the requirements or objectives; [●] partially suitable to fulfil some of the objectives or requirements [●] unsuitable to fulfil most or some of the objectives or requirements. The attribution of each adequacy category is based on subjective judgement and the most recent information available.

Spatial domain / Name		Type	Biodiversity components			Temporal domain of assessment	Approach		
			Level	Scale	Facet				
			Genes Populations Communities Ecosystems Landscapes	Coarse (global to regional) Fine (local)	Composition Structure Function	Past Current Future	Detection	Modelling	Combined
Global	GEOBON	Initiative / Observation Network	P, C, E	C	C, S, F	P, C, F	●	●	●
	ILTER	Initiative / Observation Network	P, C, E	F	C, S, F	P, C	●	●	●
	IPBES	Organization / Initiative	G, P, C, E, L	C, F	C, S, F	P, C, F	●	●	●
	CBD / Aichi Biodiversity Targets	Organization / Initiative	G, P, C, E, L	C, F	C, S, F	P, C, F	●	●	●
Continental (Pan-European)	EUBON	Initiative / Observation Network	P, C	C	C, S	P, C, F	●	●	●
	ESA Copernicus	Observation programme	E, L	C, F	C, S, F	P, C	●	●	●
	CAP	Policy / Strategic outlook	P, C, E, L	C	C, S	P, C	●	●	●
	IRENA	Monitoring / Indicator set	P, C, E, L	C	C, S	P, C	●	●	●
	Habitats Directive / Natura 2000	Policy / Conservation Network	P, C, E	C, (F)	C, S	C	●	●	●
	SEBI	Monitoring / Indicator set	G, P, E	C	C, S	C	●	●	●
	LUCAS	Observation programme	L, E	F	C, S	C	●	●	●
	ECOPOTENTIAL	Research project	P, C, E, L	F	C, S, F	C, F	●	●	●
	SWOS	Research project	E	F	C, S, F	P, C	●	●	●
National (Portugal)	NSBC monitoring	Policy / Strategic outlook	P, C, E, L	C, (F)	C, S	P, C, (F)	●	●	●
	Impact assessment monitoring	Observation programme(s)	P, C, E	F	C, S	P, C, (F)	●	●	●
	Common birds monitoring	Citizen-based monitoring programmes	P, C	C	C, S	P, C	●	●	●

CHAPTER 11 - Conclusions and outlook

Based on a comprehensive framework including multiple levels of biological and ecological organization, various scales and different facets of biodiversity, this thesis aimed to improve the available methods and toolset to evaluate biodiversity patterns and their change, and to provide insights regarding the adoption of EO technologies for that endeavour. From a methodological viewpoint, three complementary approaches were explored during the research plan: detection, modelling and combined; each with its own set of advantages and shortcomings.

In this final chapter we provide a general summary of research contributions of the several studies, from the advancement in methods and the state of knowledge up to operational features surrounding the adoption of developed concepts, methodologies and tools for biodiversity monitoring and assessment. Along this chapter, we also highlight some potential ways to advance the work initiated in this thesis and provide an outlook to potential connections with current challenges in each topic.

11.1. Summary of contributions and future developments

Study S1 explores the dynamics and conservation of Mediterranean habitats, revealing a positive effect of structural heterogeneity on gene flow in pond-breeding amphibians. More generally, it illustrates how continuous spectral indices related to vegetation cover and water content (e.g., NDVI, NDMI) have great potential to offer insights about major drivers of (meta-)population connectivity in landscape genetics studies. In our study area, variables associated to fine-scale structural habitat heterogeneity/complexity proved to have a major impact on regional patterns of genetic differentiation in two syntopic pond breeding amphibians. This heterogeneity is a characteristic of Mediterranean landscapes at low to medium elevations, which include extensively managed areas together with natural and/or semi-natural habitats. While it remains to be seen whether our results are generalizable to other taxa, the differences observed between two taxonomically and ecologically close taxa highlight the conservation value of these areas and point to the need of considering species individually when identifying and designing corridors connecting local populations in Mediterranean habitats. For this challenge EO-based data may provide important supporting information linking species functional connectivity to landscape pattern and process.

As new sensors and EO platforms come into play these will be able to provide more insights for landscape genetics studies. These new systems will be capable of describing even more detailed structural, compositional and functional attributes of habitats and environments linked to amphibian species. In turn, this could improve the ability of assessing factors controlling gene flow and genetic structure of populations, with benefits for both theoretical and applied ecological domains. As an example, new SAR and spaceborne LiDAR missions might further improve the characterization of functional connectivity and habitat suitability (Betbeder et al. 2017). Also, for further refining this kind of studies, and especially considering species with low dispersal abilities, higher-detail land cover/use products may be required to test assumptions regarding landscape composition and structure effects. Still, despite the advances attained in this study regarding the integration with EO, we think that much remains to be done. One particular aspect is the inclusion of the temporal dimension in landscape genetic studies using EO data. In this sense, we suggest that EO time-series can be used to address how the 'resistance landscape' of species has evolved through very-recent times, allowing to characterize the spatiotemporal change of resistance and functional connectivity conditions. This, in turn, may hold many benefits for the conservation of threatened species, and clarify why some populations may undergo higher risks of genetic diversity loss.

Study S2 explored the integration of EO-based indices of vegetation functioning and evapotranspiration in SDMs, in order to convey better predictions and to evaluate spatiotemporal habitat suitability dynamics. This has several obvious implications for improving the effectiveness of biodiversity assessment and monitoring (Kerr and Ostrovsky 2003, Pettorelli et al. 2014, Skidmore et al. 2015). First, it provides evidence that EO-based functional metrics can signal changes in ecosystems affecting habitat suitability, well before assessments based on structural metrics (Bradley and Fleishman 2008, Cabello et al. 2012, Cord et al. 2014). Second, since the latter typically have lower update frequencies (e.g., due to higher dependence of ground-based data) as well as higher production costs (related, for example, to the acquisition of very-high resolution satellite or airborne imagery), an EO-based functional approach using freely accessible data (e.g., MODIS, Landsat, Sentinel-2) could also improve the cost-efficiency of monitoring. Third, the spatiotemporal dynamics of habitat suitability and the EO variables used in SDMs can be employed by regional or local authorities to devise monitoring schemes that inform on useful vegetation or ecosystem functioning indicators aimed to

track (or even anticipate) shifts in biodiversity (Cabello et al. 2012, Nagendra et al. 2013, Pettorelli et al. 2014). Fourth, reporting on threatened species could potentially benefit from the proposed framework to develop comprehensive indicators based on species' spatiotemporal dynamics and to detail pressures affecting them. Finally, by taking advantage of an iterative and model-based design (as implemented in this study), existing data on species occurrence can be used to improve species detectability and cover data gaps (Guisan et al. 2006, Le Lay et al. 2010).

Although providing relevant insights into the spatiotemporal variability of habitat suitability, this study may be understood as a pilot for further research. For example, we should broaden the scale of analyses and include more species to verify if some of these findings hold true (e.g. (Alcaraz-Segura et al. 2017)). The inclusion of time-series of species presence/absence or abundance may provide additional clues to understand if, in fact, EO-based 'functional' variables are capable of predicting species responses to land use changes. Linking habitat suitability to plant population parameters may also provide additional clues (Fois et al. 2018). Advancing these aspects will provide a better basis to select which indicators are in fact more suitable for tracking species responses, thus improving their relevance for conservation and monitoring. The use of data collected by citizen-science projects, some of them with already large collections or time-series of species surveillance (e.g., SPEA/CAC the Portuguese common bird census or AHE/SARE the Spanish survey of reptiles and amphibians), may provide an opportunity for addressing such challenge. This way, instead of simply relying on presence-absence data, modellers can actually access the ability of EO time-series to predict actual trends observed in species or communities. Providing a more 'mechanistic' basis for the understanding of how compositional, structural and functional attributes actually affect species occurrences may also contribute to deepen the understanding of such links.

Study S3 described a framework to analyse species range shifts derived from environmental change and to assess their vulnerability to landscape fragmentation. Our multispecies approach, based on a set of specifically developed fragmentation metrics and model forecasts, provides useful information for conservation and management. It allows identifying priority areas for conservation together with a deeper understanding of how landscape resistance will promote or hinder species movements. On the other hand, connectivity analyses improve the identification of potential migration corridors, essential when designing appropriate conservation or protection measures for multi-objective environmental planning (Dennis et al. 2013, Nunez et al. 2013). More broadly, our approach can potentially be used to define ecological networks for long-term

metapopulation persistence, and to assess the impacts of infrastructures on species movements.

Likewise, our approach can be used to design management interventions and set priorities aiming to increase landscape connectivity, thereby contributing to climate change adaptation (Heller and Zavaleta 2009, Krosby et al. 2010) by facilitating dispersal and mitigating the impacts of land use dynamics. The design of impact mitigation actions can also be potentially improved. Mapping the intersections between key migration corridors and motorways can guide managers and planners in determining which motorway segments will most likely act as barriers, thus having the greatest impact on wildlife movement (McRae et al. 2012). This information can be used to plan and implement conservation measures intended to mitigate fragmentation effects, for example, specific road-crossing structures. Finally, the application of our framework can improve the effectiveness of monitoring schemes, a main component of adaptive conservation management under global change (Lindenmayer and Likens 2009), specifically by guiding the design of efficient observation networks. More broadly, the identification of potential dispersal corridors or areas of the landscape promoting dispersal is crucial for effectively long-term monitoring and adaptive management of wildlife populations (Bennett and Saunders 2010).

Despite the advances made, some aspects of this study could be improved in future applications of the framework. First, the inclusion of fine-scale land use data could enhance model predictions and deliver a better understanding of the effect of land use changes. Second, covering data gaps and updating species records to reflect current distribution patters is crucial to obtain robust model predictions. Because models are contingent on data quality, improving databases and atlases is crucial to obtain informative forecasts and reduce uncertainty. Third, although our approach showed great advantages to address data-deficient species, including more realistic representation of ecological processes (e.g., dispersal) and demography could further improve the proposed methodology.

Study S4 offered insights related to the exploitation of UAV platforms for the purpose of mapping and monitoring natural habitats of conservation interest. The results obtained in our test were robust, despite the low-spectral resolution of the tested platform, revealing that it is possible to successfully discriminate a relatively large number of classes with high to very-high levels of accuracy. This suggests that UAV-based approaches can provide robust estimates of class/habitat diversity as well as of the

extent (and connectivity) of habitat types. In turn, this may be particularly useful for supporting mandatory Natura 2000 reporting obligations (Vanden Borre et al. 2011). UAV-based assessments show a large potential to complement previous research in the detection and mapping of Natura 2000 habitats currently employing satellite imagery from moderate spatial resolution (Díaz Varela et al. 2008) to very-high spatial resolution (Förster et al. 2008; Hernando et al. 2012; Schmidt et al. 2014; Buck et al. 2015), hyperspectral sensors (Haest et al. 2010; Chan et al. 2012; Spanhove et al. 2012), radar satellite data (Schuster et al. 2011; Schuster et al. 2015) and LiDAR (Bässler et al. 2011; Zlinszky et al. 2014).

We argue that well planned, standardized and systematic UAV surveying over a statistically sound selection of sites could help to develop a monitoring system that could inform on the extent, connectivity, habitat condition and trends of Natura 2000 habitats in a reproducible fashion and allowing a reduction in running costs and operational complexity of image acquisition (Anderson & Gaston 2013; Mancini et al. 2013; Calviño-Cancela et al. 2014). In order to adequately accomplish this, nature protection agencies and/or they partner stakeholders should acquire suitable UAV equipment, train their staff in using this type of technology, and develop semi-automated procedures for image post-processing and classification, thus making it easier and faster to analyse UAV data. In turn, long-term advantages of UAV-based ecological monitoring related to flexible flight scheduling, prompt availability of very-high resolution images, reduced acquisition costs, low or absent cloud contamination (Getzin et al. 2012; Anderson & Gaston 2013), along with other factors, could provide a cost-effective solution for conservation agencies.

Future developments of this study should include the exploitation of GEOBIA techniques for improved handling, processing and classification of UAV images (see study S6). Very recent advances in image processing based on deep-learning classification are also offering powerful analytical pipelines to improve the analysis of EO data (e.g., (Guirado et al. 2017)). Moreover, testing the ability of UAVs to cover seasonal variation and phenological dimensions of vegetation may also constitute an interesting focal point for future research. In addition, developing methods to enlarge the set of currently available vegetation and biophysical parameters (beyond the classification of images into land cover or habitat maps) may also constitute a promising follow-up for this study. Finally, cross-platform integration (considering available satellite-based platforms) and data fusion are other interesting topics to include in the research agenda.

Study S5 assessed the stability of forest ecosystems and the role of PAs for promoting it. Using a time-series of MODIS EVI spectral vegetation index between 2000 and 2016

we were able to rank the effectiveness of a national PA network to promote forest stability. Moreover, models were used to uncover the factors underlying this ranking. Based on the factors evidenced in our analyses we argue that is possible to extract robust measures to improve the performance of PAs in ensuring forest stability and to reduce risks and pressures linked to disturbance phenomena. We provide a detailed description of these findings together with some possible recommendations to improve the current status of forest ecosystems. By using a functionally-oriented approach, we believe that it is possible to assess and monitor how forest ecosystems cope with disturbance regimes and to characterize their resilience. In turn, stabilizing undesired dynamics will translate into a higher likelihood of natural systems keeping their current stable state, in this case a forest-type structural and functional dynamics (see Figure 8 - 2) (Johnstone et al. 2016).

We argue that adopting our EO-based functional framework to assess and monitor the 'disturbance - response' binomial of stability will hold advantages for forest management and conservation planning. Current and future management goals for PAs should embrace both ends of the equation, namely by fostering a 'smart' disturbance regime (Fernandes 2013) while simultaneously promoting forest resilience and adaptive capacity to minimize the risks related to potential regime shifts (which increase uncertainty and vulnerability). Improving conservation measures in PA networks will require addressing the several components of disturbance regimes and recognizing their multi-scalar socio-ecological ramifications. Disturbances generate biological legacies that interact with environmental conditions shaping ecosystem recovery (Franklin et al. 2000). Currently, global changes involving climate, land use and biological invasions are rapidly altering disturbance regimes and legacies as well as the context in which ecosystems recover from damaging events (Trumbore et al. 2015). This may trigger abrupt shifts to different states (Frelich 2002; Hughes et al. 2013) and even originate novel environments and ecosystems (Williams and Jackson 2007).

In face of such challenges, managers and stakeholders must take into account the non-linear and complex dynamics of ecosystems and the potential occurrence of regime shifts that may drive ecosystems into undesired (or less desirable) states. As a consequence, it is crucial to look both to disturbance regime and to the ecosystem state and conditions that support recovery. For this endeavour, we showed that EO platforms provide useful data to support ecosystem monitoring with high temporal coverage and update frequency, thus providing a deeper understanding of systems' dynamics. As more data becomes available to feed robust modelling frameworks, from specialists on the

field up to satellites on orbit, this new paradigm opens up new and unforeseen opportunities to develop better tools to support decision making and conservation policies.

Future developments of these methods should exploit other EO platforms as well as different variables/products which physical meaning can be translated into the multidimensional concept of stability. These could include, besides vegetation indices, measures of water indices, land surface temperature, albedo, etc. These would allow to characterize other dimensions of change that can improve the detection of ecosystem changes. From the point of view of modelling and understanding factors shaping (relative) stability dynamics, we consider important to include data related to a finer characterization of forest structure and composition as well as data describing relevant socio-ecological dimensions related to PA expenditure, land use and management.

Finally, **study S6** made substantial contributions to the improvement of GEOBIA methods for processing of EO imagery. We have developed and tested an R package that facilitates the process of image segmentation by automatically optimizing its parameters. In turn, this was found to improve the process of image classification and the comparison and selection of the most suited algorithms depending on the task. The cornerstone of our approach was based on a close integration between the image segmentation and the classification steps that are common in GEOBIA workflows (Baatz et al. 2008, Lang 2008, Blaschke 2010). Hence, the objective was to use GA for optimizing image segmentation parameters with the aim of maximizing the thematic accuracy of supervised classification. This way we provide a relatively simple and generalizable approach for optimizing object-based image analysis and compare multiple techniques. From our tests, we observed that this approach allows to define segmentation parameters which balance between the over- and under-segmentation spectrum across all target classes, without a relevant loss in overall classification performance. Such results also support the notion that our package can be used by ecologists and practitioners to facilitate and improve their GEOBIA analyses with benefits for ecological change evaluation. Although GA-based optimization may help to improve object-based analyses, it is still crucial that the human operator carefully defines every input and monitors the optimization process.

Still, *SegOptim* is only giving its first steps as a computational solution for such a complex problem. The roadmap of future developments includes (among others) user-defined fitness functions based on cross-validation results, integrating and testing more algorithms already available (for segmentation but mostly for classification), multi-

classifier stacking/fusion, calculation of shape and context metrics for segments, the possibility of evaluating and performing optimization through supervised discrepancy measures or even unsupervised techniques. We are hopeful that researchers and practitioners may find the package useful for their activities and research, allowing to test, adjust and improve its functionalities over time.

11.2. Final remarks and outlook

Earth Observation (EO) technologies are a powerful tool and data source to monitor the status and change of ecosystems, with a vast collection of available sensors and platforms with different spatial, spectral and temporal resolutions. This variety of EO data sources means that a multi-level (from genes to landscapes), multi-scalar (from local to global) and multi-faceted (composition, structure, function) monitoring systems can be developed and supported by these data and the related toolset (see Table 10 - 1). Together with robust modelling frameworks, this can (and already is) advancing the scientific knowledge regarding the causes underlying the accelerated changes in biodiversity. Throughout this thesis we supported this notion through a series of research papers that individually constitute building blocks to develop a EO-supported and model-assisted biodiversity monitoring system. In its essence that system could respond to the demands of national and international efforts aiming to halt biodiversity loss by informing on meaningful sets of indicators able to track the implementation of measures and policies in this regard.

As final and overarching remarks stemming from this thesis, we highlight the following **ten points**, organized under two main topics: (i) advances in the state of knowledge, and (ii) methods, and operational challenges towards EO-based biodiversity monitoring.

Thus, in terms of **advances in the state of knowledge and methods**, we highlight the following ideas:

- **In order to effectively assess and monitor biodiversity, national and international initiatives, programmes or policies should consider biodiversity in all its dimensions and complexity.** This must encompass its multiple levels, scales and attributes/facets (structure, composition, function). Failing to address some or most of these dimensions will potentially result in partial, biased or incomplete evaluations of biodiversity status and change.

- EO systems and platforms in all their variety of sources currently provide repeatable, synoptic and cost-effective data and products regarding Earth's surface that can effectively support, or contribute, either directly or indirectly, to the monitoring of several (almost all) levels, scales and facets of biodiversity. In fact, **the reach of EO data, in combination with models, to support biodiversity assessment and monitoring ranges from gene flow up to ecosystem and landscape stability**. However, perhaps one of the major benefits is not only addressing specific components at specific levels or scales but in fact to perform **cross-scalar and cross-level analyses** that link processes at a fine-scale (such as gene flow) up to dynamics happening at much broader scales (e.g., habitat fragmentation).

- Although most efforts in EO and ecology integration focus on applied research aspects, we argue and (partially) showed throughout this thesis that **many fundamental or theoretical aspects in ecology can also be investigated using EO as a primary data source**. In particular, research developments relying on empirical/observational approaches studying topics such as functional connectivity or ecosystem stability/resilience can be addressed with EO products.

- **Fostering and improving the integration between models and EO data is crucial to obtain a bridge between fundamental and applied research and to tackle many challenges in biodiversity monitoring.** In particular, the integration of EO and SDMs may provide additional benefits for assessing biodiversity status and change, but modellers should be well aware of the (bio)physical meaning and interpretation of EO products. In this regard, modellers should be able to understand the 'language' of remote sensing experts as well as the characteristics and limitations of EO data.

- **Providing open-source state-of-the-art tools will further open the range of improved methods in biodiversity research.** In this thesis, we followed this principle and provide new methods in the GEOBIA paradigm. Despite recent (and not so recent) efforts to open up the access to novel tools and methods, still many researchers in the RS/EO field do not openly and transparently publish their code and software packages and, as consequence, this makes impossible to profit from many advances in this field.

Concerning the **operational challenges towards EO-based biodiversity monitoring**, we highlight the following points:

- **To truly benefit from EO opportunities in biodiversity science and conservation will require a close integration and communication between ecologists, remote sensing specialists and large-scale data providers** (e.g., ESA, NASA). Moreover, we argue that fostering the communication between EO specialists, ecologists and modellers may further improve the usable range of EO products and improve their integration and assimilation into models. Still, to profit from EO, its link to underlying patterns and processes under consideration or analysis should be clear and working hypothesis should be meaningful and tangible. This means, for example, that the scale of EO variables should be connected to the patterns and processes under examination. Failing to establish this connection may lead to poor results which potentially undermine the value of EO-based approaches.

- Despite the wide availability of free EO products and powerful open-source software for GIS/RS analysis, **national organisms related to nature protection and conservation have still not yet fully realized the potential of this data source for their activities**, still relying primordially in 'traditional' field-based methods (typically at the species or community levels) that only encompass a portion of biodiversity dimensions. For better harnessing EO advantages, nature conservation organisms should be trained and capacitated to use these technologies; training actions could potentially be promoted by research entities and EO data providers such as ESA.

- As an illustration of the previous point, and despite some survey limitations derived from the small footprint, if used with a proper sampling scheme and appropriated semi-automated technologies for image processing, **UAV technologies hold strong advantages for monitoring fine-scale natural habitats**. These may allow to cover Natura 2000 reporting requirements by making a systematic assessment of target habitat types, thus improving official reports on the extent and condition of habitats.

- Due to their characteristics (e.g., synoptic coverage, repeatability, high-temporal frequency) **EO is perhaps one of the most important data sources for evaluating the effectiveness of Protected Areas.** Although hard to set baseline conditions and reference areas, remotely-sensed indicators can decisively contribute to tackle this challenge. However, to accomplish this, systematic approaches are required as well as meaningful indicators as we suggest in this thesis.

- Picking up from the concept of 'safe operating space' (Rockstrom et al. 2009, Scheffer et al. 2015), we argue that **EO is well-equipped to characterize several dimensions of planetary and ecosystem boundary conditions**, allowing to understand if systems are in fact operating under 'safe' conditions. Currently, most research on Anthropocene rates of biodiversity decline focused on the species level, however we claim that this is insufficient to fully characterize and encapsulate biodiversity in all its dimensions. In fact, we still need to improve our understanding of how certain ecosystems are disappearing, how their functioning is being altered or if and how their distribution is changing across the globe or at the regional scale. A robust integration between models and EO data may contribute to elucidate these trends.

Despite the remarkable value of EO detection or combined approaches for biodiversity monitoring and ecological change assessment, we should not expect that these provide a 'magic wand' capable of solving all or even most of the problems in these domains. Although valuable, EO is not a panacea for tackling all issues in conservation monitoring and management and should perhaps (depending on the specific goals) be seen as a complementary technology and data source capable of adding many relevant inputs to the contemporary ecologist 'toolkit'. In addition, the acceptance of these technologies by environmental or conservation-related agencies is typically slow-paced (although exceptions obviously exist), and therefore scientists should have reasonable expectations regarding operational-use and 'technological' adoption.

There are however many possible steps to improve this situation (here excluding the obvious need to improve the '*technological readiness level'* of some approaches and applications). Besides enhancing intersectoral communication, promoting outreach, training and capacity-building, another important strategy to foster a more 'EO-supported paradigm' is perhaps to strengthen the bridge between field-based assessments (still traditionally more used in biodiversity surveys) and EO-based approaches. The vast

advances in automated field- or ground-based recording devices (e.g., camera traps, sound recorders, GPS telemetry, wireless sensor networks), but also high-throughput DNA sequencing and modern ecological modelling, will further improve the ability to extract valuable information from EO data. Such an approach would potentially offer a more efficient, complete and near-real-time monitoring of management and conservation impacts on biodiversity and ecosystem functions and services. Appropriate cyber-infrastructures and high-performance/distributed computing resources are required to store, manage, share and process large amounts of data (such as those coming from EO spaceborne platforms) and thus harness the potential of integrating all these data sources.

References

Alcaraz-Segura, D., A. Lomba, R. Sousa-Silva, D. Nieto-Lugilde, P. Alves, D. Georges, J. R. Vicente, and J. P. Honrado. 2017. Potential of satellite-derived ecosystem functional attributes to anticipate species range shifts. International Journal of Applied Earth Observation and Geoinformation 57:86-92.

Allen, T. F. H., and T. W. Hoekstra. 1990. The confusion between scale-defined levels and conventional levels of organization in ecology. Journal of Vegetation Science 1:5-12.

Almeida, C. M. D., A. M. V. Monteiro, G. Câmara, B. S. Soares-Filho, G. C. Cerqueira, C. L. Pennachin, and M. Batty. 2005. GIS and remote sensing as tools for the simulation of urban land-use change. International Journal of Remote Sensing 26:759-774.

Anderson, K., and K. J. Gaston. 2013. Lightweight unmanned aerial vehicles will revolutionize spatial ecology. Frontiers in Ecology and the Environment 11:138-146.

Andrews, K. M., J. W. Gibbons, and D. M. Jochimsen. 2008. Ecological effects of roads on amphibians and reptiles: a literature review. Pages 121-143 *in* J. C. Mitchell, R. E. J. Brown, and B. Bartholomew, editors. Urban Herpetology. Society for the Study of Amphibians & Reptiles, Salt Lake City, UT.

Araújo, M. B., W. Thuiller, and R. G. Pearson. 2006. Climate warming and the decline of amphibians and reptiles in Europe. Journal of Biogeography 33:1712-1728.

Auffret, A. G., J. Plue, and S. A. Cousins. 2015. The spatial and temporal components of functional connectivity in fragmented landscapes. Ambio 44 Suppl 1:S51-59.

Baatz, M., C. Hoffmann, and G. Willhauck. 2008. Progressing from object-based to object-oriented image analysis.*in* T. Blaschke, S. Lang, and G. J. Hay, editors. Object-Based Image Analysis - Spatial Concepts for Knowledge-Driven Remote Sensing Applications. Springer-Verlag, Berlin.

Baguette, M., and H. Van Dyck. 2007. Landscape connectivity and animal behavior: functional grain as a key determinant for dispersal. Landscape Ecology 22:1117-1129.

Bai, Y., J. Wu, Q. Pan, J. Huang, Q. Wang, F. Li, A. Buyantuyev, and X. Han. 2007. Positive linear relationship between productivity and diversity: evidence from the Eurasian Steppe. Journal of Applied Ecology 44:1023-1034.

Bastos, R., M. D'Amen, J. Vicente, M. Santos, H. Yu, D. Eitelberg, J. Gonçalves, E. Civantos, J. Honrado, and J. A. Cabral. 2016. A multi-scale looping approach to predict spatially dynamic patterns of functional species richness in changing landscapes. Ecological Indicators 64:92-104.

Bennett, A. F., and D. A. Saunders. 2010. Habitat fragmentation and landscape change. Pages 88-106 *in* N. S. Sodhi and P. R. Ehrlich, editors. Conservation Biology for All. Oxford University Press, New York, US.

Betbeder, J., M. Laslier, L. Hubert-Moy, F. Burel, and J. Baudry. 2017. Synthetic Aperture Radar (SAR) images improve habitat suitability models. Landscape Ecology.

Blaschke, T. 2010. Object based image analysis for remote sensing. ISPRS Journal of Photogrammetry and Remote Sensing 65:2-16.

Bradley, B. A., and E. Fleishman. 2008. Can remote sensing of land cover improve species distribution modelling? Journal of Biogeography 35:1158-1159.

Bradley, B. A., A. D. Olsson, O. Wang, B. G. Dickson, L. Pelech, S. E. Sesnie, and L. J. Zachmann. 2012. Species detection vs. habitat suitability: Are we biasing habitat suitability models with remotely sensed data? Ecological Modelling 244:57-64.

Carvalho, S. B., J. C. Brito, E. J. Crespo, and H. P. Possingham. 2010. From climate change predictions to actions - conserving vulnerable animal groups in hotspots at a regional scale. Global Change Biology 16:3257-3270.

Colgan, S. M., A. C. Baldeck, J.-B. Féret, and P. G. Asner. 2012. Mapping Savanna Tree Species at Ecosystem Scales Using Support Vector Machine Classification and BRDF Correction on Airborne Hyperspectral and LiDAR Data. Remote Sensing 4.

Cord, A. F., D. Klein, F. Mora, and S. Dech. 2014. Comparing the suitability of classified land cover data and remote sensing variables for modeling distribution patterns of plants. Ecological Modelling 272:129-140.

Cushman, S. A., K. Gutzweiler, J. S. Evans, and K. McGarigal. 2010. The Gradient Paradigm: A Conceptual and Analytical Framework for Landscape Ecology.*in* S. A. Cushman and F. Huettmann, editors. Spatial Complexity, Informatics, and Wildlife Conservation. Springer.

Decout, S., S. Manel, C. Miaud, and S. Luque. 2012. Integrative approach for landscape-based graph connectivity analysis: a case study with the common frog (Rana temporaria) in human-dominated landscapes. Landscape Ecology 27:267-279.

Dennis, R. L. H., L. Dapporto, J. W. Dover, and T. G. Shreeve. 2013. Corridors and barriers in biodiversity conservation: a novel resource-based habitat perspective for butterflies. Biodiversity and Conservation 22:2709-2734.

Elith, J., M. Kearney, and S. Phillips. 2010. The art of modelling range-shifting species. Methods in Ecology and Evolution 1:330-342.

Elith, J., and J. Leathwick. 2009. Species Distribution Models: Ecological Explanation and Prediction Across Space and Time. Annual Review of Ecology, Evolution, and Systematics 40:677-697.

Fisher, J. B., R. J. Whittaker, and Y. Malhi. 2011. ET come home: potential evapotranspiration in geographical ecology. Global Ecology and Biogeography 20:1-18.

Fois, M., A. Cuena-Lombraña, G. Fenu, D. Cogoni, and G. Bacchetta. 2018. Does a correlation exist between environmental suitability models and plant population parameters? An experimental approach to measure the influence of disturbances and environmental changes. Ecological Indicators 86:1-8.

Forman, R. T. T., and E. O. Wilson. 1995. Land Mosaics: The Ecology of Landscapes and Regions. Cambridge University Press.

Guirado, E., S. Tabik, D. Alcaraz-Segura, J. Cabello, and F. Herrera. 2017. Deep-learning Versus OBIA for Scattered Shrub Detection with Google Earth Imagery: Ziziphus lotus as Case Study. Remote Sensing 9:1220.

Guisan, A., and W. Thuiller. 2005. Predicting species distribution: offering more than simple habitat models. Ecology Letters 8:993-1009.

Guisan, A., R. Tingley, J. B. Baumgartner, I. Naujokaitis-Lewis, P. R. Sutcliffe, A. I. T. Tulloch, T. J. Regan, L. Brotons, E. McDonald-Madden, C. Mantyka-Pringle, T. G. Martin, J. R. Rhodes, R. Maggini, S. A. Setterfield, J. Elith, M. W. Schwartz, B. A. Wintle, O. Broennimann, M. Austin, S. Ferrier, M. R. Kearney, H. P. Possingham, and Y. M. Buckley. 2013. Predicting species distributions for conservation decisions. Ecology Letters 16:1424-1435.

Hawkins, B. A., R. Field, H. V. Cornell, D. J. Currie, J.-F. Guégan, D. M. Kaufman, J. T. Kerr, G. G. Mittelbach, T. Oberdorff, E. M. O'Brien, E. E. Porter, and J. R. G. Turner. 2003. Energy, water, and broadscale geographic patterns of species richness. Ecology 84:3105-3117.

Hay, G. J., and G. Castilla. 2008. Geographic Object-Based Image Analysis (GEOBIA): A new name for a new discipline.*in* T. Blaschke, S. Lang, and G. J. Hay, editors. Object-Based Image Analysis - Spatial Concepts for Knowledge-Driven Remote Sensing Applications. Springer-Verlag, Berlin.

He, K. S., D. Rocchini, M. Neteler, and H. Nagendra. 2011. Benefits of hyperspectral remote sensing for tracking plant invasions. Diversity and Distributions 17:381-392.

Heller, N. E., and E. S. Zavaleta. 2009. Biodiversity management in the face of climate change: A review of 22 years of recommendations. Biological Conservation 142:14-32.

Hodgson, J. A., C. D. Thomas, C. Dytham, J. M. Travis, and S. J. Cornell. 2012. The speed of range shifts in fragmented landscapes. PLoS ONE 7:e47141.

Hodgson, J. A., C. D. Thomas, B. A. Wintle, and A. Moilanen. 2009. Climate change, connectivity and conservation decision making: back to basics. Journal of Applied Ecology 46:964-969.

IUCN. 2014. The IUCN Red List of Threatened Species. Version 2014.3.

Jackson, L. J., A. S. Trebitz, and K. L. Cottingham. 2000. An Introduction to the Practice of Ecological Modeling. BioScience 50:694-706.

Johnstone, J. F., C. D. Allen, J. F. Franklin, L. E. Frelich, B. J. Harvey, P. E. Higuera, M. C. Mack, R. K. Meentemeyer, M. R. Metz, G. L. W. Perry, T. Schoennagel, and M. G. Turner. 2016. Changing disturbance regimes, ecological memory, and forest resilience. Frontiers in Ecology and the Environment 14:369-378.

Krosby, M., J. Tewksbury, N. M. Haddad, and J. Hoekstra. 2010. Ecological connectivity for a changing climate. Conserv Biol 24:1686-1689.

Lang, S. 2008. Object-based image analysis for remote sensing applications: modeling reality – dealing with complexity.*in* T. Blaschke, S. Lang, and G. J. Hay, editors. Object-Based Image Analysis - Spatial Concepts for Knowledge-Driven Remote Sensing Applications. Springer-Verlag, Berlin.

Lausch, A., L. Bannehr, M. Beckmann, C. Boehm, H. Feilhauer, J. M. Hacker, M. Heurich, A. Jung, R. Klenke, C. Neumann, M. Pause, D. Rocchini, M. E. Schaepman, S. Schmidtlein, K. Schulz, P. Selsam, J. Settele, A. K. Skidmore, and A. F. Cord. 2016. Linking Earth Observation and taxonomic, structural and functional biodiversity: Local to ecosystem perspectives. Ecological Indicators 70:317-339.

Li, M., L. Ma, T. Blaschke, L. Cheng, and D. Tiede. 2016. A systematic comparison of different object-based classification techniques using high spatial resolution imagery in agricultural environments. International Journal of Applied Earth Observation and Geoinformation 49:87-98.

Lindenmayer, D. B., and G. E. Likens. 2009. Adaptive monitoring: a new paradigm for long-term research and monitoring. Trends in Ecology & Evolution 24:482-486.

Lu, X., G. Zheng, C. Miller, and E. Alvarado. 2017. Combining Multi-Source Remotely Sensed Data and a Process-Based Model for Forest Aboveground Biomass Updating. Sensors (Basel, Switzerland) 17:2062.

Lucas, R., P. Blonda, P. Bunting, G. Jones, J. Inglada, M. Arias, V. Kosmidou, Z. I. Petrou, I. Manakos, M. Adamo, R. Charnock, C. Tarantino, C. A. Mücher, R. H. G. Jongman, H. Kramer, D. Arvor, J. P. Honrado, and P. Mairota. 2015. The Earth Observation Data for Habitat Monitoring (EODHaM) system. International Journal of Applied Earth Observation and Geoinformation 37:17-28.

Mairota, P., B. Cafarelli, R. K. Didham, F. P. Lovergine, R. M. Lucas, H. Nagendra, D. Rocchini, and C. Tarantino. 2015. Challenges and opportunities in harnessing satellite remote-sensing for biodiversity monitoring. Ecological Informatics 30:207-214.

Marpu, P. R., M. Neubert, H. Herold, and I. Niemeyer. 2010. Enhanced evaluation of image segmentation results. Journal of Spatial Science 55:55-68.

McRae, B. H., S. A. Hall, P. Beier, and D. M. Theobald. 2012. Where to Restore Ecological Connectivity? Detecting Barriers and Quantifying Restoration Benefits. PLoS ONE 7:e52604.

Meinel, G., and M. Neubert. 2004. A comparison of segmentation programs for high resolution remote sensing data. International Archives of the Photogrammetry, Remote Sensing and Spatial Information Sciences 35:1097-1105.

Minor, E. S., and D. L. Urban. 2008. A graph-theory framework for evaluating landscape connectivity and conservation planning. Conserv Biol 22:297-307.

Mücher, C. A., L. Kooistra, M. Vermeulen, J. V. Borre, B. Haest, and R. Haveman. 2013. Quantifying structure of Natura 2000 heathland habitats using spectral mixture analysis and segmentation techniques on hyperspectral imagery. Ecological Indicators 33:71-81.

Mücher, C. A., L. Roupioz, H. Kramer, M. M. B. Bogers, R. H. G. Jongman, R. M. Lucas, V. E. Kosmidou, Z. Petrou, I. Manakos, E. Padoa-Schioppa, M. Adamo, and P. Blonda. 2015. Synergy of airborne LiDAR and Worldview-2 satellite imagery for land cover and habitat mapping: A BIO_SOS-EODHaM case study for the Netherlands. International Journal of Applied Earth Observation and Geoinformation 37:48-55.

Nagendra, H., R. Lucas, J. P. Honrado, R. H. G. Jongman, C. Tarantino, M. Adamo, and P. Mairota. 2013. Remote sensing for conservation monitoring: Assessing protected areas, habitat extent, habitat condition, species diversity, and threats. Ecological Indicators 33:45-59.

Nunez, T. A., J. J. Lawler, B. H. McRae, D. J. Pierce, M. B. Krosby, D. M. Kavanagh, P. H. Singleton, and J. J. Tewksbury. 2013. Connectivity planning to address climate change. Conserv Biol 27:407-416.

Pascual-Hortal, L., and S. Saura. 2008. Integrating landscape connectivity in broad-scale forest planning through a new graph-based habitat availability methodology: application to capercaillie (Tetrao urogallus) in Catalonia (NE Spain). European Journal of Forest Research 127:23-31.

Pecl, G. T., M. B. Araújo, J. D. Bell, J. Blanchard, T. C. Bonebrake, I.-C. Chen, T. D. Clark, R. K. Colwell, F. Danielsen, B. Evengård, L. Falconi, S. Ferrier, S. Frusher, R. A. Garcia, R. B. Griffis, A. J. Hobday, C. Janion-Scheepers, M. A. Jarzyna, S. Jennings, J. Lenoir, H. I. Linnetved, V. Y. Martin, P. C. McCormack, J. McDonald, N. J. Mitchell, T. Mustonen, J. M. Pandolfi, N. Pettorelli, E. Popova, S. A. Robinson, B. R. Scheffers, J. D. Shaw, C. J. B. Sorte, J. M. Strugnell, J. M. Sunday, M.-N. Tuanmu, A. Vergés, C. Villanueva, T. Wernberg, E. Wapstra, and S. E. Williams. 2017. Biodiversity redistribution under climate change: Impacts on ecosystems and human well-being. Science 355.

R Development Core Team. 2017. R: A Language and Environment for Statistical Computing; URL: https://www.R-project.org/. R Foundation for Statistical Computing, Vienna, Austria.

Rocchini, D., D. S. Boyd, J.-B. Féret, G. M. Foody, K. S. He, A. Lausch, H. Nagendra, M. Wegmann, and N. Pettorelli. 2016. Satellite remote sensing to monitor species diversity: potential and pitfalls. Remote Sensing in Ecology and Conservation 2:25-36.

Rockstrom, J., W. Steffen, K. Noone, A. Persson, F. S. Chapin, E. F. Lambin, T. M. Lenton, M. Scheffer, C. Folke, H. J. Schellnhuber, B. Nykvist, C. A. de Wit, T. Hughes, S. van der Leeuw, H. Rodhe, S. Sorlin, P. K. Snyder, R. Costanza, U. Svedin, M. Falkenmark, L. Karlberg, R. W. Corell, V. J. Fabry, J. Hansen, B. Walker, D. Liverman, K. Richardson, P. Crutzen, and J. A. Foley. 2009. A safe operating space for humanity. Nature 461:472-475.

Sayer, J., T. Sunderland, J. Ghazoul, J.-L. Pfund, D. Sheil, E. Meijaard, M. Venter, A. K. Boedhihartono, M. Day, C. Garcia, C. van Oosten, and L. E. Buck. 2013. Ten principles for a landscape approach to reconciling agriculture, conservation, and other competing land uses. Proceedings of the National Academy of Sciences 110:8349-8356.

Scheffer, M., S. Barrett, S. R. Carpenter, C. Folke, A. J. Green, M. Holmgren, T. P. Hughes, S. Kosten, I. A. van de Leemput, D. C. Nepstad, E. H. van Nes, E. T. H. M. Peeters, and B. Walker. 2015. Creating a safe operating space for iconic ecosystems. Science 347:1317-1319.

Simonson, W. D., H. D. Allen, and D. A. Coomes. 2012. Use of an Airborne Lidar System to Model Plant Species Composition and Diversity of Mediterranean Oak Forests

Utilización de un Sistema Lidar Aerotransportado para Modelar la Composición y Diversidad de Especies de Plantas en Bosques Mediterráneos de Roble. Conservation Biology 26:840-850.

Skidmore, A. K., N. Pettorelli, N. C. Coops, G. N. Geller, M. Hansen, R. Lucas, C. A. Mücher, B. O'Connor, M. Paganini, H. M. Pereira, M. E. Schaepman, W. Turner, T. Wang, and M. Wegmann. 2015. Agree on biodiversity metrics to track from space. Nature 523.

Teodoro, A. C., and R. Araújo. 2016. Comparison of performance of object-based image analysis techniques available in open source software (Spring and Orfeo Toolbox/Monteverdi) considering very high spatial resolution data. Journal of Applied Remote Sensing 10:1-22.

Turner, W., S. Spector, N. Gardiner, M. Fladeland, E. Sterling, and M. Steininger. 2003. Remote sensing for biodiversity science and conservation. Trends in Ecology & Evolution 18:306-314.

UNEP-WCMC, and IUCN. 2016. Protected Planet Report 2016 - Update on global statistics December 2016, CBD COP13. Cambridge, UK

Gland, Switzerland.

Vanden Borre, J., T. Spanhove, and B. Haest. 2017. Towards a Mature Age of Remote Sensing for Natura 2000 Habitat Conservation: Poor Method Transferability as a Prime Obstacle. Pages 11-37 *in* R. Díaz-Delgado, R. Lucas, and C. Hurford, editors. The Roles of Remote Sensing in Nature Conservation: A Practical Guide and Case Studies. Springer International Publishing, Cham.

Vaz, A. S., B. Marcos, J. Gonçalves, A. Monteiro, P. Alves, E. Civantos, R. Lucas, P. Mairota, J. Garcia-Robles, J. Alonso, P. Blonda, A. Lomba, and J. P. Honrado. 2015. Can we predict habitat quality from space? A multi-indicator assessment based on an automated knowledge-driven system. International Journal of Applied Earth Observation and Geoinformation 37:106-113.

Wang, K., S. E. Franklin, X. Guo, and M. Cattet. 2010. Remote Sensing of Ecology, Biodiversity and Conservation: A Review from the Perspective of Remote Sensing Specialists. Sensors 10:9647.

Wolpert, D. H. 1996. The Lack of A Priori Distinctions Between Learning Algorithms. Neural Computation 8:1341-1390.

Wolpert, D. H., and W. G. Macready. 1997. No free lunch theorems for optimization. IEEE Transactions on Evolutionary Computation 1:67-82.

Zhang, Y., X. Xiao, X. Wu, S. Zhou, G. Zhang, Y. Qin, and J. Dong. 2017. A global moderate resolution dataset of gross primary production of vegetation for 2000–2016. Scientific Data 4:170165.

Zimmermann, N. E., T. C. Edwards, G. G. Moisen, T. S. Frescino, and J. A. Blackard. 2007. Remote sensing-based predictors improve distribution models of rare, early successional and broadleaf tree species in Utah. Journal of Applied Ecology 44:1057-1067.

SECTION IV. Appendices

Appendix I | Chapter 4 - Comparative landscape genetics of pond-breeding amphibians in Mediterranean temporal wetlands: the positive role of structural heterogeneity in promoting gene flow

Supplemental Table 1. Geographic distances (in km) between sampled *P. cultripes* populations.

Pop/km	C1	C2	C3	C4	C5	C6	C7	C8	C9	C10	C11	C12	C13	C14	C15	C16
C1	0.00															
C2	39.64	0.00														
C3	56.17	21.61	0.00													
C4	53.05	13.43	17.27	0.00												
C5	62.29	29.30	39.49	22.54	0.00											
C6	62.04	23.26	25.43	10.98	15.49	0.00										
C7	64.17	24.57	17.92	11.42	25.45	9.96	0.00									
C8	76.11	37.45	35.43	24.69	20.49	14.21	17.53	0.00								
C9	80.20	41.57	25.65	29.53	41.63	27.21	18.68	25.06	0.00							
C10	86.27	50.27	30.15	40.30	55.61	40.58	31.06	39.70	14.65	0.00						
C11	97.31	60.29	41.15	49.21	61.43	47.40	38.80	43.12	20.22	11.59	0.00					
C12	114.10	74.73	65.72	61.35	56.97	52.13	51.01	38.43	41.79	49.58	43.02	0.00				
C13	120.45	81.09	66.33	68.01	70.93	61.51	56.61	50.49	40.76	41.16	30.73	23.26	0.00			
C14	121.13	81.75	67.03	68.66	71.45	62.11	57.26	51.03	41.46	41.87	31.41	23.29	0.71	0.00		
C15	126.86	88.64	70.95	76.37	83.21	71.79	65.11	62.82	47.07	41.89	30.30	40.12	16.87	16.89	0.00	
C16	125.04	85.74	70.61	72.71	75.75	66.32	61.30	55.32	45.14	44.61	33.73	26.63	4.83	4.30	14.44	0.00

Supplemental Table 2. Geographic distances (in km) between sampled *P. waltl* populations.

Pop/km	W1	W2	W3	W4	W5	W6	W7	W8	W9	W10	W11	W12	W13	W14	W15	W16	W17	W18	W19	W20
W1	0.00																			
W2	21.90	0.00																		
W3	25.67	4.22	0.00																	
W4	41.18	19.36	16.12	0.00																
W5	38.95	17.68	13.52	8.83	0.00															
W6	41.14	22.09	17.99	17.08	8.45	0.00														
W7	47.47	32.82	29.33	31.13	22.54	14.10	0.00													
W8	45.95	25.70	21.49	15.53	8.84	5.85	16.91	0.00												
W9	47.43	27.54	23.33	17.67	10.98	6.56	15.49	2.20	0.00											
W10	50.28	28.68	24.67	12.24	11.42	14.14	25.45	8.87	9.96	0.00										
W11	67.16	45.27	41.67	26.08	29.53	32.60	41.63	26.90	27.21	18.68	0.00									
W12	76.25	54.95	52.04	35.97	42.01	46.84	57.20	41.52	42.22	32.73	16.06	0.00								
W13	85.24	63.60	60.39	44.30	49.21	52.80	61.43	47.12	47.40	38.80	20.22	10.43	0.00							
W14	98.65	77.13	74.00	57.88	62.92	66.38	74.44	60.65	60.82	52.44	33.79	22.61	13.70	0.00						
W15	88.32	68.99	64.77	55.21	51.79	47.34	43.31	43.30	41.45	42.98	39.65	51.82	47.94	55.20	0.00					
W16	106.85	85.08	81.19	66.44	68.01	68.02	70.93	62.32	61.51	56.61	40.76	40.50	30.73	27.88	36.82	0.00				
W17	107.51	85.75	81.85	67.12	68.66	68.63	71.45	62.94	62.11	57.26	41.46	41.20	31.41	28.40	37.04	0.71	0.00			
W18	108.33	89.82	85.63	76.67	72.93	67.87	61.71	64.28	62.32	64.44	60.09	70.42	64.61	68.61	21.49	43.75	43.60	0.00		
W19	109.05	87.32	83.40	68.76	70.17	69.99	72.53	64.32	63.45	58.78	43.18	43.09	33.31	30.08	37.23	2.59	1.90	42.83	0.00	
W20	111.51	89.71	85.84	70.96	72.71	72.82	75.75	67.11	66.32	61.30	45.14	43.82	33.73	28.99	40.88	4.83	4.30	46.05	3.66	0.00

Supplemental Table 3. Reclassification table for Corine Land Cover 2006. Given that CLC is a hierarchical dataset, we maintained some relevant classes maximally disaggregated (e.g., different types of vegetated areas), while others were merged into their broader supra-category (e.g., similar types of impervious or artificial areas).

CLC code	Corine Land Cover class	New code	New category
111	Continuous urban fabric	1	Urban/artificial
112	Discontinuous urban fabric	1	Urban/artificial
121	Industrial or commercial units	1	Urban/artificial
122	Road and rail networks and associated land	1	Urban/artificial
124	Airports	1	Urban/artificial
131	Mineral extraction sites	1	Urban/artificial
132	Dump sites	1	Urban/artificial
133	Construction sites	1	Urban/artificial
141	Green urban areas	1	Urban/artificial
142	Sport and leisure facilities	1	Urban/artificial
211	Non-irrigated arable land	2	Non-irrigated arable land
212	Permanently irrigated land	3	Permanently irrigated land
221	Vineyards	4	Permanent crops
222	Fruit trees and berry plantations	4	Permanent crops
223	Olive groves	4	Permanent crops
231	Pastures	5	Pastures
242	Complex cultivation patterns	6	Complex cultivation patterns
243	Land principally occupied by agriculture and natural vegetation	7	Land principally occupied by agriculture and natural vegetation
244	Agro-forestry areas	8	Agro-forestry areas
311	Broad-leaved forest	9	Broad-leaved forest
312	Coniferous forest	10	Coniferous forest
313	Mixed forest	11	Mixed forest
321	Natural grasslands	12	Natural grasslands
322	Moors and heathland	13	Scrub and/or herbaceous vegetation

323	Sclerophyllous vegetation	13	Scrub and/or herbaceous vegetation
324	Transitional woodland-shrub	13	Scrub and/or herbaceous vegetation
332	Bare rocks	14	Open spaces with little or no vegetation
333	Sparsely vegetated areas	14	Open spaces with little or no vegetation
334	Burnt areas	14	Open spaces with little or no vegetation
512	Water bodies	15	Water bodies

Supplemental Table 4. Full reclassification table for SIOSE (*Sistema de Información sobre Ocupación del Suelo de España*), available from the Spanish *Centro Nacional de Información Geográfica* for year 2005 (CNIG; URL: http://centrodedescargas.cnig.es) considering all classes for Spain (total of 116 initial classes and 54 new). From the reclassified data, a total of 29 classes were found in the study area.

SIOSE ID	SIOSE code	SIOSE class description	New class
831	PAG	Agrícola, Ganadero	Agriculture/livestock farm
103	LAA	Lámina de Agua Artificial	Artificial water line
331	PDA	Playas, dunas y arenales	Beach/sand dunes
311	-	Frondosas	Broadleaf
312	FDC	Frondosas Caducifolias	Broadleaf deciduous
313	FDP	Frondosas Perennifolias	Broadleaf evergreen
334	ZQM	Zonas Quemadas	Burnt areas
844	TCG	Camping	Camping
211	CHA	Arroz	Cereal crops
212	CHL	Cultivos Herbáceos distintos de Arroz	Cereal crops
521	ALC	Lagunas Costeras	Coastal lagoons
599	-	Compuestas	Composite types
316	CNF	Coniferas	Coniferous
413	HSA	Salinas Continentales	Continental salt pit
410	-	Humedales Continentales	Continental wetlands
336	RMB	Ramblas	Creek/stream bed
200	-	Cultivos	Crops
701	DHS	Dehesa	Dehesa
522	AES	Estuarios	Estuary
833	PMX	Minero Extractivo	Extractive mining
834	PPS	Piscifactoria	Fish farm
310	-	Arbolado Forestal	Forest tree cover
335	GNP	Glaciares y Nieves permanentes	Glaciers/permanent snow
859	ECG	Campo de Golf	Golf course
320	MTR	Matorral	Heathland/shrubland
210	-	Cultivos Herbáceos	Herbaceous crops
510	-	Aguas Continentales	Inland waters
513	ALG	Lagos y Lagunas	Lakes and lagoons
921	NVE	Vertederos y Escombreras	Landfills/slagheaps
422	HSM	Salinas Marinas	Marine salt pit
520	-	Aguas Marinas	Marine waters
420	-	Humedales Marinos	Marine wetlands
411	HPA	Zonas Pantanosas	Marshes/swamps
421	HMA	Marismas	Marshes/swamps
290	PRD	Prados	Meadows
412	HTU	Turberas	Mire/peatland
600	-	No Predefinida	Non-predefined
330	-	Terrenos sin Vegetación	Non-vegetated
333	SDN	Suelo Desnudo	Open soil

300	PST	Pastizal	Pastureland
700	-	Predefinida	Predefined
832	PFT	Forestal Primario	Production forest
880	-	Transporte	Roads/railways
881	NRV	Red Viaria	Roads/railways
882	NRF	Red Ferroviaria	Roads/railways
350	-	Roquedos	Rocky outcrops
351	ACM	Acantilados Marinos	Rocky outcrops
352	ARR	Afloramientos Rocosos y Roquedos	Rocky outcrops
353	CCH	Canchales	Rocky outcrops
354	CLC	Coladas Lávicas	Rocky outcrops
523	AMO	Mares y Océanos	Sea and ocean
99	-	Simples	Simple cover types
840	-	Terciario	Tertiary sector
102	ZAU	Zona Verde Artificial y Arbolado Urbano	Urban green/woodland
860	EPU	Parque Urbano	Urban park
100	-	Coberturas Artificiales	Urban/artificial
101	EDF	Edificación	Urban/artificial
104	VAP	Vial, Aparcamiento o Zona Peatonal sin Vegetación	Urban/artificial
111	OCT	Otras Construcciones	Urban/artificial
121	SNE	Suelo No Edificado	Urban/artificial
131	ZEV	Zonas de Extracción o Vertido	Urban/artificial
703	AAR	Asentamiento Agrícola Residencial	Urban/artificial
800	-	Artificial	Urban/artificial
810	-	Urbano Mixto	Urban/artificial
811	UCS	Casco	Urban/artificial
812	UEN	Ensanche	Urban/artificial
813	UDS	Discontinuo	Urban/artificial
820	-	Industrial	Urban/artificial
821	IPO	Polígono Industrial Ordenado	Urban/artificial
822	IPS	Polígono Industrial sin Ordenar	Urban/artificial
823	IAS	Industrial Aislada	Urban/artificial
830	-	Primario	Urban/artificial
841	TCO	Comercial y Oficinas	Urban/artificial
842	TCH	Complejo Hotelero	Urban/artificial
843	TPR	Parque Recreativo	Urban/artificial
850	-	Equipamiento Dotacional	Urban/artificial
851	EAI	Administrativo Institucional	Urban/artificial
852	ESN	Sanitario	Urban/artificial
853	ECM	Cementerio	Urban/artificial
854	EDU	Educación	Urban/artificial
855	EPN	Penitenciario	Urban/artificial
856	ERG	Religioso	Urban/artificial
857	ECL	Cultural	Urban/artificial
858	EDP	Deportivo	Urban/artificial
870	-	Infraestructuras	Urban/artificial

883	NPO	Portuario	Urban/artificial
884	NAP	Aeroportuario	Urban/artificial
890	-	Energía	Urban/artificial
891	NEO	Eólica	Urban/artificial
892	NSL	Solar	Urban/artificial
893	NCL	Nuclear	Urban/artificial
894	NEL	Eléctrica	Urban/artificial
895	NTM	Térmica	Urban/artificial
896	NHD	Hidroeléctrica	Urban/artificial
897	NGO	Gaseoducto Oleoducto	Urban/artificial
900	NTC	Telecomunicaciones	Urban/artificial
910	-	Suministro de Agua	Urban/artificial
911	NDP	Depuradoras y Potabilizadoras	Urban/artificial
912	NCC	Conducciones y Canales	Urban/artificial
913	NDS	Desalinizadora	Urban/artificial
920	-	Residuos	Urban/artificial
922	NPT	Plantas de Tratamiento	Urban/artificial
704	UER	Huerta Familiar	Urban/vegetable crops
514	AEM	Embalses	Water dam/reservoir
500	-	Coberturas de Agua	Water surface
511	ACU	Cursos de Agua	Water surface/line
512	-	Láminas de Agua	Water surface/line
400	-	Coberturas Húmedas	Wetlands
220	-	Leñosos	Woody crops
221	-	Frutales	Woody crops
222	LFC	Frutales Cítricos	Woody crops
223	LFN	Frutales No Cítricos	Woody crops
231	LVI	Viñedo	Woody crops
232	LOL	Olivar	Woody crops
241	LOC	Otros Leñosos	Woody crops
702	OVD	Olivar-Viñedo	Woody crops

Supplemental Table 5. Resistance values/weights attributed to each new SIOSE class (total 29) in the study area. These *a priori* weights were later transformed by the resistance surface optimization procedure (see main text) to better reflect land use effects. Because SIOSE data also provides composite/multiclass patches with a proportion given for each class represented in a given patch, the total resistance weight of each LUC patch (i) was given by: $t = \sum p_c w_c$, with p_c, equal to the proportion of class c in the patch and w_c, equal to the weight attributed to that class (Supp. Tables 4 and 5). Values at patch-level were then averaged for each pixel at 100m.

SIOSE 2005 new class	Resistance weight
Agriculture/livestock farm	1
Artificial water line	1
Broadleaf deciduous	1
Broadleaf evergreen	1
Burnt areas	10
Camping	25
Cereal crops	1
Coniferous	1
Continental salt pit	50
Creek/stream bed	1
Dehesa	1
Extractive mining	25
Golf course	25
Heathland/shrubland	1
Landfills/slagheaps	25
Marshes/swamps	1
Meadows	1
Open soil	1
Pastureland	1
Production forest	1
Roads/railways	75
Rocky outcrops	25
Urban green/woodland	1
Urban park	25
Urban/artificial	100
Urban/vegetable crops	50
Water dam/reservoir	50
Water surface/line	1
Woody crops	25

Supplemental Table 6. Pairwise F_{ST} values between sampled *P. cultripes* populations.

Pop/Fst	C1	C2	C3	C4	C5	C6	C7	C8	C9	C10	C11	C12	C13	C14	C15	C16
C1																
C2	0.166															
C3	0.394	0.231														
C4	0.136	0.066	0.239													
C5	0.130	0.036	0.246	0.021												
C6	0.100	0.046	0.200	0.032	0.021											
C7	0.132	0.036	0.246	0.047	0.019	0.031										
C8	0.097	0.089	0.273	0.034	0.030	0.023	0.049									
C9	0.101	0.040	0.240	0.053	0.028	0.043	0.016	0.050								
C10	0.305	0.149	0.359	0.196	0.133	0.174	0.130	0.212	0.146							
C11	0.137	0.073	0.283	0.073	0.043	0.045	0.039	0.048	0.030	0.189						
C12	0.211	0.143	0.230	0.145	0.138	0.087	0.149	0.153	0.130	0.270	0.150					
C13	0.126	0.077	0.240	0.052	0.052	0.044	0.076	0.050	0.041	0.204	0.049	0.122				
C14	0.131	0.111	0.271	0.066	0.062	0.068	0.080	0.054	0.058	0.208	0.061	0.155	0.001			
C15	0.163	0.147	0.341	0.145	0.098	0.108	0.086	0.125	0.083	0.208	0.113	0.211	0.136	0.132		
C16	0.114	0.079	0.225	0.044	0.054	0.065	0.054	0.051	0.026	0.171	0.041	0.123	0.011	0.017	0.120	

Supplemental Table 7. Pairwise G''_{ST} values between sampled *P. cultripes* populations.

Pop/G"st	C1	C2	C3	C4	C5	C6	C7	C8	C9	C10	C11	C12	C13	C14	C15	C16
C1	0.000															
C2	0.267	0.000														
C3	0.522	0.332	0.000													
C4	0.247	0.115	0.381	0.000												
C5	0.222	0.060	0.357	0.039	0.000											
C6	0.180	0.080	0.317	0.060	0.039	0.000										
C7	0.216	0.059	0.355	0.083	0.033	0.055	0.000									
C8	0.164	0.148	0.397	0.062	0.052	0.041	0.083	0.000								
C9	0.171	0.067	0.349	0.097	0.049	0.077	0.027	0.087	0.000							
C10	0.456	0.227	0.477	0.329	0.210	0.290	0.202	0.333	0.229	0.000						
C11	0.238	0.123	0.428	0.134	0.076	0.083	0.067	0.086	0.054	0.305	0.000					
C12	0.339	0.228	0.323	0.256	0.233	0.151	0.242	0.253	0.216	0.408	0.254	0.000				
C13	0.238	0.138	0.384	0.102	0.099	0.085	0.138	0.093	0.077	0.349	0.093	0.220	0.000			
C14	0.243	0.197	0.432	0.128	0.118	0.129	0.145	0.102	0.109	0.354	0.114	0.278	0.001	0.000		
C15	0.249	0.228	0.470	0.246	0.157	0.181	0.135	0.199	0.133	0.307	0.184	0.325	0.235	0.227	0.000	
C16	0.226	0.147	0.380	0.089	0.109	0.130	0.103	0.100	0.052	0.306	0.081	0.231	0.023	0.034	0.216	0.000

Supplemental Table 8. Pairwise D_{EST} values between sampled *P. cultripes* populations.

Pop/Dest	C1	C2	C3	C4	C5	C6	C7	C8	C9	C10	C11	C12	C13	C14	C15	C16
C1	0.000															
C2	0.086	0.000														
C3	0.146	0.046	0.000													
C4	0.104	0.016	0.086	0.000												
C5	0.071	0.005	0.055	0.004	0.000											
C6	0.061	0.027	0.055	0.010	0.004	0.000										
C7	0.067	0.006	0.038	0.016	0.003	0.009	0.000									
C8	0.050	0.033	0.081	0.012	0.004	0.005	0.010	0.000								
C9	0.047	0.008	0.059	0.008	0.003	0.008	0.003	0.015	0.000							
C10	0.146	0.038	0.065	0.100	0.042	0.082	0.028	0.068	0.049	0.000						
C11	0.062	0.015	0.083	0.025	0.017	0.014	0.007	0.013	0.006	0.074	0.000					
C12	0.103	0.041	0.048	0.064	0.039	0.031	0.049	0.048	0.057	0.100	0.073	0.000				
C13	0.089	0.041	0.083	0.019	0.015	0.013	0.023	0.011	0.010	0.114	0.015	0.070	0.000			
C14	0.073	0.055	0.115	0.036	0.024	0.046	0.031	0.016	0.024	0.119	0.027	0.095	0.000	0.000		
C15	0.055	0.053	0.065	0.076	0.023	0.045	0.030	0.028	0.025	0.056	0.047	0.066	0.063	0.059	0.000	
C16	0.074	0.033	0.088	0.014	0.022	0.042	0.018	0.022	0.004	0.084	0.018	0.062	0.002	0.006	0.087	0.000

Supplemental Table 9. Pairwise F_{ST} values between sampled *P. waltl* populations.

Pop/Fst	W1	W2	W3	W4	W5	W6	W7	W8	W9	W10	W11	W12	W13	W14	W15	W16	W17	W18	W19	W20
W1	0.000																			
W2	0.133	0.000																		
W3	0.189	0.004	0.000																	
W4	0.236	0.217	0.278	0.000																
W5	0.124	0.122	0.152	0.099	0.000															
W6	0.280	0.266	0.332	0.293	0.187	0.000														
W7	0.112	0.097	0.138	0.170	0.079	0.162	0.000													
W8	0.099	0.116	0.164	0.146	0.095	0.186	0.033	0.000												
W9	0.121	0.120	0.155	0.156	0.111	0.261	0.050	0.033	0.000											
W10	0.208	0.159	0.212	0.063	0.090	0.225	0.120	0.104	0.121	0.000										
W11	0.198	0.166	0.217	0.093	0.111	0.202	0.101	0.081	0.109	0.037	0.000									
W12	0.246	0.227	0.273	0.140	0.157	0.237	0.146	0.119	0.166	0.072	0.080	0.000								
W13	0.313	0.274	0.315	0.192	0.194	0.255	0.188	0.176	0.211	0.124	0.153	0.069	0.000							
W14	0.295	0.259	0.309	0.216	0.213	0.294	0.180	0.163	0.208	0.121	0.095	0.107	0.191	0.000						
W15	0.239	0.230	0.279	0.204	0.148	0.282	0.137	0.118	0.142	0.122	0.110	0.115	0.164	0.172	0.000					
W16	0.322	0.270	0.308	0.196	0.187	0.251	0.199	0.187	0.230	0.107	0.111	0.110	0.112	0.153	0.187	0.000				
W17	0.295	0.250	0.291	0.168	0.167	0.234	0.169	0.148	0.203	0.086	0.101	0.064	0.086	0.128	0.164	0.007	0.000			
W18	0.336	0.307	0.394	0.384	0.292	0.427	0.271	0.252	0.268	0.306	0.266	0.372	0.384	0.386	0.337	0.370	0.369	0.000		
W19	0.268	0.222	0.259	0.178	0.174	0.224	0.151	0.135	0.190	0.094	0.093	0.108	0.116	0.138	0.176	0.029	0.031	0.324	0.000	
W20	0.309	0.282	0.333	0.252	0.235	0.270	0.217	0.154	0.230	0.146	0.138	0.129	0.186	0.147	0.167	0.124	0.107	0.392	0.109	0.000

Supplemental Table 10. Pairwise G''_{ST} values between sampled *P. waltl* populations.

Pop/G"st	W1	W2	W3	W4	W5	W6	W7	W8	W9	W10	W11	W12	W13	W14	W15	W16	W17	W18	W19	W20
W1	0.000																			
W2	0.272	0.000																		
W3	0.366	0.010	0.000																	
W4	0.482	0.463	0.564	0.000																
W5	0.274	0.283	0.344	0.229	0.000															
W6	0.544	0.542	0.628	0.594	0.419	0.000														
W7	0.248	0.225	0.315	0.399	0.197	0.364	0.000													
W8	0.216	0.268	0.369	0.339	0.233	0.413	0.087	0.000												
W9	0.255	0.265	0.328	0.345	0.266	0.549	0.122	0.081	0.000											
W10	0.460	0.370	0.477	0.146	0.227	0.500	0.311	0.268	0.293	0.000										
W11	0.442	0.390	0.496	0.220	0.282	0.459	0.265	0.214	0.268	0.097	0.000									
W12	0.532	0.515	0.597	0.319	0.385	0.516	0.367	0.298	0.393	0.180	0.204	0.000								
W13	0.645	0.590	0.647	0.415	0.453	0.524	0.444	0.413	0.470	0.291	0.364	0.158	0.000							
W14	0.613	0.565	0.643	0.471	0.501	0.611	0.433	0.390	0.470	0.290	0.230	0.250	0.421	0.000						
W15	0.480	0.485	0.555	0.430	0.338	0.564	0.316	0.269	0.310	0.279	0.256	0.259	0.348	0.369	0.000					
W16	0.674	0.593	0.646	0.430	0.444	0.528	0.483	0.453	0.526	0.258	0.271	0.258	0.248	0.344	0.406	0.000				
W17	0.630	0.560	0.625	0.377	0.403	0.504	0.415	0.362	0.472	0.211	0.252	0.153	0.196	0.294	0.363	0.016	0.000			
W18	0.580	0.549	0.632	0.682	0.576	0.701	0.518	0.477	0.486	0.579	0.516	0.700	0.686	0.695	0.589	0.665	0.684	0.000		
W19	0.579	0.503	0.564	0.404	0.424	0.487	0.377	0.337	0.447	0.234	0.233	0.260	0.265	0.320	0.394	0.069	0.073	0.608	0.000	
W20	0.613	0.583	0.651	0.521	0.527	0.531	0.488	0.344	0.491	0.326	0.313	0.282	0.389	0.309	0.341	0.263	0.231	0.675	0.239	0.000

Supplemental Table 11. Pairwise D_{EST} values between sampled *P. waltl* populations.

Pop/Dest	W1	W2	W3	W4	W5	W6	W7	W8	W9	W10	W11	W12	W13	W14	W15	W16	W17	W18	W19	W20
W1	0.000																			
W2	0.091	0.000																		
W3	0.141	0.000	0.000																	
W4	0.194	0.219	0.273	0.000																
W5	0.067	0.104	0.145	0.093	0.000															
W6	0.216	0.233	0.301	0.276	0.165	0.000														
W7	0.081	0.066	0.110	0.190	0.078	0.153	0.000													
W8	0.084	0.114	0.151	0.096	0.051	0.192	0.030	0.000												
W9	0.086	0.092	0.120	0.118	0.090	0.281	0.043	0.019	0.000											
W10	0.242	0.138	0.193	0.063	0.088	0.256	0.139	0.058	0.077	0.000										
W11	0.207	0.170	0.222	0.065	0.080	0.185	0.094	0.063	0.099	0.021	0.000									
W12	0.324	0.325	0.333	0.118	0.220	0.247	0.202	0.153	0.199	0.069	0.082	0.000								
W13	0.339	0.303	0.298	0.185	0.244	0.235	0.225	0.186	0.216	0.154	0.191	0.048	0.000							
W14	0.334	0.299	0.309	0.211	0.238	0.302	0.188	0.149	0.245	0.110	0.098	0.127	0.203	0.000						
W15	0.171	0.197	0.221	0.199	0.092	0.237	0.097	0.047	0.093	0.085	0.067	0.090	0.149	0.149	0.000					
W16	0.425	0.358	0.387	0.182	0.257	0.264	0.299	0.196	0.273	0.103	0.105	0.089	0.102	0.148	0.177	0.000				
W17	0.374	0.307	0.322	0.163	0.222	0.251	0.259	0.162	0.254	0.086	0.103	0.046	0.071	0.103	0.153	0.001	0.000			
W18	0.256	0.261	0.307	0.363	0.298	0.351	0.243	0.234	0.206	0.270	0.232	0.399	0.389	0.381	0.253	0.307	0.393	0.000		
W19	0.322	0.250	0.236	0.160	0.232	0.230	0.214	0.158	0.254	0.107	0.106	0.080	0.105	0.128	0.165	0.015	0.014	0.289	0.000	
W20	0.346	0.311	0.323	0.242	0.297	0.226	0.260	0.158	0.223	0.142	0.127	0.091	0.139	0.117	0.120	0.068	0.069	0.289	0.071	0.0000

Supplemental Table 12. Pairwise migration rates between populations of *P. cultripes* as estimated by BayesAss. Direction of migration (from population X to population Y) indicated in rows. Population numbers as in Table 1.

Pc/Nm	C1	C2	C3	C4	C5	C6	C7	C8	C9	C10	C11	C12	C13	C14	C15	C16
C1	0.7878	0.0133	0.0136	0.0133	0.0134	0.0134	0.0133	0.0133	0.0180	0.0140	0.0132	0.0138	0.0158	0.0135	0.0168	0.0134
C2	0.0126	0.6771	0.0158	0.0105	0.0104	0.0103	0.0102	0.0106	0.1623	0.0122	0.0103	0.0112	0.0125	0.0106	0.0130	0.0104
C3	0.0121	0.0117	0.8193	0.0118	0.0121	0.0117	0.0118	0.0121	0.0129	0.0122	0.0123	0.0120	0.0120	0.0119	0.0121	0.0119
C4	0.0100	0.0098	0.0100	0.6766	0.0099	0.0098	0.0099	0.0097	0.1813	0.0099	0.0098	0.0118	0.0111	0.0099	0.0105	0.0100
C5	0.0121	0.0113	0.0117	0.0116	0.6784	0.0118	0.0114	0.0116	0.1386	0.0119	0.0114	0.0116	0.0162	0.0118	0.0273	0.0115
C6	0.0098	0.0099	0.0097	0.0098	0.0096	0.6765	0.0098	0.0098	0.1727	0.0098	0.0097	0.0104	0.0110	0.0098	0.0217	0.0100
C7	0.0110	0.0108	0.0189	0.0108	0.0110	0.0106	0.6775	0.0106	0.1473	0.0130	0.0107	0.0108	0.0167	0.0107	0.0190	0.0107
C8	0.0118	0.0111	0.0111	0.0112	0.0111	0.0109	0.0111	0.6777	0.1571	0.0122	0.0111	0.0110	0.0142	0.0111	0.0165	0.0110
C9	0.0246	0.0113	0.0199	0.0114	0.0110	0.0114	0.0111	0.0109	0.7299	0.0174	0.0111	0.0197	0.0445	0.0113	0.0428	0.0116
C10	0.0111	0.0111	0.0163	0.0113	0.0113	0.0110	0.0111	0.0110	0.0166	0.8156	0.0112	0.0116	0.0119	0.0112	0.0166	0.0112
C11	0.0117	0.0105	0.0105	0.0103	0.0103	0.0104	0.0105	0.0102	0.0919	0.0107	0.6770	0.0110	0.0621	0.0105	0.0418	0.0106
C12	0.0112	0.0111	0.0187	0.0110	0.0113	0.0113	0.0111	0.0109	0.0336	0.0155	0.0109	0.7950	0.0128	0.0111	0.0136	0.0111
C13	0.0109	0.0105	0.0116	0.0104	0.0103	0.0104	0.0105	0.0104	0.0258	0.0119	0.0106	0.0186	0.8137	0.0103	0.0137	0.0105
C14	0.0098	0.0101	0.0103	0.0098	0.0099	0.0101	0.0102	0.0101	0.0133	0.0102	0.0100	0.0105	0.1733	0.6769	0.0153	0.0102
C15	0.0106	0.0104	0.0106	0.0103	0.0102	0.0105	0.0103	0.0105	0.0129	0.0130	0.0105	0.0106	0.0112	0.0103	0.8380	0.0103
C16	0.0110	0.0099	0.0132	0.0098	0.0098	0.0098	0.0100	0.0098	0.0243	0.0109	0.0095	0.0112	0.1618	0.0099	0.0126	0.6765

Supplemental Table 13. Pairwise migration rates between populations of *P. waltl* as estimated by BayesAss. Direction of migration (from population X to population Y) indicated in rows. Population numbers as in Table 1.

Pw/Nm	W1	W2	W3	W4	W5	W6	W7	W8	W9	W10	W11	W12	W13	W14	W15	W16	W17	W18	W19	W20
W1	0.8296	0.0200	0.0083	0.0086	0.0087	0.0083	0.0084	0.0084	0.0085	0.0081	0.0083	0.0083	0.0082	0.0085	0.0084	0.0083	0.0083	0.0084	0.0082	0.0083
W2	0.0140	0.8284	0.0082	0.0116	0.0090	0.0083	0.0084	0.0085	0.0111	0.0083	0.0083	0.0083	0.0082	0.0082	0.0083	0.0084	0.0083	0.0091	0.0085	0.0085
W3	0.0114	0.1151	0.6780	0.0118	0.0114	0.0114	0.0113	0.0113	0.0116	0.0115	0.0116	0.0115	0.0116	0.0115	0.0113	0.0114	0.0115	0.0115	0.0116	0.0117
W4	0.0092	0.0094	0.0091	0.8212	0.0123	0.0092	0.0091	0.0090	0.0126	0.0089	0.0091	0.0089	0.0091	0.0089	0.0091	0.0090	0.0089	0.0091	0.0091	0.0089
W5	0.0132	0.0084	0.0070	0.0239	0.8223	0.0092	0.0070	0.0069	0.0247	0.0069	0.0069	0.0073	0.0070	0.0069	0.0073	0.0069	0.0070	0.0070	0.0072	0.0071
W6	0.0106	0.0105	0.0103	0.0113	0.0104	0.7980	0.0105	0.0102	0.0135	0.0103	0.0105	0.0103	0.0105	0.0104	0.0107	0.0103	0.0104	0.0103	0.0105	0.0105
W7	0.0091	0.0090	0.0091	0.0092	0.0095	0.0089	0.6757	0.0090	0.1614	0.0089	0.0090	0.0090	0.0091	0.0091	0.0091	0.0092	0.0089	0.0089	0.0089	0.0089
W8	0.0110	0.0181	0.0101	0.0217	0.0114	0.0100	0.0100	0.6768	0.1223	0.0099	0.0097	0.0099	0.0098	0.0100	0.0101	0.0097	0.0098	0.0101	0.0099	0.0098
W9	0.0204	0.0132	0.0093	0.0197	0.0133	0.0092	0.0092	0.0093	0.7902	0.0091	0.0094	0.0093	0.0092	0.0094	0.0136	0.0092	0.0092	0.0093	0.0094	0.0091
W10	0.0092	0.0094	0.0090	0.1561	0.0092	0.0092	0.0094	0.0095	0.0103	0.6759	0.0094	0.0094	0.0093	0.0091	0.0094	0.0093	0.0094	0.0091	0.0093	0.0093
W11	0.0090	0.0091	0.0090	0.1594	0.0090	0.0089	0.0089	0.0089	0.0110	0.0089	0.6757	0.0090	0.0089	0.0087	0.0097	0.0088	0.0092	0.0089	0.0097	0.0091
W12	0.0104	0.0093	0.0087	0.0640	0.0097	0.0088	0.0090	0.0085	0.0137	0.0089	0.0089	0.6929	0.0273	0.0118	0.0596	0.0087	0.0089	0.0087	0.0113	0.0109
W13	0.0087	0.0086	0.0089	0.0094	0.0090	0.0086	0.0087	0.0086	0.0088	0.0088	0.0089	0.0097	0.8301	0.0089	0.0091	0.0087	0.0087	0.0088	0.0096	0.0093
W14	0.0091	0.0094	0.0094	0.0110	0.0095	0.0093	0.0094	0.0095	0.0094	0.0092	0.0093	0.0108	0.0100	0.7868	0.0100	0.0093	0.0091	0.0093	0.0339	0.0162
W15	0.0091	0.0091	0.0089	0.0103	0.0115	0.0092	0.0090	0.0090	0.0140	0.0089	0.0090	0.0093	0.0093	0.0092	0.8188	0.0091	0.0089	0.0091	0.0090	0.0093
W16	0.0090	0.0091	0.0090	0.0090	0.0091	0.0089	0.0092	0.0091	0.0090	0.0091	0.0092	0.0093	0.0090	0.0090	0.0092	0.6757	0.0091	0.0090	0.1610	0.0091
W17	0.0086	0.0086	0.0088	0.0085	0.0086	0.0086	0.0085	0.0086	0.0086	0.0083	0.0087	0.0086	0.0087	0.0087	0.0087	0.0086	0.6751	0.0087	0.1684	0.0102
W18	0.0091	0.0089	0.0112	0.0091	0.0090	0.0089	0.0108	0.0110	0.0091	0.0114	0.0106	0.0089	0.0090	0.0091	0.0089	0.0102	0.0109	0.8159	0.0091	0.0089
W19	0.0085	0.0086	0.0087	0.0105	0.0085	0.0083	0.0085	0.0084	0.0087	0.0086	0.0087	0.0086	0.0098	0.0094	0.0088	0.0087	0.0087	0.0085	0.8317	0.0098
W20	0.0087	0.0087	0.0086	0.0138	0.0085	0.0085	0.0086	0.0085	0.0086	0.0084	0.0086	0.0089	0.0088	0.0093	0.0137	0.0085	0.0088	0.0086	0.0209	0.8130

Appendix II | Chapter 5 - Exploring the spatiotemporal dynamics of habitat suitability to improve conservation management of a vulnerable plant species

Appendix S1 – Description of the study area

Climate

According to the Köppen-Geiger classification (Kottek et al. 2006), the climate is Mediterranean (type Csb) with strong yearly amplitudes, i.e. cold and wet winters (with occasional snow above 900m) and hot summers. In the warmer months of the year, July and August, temperatures reach maximum values of approximately 24 to 39°C, while in the colder months of December and January minimum temperatures range from -3 to 8°C (IM 2012). On average, the wettest month is December (c.a. 130mm), followed by January (111mm), and February (86mm), whereas the minimum values of precipitation occur in the months of July (12mm) and August (18mm), corresponding to the summer drought months (IM 2012).

Land cover/land use

According to the Corine Land Cover 2006 (CLC06; Caetano et al. 2009a, Caetano et al. 2009b) the study-area is dominated by shrubby and herbaceous natural and semi-natural vegetation, corresponding to 51.6% of the territory. Forest areas occupy 16.5% and are dominated by coniferous forests (11.2%) followed by mixed (3.6%) and broadleaved (1.7%) forests. Agro-forestry and agricultural areas occupy 28.9% of the land, composed mainly by non-irrigated crops (12.0%) and heterogeneous agro-forestry mosaics (15.2%). Urban areas (dispersed, small rural villages, plus the town of Vila Pouca de Aguiar) in combination with transportation networks fill up 2.3% of the landscape. In recent years two large motorways were built: the A24 (opened in 2005) and the A7 (opened in 2006).

From 1984 to 2009, an area equal to 1667ha (ca. 3.8% of the region) was on average affected by wildfires each year (AFN 2011) leading to considerable losses on forested areas. In this period, five very critical years recorded more than 10% of affected area, specifically the years of 1985, 1990, 1996, 1998 and 2005; in 2005 alone, 25% of the area, mostly with shrublands/heathlands and forest, was burned.

Appendix S2 – Preliminary Maxent model used for sampling design

A preliminary model was used for devising the model-based sampling scheme (Guisan et al. 2006, Le Lay et al. 2010) for in-field surveys. For this purpose, *Maxent v.3.3.3k* software (Phillips et al. 2006, Phillips and Dudík 2008, Elith et al. 2011) was used as an exploratory tool for producing spatial predictions of habitat suitability for *V. micrantha* with a spatial resolution of 1km and based on preliminary presence-only data. A total of 38 records for the Northern region of Portugal were collected from multiple sources (mostly from herbaria) and corresponding to different collectors and dates. A total of eight predictor variables were initially considered as good candidates for model development (Table S 1) based on preliminary knowledge on the species distribution. Selected variables were indirectly tested for multicollinearity through Spearman correlation (Table S 2). No absolute pairwise correlations above 0.7 were found thus signalling low to moderate inter-correlation effects. Although a relatively large number of variables were considered, Maxent robust performance in cases of low sample size may be partially explained by the use of regularization to avoid over-fitting. The determined amount of regularization varies with sample size to guarantee good performance, while the type of regularization implemented (L-1) tends to omit irrelevant variables in the model (Wisz et al. 2008). Maxent was parametrized to include only linear and hinge features, 2000 iterations for model fitting and a convergence threshold equal to 1.0E-7. Evaluation was performed through 10-fold cross-validation. Overall test results showed a good model performance with an average test AUC equal to 0.811, and a standard deviation of 0.148 across the 10 evaluation rounds (Figure 1). Variable importance contributions to the model are presented in Figure 2, while response plots are represented in Figure 3. Spatial predictions for the study-area are shown in Figure 4.

Table S 1 – Environmental variables used for developing the preliminary model and estimates of their relative predictive contributions as calculated by Maxent.

Variable name/acronym	**Percent contribution**	**Permutation importance**
% covered by agroforestry (cos02_agr)	25.2	18.1
Mean Shape Index (ldscos02_msi)	23.7	18.5

% covered by Cambisoils (soil_cambis)	15.5	24.5
% covered by discontinuous/low-density urban areas (cos02_urb)	10.4	1
Density of large rivers with Sthraler order between 4 and 5 (hidro_4_5) in m/km^2	8.7	13.6
Annual NDVI minimum/base value for 2010 (fmbasevalue_max)	7.2	9.4
Actual Evapotranspiration – annual range for 2010 (evap_trange)	5.9	8.9
% covered by convex topographic forms (gmorf_g10)	3.3	6.1

Table S 2 – Spearman correlation matrix for the selected environmental variables used for developing the preliminary model.

	cos02_urb	cos02_agr	evap_trange	gmorf_g10	hidro_4_5	ldscos02_msi	soil_cambis	fmbasevalue_max
cos02_urb	-							
cos02_agr	0.60	-						
evap_trange	0.26	0.35	-					
gmorf_g10	-0.27	-0.48	-0.33	-				
hidro_4_5	-0.03	-0.01	-0.01	-0.29	-			
ldscos02_msi	0.37	0.62	0.22	-0.26	0.04	-		
soil_cambis	0.30	0.64	0.07	-0.18	0.01	0.49	-	
fmbasevalue_max	0.02	0.04	0.07	-0.02	0.21	0.11	0.06	-

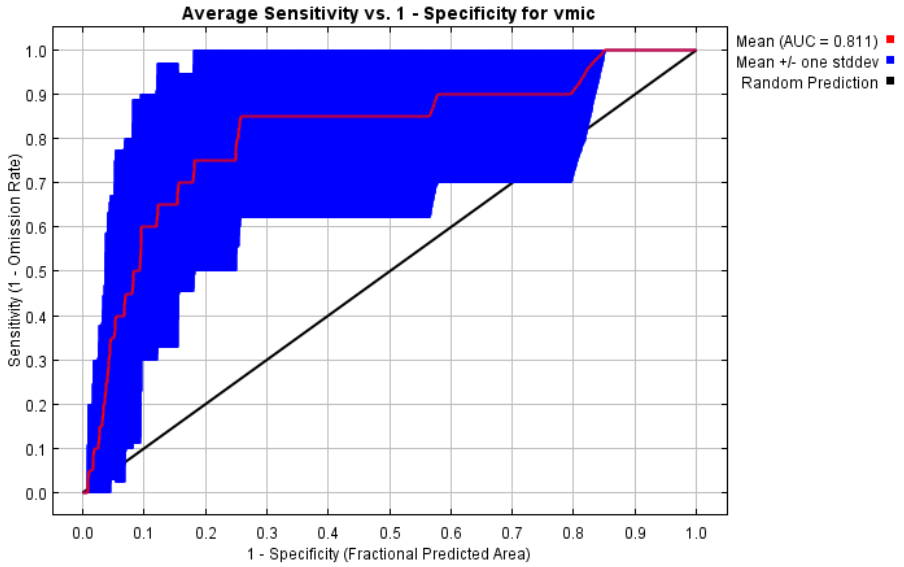

Figure 1 – Model evaluation results for the Receiver Operating Characteristic (ROC) plot showing Sensitivity (or True Positive Rate, y-axis) vs. 1- Specificity (or False Positive Rate; x-axis) and the Area Under the Curve (AUC). The average test AUC for the replicate runs is 0.811, and the standard deviation is 0.148.

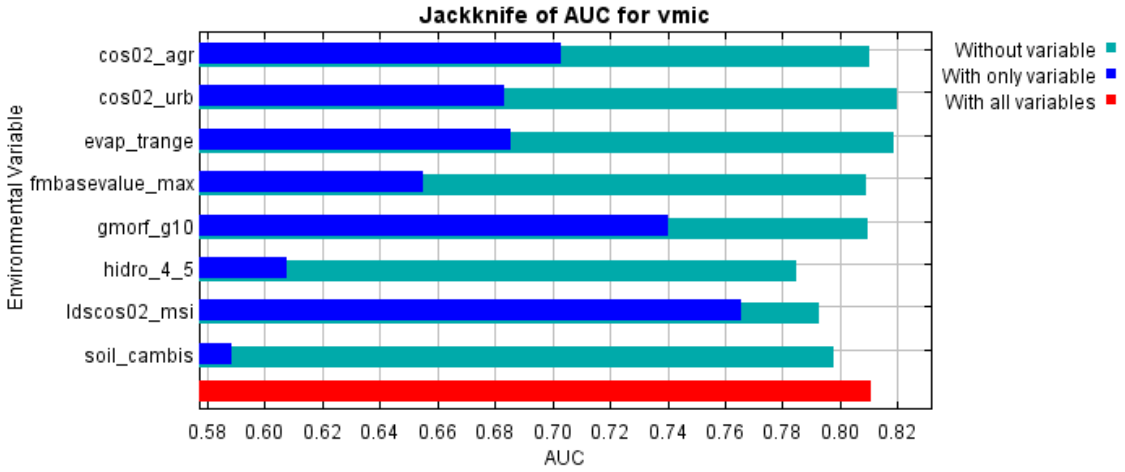

Figure 2 – Results for the jackknife test of variable importance using AUC on test data.

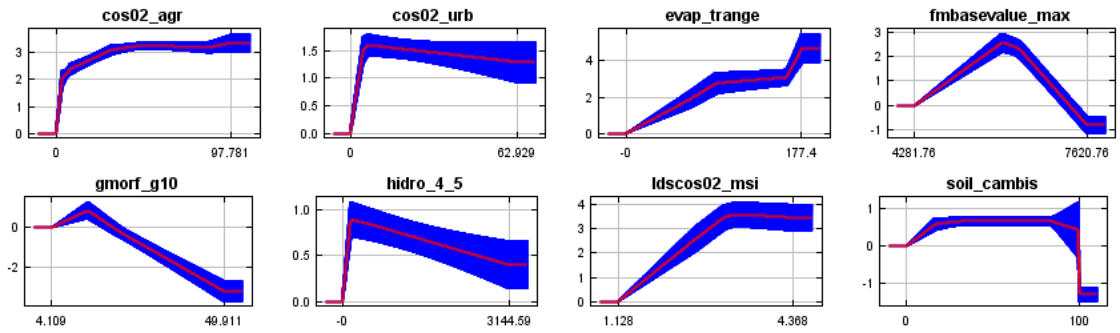

Figure 3 – Response curves showing how each environmental variable affects the Maxent prediction. These curves were generated by a Maxent model using only the corresponding variable.

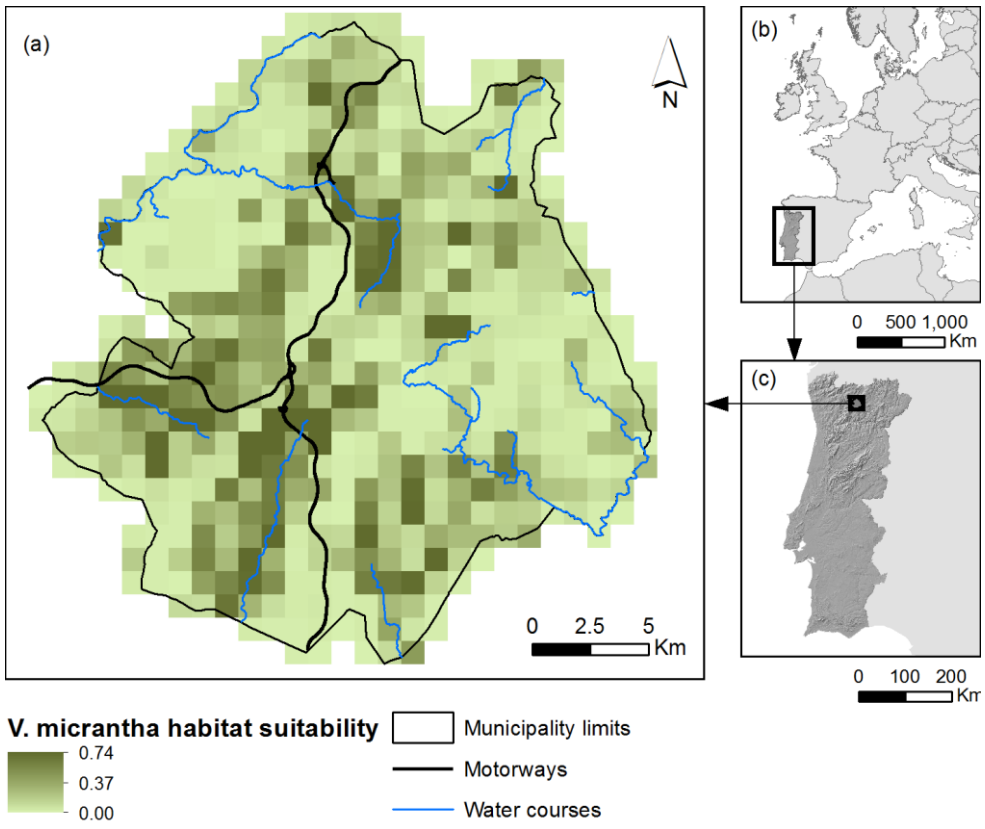

Figure 4 – (a) Map representation of *V. micrantha* habitat suitability for the study-area of Vila Pouca de Aguiar municipality as calculated by the Maxent model; (b, c) show the location of the study-area in a larger extent.

Appendix S3 – Competing hypotheses definition, justification and support

H1 – Vegetation functioning dynamics: productivity, and, H2 – Vegetation functioning dynamics: phenology. The properties of annual NDVI time-series, can be used as proxies for vegetation functioning dynamics (VFD) when summarized into a set of metrics. These metrics have the ability to dynamically and synoptically capture changes in phenology and productivity of earth ecosystems and provide insights about habitat quality (Bradley and Fleishman 2008). Nevertheless, their use in SDM applications is still recent. Coops et al. (2009) shown that, although land cover information may be important to predict breeding bird species richness, data on vegetation productivity and energy was also critical to define how many species occur in each habitat type. Jönsson et al. (2010) argue that vegetation indices calculated from the Moderate Resolution Imaging Spectroradiometer (MODIS) data can be useful for monitoring climate change impacts on forest tree phenology. Tuanmu et al. (2010) successfully used TIMESATs' (Jönsson and Eklundh 2004) phenological indices based

on Wide Dynamic Range Vegetation Index (also calculated from MODIS data products) to map understory vegetation. Beck et al. (2008) also used TIMESATs' VFD indices to correlate with the altitudinal movement of giant pandas in the Foping Biosphere Reserve in southwestern China. Several authors (e.g.: Pettorelli et al. 2005, Alcaraz et al. 2006) integrate these indices in two main groups, one related with measures of overall productivity/biomass and of variability in productivity (e.g., the annual maximum NDVI value and the relative range or amplitude of the NVDI) and another related with phenological measures (e.g., the dates of the beginning, end and peak(s) of the growing season). Following this rationale and in order to improve the construction of hypotheses related to VFD we sub-divided them into two separate blocks thus considering productivity (H1) and phenology (H2) separately.

H3 – Landscape composition, and, H4 – Landscape configuration. Explaining the role of large and small-scale heterogeneity on species distribution and abundance is currently one of the major motivations of landscape ecology research (Thornton et al. 2011). Analyses performed at multiple scales have shown the importance of landscape pattern for many taxa (Atauri and Lucio 2001, Turner 2005). Hamer et al. (2006) and Renfrew and Ribic (2008) showed the importance of landscape composition and configuration and their interplay for predicting the distribution, relative abundance and richness of grassland bird species. Dumortier et al. (2002) used features related to landscape composition and configuration to predict vascular plant species richness of fragmented forests in agricultural landscapes in central Belgium. Lomba et al. (2010) used features related both to landscape composition and configuration to predict local scale habitat suitability for cyclamen-flowered daffodil (Narcissus cyclamineus) a rare, endemic plant species from the Iberian Peninsula. As in the case of the two former hypotheses we have also considered two separate effects (following Turner (2005) definition) related to landscape composition (H3; what and how much is present, such as the number and amount of different habitat or land use/land cover types), and configuration (H4; how those types are spatially organized).

H5 – Soil types. Soil properties, such as texture and drainage, can modify water availability and thus productivity (Begon et al. 2006) with an direct effect on resource availability to plant species. Klironomos (2002) found that feedbacks with soil biota contributed to explain plant rarity and invasiveness, showing that such interactions play a major role for explaining the variance in the relative abundance of species in plant

communities. Several SDM applications, e.g., Aitken et al. (2007), Gogol-Prokurat (2011), Lomba et al. (2010) and Wiser et al. (1998) have also used predictor variables related to soil type or soil attributes (texture, mineralogical and/or chemical properties) to enhance rare species predictions at a local scale.

H6 – Water availability. Actual evapotranspiration (EVPTR) reflects both the energy and the water regimes, i.e., it provides an indication of ecologically climatic relevant features related to energy supply (since EVPTR is an important energy flux) and to water balance thereby conveying an important constraint on water availability at the land surface (Fisher et al. 2011). Therefore, EVPTR influences ecosystem parameters and processes such as soil moisture content, vegetation productivity, water balance, and ecosystem nutrient, which highlights the interactions between evapotranspiration and several other earth system processes (Wever et al. 2002). Moreover, Hawkins et al. (2003) found that measures of energy, water, or water-energy balance explained on average over 60% of the variation in species richness for a wide range of plant and animal groups. Remote sensing has been recognized as a feasible tool to provide continuous information on temporally and spatially distributed regional evapotranspiration over land surface. The MODIS sensor currently provides unprecedented information regarding vegetation and surface energy which can be used for global and regional scale evapotranspiration estimation in near real-time (e.g., Mu et al. 2011).

H7 – Fire regime. The effects of wildfires are of particular importance in Mediterranean landscapes where they exert a strong influence on its structure, functioning and dynamics (Bajocco and Ricotta 2008, Silva et al. 2011). Fire regime components (frequency, season, intensity) significantly influence the composition and diversity of plant communities at the local scale and may cause the loss of many species (Bond and Wilgen 1996, Bowman and Murphy 2010). Reside et al. (2012) used fire frequency and its shifts to analyse its effect on the distribution of 44 bird species in Australia tropical savannas. Gogol-Prokurat (2011) used fire history, along with other relevant variables, to predict local scale habitat suitability for four endemic rare plant species in El Dorado, California. Bourg et al. (2005) also used fire frequency data to predict suitable habitat and potential new population occurrences for turkeybeard (Xerophyllum asphodeloides), a rare liliaceous understory herb associated with southern Appalachian pine-oak forests, in northwestern Virginia.

Appendix S4 – Correlation matrix for predictor variables used in model fitting

Table S 3 – Spearman correlation matrix for all the variables used in model fitting (Note: the three highest absolute pairwise-correlation values were highlighted in grey color and bold lettering).

	MAXVL	AMPLT	START	MIDSN	PAGFO	PURBD	MEDPS	TEDGE	PCAMB	EVPTR	RDENS	ABURN	BTRND
MAXVL	1.00												
AMPLT	**0.53**	1.00											
START	0.25	0.14	1.00										
MIDSN	0.10	-0.22	0.48	1.00									
PAGFO	0.13	0.22	-0.41	-0.38	1.00								
PURBD	0.07	0.12	-0.26	-0.24	0.53	1.00							
MEDPS	-0.17	-0.14	0.11	0.02	-0.32	-0.47	1.00						
TEDGE	0.21	0.10	-0.11	0.07	0.40	0.45	**-0.59**	1.00					
PCAMB	0.04	0.07	-0.29	-0.04	**0.59**	0.30	-0.39	**0.54**	1.00				
EVPTR	0.02	0.10	-0.08	-0.30	0.31	0.24	0.00	0.00	0.18	1.00			
RDENS	0.12	-0.07	0.03	0.04	-0.02	-0.01	-0.15	0.17	0.01	0.00	1.00		
ABURN	-0.10	-0.08	0.21	0.06	-0.45	-0.34	0.26	-0.42	-0.45	-0.19	0.09	1.00	
BTRND	0.02	0.01	0.15	0.23	-0.09	0.02	-0.04	0.09	0.05	-0.10	-0.06	-0.08	1.00

Variables description

PCAMB – percentage cover of cambisols for each 1km^2 grid unit

RDENS – density of main rivers (in m.km^{-2})

ABURN – average area burnt between 2000 and 2010, for each grid unit (in m^2)

BTRND – temporal tendency of burnt area using the trend slope (in m^2.year^{-1}) for the period 2001-2010 using Sen-Theil's method (Theil 1950, Sen 1968)

MAXVL – maximum value for the fitted function during the growing season (Jönsson and Eklundh 2002, Jönsson and Eklundh 2004)

AMPLT – seasonal amplitude (Jönsson and Eklundh 2002, Jönsson and Eklundh 2004)

START – time for the start of the growing season (in days) (Jönsson and Eklundh 2002, Jönsson and Eklundh 2004)

MIDSN – time for the mid of the growing season (in days) (Jönsson and Eklundh 2002, Jönsson and Eklundh 2004)

EVPTR – actual evapotranspiration (in mm.year^{-1}) used to characterize water availability from MODIS MOD16A3 product, computed according to Mu et al. (2011).

PAGFO – percentage covered by agricultural/agroforestry mosaics

PURBD – percentage cover of discontinuous/low-density urban areas for each 1km^2 grid unit

MEDPS – median patch size landscape spatial configuration (in m^2)

TEDGE – total length of patch edges (in meters)

Predictor variables types

Predictor variables were categorized into three groups: (i) static, (ii) semi-dynamic, and (iii) dynamic, following Stanton et al. (2011).

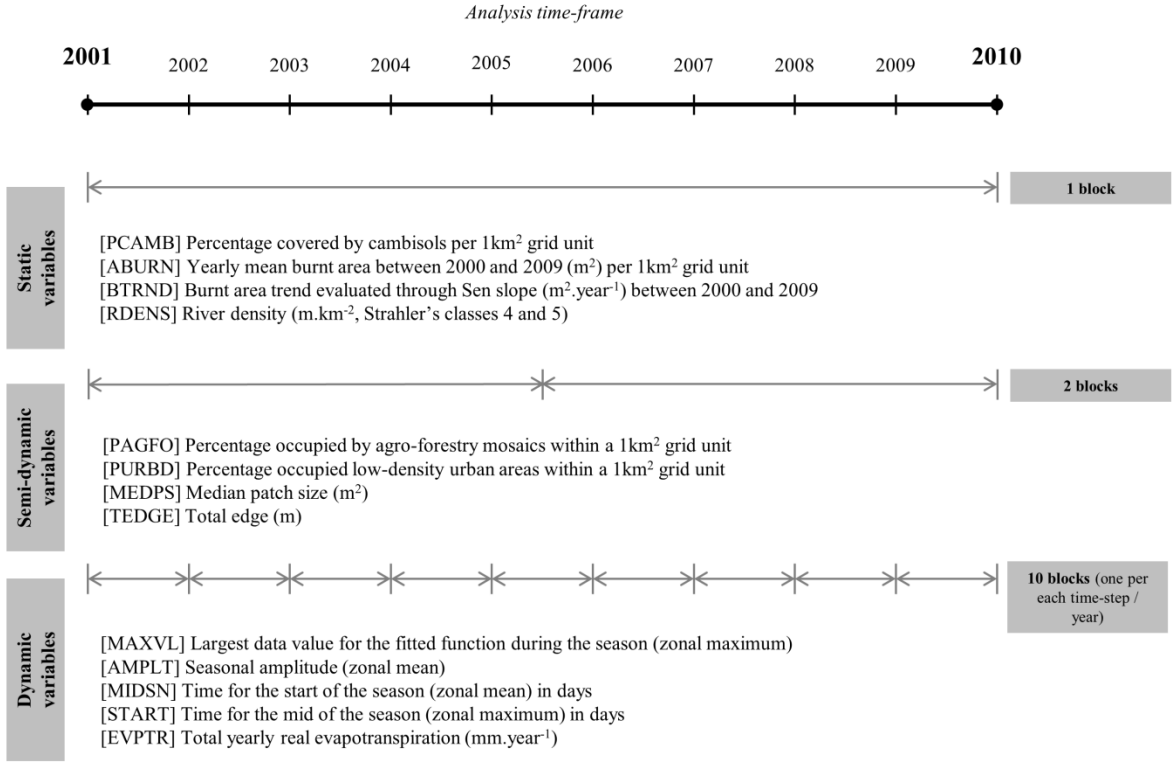

Appendix S5 – Model diagnostics

Several tests were used to produce a more complete diagnostic of modelling results. These included a Chi-square test for over-dispersion (

Table S 1; column 3). This problem happens if the observed variance of the response variable is larger than what would be expected from a binomial distribution. Over-

dispersion error can cause distorted test standard errors and inaccuracies in significance testing. For evaluation this effect we applied the test used in Kabacoff (2011).

We also tested for multicollinearity in each model by calculating Variance Inflation Factors (VIF) as implemented in the R package *car* using function *vif()*. Multicollinearity leads to large confidence intervals in model parameters and hinders the interpretation of individual model coefficients. For each predictor, the square-root of VIF shows the degree to which the confidence interval for that variable's regression parameter is increased in relation to a model with non-correlated predictors (Kabacoff 2011). In general, if $\sqrt{VIF} > 2$ is indicative of multicollinearity problems (

Table S 1; column 4).

In order to test for autocorrelation the Durbin-Watson test was used (

Table S 1; column 5). Observations were ordered according to longitude and tested for autocorrelation using function *durbinWatsonTest ()* at lag=1 implemented in R package *car*.

According to the diagnostic measures no significant problems were detected for the three tests, including over-dispersion (all test p-values > 0.05), multicollinearity (all values were under 2), and autocorrelation (all p-values > 0.05).

Table S 4 – Model diagnostics for each candidate model used in MMI testing. P-values use the following symbols (ns) p>0.05, (*) p<0.05, (**) p<0.01, (***) p<0.001. In VIF column only one value is shown since these are equal for bivariate models.

Model code	Model description	Chi-sq. test over-dispersion p-value	Square-root of VIF	Durbin-Watson test on autocorrelation at lag=1	
				Autocorrelation	p-value
M1	VFD (productivity)	0.264 (ns)	1.019	0.144	0.150 (ns)
M2	VFD (phenology)	0.304 (ns)	1.258	0.141	0.142 (ns)
M3	Landscape composition	0.266 (ns)	1.036	-0.266	0.390 (ns)
M4	Landscape configuration	0.304 (ns)	1.027	0.030	0.304 (ns)
M5	Soils	0.356 (ns)	-	-0.205	0.726 (ns)
M6	Water availability	0.266 (ns)	1.000	-0.068	0.738 (ns)
M7	Fire disturbance	0.266 (ns)	1.020	0.152	0.128 (ns)

Appendix S6 – Modified Corine Land Cover (CLC): methodological notes

In order to include land use/land cover (LULC) categories initially absent from the Corine Land Cover (CLC) dataset due to the minimum mapping unit (MMU, 25ha) of the product, we produced a modified CLC version integrating these categories.

The rationale behind this procedure relates also to the need of building a new LULC dataset that could better characterize landscape features that closely resemble present-day conditions and at the same time enhance the representation of landscape elements that were hypothesized as relevant for the test-species distribution.

Considering this, we performed an update on the original CLC 2000 and 2006 products using ancillary GIS data regarding:

a) Finer-scale land use/cover product (MMU = 1ha) for the year 2002 (hereafter named COS2002) considering the whole extent of the study-area;

b) Transportation networks namely roads and railways; and,

c) Strahler hierarchized river/hydrographic network at the municipal level.

All operations were performed with ESRI ArcGIS/ArcMap software using a vector representation of data. Regarding linear data (roads and hydrographic network) we used a buffer expansion on the original geometry to obtain a polygon representation of these features compatible with the CLC product. Buffer sizes/lengths are defined below on subsections b) and c) and were estimated through visual inspection and measurements (mean values) based on orthoimagery for the study area.

CLC updated features and procedures

a) Based on the COS2002 product the following categories were updated/inserted into the original CLC products:

   - Quarries
   - Water dams/water surfaces associated with irrigation infrastructures;
   - Discontinuous and low to very-low density urban areas (category URBD)

b) Based on the municipal hydrographic network:

   - Only rivers/water courses/streams with Strahler order higher than 3 were considered. Buffer sizes (single-side) equal to 2, 5 and 10 meters were used for rivers with Strahler orders 3, 4 and 5.

c) Based on transportation infrastructures data:

- National roads (EN-2/EN-202/EN-206) – buffer size = 3m
- Railways – buffer size = 3m
- Municipal roads – buffer size = 2.5m
- Forest tracks – buffer size = 1.5m
- Motorways A7/IC5 and A24/IP3 – buffer size = 20m. Motorways were updated/inserted exclusively on the CLC 2006 map since their construction was finished in 2005 (A24/IP3) and 2006 (A7/IC5). Both roads were already present (or partially present in the case of A7/IC5) in the 2006 product in the class. “133 – Construction sites”.

After performing all geometric and database operations that lead to the new CLC version we used a reclassified version of it based on simplification of the original legend. The reclassification table is presented below (Table S 5).

Table S 5 – CLC 2000/2006 reclassification table (Note: * - after 2005/2006 this LULC category has changed into an active motorway currently opened to the public).

Initial CLC code and category	New code	New category
1.1.2 Discontinuous urban fabric	URBC	Urban areas
1.2.2 Road and rail networks and associated land	TNET	High density transportation networks (motorways, national roads and railways)
1.3.1 Mineral extraction areas	QUAR	Quarries
1.3.3 Construction sites	TNET (*)	High density transportation networks (motorways, national roads and railways)
2.1.1 Non-irrigated arable land	AGFO	Agricultural and agro-forestry areas
2.2.1 Vineyards	AGFO	Agricultural and agro-forestry areas
2.3.1 Pastures	AGFO	Agricultural and agro-forestry areas
2.4.1 Annual crops associated with permanent crops	AGFO	Agricultural and agro-forestry areas
2.4.2 Complex cultivation patterns	AGFO	Agricultural and agro-forestry areas
2.4.3 Land principally occupied by agriculture, with significant areas of natural vegetation	AGFO	Agricultural and agro-forestry areas
3.1.1 Broad-leaved forest	BLFO	Broadleaved forests
3.1.2 Coniferous forest	COFO	Coniferous forests
3.1.3 Mixed forest	MXFO	Mixed forests
3.2.1 Natural grassland	HBVG	Natural herbaceous vegetation (natural grasslands)
3.2.2 Moors and heathland	SLHL	Shrublands and heathlands

3.2.4 Transitional woodland/shrub	SLHL	Shrublands and heathlands
3.3.2 Bare rocks	SPVG	Sparsely vegetated areas
3.3.3 Sparsely vegetated areas	SPVG	Sparsely vegetated areas
3.3.4 Burnt areas	SLHL	Shrublands and heathlands

After the reclassification procedure a new and simplified geometry was generated by using ArcGIS' "*Dissolve*" command. Based on these modified datasets we calculated the areas covered by each class for 2000 and 2006 as well as its percent change in this period (see Table S 6). These modified versions of CLC were later used to calculate the percentage cover of each class per grid unit and also several landscape metrics for each grid unit.

Table S 6 – Final LULC classes/categories in the modified CLC version and related areas and percentage covered by each category for the years 2000 and 2006. Column in position five, "% change 2000 – 2006", depicts % change = [(A_{2006} - A_{2000}) / A_{2000}] × 100, with A equal to the total class area (Note: classes flagged with an asterisk (*) were originally absent from the CLC legend). Columns "AICc" and "D" show respectively the Akaike Information Criterion (with small sample size correction) and Deviance for an univariate model containing each land use/cover class used to preliminarily test the predictive performance of landscape composition categories.

Code	Description	Area (m^2)		% Cover		% change 2000 - 2006	AICc	D
		2000	2006	2000	2006			
AGFO	Agricultural and agro-forestry areas	13001.6	12919.2	25.7	25.5	-0.6	28.26	0.28
BLFO	Broadleaved forests	1360.7	786.7	2.7	1.6	-42.2	33.47	0.06
COFO	Coniferous forests	8980.1	5147.8	17.7	10.2	-42.7	32.63	0.09
HBVG	Natural herbaceous vegetation (natural grasslands)	2320.8	2261.3	4.6	4.5	-2.6	32.36	0.15
MURS*	Municipal roads	110.3	110.3	0.2	0.2	0.0	34.94	0.01
MXFO	Mixed forests	2295.2	1683.7	4.5	3.3	-26.6	34.15	0.04
QUAR	Quarries	432.7	569.6	0.9	1.1	31.7	35.06	0.06
RIVR*	Rivers (water surface and margins)	197.2	196.9	0.4	0.4	-0.2	31.10	0.14
SLHL	Shrublands and heathlands	14357.6	18953.1	28.4	37.5	32.0	32.67	0.09
SPVG	Sparsely vegetated areas	6244.6	5947.2	12.3	11.8	-4.8	34.67	0.02

TNET	High density transportation networks (motorways, national roads and railways)	54.9	768.4	0.1	1.5	1300.5	35.38	0.00
TRKS*	Tracks	110.8	110.8	0.2	0.2	0.0	34.30	0.04
URBC	High-density continuous urban areas	342.6	354.7	0.7	0.7	3.5	-	-
URBD*	Low-density discontinuous urban areas	671.7	671.3	1.3	1.3	0.0	28.79	0.21
WADM*	Water damns	119.0	119.0	0.2	0.2	0.0	-	-

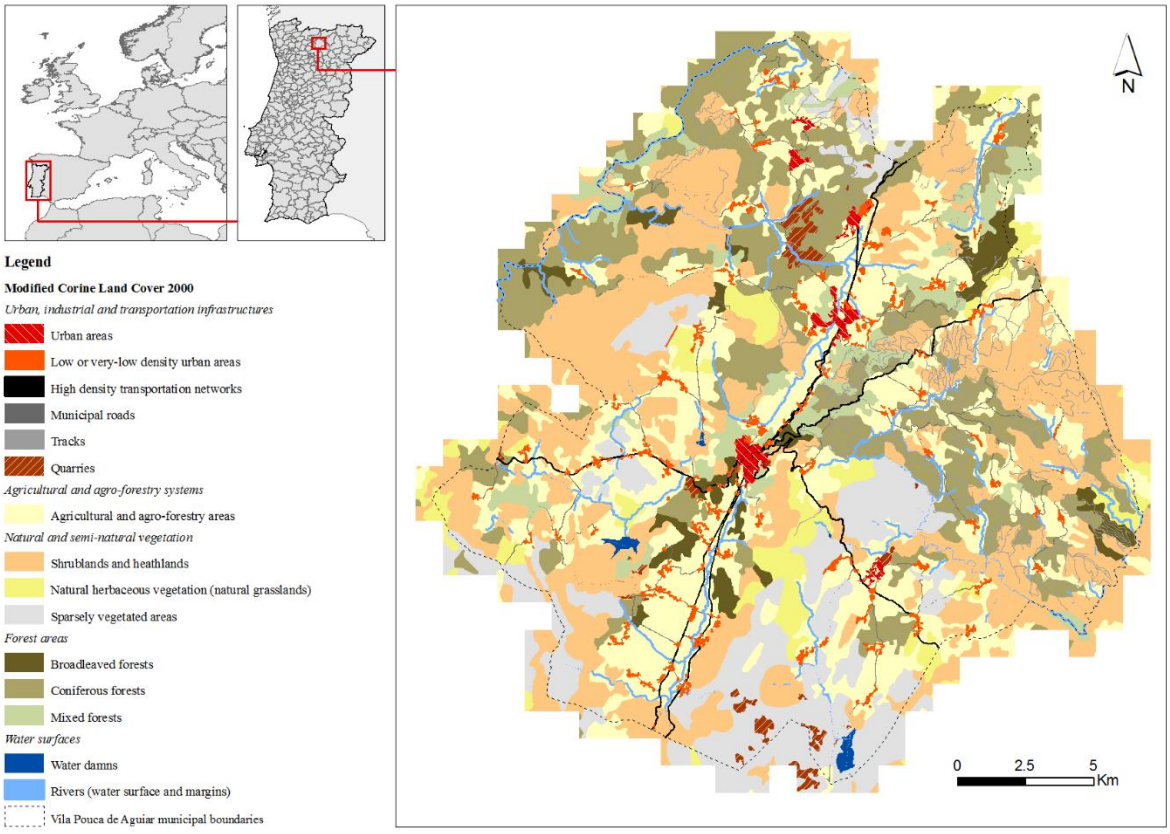

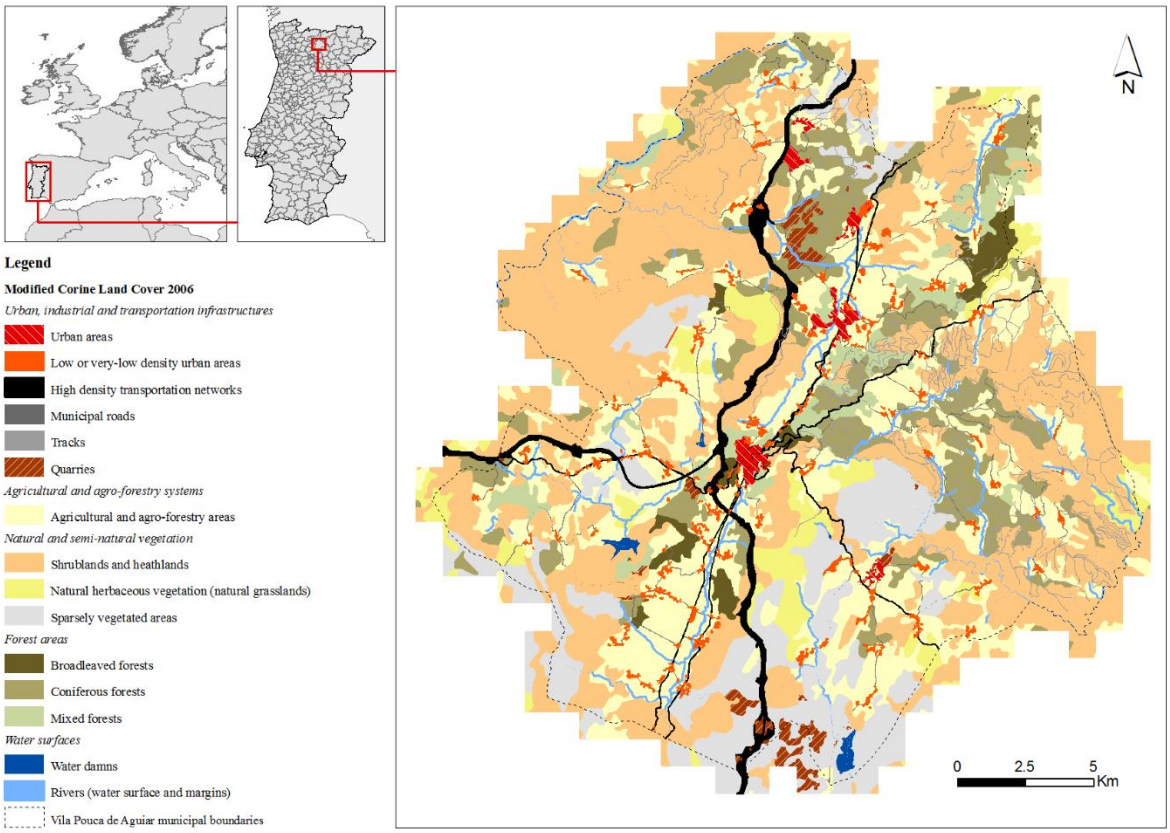

Appendix S7 – Species response curves for predictors

With the purpose of furthering the description of *V. micrantha* determinants of habitat suitability, univariate GAM models were used to devise response curves plots (RCP; (Elith et al. 2005, Heikkinen and Mäkipää 2010) allowing to analyse the response variability of the species to the gradient in a certain predictor. GAM univariate models included terms with a maximum allowed smoothing equal to 2 (as in the competing models defined for multi-model inference). Solid black lines represent GAM predicted values $\pm$ the standard error in red dashed lines. In general, RCPs showed complex and non-linear responses of the species to the environmental gradients depicted in predictor variables.

M1: Seasonal amplitude (AMPLT)

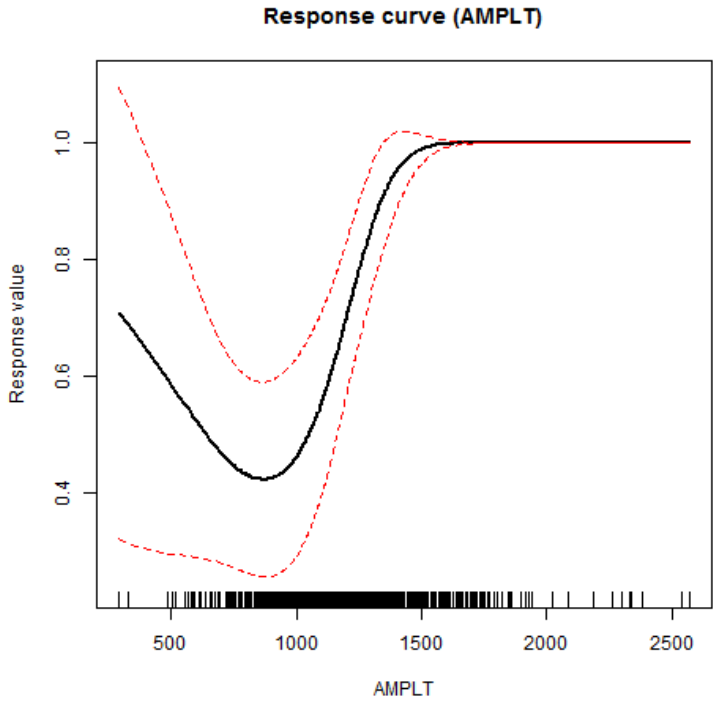

M1: Peak value of the growing season (MAXVL)

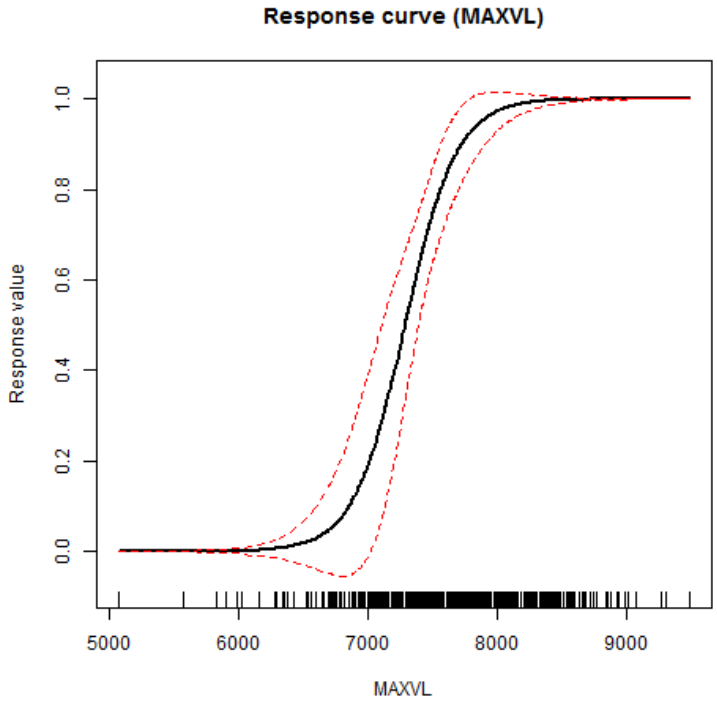

M2: Mid of growing season (MIDSN, in days)

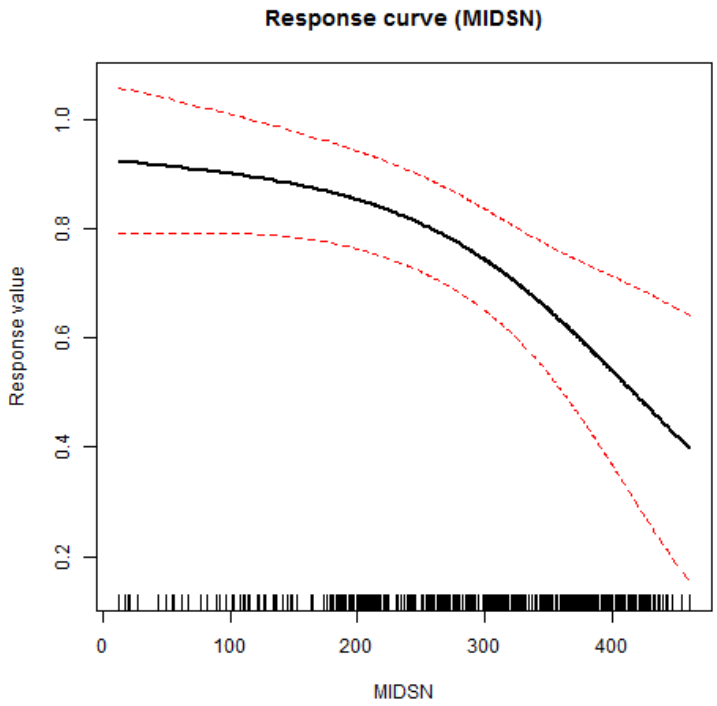

M2: Start of the growing season (START, in days)

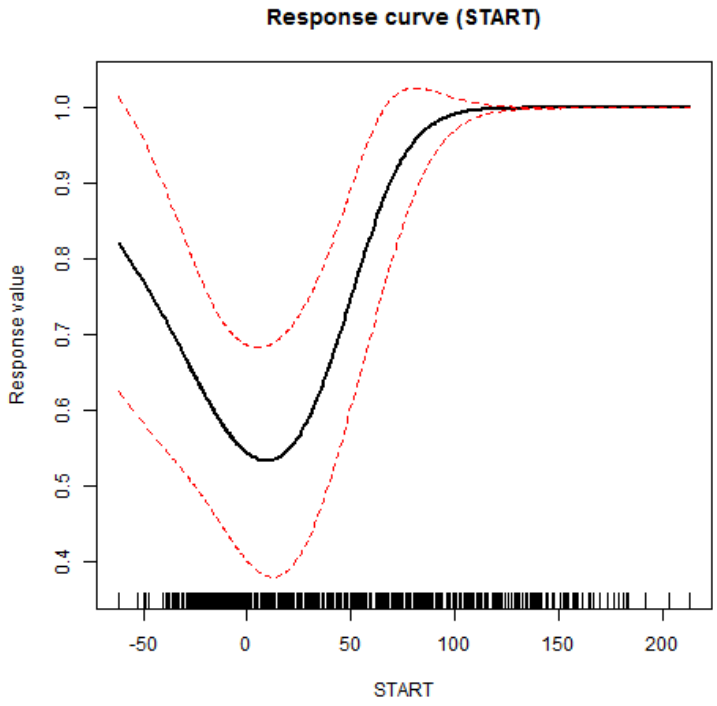

M3: % covered by agroforestry (PAGFO)

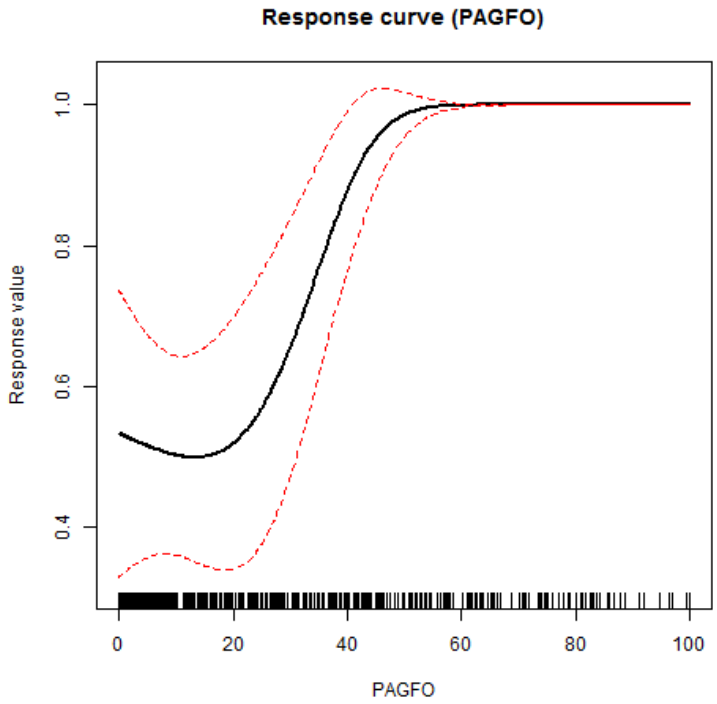

M3: % covered by discontinuous low-density urban-rural areas (PURBD)

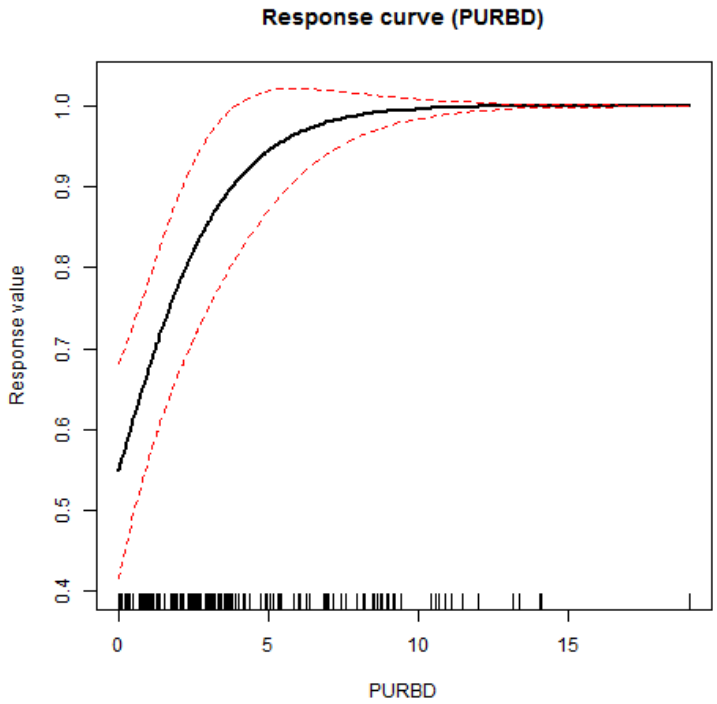

M4: Median patch size (MEDPS, in m^2)

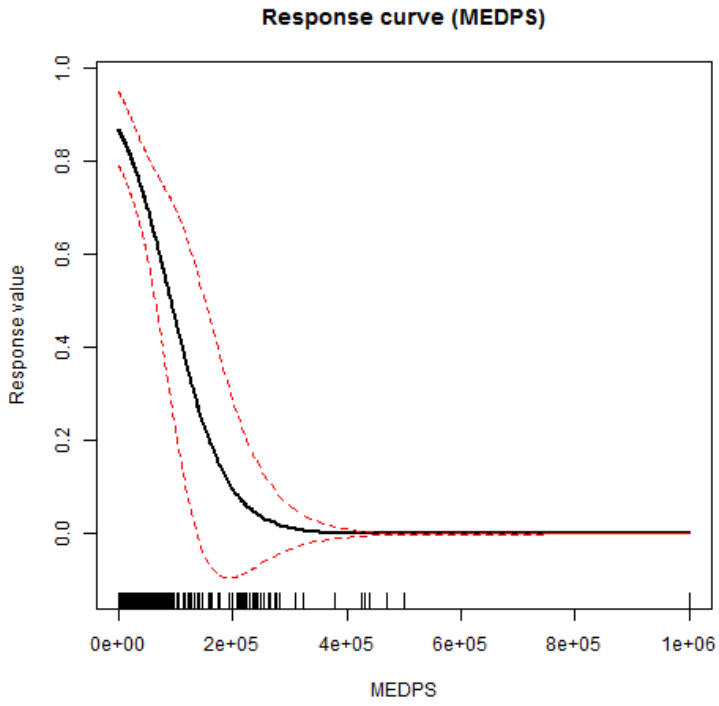

M4: Total patch edge, in meters considering all land cover/use categories (TEDGE)

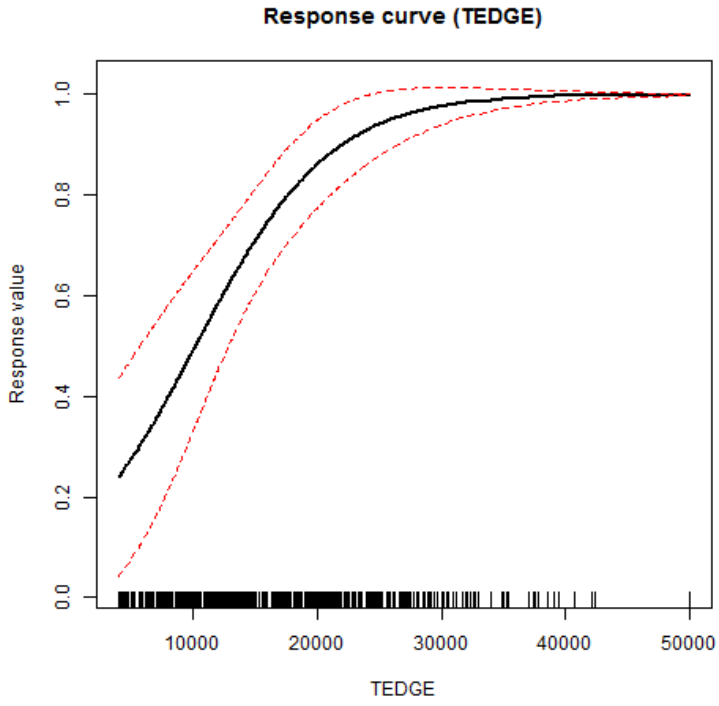

M5: % cover of cambisols (PCAMB)

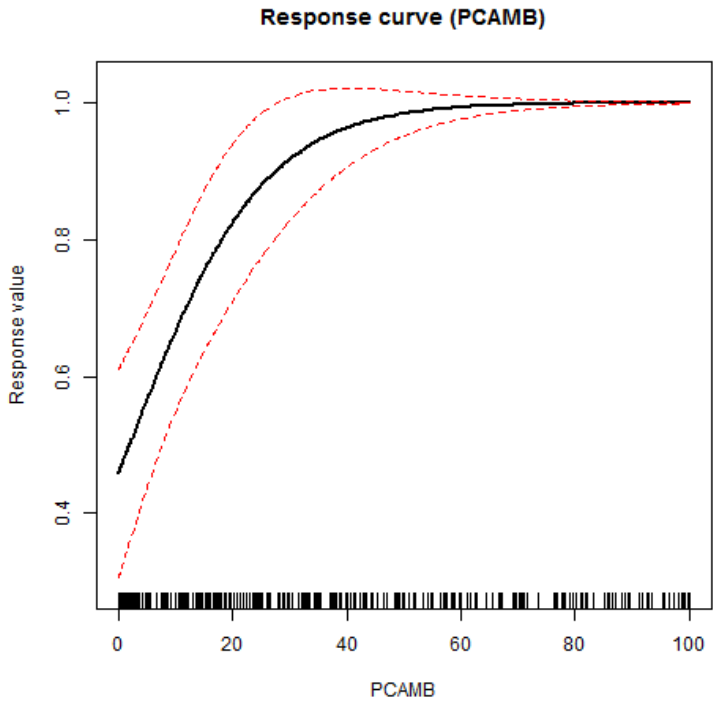

M6: Actual evapotranspiration (EVPTR)

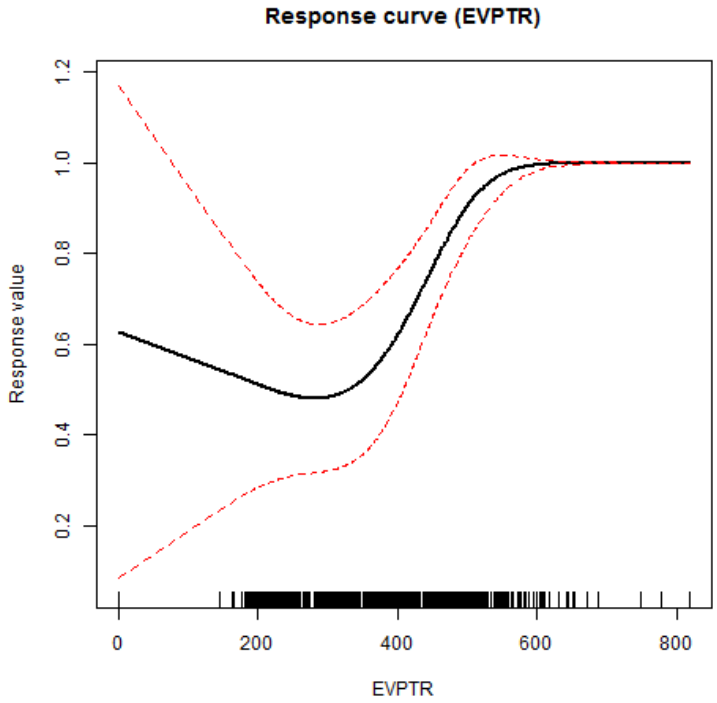

M6: River density in each grid unit (RDENS, in $m.km^{-2}$)

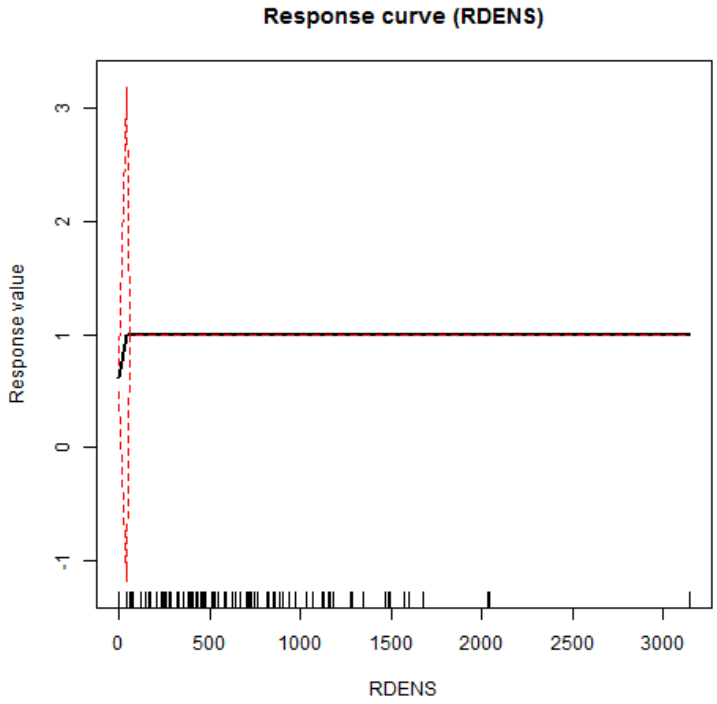

M7: ABURN – average burned area between 2001 and 2010

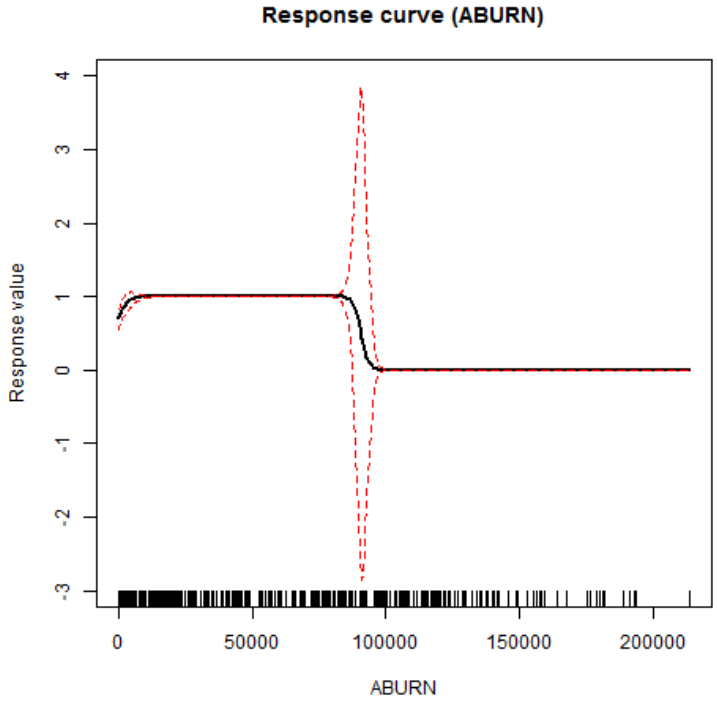

M7: BTRND – burned area trend for 2001 – 2010

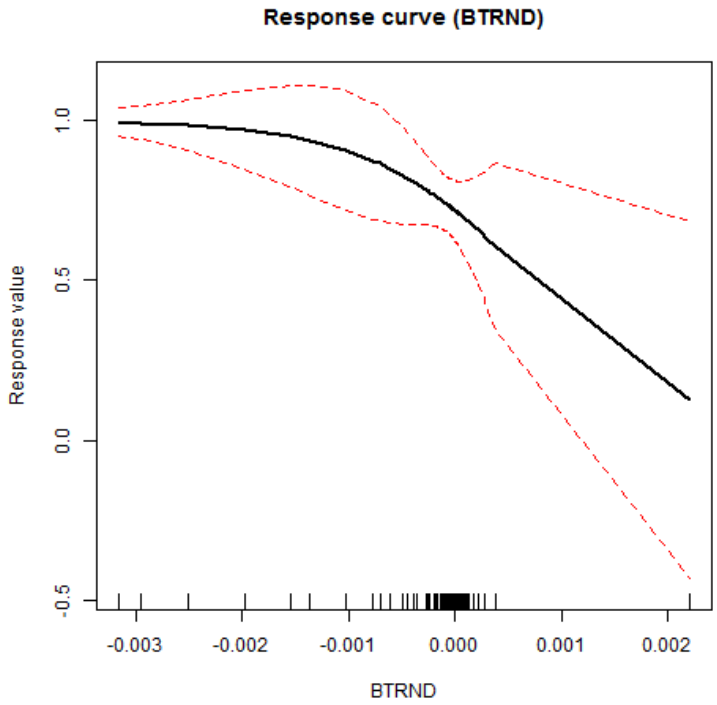

References

AFN. 2011. Cartografia nacional de áreas ardidas (national mapping of burnt areas), URL: http://www.afn.min-agricultura.pt/portal/dudf/cartografia/cartograf-areas-ardidas-1990-2009, accessed on 10-01-2011. Autoridade Florestal Nacional (National Forestry Authority).

Aitken, M., D. W. Roberts, and L. M. Shultz. 2007. Modeling distributions of rare plants in the Great Basin, Westhern North America. Western North American Naturalist 67:26-38.

Alcaraz, D., J. Paruelo, and J. Cabello. 2006. Identification of current ecosystem functional types in the Iberian Peninsula. Global Ecology and Biogeography 15:200-212.

Atauri, J. A., and J. V. d. Lucio. 2001. The role of landscape structure in species richness distribution of birds, amphibians, reptiles and lepidopterans in Mediterranean landscapes. Landscape Ecology:147-159.

Bajocco, S., and C. Ricotta. 2008. Evidence of selective burning in Sardinia (Italy): which land-cover classes do wildfires prefer? Landscape Ecology 23:241-248.

Beck, P. S. A., T. J. Wang, A. K. Skidmore, and X. H. Liu. 2008. Displaying remotely sensed vegetation dynamics along natural gradients for ecological studies. International Journal of Remote Sensing 29:4277-4283.

Begon, M., C. R. Townsend, and J. L. Harper. 2006. The Flux of Energy through Ecosystems. Pages 512-537 Ecology - From individuals to ecosystems. Blackwell Publishing Ltd, Oxford, UK.

Bond, W. J., and B. W. v. Wilgen. 1996. Plants and Fire. Chapman and Hall, London, UK.

Bourg, N. A., W. J. McShea, and D. E. Gill. 2005. Putting a CART before the search: successful habitat prediction for a rare forest herb. Ecology 86:2793-2804.

Bowman, D. M. J. S., and B. P. Murphy. 2010. Fire and biodiversity. Pages 163-180 *in* N. S. Sodhi and P. R. Ehrlich, editors. Conservation Biology for All. Oxford University Press, New York.

Bradley, B. A., and E. Fleishman. 2008. Can remote sensing of land cover improve species distribution modelling? Journal of Biogeography 35:1158-1159.

Caetano, M., A. Araújo, A. Nunes, V. Nunes, and M. Pereira. 2009a. Accuracy assessment of the CORINE Land Cover 2006 map of Continental Portugal, Technical Report. Instituto Geográfico Português.

Caetano, M., V. Nunes, and A. Nunes. 2009b. CORINE Land Cover 2006 for Continental Portugal, Technical Report. Instituto Geográfico Português.

Coops, N. C., M. A. Wulder, and D. Iwanicka. 2009. Exploring the relative importance of satellite-derived descriptors of production, topography and land cover for predicting breeding bird species richness over Ontario, Canada. Remote Sensing of Environment 113:668-679.

Dumortier, M., J. Butaye, H. Jacquemyn, N. Van Camp, N. Lust, and M. Hermy. 2002. Predicting vascular plant species richness of fragmented forests in agricultural landscapes in central Belgium. Forest Ecology and Management 158:85-102.

Elith, J., S. Ferrier, F. Huettmann, and J. Leathwick. 2005. The evaluation strip: A new and robust method for plotting predicted responses from species distribution models. Ecological Modelling 186:280-289.

Elith, J., S. J. Phillips, T. Hastie, M. Dudík, Y. E. Chee, and C. J. Yates. 2011. A statistical explanation of MaxEnt for ecologists. Diversity and Distributions 17:43-57.

Fisher, J. B., R. J. Whittaker, and Y. Malhi. 2011. ET come home: potential evapotranspiration in geographical ecology. Global Ecology and Biogeography 20:1-18.

Gogol-Prokurat, M. 2011. Predicting habitat suitability for rare plants at local spatial scales using a species distribution model. Ecological Applications 21:33-47.

Guisan, A., O. Broennimann, R. Engler, M. Vust, N. G. Yoccoz, A. Lehmann, and N. E. Zimmermann. 2006. Using Niche-Based Models to Improve the Sampling of Rare Species. Conservation Biology 20:501-511.

Hamer, T., C. Flather, and B. Noon. 2006. Factors Associated with Grassland Bird Species Richness: The Relative Roles of Grassland Area, Landscape Structure, and Prey. Landscape Ecology 21:569-583.

Hawkins, B. A., R. Field, H. V. Cornell, D. J. Currie, J.-F. Guégan, D. M. Kaufman, J. T. Kerr, G. G. Mittelbach, T. Oberdorff, E. M. O'Brien, E. E. Porter, and J. R. G. Turner. 2003. Energy, water, and broadscale geographic patterns of species richness. Ecology 84:3105-3117.

Heikkinen, J., and R. Mäkipää. 2010. Testing hypotheses on shape and distribution of ecological response curves. Ecological Modelling 221:388-399.

IM. 2012. Climate Normals 1971 - 2000 for Vila Real (Portugal) climatological station. Instituto de Meteorologia.

Jönsson, A. M., L. Eklundh, M. Hellström, L. Bärring, and P. Jönsson. 2010. Annual changes in MODIS vegetation indices of Swedish coniferous forests in relation to snow dynamics and tree phenology. Remote Sensing of Environment 114:2719-2730.

Jönsson, P., and L. Eklundh. 2002. Seasonality extraction by function fitting to time-series of satellite sensor data. Geoscience and Remote Sensing, IEEE Transactions on 40:1824-1832.

Jönsson, P., and L. Eklundh. 2004. TIMESAT - a program for analyzing time-series of satellite sensor data. Computers & Geosciences 30:833-845.

Kabacoff, R. I. 2011. R in Action - Data analysis and graphics with R. First edition. Manning Publications, Shelter Island, NY.

Klironomos, J. N. 2002. Feedback with soil biota contributes to plant rarity and invasiveness in communities. Nature 417:67-70.

Kottek, M., J. Grieser, C. Beck, B. Rudolf, and F. Rubel. 2006. World Map of the Köppen-Geiger climate classification updated. Meteorologische Zeitschrift 15:259-263.

Le Lay, G., R. Engler, E. Franc, and A. Guisan. 2010. Prospective sampling based on model ensembles improves the detection of rare species. Ecography 33:1015-1027.

Lomba, A., L. Pellissier, C. Randin, J. Vicente, F. Moreira, J. Honrado, and A. Guisan. 2010. Overcoming the rare species modelling paradox: A novel hierarchical framework applied to an Iberian endemic plant. Biological Conservation 143:2647-2657.

Mu, Q., M. Zhao, and S. W. Running. 2011. Improvements to a MODIS global terrestrial evapotranspiration algorithm. Remote Sensing of Environment 115:1781-1800.

Pettorelli, N., J. O. Vik, A. Mysterud, J.-M. Gaillard, C. J. Tucker, and N. C. Stenseth. 2005. Using the satellite-derived NDVI to assess ecological responses to environmental change. Trends in ecology & evolution (Personal edition) 20:503-510.

Phillips, S. J., R. P. Anderson, and R. E. Schapire. 2006. Maximum entropy modeling of species geographic distributions. Ecological Modelling 190:231-259.

Phillips, S. J., and M. Dudík. 2008. Modeling of species distributions with Maxent: new extensions and a comprehensive evaluation. Ecography 31:161-175.

Renfrew, R., and C. Ribic. 2008. Multi-scale models of grassland passerine abundance in a fragmented system in Wisconsin. Landscape Ecology 23:181-193.

Reside, A. E., J. VanDerWal, A. Kutt, I. Watson, and S. Williams. 2012. Fire regime shifts affect bird species distributions. Diversity and Distributions 18:213-225.

Sen, P. K. 1968. Estimates of the Regression Coefficient Based on Kendall's Tau. Journal of the American Statistical Association 63:1379-1389.

Silva, J. S., P. Vaz, F. Moreira, F. Catry, and F. C. Rego. 2011. Wildfires as a major driver of landscape dynamics in three fire-prone areas of Portugal. Landscape and Urban Planning 101:349-358.

Stanton, J. C., R. G. Pearson, N. Horning, P. Ersts, and H. R. Akçakaya. 2011. Combining static and dynamic variables in species distribution models under climate change.

Theil, H. 1950. A rank-invariant method of linear and polynomial regression analysis. Pages 1397–1412 *in* III Proceedings of the Koninklijke Nederlandse Akademie van Wetenschappen.

Thornton, D., L. Branch, and M. Sunquist. 2011. The influence of landscape, patch, and within-patch factors on species presence and abundance: a review of focal patch studies. Landscape Ecology 26:7-18.

Tuanmu, M.-N., A. Viña, S. Bearer, W. Xu, Z. Ouyang, H. Zhang, and J. Liu. 2010. Mapping understory vegetation using phenological characteristics derived from remotely sensed data. Remote Sensing of Environment 114:1833-1844.

Turner, M. G. 2005. Landscape Ecology: What Is the State of the Science? Annual Review of Ecology, Evolution, and Systematics 36:319-344.

Wever, L. A., L. B. Flanagan, and P. J. Carlson. 2002. Seasonal and interannual variation in evapotranspiration, energy balance and surface conductance in a northern temperate grassland. Agricultural and Forest Meteorology 112:31-49.

Wiser, S. K., R. K. Peet, and P. S. White. 1998. Prediction of rare-plant occurrence: A southern Appalachian example. Ecological Applications 8:909-920.

Wisz, M. S., R. J. Hijmans, J. Li, A. T. Peterson, C. H. Graham, and A. Guisan. 2008. Effects of sample size on the performance of species distribution models. Diversity and Distributions 14:763-773.

Appendix III | Chapter 6 - A model-based framework for assessing the vulnerability of low dispersal vertebrates to landscape fragmentation under environmental change

Appendix S1 – Study-area description, species occurrence points and description of the test species

Study-area description

According to the Köppen-Geiger classification (Peel et al. 2007) the study-area, including the full extent of mainland Portugal, presents a Mediterranean climate type with subtype *Csb* ("warm-summer") mainly in the north and subtype *Csa* ("hot-summer") mainly in the south. Mean annual temperature ranges from approximately 7ºC in the northern mountains to 18ºC in the southern lowlands. Mean total annual precipitation ranges from approximately 400mm in the southern areas and in the upper Douro valley up to 2800mm in the northwest mountain areas.

In the global climatic classification of Metzger *et al.* (2013), most of mainland Portugal was classified as having Warm Temperate climate, xeric to mesic, with cold and wet conditions being reached in the main mountain tops.

Mainland Portugal is largely included in the Mediterranean biogeographic region and only the north-western part of the country belongs to the Eurosiberian region (Costa et al. 2012).

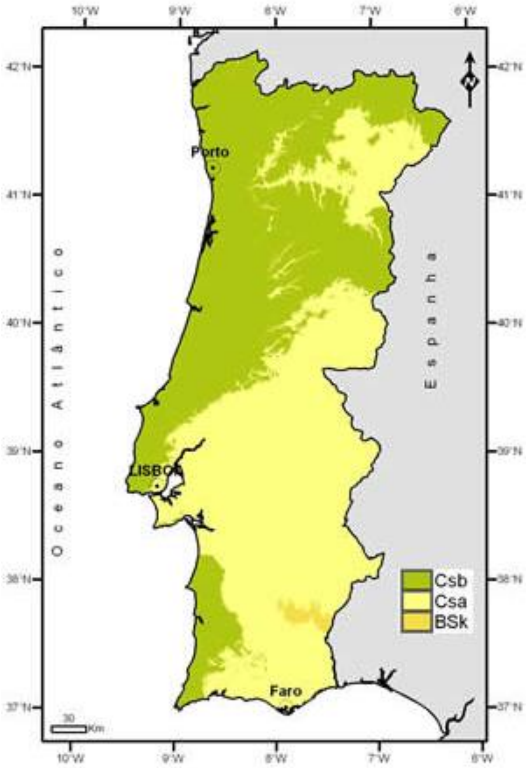

Figure 5 - Koppën climatic classification for mainland Portugal (source: https://www.ipma.pt/pt/oclima/normais.clima/, visited October 2014)

In terms of lithology, schist and granite are the predominant bedrock types, with limestone and other sedimentary formations strongly represented in the centre-west and southwest areas.

According to Corine Land Cover 2006 (EEA 2007, Caetano et al. 2009a, Caetano et al. 2009b) the country is composed by 47.05% of agricultural and agroforestry areas, 22.59% by forest areas, 19.37% is occupied by heathlands, shrublands, moors and/or early-successional vegetation, 5.77% by open spaces sparsely or non-vegetated, 3.47% by artificial surfaces, and, 1.74% by wetlands and inland water bodies.

Description of selected species

Lacerta schreiberi (Schreiber's Green Lizard) is an Iberian endemism considered as Near Threatened by IUCN (Sá-Sousa et al. 2009) as their population trend is decreasing. This species lives in humid, bushy areas of shrubland, woodland edges, open woodland (deciduous, mixed and pine), along river and stream sides, overgrown sites and close to fences in pasture land. It is tightly linked to streams in the southern part of its distribution. Populations of this species are considered isolated if there is no

other population within a distance of 10 km (Brito 1999), thus we considered it as a high dispersal capacity reptile species.

As the opposite, *Anguis fragilis* has a very extensive worldwide distribution that occupies most part of Europe, from the Iberian Peninsula and Britain (though absent in Ireland) to Russia (Galán and Salvador 2009). In Portugal, this species is distributed widely through the North of the country and so more located at center (Loureiro et al. 2008). Its abundance decreases from North to the central and eastern regions, and is absent in the South. We considered this species as low dispersal capacity since the reported maximum annual dispersal distance for adult individuals is around 1000m (Popescu et al. 2013).

Chioglossa lusitanica (Golden-striped Salamander) is another Iberian endemism considered as Vulnerable by IUCN (Arntzen et al. 2009) as their population trend is decreasing. The species is associated with clear, well-oxygenated, small- to medium-sized streams, with dense surrounding vegetation in mountainous and hilly areas. It is associated with broad-leaved oak forest, and occurs in secondary vegetation, but not usually in commercial plantations. Some populations in north-western Spain have disappeared following replacement of broad-leaved forest with other habitats. The major threats to the species are pollution of streams with agrochemicals, and the loss of terrestrial habitats associated with the streams through conversion to forestry plantations (mainly eucalypt and pine plantations). In Portugal, habitat is at risk due to recurrent wildfires. We considered this species as low dispersal capacity given that their migration distances are a few hundreds of meters (Arntzen 1980).

As the opposite, *Epidalea calamita* (Natterjack Toad) is a wide distributed species in Europe considered as Least Concern by IUCN (Beja et al. 2009). This species is generally found in open and unshaded light sandy soils of coastal dunes, lowland heaths, semi-desert, high mountains, pine forest glades, gardens, parks, agricultural fields, sand and gravel quarries and meadows. The main threats to this species are loss of specialized habitats by natural encroachment of scrub and woodland; afforestation, acidification of breeding pools, agricultural development and infilling of breeding sites (such as temporary pools and sand and gravel quarries). In some parts of its range (e.g. in UK and Spain) chytridiomycosis is a threat. The species is considered vulnerable to climate change, particularly in southern Europe. The maximum annual migratory range of adult natterjacks recorded is 4441m (Smith and Green 2005) placing natterjacks among the upper 10% of wide-ranging anuran species. Given this value we considered this species as high dispersal capacity.

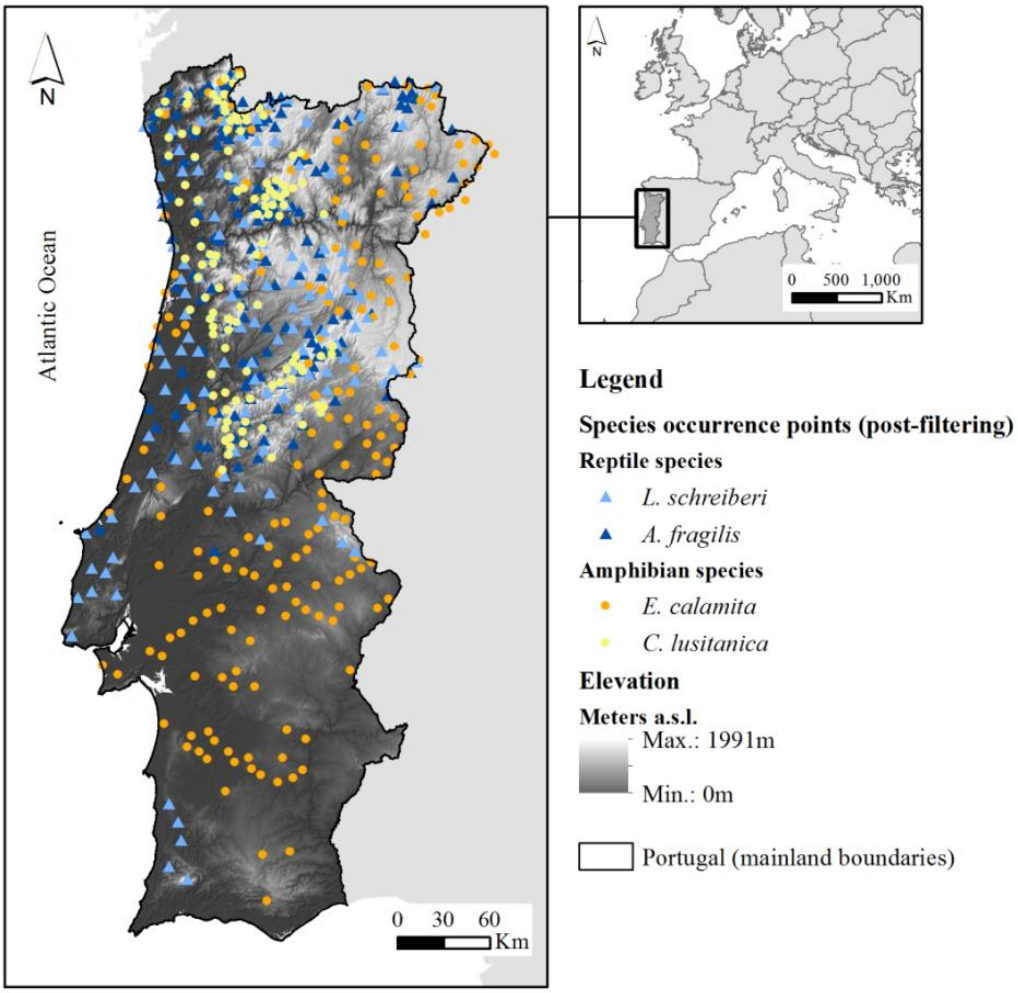

Figure 6 – Study area location and species occurrence points used for model fitting after employing the spatial filtering routine.

Appendix S2 – Results for the spatial filtering routine applied to occurrence records

The Clarck-Evans aggregation index (CEAI) was used to perform the spatial filtering of input data on species occurrence. This index provides a measure of clustering or ordering of a point pattern, calculated as the ratio of the observed mean distance between nearest neighbours in the data to that expected for a Poisson point process of the same intensity. A CEAI value equal to 1 indicates that the points are distributed randomly, whereas CEAI>1 suggests ordering, and, CEAI<1 suggests clustering. To avoid biases due to edge effects, we computed the corrected Clark and Evans index as

proposed by (Donnelly 1978). The computation was performed in R statistical software using the *spatstat* package (Baddeley and Turner 2005).

Table 1 – Results for the spatial filtering applied for reducing spatial sampling bias and spatial autocorrelation in occurrence records collected from the Portuguese Atlas of Reptiles and Amphibians. The pairwise distance (in meters) corresponds to the value for which the Clarck-Evans aggregation index was increased up to 0.9 after removing duplicated and/or clustered neighbouring points. N_0 and N_1 are, respectively, the initial and final number of points used for model fitting

Species	Pairwise distance (meters)	Clark-Evans aggregation index	N_0	N_1
ANGFR	3250	0.855	281	178
EPCAL	6500	0.856	860	191
CHALU	3250	0.872	480	112
LACSH	9500	0.853	1899	133

Appendix S3 – List of available GCMs from WorldClim

Full list of GCMs used to produce ensemble average projections for bioclimatic data concerning RCP 2.6 and RCP 8.5 for the year 2050. All data was downloaded from http://www.worldclim.org/cmip5_30s (visited at February 2014) with a spatial resolution of 30 arc-second (*ca.* 900m at the equator). Although data for GCMs: CNRM-CM5 (CN) and MIROC5 (MC) were available, some problems were detected in file integrity and decompression, and for that reason they were not used in climatic data ensembles.

GCM	Code
BCC-CSM1-1	BC
CCSM4	CC
GFDL-CM3	GF
GISS-E2-R	GS
HadGEM2-AO	HD
HadGEM2-ES	HE
IPSL-CM5A-LR	IP
MRI-CGCM3	MG
MIROC-ESM-CHEM	MI
MPI-ESM-LR	MP
MIROC-ESM	MR
NorESM1-M	NO

Appendix S4 – Land-use categories used in DynaCLUE 2050 land-use change projections for Europe based on Corine Land Cover

Dyna CLUE class	Nr	Visualization (RGB)	Land cover class description
0	0	0 (219/0/0)	Built-up area
1	1	1 (254/250/194)	Arable land (non-irrigated)
2	2	2 (163/222/133)	Pasture land
3	3***	3 (114/137/68)	(Semi-) natural vegetation (including natural grasslands, scrublands, regeneration forest below 2m and small forest patches within agricultural landscapes)
9	4*	4 (173/164/254)	Inland wetlands
9	5*	5 (160/160/160)	Glaciers and snow
4	6	6 (254/172/0)	Irrigated arable land
5	7	7 (205/205/102)	Recently abandoned arable land (i.e., "long fallow": includes very extensive farmland not reported in agricultural statistics, herbaceous vegetation, grasses and shrubs below 30cm)
6	8	8 (205/152/107)	Permanent crops
-	9**	1 (254/250/194)	Arable land devoted to the cultivation of (annual) biofuel crops
7	10	9 (1/99/0)	Forest
9	11*	5 (160/160/160)	Sparsely vegetated areas
9	12*	5 (160/160/160)	Beaches, dunes and sands
9	13*	-9999	Salines
9	14	-9999	Water and coastal flats
9	15*	3 (114/137/68)	Heather and moorlands
8	16	7 (205/205/102)	Recently abandoned pasture land (includes very extensive pasture land not reported in agricultural statistics, grasses and shrubs below 30cm)
-	17	1 (254/205/194)	Perennial crops cultivated for biodiesel production

Appendix S5 – Evaluation of species distribution dynamics and connectivity analyses (full methodological description)

Boolean comparisons between ensembled model projections for current and future conditions allowed evaluating the potential dynamics in the distribution of suitable areas for the target species. The possible outcomes of these comparisons yielded four discrete classes defined as, (i) ”unsuitable”: areas currently unsuitable that will remain unsuitable in future projections; (ii) “lost”: areas currently suitable that will lose suitability in the future; (iii) ”kept”: areas that are currently suitable that will remain with adequate conditions in the future, and, (iv) ”new”: areas that are currently unsuitable that may become suitable in the future.

In this analysis we assumed that populations affected by loss of environmental suitability (*i.e.*, inhabiting areas identified as “lost”), due to combined effects of climate and land use changes, will be forced migrate to stable areas that remain suitable under the obtained model projections (identified as “kept”). We argue that it would be also possible to apply the same reasoning to study the potential colonization of projected new suitable areas by analysing connectivity from “kept” and/or “lost” areas to “new” areas. However, we focused our attention on the likelihood of potential migrations from “lost” to “kept” areas by analysing the functional connectivity between these two instances.

In order to assess the connectivity between these areas we used LORACS software (Pinto and Keitt 2009, Pinto et al. 2012) which allowed evaluating multiple shortest paths (SP) from “lost” to “kept” areas which are assumed to form a corridor. This analysis also enables the evaluation of corridor redundancy using a graph-theoretical approach while simultaneously accounting for landscape matrix resistance.

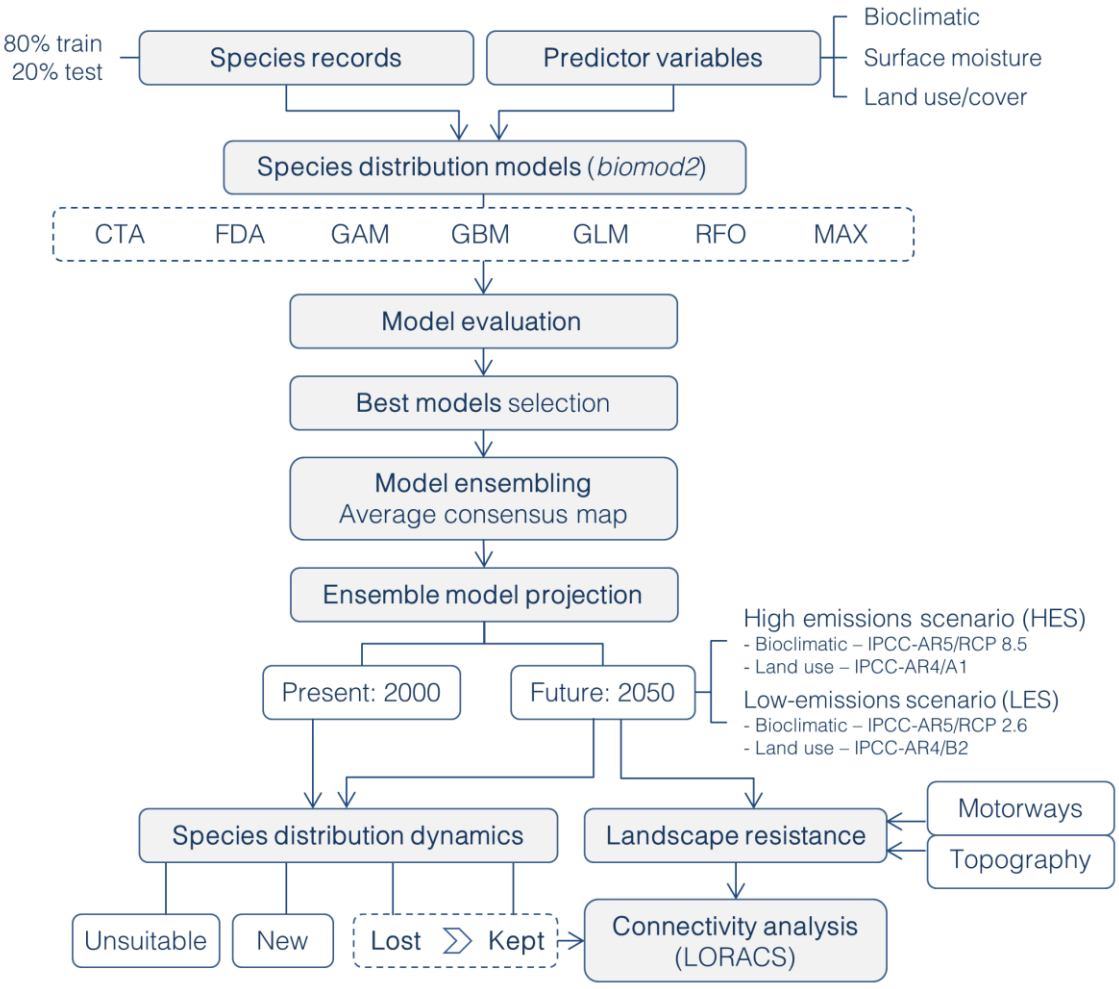

Figure 7 – Schematic representation of the methodological approach implemented

The parameterization of LORACS was set to a corridor width of 30% and 10 different SPs were calculated between each "lost" cell, hereafter denoted as a source area, $s_i, i \in \{1, \dots, m\}c$ (in this test, a pixel with 1km^2 of spatial resolution), and the closest target "kept" area, denoted as $t_j, j \in \{1, \dots, n\}$ measured by the Euclidean distance between these two sites. The results for the 10 simulated SPs were then aggregated to the average cost distance, denoted as $c(s_i, t_j)$.

In order to simulate variability in potential migration routes, we calculated the average cost distance between a source area and multiple k neighboring target areas, residing in different and spatially disjoint "kept" habitat patches, $P_u, u \in \{1, \dots, p\}$ and $t \subset P$ (Figure 6). These patches were obtained by removing pixels intersected by motorways from "kept" areas and then detecting clumps of connected pixels considering four adjacent cells ("rook's case"; see Appendix S7). For the purpose of this test we set k=5. By

averaging $c(s_i, t_j)$ values for k target areas we then calculated the Mean Functional Distance (MFD) index as a measure of functional connectivity, given by:

$$MFD_i = \frac{1}{\mathrm{k}} \sum^{\mathrm{k}} c(s_i, t_j) \qquad \text{(Equation 3)}$$

The rationale behind this index is to measure connectivity using a cost-based distance metric which explicitly incorporates landscape matrix resistance and least-cost path variability by calculating multiple pathways between a source area and multiple target Euclidean nearest-neighbours. This index varies from >0 to an undefined upper bound. MFD is greatly dependent on the spatial configuration of source/target areas and landscape traversal resistance with higher values of MFD signalling lower connectivity.

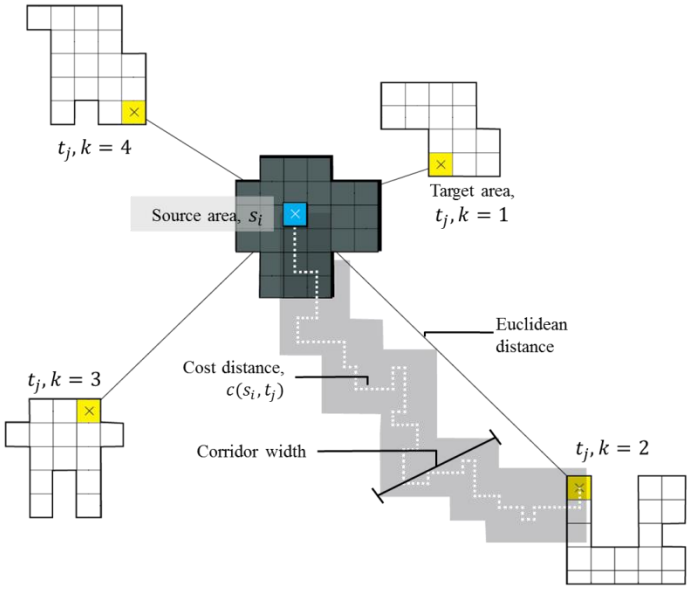

Figure 4 – Schematic representation of the connectivity analysis performed by LORACS considering four nearest stable patches (i.e., four target areas displayed in yellow) around a source area (in blue colour). Cost distance explicitly considers a cost raster determining landscape resistance in contrast to Euclidean distance.

Since LORACS calculates multiple SPs it is possible to count the number of times that a given area, a, (a cell with 1km^2) is selected for the pathway of a given SP calculation, noted as $a(s_i, t_j) \in [0, 10]$ (with the maximum value equal to the number of simulated SPs). Calculating the total summation of $a(s_i, t_j)$ across all source areas, and k neighbors, we obtained a zonation of areas important for maintaining connectivity, as well as, potential migration corridors, defined as:

$$SPsum = \sum^{\mathrm{m}} \sum^{\mathrm{k}} a(s_i, t_j) \qquad \text{(Equation 4)}$$

This index only assumes integer values and varies from 0 to an undefined upper bound depending on the spatial configuration of source/target areas and landscape resistance. In general, a higher amount of source areas cause an increase in the upper limit of $SPsum$, which in turn means that particular areas are selected more frequently in least-cost pathways; due to this, $SPsum$ must be analysed or compared in a relative fashion depending on these variables. For this index, higher values correlate to important areas for maintaining connectivity.

By mapping this index, we further analysed the intersection between important areas for connectivity or potential migration corridors for which $SPsum \geq 1$, and the motorway network (considering a buffer of 500m around each road) in order to assess vulnerability and conflicts for each species.

In order to determine shortest paths, LORACS uses a cost raster defining landscape matrix resistance to movement. In this test, this cost raster included three main components which were hypothesized to affect movement or dispersal probabilities in space and thus affect functional connectivity (Spear et al. 2010). These components were related to: (i) projected habitat suitability using biomod2 ensemble projections (h) for the year 2050 (denoted as component H) and calculated as the inverse of projected suitability outcomes since we were interested in landscape resistance to movement (and not permeability), (ii) linear structures inducing barrier or high-resistance effects; in this test we focused on the presence/vicinity of motorways (denoted as component R), calculated as the proportion of each 1km^2 cell intersected by a buffer of 500m around the motorway network (p_R), and, (iii) topographic roughness/heterogeneity (component T), calculated as the inter-quartile range in elevation (IQR) using elevation data from SRTM 90m.

Each component was then rescaled to the range [0, 1000] and attributed a weight, equal to: $w_H = 0.375$, $w_R = 0.375$, and, $w_T = 0.250$ in the final calculation (Equation 8).

$H = \frac{1}{h}$, rescaled to: $H' = \frac{H \times 1000}{arg_{max}(H)}$ (Equation 5)

$R = p_R = \frac{A_{motorways_buffer_500m}}{A_{total_cell_1km2}}$, rescaled to: $R' = \frac{R \times 1000}{arg_{max}(R)}$ (Equation 6)

$T = IQR = Q_{75\%} - Q_{25\%}$, rescaled to: $T' = \frac{T \times 1000}{arg_{max}(T)}$ (Equation 7)

The total landscape resistance cost, bounded within the interval [0, 1000] was given by a weighted sum of each rescaled partial component as:

$$Cost = w_H \cdot H' + w_R \cdot R' + w_T \cdot T' \quad \text{(Equation 8)}$$

Appendix S6 – Pearson correlation matrix for continuous predictor variables

	BIO 02	**BIO 04**	**BIO 05**	**BIO 06**	**BIO 14**	**CAR MD**	**CAR SD**	**TWI MD**	**TWI SD**
BIO 02	1.00	0.73	0.74	-0.16	-0.12	0.05	0.05	0.03	-0.07
BIO 04	0.73	1.00	0.53	-0.33	0.14	0.04	0.17	-0.12	-0.05
BIO 05	0.74	0.53	1.00	0.06	-0.64	0.18	-0.10	0.34	-0.15
BIO 06	-0.16	-0.33	0.06	1.00	-0.34	0.06	-0.18	0.26	-0.06
BIO 14	-0.12	0.14	-0.64	-0.34	1.00	-0.16	0.25	-0.47	0.15
CAR MD	0.05	0.04	0.18	0.06	-0.16	1.00	0.42	0.60	0.09
CAR SD	0.05	0.17	-0.10	-0.18	0.25	0.42	1.00	-0.11	0.36
TWI MD	0.03	-0.12	0.34	0.26	-0.47	0.60	-0.11	1.00	-0.17
TWI SD	-0.07	-0.05	-0.15	-0.06	0.15	0.09	0.36	-0.17	1.00

Appendix S7 – Habitat suitability, stable habitat patches and landscape resistance by test species and scenario

RCP 2.6 – Low-emissions scenario

RCP 8.5 – High-emissions scenario

Anguis fragilis

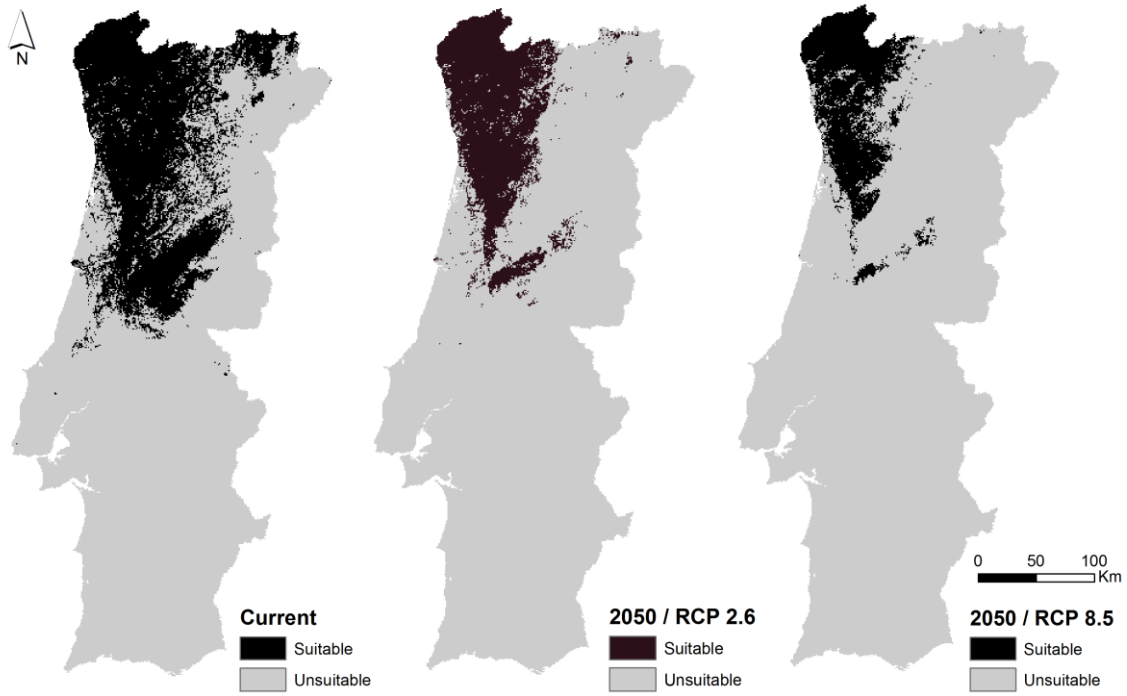

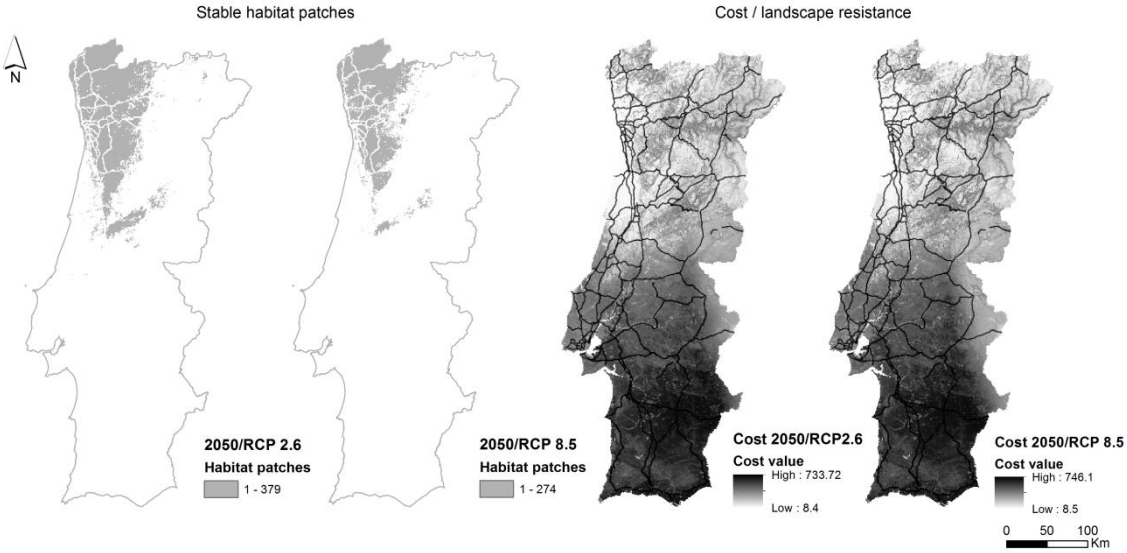

RCP 2.6 – Low-emissions scenario

RCP 8.5 – High-emissions scenario

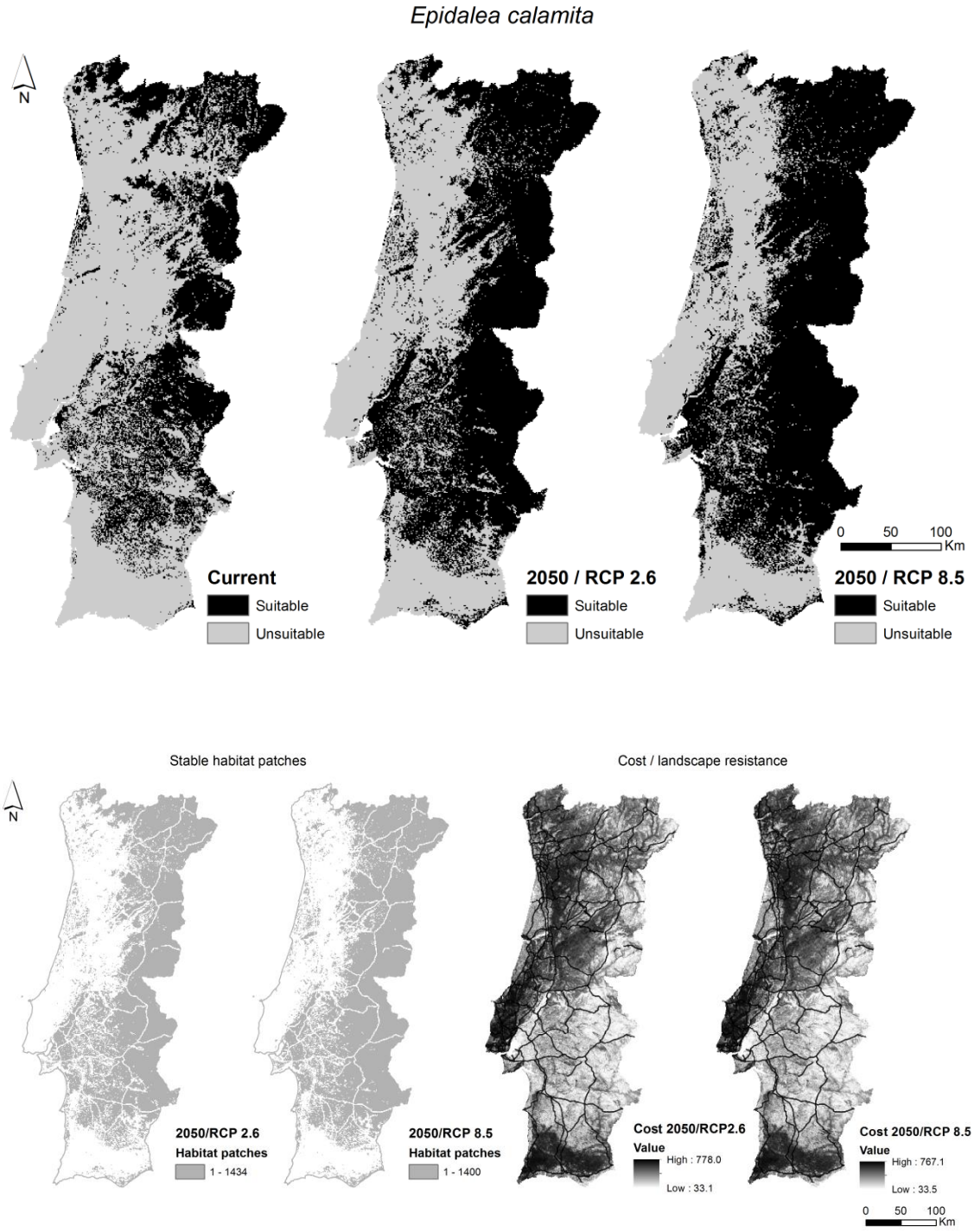

RCP 2.6 – Low-emissions scenario

RCP 8.5 – High-emissions scenario

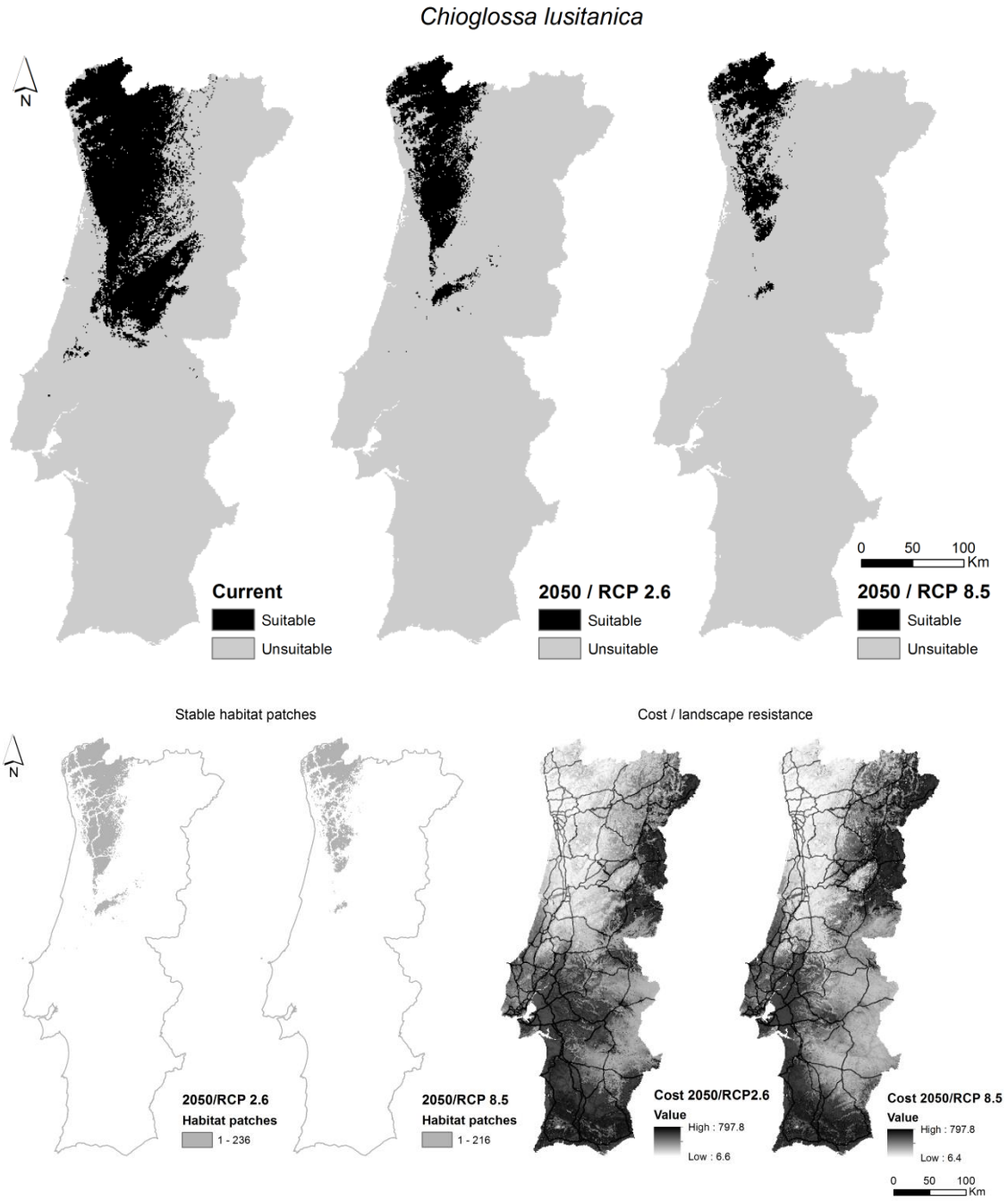

RCP 2.6 – Low-emissions scenario

RCP 8.5 – High-emissions scenario

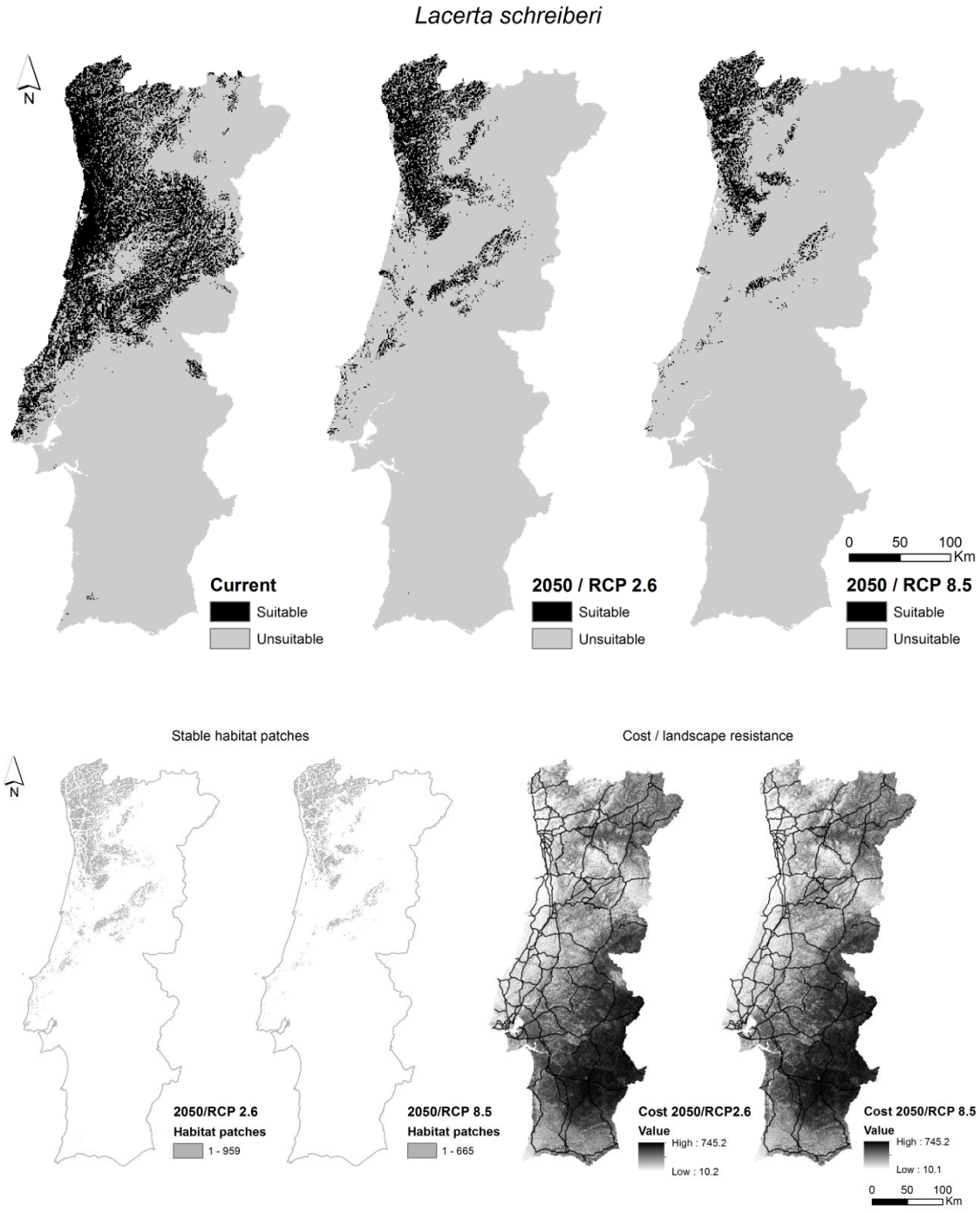

Appendix S8 – Importance of predictor variables by species and modelling technique

Table 2 – Mean variable importance for reptile species *Anguis fragilis* across all rounds by modelling technique, overall average and final rank (in decreasing importance order: 1 – most important to 10 – least important; based on overall average)

Predictor name	GLM	GBM	GAM	CTA	FDA	RFO	MAX	Average	Rank
BIO_14	7.88E-01	6.09E-01	8.86E-01	8.38E-01	7.14E-01	3.54E-01	8.36E-01	7.18E-01	1
TWI_MD	9.61E-02	7.94E-02	1.03E-01	5.48E-02	1.09E-01	6.95E-02	4.62E-02	7.98E-02	2
BIO_04	4.89E-02	5.67E-02	1.13E-01	1.14E-01	1.20E-01	4.40E-02	4.89E-02	7.78E-02	3
BIO_05	3.34E-02	1.25E-02	1.51E-01	3.55E-03	4.41E-02	2.66E-02	1.56E-02	4.10E-02	4
CAR_SD	3.54E-02	4.22E-02	4.20E-02	2.04E-02	2.72E-02	3.41E-02	1.09E-02	3.03E-02	5
LULC_CL	2.39E-02	3.39E-02	7.22E-02	1.48E-02	1.68E-02	2.58E-02	1.54E-02	2.90E-02	6
BIO_06	2.14E-02	1.95E-02	4.99E-02	9.65E-03	5.67E-02	2.70E-02	1.14E-02	2.80E-02	7
BIO_02	2.36E-02	6.16E-03	9.13E-02	6.58E-03	9.31E-03	8.86E-03	9.60E-03	2.22E-02	8
CAR_MD	9.02E-03	7.75E-03	2.23E-02	3.90E-03	1.86E-02	1.29E-02	1.15E-02	1.23E-02	9
TWI_SD	7.65E-03	1.69E-02	1.12E-02	1.19E-02	7.49E-03	2.06E-02	7.50E-03	1.19E-02	10

Table 3 – Mean variable importance for reptile species *Lacerta schreiberi* across all rounds by modelling technique, overall average and final rank (in decreasing importance order: 1 – most important to 10 – least important; based on overall average)

Predictor name	GLM	GBM	GAM	CTA	FDA	RFO	MAX	Average	Rank
BIO_05	4.39E-01	1.75E-01	4.55E-01	4.88E-01	3.86E-01	9.47E-02	1.92E-01	3.19E-01	1
BIO_14	1.80E-01	1.37E-01	2.46E-01	3.16E-01	2.08E-01	9.14E-02	2.02E-01	1.97E-01	2
TWI_MD	1.38E-01	4.54E-02	3.25E-01	4.55E-02	2.28E-01	3.07E-02	1.57E-01	1.39E-01	3
CAR_MD	9.12E-02	4.84E-02	2.20E-01	7.58E-02	1.96E-01	3.86E-02	1.13E-01	1.12E-01	4
BIO_04	2.91E-02	2.79E-02	3.25E-01	5.95E-02	2.15E-01	2.18E-02	2.16E-02	1.00E-01	5
BIO_02	6.78E-02	4.96E-02	2.58E-01	5.27E-02	1.12E-01	3.57E-02	7.94E-02	9.36E-02	6
CAR_SD	1.33E-01	1.12E-01	5.01E-02	1.07E-01	6.64E-02	7.91E-02	4.88E-02	8.52E-02	7
BIO_06	3.14E-02	1.52E-02	1.70E-01	2.56E-02	8.22E-02	1.59E-02	4.21E-02	5.47E-02	8
TWI_SD	3.71E-02	5.07E-02	4.11E-02	4.64E-02	4.10E-02	4.26E-02	9.58E-02	5.07E-02	9
LULC_CL	4.77E-04	3.49E-02	6.18E-02	2.91E-02	8.39E-03	2.30E-02	1.45E-02	2.46E-02	10

Table 4 – Mean variable importance for amphibian species *Chioglossa lusitanica* across all rounds by modelling technique, overall average and final rank (in decreasing importance order: 1 – most important to 10 – least important; based on overall average)

Predictor name	GLM	GBM	GAM	CTA	FDA	RFO	MAX	Average	Rank
BIO_14	4.61E-01	2.09E-01	6.04E-01	5.57E-01	2.31E-01	1.71E-01	3.65E-01	3.71E-01	1
TWI_MD	3.76E-01	1.76E-01	3.04E-01	1.77E-01	3.73E-01	1.44E-01	1.57E-01	2.44E-01	2
BIO_04	1.92E-01	1.25E-01	3.76E-01	2.14E-01	2.92E-01	8.35E-02	1.23E-01	2.01E-01	3
BIO_06	1.26E-01	7.07E-02	2.29E-01	7.07E-02	3.43E-01	7.32E-02	9.14E-02	1.43E-01	4
BIO_05	6.76E-02	7.74E-03	2.61E-01	7.24E-03	1.23E-01	1.66E-02	4.25E-03	6.97E-02	5
BIO_02	8.49E-02	1.50E-02	2.68E-01	2.55E-02	4.55E-02	1.34E-02	6.16E-03	6.55E-02	6
CAR_MD	4.90E-02	1.12E-02	6.04E-02	7.94E-03	8.03E-02	8.66E-03	2.26E-02	3.43E-02	7
CAR_SD	4.57E-02	3.48E-02	4.28E-02	2.67E-02	1.32E-02	2.32E-02	4.52E-03	2.73E-02	8
LULC_CL	7.35E-03	2.10E-02	7.05E-02	1.33E-02	1.30E-02	1.19E-02	8.95E-03	2.09E-02	9
TWI_SD	9.26E-03	1.39E-02	1.61E-02	7.33E-03	5.10E-03	1.16E-02	2.85E-03	9.44E-03	10

Table 5 – Mean variable importance for amphibian species *Epidalea calamita* across all rounds by modelling technique, overall average and final rank (in decreasing importance order: 1 – most important to 10 – least important; based on overall average)

Predictor name	GLM	GBM	GAM	CTA	FDA	RFO	MAX	Average	Rank
TWI_MD	4.85E-01	2.36E-01	4.92E-01	3.55E-01	4.21E-01	1.25E-01	4.36E-01	3.64E-01	1
BIO_04	4.16E-01	2.18E-01	3.94E-01	3.40E-01	3.09E-01	1.00E-01	1.73E-01	2.79E-01	2
BIO_14	3.95E-01	8.92E-02	4.30E-01	1.50E-01	2.75E-01	3.89E-02	3.94E-01	2.53E-01	3
BIO_05	6.55E-02	2.49E-02	3.09E-01	7.26E-02	2.38E-01	2.34E-02	9.84E-02	1.19E-01	4
LULC_CL	4.41E-02	1.02E-01	1.63E-01	2.01E-01	5.28E-02	6.52E-02	8.77E-02	1.02E-01	5
BIO_06	6.80E-02	2.60E-02	2.01E-01	6.15E-02	1.28E-01	2.57E-02	3.38E-02	7.78E-02	6
CAR_MD	3.27E-02	6.74E-02	2.61E-02	1.75E-01	6.24E-02	6.38E-02	8.41E-02	7.31E-02	7
TWI_SD	1.92E-02	4.57E-02	4.16E-02	8.29E-02	3.94E-02	4.53E-02	5.28E-02	4.67E-02	8
BIO_02	3.02E-02	9.80E-03	1.30E-01	3.67E-02	4.53E-02	1.45E-02	3.29E-02	4.28E-02	9
CAR_SD	3.31E-02	2.51E-02	3.24E-02	5.95E-02	2.21E-02	2.99E-02	6.92E-02	3.88E-02	10

Appendix S9 – Habitat suitability dynamics under projections of climate and land-use change

Table 6 – Outcomes for the Boolean comparison between suitable/unsuitable areas and projections for current and future environmental conditions.

Future distribution / *Current distribution*	**Unsuitable areas** [0]	**Suitable areas** [1]
Unsuitable areas [0]	Stable unsuitable areas (unsuitable)	Potential colonization areas (new)
Suitable areas [1]	Potential extinction areas (lost)	Stable suitable areas (kept)

Table 7 – Area (in km^2) for each type of projected habitat suitability dynamics between 2000 and 2050 by species and scenario (LES – low-emissions scenario: bioclimatic IPCC-AR5 RCP 2.6/ land-use IPCC AR4-B2; HES – high-emissions scenario: bioclimatic IPCC-AR5 RCP 2.6/ land-use IPCC-AR4 A1).

Species	Scenario	Unsuitable (km^2)	New (km^2)	Lost (km^2)	Kept (km^2)
ANGFR	LES	65269	125	10396	12610
	HES	65367	27	13988	9018
EPCAL	LES	38254	18028	1345	30773
	HES	33026	23256	1910	30208
CHALU	LES	69358	8	10297	8737
	HES	69361	5	13576	5458
LACSH	LES	67186	485	13174	7555
	HES	67202	469	15711	5018

Table 8 – Area (in percentage) for each type of projected habitat suitability dynamics between 2000 and 2050 by species and scenario (LES – low-emissions scenario: bioclimatic IPCC-AR5 RCP 2.6/ land-use IPCC AR4-B2; HES – high-emissions scenario: bioclimatic IPCC-AR5 RCP 2.6/ land-use IPCC-AR4 A1)

Species	Scenario	% Unsuitable	% New	% Lost	% Kept	% net variation
ANGFR	LES	73.8	0.1	11.8	14.3	-44.6
	HES	73.9	0.0	15.8	10.2	-60.7
EPCAL	LES	43.3	20.4	1.5	34.8	51.9
	HES	37.4	26.3	2.2	34.2	66.5
CHALU	LES	78.5	0.0	11.6	9.9	-54.1
	HES	78.5	0.0	15.4	6.2	-71.3
LACSH	LES	76.0	0.5	14.9	8.5	-61.2
	HES	76.0	0.5	17.8	5.7	-73.5

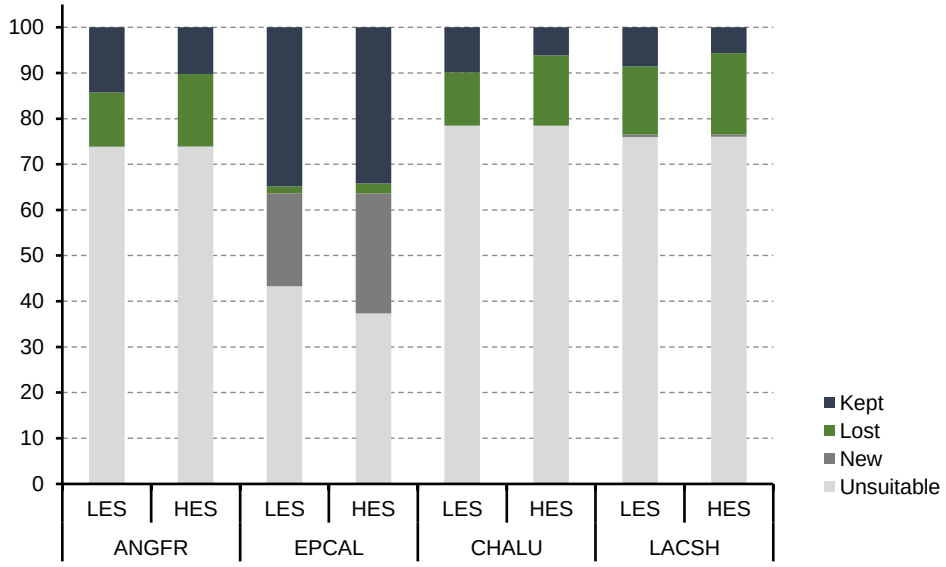

Fig. 5 – Barplot representing the percentage area for each type of projected habitat suitability dynamics between 2000 and 2050 by species and scenario (LES – low-emissions scenario: bioclimatic IPCC-AR5 RCP 2.6/ land-use IPCC AR4-B2; HES – high-emissions scenario: bioclimatic IPCC-AR5 RCP 2.6/ land-use IPCC-AR4 A1)

Appendix S10 – Connectivity metrics: summary statistics

Table 9 – Descriptive statistics (first, second/median and third quartiles and average) for the Mean Functional Distance index (MFD), for $k = 1$ and $k = 5$, by species and scenario. HES – High-emissions scenario: bioclimatic variables for IPCC-AR5 RCP 8.5 / land-use data for IPCC-AR4 A1; LES – Low-emissions scenario: bioclimatic variables for IPCC-AR5 RCP 2.6 / land-use data for IPCC-AR4 B2

		MFD (k=1)			**MFD** (k=5)		
		Q25%	Q50%	Q75%	Q25%	Q50%	Q75%
Anguis fragilis	HES	113.0	258.5	589.8	308.2	522.7	880.2
	LES	188.7	564.7	1286.7	452.4	902.3	1634.0
Lacerta schreiberi	HES	75.3	168.5	428.9	212.7	350.2	600.9
	LES	141.9	415.1	978.7	327.4	602.6	1189.0
Chioglossa lusitanica	HES	118.8	400.4	996.1	370.8	678.4	1302.3
	LES	188.8	817.3	2641.0	464.1	1143.2	2999.8
Epidalea calamita	HES	94.0	139.7	246.8	391.4	611.0	850.3
	LES	102.0	186.9	383.1	366.8	611.2	973.6

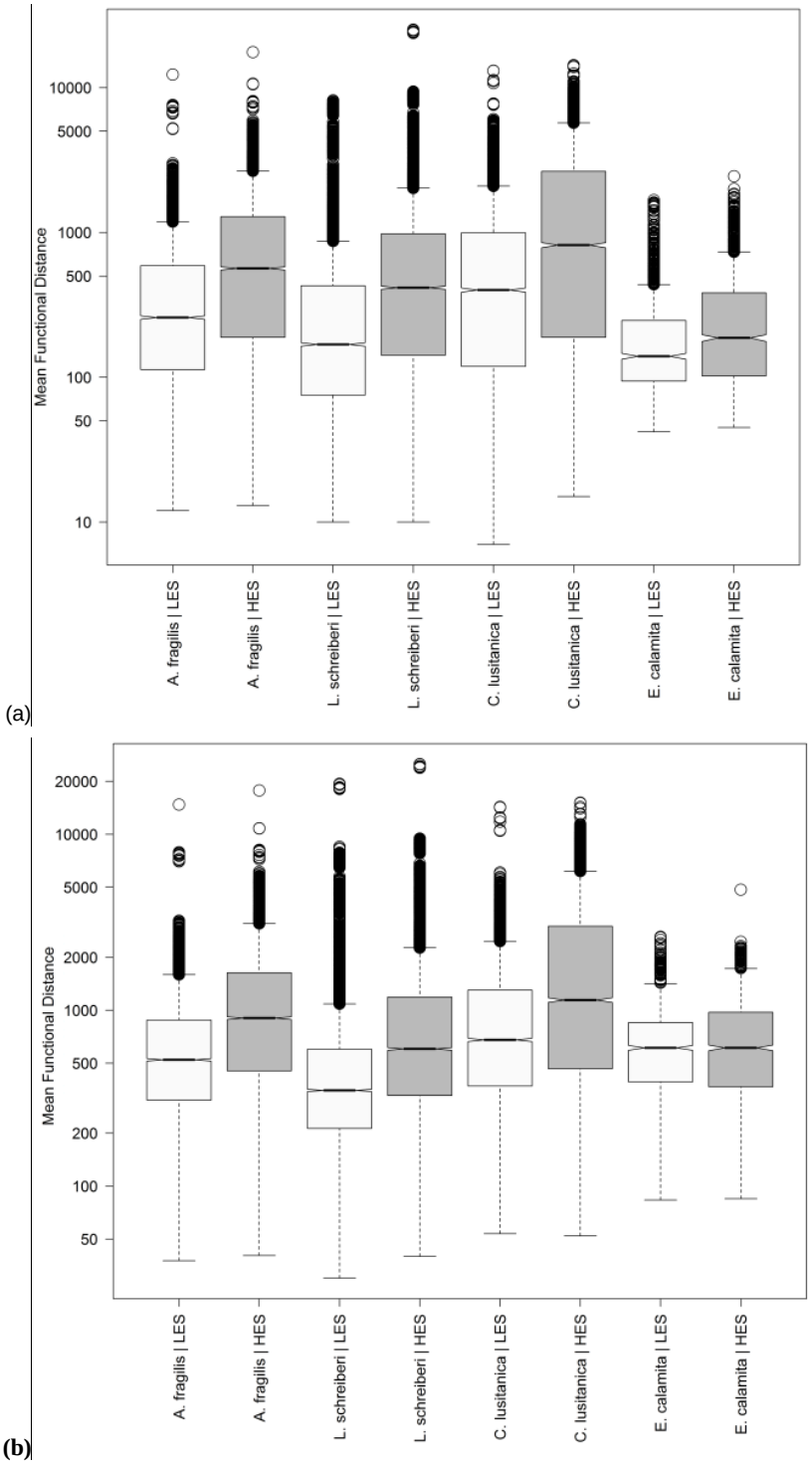

Fig. 6 (a, b) – Boxplots for the Mean Functional Distance (MFD) index of connectivity for (a) k=1 (one nearest-neighbour, no average applied), and, (b) k=5 (five nearest-neighbours) by species and scenario. LES – low-emissions scenario (white boxes), HES – high-emissions scenario (grey boxes). Outliers, *i.e.*, values 1.25 times the inter-quartile range outside the box, were represented as circles

References

Arntzen, J. W. 1980. Ecological Observations on Chioglossa lusitanica (Caudata, Salamandridae). Amphibia-Reptilia 1:187-203.

Arntzen, J. W., J. Bosch, M. Denoël, M. Tejedo, P. Edgar, M. Lizana, I. Martínez-Solano, A. Salvador, M. García-París, E. R. Gil, P. Sá-Sousa, and R. M. 2009. 2009. *Chioglossa lusitanica*. The IUCN Red List of Threatened Species. Version 2014.2. URL: http://www.iucnredlist.org/details/4657/0 (last visited: September 2014).

Baddeley, A., and R. Turner. 2005. Spatstat: an R package for analyzing spatial point patterns. Journal of Statistical Software 12:1-42.

Beja, P., S. Kuzmin, T. Beebee, M. Denoël, B. Schmidt, D. Tarkhnishvili, N. Ananjeva, N. Orlov, P. Nyström, A. Ogrodowczyk, M. Ogielska, J. Bosch, C. Miaud, M. Tejedo, M. Lizana, and I. Martínez-Solano. 2009. *Epidalea calamita*. The IUCN Red List of Threatened Species. Version 2014.2. URL: http://www.iucnredlist.org/details/54598/0 (last visited: September 2014).

Brito, J. C. 1999. Management strategies for Conservation of the lizard Lacerta Schreiberi in Portugal. Biological Conservation.

Caetano, M., A. Araújo, A. Nunes, V. Nunes, and M. Pereira. 2009a. Accuracy assessment of the CORINE Land Cover 2006 map of Continental Portugal, Technical Report. Instituto Geográfico Português.

Caetano, M., V. Nunes, and A. Nunes. 2009b. CORINE Land Cover 2006 for Continental Portugal, Technical Report. Instituto Geográfico Português.

Costa, J. C., C. Neto, C. Aguiar, J. Capelo, M. D. Espírito-Santo, J. Honrado, C. Pinto-Gomes, T. Monteiro-Henriques, M. Sequeira, and M. Lousã. 2012. Vascular plant communities in Portugal (Continental, the Azores and Madeira). Global Geobotany 2:1-180.

Donnelly, K. P. 1978. Simulations to determine the variance and edge-effect of total nearest neighbour distance. Pages 91-95 *in* I. Hodder, editor. Simulation studies in archaeology. Cambridge University Press, Cambridge/New York.

EEA. 2007. CLC2006 technical guidelines. Page 70. Office for Official Publications of the European Communities, Luxembourg.

Galán, P., and A. Salvador. 2009. Lución – Anguis fragilis.*in* A. Salvador and A. Marco, editors. Enciclopedia Virtual de los Vertebrados Españoles., Museo Nacional de Ciencias Naturales, Madrid.

Loureiro, A., N. Ferrand de Almeida, M. A. Carretero, and O. S. Paulo. 2008. Atlas dos Anfíbios e Répteis de Portugal. 1st Ed. edition. Instituto da Conservação da Natureza, Lisboa.

Metzger, M. J., D. J. Brus, R. G. H. Bunce, P. D. Carey, J. Gonçalves, J. P. Honrado, R. H. G. Jongman, A. Trabucco, and R. Zomer. 2013. Environmental stratifications as the basis for national, European and global ecological monitoring. Ecological Indicators 33:26-35.

Peel, M. C., B. L. Finlayson, and T. A. McMahon. 2007. Updated world map of the Köppen-Geiger climate classification. Hydrol. Earth Syst. Sci. 11:1633-1644.

Pinto, N., and T. Keitt. 2009. Beyond the least-cost path: evaluating corridor redundancy using a graph-theoretic approach. Landscape Ecology 24:253-266.

Pinto, N., T. H. Keitt, and M. Wainright. 2012. LORACS: JAVA software for modeling landscape connectivity and matrix permeability. Ecography 35:388-392.

Popescu, V. D., L. Rozylowicz, D. Cogalniceanu, I. M. Niculae, and A. L. Cucu. 2013. Moving into protected areas? Setting conservation priorities for Romanian reptiles and amphibians at risk from climate change. PLoS One 8:e79330.

Sá-Sousa, P., R. Marquez, V. Pérez-Mellado, and I. M.-S. . 2009. *Lacerta schreiberi*. The IUCN Red List of Threatened Species. Version 2014.2. URL: http://www.iucnredlist.org/details/11113/0 (last visited: September 2014).

Smith, M. A., and D. M. Green. 2005. Dispersal and the metapopulation paradigm in amphibian ecology and conservation: are all amphibian populations metapopulations? Ecography 28:110-128.

Spear, S. F., N. Balkenhol, M.-J. Fortin, B. H. McRae, and K. I. M. Scribner. 2010. Use of resistance surfaces for landscape genetic studies: considerations for parameterization and analysis. Molecular Ecology 19:3576-3591.

Appendix IV | Chapter 7 – Evaluating an unmanned aerial vehicle-based approach for assessing habitat extent and condition in fine-scale early successional mountain mosaics

Appendix S1 – Test-site photographs recorded during in-field campaigns

Figure S1.1 - Panoramic photography of the test-site showing grassland 6230* and wet heath 4020* habitat types in the first plane and rocky outcrops in higher elevation areas (date: 17-04-2013, during UAV image collection and fieldwork).

Figure S1.2 - Oligotrophic water course with aquatic vegetation (habitat 3130) in mosaic with temperate wet heathlands 4020* dominated by the narrow endemic *Genista berberidea* (date: 17-04-2013)

Figure S1.3 – Mosaic of oligotrophic water course with aquatic vegetation (habitat 3130) temperate wet heathlands (habitat 4020*), and rich species Nardus grasslands (habitat 6230*). In the background a mosaic of dry heathlands (habitat 4030) and Oro-Iberian grasslands (date: 17-04-2013).

Figure S1.4 – Rock outcrops with a mosaic of dry heathlands (habitat 4030) and Oro-Iberian grasslands.

Figure S1.5 (top) – oligotrophic water course with aquatic vegetation (habitat 3130) in mosaic with temperate wet heathlands (habitat 4020*), and rich species Nardus grasslands (habitat 6230*).

Figure S1.6 – Bovine (top) and equine cattle (bottom) grazing on grassland areas on the test-site (date: 30-10-2013; during evaluation/validation fieldwork).

Appendix S2 – Spectral sensitivity data for Canon cameras

Table S2.1 – Camera specifications for Canon models indicating production year, sensor type and size (mm), maximum resolution (in pixels), processor type/family and band centres for the red, green and blue bands (wavelength values in nm). The first row shows the camera model used by the UAV device for image collection.

Model	Year	Sensor type	Sensor size	Maximum resolution	Processor	Red band (nm)	Green band (nm)	Blue band (nm)	Source/ Reference
Canon Ixus 220 HS	***2011***	***BSI-CMOS***	***1/2.3" (6.17 x 4.55 mm)***	***4000 x 3000***	***DIGIC 4***	**-**	**-**	**-**	-
Canon S110	2012	CMOS	1/1.7" (7.44 x 5.58 mm)	4000 x 3000	DIGIC 5	596	515	454	SenseFly (2015)
Canon 10D	2003	CMOS	APS-C (22.7 x 15.1 mm)	3072 x 2048	DIGIC	600	528	476	Kawakami et al. (2013)
Canon 400D	2006	CMOS	APS-C (22.2 x 14.8 mm)	3888 x 2592	DIGIC II	596	532	456	
Canon 1D Mark III	2007	CMOS	APS-H (28.7 x 18.7 mm)	3888 x 2592	DIGIC III	590	530	460	Jiang et al. (2013)
Canon 20D	2004	CMOS	APS-C (22.5 x 15 mm)	3504 x 2336	DIGIC II	600	530	470	
Canon 300D	2003	CMOS	APS-C (22.7 x 15.1 mm)	3072 x 2048	DIGIC	590	530	470	
Canon 40D	2007	CMOS	APS-C (22.2 x 14.8 mm)	3888 x 2592	DIGIC III	600	530	460	
Canon 500D	2009	CMOS	APS-C (22.3 x 14.9 mm)	4752 x 3168	DIGIC 4	580	530	460	
Canon 50D	2008	CMOS	APS-C (22.3 x 14.9 mm)	4752 x 3168	DIGIC 4	590	530	460	
Canon 5D Mark II	2008	CMOS	Full frame (36 x 24 mm)	5616 x 3744	DIGIC 4	600	510	460	
Canon 600D	2011	CMOS	APS-C (22.3 x 14.9 mm)	5184 x 3456	DIGIC 4	590	530	460	
Canon 60D	2010	CMOS	APS-C (22.3 x 14.9 mm)	5184 x 3456	DIGIC 4	590	530	460	
					Mean ± Std. Error	594 ± 2	527 ± 2	462 ± 2	

Figure S2.1 (a, l) – Spectral sensitivity for Canon models in Table S2.1. Values were smoothed using the *loess* function implemented in R statistical analysis software.

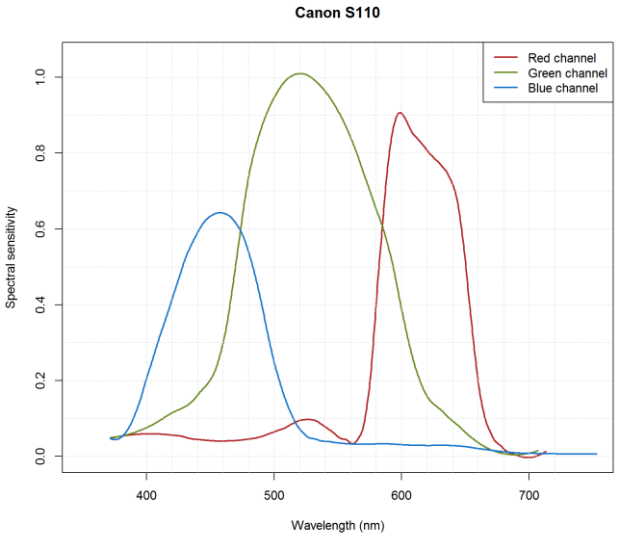

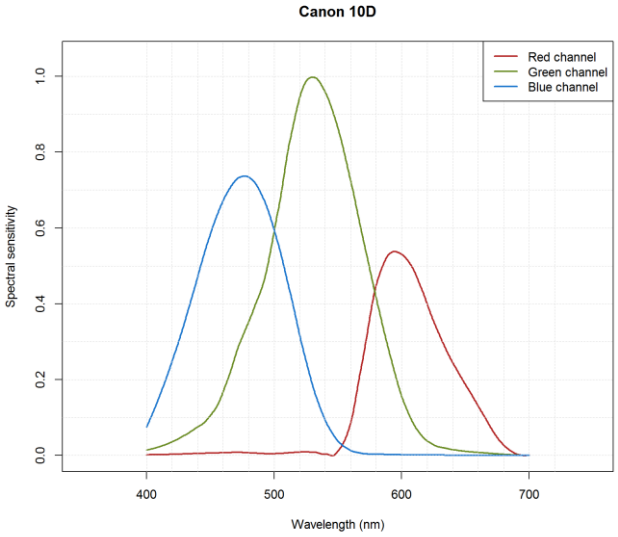

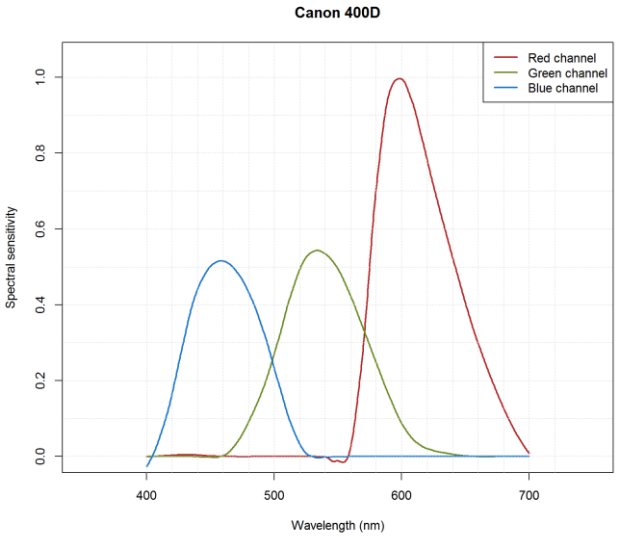

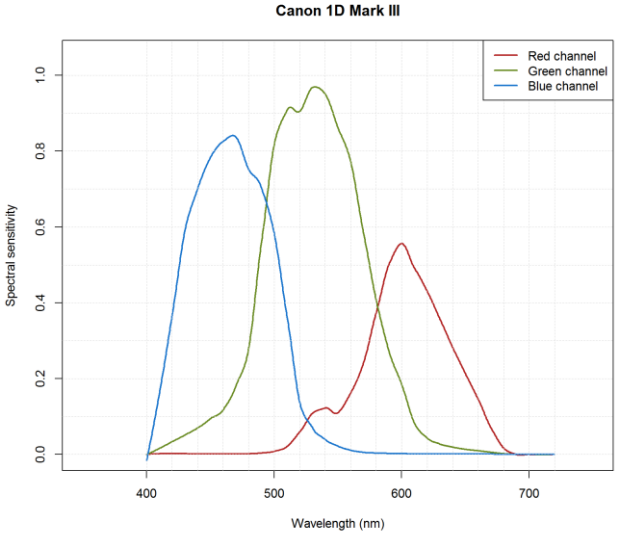
Canon 1D Mark III
Red channel
Green channel
Blue channel
Spectral sensitivity
0.0
0.2
0.4
0.6
0.8
1.0
400
500
600
700
Wavelength (nm)

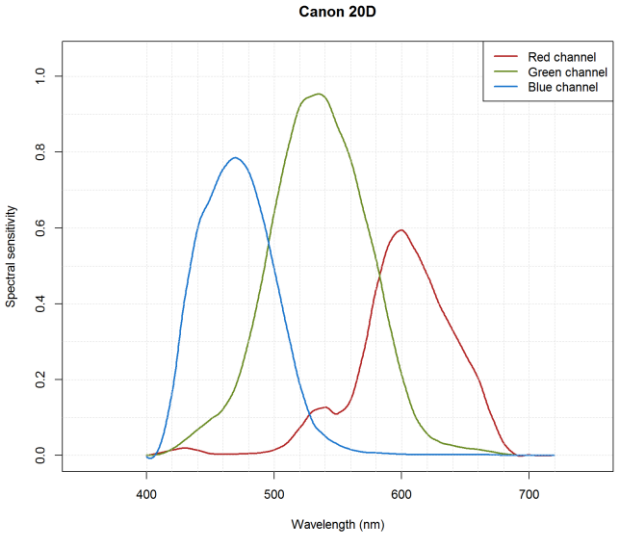
Canon 20D
Red channel
Green channel
Blue channel
Spectral sensitivity
0.0
0.2
0.4
0.6
0.8
1.0
400
500
600
700
Wavelength (nm)

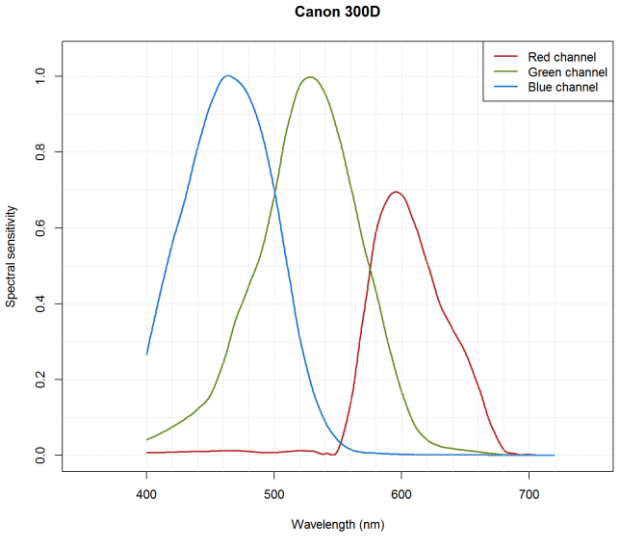
Canon 300D
Red channel
Green channel
Blue channel
Spectral sensitivity
0.0
0.2
0.4
0.6
0.8
1.0
400
500
600
700
Wavelength (nm)

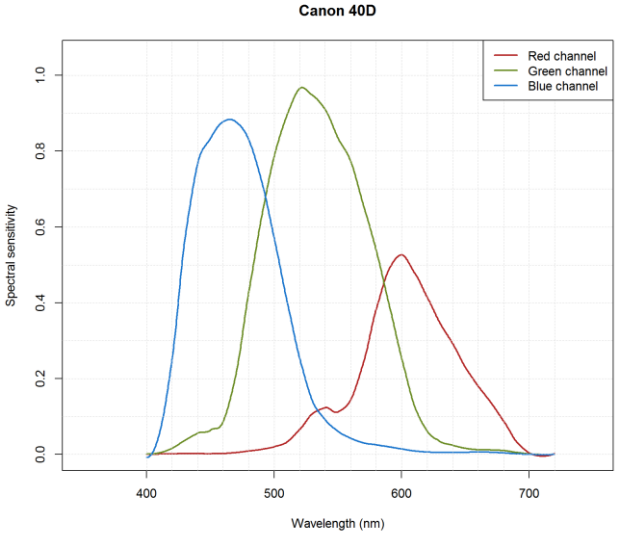
Canon 40D
Red channel
Green channel
Blue channel
Spectral sensitivity
0.0
0.2
0.4
0.6
0.8
1.0
400
500
600
700
Wavelength (nm)

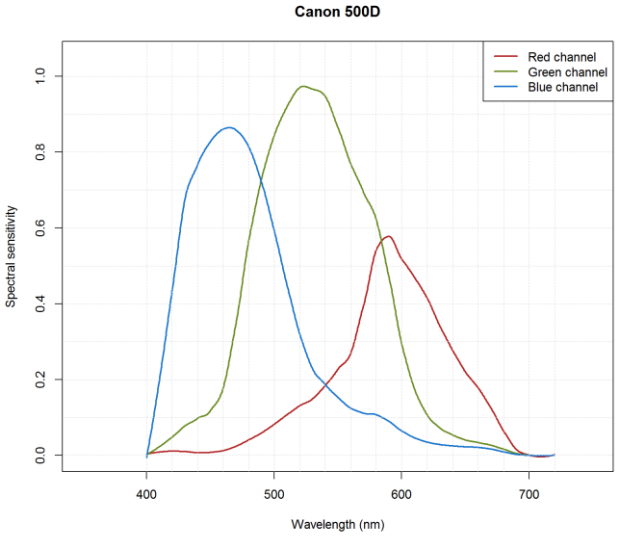
Canon 500D
Red channel
Green channel
Blue channel
Spectral sensitivity
0.0
0.2
0.4
0.6
0.8
1.0
400
500
600
700
Wavelength (nm)

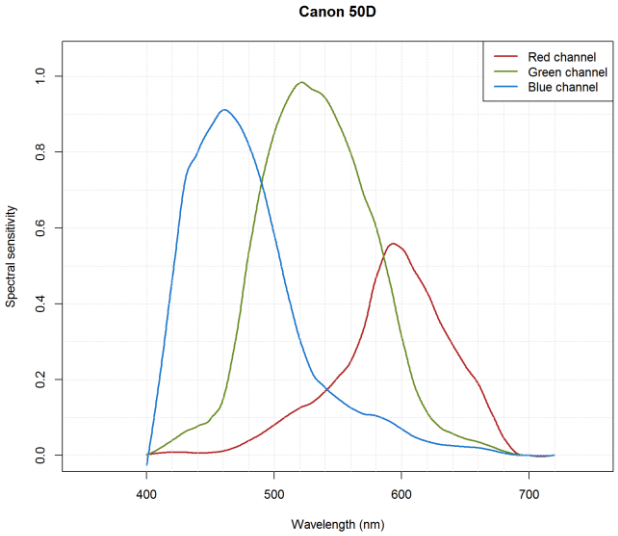
Canon 50D
Red channel
Green channel
Blue channel
Spectral sensitivity
0.0
0.2
0.4
0.6
0.8
1.0
400
500
600
700
Wavelength (nm)

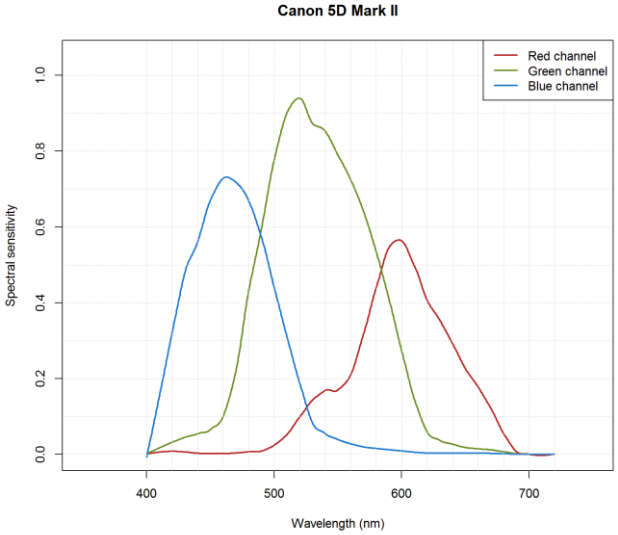
Canon 5D Mark II
Red channel
Green channel
Blue channel
Spectral sensitivity
0.0
0.2
0.4
0.6
0.8
1.0
400
500
600
700
Wavelength (nm)

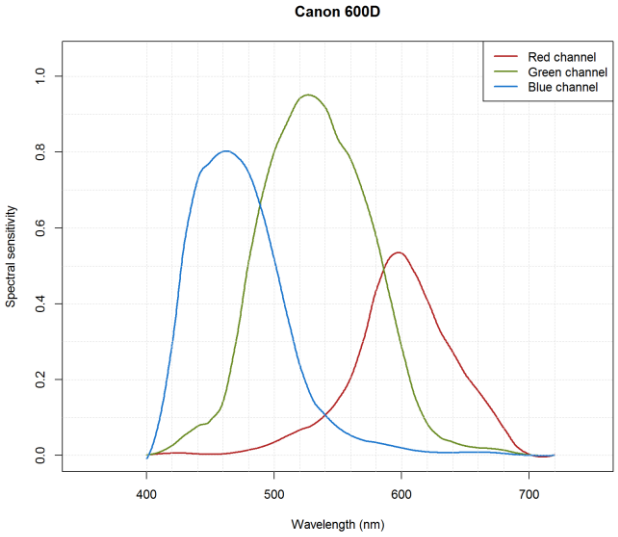
Canon 600D
Red channel
Green channel
Blue channel
Spectral sensitivity
0.0
0.2
0.4
0.6
0.8
1.0
400
500
600
700
Wavelength (nm)

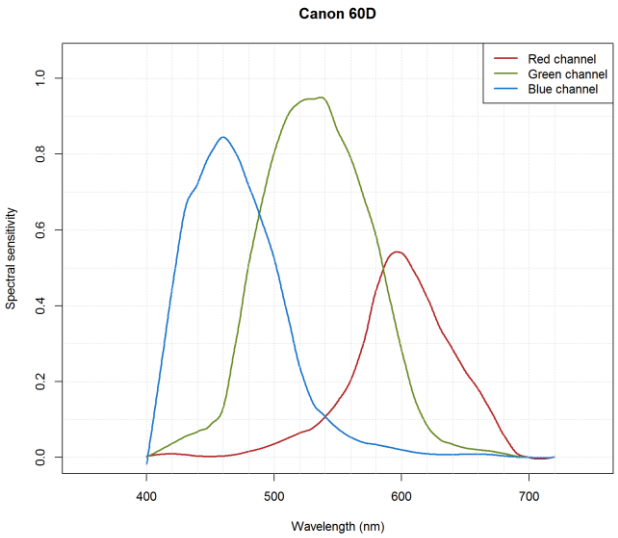
Canon 60D
Red channel
Green channel
Blue channel
Spectral sensitivity
0.0
0.2
0.4
0.6
0.8
1.0
400
500
600
700
Wavelength (nm)

Appendix S3 – Features used for supervised image classification

Table S3.1. Complete list of features calculated from RGB imagery

Input data	Feature name/accronym		Function	Kernel size (pixels)	Other parameters
RGB image	**Color bands**	R_Band	-	-	-
		G_Band			
		B_Band			
Color bands	**Band ratios / vegetation indices**	R_G_Ratio	R / G	-	-
		R_B_Ratio	R / B		
		G_R_Ratio	G / R		
		G_B_Ratio	G / B		
		B_R_Ratio	B / R		
		B_G_Ratio	B / G		
		B_RGB_Ratio	B / (R + G + B)		
		R_BG_Ratio	R / (B + G)		
		BRG_3_Ratio	(B + G + R) / 3		
		B_GR_Ratio	B / (G + R)		
		R_RGB_Ratio	R / (R + G + B)		
		VV_Index_Ratio	[1 - |(R - 30) / (R + 30)|] x [1 - |(G - 50) / (G + 50)|] x [1 - |(B - 10) / (B + 10)|]		
Band ratios / vegetation indices	**Band ratios /vegetation indices local statistics / texture**	R_G_AVG_K5	Mean	5x5	-
		R_G_VAR_K5	Variance		
		R_G_AVG_K11	Mean	11x11	-
		R_G_VAR_K11	Variance		
		R_B_AVG_K5	Mean	5x5	-
		R_B_VAR_K5	Variance		
		R_B_AVG_K11	Mean	11x11	-
		R_B_VAR_K11	Variance		
		G_R_AVG_K5	Mean	5x5	-
		G_R_VAR_K5	Variance		
		G_R_AVG_K11	Mean	11x11	-
		G_R_VAR_K11	Variance		
		G_B_AVG_K5	Mean	5x5	-
		G_B_VAR_K5	Variance		
		G_B_AVG_K11	Mean	11x11	-
		G_B_VAR_K11	Variance		
		B_R_AVG_K5	Mean	5x5	-
		B_R_VAR_K5	Variance		
		B_R_AVG_K11	Mean	11x11	-
		B_R_VAR_K11	Variance		
		B_G_AVG_K5	Mean	5x5	-
		B_G_VAR_K5	Variance		
		B_G_AVG_K11	Mean	11x11	-
		B_G_VAR_K11	Variance		

		B_RGB_AVG_K5	Mean	5x5	-
		B_RGB_VAR_K5	Variance		
		B_RGB_AVG_K11	Mean	11x11	-
		B_RGB_VAR_K11	Variance		
		R_BG_AVG_K5	Mean	5x5	-
		R_BG_VAR_K5	Variance		
		R_BG_AVG_K11	Mean	11x11	-
		R_BG_VAR_K11	Variance		
		BRG_3_AVG_K5	Mean	5x5	-
		BRG_3_VAR_K5	Variance		
		BRG_3_AVG_K11	Mean	11x11	-
		BRG_3_VAR_K11	Variance		
		B_GR_AVG_K5	Mean	5x5	-
		B_GR_VAR_K5	Variance		
		B_GR_AVG_K11	Mean	11x11	-
		B_GR_VAR_K11	Variance		
		R_RGB_AVG_K5	Mean	5x5	-
		R_RGB_VAR_K5	Variance		
		R_RGB_AVG_K11	Mean	11x11	-
		R_RGB_VAR_K11	Variance		
		VV_Index_AVG_K5	Mean	5x5	-
		VV_Index_VAR_K5	Variance		
		VV_Index_AVG_K11	Mean	11x11	-
		VV_Index_VAR_K11	Variance		
R_Band (CH1)	**Local statistics texture**	LS_CH1_Mean_RD3	Mean	3x3	-
		LS_CH1_Var_RD3	Variance		
		LS_CH1_Skew_RD3	Skewness		
		LS_CH1_Kurt_RD3	Kurtosis		
		LS_CH1_Mean_RD5	Mean	5x5	-
		LS_CH1_Var_RD5	Variance		
		LS_CH1_Skew_RD5	Skewness		
		LS_CH1_Kurt_RD5	Kurtosis		
		LS_CH1_Mean_RD9	Mean	9x9	-
		LS_CH1_Var_RD9	Variance		
		LS_CH1_Skew_RD9	Skewness		
		LS_CH1_Kurt_RD9	Kurtosis		
G_Band (CH2)	**Local statistics texture**	LS_CH2_Mean_RD3	Mean	3x3	-
		LS_CH2_Var_RD3	Variance		
		LS_CH2_Skew_RD3	Skewness		
		LS_CH2_Kurt_RD3	Kurtosis		
		LS_CH2_Mean_RD5	Mean	5x5	-
		LS_CH2_Var_RD5	Variance		
		LS_CH2_Skew_RD5	Skewness		
		LS_CH2_Kurt_RD5	Kurtosis		
		LS_CH2_Mean_RD9	Mean	9x9	-
		LS_CH2_Var_RD9	Variance		
		LS_CH2_Skew_RD9	Skewness		

		LS_CH2_Kurt_RD9	Kurtosis		
B_Band (CH3)	**Local statistics texture**	LS_CH3_Mean_RD3	Mean	3x3	-
		LS_CH3_Var_RD3	Variance		
		LS_CH3_Skew_RD3	Skewness		
		LS_CH3_Kurt_RD3	Kurtosis		
		LS_CH3_Mean_RD5	Mean	5x5	-
		LS_CH3_Var_RD5	Variance		
		LS_CH3_Skew_RD5	Skewness		
		LS_CH3_Kurt_RD5	Kurtosis		
		LS_CH3_Mean_RD9	Mean	9x9	-
		LS_CH3_Var_RD9	Variance		
		LS_CH3_Skew_RD9	Skewness		
		LS_CH3_Kurt_RD9	Kurtosis		
Brightness transformation (BRG) [*]	**Haralick texture (simple)**	HC_SP_Energy_BRG_XR3_YR3	Energy	3x3	X offset = 1; Y Offset = 1; Number of bins = 8
		HC_SP_Entropy_BRG_XR3_YR3	Entropy		
		HC_SP_Corr_BRG_XR3_YR3	Correlation		
		HC_SP_InvDiffM_BRG_XR3_YR3	Inverse Difference Moment		
		HC_SP_Inertia_BRG_XR3_YR3	Inertia		
		HC_SP_ClustShade_BRG_XR3_YR3	Cluster Shade		
		HC_SP_ClustP_BRG_XR3_YR3	Cluster Prominence		
		HC_SP_HCorr_BRG_XR3_YR3	Haralick's Correlation		
	Haralick texture (advanced)	HC_AD_Mean_BRG_XR3_YR3	Mean		
		HC_AD_Var_BRG_XR3_YR3	Variance		
		HC_AD_SAvg_BRG_XR3_YR3	Sum Average		
		HC_AD_SVar_BRG_XR3_YR3	Sum Variance		
		HC_AD_SEntr_BRG_XR3_YR3	Sum Entropy		
		HC_AD_DiffEntr_BRG_XR3_YR3	Difference of Entropies		
		HC_AD_DiffVar_BRG_XR3_YR3	Difference of Variances		
		HC_AD_IC1_BRG_XR3_YR3	I. Correlation (IC1)		
		HC_AD_IC2_BRG_XR3_YR3	I. Correlation (IC2)		
	Haralick texture (higher)	HC_HG_SRE_BRG_XR3_YR3	Short Run Emphasis		
		HC_HG_LRE_BRG_XR3_YR3	Long Run Emphasis		
		HC_HG_GLN_BRG_XR3_YR3	Grey-Level Nonuniformity		
		HC_HG_RLN_BRG_XR3_YR3	Run Length Nonuniformity		
		HC_HG_RP_BRG_XR3_YR3	Run Percentage		
		HC_HG_LGRE_BRG_XR3_YR3	Low Grey-Level Run Emphasis		
		HC_HG_HGRE_BRG_XR3_YR3	High Grey-Level Run Emphasis		
		HC_HG_SRLGE_BRG_XR3_YR3	Short Run Low Grey-Level Emphasis		
		HC_HG_SRHGE_BRG_XR3_YR3	Short Run High Grey-Level Emphasis		
		HC_HG_LRLGE_BRG_XR3_YR3	Long Run Low Grey-Level Emphasis		
		HC_HG_LRHGE_BRG_XR3_YR3	Long Run High Grey-Level Emphasis		
Brightness transformation (BRG) [*]	**Haraclick texture (simple)**	HC_SP_Energy_BRG_XR9_YR9	Energy	9x9	X offset = 1; Y Offset = 1; Number of bins = 8
		HC_SP_Entropy_BRG_XR9_YR9	Entropy		
		HC_SP_Corr_BRG_XR9_YR9	Correlation		
		HC_SP_InvDiffM_BRG_XR9_YR9	Inverse Difference Moment		
		HC_SP_Inertia_BRG_XR9_YR9	Inertia		
		HC_SP_ClustShade_BRG_XR9_YR9	Cluster Shade		
		HC_SP_ClustP_BRG_XR9_YR9	Cluster Prominence		

		HC_SP_HCorr_BRG_XR9_YR9	Haralick's Correlation		
	Haralick texture (advanced)	HC_AD_Mean_BRG_XR9_YR9	Mean		
		HC_AD_Var_BRG_XR9_YR9	Variance		
		HC_AD_SAvg_BRG_XR9_YR9	Sum Average		
		HC_AD_SVar_BRG_XR9_YR9	Sum Variance		
		HC_AD_SEntr_BRG_XR9_YR9	Sum Entropy		
		HC_AD_DiffEntr_BRG_XR9_YR9	Difference of Entropies		
		HC_AD_DiffVar_BRG_XR9_YR9	Difference of Variances		
		HC_AD_IC1_BRG_XR9_YR9	I. Correlation (IC1)		
		HC_AD_IC2_BRG_XR9_YR9	I. Correlation (IC2)		
	Haralick texture (higher)	HC_HG_SRE_BRG_XR9_YR9	Short Run Emphasis		
		HC_HG_LRE_BRG_XR9_YR9	Long Run Emphasis		
		HC_HG_GLN_BRG_XR9_YR9	Grey-Level Nonuniformity		
		HC_HG_RLN_BRG_XR9_YR9	Run Length Nonuniformity		
		HC_HG_RP_BRG_XR9_YR9	Run Percentage		
		HC_HG_LGRE_BRG_XR9_YR9	Low Grey-Level Run Emphasis		
		HC_HG_HGRE_BRG_XR9_YR9	High Grey-Level Run Emphasis		
		HC_HG_SRLGE_BRG_XR9_YR9	Short Run Low Grey-Level Emphasis		
		HC_HG_SRHGE_BRG_XR9_YR9	Short Run High Grey-Level Emphasis		
		HC_HG_LRLGE_BRG_XR9_YR9	Long Run Low Grey-Level Emphasis		
		HC_HG_LRHGE_BRG_XR9_YR9	Long Run High Grey-Level Emphasis		
Brightness transformation (BRG) [*]	**Structural Feature Set texture (SFS)**	SFS_Len_BRG_LT70	Length	-	Spectral threshold = 70; Spatial threshold = 100; Number directions = 20; Alpha = 1
		SFS_Width_BRG_LT70	Width		
		SFS_PSI_BRG_LT70	PSI		
		SFS_WMean_BRG_LT70	Weighted-mean		
		SFS_Ratio_BRG_LT70	Ratio		
		SFS_SD_BRG_LT70	Standard-deviation		
		SFS_Len_BRG_LT100	Length	-	Spectral threshold = 100; Spatial threshold = 100; Number directions = 20; Alpha = 1
		SFS_Width_BRG_LT100	Width		
		SFS_PSI_BRG_LT100	PSI		
		SFS_WMean_BRG_LT100	Weighted-mean		
		SFS_Ratio_BRG_LT100	Ratio		
		SFS_SD_BRG_LT100	Standard-deviation		

[*] The brightness transformation used as input to calculate Haralick and Structural Feature Set features was calculated as: $BRG = [(299 \times R) + (587 \times G) + (114 \times B)]/1000$, with R,G,B being the red, green and blue color channels.

Table S3.2. Complete list of features calculated from the Digital Surface Model

Input data	Feature name/accronym	Function	Kernel size (pixels)	Other parameters

Digital Surface Model (meters a.s.l.)	**Surface elevation texture/ roughness**	DSM_SurfElevation_MN_R5	Mean	5x5	-
		DSM_SurfElevation_MN_R9		9x9	
		DSM_SurfElevation_MN_R15		15x15	
		DSM_SurfElevation_SD_R5	Standard-deviation	5x5	-
		DSM_SurfElevation_SD_R9		9x9	
		DSM_SurfElevation_SD_R15		15x15	
Surface elevation (DSM_SurfElevation_MN_R15)	**Surface curvature**	Plan curvature		-	-
		Total curvature			
		Profile curvature			

Appendix S4 – Preliminary cross-validation results

Compares the performance of candidate classification algorithms: Random Forests, Support Vector Machines, Neural Networks, k-Nearest Neighbour, Generalized Boosted Model, and C5.0. Table S4.1 shows performance statistics for the test set: overall accuracy and Kappa were used to select the best performing algorithm. The '*Parameters'* column presents which parameters were modified during classification tuning and the respective tuning grid (bold lettering shows the best parameterization for each tested algorithm). Overall, comparison results highlighted Random Forests as the best performing method with highest values for both overall accuracy and Kappa. All tests were developed in *R* statistical software v.3.1.2-x64 using '*caret*' package (Kuhn 2016) which is dedicated to multi-algorithm tuning, calibration and evaluation.

Table S4.1 – Performance statistics for the different classification algorithms tested. Values present the average overall accuracy and Kappa across 5-fold cross-validation.

Classification algorithm	**Parameters**		**Performance**	
	mtry		***Accuracy***	***Kappa***
Random Forests	3		0.865	0.811
	5		0.871	0.819
	8		**0.872**	**0.820**
Support Vector Machines (radial basis function)	***sigma***	***C***	***Accuracy***	***Kappa***
	0.136	0.25	0.810	0.728
	0.136	0.50	0.818	0.741
	0.136	1.00	0.826	0.753
	0.136	2.00	0.833	0.763
	0.136	**4.00**	**0.839**	**0.772**
Neural networks	***size***	***decay***	***Accuracy***	***Kappa***

(1 hidden layer with PCA pre-processing)	1	0.0000	0.098	-0.001
	1	0.0001	0.460	0.101
	1	0.0010	0.419	0.252
	1	0.0100	0.591	0.364
	1	0.1000	0.616	0.395
	3	0.0000	0.480	0.000
	3	0.0001	0.484	0.099
	3	0.0010	0.445	0.305
	3	0.0100	0.691	0.554
	3	0.1000	0.702	0.570
	5	0.0000	0.480	0.000
	5	0.0001	0.615	0.464
	5	0.0010	0.477	0.207
	5	0.0100	0.451	0.340
	5	0.1000	0.741	0.626
	7	0.0000	0.296	0.111
	7	0.0001	0.526	0.276
	7	0.0010	0.457	0.269
	7	0.0100	0.708	0.579
	7	**0.1000**	**0.756**	**0.650**
	9	0.0000	0.099	-0.001
	9	0.0001	0.332	0.065
	9	0.0010	0.418	0.282
	9	0.0100	0.648	0.501
	9	0.1000	0.750	0.642
	size	***decay***	***Accuracy***	***Kappa***
Neural networks (1 hidden layer)	1	0.0000	0.645	0.459
	1	0.0001	0.643	0.461
	1	0.0010	0.644	0.456
	1	0.0100	0.642	0.456
	1	0.1000	0.637	0.444
	3	0.0000	0.724	0.601
	3	0.0001	0.718	0.593
	3	0.0010	0.726	0.604
	3	0.0100	0.721	0.599
	3	0.1000	0.716	0.588
	5	0.0000	0.739	0.626
	5	0.0001	0.739	0.626
	5	0.0010	0.735	0.620
	5	0.0100	0.720	0.597
	5	0.1000	0.748	0.638
	7	0.0000	0.733	0.615
	7	0.0001	0.738	0.622
	7	0.0010	0.722	0.597
	7	0.0100	0.729	0.609
	7	0.1000	0.740	0.625

	9	0.0000	0.757	0.653
	9	0.0001	0.767	0.669
	9	0.0010	0.762	0.660
	9	0.0100	0.754	0.650
	9	**0.1000**	**0.768**	**0.668**
k-Nearest Neighbour	***kmax***	***distance***	***Accuracy***	***Kappa***
	5	2	0.826	0.758
	7	2	0.829	0.763
	9	2	0.832	0.766
	11	2	0.834	0.768
	13	**2**	**0.834**	**0.768**
Generalized Boosted Model	***interaction.depth***	***n.trees***	***Accuracy***	***Kappa***
	1	50	0.735	0.610
	2	50	0.780	0.685
	4	50	0.805	0.724
	5	50	0.814	0.738
	1	100	0.759	0.652
	2	100	0.799	0.714
	4	100	0.822	0.749
	5	100	0.830	0.761
	1	150	0.771	0.671
	2	150	0.808	0.728
	4	150	0.830	0.761
	5	150	0.837	0.771
	1	200	0.777	0.681
	2	200	0.814	0.737
	4	200	0.836	0.770
	5	200	0.841	0.777
	1	250	0.781	0.687
	2	250	0.818	0.743
	4	250	0.839	0.775
	5	**250**	**0.844**	**0.782**
C5.0 Tree	**Rule type**		**Accuracy**	**Kappa**
	Tree		**0.823**	**0.755**

Appendix S5 – Overall classification performance measures

Consider the following notation for the confusion matrix (or, contingency table) of a given multiclass prediction problem:

		Observed class				
	i,j	1	2	...	K	Total
Predicted class	1	$n(P_1, O_1)$	$n(P_1, O_2)$	...	$n(P_1, O_K)$	$N(P_1)$
	2	$n(P_2, O_1)$	$n(P_2, O_2)$	...	$n(P_2, O_K)$	$N(P_2)$
	...	...	...	...	...	...
	K	$n(P_k, O_1)$	$n(P_k, O_2)$	...	$n(P_K, O_K)$	$N(P_K)$
	Total	$N(O_1)$	$N(O_2)$	...	$N(O_K)$	N

In the above confusion matrix, $n(P_i, O_j)$ denotes the number of predictions belonging to class i that had observations in class j, $N(P_i)$ denotes the total number of predictions in class i, $N(O_j)$ denotes the total number of observations in category j, and N is the total number of predictions.

With the purpose of quantifying the overall classification performance at producer level the following measures were calculated:

Accuracy (ACC) – provides an overall measure that quantifies the fraction of predictions in the correct class. It is a simple and intuitive measure although it can be somewhat misleading since it is heavely influenced by the most common class. Ranges from [0,1] and a value of 1 indicates perfect score.

$$ACC = \frac{1}{N}\sum_{i=1}^{K} n(P_i, O_i)$$

Heidke skill score (HSS) – measures the accuracy of a given algorithm in predicting the correct class relative to that of random chance. This measure is one form of a generalized skill score, where the score in the numerator is the number of correct

predictions, and the reference prediction is, in this case, given by random chance. Requires a rather large sample size to ensure that all elements of the contingency table are adequately sampled. Ranges from]-∞, 1] with 0 indicating no skill and 1 a perfect score.

$$HSS = \frac{\frac{1}{N}\sum_{i=1}^{K} n(P_i, O_i) - \frac{1}{N^2}\sum_{i=1}^{K} N(P_i)N(O_i)}{1 - \frac{1}{N^2}\sum_{i=1}^{K} N(P_i)N(O_i)}$$

Peirce's skill score (PSS) – measures the accuracy of a given algorithm in predicting the correct class relative to that of random chance. This measure is similar to the Heidke skill score (above), except that in the denominator the fraction of correct predictions due to random chance is for an unbiased prediction. Varies from [-1,1] with 0 indicating no skill and 1 a perfect score.

$$PSS = \frac{\frac{1}{N}\sum_{i=1}^{K} n(P_i, O_i) - \frac{1}{N^2}\sum_{i=1}^{K} N(P_i)N(O_i)}{1 - \frac{1}{N^2}\sum_{i=1}^{K} (N(O_i))^2}$$

Gerrity skill score (GSS) – measures the accuracy of a given algorithm in predicting the correct class relative to that of random chance. Gerrity score uses all entries in the confusion matrix, does not depend on the prediction distribution and is equitable (*i.e.,* random and constant forecasts score a value of 0). This measure, unlike HSS and PSS, does not reward conservative predictions instead it rewards predictions for correctly determining the less likely classes. Smaller errors are penalized less than larger forecast errors. This is achieved through the use of the scoring matrix. GSS ranges from [-1,1] with 0 indicating no skill and 1 a perfect score.

$$GSS = \frac{1}{N}\sum_{i=1}^{K}\sum_{j=1}^{K} n(P_i, O_j)\, s_{ij}$$

where s_{ij} are elements of a scoring matrix given by:

$s_{ij} = \frac{1}{K-1}\left(\sum_{r=1}^{i-1} a_r^{-1} + \sum_{r=1}^{K-1} a_r\right)$, if $(i = j)$, i.e., diagonal,

$s_{ij} = s_{ji} = \frac{1}{K-1}\left(\sum_{r=1}^{i-1} a_r^{-1} - (j-i) + \sum_{r=1}^{K-1} a_r\right)$, if $(i \neq j)$, i.e., off-diagonal, and,

$a_i = \frac{(1-\sum_{r=1}^{i} p_r)}{\sum_{r=1}^{i} p_r}$, with sample probabilities (observed frequencies) given by: $p_i = \frac{N(O_i)}{N}$

Adapted from: Jolliffe, I.T., Stephenson, D.B. (eds.), 2003. Forecast Verification - A Practitioner's Guide in Atmospheric Science, 1st ed. John Wiley & Sons, Chichester, West Sussex, England.

Appendix S6 – References used for comparing producer and user accuracy values

Table S6.1 – Summary table showing values for producer and user accuracies assembled for comparison purposes. Classification performance metrics were compiled for similar habitat types including grasslands/meadows: 62xx, 64xx and 65xx, and, heathlands: 40xx and included a large variety of application contexts, classification approaches, input imagery data but all developed in the scope of Natura 2000 network. Performance metrics were collected from a semi-systematic literature review using the search term/expressions: "Natura 2000" combined, in alternation, with: "remote sensing", and, "habitat mapping". The search expressions were purposely wide-ranged to cover a large number of research papers or conference proceedings. Article searches were conducted at Scopus (http://www.scopus.com/) and Google Scholar (https://scholar.google.pt/) in May 2015. In cases where more than one value was shown (*e.g.,* more than one classification approach/method tested in the paper) then only the highest/best value was recorded in the table.

Notes:

(*1) Accuracy values in the paper referred to single-class classification approaches and were discarded for comparison purposes.

(*2) In this case more than one test site was used in the paper hence we recorded the range for producer and user accuracies across sites. For comparison, the mid value (of the range) was used.

Reference	Satellite /sensor /image data	Classification approach/algorithm	Vegetation class(es) reported	Habitat type(s) reported	Producer accuracy	User accuracy
Buck et al., 2015	RapidEye	Approach: object-based Classification algorithms: - Maximum likelihood - Support Vector Machines	Dry grasslands	62xx	**0.99**	**0.79**
			Wet grasslands	64xx	**0.38**	**0.81**
			Mesophilic grasslands	65xx	**0.57**	**0.41**
Chan et al., 2012	Hyperspectral CHRIS/Proba	Approach: pixel-based Classification algorithms: - Random Forest - Adaboost - Support Vector Machines	Temporary and permanent grassland	-	**0.65 (*1)**	
			Calluna-dominated heath	2310 / 4030	**0.45 (*1)**	
			Erica-dominated heath	4010	**0.48 (*1)**	
			Molinia-dominated heath	2310 / 2330 / 4010 / 4030	**0.81 (*1)**	
Corbane et al., 2013	RapidEye	Approach: object-based Classification algorithm: - Sparse Partial Least Square Discriminant Analysis	Semi-natural dry grasslands and scrubland facies on calcareous substrates	6210	**0.68**	**0.92**
			Extensively managed hay meadows of the planar to submountain zones	6510	**0.67**	**0.66**
Díaz Varela et al., 2008	Landsat TM	Approaches: object and pixel-based Classification algorithms: - Maximum likelihood - Nearest neighbour	Extensive Grasslands	-	**0.42**	**0.75**
			Sparse wet heathlands	4020* (4030; 7110*; 6230*; 7140; 7150)	**0.56**	**0.56**

			Mid-dense wet heathlands	4020* (4030; 7110*; 6230*; 7140; 7150)	**0.65**	**0.62**
			Dense wet heathlands	4020* (4030; 7110*; 6230*; 7140; 7150)	**0.76**	**0.63**
			Dry heathlands and scrubs	4030	**0.51**	**0.52**
Feilhauer et al., 2014	AISA Dual	Approaches: pixel-based Classification algorithms: - Random Forest	*Molinia* meadows	6410	**0.75**	**0.71**
	RapidEye		*Molinia* meadows	6410	**0.69**	**0.69**
	Sentinel-2		*Molinia* meadows	6410	**0.75**	**0.68**
Förster et al., 2008	QuickBird	Approaches: pixel, object and knowledge-based Classification algorithms: - Maximum likelihood - Knowledge-based system	Xeric sand calcareous grasslands	6120*	**0.80 - 1.00**	**0.77 - 1.00 (*2)**
			Heathland	4030	**0.95 - 1.00**	**0.92 - 0.95 (*2)**
Förster et al., 2010	RapidEye	Approach: object-based Classification algorithms: - Nearest neighbour	Dry grasslands	62xx	**0.90 (*1)**	
			Heathland	40xx	**0.98 (*1)**	
Haest et al., 2010	Hyperspectral AHS	Approaches: pixel, object and knowledge-based Classification algorithms: - Linear Discriminant Analysis with Sequential-Floating-Forward-Selection	Northern Atlantic wet heaths	4010	**0.20**	**0.49**
			Dry heaths	4030	**0.46**	**0.34**
Hernando et al., 2012	QuickBird	Approaches: object and knowledge-based Classification algorithm: - Fuzzy logic knowledge-based system	*Nardus* grasslands	6230*	**0.97**	**0.93**
			Heathland	4090	**0.90**	**0.57**
Stenzel et al., 2014	RapidEye	Approach: pixel-based Classification algorithm: Maximum Entropy One-class Classifier	*Molinia* meadows	6410	**0.76**	**0.73**
Zlinszky et al., 2014	LiDAR	Approach: pixel-based Classification algorithms: - Random Forest	Lowland hay meadow	6510	**0.42**	**0.54**
			Molinia meadows	6410	**0.62**	**0.79**
			Dry meadow	6210	**0.79**	**0.66**

Table S6.2 – Summary table showing some descriptive statistics for producer and user accuracy values collected from the literature revision.

Vegetation type	Habitat types reported	Statistical descriptor	Producer accuracy	User accuracy
Grasslands/ meadows (n=15)	62xx / 64xx / 65xx	Minimum	0.38	0.41
		25% Quartile	0.60	0.67
		Median	0.69	0.73
		75% Quartile	0.78	0.80
		Maximum	0.99	0.93
		Mean ± Std. Error	0.69 ± 0.05	0.73 ± 0.04
Heathlands (n=8)	40xx	Minimum	0.20	0.34
		25% Quartile	0.50	0.51
		Median	0.61	0.57
		75% Quartile	0.80	0.62
		Maximum	0.98	0.94
		Mean ± Std. Error	0.61 ± 0.09	0.57 ± 0.06

Appendix S7 – Confusion matrix calculated from validation/test set 1

Table S7 - Confusion matrix calculated from validation/test set 1

		Observed										
		4020	**4030**	**6230**	**Bare rock**	**Bare soil**	**Tracks**	**Water surfaces / water lines**	**Bare soil / 4030 degraded**	**Ponds**	**6230 degraded**	$N(P_i)$
Predicted	**4020**	**3896**	196	499	36	219	15	61	73	14	33	**5042**
	4030	305	**11119**	789	177	440	13	83	474	0	64	**13464**
	6230	1147	1256	**48250**	63	969	117	58	206	0	725	**52791**
	Bare rock	10	147	50	**11150**	27	2	0	370	2	0	**11758**
	Bare soil	142	172	380	19	**4091**	94	31	106	4	46	**5085**
	Tracks	6	27	86	44	69	**2781**	0	55	0	0	**3068**
	Water surfaces / water lines	48	44	43	0	22	0	**767**	0	0	2	**926**
	Bare soil / 4030 degraded	18	386	137	321	120	76	0	**5127**	0	0	**6185**
	Ponds	8	0	0	7	1	0	0	0	**639**	0	**655**
	6230 degraded	69	17	156	0	124	0	0	0	0	**5685**	**6051**
	$N(O_i)$	**5649**	**13364**	**50390**	**11817**	**6082**	**3098**	**1000**	**6411**	**659**	**6555**	**(N=105 025)**

References

Buck, O., V. E. G. Millán, A. Klink, and K. Pakzad. 2015. Using information layers for mapping grassland habitat distribution at local to regional scales. International Journal of Applied Earth Observation and Geoinformation 37:83-89.

Chan, J. C.-W., P. Beckers, T. Spanhove, and J. V. Borre. 2012. An evaluation of ensemble classifiers for mapping Natura 2000 heathland in Belgium using spaceborne angular hyperspectral (CHRIS/Proba) imagery. International Journal of Applied Earth Observation and Geoinformation 18:13-22.

Corbane, C., S. Alleaume, and M. Deshayes. 2013. Mapping natural habitats using remote sensing and sparse partial least square discriminant analysis. International Journal of Remote Sensing 34:7625-7647.

Díaz Varela, R. A., P. Ramil Rego, S. Calvo Iglesias, and C. Muñoz Sobrino. 2008. Automatic habitat classification methods based on satellite images: A practical assessment in the NW Iberia coastal mountains. Environmental Monitoring and Assessment 144:229-250.

Feilhauer, H., C. Dahlke, D. Doktor, A. Lausch, S. Schmidtlein, G. Schulz, and S. Stenzel. 2014. Mapping the local variability of Natura 2000 habitats with remote sensing. Applied Vegetation Science 17:765-779.

Förster, M., A. Frick, C. Schuster, and B. Kleinschmit. 2010. Object-based change detection analysis for the monitoring of habitats in the framework of the Natura 2000 directive with multi-temporal satellite data. Page 5 *in* GEOBIA 2010: Geographic Object-Based Image Analysis, Ghent, Belgium.

Förster, M., A. Frick, H. Walentowski, and B. Kleinschmit. 2008. Approaches to utilising QuickBird data for the monitoring of NATURA 2000 habitats. Community Ecology 9:155-168.

Haest, B., G. Thoonen, J. V. Borre, T. Spanhove, S. Delalieux, L. Bertels, L. Kooistra, C. A. Mücher, and P. Scheunders. 2010. An object-based approach to quantity and quality assessment of heathland habitats in the framework of Natura 2000 using hyperspectral airborne images. Page 6 *in* E. A. Addink and F. M. B. V. Coillie, editors. GEOBIA 2010: Geographic Object-Based Image Analysis, Ghent, Belgium.

Hernando, A., L. A. Arroyo, J. Velázquez, and R. Tejera. 2012. Objects-based Image Analysis for Mapping Natura 2000 Habitats to Improve Forest Management. Photogrammetric Engineering & Remote Sensing 78:991-999.

Jiang, J., D. Liu, J. Gu, and S. Susstrunk. 2013. What is the Space of Spectral Sensitivity Functions for Digital Color Cameras?*in* IEEE Workshop on the Applications of Computer Vision (WACV).

Kawakami, R., Z. Hongxun, R. T. Tan, and K. Ikeuchi. 2013. Camera Spectral Sensitivity and White Balance Estimation from Sky Images. International Journal of Computer Vision.

Kuhn, M. 2016. caret: Classification and Regression Training. R package version 6.0-70. http://CRAN.R-project.org/package=caret.

SenseFly. 2015. SenseFly: Drones Accessories, S110 RGB. URL: https://www.sensefly.com/drones/accessories.html (visited in 20/05/2015).

Stenzel, S., H. Feilhauer, B. Mack, A. Metz, and S. Schmidtlein. 2014. Remote sensing of scattered Natura 2000 habitats using a one-class classifier. International Journal of Applied Earth Observation and Geoinformation 33:211-217.

Zlinszky, A., A. Schroiff, A. Kania, B. Deák, W. Mücke, Á. Vári, B. Székely, and N. Pfeifer. 2014. Categorizing Grassland Vegetation with Full-Waveform Airborne Laser

Scanning: A Feasibility Study for Detecting Natura 2000 Habitat Types. Remote Sensing 6:8056-8087.

Appendix V | Chapter 8 – Assessing the effectiveness of Protected Areas to ensure the stability of forests – a methodological approach employing MODIS EVI time-series data

Appendix S1 – List of selected Protected-areas in mainland Portugal

(source: http://www.icnf.pt/portal/naturaclas/cart/resource/doc/ap-rn-ramsar/AP-00AP-JUN-2016)

Selected	Classification type	Protected Area name	Area type	Creation year	Area (hectares)
Yes	Regional Protected Landscape	*Açude do Monte da Barca*	Terrestrial	1980	867.80
Yes	Regional Protected Landscape	*Albufeira do Azibo*	Terrestrial	1999	3277.19
Yes	Natural Park	*Alvão*	Terrestrial	1983	7238.30
Yes	Natural Park	*Arrábida*	Terrestrial	1976	12381.67
Yes	Protected Landscape	*Arriba Fóssil da Costa da Caparica*	Terrestrial	1984	1551.55
Yes	Regional Protected Landscape	*Corno do Bico*	Terrestrial	1999	2070.83
Yes	Natural Park	*Douro Internacional*	Terrestrial	1998	86834.82
Yes	Natural Reserve	*Dunas de São Jacinto*	Terrestrial	1979	733.46
Yes	Natural Reserve	*Estuário do Sado*	Estuarine	1980	23971.55
Yes	Natural Reserve	*Lagoas de Santo André e Sancha*	Terrestrial	2000	3123.48
Yes	Natural Park	*Litoral Norte*	Terrestrial	1987	1316.48
Yes	Natural Park	*Montesinho*	Terrestrial	1979	74224.89
Yes	Natural Reserve	*Paul de Arzila*	Terrestrial	1988	586.73
Yes	National Park	*Peneda-Geres*	Terrestrial	1971	69594.48
Yes	Natural Park	*Ria Formosa*	Terrestrial	1978	17900.77
Yes	Natural Park	*Serra da Estrela*	Terrestrial	1976	89132.21
Yes	Regional Protected Landscape	*Serra de Montejunto*	Terrestrial	1999	4897.45
Yes	Natural Park	*Serra de São Mamede*	Terrestrial	1989	56061.31
Yes	Protected Landscape	*Serra do Açor*	Terrestrial	1982	373.39
Yes	Natural Reserve	*Serra Malcata*	Terrestrial	1981	16157.98
Yes	Natural Park	*Serras de Aire e Candeeiros*	Terrestrial	1979	38392.91

Yes	Natural Park	*Sintra-Cascais*	Terrestrial	1981	14450.84
Yes	Natural Park	*Sudoeste Alentejano e Costa Vicentina*	Terrestrial	1988	60571.97
Yes	Natural Park	*Tejo Internacional*	Terrestrial	2000	26490.43
Yes	Natural Park	*Vale do Guadiana*	Terrestrial	1995	69665.94
No	Regional Protected Landscape	*Açude da Agolada*	Terrestrial	1980	266.40
No	Natural Park	*Arrábida*	Marine	1976	5271.65
No	Natural Reserve	*Berlengas*	Marine	1981	9441.97
No	Natural Reserve	*Berlengas*	Terrestrial	1981	98.76
No	Natural Monument	*Cabo Mondego*	Marine	2007	61.26
No	Natural Monument	*Cabo Mondego*	Terrestrial	2007	56.42
No	Natural Monument	*Carenque*	Terrestrial	1997	6.09
No	Natural Reserve	*Dunas de São Jacinto*	Marine	1979	262.23
No	Local Natural Reserve	*Estuário do Douro*	Terrestrial	2009	66.35
No	Natural Reserve	*Estuário do Tejo*	Estuarine	1976	2889.29
No	Natural Reserve	*Estuário do Tejo*	Terrestrial	1976	11526.92
No	Private Protected Area	*Faia Brava*	Terrestrial	2010	214.65
No	Regional Protected Landscape	*Fonte Benemola*	Terrestrial	1991	406.38
No	Regional Protected Landscape	*Lagoas de Bertiandos e São Pedro de Arcos*	Terrestrial	2000	345.87
No	Natural Reserve	*Lagoas de Santo André e Sancha*	Marine	2000	2142.02
No	Regional Protected Landscape	*Litoral de Vila do Conde e Reserva Ornitológica do Mindelo*	Terrestrial	2009	379.57
No	Natural Park	*Litoral Norte*	Marine	1987	7445.33
No	Local Natural Reserve	*Paul da Tornada*	Terrestrial	2009	53.65
No	Natural Reserve	*Paul do Boquilobo*	Terrestrial	1980	817.63
No	Natural Monument	*Pedreira do Avelino*	Terrestrial	1997	1.66
No	Natural Monument	*Portas de Ródão*	Terrestrial	2009	965.38
No	Regional Protected Landscape	*Rocha da Pena*	Terrestrial	1991	671.82
No	Natural Reserve	*Sapal de Castro Marim e Vila Real de Santo António*	Terrestrial	1975	2307.99
No	Regional Protected Landscape	*Serra da Gardunha*	Terrestrial	2014	10507.49

No	Natural Park	*Sudoeste Alentejano e Costa Vicentina*	Marine	1988	28996.80
No	Regional Natural Park	*Vale do Tua*	Terrestrial	2013	24769.07

Appendix S2 – Demographic changes in selected protected areas

Data source: Portuguese National Statistics Institute (INE, https://www.ine.pt)

Population/demography censuses at the most disaggregated statistical unit level (BGRI)

Year 1991: http://mapas.ine.pt/download/index1991.phtml

Year 2001: http://mapas.ine.pt/download/index2001.phtml

Year 2011: http://mapas.ine.pt/download/index2011.phtml

Protected area name	Average PA elevation (m)	Resident population 1991 (# individuals)	Resident population 2001 (# individuals)	Resident population 2011 (# individuals)	% Population change 1991 - 2011	% Population change 2001 - 2011
Açude do Monte da Barca	59	844	477	529	-37.32	10.90
Albufeira do Azibo	643	3477	2879	2528	-27.29	-12.19
Alvão	950	6748	5474	4376	-35.15	-20.06
Arrábida	146	20321	20094	25047	23.26	24.65
Arriba Fóssil da Costa da Caparica	53	5216	8279	10409	99.56	25.73
Corno do Bico	590	5394	4707	3580	-33.63	-23.94
Douro Internacional	611	25194	21624	18395	-26.99	-14.93
Dunas de São Jacinto	6	1185	1126	1129	-4.73	0.27
Estuário do Sado	10	11964	10627	12879	7.65	21.19
Lagoas de Santo André e Sancha	22	3472	2735	4360	25.58	59.41
Litoral Norte	7	18240	19459	15342	-15.89	-21.16
Montesinho	827	14476	12520	11286	-22.04	-9.86
Paul de Arzila	29	3004	2866	3338	11.12	16.47
Peneda-Geres	866	19995	16838	12788	-36.04	-24.05
Ria Formosa	8	39953	39034	47113	17.92	20.70
Serra da Estrela	986	58393	50208	39710	-32.00	-20.91
Serra de Montejunto	297	8148	8421	7382	-9.40	-12.34
Serra de São Mamede	479	29849	28888	24672	-17.34	-14.59
Serra do Açor	634	1156	859	244	-78.89	-71.59
Serra Malcata	801	3662	2964	2665	-27.23	-10.09
Serras de Aire e Candeeiros	339	50565	49791	46736	-7.57	-6.14
Sintra-Cascais	151	44534	50276	55894	25.51	11.17
Sudoeste Alentejano e Costa Vicentina	68	29180	29642	29775	2.04	0.45
Tejo Internacional	234	6436	7369	3110	-51.68	-57.80
Vale do Guadiana	140	10883	9628	7866	-27.72	-18.30

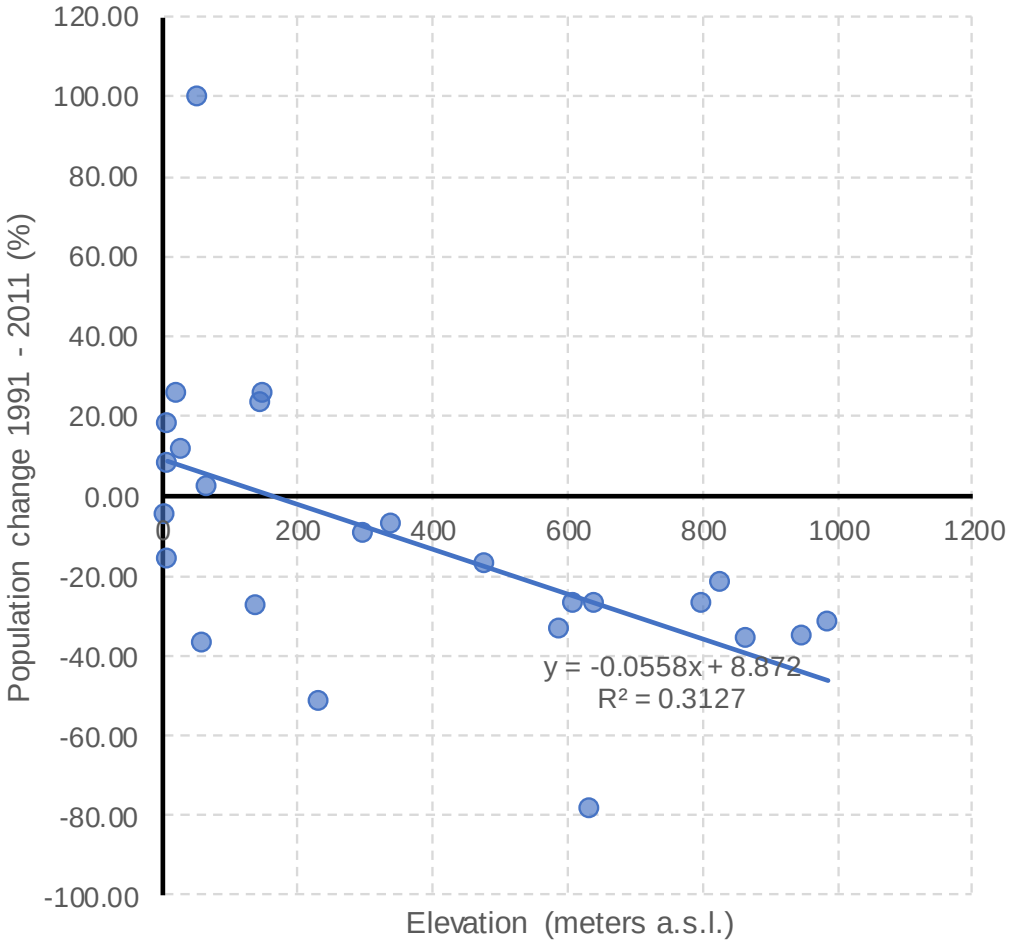

Figure S2 - 1 – % Population change between 1991 and 2011 as a function of PA average elevation. Notice that mountainous PAs suffered the strongest population decreases. In contrast, low-land PAs (especially near the coastline) recorded increases in population.

Appendix S3 – Description of common species in Corine Land cover forest classes

Class	Description
Broad-leaved forests (CLC 311)	Vegetation formations composed mainly of trees, including shrub and bush understory, where broad-leaved species predominate (> 75 % of the area); Typical native broadleaf species are the is also common in some northern regions. Southern-Mediterranean areas are typically dominated by Cork oak (*Q. suber*) and holm oak (*Q. ilex*). Common non-native broadleaf species include Eucalypt (*Eucalyptus* spp.) used for pulp production and typically planted throughout the north and center of the country. In recent years, invasive species of the Acacia genus (e.g., *A. dealbata*, A. *melanoxylon, A. longifolia*) have also increased their coverage mainly as a consequence of high wildfire frequency and/or motorway development (Vicente et al. 2010, ICNF 2013, Vicente et al. 2014).
Coniferous forests (CLC 312)	Vegetation formation composed principally of trees, including shrub and bush understory, where coniferous species predominate (> 75 % of the area); Regarding native coniferous species, maritime pine (*Pinus pinaster*), although its decrease in the last decades, is still widespread in the north and center regions of Portugal. Stone pine (*P. pinea*) is most common in southern regions. Non-native species from the genus Cedrus (e.g., *C. atlantica* or *C. deodora*), Cupressus (e.g., *C. macrocarpa*, *C. sempervirens*), and other such as *Chamaecyparis lawsoniana* and *Pseudotsuga menziesii* are some examples of planted non-native coniferous species used for production purposes.
Mixed forests (CLC 313)	Vegetation formation composed principally of trees, including shrub and bush understory, where neither broad-leaved nor coniferous species predominate. The share of coniferous or broad-leaved species does not exceed 25% in the canopy closure.

Appendix S4 – Details of smoothing algorithms

The filtering method is considered a moving-window implementation of the Hampel identifier (Hampel 1974, Davies and Gather 1993) which defines the central point (x_k) in a given data window that is considered an outlier and is replaced if it lies more than t times the moving data window's mean absolute deviation (MAD) scale estimate from its median:

$$y_k = \begin{cases} x_k \; if \; |x_k - m_k| \leq tS_k \\ else \; m_k \end{cases}$$

Where m_k is the window median value and S_k is the MAD scale estimate as given by: $S_k = 1.4826 \times median(|x_k - m_k|)$.

The smoothing method applied to the data presents several advantages, since it is computationally fast, gives continuous control over smoothness and allows for automatic interpolation (Eilers 2003). It is based on penalized least squares given by the minimization of a cost function describing the balance between fidelity, as the quadratic difference between estimates and actual observations, and roughness, expressed as the quadratic difference between successive estimates (Eilers 2003). This balance is controlled by a smoothing parameter (lambda); larger lambda values lead to more smoothing but at the expense of fidelity. Determining a suitable lambda value required some fine tuning and inspection since it depends on the data. After some experimentation, this parameter was set to 2. The smoothness is also controlled by the order of differentiation which was fixed to a second order finite difference penalty as implemented in R package ptw (Bloemberg et al. 2010, Wehrens et al. 2015). By controlling the weights attributed to each data point in the time-series, the smoothing was applied to fit the annual "upper envelope" of the time-series under the assumption that atmospheric effects mainly result in a decrease of the vegetation index (Beck et al. 2006).

References

Beck, P. S. A., C. Atzberger, K. A. Høgda, B. Johansen, and A. K. Skidmore. 2006. Improved monitoring of vegetation dynamics at very high latitudes: A new method using MODIS NDVI. Remote Sensing of Environment 100:321-334.

Bloemberg, T. G., J. Gerretzen, H. J. P. Wouters, J. Gloerich, M. van Dael, H. J. C. T. Wessels, L. P. van den Heuvel, P. H. C. Eilers, L. M. C. Buydens, and R. Wehrens. 2010. Improved parametric time warping for proteomics. Chemometrics and Intelligent Laboratory Systems 104:65-74.

Davies, L., and U. Gather. 1993. The Identification of Multiple Outliers. Journal of the American Statistical Association 88:782-792.

Eilers, P. H. C. 2003. A Perfect Smoother. Analytical Chemistry 75:3631-3636.

Hampel, F. R. 1974. The Influence Curve and Its Role in Robust Estimation. Journal of the American Statistical Association 69:383-393.

ICNF. 2013. 6.º Inventário Florestal Nacional - Resultados preliminares (v1.1). Instituto da Conservação da Natureza e das Florestas, Lisboa.

Vicente, J., P. Alves, C. Randin, A. Guisan, and J. Honrado. 2010. What drives invasibility? A multi-model inference test and spatial modelling of alien plant species richness patterns in northern Portugal. Ecography 33:1081-1092.

Vicente, J. R., H. M. Pereira, C. F. Randin, J. Gonçalves, A. Lomba, P. Alves, J. Metzger, M. Cezar, A. Guisan, and J. Honrado. 2014. Environment and dispersal paths override life strategies and residence time in determining regional patterns of invasion by alien plants. Perspectives in Plant Ecology, Evolution and Systematics 16:1-10.

Wehrens, R., T. G. Bloemberg, and P. H. C. Eilers. 2015. Fast parametric time warping of peak lists. Bioinformatics 31:3063-3065.

Appendix S5 – Search buffer distances by protected area

Protected area name	Total forest area (km^2)	Buffer distance (km)
Açude do Monte da Barca	6.88	1.50
Albufeira do Azibo	3.44	3.50
Alvão	9.81	3.25
Arrábida	20.63	21.00
Arriba Fóssil da Costa da Caparica	6.56	8.50
Corno do Bico	9.81	4.75
Douro Internacional	85.50	11.50
Dunas de São Jacinto	4.19	6.00
Estuário do Sado	51.00	4.50
Lagoas de Santo André e Sancha	14.56	2.75
Litoral Norte	3.50	3.25
Montesinho	126.25	9.75
Paul de Arzila	2.19	1.25
Peneda-Geres	87.44	9.50
Ria Formosa	8.00	14.75
Serra da Estrela	202.25	13.75
Serra de Montejunto	9.13	17.25
Serra de São Mamede	169.56	36.50
Serra do Açor	2.81	2.25
Serra Malcata	52.19	9.75
Serras de Aire e Candeeiros	26.69	6.75
Sintra-Cascais	39.50	29.75
Sudoeste Alentejano e Costa Vicentina	84.38	10.50
Tejo Internacional	127.69	6.00
Vale do Guadiana	31.94	29.50

Appendix S6 – Full list of models calibrated and ranked using AICc

Results for AICc-based model ranking for each response stability metric: annual coefficient of variation of the annual 5% quantile (Q05), median (MED), 95% quantile (Q95), annual difference between 95 and 5% quantiles (DQT), and "summerness" (sine) transformation of the day of maximum (SMN). STL decomposition – trend component coefficient of variation (TRD), and maximum Lyapunov exponent (MLE). ΔAICc – Delta AIC (greater values translate lower model support; typically, values above 2 or 3 have low support); w_i – Akaike weights (higher values represent greater relative model support within [0, 1]); and, D2 – explained deviance; symbols within parenthesis represent model significance: (***) p<0.001, (**) p<0.01, (*) p<0.05, (.) p<0.1. Bold-highlighted models attained the best support to explain differences between stable vs. unstable areas considering each metric.

Hypothesis	**Model code / predictor variables**	**Response variable/ stability metric**											
		Q05			**MED**			**Q95**			**DQT**		
		ΔAICc	**w_i**	**D2**	**ΔAICc**	**w_i**	**D2**	**ΔAICc**	**w_i**	**D2**	**ΔAICc**	**w_i**	**D2**
I. Climatic anomalies	M1.1 = PREC_ANOM	3.62	0.02	-	9.54	0.00	0.14 (*)	10.65	0.00	0.1 (.)	6.03	0.01	-
	M1.2 = TMAX_ANOM + TMIN_ANOM	4.75	0.01	0.06	13.65	0.00	0.09	15.81	0.00	0.02	7.79	0.00	0.02
II. Protected area attributes	M2.1 = PA_SIZE	**1.96**	**0.04**	**0.06**	9.33	0.01	0.14 (*)	12.26	0.00	0.05	5.38	0.01	0.02
	M2.2 = PA_ELEV	3.57	0.02	0.01	14.05	0.00	0.01	14.07	0.00	-	5.63	0.01	0.01
	M2.3 = PA_AGE	3.39	0.02	0.01	13.85	0.00	0.01	14.07	0.00	-	5.86	0.01	0.01
	M2.4 = PA_CIRC	3.16	0.02	0.02	11.43	0.00	0.08 (.)	12.67	0.00	0.04	5.38	0.01	0.02
	M2.5 = PA_SAC	3.72	0.02	-	13.73	0.00	0.01	13.24	0.00	0.02	4.34	0.02	0.05
	M2.6 = PA_SPA	**2.11**	**0.04**	**0.06**	13.69	0.00	0.02	13.72	0.00	0.01	5.06	0.01	0.03
III. Human pressure	M3.1 = POP_DENS	3.08	0.03	0.02	11.54	0.00	0.08	13.05	0.00	0.03	5.86	0.01	0.01
	M3.2 = POP_CHANGE	3.55	0.02	0.01	13.30	0.00	0.03	13.56	0.00	0.01	4.20	0.02	0.05
	M3.3 = ROAD_DENS	3.59	0.02	-	14.13	0.00	-	13.78	0.00	0.01	3.60	0.03	0.07
IV. Landscape and forest composition	M4.1 = LC_SIDI	3.36	0.02	0.01	11.77	0.00	0.07	11.94	0.00	0.06	4.51	0.02	0.04
	M4.2 = LC_BRLF	**0.00**	**0.12**	**0.13 (.)**	7.94	0.01	0.18 (*)	8.38	0.01	0.16 (*)	**1.23**	**0.09**	**0.14 (*)**
	M4.3 = LC_CONF	**2.11**	**0.04**	**0.06**	11.88	0.00	0.07	10.06	0.00	0.12 (*)	**1.94**	**0.07**	**0.12 (*)**
	M4.4 = LC_MIXF	3.39	0.02	0.01	13.74	0.00	0.01	14.01	0.00	-	5.37	0.01	0.02
V. Forest structure	M5.1 = FOR_AREA	3.16	0.02	0.02	11.12	0.00	0.09 (.)	13.48	0.00	0.02	4.74	0.02	0.04
	M5.2 = FOR_COHES	**1.99**	**0.04**	**0.06**	12.16	0.00	0.06	13.76	0.00	0.01	4.49	0.02	0.05
	M5.4 = FCH_AVG	3.69	0.02	-	14.09	0.00	-	14.04	0.00	-	4.00	0.02	0.06
	M5.5 = FCH_STD	**1.38**	**0.06**	**0.08**	5.56	0.04	0.25 (**)	5.16	0.06	0.26 (**)	**0.48**	**0.14**	**0.16 (*)**
	M5.6 = FCH_AVG + FCH_STD	3.95	0.02	0.09	7.84	0.01	0.26 (*)	7.71	0.02	0.26 (*)	**0.20**	**0.16**	**0.25 (*)**
VI. Forest disturbance	M6.1 = BURN_PA	2.55	0.03	0.04	13.31	0.00	0.03	13.91	0.00	-	6.05	0.01	-
	M6.2 = BURN_FOR	**1.91**	**0.05**	**0.07**	12.77	0.00	0.04	13.94	0.00	-	6.04	0.01	-
	M6.3 = PWN_PERC	3.68	0.02	-	14.10	0.00	-	14.07	0.00	-	6.04	0.01	-
	M7.1 = LC_BRLF + PA_SIZE	**0.04**	**0.12**	**0.23 (*)**	**3.17**	**0.12**	**0.40 (**)**	9.02	0.01	0.22 (*)	**3.02**	**0.04**	**0.16 (.)**

VII. 'Combined' models	M7.2 = PA_SIZE + LC_BRLF + BURN_FOR:PA_ELEV	**1.10**	**0.07**	**0.29 (*)**	**0.00**	**0.58**	**0.57 (***)**	8.77	0.01	0.31 (*)	5.87	0.01	0.16
	M7.3 = PA_SIZE + FCH_STD + BURN_FOR:PA_ELEV	4.00	0.02	0.19	3.96	0.08	0.46 (**)	6.24	0.03	0.38 (**)	5.77	0.01	0.17
	M7.4 = BURN_FOR + PA_SIZE + FCH_AVG	**2.46**	**0.03**	**0.24 (.)**	6.23	0.03	0.39 (**)	16.61	0.00	0.08	8.06	0.00	0.10
	M7.5 = LC_BRLF + FCH_AVG + FCH_STD	3.18	0.02	0.22	3.93	0.08	0.46 (**)	3.97	0.10	0.45 (**)	**0.00**	**0.17**	**0.34 (**)**
	M7.6 = PWN_PERC + PWN_PERC:LC_CON	4.99	0.01	0.05	6.91	0.02	0.29 (**)	**0.00**	**0.74**	**0.48 (***)**	**2.69**	**0.05**	**0.17 (.)**

Hypothesis	**Model code / predictor variables**	**Response variable/ stability metric**											
		SMN			**MLE**			**TRD**			**HUP**		
		ΔAICc	**w_i**	**D2**	**ΔAICc**	**w_i**	**D2**	**ΔAICc**	**w_i**	**D2**	**ΔAICc**	**w_i**	**D2**
I. Climatic anomalies	M1.1 = PREC_ANOM	6.21	0.02	0.01	**0.53**	**0.11**	**0.15 (*)**	10.06	0.00	0.13 (*)	2.41	0.03	-
	M1.2 = TMAX_ANOM + TMIN_ANOM	6.02	0.02	0.09	3.84	0.02	0.13	13.37	0.00	0.11	3.80	0.02	0.04
II. Protected area attributes	M2.1 = PA_SIZE	6.37	0.02	-	3.54	0.02	0.06	10.76	0.00	0.11 (.)	0.93	0.06	0.05
	M2.2 = PA_ELEV	6.35	0.02	-	4.81	0.01	0.02	14.14	0.00	0.01	2.44	0.03	-
	M2.3 = PA_AGE	5.03	0.04	0.04	5.24	0.01	0.01	14.26	0.00	-	2.06	0.04	0.01
	M2.4 = PA_CIRC	6.32	0.02	-	**1.82**	**0.06**	**0.11 (.)**	11.40	0.00	0.09 (.)	2.47	0.03	-
	M2.5 = PA_SAC	6.17	0.02	0.01	5.45	0.01	-	14.19	0.00	-	1.76	0.04	0.02
	M2.6 = PA_SPA	5.48	0.03	0.03	5.04	0.01	0.01	13.07	0.00	0.04	2.47	0.03	-
III. Human pressure	M3.1 = POP_DENS	6.40	0.02	-	4.52	0.02	0.03	11.78	0.00	0.08	2.43	0.03	-
	M3.2 = POP_CHANGE	6.40	0.02	-	4.26	0.02	0.04	13.40	0.00	0.03	2.10	0.04	0.01
	M3.3 = ROAD_DENS	**0.00**	**0.46**	**0.19 (*)**	5.35	0.01	-	14.31	0.00	-	2.23	0.03	0.01
IV. Landscape and forest composition	M4.1 = LC_SIDI	6.20	0.02	0.01	4.58	0.01	0.03	13.00	0.00	0.04	**0.00**	**0.10**	**0.08**
	M4.2 = LC_BRLF	6.21	0.02	0.01	**1.26**	**0.08**	**0.13 (*)**	6.44	0.02	0.24 (**)	1.90	0.04	0.02
	M4.3 = LC_CONF	6.18	0.02	0.01	4.26	0.02	0.04	12.67	0.00	0.05	**0.73**	**0.07**	**0.05**
	M4.4 = LC_MIXF	6.41	0.02	-	5.34	0.01	-	14.06	0.00	0.01	2.44	0.03	-
V. Forest structure	M5.1 = FOR_AREA	6.16	0.02	0.01	**0.00**	**0.14**	**0.17 (*)**	9.46	0.01	0.15 (*)	2.46	0.03	-
	M5.2 = FOR_COHES	6.38	0.02	-	**3.01**	**0.03**	**0.08**	9.67	0.00	0.14 (*)	2.43	0.03	-
	M5.4 = FCH_AVG	6.20	0.02	0.01	4.91	0.01	0.02	14.15	0.00	0.01	2.46	0.03	-
	M5.5 = FCH_STD	3.86	0.07	0.07	**1.83**	**0.06**	**0.11 (.)**	7.01	0.02	0.22 (**)	1.60	0.05	0.03
	M5.6 = FCH_AVG + FCH_STD	6.26	0.02	0.08	3.65	0.02	0.14	9.18	0.01	0.23 (*)	4.19	0.01	0.03
VI. Forest disturbance	M6.1 = BURN_PA	6.26	0.02	-	4.35	0.02	0.03	12.57	0.00	0.05	2.45	0.03	-
	M6.2 = BURN_FOR	6.09	0.02	0.01	5.02	0.01	0.01	12.11	0.00	0.07	2.04	0.04	0.01
	M6.3 = PWN_PERC	6.41	0.02	-	4.25	0.02	0.04	14.22	0.00	-	**0.55**	**0.08**	**0.06**
VII. 'Combined' models	M7.1 = LC_BRLF + PA_SIZE	8.77	0.01	0.01	**1.18**	**0.08**	**0.21 (*)**	**2.64**	**0.16**	**0.43 (***)**	2.87	0.02	0.07
	M7.2 = PA_SIZE + LC_BRLF + BURN_FOR:PA_ELEV	11.62	0.00	0.01	**1.59**	**0.07**	**0.29 (*)**	**0.00**	**0.60**	**0.59 (***)**	5.63	0.01	0.07
	M7.3 = PA_SIZE + FCH_STD + BURN_FOR:PA_ELEV	7.97	0.01	0.11	4.15	0.02	0.21 (.)	6.69	0.02	0.39 (**)	6.21	0.00	0.05
	M7.4 = BURN_FOR + PA_SIZE + FCH_AVG	11.31	0.00	0.02	5.26	0.01	0.17	5.31	0.04	0.43 (**)	6.30	0.00	0.05
	M7.5 = LC_BRLF + FCH_AVG + FCH_STD	8.44	0.01	0.10	**3.34**	**0.03**	**0.23 (.)**	3.89	0.09	0.47 (**)	6.15	0.00	0.05
	M7.6 = PWN_PERC + PWN_PERC:LC_CON	8.73	0.01	0.01	**1.68**	**0.06**	**0.2 (*)**	9.32	0.01	0.23 (*)	2.54	0.03	0.08

Appendix S7 – Area covered by different forest species according to 1995 forest inventory by PA and NPA

Data source: ICNF (Portuguese Institute for Nature Conservation and Forestry)

URL: http://www.icnf.pt/portal/florestas/ifn/ifn4/dad-base95-98

PA – selected Protected Areas

NPA – Areas not covered by selected Protected Areas

Species	Total area in NPA (ha)	Total area in selected PAs (ha)	% area in NPA	% area in selected PAs
Holm oak (*Quercus ilex*)	443079.2	26065.5	14.5	14.2
Cork oak (*Quercus suber*)	693036.2	21734.7	22.6	11.8
Other Quercus species (*Q. robur, Q. pyrenaica*, etc.)	127390.0	21730.8	4.2	11.8
Chestnut (*Castanea sativa*)	36212.7	4976.6	1.2	2.7
***Eucalyptus* spp.**	650645.3	20356.6	21.3	11.1
Other broadleaf species *(Fraxinus* spp., *Salix* spp., etc)	101321.3	13328.5	3.3	7.3
Maritime pine (*Pinus pinaster*)	919525.2	58105.8	30.1	31.7
Stone pine (*Pinus pinea*)	71463.1	6104.4	2.3	3.3
Other coniferous species (*Pinus* spp., *Cupressus* spp., *Chamaecyparis* spp., etc)	17261.8	11144.6	0.6	6.1
Total area	**3059934.6**	**183547.4**		

Appendix VI | Chapter 9 – *SegOptim* – a R package for optimizing image segmentation parameters with evolutionary algorithms in the context of supervised classification

Appendix S1 – List of reviewed papers in the context of OBIA and supervised classification

We used the *ISI Web Of Science*™ application (URL: http://apps.webofknowledge.com) to search for articles between 2007-2016 referring OBIA (a term more frequent than GEOBIA and contained in the latter) in the contexts of Remote Sensing/Earth Observation and for the purpose of classification. We used the following query: *(TS=("OBIA" OR "segmentation" OR "object-based")) AND (TS=("remote sensing" OR "earth observation" OR "satellite")) AND (TS=("classification")).* Results were then filtered to particular application areas corresponding to the major following categories: ("*Remote Sensing"* OR "*Plant Sciences"* OR "*Biodiversity Conservation"* OR "*Ecology"* OR "*Agronomy"* OR "*Forestry"*). A total of 1067 articles were found and from this set, 72 (ca. 7%) were randomly selected for further screening and analysis (Table S1 - 1).
For reviewing the selected papers, we defined and used a set of questions and criteria (Table S1 - 2) which allowed standardizing the collection of data from each article.

Table S1 - 1 – List of reviewed publications randomly selected.

Ref/ID	Publication year	Authors	Title	Journal
11	2016	Zheng, C; Zhang, Y; Wang, LG	Multilayer semantic segmentation of remote-sensing imagery using a hybrid object-based Markov random field model	INTERNATIONAL JOURNAL OF REMOTE SENSING
14	2016	Li, ST; Lu, T; Fang, LY; Jia, XP; Benediktsson, JA	Probabilistic Fusion of Pixel-Level and Superpixel-Level Hyperspectral Image Classification	IEEE TRANSACTIONS ON GEOSCIENCE AND REMOTE SENSING
15	2016	Ng, WT; Meroni, M; Immitzer, M; Bock, S; Leonardi, U; Rembold, F; Gadain, H; Atzberger, C	Mapping Prosopis spp. with Landsat 8 data in arid environments: Evaluating effectiveness of different methods and temporal imagery selection for Hargeisa, Somaliland	INTERNATIONAL JOURNAL OF APPLIED EARTH OBSERVATION AND GEOINFORMATION
26	2016	Zheng, XY; Wang, Y; Gan, MY; Zhang, J; Teng, LM; Wang, K; Shen, ZQ; Zhang, L	Discrimination of Settlement and Industrial Area Using Landscape Metrics in Rural Region	REMOTE SENSING
42	2016	Hao, M; Shi, WZ; Zhang, H; Wang, QM; Deng, KZ	A Scale-Driven Change Detection Method Incorporating Uncertainty Analysis for Remote Sensing Images	REMOTE SENSING
43	2016	Husson, E; Ecke, F; Reese, H	Comparison of Manual Mapping and Automated Object-Based Image Analysis of Non-Submerged Aquatic Vegetation from Very-High-Resolution UAS Images	REMOTE SENSING
46	2016	Martinez-Lopez, J; Bertzky, B; Bonet-Garcia, FJ; Bastin, L; Dubois, G	Biophysical Characterization of Protected Areas Globally through Optimized Image Segmentation and Classification	REMOTE SENSING
48	2016	Zhang, XR; Song, Q; Gao, ZY; Zheng, YG; Weng, P; Jiao, LC	Spectral-Spatial Feature Learning Using Cluster-Based Group Sparse Coding for Hyperspectral Image Classification	IEEE JOURNAL OF SELECTED TOPICS IN APPLIED EARTH

				OBSERVATIONS AND REMOTE SENSING
52	2016	Wieland, M; Pittore, M	Large-area settlement pattern recognition from Landsat-8 data	ISPRS JOURNAL OF PHOTOGRAMMETRY AND REMOTE SENSING
56	2016	Debonnaire, N; Stumpf, A; Puissant, A	Spatio-Temporal Clustering and Active Learning for Change Classification in Satellite Image Time Series	IEEE JOURNAL OF SELECTED TOPICS IN APPLIED EARTH OBSERVATIONS AND REMOTE SENSING
70	2016	Wang, ZH; Liu, LY; Peng, DL; Liu, XJ; Zhang, S; Wang, YJ	Estimating woody aboveground biomass in an area of agroforestry using airborne light detection and ranging and compact airborne spectrographic imager hyperspectral data: individual tree analysis incorporating tree species information	JOURNAL OF APPLIED REMOTE SENSING
76	2016	Chen, Q; Chen, YH	Multi-Feature Object-Based Change Detection Using Self-Adaptive Weight Change Vector Analysis	REMOTE SENSING
90	2016	Li, XJ; Chen, WT; Cheng, XW; Wang, LZ	A Comparison of Machine Learning Algorithms for Mapping of Complex Surface-Mined and Agricultural Landscapes Using ZiYuan-3 Stereo Satellite Imagery	REMOTE SENSING
103	2016	Vermeulen, D; van Niekerk, A	Evaluation of a WorldView-2 image for soil salinity monitoring in a moderately affected irrigated area	JOURNAL OF APPLIED REMOTE SENSING
121	2016	Hamedianfar, A; Shafri, HZM	Integrated approach using data mining-based decision tree and object-based image analysis for high-resolution urban mapping of WorldView-2 satellite sensor data	JOURNAL OF APPLIED REMOTE SENSING
122	2016	Mylonas, SK; Stavrakoudis, DG; Theocharis, JB; Zalidis, GC; Gitas, IZ	Local Search-Based GeneSIS algorithm for the Segmentation and Classification of Remote-Sensing Images	IEEE JOURNAL OF SELECTED TOPICS IN APPLIED EARTH OBSERVATIONS AND REMOTE SENSING
129	2016	Hussain, E; Shan, J	Object-based urban land cover classification using rule inheritance over very high-resolution multisensor and multitemporal data	GISCIENCE & REMOTE SENSING
131	2016	Guo, B; Huang, XF; Li, QQ; Zhang, F; Zhu, JS; Wang, CS	A Stochastic Geometry Method for Pylon Reconstruction from Airborne LiDAR Data	REMOTE SENSING
141	2016	Chretien, LP; Theau, J; Menard, P	Visible and thermal infrared remote sensing for the detection of white-tailed deer using an unmanned aerial system	WILDLIFE SOCIETY BULLETIN
155	2016	Momeni, R; Aplin, P; Boyd, DS	Mapping Complex Urban Land Cover from Spaceborne Imagery: The Influence of Spatial Resolution, Spectral Band Set and Classification Approach	REMOTE SENSING
157	2016	Cheng, GL; Zhu, FY; Xiang, SM; Wang, Y; Pan, CH	Semisupervised Hyperspectral Image Classification via Discriminant Analysis and Robust Regression	IEEE JOURNAL OF SELECTED TOPICS IN APPLIED EARTH OBSERVATIONS AND REMOTE SENSING
163	2016	Li, MM; Stein, A; Bijker, W; Zhan, QM	Region-based urban road extraction from VHR satellite images using Binary Partition Tree	INTERNATIONAL JOURNAL OF APPLIED EARTH OBSERVATION AND GEOINFORMATION
167	2016	Mueller-Warrant, GW; Sullivan, C; Anderson, N; Whittaker, GW	Detecting and correcting logically inconsistent crop rotations and other land-use sequences	INTERNATIONAL JOURNAL OF REMOTE SENSING
177	2016	Guo, Z; Du, SH; Li, M; Zhao, WZ	Exploring GIS knowledge to improve building extraction and change detection from VHR imagery in urban areas	INTERNATIONAL JOURNAL OF IMAGE AND DATA FUSION
188	2016	Salas, EAL; Boykin, KG; Valdez, R	Multispectral and Texture Feature Application in Image-Object Analysis of Summer Vegetation in Eastern Tajikistan Pamirs	REMOTE SENSING
193	2016	Wen, DW; Huang, X; Zhang, LP; Benediktsson, JA	A Novel Automatic Change Detection Method for Urban High-Resolution Remotely Sensed Imagery Based on Multiindex Scene Representation	IEEE TRANSACTIONS ON GEOSCIENCE AND REMOTE SENSING
196	2015	Li, G; Wan, YC	A new combination classification of pixel- and object-based methods	INTERNATIONAL JOURNAL OF REMOTE SENSING
208	2015	Bekaddour, A; Bessaid, A; Bendimerad, FT	Multi Spectral Satellite Image Ensembles Classification Combining k-means, LVQ and SVM Classification Techniques	JOURNAL OF THE INDIAN SOCIETY OF REMOTE SENSING
229	2015	Zhang, YG; Zhang, LB; Yu, XC	Region of interest extraction based on multiscale visual saliency analysis for remote sensing images	JOURNAL OF APPLIED REMOTE SENSING

240	2015	Whiteside, TG; Bartolo, RE	Mapping Aquatic Vegetation in a Tropical Wetland Using High Spatial Resolution Multispectral Satellite Imagery	REMOTE SENSING
244	2015	Huang, YS	Detecting the changes in rural communities in Taiwan by applying multiphase segmentation on FORMOSA-2 satellite imagery	INTERNATIONAL JOURNAL OF APPLIED EARTH OBSERVATION AND GEOINFORMATION
247	2015	Bachofer, F; Queneherve, G; Hochschild, V; Maerker, M	Multisensoral Topsoil Mapping in the Semiarid Lake Manyara Region, Northern Tanzania	REMOTE SENSING
249	2015	Hess, LL; Melack, JM; Affonso, AG; Barbosa, C; Gastil-Buhl, M; Novo, EMLM	Wetlands of the Lowland Amazon Basin: Extent, Vegetative Cover, and Dual-season Inundated Area as Mapped with JERS-1 Synthetic Aperture Radar	WETLANDS
267	2015	Khodadadzadeh, M; Li, J; Prasad, S; Plaza, A	Fusion of Hyperspectral and LiDAR Remote Sensing Data Using Multiple Feature Learning	IEEE JOURNAL OF SELECTED TOPICS IN APPLIED EARTH OBSERVATIONS AND REMOTE SENSING
275	2015	Callaghan, K; Engelbrecht, J; Kemp, J	The Use of Landsat and Aerial Photography for the Assessment of Coastal Erosion and Erosion Susceptibility in False Bay, South Africa	SOUTH AFRICAN JOURNAL OF GEOMATICS
281	2015	Furtado, LFD; Silva, TSF; Fernandes, PJF; Novo, EMLD	Land cover classification of Lago Grande de Curuai floodplain (Amazon, Brazil) using multi-sensor and image fusion techniques	ACTA AMAZONICA
292	2015	Gianinetto, M; Rusmini, M; Marchesi, A; Maianti, P; Frassy, F; Dalla Via, G; Dini, L; Nodari, FR	Integration of COSMO-SkyMed and GeoEye-1 Data With Object-Based Image Analysis	IEEE JOURNAL OF SELECTED TOPICS IN APPLIED EARTH OBSERVATIONS AND REMOTE SENSING
299	2015	Zhao, J; Zhong, YF; Zhang, LP	Detail-Preserving Smoothing Classifier Based on Conditional Random Fields for High Spatial Resolution Remote Sensing Imagery	IEEE TRANSACTIONS ON GEOSCIENCE AND REMOTE SENSING
301	2015	Lucas, R; Blonda, P; Bunting, P; Jones, G; Inglada, J; Arias, M; Kosmidou, V; Petrou, ZI; Manakos, I; Adamo, M; Charnock, R; Tarantino, C; Mucher, CA; Jongman, RHG; Kramer, H; Arvor, D; Honrado, JP; Mairota, P	The Earth Observation Data for Habitat Monitoring (EODHaM) system	INTERNATIONAL JOURNAL OF APPLIED EARTH OBSERVATION AND GEOINFORMATION
305	2015	Abdullahi, S; Pradhan, B; Jebur, MN	GIS-based sustainable city compactness assessment using integration of MCDM, Bayes theorem and RADAR technology	GEOCARTO INTERNATIONAL
308	2015	Kamal, M; Phinn, S; Johansen, K	Object-Based Approach for Multi-Scale Mangrove Composition Mapping Using Multi-Resolution Image Datasets	REMOTE SENSING
309	2015	Crichton, KA; Anderson, K; Bennie, JJ; Milton, EJ	Characterizing peatland carbon balance estimates using freely available Landsat ETM plus data	ECOHYDROLOGY
315	2015	Banerjee, B; Bovolo, F; Bhattacharya, A; Bruzzone, L; Chaudhuri, S; Mohan, BK	A New Self-Training-Based Unsupervised Satellite Image Classification Technique Using Cluster Ensemble Strategy	IEEE GEOSCIENCE AND REMOTE SENSING LETTERS
316	2015	Zehtabian, A; Ghassemian, H	An Adaptive Pixon Extraction Technique for Multispectral/Hyperspectral Image Classification	IEEE GEOSCIENCE AND REMOTE SENSING LETTERS
317	2015	Tamim, A; Minaoui, K; Daoudi, K; Yahia, H; Atillah, A; Aboutajdine, D	An Efficient Tool for Automatic Delimitation of Moroccan Coastal Upwelling Using SST Images	IEEE GEOSCIENCE AND REMOTE SENSING LETTERS
318	2015	Meka, A; Chaudhuri, S	A Technique for Simultaneous Visualization and Segmentation of Hyperspectral Data	IEEE TRANSACTIONS ON GEOSCIENCE AND REMOTE SENSING
319	2015	Gueguen, L	Classifying Compound Structures in Satellite Images: A Compressed Representation for Fast Queries	IEEE TRANSACTIONS ON GEOSCIENCE AND REMOTE SENSING
320	2015	Quinn, NWT; Burns, JR	Use of a hybrid optical remote sensing classification technique for seasonal wetland habitat degradation assessment resulting from adoption of real-time salinity management practices	JOURNAL OF APPLIED REMOTE SENSING
332	2015	Dronova, I; Gong, P; Wang, L; Zhong, LH	Mapping dynamic cover types in a large seasonally flooded wetland using extended principal component analysis and object-based classification	REMOTE SENSING OF ENVIRONMENT
338	2015	Son, NT; Chen, CF; Chang, NB; Chen, CR; Chang, LY; Thanh, BX	Mangrove Mapping and Change Detection in Ca Mau Peninsula, Vietnam, Using Landsat Data and Object-Based Image Analysis	IEEE JOURNAL OF SELECTED TOPICS IN APPLIED EARTH OBSERVATIONS AND REMOTE SENSING

375	2015	Campbell, M; Congalton, RG; Hartter, J; Ducey, M	Optimal Land Cover Mapping and Change Analysis in Northeastern Oregon Using Landsat Imagery	PHOTOGRAMMETRIC ENGINEERING AND REMOTE SENSING
381	2014	Huang, X; Guan, XH; Benediktsson, JA; Zhang, LP; Li, J; Plaza, A; Dalla Mura, M	Multiple Morphological Profiles From Multicomponent-Base Images for Hyperspectral Image Classification	IEEE JOURNAL OF SELECTED TOPICS IN APPLIED EARTH OBSERVATIONS AND REMOTE SENSING
383	2014	Blaschke, T; Feizizadeh, B; Holbling, D	Object-Based Image Analysis and Digital Terrain Analysis for Locating Landslides in the Urmia Lake Basin, Iran	IEEE JOURNAL OF SELECTED TOPICS IN APPLIED EARTH OBSERVATIONS AND REMOTE SENSING
466	2014	Zhang, Y; Guindon, B; Lantz, N; Shipman, T; Chao, D; Raymond, D	Quantification of anthropogenic and natural changes in oil sands mining infrastructure land based on RapidEye and SPOT5	INTERNATIONAL JOURNAL OF APPLIED EARTH OBSERVATION AND GEOINFORMATION
473	2014	Aguilar, MA; Bianconi, F; Aguilar, FJ; Fernandez, I	Object-Based Greenhouse Classification from GeoEye-1 and WorldView-2 Stereo Imagery	REMOTE SENSING
495	2014	Chmielewski, S; Chmielewski, TJ; Tompalski, P	Land cover and landscape diversity analysis in the West Polesie Biosphere Reserve	INTERNATIONAL AGROPHYSICS
498	2014	Ruiz, P; Mateos, J; Camps-Valls, G; Molina, R; Katsaggelos, AK	Bayesian Active Remote Sensing Image Classification	IEEE TRANSACTIONS ON GEOSCIENCE AND REMOTE SENSING
500	2014	Virtanen, T; Ek, M	The fragmented nature of tundra landscape	INTERNATIONAL JOURNAL OF APPLIED EARTH OBSERVATION AND GEOINFORMATION
509	2014	Kim, Y; Kim, Y	Improved Classification Accuracy Based on the Output-Level Fusion of High-Resolution Satellite Images and Airborne LiDAR Data in Urban Area	IEEE GEOSCIENCE AND REMOTE SENSING LETTERS
510	2014	Hof, A; Wolf, N	Estimating potential outdoor water consumption in private urban landscapes by coupling high-resolution image analysis, irrigation water needs and evaporation estimation in Spain	LANDSCAPE AND URBAN PLANNING
512	2014	Dragut, L; Csillik, O; Eisank, C; Tiede, D	Automated parameterisation for multi-scale image segmentation on multiple layers	ISPRS JOURNAL OF PHOTOGRAMMETRY AND REMOTE SENSING
514	2014	Strasser, T; Lang, S; Riedler, B; Pernkopf, L; Paccagnel, K	Multiscale Object Feature Library for Habitat Quality Monitoring in Riparian Forests	IEEE GEOSCIENCE AND REMOTE SENSING LETTERS
516	2014	Mishra, NB; Crews, KA	Mapping vegetation morphology types in a dry savanna ecosystem: integrating hierarchical object-based image analysis with Random Forest	INTERNATIONAL JOURNAL OF REMOTE SENSING
525	2014	Costa, H; Carrao, H; Bacao, F; Caetano, M	Combining per-pixel and object-based classifications for mapping land cover over large areas	INTERNATIONAL JOURNAL OF REMOTE SENSING
536	2014	Polychronaki, A; Gitas, IZ; Minchella, A	Monitoring post-fire vegetation recovery in the Mediterranean using SPOT and ERS imagery	INTERNATIONAL JOURNAL OF WILDLAND FIRE
545	2014	Borna, K; Moore, AB; Sirguey, P	Towards a vector agent modelling approach for remote sensing image classification	JOURNAL OF SPATIAL SCIENCE
548	2014	Cheng, JH; Bo, YC; Zhu, YX; Ji, XL	A novel method for assessing the segmentation quality of high-spatial resolution remote-sensing images	INTERNATIONAL JOURNAL OF REMOTE SENSING
557	2014	Witharana, C; Civco, DL	Optimizing multi-resolution segmentation scale using empirical methods: Exploring the sensitivity of the supervised discrepancy measure Euclidean distance 2 (ED2)	ISPRS JOURNAL OF PHOTOGRAMMETRY AND REMOTE SENSING
564	2014	Baraldi, A; Boschetti, L; Humber, ML	Probability Sampling Protocol for Thematic and Spatial Quality Assessment of Classification Maps Generated From Spaceborne/Airborne Very High Resolution Images	IEEE TRANSACTIONS ON GEOSCIENCE AND REMOTE SENSING
569	2013	Moller, M; Birger, J; Gidudu, A; Glasser, C	A framework for the geometric accuracy assessment of classified objects	INTERNATIONAL JOURNAL OF REMOTE SENSING
576	2013	Westergaard-Nielsen, A; Lund, M; Hansen, BU; Tamstorf, MP	Camera derived vegetation greenness index as proxy for gross primary production in a low Arctic wetland area	ISPRS JOURNAL OF PHOTOGRAMMETRY AND REMOTE SENSING
637	2013	Rajesh, S; Arivazhagan, S; Moses, KP; Abisekaraj, R	Genetic Algorithm Based Feature Subset Selection for Land Cover/Land Use Mapping Using Wavelet Packet Transform	JOURNAL OF THE INDIAN SOCIETY OF REMOTE SENSING

Table S1 - 2 – Criteria used to analyse each paper.

Question/ column	***Application context***	***Definition or criteria for evaluation***
#1	*Application context*	A brief description stating the context and objectives of the study.
#2	*Relevant?*	Is the publication relevant or usable for the study? (yes / no) To be usable it must employ both an object-based/image segmentation algorithm and supervised or unsupervised classification. If a paper is not relevant it is not required to collect more data/metadata about it.
#3	*Optical/SAR/HySR*	What kind of data was used in the study: Optical, Hyperspectral, LiDAR or SAR?
#4	*Segmentation?*	Was image segmentation/OBIA used in the study? (yes / no)
#5	*Classification?*	Was supervised or unsupervised classification used in the study? (yes / no)
#6	*Classification Type*	Type of classification used, either: supervised, unsupervised or both
#7	*Segmentation algorithm*	Acronym name of the segmentation algorithm, e.g.: Seed Region Growing, Mean Shift, Baatz-Schape, Graph-based. If it is a particular type of algorithm put the reference in curly brackets
#8	*Segmentation software*	Name of the software where the segmentation/OBIA algorithm is implemented
#9	*Classification algorithm*	Acronym name of the classification algorithm used in the paper, e.g., SVM, RF, C45, J48, KNN
#10	*Classification software*	Name of the software where the classification algorithm is implemented
#11	*Segmentation parameters defined on the paper?*	Are segmentation parameters clearly defined and stated on the paper? (yes / no) E.g., "*we used GRASS region growing algorithm with a threshold value of 0.345 and a minimum segment size of 20 (pixels)...*"
#12	*Procedure for defining or optimizing segmentation parameters*	Was any procedure or methodology used for defining, optimizing, improving or checking segmentation parameters? If not then use: Not defined or N/A if not applicable. If yes, then put a brief description of the method used.
#13	*Integrates segmentation with classification results for parameter definition or optimization?*	Were classification performance metrics/indices (e.g., accuracy, Kappa, F1, AUC) or unsupervised clustering quality (e.g., Silhouette index, Dunn index, Calinski-Harabasz, C-index) anyhow used to improve, change, tune or optimize segmentation parameters?

A summary of the type of procedures defined or tuned for image segmentation parameters, as well as the software used for image segmentation in the set of papers analysed is presented in Figure S1-1.

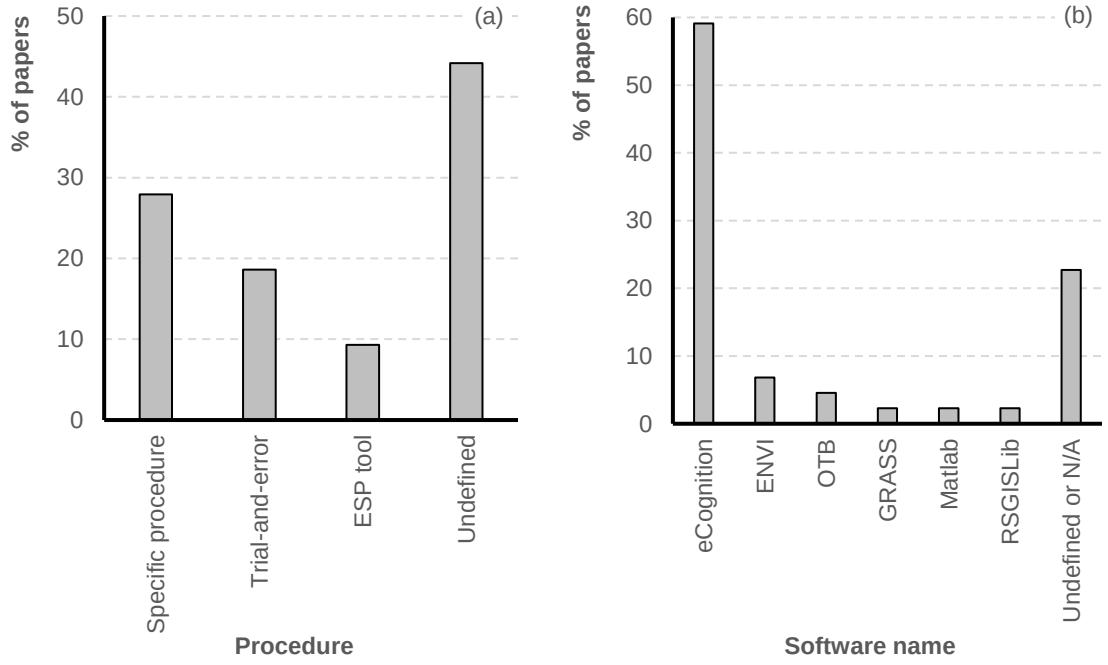

Figure S1 - 1 (a) – Type of procedure used for defining/tuning image segmentation parameters by % of papers reviewed; and, (b) software used for image segmentation by % of papers reviewed (*eCognition*, *ENVI* and *Matlab* are commercial applications while *GRASS*, *OTB* and *RSGISLib* are open-source).

Appendix S2 – Ranges of image segmentation parameters by test site

Table S2 - 1 – List of parameter ranges used for genetic algorithm optimization by test site (E1 to E6). The order of values follows that of parameter names in column #2 ("Algorithms and parameters").

Software	Algorithm and parameters	Upper / lower bound	Test site					
			E1	E2	E3	E4	E5	E6
ArcGIS	**Mean-shift:** 1) Spatial detail 2) Spectral detail 3) Minimum segment size	min	12, 12, 5	12, 12, 5	12, 12, 3	12, 12, 3	12, 12, 3	17, 17, 5
		max	20, 20, 60	20, 20, 60	20, 20, 40	20, 20, 40	20, 20, 40	20, 20, 50
SAGA GIS	**Region growing:** 1) merge threshold 2) minimum segment size	min	5, 1, 0.3, 0.3	5, 1, 0.3, 0.3	5, 1, 0.3, 0.3	5, 1, 0.3, 0.3	5, 1, 0.3, 0.3	5, 3, 0.5, 0.5
		max	30, 10, 1.5, 1.5	30, 10, 1.5, 1.5	30, 10, 1.5, 1.5	30, 10, 1.5, 1.5	30, 10, 1.5, 1.5	8, 10, 1.2, 1.2
GRASS GIS	**Region growing:** 1) merge threshold 2) minimum segment size	min	0.1, 10	0.05, 5	0.05, 3	0.01, 3	0.05, 3	0.005, 5
		max	0.5, 60	0.35, 60	0.4, 40	0.2, 40	0.4, 40	0.1, 50
RSGISLib	**Shepherd k-means iterative elimination:** 1) Nr of clusters 2) Spectral threshold 3) Minimum segment size	min	10, 40, 40	5, 15, 20	5, 5, 3	5, 5, 3	5, 3, 3	5, 3, 5
		max	20, 60, 80	20, 80, 80	20, 60, 40	20, 60, 40	20, 60, 40	20, 20, 50
OTB	**Large-scale mean-shift:** 1) Spatial detail 2) Spectral detail 3) Minimum segment size	min	10, 10, 30	3, 3, 10	3, 3, 3	3, 3, 3	3, 3, 3	3, 3, 5
		max	20, 20, 75	20, 20, 80	12, 10, 40	12, 10, 40	12, 10, 40	15, 15, 50
TerraLib	**Mean region growing:** 1) merge threshold 2) minimum segment size	min	0.005, 5	0.01, 5	0.01, 3	0.005, 3	0.005, 3	0.005, 5
		max	0.15, 40	0.2, 60	0.1, 40	0.075, 30	0.02, 20	0.01, 20
TerraLib	**Baatz-Schäpe multiresolution:** 1) Compact. weight 2) Colour weight 3) Minimum segment size 4) Merging threshold	min	0.5, 0.5, 0.01, 5	0.25, 0.25, 0.1, 10	0.5, 0.5, 0.01, 3	0.5, 0.5, 0.005, 3	0.5, 0.5, 0.01, 3	0.5, 0.5, 0.005, 3
		max	1, 1, 0.25, 60	1, 1, 0.5, 80	1, 1, 0.25, 30	1, 1, 0.01, 30	1, 1, 0.25, 20	1, 1, 0.025, 20

Appendix S3 – List of land cover/use classes for multi-class test sites

Table S3 - 1 – List of land cover/use classes by test site for multi-class problems: E2 (UAV image data), E4 (RapidEye) and E6 (Sentinel-2).

Test site	Description	Class ID/code
E2 Serra d'Arga mountain range, Caminha UL: (41°49'16.93"N, 8°42'51.53"W) LR: (41°49'14.98"N, 8°42'48.95"W)	Wet heath (Habitat Type 4020* - Temperate Atlantic wet heaths with *Erica ciliaris* and *Erica tetralix*	1
	Dry heath (Habitat Type 4030 European dry heaths)	2
	Nardus grasslands (Habitat Type 6230* Species-rich *Nardus* grassland, on siliceous substrates in mountain areas)	4
	Bare rock	6
	Bare soil	7
	Water lines	9
E4 Viana do Castelo city UL: (41°42'51.48"N, 8°51'53.13"W) LR: (41°40'9.05"N, 8°48'17.26"W)	Urban continuous	7
	Urban discontinuous	9
	Cropland	8
	Forest areas	6
	Semi-natural vegetation (shrubland, heathland)	2
	Bare soil	1
	Sand	3
	Shoreline rock outcrops or sandy sediments	4
	Water surfaces	5
E6 Vez river watershed, Arcos de Valdevez municipality UL: (42°1'3.7"N, 8°31'31.62"W) LR: (41°48'16.6"N, 8°15'22.24"W)	Urban / artificial areas / roads	1
	Annual crops	9
	Permanent crops	10
	Pine forest / woodlands	4
	Eucalyptus forest / woodlands	6
	Oak forest / woodlands	7
	Shrubland / heathland	3
	Low shrubland / rock outcrops	8
	Burnt areas / very-low vegetation cover	5
	Water surfaces	2

Appendix S4 – Confusion matrices for multi-class tests

Table S4 - 1 – Confusion matrix for test site E2

		Observed						
		Wet heath	**Dry heath**	***Nardus* grasslands**	**Bare rock**	**Bare soil**	**Water lines**	**User accuracy**
Predicted	**Wet heath**	**5892**	188	407	0	23	35	**0.90**
	Dry heath	155	**11835**	597	143	114	98	**0.91**
	***Nardus* grasslands**	945	1097	**24393**	28	125	84	**0.92**
	Bare rock	0	84	44	**1032**	12	2	**0.88**
	Bare soil	0	14	9	0	**414**	1	**0.95**
	Water lines	10	69	85	0	3	**1174**	**0.88**
	Producer accuracy	**0.84**	**0.89**	**0.96**	**0.86**	**0.60**	**0.84**	

Table S4 - 2 – Confusion matrix for test site E4

		Observed									
		Bare soil	**Semi-natural vegetation**	**Sand**	**Rock outcrops**	**Water surfaces**	**Forest**	**Urban continuous**	**Cropland**	**Urban discont.**	**User accuracy**
Predicted	**Bare soil**	**3**	8	0	0	0	1	3	3	5	**0.13**
	Semi-natural vegetation	10	**38**	0	0	1	12	17	27	9	**0.33**
	Sand	0	0	**7**	0	0	0	1	0	0	**0.88**
	Rock outcrops	0	0	0	**19**	4	1	13	0	0	**0.51**
	Water surfaces	0	0	0	12	**9153**	0	3	0	0	**1.00**
	Forest	0	56	0	2	0	**2870**	11	7	3	**0.97**
	Urban continuous	6	26	43	33	0	19	**1501**	7	123	**0.85**
	Cropland	6	36	0	0	0	4	7	**103**	6	**0.64**
	Urban discont.	9	16	1	0	0	2	73	8	**113**	**0.51**
	Producer accuracy	**0.09**	**0.21**	**0.14**	**0.29**	**1.00**	**0.99**	**0.92**	**0.67**	**0.44**	

Table S4 - 3 – Confusion matrix for test site E6

		Observed										
		Urban / artificial areas / roads	**Water surfaces**	**Shrubland / heathland**	**Pine forest / woodlands**	**Burnt areas**	**Eucalyptus forest/woodlands**	**Oak forest / woodlands**	**Low shrubland / rock outcrops**	**Annual crops**	**Permanent crops**	**User accuracy**
Predicted	**Urban / artificial areas / roads**	**235**	0	0	0	0	0	0	0	1	4	0.98
	Water surfaces	0	**108**	0	0	0	0	0	0	0	0	1.00
	Shrubland / heathland	0	0	**1718**	21	11	2	31	18	3	1	0.95
	Pine forest / woodlands	0	0	6	**244**	16	23	1	0	0	0	0.84
	Burnt areas	0	0	3	5	**215**	1	0	1	0	1	0.95
	Eucalyptus forest / woodlands	0	0	0	4	0	**24**	0	0	0	0	0.86
	Oak forest / woodlands	0	0	7	4	8	0	**679**	0	0	1	0.97
	Low shrubland / rock outcrops	1	0	25	0	1	0	7	**1348**	4	0	0.97
	Annual crops	2	0	1	0	0	0	0	2	**298**	19	0.93
	Permanent crops	0	0	0	0	0	0	0	0	15	**71**	0.83
	Producer accuracy	0.99	1.00	0.98	0.88	0.86	0.48	0.95	0.99	0.93	0.73	

Appendix S5 – Full list of optimized parameters by test site and algorithm

Test site	Segmentation algorithm	Classification algorithm	Optimized image segmentation parameters
E1	ArcGIS_MShift	GBM	SpectralDetail=12.861, SpatialDetail=14.945, MinSegmentSize=37.22
E1	ArcGIS_MShift	RF	SpectralDetail=13.084, SpatialDetail=14.139, MinSegmentSize=50.152
E1	ArcGIS_MShift	SVM	SpectralDetail=12.924, SpatialDetail=13.322, MinSegmentSize=32.985
E1	GRASS_RG	GBM	Threshold=0.432, MinSize=51.444
E1	GRASS_RG	RF	Threshold=0.442, MinSize=53.501
E1	GRASS_RG	SVM	Threshold=0.451, MinSize=51.007
E1	OTB_LSMS	GBM	SpectralRange=17.088, SpatialRange=11.509, MinSize=72.125
E1	OTB_LSMS	RF	SpectralRange=17.257, SpatialRange=16.638, MinSize=64.093
E1	OTB_LSMS	SVM	SpectralRange=18.474, SpatialRange=12.672, MinSize=63.914
E1	RSGISLib_Shep	GBM	NumClust=11.99, MinSize=59.216, SpectralThresh=78.694
E1	RSGISLib_Shep	RF	NumClust=5.682, MinSize=46.789, SpectralThresh=71.65
E1	RSGISLib_Shep	SVM	NumClust=12.119, MinSize=47.446, SpectralThresh=67.598
E1	SAGA_SRG	GBM	Bandwidth=25.751, GaussianWeightingBW=6.319, VarFeatSpace=0.763, VarPosSpace=0.755
E1	SAGA_SRG	RF	Bandwidth=25.779, GaussianWeightingBW=4.014, VarFeatSpace=0.964, VarPosSpace=0.4
E1	SAGA_SRG	SVM	Bandwidth=26.237, GaussianWeightingBW=8.087, VarFeatSpace=0.52, VarPosSpace=0.91
E1	Terralib_Baatz	GBM	CompactnessWeight=0.878, SpectralWeight=0.558, Threshold=0.234, MinSize=54.549
E1	Terralib_Baatz	RF	CompactnessWeight=0.593, SpectralWeight=0.563, Threshold=0.09, MinSize=56.254
E1	Terralib_Baatz	SVM	CompactnessWeight=0.867, SpectralWeight=0.538, Threshold=0.24, MinSize=39.235
E1	Terralib_MRGrow	GBM	Threshold=0.062, MinSize=23.962
E1	Terralib_MRGrow	RF	Threshold=0.069, MinSize=18.058
E1	Terralib_MRGrow	SVM	Threshold=0.085, MinSize=30.443
E2	ArcGIS_MShift	GBM	SpectralDetail=15.586, SpatialDetail=18.032, MinSegmentSize=5.956
E2	ArcGIS_MShift	RF	SpectralDetail=16.49, SpatialDetail=15.118, MinSegmentSize=5.275
E2	ArcGIS_MShift	SVM	SpectralDetail=18.928, SpatialDetail=15.5, MinSegmentSize=6.649
E2	GRASS_RG	GBM	Threshold=0.166, MinSize=16.078
E2	GRASS_RG	RF	Threshold=0.051, MinSize=7.785
E2	GRASS_RG	SVM	Threshold=0.179, MinSize=6.993
E2	OTB_LSMS	GBM	SpectralRange=8.688, SpatialRange=9.07, MinSize=76.495
E2	OTB_LSMS	RF	SpectralRange=4.63, SpatialRange=10.947, MinSize=20.556
E2	OTB_LSMS	SVM	SpectralRange=5.066, SpatialRange=16.328, MinSize=45.433
E2	RSGISLib_Shep	GBM	NumClust=15.705, MinSize=69.776, SpectralThresh=46.432

E2	RSGISLib_Shep	RF	NumClust=10.299, MinSize=19.922, SpectralThresh=20.56
E2	RSGISLib_Shep	SVM	NumClust=15.215, MinSize=52.454, SpectralThresh=21.019
E2	SAGA_SRG	GBM	Bandwidth=13.657, GaussianWeightingBW=1.242, VarFeatSpace=1.288, VarPosSpace=0.845
E2	SAGA_SRG	RF	Bandwidth=8.483, GaussianWeightingBW=5.069, VarFeatSpace=1.074, VarPosSpace=0.675
E2	SAGA_SRG	SVM	Bandwidth=11.105, GaussianWeightingBW=5.387, VarFeatSpace=1.03, VarPosSpace=0.519
E2	Terralib_Baatz	GBM	CompactnessWeight=0.367, SpectralWeight=0.676, Threshold=0.336, MinSize=64.421
E2	Terralib_Baatz	RF	CompactnessWeight=0.489, SpectralWeight=0.295, Threshold=0.185, MinSize=21.537
E2	Terralib_Baatz	SVM	CompactnessWeight=0.588, SpectralWeight=0.333, Threshold=0.206, MinSize=11.503
E2	Terralib_MRGrow	GBM	Threshold=0.029, MinSize=31.278
E2	Terralib_MRGrow	RF	Threshold=0.013, MinSize=11.836
E2	Terralib_MRGrow	SVM	Threshold=0.012, MinSize=19.966
E3	ArcGIS_MShift	GBM	SpectralDetail=19.075, SpatialDetail=17.009, MinSegmentSize=28.677
E3	ArcGIS_MShift	RF	SpectralDetail=18.016, SpatialDetail=15.321, MinSegmentSize=9.845
E3	ArcGIS_MShift	SVM	SpectralDetail=18.226, SpatialDetail=18.13, MinSegmentSize=24.195
E3	GRASS_RG	GBM	Threshold=0.345, MinSize=37.127
E3	GRASS_RG	RF	Threshold=0.082, MinSize=36.222
E3	GRASS_RG	SVM	Threshold=0.266, MinSize=31.77
E3	OTB_LSMS	GBM	SpectralRange=4.011, SpatialRange=8.738, MinSize=15.674
E3	OTB_LSMS	RF	SpectralRange=3.087, SpatialRange=4.465, MinSize=21.225
E3	OTB_LSMS	SVM	SpectralRange=5.741, SpatialRange=5.65, MinSize=9.267
E3	RSGISLib_Shep	GBM	NumClust=9.966, MinSize=47.813, SpectralThresh=33.182
E3	RSGISLib_Shep	RF	NumClust=10.682, MinSize=46.514, SpectralThresh=34.632
E3	RSGISLib_Shep	SVM	NumClust=9.91, MinSize=33.562, SpectralThresh=32.235
E3	SAGA_SRG	GBM	Bandwidth=16.366, GaussianWeightingBW=6.407, VarFeatSpace=1.08, VarPosSpace=0.7
E3	SAGA_SRG	RF	Bandwidth=27.103, GaussianWeightingBW=4.323, VarFeatSpace=1.233, VarPosSpace=1.158
E3	SAGA_SRG	SVM	Bandwidth=23.523, GaussianWeightingBW=4.713, VarFeatSpace=0.961, VarPosSpace=0.586
E3	Terralib_Baatz	GBM	CompactnessWeight=0.765, SpectralWeight=0.724, Threshold=0.124, MinSize=13.46
E3	Terralib_Baatz	RF	CompactnessWeight=0.793, SpectralWeight=0.728, Threshold=0.118, MinSize=16.956
E3	Terralib_Baatz	SVM	CompactnessWeight=0.819, SpectralWeight=0.718, Threshold=0.123, MinSize=18.573
E3	Terralib_MRGrow	GBM	Threshold=0.025, MinSize=3.234
E3	Terralib_MRGrow	RF	Threshold=0.03, MinSize=12.326
E3	Terralib_MRGrow	SVM	Threshold=0.032, MinSize=8.871
E4	ArcGIS_MShift	GBM	SpectralDetail=19.977, SpatialDetail=16.345, MinSegmentSize=20.647
E4	ArcGIS_MShift	RF	SpectralDetail=19.84, SpatialDetail=17.235, MinSegmentSize=35.072

E4	ArcGIS_MShift	SVM	SpectralDetail=19.394, SpatialDetail=16.387, MinSegmentSize=25.314
E4	GRASS_RG	GBM	Threshold=0.027, MinSize=3.291
E4	GRASS_RG	RF	Threshold=0.058, MinSize=4.96
E4	GRASS_RG	SVM	Threshold=0.062, MinSize=9.648
E4	OTB_LSMS	GBM	SpectralRange=9.873, SpatialRange=4.201, MinSize=38.262
E4	OTB_LSMS	RF	SpectralRange=11.314, SpatialRange=3.198, MinSize=35.541
E4	OTB_LSMS	SVM	SpectralRange=10.891, SpatialRange=4.7, MinSize=34.729
E4	RSGISLib_Shep	GBM	NumClust=14.822, MinSize=34.598, SpectralThresh=13.794
E4	RSGISLib_Shep	RF	NumClust=15.486, MinSize=33.24, SpectralThresh=26.473
E4	RSGISLib_Shep	SVM	NumClust=14.715, MinSize=23.696, SpectralThresh=12.106
E4	SAGA_SRG	GBM	Bandwidth=9.386, GaussianWeightingBW=5.341, VarFeatSpace=0.84, VarPosSpace=0.847
E4	SAGA_SRG	RF	Bandwidth=6.884, GaussianWeightingBW=4.205, VarFeatSpace=0.974, VarPosSpace=0.915
E4	SAGA_SRG	SVM	Bandwidth=5.714, GaussianWeightingBW=6.302, VarFeatSpace=0.812, VarPosSpace=0.516
E4	Terralib_Baatz	GBM	CompactnessWeight=0.585, SpectralWeight=0.685, Threshold=0.006, MinSize=27.195
E4	Terralib_Baatz	RF	CompactnessWeight=0.531, SpectralWeight=0.65, Threshold=0.006, MinSize=28.182
E4	Terralib_Baatz	SVM	CompactnessWeight=0.736, SpectralWeight=0.834, Threshold=0.007, MinSize=28.398
E4	Terralib_MRGrow	GBM	Threshold=0.006, MinSize=28.089
E4	Terralib_MRGrow	RF	Threshold=0.006, MinSize=27.194
E4	Terralib_MRGrow	SVM	Threshold=0.006, MinSize=29.261
E5	ArcGIS_MShift	GBM	SpectralDetail=19.599, SpatialDetail=19.197, MinSegmentSize=24.852
E5	ArcGIS_MShift	RF	SpectralDetail=19.411, SpatialDetail=19.828, MinSegmentSize=19.746
E5	ArcGIS_MShift	SVM	SpectralDetail=19.474, SpatialDetail=19.513, MinSegmentSize=19.969
E5	GRASS_RG	GBM	Threshold=0.015, MinSize=11.009
E5	GRASS_RG	RF	Threshold=0.015, MinSize=13.173
E5	GRASS_RG	SVM	Threshold=0.01, MinSize=14.857
E5	OTB_LSMS	GBM	SpectralRange=10.762, SpatialRange=12.27, MinSize=34.155
E5	OTB_LSMS	RF	SpectralRange=14.318, SpatialRange=6.748, MinSize=39.988
E5	OTB_LSMS	SVM	SpectralRange=10.878, SpatialRange=3.551, MinSize=32.681
E5	RSGISLib_Shep	GBM	NumClust=11.402, MinSize=16.076, SpectralThresh=21.135
E5	RSGISLib_Shep	RF	NumClust=10.45, MinSize=35.633, SpectralThresh=26.415
E5	RSGISLib_Shep	SVM	NumClust=11.437, MinSize=50.681, SpectralThresh=32.081
E5	SAGA_SRG	GBM	Bandwidth=6.265, GaussianWeightingBW=5.399, VarFeatSpace=1.204, VarPosSpace=1.056
E5	SAGA_SRG	RF	Bandwidth=5.343, GaussianWeightingBW=5.622, VarFeatSpace=0.945, VarPosSpace=0.657
E5	SAGA_SRG	SVM	Bandwidth=6.126, GaussianWeightingBW=5.438, VarFeatSpace=0.856, VarPosSpace=1.117

E5	Terralib_Baatz	GBM	CompactnessWeight=0.829, SpectralWeight=0.836, Threshold=0.094, MinSize=15.385
E5	Terralib_Baatz	RF	CompactnessWeight=0.864, SpectralWeight=0.629, Threshold=0.154, MinSize=16.915
E5	Terralib_Baatz	SVM	CompactnessWeight=0.67, SpectralWeight=0.795, Threshold=0.093, MinSize=15.85
E5	Terralib_MRGrow	GBM	Threshold=0.007, MinSize=7.924
E5	Terralib_MRGrow	RF	Threshold=0.007, MinSize=4.357
E5	Terralib_MRGrow	SVM	Threshold=0.006, MinSize=11.339
E6	ArcGIS_MShift	GBM	SpectralDetail=19.031, SpatialDetail=19.529, MinSegmentSize=41.708
E6	ArcGIS_MShift	RF	SpectralDetail=19.284, SpatialDetail=18.443, MinSegmentSize=29.372
E6	ArcGIS_MShift	SVM	SpectralDetail=19.832, SpatialDetail=17.11, MinSegmentSize=44.711
E6	GRASS_RG	GBM	Threshold=0.025, MinSize=6.26
E6	GRASS_RG	RF	Threshold=0.008, MinSize=12.87
E6	GRASS_RG	SVM	Threshold=0.006, MinSize=17.378
E6	OTB_LSMS	GBM	SpectralRange=8.183, SpatialRange=11, MinSize=47.527
E6	OTB_LSMS	RF	SpectralRange=10.031, SpatialRange=11.875, MinSize=49.553
E6	OTB_LSMS	SVM	SpectralRange=7.269, SpatialRange=11.39, MinSize=48.101
E6	RSGISLib_Shep	GBM	NumClust=13.809, MinSize=8.398, SpectralThresh=19.818
E6	RSGISLib_Shep	RF	NumClust=11.303, MinSize=9.338, SpectralThresh=34.617
E6	RSGISLib_Shep	SVM	NumClust=14.198, MinSize=14.535, SpectralThresh=41.497
E6	SAGA_SRG	GBM	Bandwidth=6.855, GaussianWeightingBW=3.354, VarFeatSpace=0.788, VarPosSpace=0.561
E6	SAGA_SRG	RF	Bandwidth=6.517, GaussianWeightingBW=5.775, VarFeatSpace=0.764, VarPosSpace=0.913
E6	SAGA_SRG	SVM	Bandwidth=5.039, GaussianWeightingBW=9.346, VarFeatSpace=1.015, VarPosSpace=1.154
E6	Terralib_Baatz	GBM	CompactnessWeight=0.607, SpectralWeight=0.684, Threshold=0.005, MinSize=18.001
E6	Terralib_Baatz	RF	CompactnessWeight=0.879, SpectralWeight=0.865, Threshold=0.011, MinSize=19.712
E6	Terralib_Baatz	SVM	CompactnessWeight=0.611, SpectralWeight=0.737, Threshold=0.023, MinSize=19.794
E6	Terralib_MRGrow	GBM	Threshold=0.005, MinSize=6.284
E6	Terralib_MRGrow	RF	Threshold=0.006, MinSize=5.713
E6	Terralib_MRGrow	SVM	Threshold=0.006, MinSize=10.419